THE UNIVERSITY OF STRATHCLYDE IN GLASGOW

CONTRIBUTION OF CORTICOMUSCULAR SYNCHRONY TO HUMAN MOVEMENT AND ITS POTENTIAL USE IN NEUROPROSTHETIC CONTROL

VOLUME 2

VASILEIOS G. STAMATOPOULOS

JUNE 2005

5 RESULTS

5.1 TEMPORAL AND SPATIAL CHARACTERISTICS OF EMG, EEG, EMG\EEG COUPLING

5.1.1 Introduction

The results that will be presented were acquired from experiments carried out on a group of 9 normal subjects. All subjects provided informed written consent with the ethical approval of the University of Strathclyde's Ethics Committee.

The main aim of the experiment was to identify movement dependent features in the temporal characteristics of EMG and EEG as well as spatial characteristics of the EEG frequency estimates by using frequency domain and time-frequency analysis techniques.

Multichannel monopolar EEG signals from 28 cortical electrodes and bipolar EMG signals from Extensor Carpi Radialis Longus (ECRL) muscle, Flexor Carpi Radialis (FCR) muscle and Biceps Brachii, Long Head (BBLH) were recorded during the repetition of the move-hold sequence. Angle rate (angular velocity) information was also recorded by a rate goniometer attached on the upper palm of the subject's hand. The move-hold sequence involved the sequential performance of four phases:

- movement flexion movement
- posture flexion posture
- movement extension
- posture extension

The duration of each movement or posture phase was 2.1s. The tasks were performed in an unconstrained manner without wrist or forearm support. Thus the elbow flexor (BBLH) plays a crucial role in stabilising forearm position throughout the task. Instructions to the subject on when to move or to hold a position were cued by auditory stimuli. For each subject 21 continuous complete move-hold sequence trials were completed. Each trial contained four phases which resulted in a 176.4sec recording.

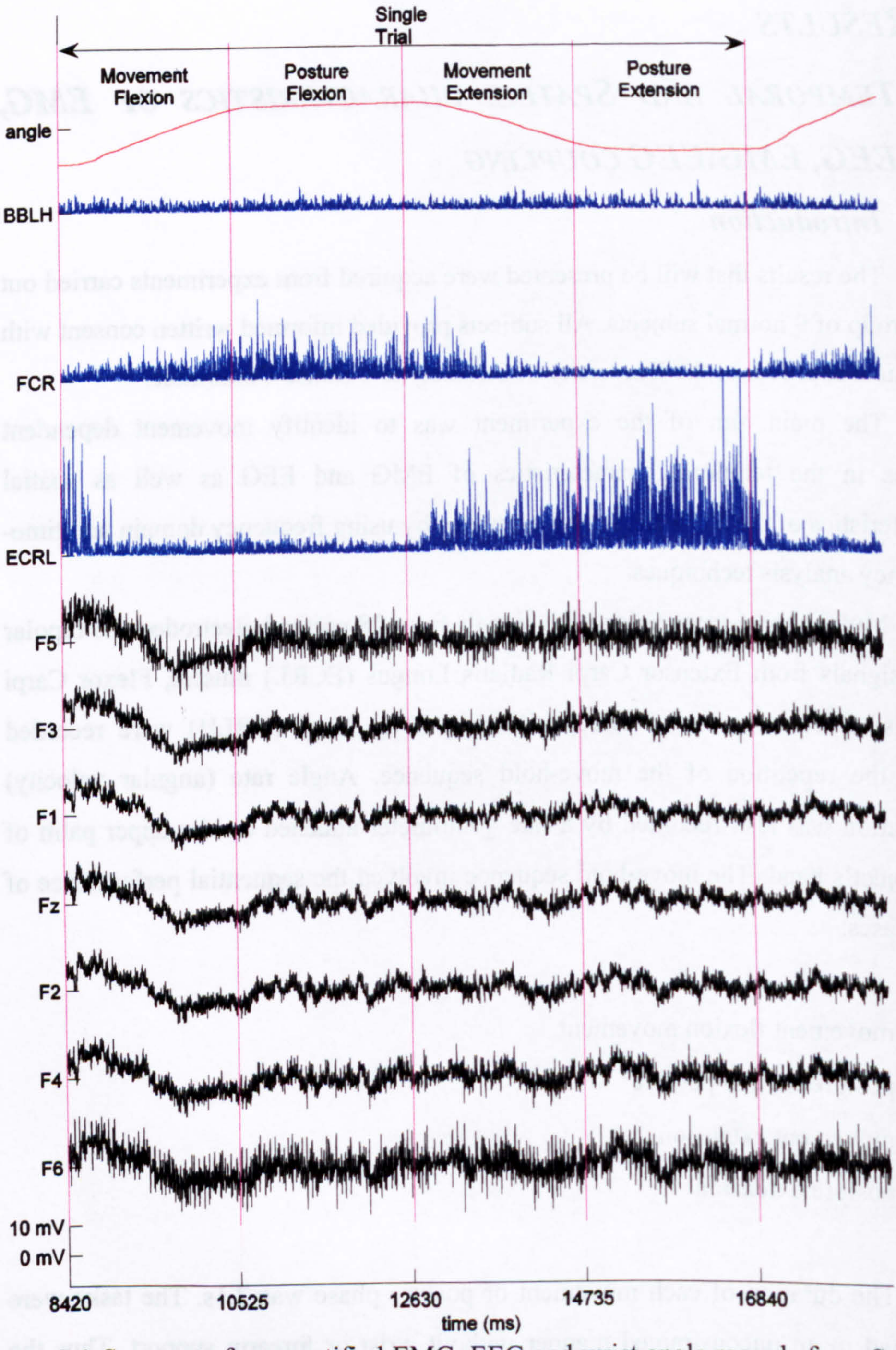

Fig.5.1 Segment of raw rectified EMG, EEG and wrist angle records from Subject 5. BBLH, FCR and ECRL EMGs and 7 from a total of 28 recorded EEG channels are displayed. The audio cues instructing the subject to move or hold are displayed in the plot as the magenta lines.

Wrist angle information and the wrist flexor (FCR), extensor (ECRL) and elbow flexor (BBLH) EMGs, as well as 28 EEG channels were recorded and analysed (Fig.5.1). Fig. 5.2 shows a detail from Fig.5.1 illustrating only the rectified EMGs during the movement extension phase.

5.1.2 Data Pre-Processing and analysis

Before the main analysis, the move-hold data were organised according to task phase. The records for each one of the four phases (for all 21 trials and all 9 subjects) were segmented and pooled to produce 4 separate records, one for each of the 4 phases (movement flexion, posture flexion, movement extension, and posture extension). The frequency domain estimates therefore correspond to the pooled across subjects and trials for each phase of the task.

Given the variability in reaction times after the audio cues, it is important to ensure that the data encompassing the transition between move and hold phases do not contaminate the pooled, phase specific datasets. Accordingly, in order to avoid including transitional states in this analysis, data occurring within ±200ms of the auditory cues were discarded. Once data sets were pooled in this way power spectra, pairwise intermuscular coherence, cumulant and phase for all recorded electrophysiological signals were calculated.

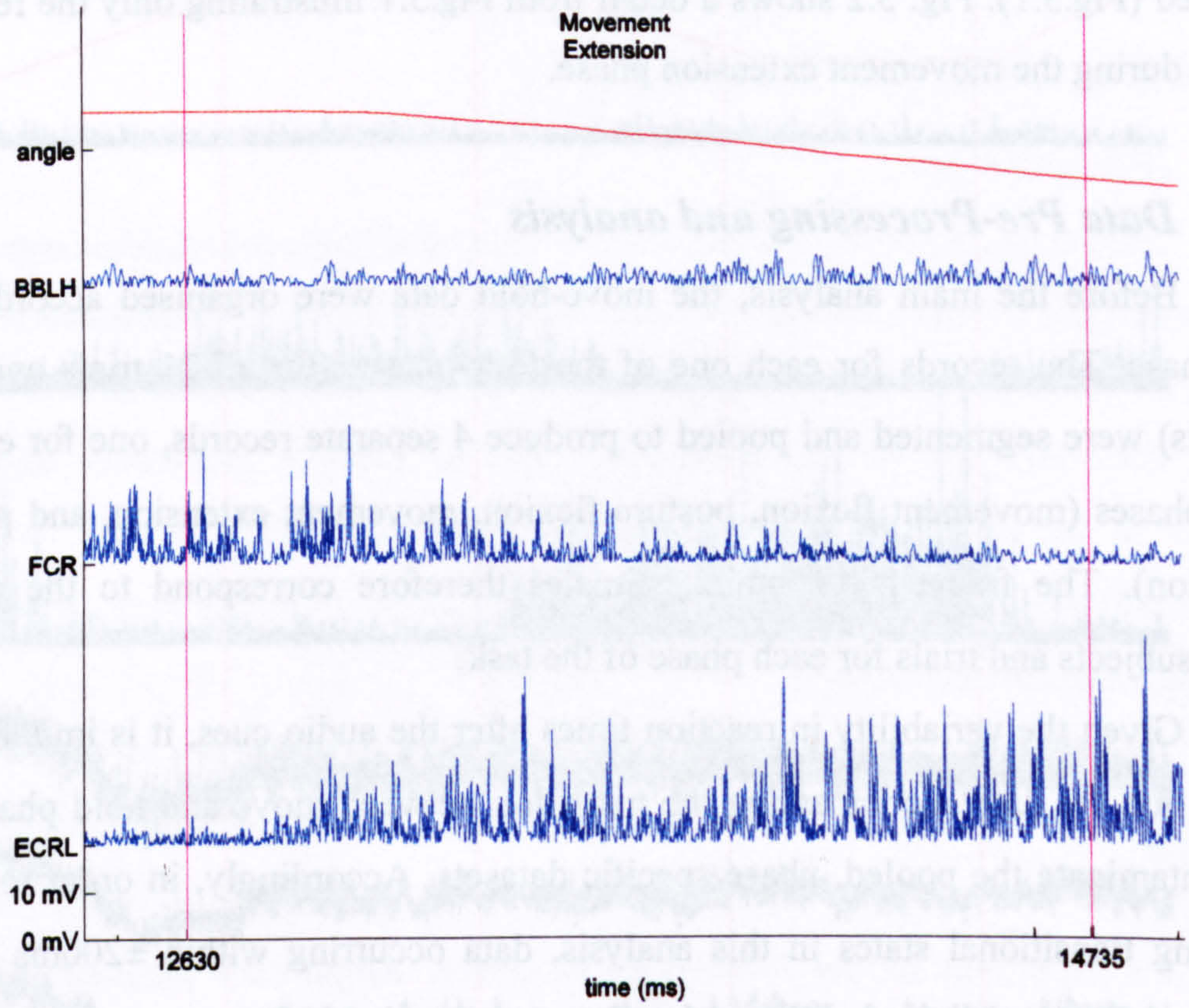

Fig. 5.2 EMG bursting during movement. Detail from Fig.5.1 where rectified EMGs of FCR and ECRL muscles demonstrate clear EMG bursting during movement extension. Angle information and audio cues are also shown.

5.1.3 Temporal EMG frequency characteristics.

To best illustrate any task dependent characteristics within the EMG signals the results of the analysis are presented as illustrated in Fig. 5.3 which shows a matrix of plots relating to single phase autospectra for each EMG channel (row 1, Fig. 5.3*a,b,c*), the respective pairwise coherences (row 2, Fig. 5.3*d,e,f*), cumulant densities (row 3, Fig. 5.3*g,h,i*) and phase plots (row 4, Fig. 5.3*j,k,f*). Statistical parameters illustrating the estimated magnitude of a 95% confidence interval for each spectral estimate are shown by the small vertical lines at the top right of each power spectrum. The green horizontal lines in the coherence plots represent the estimated upper 95% confidence limit. In the cumulant estimate plots the horizontal line at zero is the asymptotic value and the green horizontal lines are the estimated upper and lower 95% confidence limits. Finally, the phase is only shown at frequencies where statistically significant coherence (over the 95% confidence limit) is identified. The blue plot represents the phase of the rectified EMG signals while red represents the phase when the second of the rectified signals was inverted. When normal phase can not be interpreted according the model described in analytical methods chapter, the phase curve when one of the two signals has been inverted can derive the correct delay, especially when signals are coupled in an "out of phase" fashion. The power spectral and coherence estimates have been further smoothed, using a 3 point Hanning filter (Halliday and Rosenberg 1999). Smoothing was not used for the cumulant density and phase.

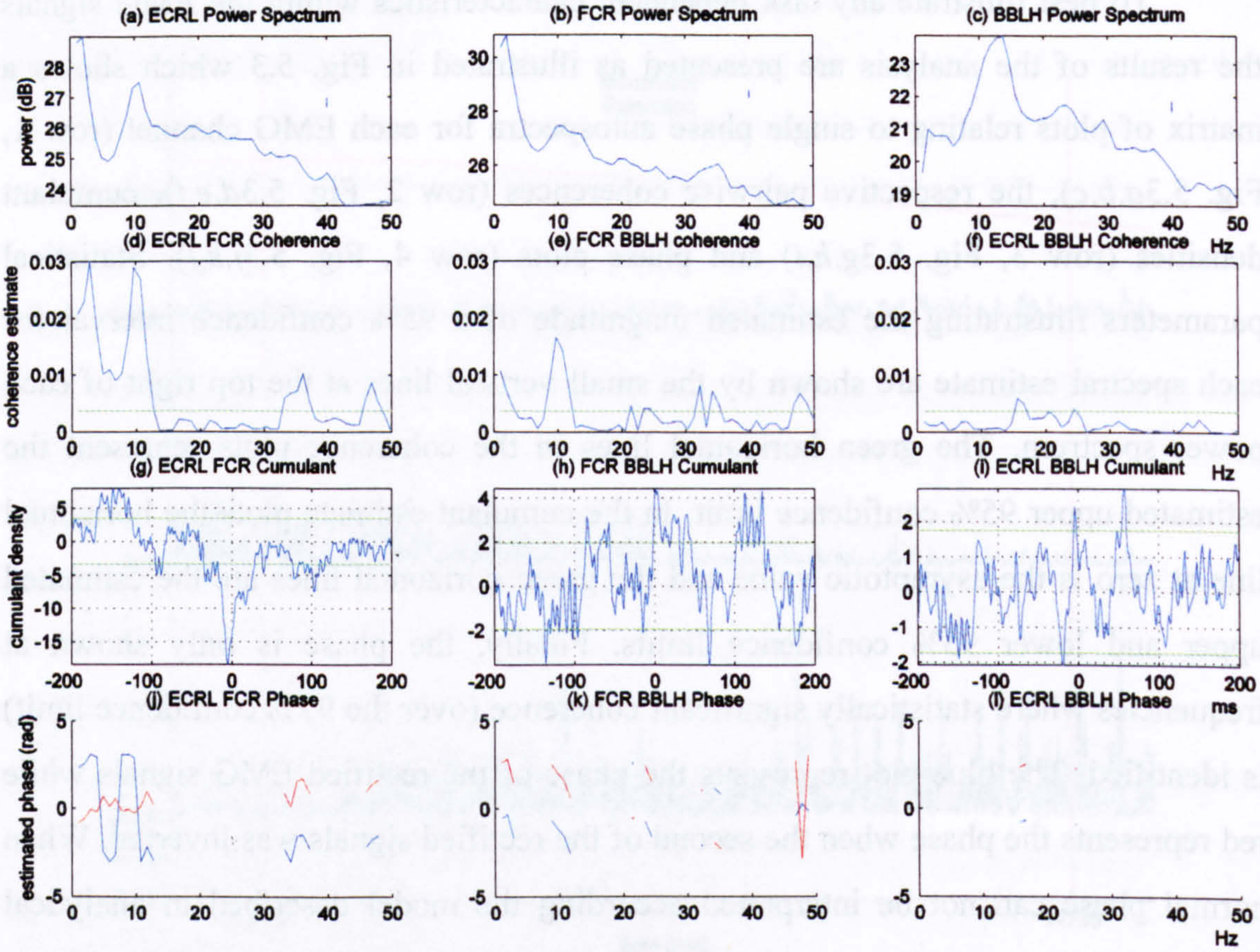

Fig. 5.3 Frequency characteristics of ECRL, FCR and BBLH EMGs, during movement flexion. The frequency characteristics include powers spectral estimates for the three EMGs on the first row of plots (a, b, c), with the small vertical lines at the top right give the estimated magnitude of a 95% confidence interval. The second row of plots (d, e, f) gives the coherence estimates between all three pairs of EMGs. The green horizontal line represents the estimated upper 95% confidence limit. The third row of plots (g, h, i) corresponds to the cumulant estimates for the current phase for the same pairs of muscles corresponding to coherence plots. The horizontal line at zero is the asymptotic value and the green horizontal lines are the estimated upper and lower 95% confidence limits. The fourth row (j, k, l) represents the phase estimate for the same pairs, where there is significant coherence. The blue line represents the phase as calculated and the red is the phase calculated when one of the rectified EMG records was inverted.

5.1.3.1 Movement flexion phase EMG coupling.

In Fig. 5.3 the frequency characteristics of the recorded EMGs during movement flexion are shown. The FCR acts as agonist and the ECRL as antagonist while the BBLH is coactive throughout the task and aids in supporting the arm (see also Fig.5.1).

The power spectra of ECRL and FCR EMGs (Fig. 5.3*a,b*) show a low frequency (0-6Hz) component with a peak at 4Hz. This feature is absent from the BBLH spectrum (Fig. 5.3*c*).

Strong 5-15Hz features appear in the power spectra of all three muscles. 10Hz activity during movement has been reported to occur in agonist and antagonist during movement (Vallbo and Wessberg 1993; Wessberg and Vallbo 1996). Indeed the spectral features for ECRL and FCR have a peak at 10Hz. The large 14Hz power feature in the BBLH could also reflect a neurogenic source of motor unit synchronisation related to normal physiological tremor (Halliday, Conway et al. 1999). BBLH also contains clear spectral features in the beta band. Such activity is often observed in muscles contributing to a postural task. Importantly, both ECRL and FCR do not have any distinct feature in this band. The FCR power spectrum contains a small but distinct gamma feature (30-40Hz).

The low 0-6Hz frequency modulation of ECRL and FCR EMGs observed earlier (Fig. 5.3*a,b*) is also evident in the coherence estimate between the two EMGs (Fig. 5.3*d*). The coherence plot between these two muscles shows a peak in the 2-4Hz band. This indicates a common modulation of the EMGs in this frequency range. Smaller coherence in the 0-6Hz band (with no peak appearing at 2-4Hz) is also apparent between FCR and BBLH (Fig. 5.3*e*) but not between ECRL\BBLH (Fig. 5.3*f*).

The intermuscular coherence between ECRL and FCR also shows a clear and prominent 10Hz coupling feature. The agonist antagonist bursts during movement are visible in the raw rectified EMG as illustrated in Fig. 5.2. This is interpreted to represent the process reported by Vallbo (1993) who demonstrated that during slow movements a 10Hz reciprocal bursting occurs between antagonistic ECRL and FCR. The agonist produces a driving pulse and the antagonist responds by producing a braking pulse out of phase with the agonist burst. The reciprocal nature of this

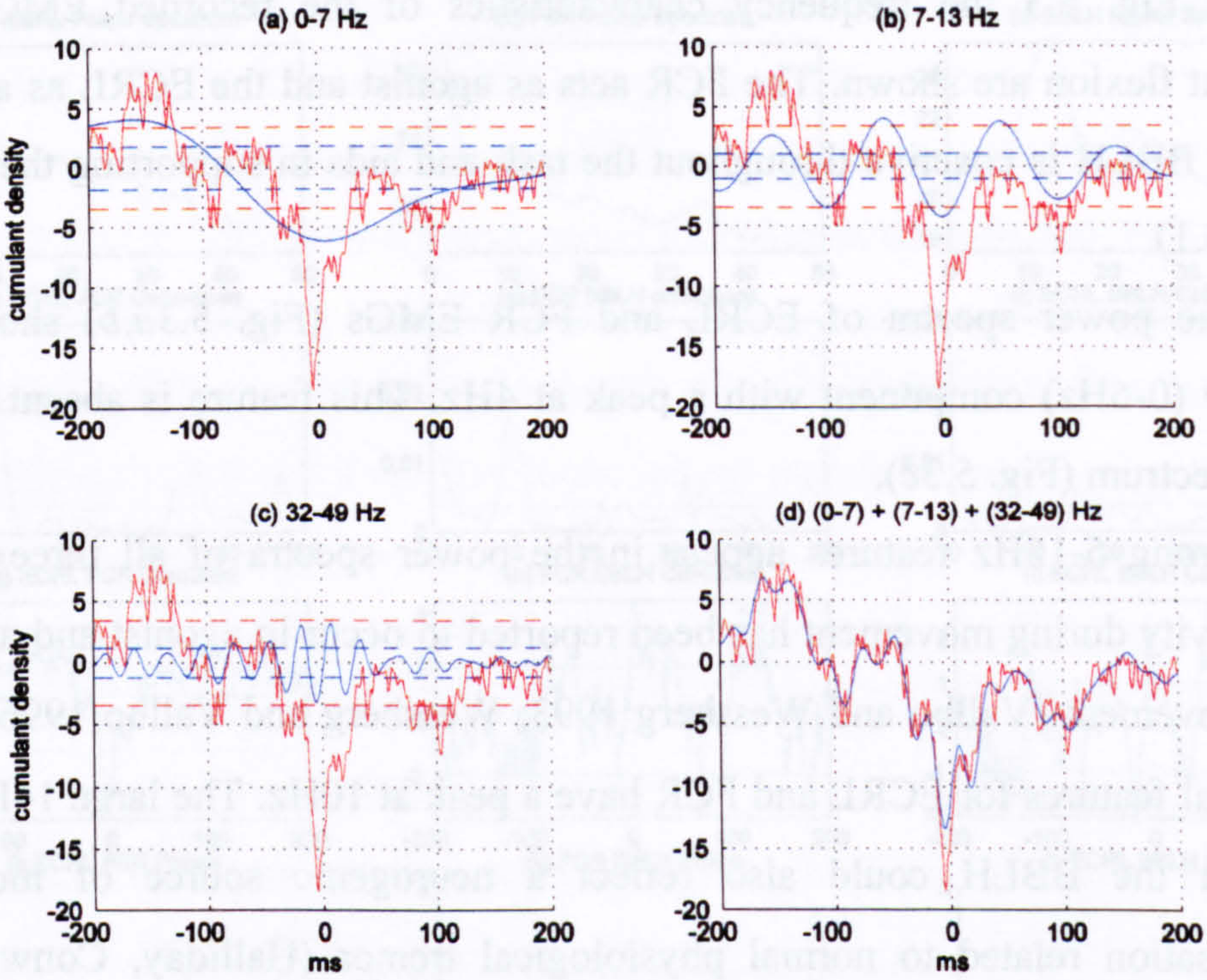

Fig. 5.4 Cumulant plots for ECRL\FCR EMGs during movement flexion. The red plot represents the cumulant estimate for the whole 0-500Hz spectrum and the blue plot represents the estimate for the frequency band indicated at the top of each plot. The confidence limits are represented by the corresponding colour dashed horizontal lines.

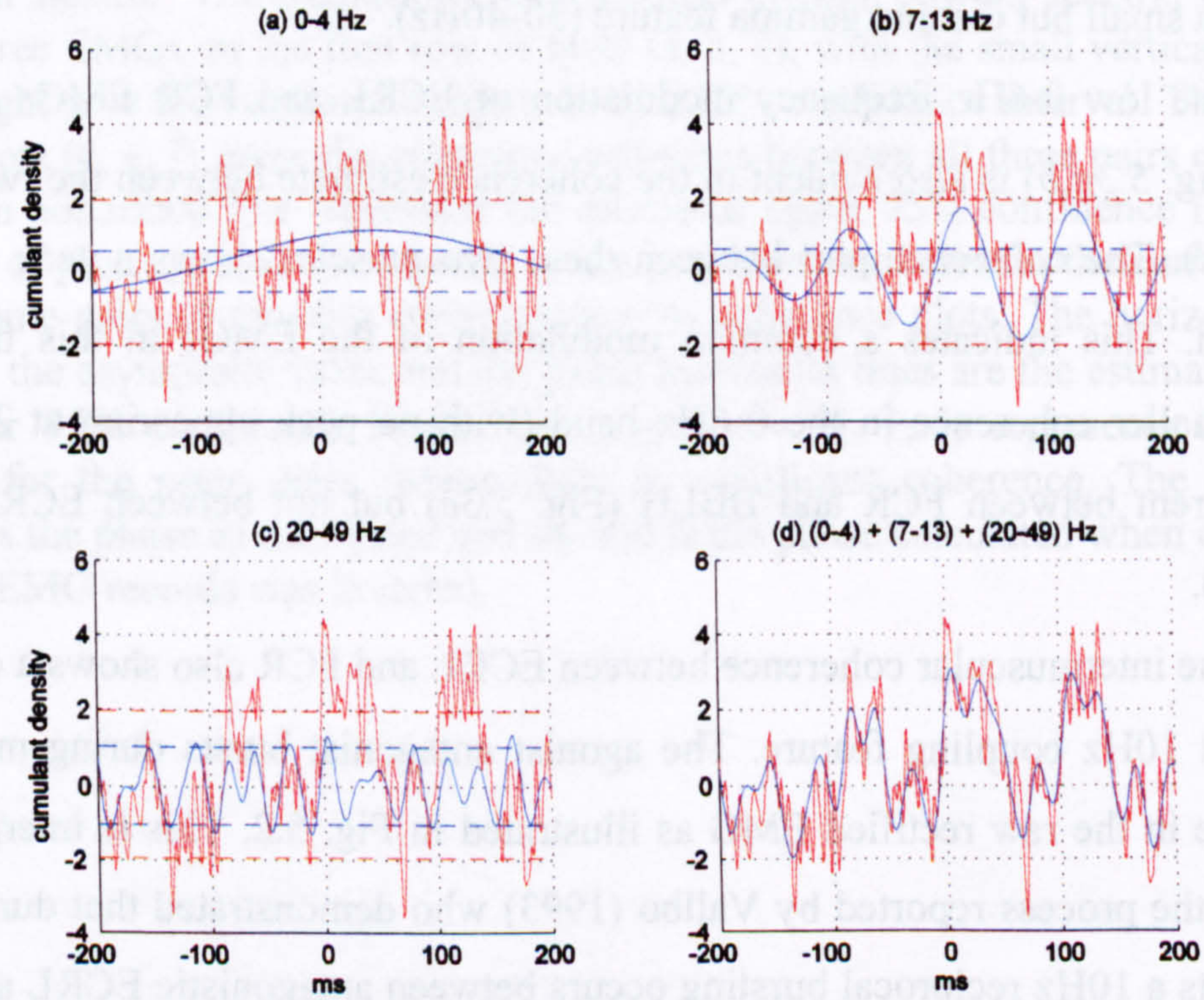

Fig. 5.5 Cumulant plots for FCR\BBLH EMGs during movement flexion. The red plot represents the cumulant estimate for the whole 0-500Hz spectrum and the blue plot represents the estimate for the frequency band indicated at the top of each plot.

feature is apparent from the respective cumulant shown in Fig. 5.3*g*. This characteristic will be further examined in Fig. 5.3.

Importantly, 10Hz coupling occurs between FCR and BBLH (Fig. 5.3*e*) but a similar relationship cannot be seen in the ECRL\BBLH coherence (Fig. 5.3*f*) as would be expected considering the presence of strong coupling of ECRL\FCR and FCR\BBLH EMGs.

In addition, the ECRL\FCR coherence plot (Fig. 5.3*d*) also demonstrates small gamma coupling in the frequency range 34-37Hz. Further gamma coupling is also evident between FCR\BBLH (Fig. 5.3*e*) within the 30-37Hz and 46-50Hz ranges. Apart from a small feature of beta coupling (15Hz) no other statistically significant coherence over the confidence limit exists between ECRL\BBLH (Fig. 5.3*f*) during this phase of the task. The 15Hz frequency coupling seen in ECRL\BBLH coherence can also be identified in the corresponding cumulant plot estimate (Fig. 5.3*f*).

The cumulant densities confirm the presence of "out of phase" 10Hz synchronisation for ECRL\FCR (Fig. 5.3*g*) and short-term synchronisation between FCR\BBLH (Fig. 5.3*h*) as indicated by the side band periodicity around the narrow central trough and peak respectively. Despite the common frequency range in coherence seen between ECRL\FCR and FCR\BBLH the differences in the cumulant plots suggest that different mechanisms may be responsible. If the same oscillatory input accounted for the coupling of the two out muscle pairs in the same frequency range (ECRL\FCR, FCR\BBLH), the third pair (ECRL\BBLH) should behave in a similar way, showing statistically significant coupling at 10Hz, which is not the case.

Since the cumulant and coherence estimates are closely linked it is important to examine the cumulant in relation to the distinct coupling features present in the coherence plots. The cumulant components analysis was used here to isolate frequency components in the cumulant plots according to the corresponding statistically significant coherence features and determine their contribution to the overall coupling process.

Fig. 5.4 contains the independent cumulant estimate components for ECRL FCR EMGs, for three frequency bands that demonstrate coupling over the statistical

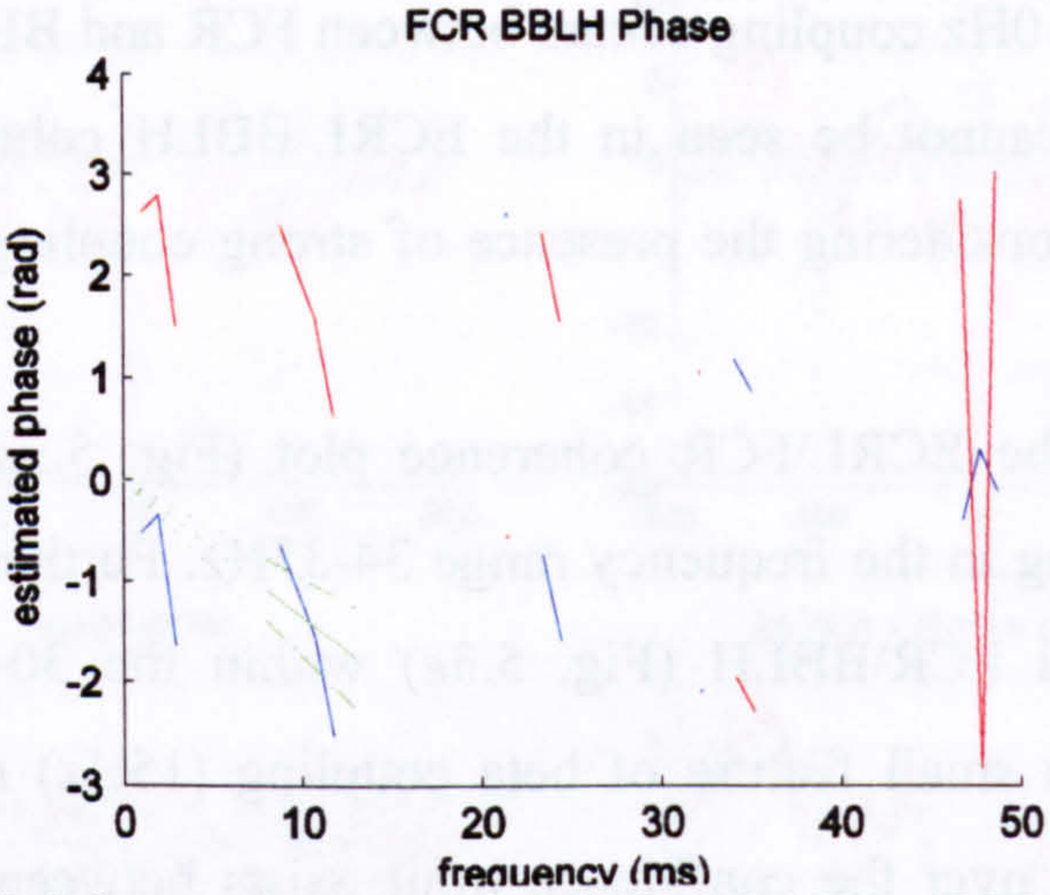

Fig. 5.6 Example of delay estimation from the 7-13Hz FCR\BBLH phase curve, based on weighted least squares regression. The solid line shows the delay estimate while the dashed lines show the error. The dotted lines highlight the fact that the extension of the delay estimate fit should cross zero. The red plot indicates the phase when one of the two EMGs is inverted. This would give a valid result when signals where synchronised in an out of phase fashion, which is not the case here.

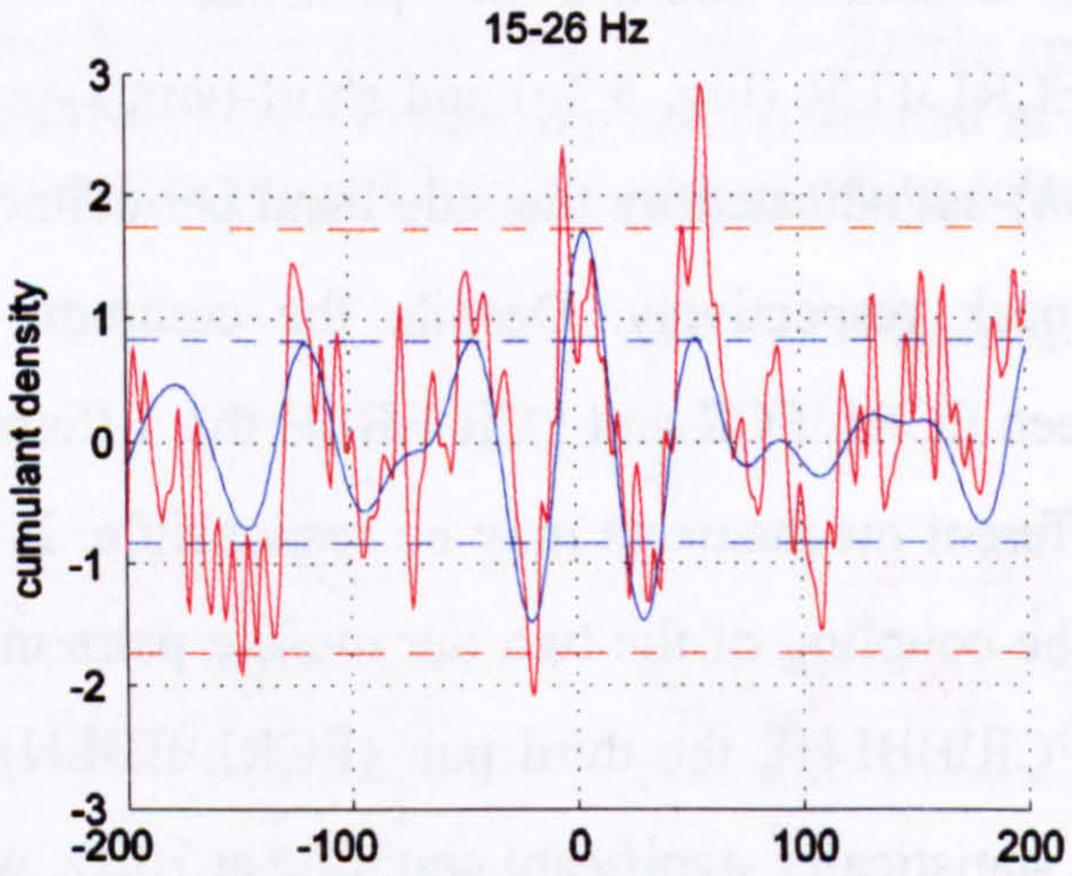

Fig. 5.7 Cumulant plots for ECRL\BBLH EMGs during movement flexion. The red plot represents the cumulant estimate for the whole 0-500Hz spectrum and the blue plot represents the estimate for the frequency band indicated at the top of the plot.

significance limit in the corresponding coherence plot in Fig. 5.3*d*. In the lower frequency 0-7Hz band (Fig. 5.4*a*) a wide trough can be seen (blue plot) that is linked to the out of phase modulation that occurs between the antagonistic muscles during active slow flexion. The dominant synchronisation frequency indicated by the secondary features is approximately 3Hz. The peak in the corresponding coherence plot appeared at the same frequency (Fig. 5.3*d*). The delay revealed by the cumulant is 5ms while the phase estimate of the delay is 1.1±2ms as calculated after inverting the FCR EMG signal.

The cumulant estimated for the 7-13Hz band shows synchronisation features that associate with the original wideband estimate (Fig. 5.4*b*). With secondary features at -51 and 52ms corresponding to 9.7Hz, the frequency closely matches the 9.8Hz frequency where maximum coupling is seen in the coherence plot (Fig. 5.3*d*). There is a central trough at 0ms showing seamless "out of phase" synchronisation. This can be explained by the agonist antagonist double pulse model (Vallbo and Wessberg 1993) which however had not identified the exact "out of phase" nature and the zero delay between signals that are evident in the present analysis. The phase between 7-13Hz between ECRL and the inverted FCR (Fig. 5.3*j*) derives 0.2±3.8ms phase difference, very close to the 0ms estimate of the delay derived by the cumulant. For deriving the phase, the FCR EMG was inverted because for rectified out of phase synchronised signals, phase estimates can give a valid result only when one of the two signals is inverted. In this way the "out of phase" synchronisation is converted into "in phase" synchronisation.

The close to zero phase difference for the 10Hz agonist antagonist modulation during slow movement is an important observation as it gives clues on the origin and the generation mechanism of the discussed modulation. It suggests that no simple feedback loop mechanism, such as the stretch reflex, is involved as this might be expected to introduce a measurable non-zero delay. A descending spinal modulation or supra-spinal mechanisms may therefore be more likely to be responsible for this flexor extensor interaction.

Within the 32-49Hz gamma band component of the intermuscular coupling (Fig. 5.4*c*), there is also a narrow negative feature at the lag time of -5ms. The phase between ECRL and inverted FCR EMGs confirms the above result deriving a -

5.2±1.0ms delay. This trough also indicates "out of phase" synchronisation between muscles meaning that the agonist is lagging behind the antagonist by 5ms. The positive sidepeaks at -18 and 8ms indicate a 37Hz frequency, very close to the 36Hz peak in the corresponding coherence plot (Fig. 5.3*e*).

Each cumulant estimated for each band can be combined by simple arithmetic addition as in Fig. 5.4*d* which shows that the main features of the full cumulant (red line) is adequately captured by consideration of these separable spectral features.

Using the same approach it is possible to analyse the FCR\BBLH cumulant (Fig. 5.3*h*) in relation to the features appearing in the corresponding coherence plot (Fig. 5.5). The low frequency 0-4Hz (Fig. 5.5*a*) cumulant shows 51ms delay, the short phase curve did not derive a similar delay with a high error margin (42.2±75.7ms) because the weighted least squares regression method for calculating the phase is quite sensitive to high error in low frequencies smaller than 8Hz. The high frequency 20-49Hz frequency components affect the original cumulant plot, without however being statistically significant on their own.

The 7-13Hz feature is dominant, confirming the large 10Hz peak in the coherence plot seen in Fig. 5.3*e*. As with the ECRL\FCR pairing the coupling arises at 9.8Hz. A negative trough at +70ms and a positive peak at 21ms having similar absolute magnitude are the main features. A +21.0±9.4ms phase difference is derived for the 7-13Hz band (Fig. 5.3*k* & Fig. 5.6) which suggests the cumulant 21ms peak expresses the lag for the cumulant plot, indicating "in phase" synchronisation. Thus both cumulant and phase suggest that the FCR EMG leads the BBLH signal by +21ms. This is unlikely to reflect processes associated with short term synchronisation between these muscles as the lag time for this would be expected to be less and as BBLH is the more proximal muscle to the CNS it might also be expected that BBLH EMG would lead FCR.

As far as the generation mechanism for FCR\BBLH 10Hz coupling it is feasible that a reflex loop is possibly involved. This might arise as afferent feedback driven by the 10Hz movement tremor act to modulate BBLH activity.

The ECRL\BBLH cumulant (Fig. 5.7) contains weak beta oscillatory features but no alpha features showing 5ms delay and 20Hz coupling frequency. The different attributes of the ECRL\FCR (Fig. 5.5*b*) and FCR\BBLH (Fig. 5.6*b*) cumulant plots

and the different delays, strongly suggest different underlying mechanisms. This is further suggested by the lack of coupling for the ECRL\BBLH pair. However, the lack of coupling for the ECRL\BBLH specifically in the 10Hz band may also indicate that a simple reflex mechanism does not account for the 10Hz FCR/BBLH coupling.

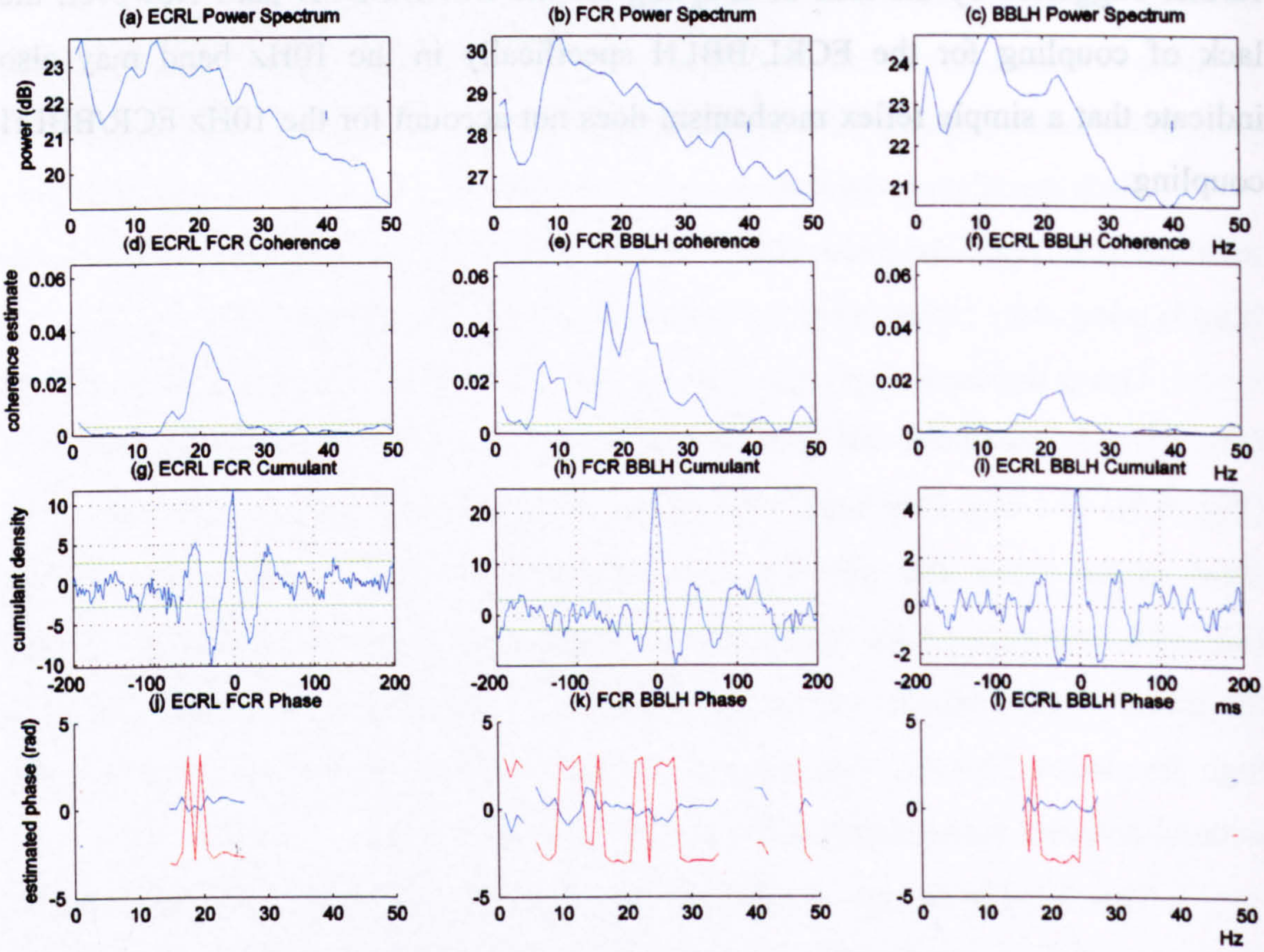

Fig. 5.8 Frequency characteristics of ECRL, FCR and BBLH EMGs, during posture flexion. The frequency characteristics include powers spectral estimates for the three EMGs on the first row of plots (a, b, c), with the small vertical lines at the top right give the estimated magnitude of a 95% confidence interval. The second row of plots (d, e, f) gives the coherence estimates between all three pairs of EMGs. The green horizontal line represents the estimated upper 95% confidence limit. The third row of plots (g, h, i) corresponds to the cumulant estimates for the current phase for the same pairs of muscles corresponding to coherence plots. The horizontal line at zero is the asymptotic value and the green horizontal lines are the estimated upper and lower 95% confidence limits. The fourth row (j, k, l) represents the phase estimate for the same pairs, where there is significant coherence. The blue line represents the phase as calculated and the red is the phase calculated when one of the rectified EMG records was inverted.

5.1.3.2 Posture flexion phase EMG coupling.

Following the end of the active flexion phase the subjects held their wrist in the flexed position. In this posture a degree of co-activation between FCR and ECRL can be expected given the need to stabilise the position of the hand against gravitational influences. Fig. 5.8 illustrates the characteristics of the intermuscular coupling during this postural phase of the trial.

All three EMG power spectra contain 1-6Hz features (Fig. 5.8*a,b,c*). Most likely this reflects low frequency tremor signals or the biomechanical properties of the wrist-forearm. The EMG power spectra for ECRL, FCR and BBLH are dominated by peaks close to 10Hz. ECRL and BBLH spectra also show distinguishable features around 20Hz. This is typical for muscles performing voluntary postural tasks. A clear beta peak in the FCR spectrum is not present, but there is generally high activation in the 10 to 30Hz area. Some gamma features are also present in the FCR spectrum.

The coherence plots show distinct coupling between all three muscles with peaks at 20Hz and 22Hz respectively for ECRL\FCR, FCR\BBLH and ECRL\BBLH muscle pairs (Fig. 5.8*d,e,f*). The coherences are statistically significant and strong especially between the FCR and BBLH EMGs. The shape of the coherence peaks in the 15-30Hz band is similar for all three muscle pairs. However, while all three pairs are strongly coupled in the 15-30Hz frequency band, only FCR\BBLH pair is strongly coupled in the 5-15Hz band. In the same plot, 35-50Hz features are also present. A small feature at 48Hz is present in each plot but is only statisticaly significant in FCR/BBLH and ECRL/BBLH coherences.

The cumulant plots confirm the near 20Hz coupling. All plots (Fig. 5.8*g,h,i*) have positive narrow peak and each EMG appears to be synchronised and "in phase", with lags very close to zero. The narrow peak and the highly dumped oscillatory features indicate a degree of short term synchronisation between each motor pool, rather that common rhythmic oscillatory input. During the posture flexion the cumulant for FCR\BBLH shows the strongest coupling. As with the corresponding coherence plots the FCR\BBLH cumulant plot resembles the ECRL\BBLH cumulant.

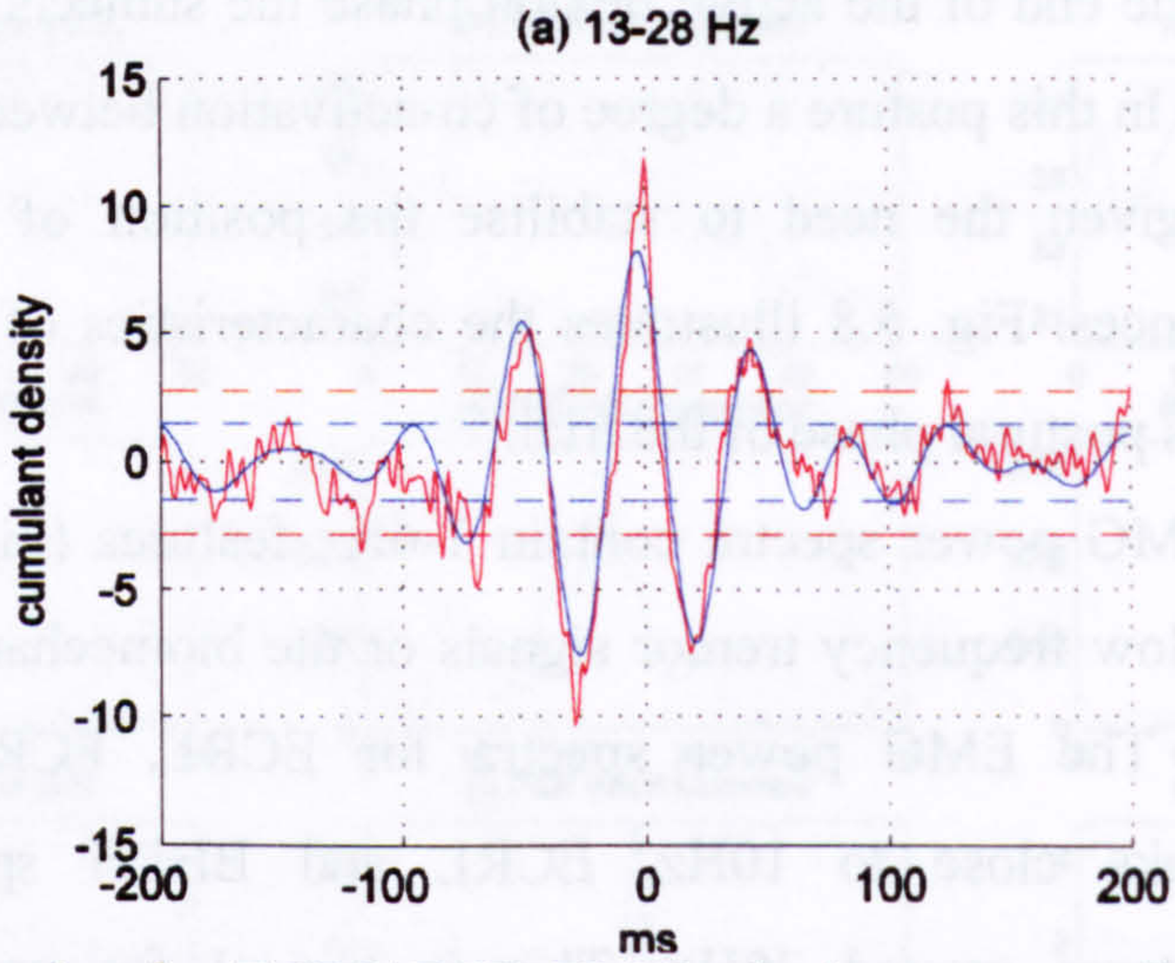

Fig. 5.9 Cumulant plot for ECRL\FCR EMGs during posture flexion. The red plot represents the cumulant estimate for the whole 0-500Hz spectrum and the blue plot represents the estimate for the frequency band indicated at the top of the plot.

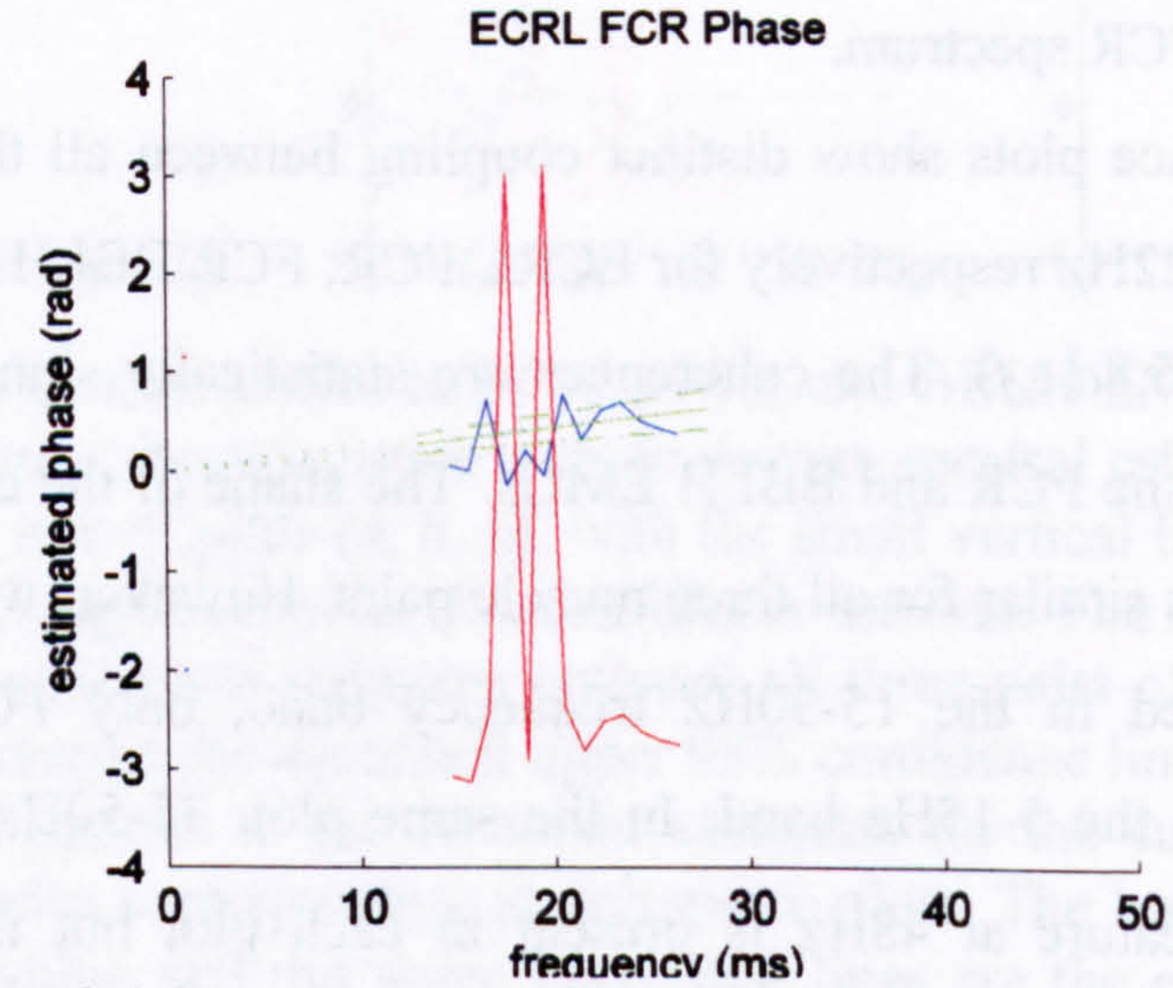

Fig. 5.10 Example of delay estimation from the 13-28Hz ECRL\FCR phase curve, based on weighted least squares regression. The solid line shows the delay estimate while the dashed lines show the error. The dotted lines highlight the fact that the extension of the delay estimate fit should cross zero. The red plot indicates the phase when one of the two EMGs is inverted. This would give a valid result when signals where synchronised in an out of phase fashion, which is not the case here.

Closer examination of the cumulant density estimates illustrates that for ECRL\FCR cumulant (Fig. 5.9, blue line) the components within the 20Hz range provide most of the statisticaly significant features apparent in wideband full cumulant (Fig. 5.9 red line). The original plot, reveals zero lag between the two signals. The cumulant for the 13-28Hz band, represented in the blue plot, reveals a very small lead for the FCR over the ECRL of -3ms. The dominant coupling frequency derived by the secondary peaks, is 20Hz, while for the coherence plot shows maximum coherence at 20.50Hz. The phase plot (Fig. 5.8*j* and Fig. 5.10) for 13-28 Hz derives -3.7±1.2 ms, very close to the -3ms predicted by the cumulant plot. The latency detected is too short to be the result of any reflex mechanism and most likely can be accounted for by differences in EMG conduction velocities. The short lag time combined with the sharp shape of cumulant plot and the coherence plots suggest that short term synchronisation of central origin is a likely explanation. In addition, and in light of the results from the simulation study in Appendix 8.3 it is highly likely that this common drive is oscillatory in nature.

The origin of this common oscillation could be supraspinal structures, and more specifically the motor cortex, considering the fact that as coherence between cortical activity and EMG occurs during posture for a similar range of frequencies (Conway, Halliday et al. 1995).

For the FCR\BBLH muscles (Fig. 5.8*e*), statisticaly significant coherence was present within the 0-5Hz, 5-13Hz and 13-35Hz ranges. The 0-5Hz cumulant (Fig. 5.11*a*) showed "in phase" synchronisation and delay at 36ms while the phase curve derived a similar delay estimate of 32.6±15.8ms. The main feature that the cumulant reveals for the 5-13Hz band is a trough at +58ms with positive side-peaks at +3 and +111ms (Fig. 5.11*b*). The phase plot can not be interpreted according to the model described in the analytical methods chapter while the shape of the cumulant reveals out of phase synchronisation. By inverting one of the two EMGs, the 5-13Hz band was "out of phase" synchronised in the respective phase plot (Fig. 5.8*k*), which derived 58.5±13.5ms, delay remarkably close to the 58ms derived by the central trough in the corresponding cumulant (Fig. 5.11*b*). The almost identical phase estimation from cumulant plot and inverted EMG phase estimation is reassuring for

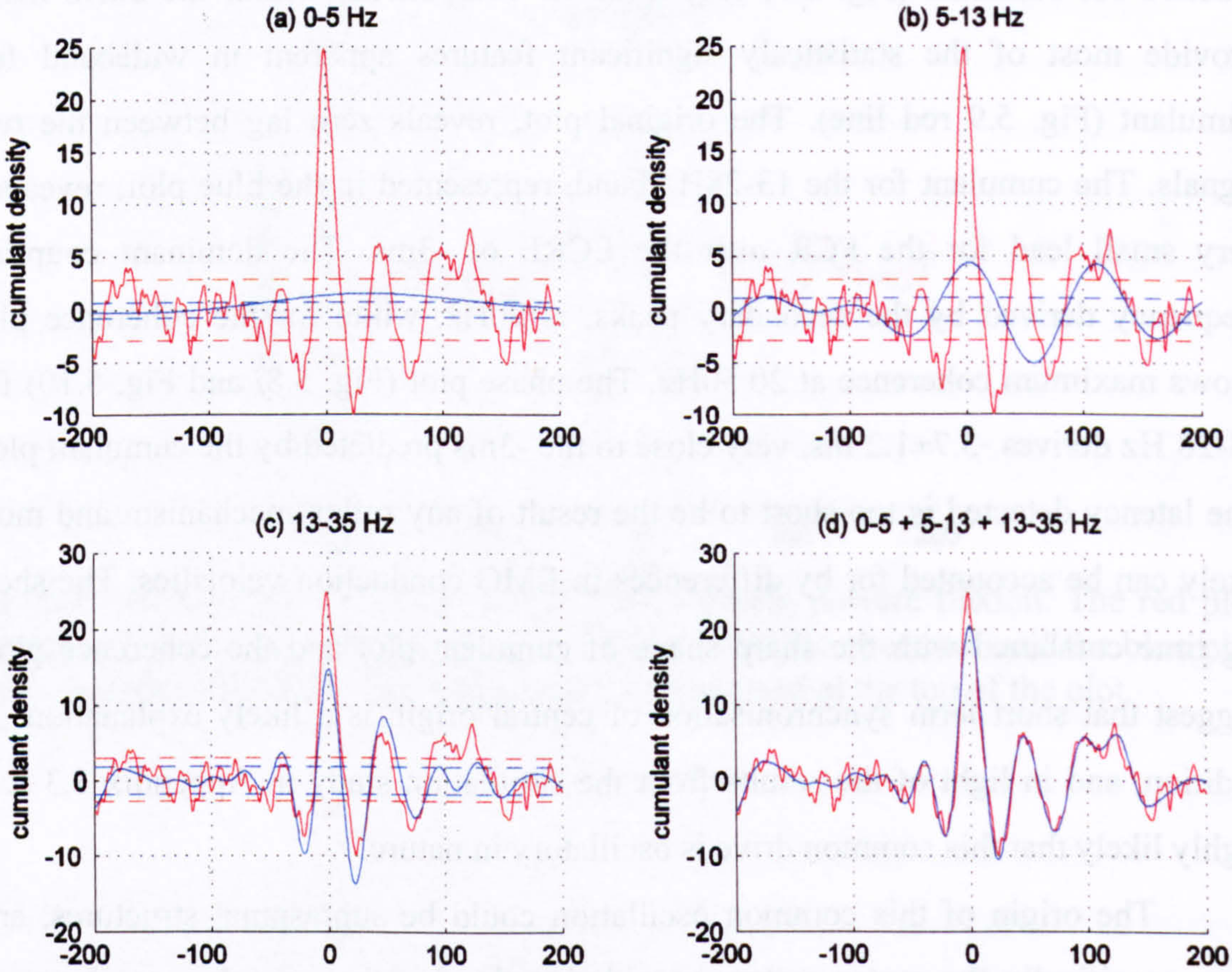

Fig. 5.11 Cumulant plots for FCR\BBLH EMGs during posture flexion. The red plot represents the cumulant estimate for the whole 0-500Hz spectrum and the blue plot represents the estimate for the frequency band indicated at the top of each plot.

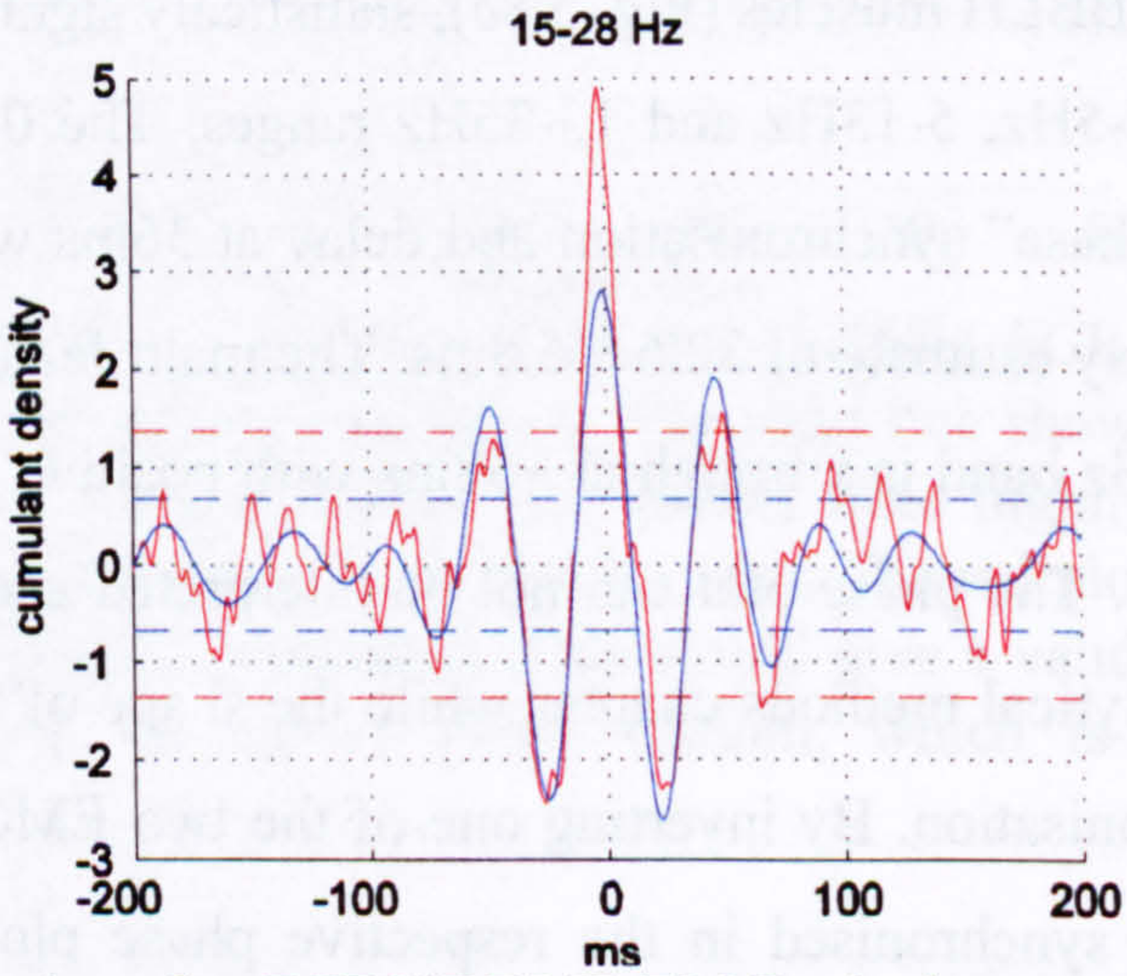

Fig. 5.12 Cumulant plots for ECRL\BBLH EMGs during posture flexion. The red plot represents the cumulant estimate for the whole 0-500Hz spectrum and the blue plot represents the estimate for the frequency band indicated at the top of the plot.

the "out of phase" synchronisation and the reliable delay estimate between the signals.

5-15Hz coupling between FCR and BBLH appears to be present during either maintained flexion and during active flexion (Fig. 5.7*e*, Fig. 5.13*e*). The oscillatory features of the cumulant are different, supporting the view of a different coupling mechanism during the different phases. The absence of 10Hz in the ECRL\FCR posture flexion coupling (Fig. 5.8*f*) and its presence during movement coupling further supports the above suggestion.

The 13-35Hz band cumulant plot (Fig. 5.11*c*) gives +0ms phase lag and a frequency of 22Hz. The corresponding phase plot (Fig. 5.8*k*), estimates a lag of 0.6±1.1ms and is therefore in agreement with the cumulant. Because of the sharp cumulant and near zero lag, it is likely that the central peak in the cumulant plot represents short term synchronisation of central origin.

The ECRL\BBLH cumulant in Fig. 5.12 demonstrates strong coupling. The corresponding coherence plot (Fig. 5.8*f*) shows coherence in the 15-28Hz band. The cumulant density component for this frequency range shows a positive peak at -2ms with the BBLH leading the ECRL. The phase plot (Fig. 5.8*l*) gave a similar delay with -1.3±0.9ms and for all intent and purposes this can be considered to be indicative of synchronisation at approximately 22Hz as indicated by the sidebands.

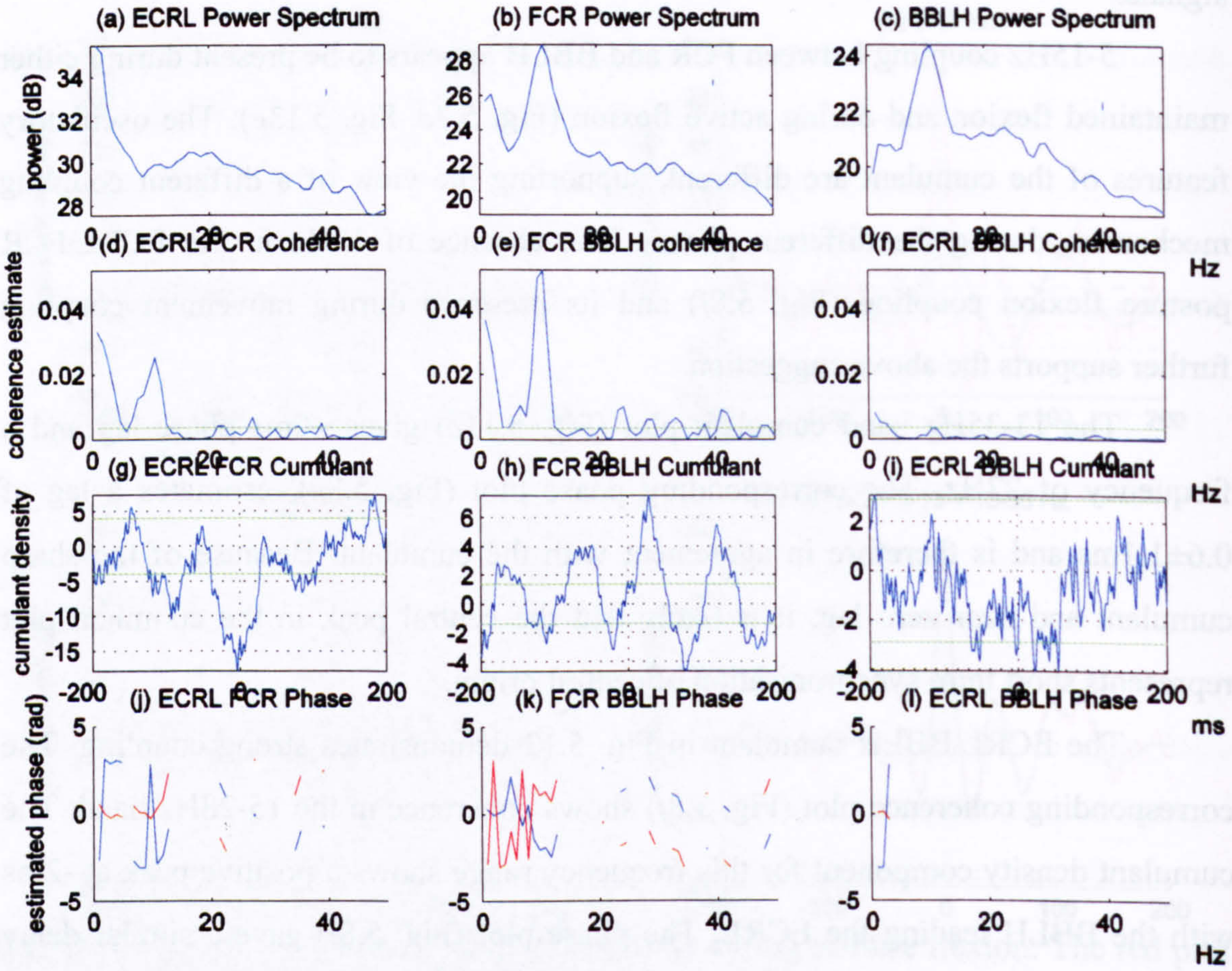

Fig. 5.13 Frequency characteristics of ECRL, FCR and BBLH EMGs, during movement extension. The frequency characteristics include powers spectral estimates for the three EMGs on the first row of plots (a, b, c), with the small vertical lines at the top right give the estimated magnitude of a 95% confidence interval. The second row of plots (d, e, f) gives the coherence estimates between all three pairs of EMGs. The green horizontal line represents the estimated upper 95% confidence limit. The third row of plots (g, h, i) corresponds to the cumulant estimates for the current phase for the same pairs of muscles corresponding to coherence plots. The horizontal line at zero is the asymptotic value and the green horizontal lines are the estimated upper and lower 95% confidence limits. The fourth row (j, k, l) represents the phase estimate for the same pairs, where there is significant coherence. The blue line represents the phase as calculated and the red is the phase calculated when one of the rectified EMG records was inverted.

5.1.3.3 Movement extension phase EMG coupling

Fig. 5.13 shows the characteristics of the EMG spectra, coherence cumulant and phase estimate during movement extension phase. As in the flexion phase of movement, during extension statisticaly significant coherence occurs in the low frequency 0-6Hz band between ECRL and FCR. The neurogenic or biomechanical origin of this activity is not clear.

During extension movement there is high activation in the ECRL muscle especially in the 0-8Hz spectral range (Fig. 5.13*a*). An 8-12Hz feature is not as large as expected, and the spectra are dominated by low frequencies. The FCR and BBLH spectra (Fig. 5.13*b,c*) show prominent peaks close to 10Hz. Beta features are also present in the BBLH plot. ECRL\FCR and FCR\BBLH EMGs show statisticaly significant 10Hz coupling for but as seen in Fig. 5.13*f*, the ECRL\BBLH pair lacks any strong coupling in the same band. No 20Hz coherence is observed in Fig. 5.13*f*. As seen in Fig. 5.13*d,e*, 15-35Hz coherence has been suppressed compared with the previous flexion posture. However small coherence, just over the confidence limit can be observed in both plots for 15-35Hz and 35-50Hz bands.

While the cumulant for ECRL\BBLH muscles in Fig. 5.13*i* shows no statisticaly significant synchronisation features, the ECRL\FCR and FCR\BBLH pairs (Fig. 5.13*g,h*) show statisticaly significant 10Hz coupling in agreement with the corresponding coherence plots. Similar to the movement flexion phase both plots contain a central trough. However differences in the shape and the timing of the overall plot suggest differences in the nature of synchronisation. The cumulant plots and their frequency components will be examined in detail later.

Fig. 5.14 illustrates that ECRL\FCR EMGs are coupled in the 0-6Hz band. The synchronisation is out of phase and the delay given by the central trough of the cumulant (Fig. 5.14*a*) is -2ms while the corresponding phase estimate is similar at -2.0±27.0ms despite the high error.

The cumulant density component is also shown for the 6-13Hz band for the ECRL\FCR muscle pair in Fig. 5.14*b*. There is a central broad trough at -3 ms, revealing "out of phase" synchronisation. The two positive sidebands are located at -53ms and +50ms. The phase of the ECRL with the inverted FCR EMG is -4.7±4.5, similar to the cumulant prediction, which means that the FCR has a small lead over

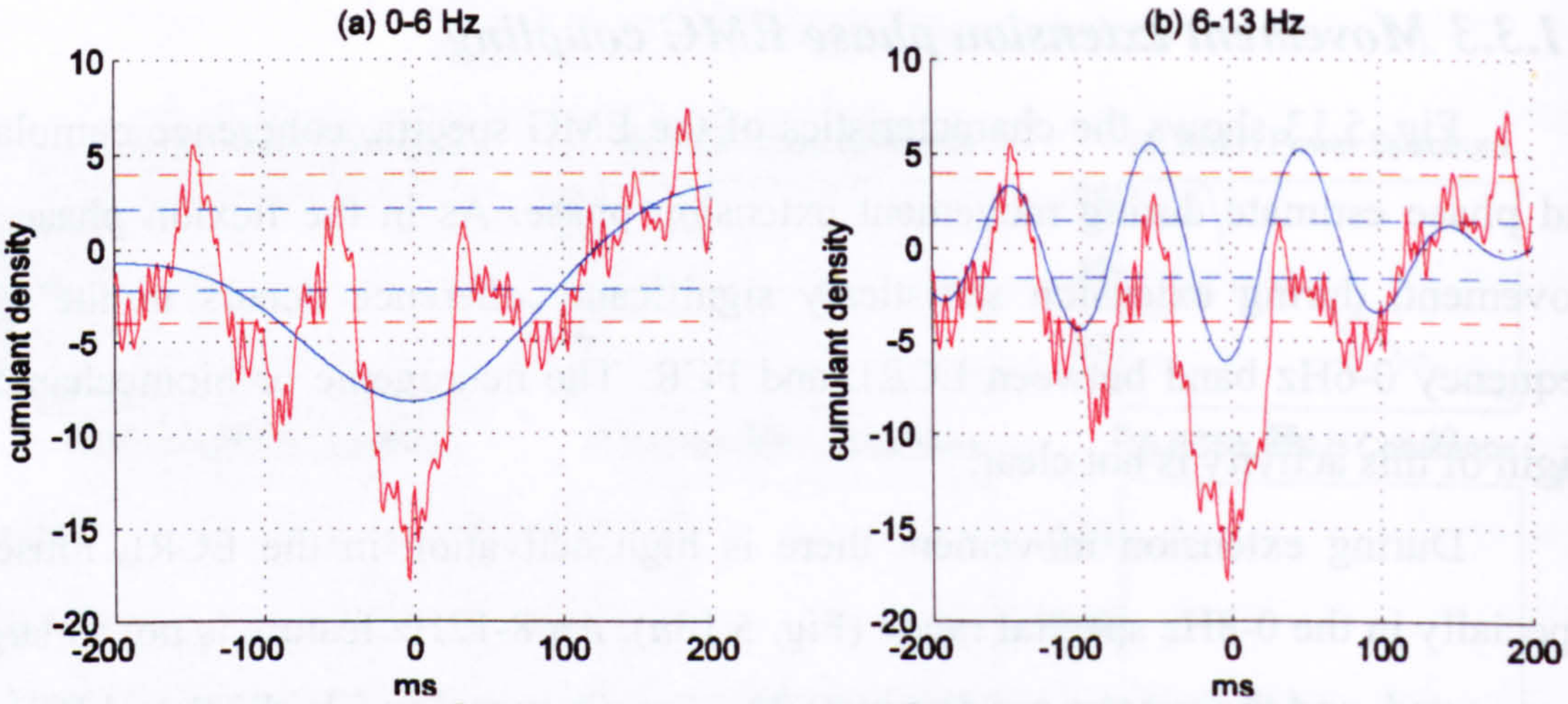

Fig. 5.14 Cumulant plot for ECRL\FCR EMGs during movement extension. The red plot represents the cumulant estimate for the whole 0-500Hz spectrum and the blue plot represents the estimate for the frequency band indicated at the top of the plot.

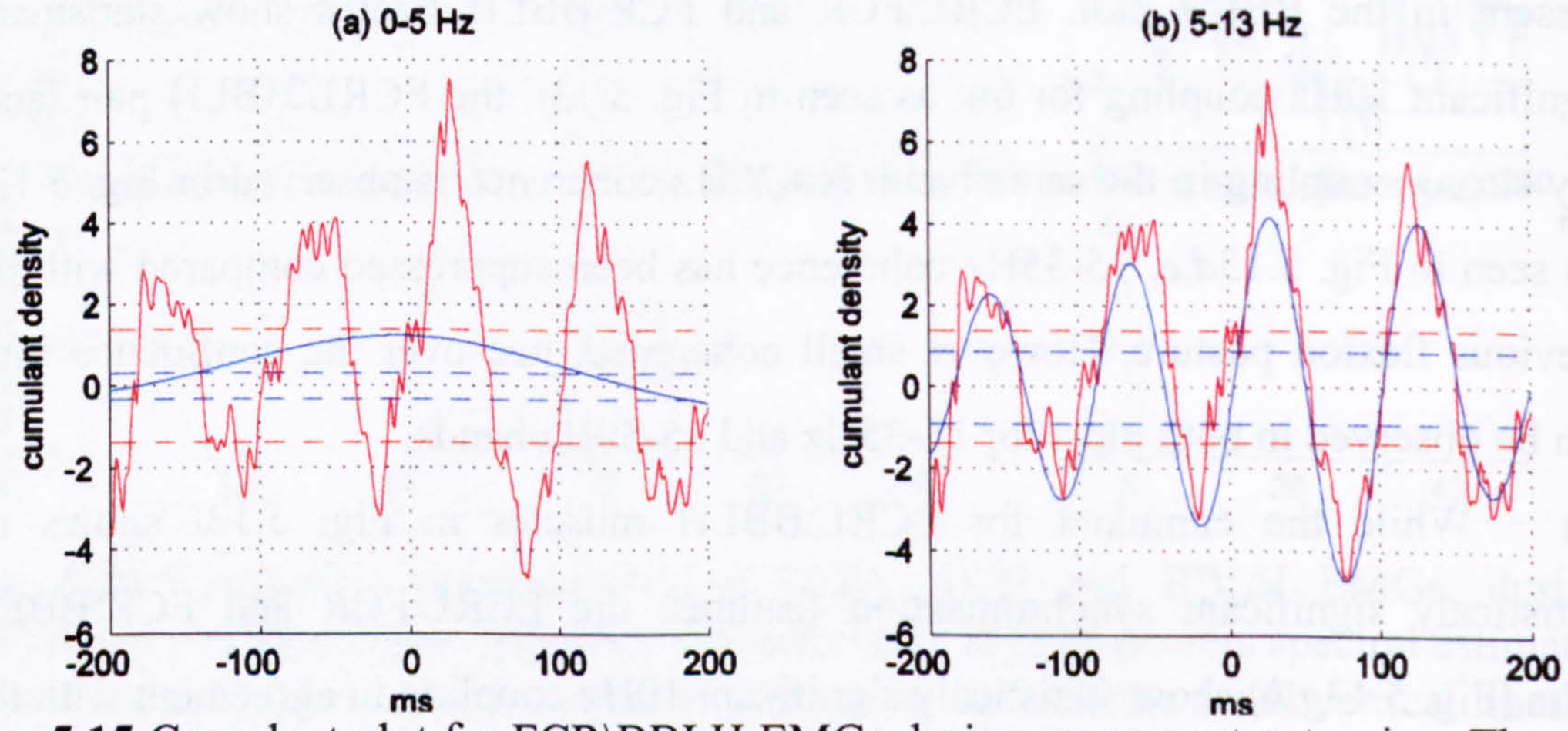

Fig. 5.15 Cumulant plot for FCR\BBLH EMGs during movement extension. The red plot represents the cumulant estimate for the whole 0-500Hz spectrum and the blue plot represents the estimate for the frequency band indicated at the top of the plot.

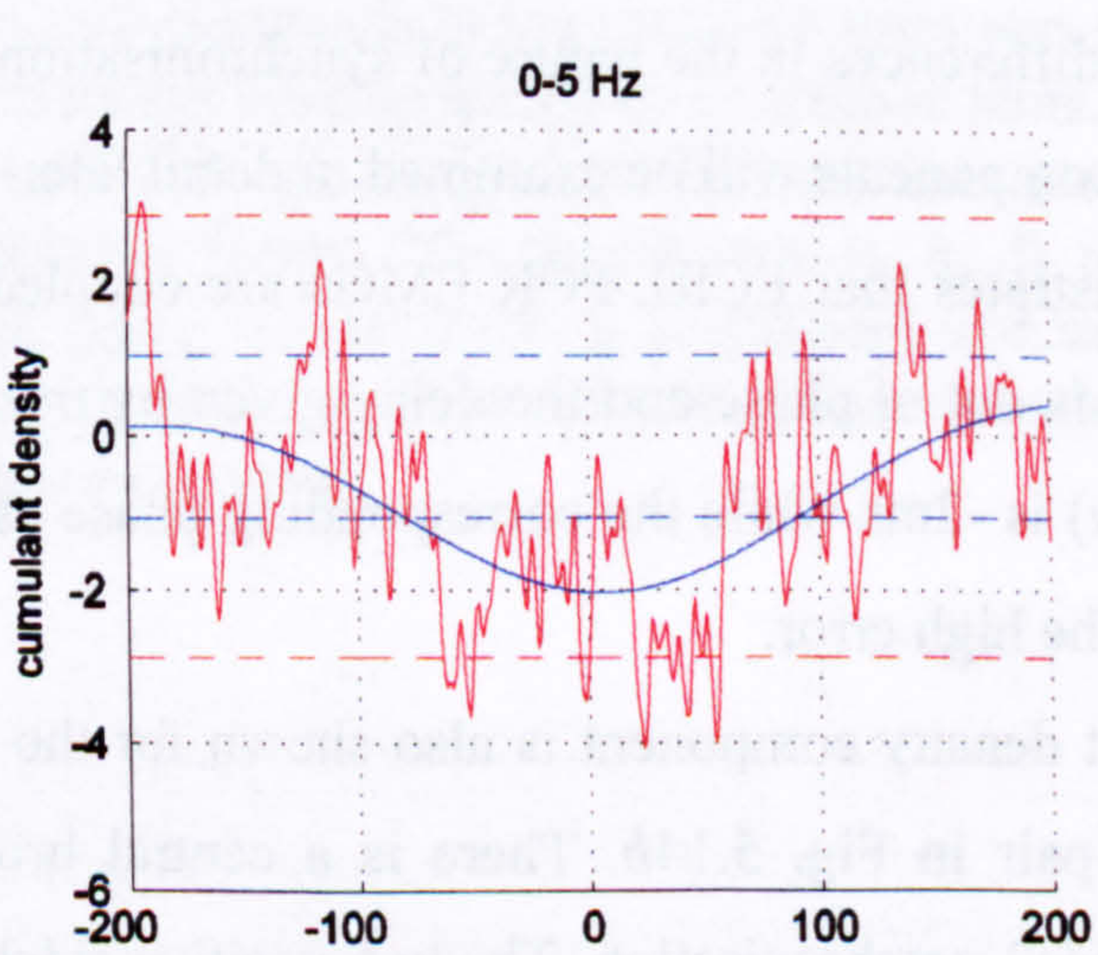

Fig. 5.16 Cumulant plot for ECRL\BBLH EMGs during posture flexion. The red plot represents the cumulant estimate for the whole 0-500Hz spectrum and the blue plot represents the estimate for the frequency band indicated at the top of the plot.

the ECRL EMG. During movement extension (Fig. 5.14*b*) and movement flexion (Fig. 5.4*b*) the cumulant plots appear very similar. The amplitude lag is close to 0ms for both cases and the negative peak may indicate inhibitory interaction between the two EMGs. Also considering the lack of strong 10Hz content in the driving agonist ECRL spectral estimate, it is unlikely that a loop mechanism is responsible for the very strong FCR 10Hz content, and the resulting coherence. It is more likely that the CNS is driving directly the ECRL and FCR, by two out of phase signals of central origin.

The 0-5Hz band in Fig. 5.15*a* illustrates strong "in phase" synchronisation with delay of -8ms according to the cumulant. The phase derived a similar estimate of -9.7±34.3ms, however the error was high, which is often the case when for the method is used for frequencies below 8Hz. Fig. 5.15*b* shows the cumulant plot for the 5-13Hz band for the FCR\BBLH pair. The main coupling feature appeared at 11Hz in the corresponding coherence plot (Fig. 5.13*e*). The main cumulant component features are a trough at 78ms and a peak at 28ms of similar absolute magnitude. The phase plot derives a latency of 29.5±2.8ms which suggests that the second value expresses the lag between the "in phase" synchronised EMG signals. The shape of the cumulant has a highly oscillatory form which suggests that a common oscillatory input (in a form of a reflex loop) rather than short term synchronisation could be responsible for the observed phenomenon. A similar cumulant plot was observed for the same pair during flexion movement with a 21ms lag (Fig. 5.5*b*).

Fig. 5.16 illustrates out of phase coupling between ECRL\BBLH within 1-6Hz during movement extension. The cumulant suggests a 6ms delay while the corresponding phase was too large (2.9±21.5ms). There was no coupling in the same band during movement flexion (Fig. 5.5*l*).

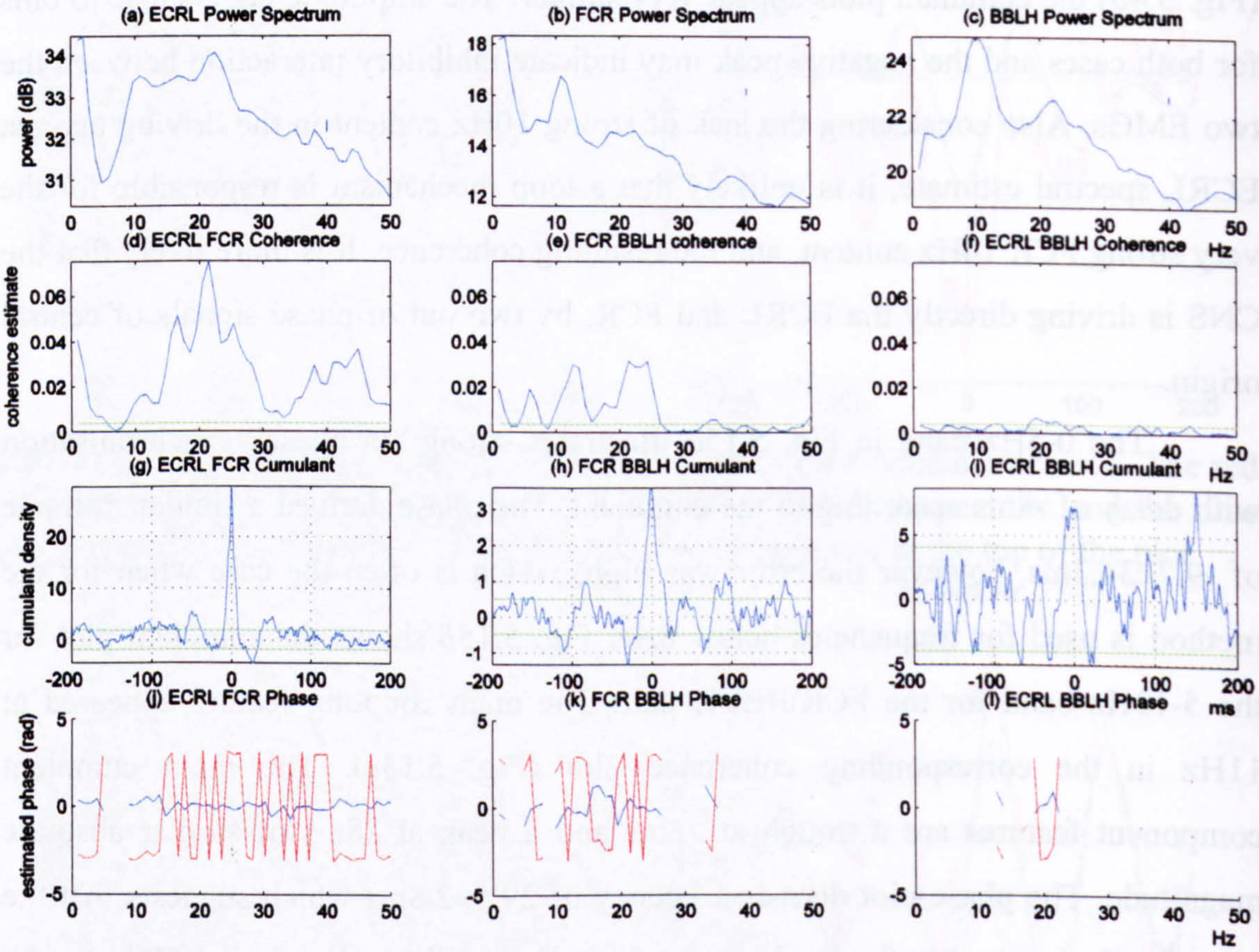

Fig. 5.17 Frequency characteristics of ECRL, FCR and BBLH EMGs, during posture extension. The frequency characteristics include powers spectral estimates for the three EMGs on the first row of plots (a, b, c), with the small vertical lines at the top right give the estimated magnitude of a 95% confidence interval. The second row of plots (d, e, f) gives the coherence estimates between all three pairs of EMGs. The green horizontal line represents the estimated upper 95% confidence limit. The third row of plots (g, h, i) corresponds to the cumulant estimates for the current phase for the same pairs of muscles corresponding to coherence plots. The horizontal line at zero is the asymptotic value and the green horizontal lines are the estimated upper and lower 95% confidence limits. The fourth row (j, k, l) represents the phase estimate for the same pairs, where there is significant coherence. The blue line represents the phase as calculated and the red is the phase calculated when one of the rectified EMG records was inverted.

5.1.3.4 Posture extension phase EMG coupling

Fig. 5.17 demonstrates the pooled results for the three recorded EMGs; (ECRL, FCR and BBLH) during extension posture. A low frequency component (0-6Hz) is seen in the ECRL and FCR spectra (Fig. 5.17*a,b*) while it is absent from the BBLH spectrum (Fig. 5.17*c*). This feature could either be of neurological origin or the result of low frequency modulation of the EMG due to biomechanical properties of the wrist (Lakie, Walsh et al. 1984; Milner 2002). This low frequency activity is also illustrated as comodulation in ECRL\FCR coherence (Fig. 5.17*d*). Power spectra show 8-12Hz and 15-25Hz peaks for all 3 muscles with 15-25Hz band dominating the spectrum of the ECRL (Fig. 5.17*a*) and 10Hz dominance for the spectra of FCR and BBLH (Fig. 5.17*b,c*).

The ECRL\FCR pair appears synchronised for a wide range of the beta band (10-30Hz) and the gamma band (35-48Hz) (Fig. 5.17*d*). FCR and BBLH show statisticaly significant coherence in the 20Hz area but also a prominent peak at 14Hz and 6Hz. The coherence for the ECRL and BBLH muscles is smaller than the other two pairs but still statisticaly significant in the region of 20Hz. A small coherence peak is also seen at 14Hz for the same pair. It is important that high coherence at 15-25Hz can be observed for the two muscle pairs (ECRL\FCR in Fig. 5.17*d*, FCR\BBLH in Fig. 5.17*e*) but it is much lower for the ECRL\BBLH pair. The frequency distributions of the coherence features are also different. In the corresponding plots for flexion posture (Fig. 5.8*d,e,f*) the coherence features were all strong and with a similar frequency distribution. Therefore a functional differentiation emerges in the way the muscles are synchronised between the two phases of posture; posture flexion and posture extension.

Observing the cumulant plots for ECRL\FCR and FCR\BBLH (Fig. 5.17*g,h*) it emerges that both contain a statisticaly significant narrow central peak, suggesting short term synchronisation with The ECRL\FCR peak showing the strongest synchronysation. The ECRL\BBLH shows weak synchronisation (Fig. 5.17*i*).

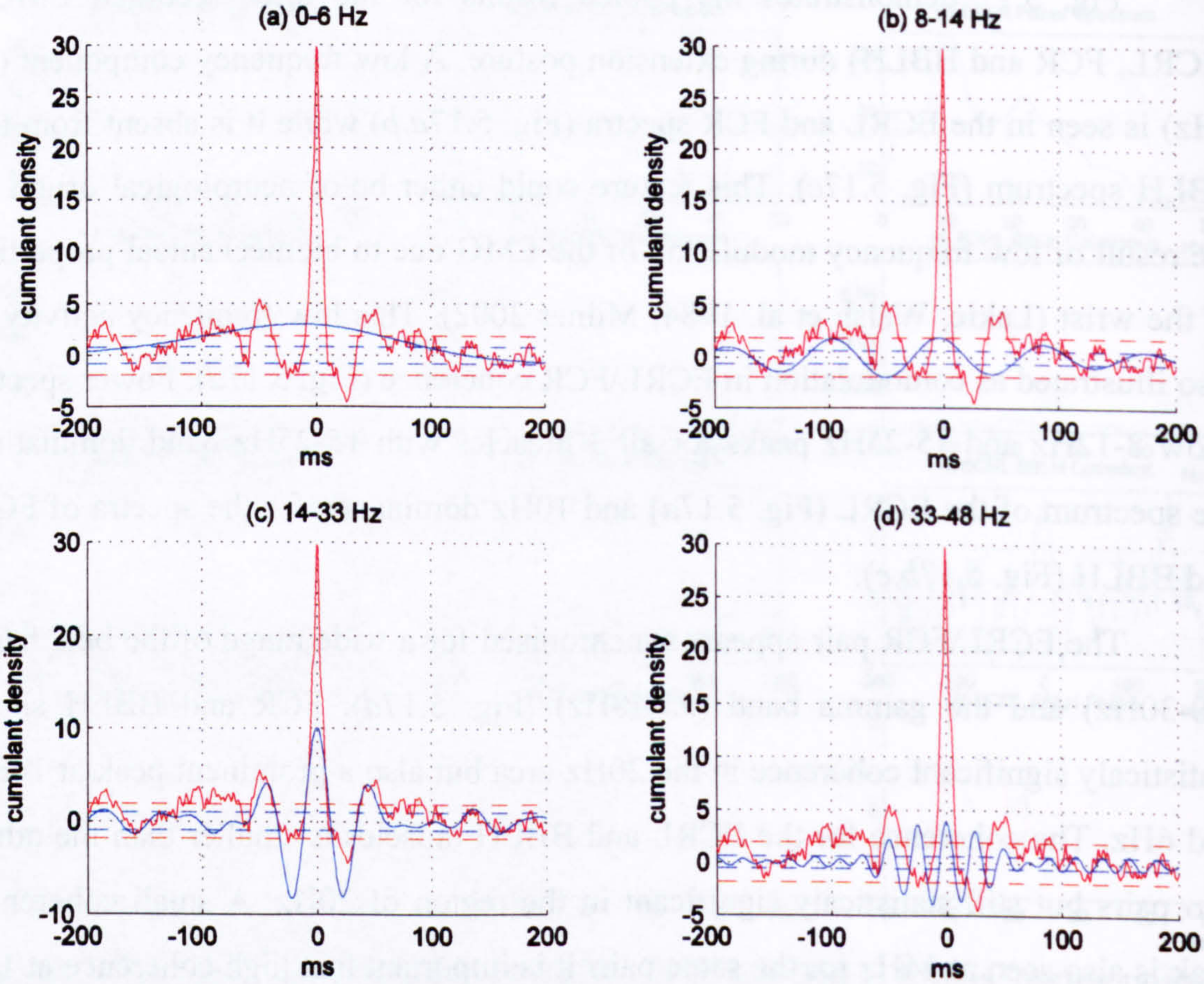

Fig. 5.18 Cumulant plots for ECRL\FCR EMGs during posture extension. The red plot represents the cumulant estimate for the whole 0-500Hz spectrum and the blue plot represents the estimate for the frequency band indicated at the top of each plot.

Examining the ECRL\FCR pair cumulant estimates in detail in Fig. 5.18*a*, low frequency "in phase" EMG comodulation can be observed within the 0-6Hz band the cumulant shows a -15ms delay while the phase gives -16.0±25.1ms suggesting that FCR is leading ECRL.

Examining the same ECRL\FCR cumulant within the 8-14Hz band in Fig. 5.18*b* a feature of approximately 10Hz is present, not obvious in the wideband cumulant plot. There are two main features with similar absolute amplitude, a trough at -51ms and a peak at -5ms. The phase estimates derives -6.0±3.7ms delay which indicates that -5ms the peak is the dominant feature. This suggests "in phase" synchronisation in this frequency band with FCR having a slight lead over the ECRL EMG.

For the main coherence feature seen at 14-33Hz in Fig. 5.18*c* the cumulant shows a 0ms lag and secondary features associated with 22Hz synchronisation. The phase plot also derives a similar delay at 0.0±0.6ms. The cumulant for the 33-48Hz feature in Fig. 5.18*d* gives statisticaly significant coupling indicating synchronisation around 37Hz, with a central peak at 0ms. The corresponding phase gives a similar near zero delay estimate at -0.3±0.4ms.

The FCR\BBLH coherence plot (Fig. 5.17*e*) contains a number of distinct features. Fig. 5.19 illustrates the cumulant density analysis for the different frequency bands. Within the 0-4Hz range the cumulant peak shows a 31ms delay while the corresponding phase gives 29.3±34.3ms. This suggests that FCR is leading the BBLH for the specific frequency band. That makes it unlikely to be of central origin because of the closer proximity of BBLH to CNS than of FCR. If central descending command was underling the coupling in this band BBLH should be leading FCR. Therefore some sort of reflex mechanism should be generating this synchronisation.

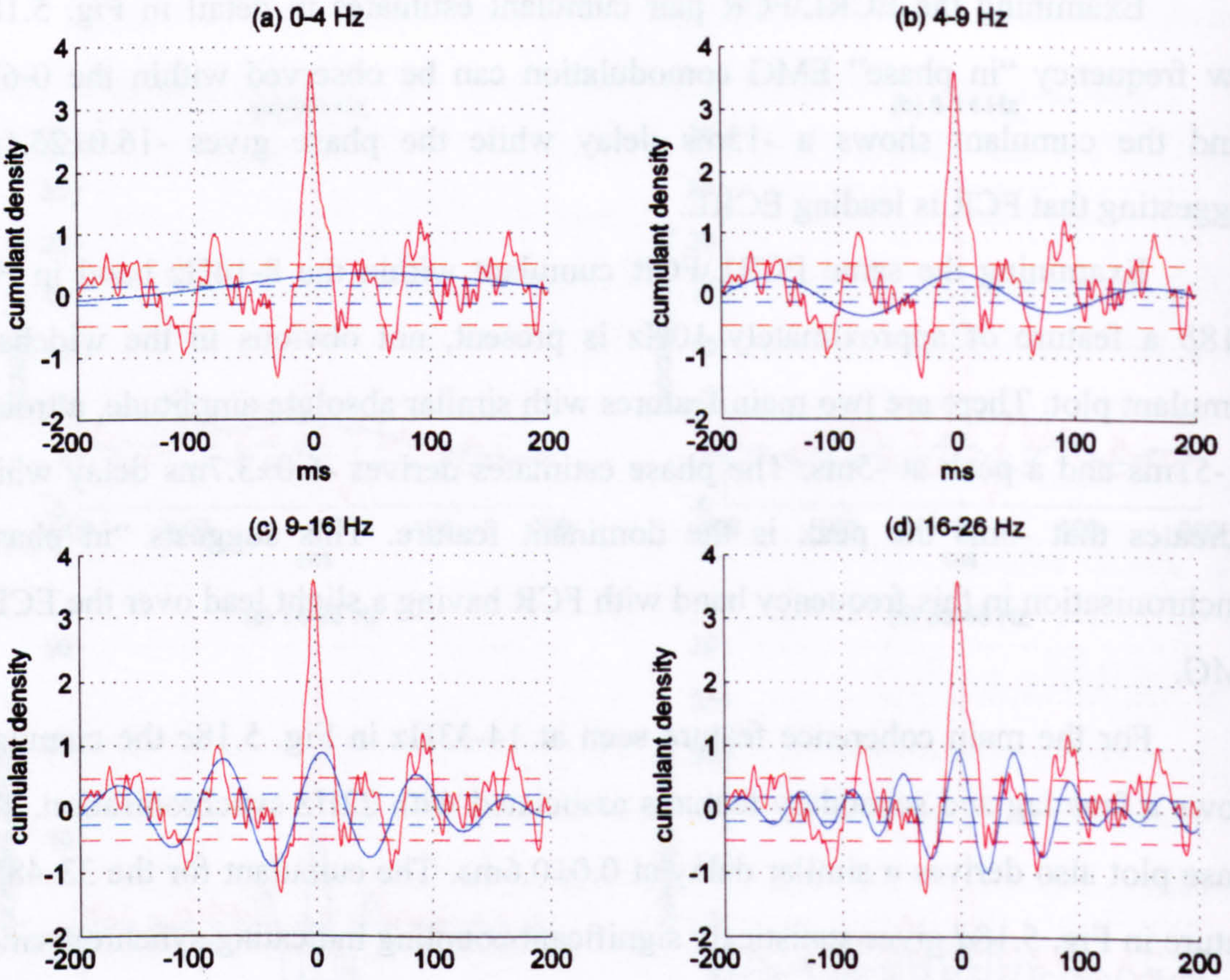

Fig. 5.19 Cumulant plots for FCR\BBLH EMGs during posture extension. The red plot represents the cumulant estimate for the whole 0-500Hz spectrum and the blue plot represents the estimate for the frequency band indicated at the top of each plot.

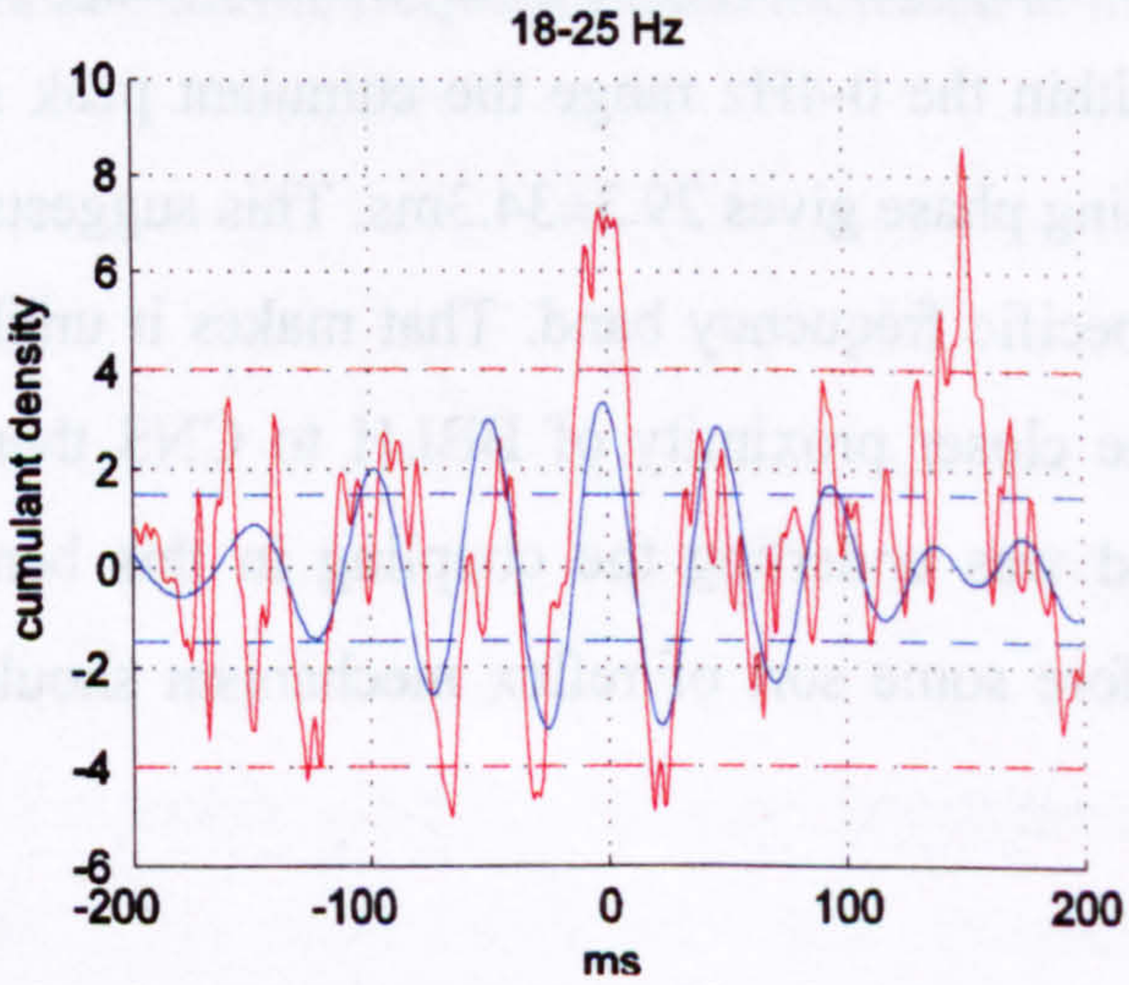

Fig. 5.20 Cumulant plot for ECRL\BBLH EMGs during posture extension. The red plot represents the cumulant estimate for the whole 0-500Hz spectrum and the blue plot represents the estimate for the frequency band indicated at the top of the plot.

The cumulant estimate for the 4-9Hz band (Fig. 5.19*b*) reveals a central peak at 0ms and suggests 6Hz coupling. The phase does not give a valid result and contains a large error. The cumulant for the 9-16Hz band (Fig. 5.19*c*) shows a peak at 5ms and has a highly oscillatory shape. The phase plot gives a fairly close estimate at 3.4±3.0ms. The last statisticaly significant feature lies in the 16-26Hz band (Fig. 5.19*d*) and the cumulant estimate gives a positive peak at -1ms and an oscillatory form. The phase derives a similar value of 0.4 ± 1.9ms.

Comparing the coherences for ECRL\FCR and FCR\BBLH pairs in Fig. 5.17, a symmetric shape of the coherence plot around the dominant frequency for the first pair is apparent. This is not the case for the second where a rapid decline is observed after the 24Hz.

The ECRL\BBLH coupling shows a weak coherence feature in the 17-25Hz band (Fig. 5.20). The cumulant plot shows synchronisation features just over the confidence limit. It shows a positive peak and a latency of -2ms. The dominant coupling frequency is at 20Hz. The phase plot gives a similar delay at -1.5±3.2ms. The corresponding coupling feature during flexion posture for the same pair of muscles was considerably stronger.

TEXT BOUND INTO

THE SPINE

	ECRL				FCR				BBLH			
	0-5 Hz	5-15 Hz	15-35 Hz	35-50 Hz	0-5 Hz	5-15 Hz	15-35 H	35-50 Hz	0-5 Hz	5-15 Hz	15-35 Hz	35-50
Movement Flexion	2Hz	11Hz			2Hz	11Hz				14Hz	23Hz	
Posture Flexion	2Hz	14Hz	27Hz		2Hz	11Hz	22Hz		2Hz	12Hz	23Hz	
Movement Extension	1Hz		21Hz	39Hz	2Hz	11Hz				11Hz		
Posture Extension	2Hz	11Hz	22Hz		2Hz	11Hz	22Hz	37Hz		9Hz	22Hz	

Table 5.1 Power spectral features appearing in EMG during the four motion phases. The frequency spectrum has been separated in four bands and the central frequency of the most important feature in each band is shown.

	ECRL\FCR				FCR\BBLH				ECRL\BBLH			
Frequency / Delay	0-5 Hz	5-15 Hz	15-35 Hz	35-50 Hz	0-5 Hz	5-15 Hz	15-35 Hz	35-50 Hz	0-5 Hz	5-15 Hz	15-35 Hz	35-50
Movement Flexion	3Hz / 5ms	10Hz / 0ms		36Hz / -5ms	1Hz / 51ms	10Hz / 22ms						
Posture Flexion			21Hz / -3ms		1Hz / 3ms	8Hz / 53ms	22Hz / 0ms	48Hz / 0ms			22Hz / -2ms	
Movement Extension	1Hz / -2ms	11Hz / -3ms			1Hz / -2ms	11Hz / 28ms			1Hz / 5ms			
Posture Extension	1Hz / -15ms	11Hz / -5ms	21Hz / 0ms	45Hz / 0ms	1Hz / 50ms	13Hz / 5ms	22Hz / -1ms				20Hz / -2ms	

Table 5.2 Intermuscular coupling features appearing during the four motion phases (ECRL\FCR, FCR\. The frequency spectrum has been separated in four bands and the central frequency and delay of the most important feature in each band is shown. Black colour represents in phase coupling while red colour represents out of phase intermuscular coupling.

5.1.3.5 Summary

Table 5.1 and Table 5.2 contain the summarised results from the current experiment. The frequency spectrum has been separated in 4 different bands: 0-5Hz, 5-15Hz, 15-35Hz and 35-50Hz. The peak frequency of the main coherence features in each band appears in each cell. The delay derived by the cumulant central peak or trough is also included, when verified by the phase curve delay estimation based on the weighted least squares regression. Only the main features were included; the magnitude of the coherence peak had to be at least two times greater than the confidence limit. The main findings of the results were:

- High coupling was observed centred around 10Hz between wrist agonist and antagonist during flexion and extension movements, which is probably of central origin. The ECRL\FCR EMGs were coupled "out of phase" and with zero delay. This coherence was completely suppressed during posture flexion. The kind of synchronisation appears to be a common oscillatory input with independent Poisson processes as it appears in Appendix 8.4.4-Example 4 (Fig.8.30, Fig.8.31). A model that can better describe the out of phase nature of the signals can be seen in Analytical Methods 4.4.3 (Fig.4.6, Fig.4.7)
- ECRL\FCR and FCR\BBLH EMG pairs showed strong coupling during movement at 10Hz, but no coupling was observed in the same frequency between ECRL\BBLH. FCR\BBLH coupling was "in phase" and delay suggested that FCR leads BBLH by 22-28ms during movement flexion-extension despite the fact that BBLH is located closer to the CNS, suggesting that a peripheral reflex mechanism may be the underlying cause. The kind of synchronisation appears to be a common oscillatory input with independent Poisson processes as it appears in Appendix 8.4.4-Example 4 (Fig.8.30, Fig.8.31) with the only difference that delay is also introduced.
- High coherence was present between agonist and antagonist in the 15-35Hz band, centred around 21Hz occurred during posture extension and posture flexion between ECRL\FCR agonist and antagonist. The coupling was "in phase" with delays between the signals close to zero. Short term synchronisation of central origin appears to cause this activity. This coupling was suppressed during movement. The kind of synchronisation appears to be short term synchronisation. This appears similar to a common oscillatory input with common Poisson processes model as it

appears in Appendix 8.4.4-Example 4 (Fig.8.29, Fig.8.30). There is also some resemblance with the model presented in Appendix 8.4.3-Example 3-Non oscillatory inputs producing oscillatory output. However the strong power spectra harmonics and the not well defined coupling features appearing in the simulated data do not suggest this model as a valid explanation of the coherence behaviour.

- FCR\BBLH were synchronised at 10Hz during posture and movement but with different coupling characteristics for posture and movement indicating that different physiological mechanisms may be involved.
- High 1-5Hz ECRL\FCR coupling was present during posture and movement. During movement it had "out of phase" synchronisation properties while during posture it was "in phase" synchronisation. The neurogenic or biomechanical origin is not clear and needs to be further investigated.
- High ECRL\FCR coherence between 35-50Hz was present during posture extension, while absent during posture flexion.
- The most statisticaly significant power feature was the high antagonist FCR 10Hz feature during movement and the absence of a clear 10Hz feature for the ECRL agonist during extension movement. Similarly ECRL demonstrated high 10Hz during flexion movement.

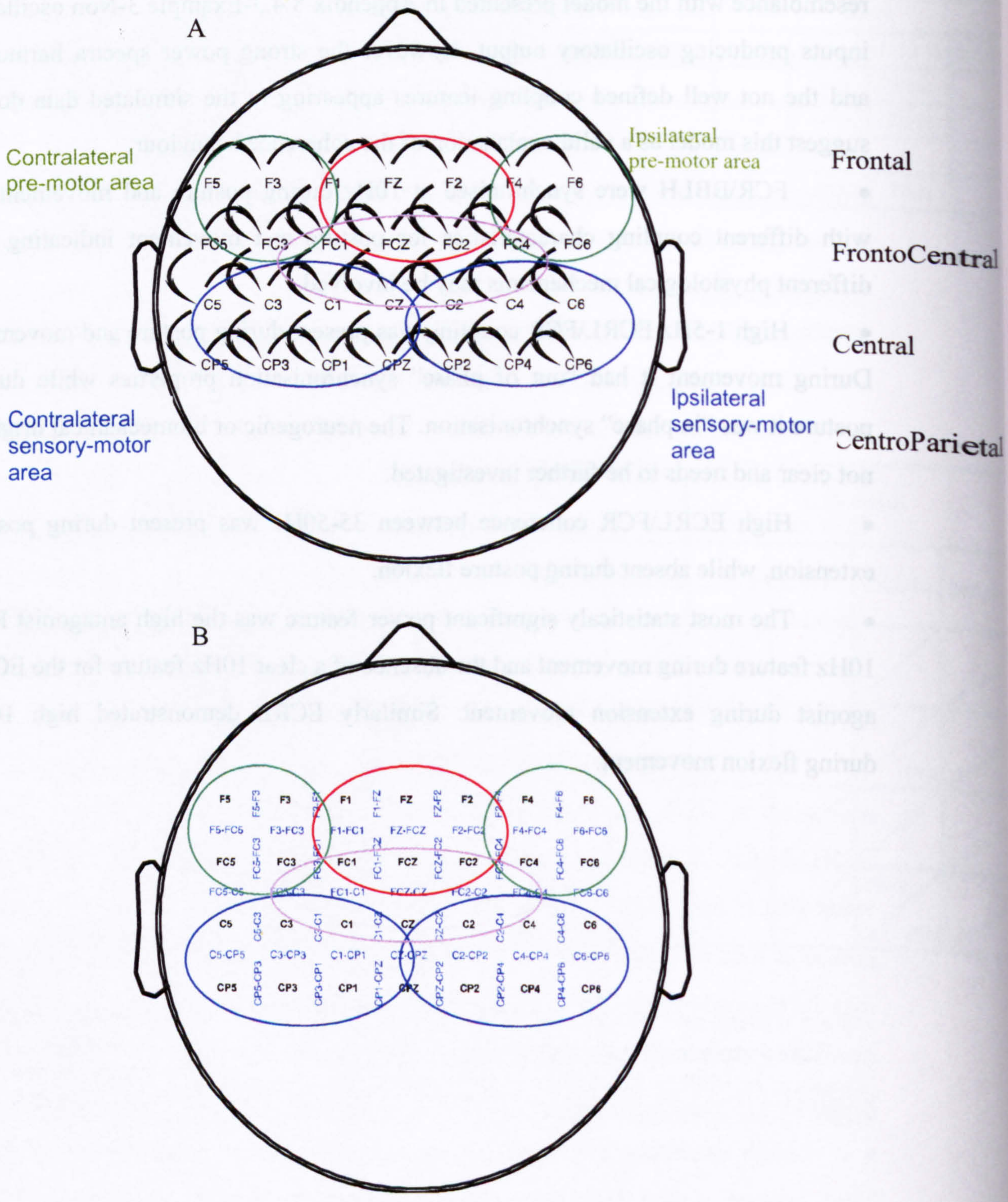

Fig. 5.21 Monopolar (A) and bipolar (B) multichannel EEG montages showing the main motor anatomical motor areas.

5.1.4 Cortical and Corticomuscular frequency characteristics.

As shown before, task dependent synchronisation occurs between muscles involved in postural or movement tasks. During posture, synchronisation occurs centred around the 10Hz and 20Hz bands while for movement the 20Hz coupling may get suppressed while there is still coupling at 10Hz. Various groups have suggested the supraspinal origin of the 10Hz and 20Hz EMG frequency modulations (Vallbo and Wessberg 1993; Salenius, Portin et al. 1997). Some evidence supporting the central origin or contribution of the under discussion frequencies has already been presented in the previous section examining EMG signals. The frequency characteristics of the EEG signal in relation with the EMG signal are now going to be examined. Similar analysis methods with the ones previously used for EMG signals were employed

Before the application of the analytical methods that have already been described, the move-hold data had to be prepared and organised according to the individual phases in the same way that the data was prepared for the analysis of the EMG. Data from the same move hold sequence were used so the results are directly comparable with the previous section. The data for each one of the four phases, for each of the 21 trials and for every subject, were segmented and reshaped to produce a single record representing one specific task phase. The frequency estimate of that record corresponded the specific task and to the pooled estimate representing common intersubject characteristics. Only the data 200ms after the audio cue (indicating the start of a phase) to 200ms before the next cue (indicating the end of the phase) were used. In this way 400ms from each phase were discarded, in order to ensure the subject was actually performing the current task and avoid any effect of poor synchronisation with the audio cues and reaction time lag.

The spatial characteristics (distribution of features over the scalp) of the cortical signals are also of great interest. For this reason multiple monopolar channels (Fig. 5.21*A*) over the ipsilateral and contralateral motor cortex were recorded in order to examine the variations of localised signals over a wide area. Bipolar recordings were also produced by generating montages of bipolar electrodes in both vertical and horizontal directions by means of subtracting the records corresponding to the bipolar electrode pairs as shown in Fig. 5.21*B*. In this way the identification

frequency characteristics and corticomuscular coupling between individual muscles and a widespread area over the motor cortex was possible. The cortical area examined included the contralateral and ipsilateral primary motor and sensory cortices, the premotor area and the SMA.

During the analysis a number of parameters were calculated, corticomuscular coherences between all three muscles and monopolar or bipolar EEG channels as well as cumulant densities and phases. Intracortical spectral estimates were also calculated. Given the sheer scale of the number of graphs generated, only the most representative have been included.

5.1.4.1 EEG Power Spectral density task dependent features

During the move-hold sequence task EEG recordings were acquired. In order to examine task dependent changes in the power spectral power of EEG signals the corresponding to the movement phase, monopolar and bipolar power spectral density plots were created and they are included in Appendix 8.2. These plots demonstrated some interesting features throughout the whole examined power spectrum:

- Very high delta (0-3Hz) and high theta (4-7Hz) frequency content during all move-hold sequence phases.
- Distinct alpha (8-13Hz) features during all move-hold sequence phases that appear in central electrodes and reach a maximum in centroparietal electrodes. These features were laterally symmetrical.
- Beta features were always present and increased mainly during posture.
- Gamma features did appear but with no clear organisation and task dependency.

It was not possible to extract more information in the way the EEG power spectral plots were presented. Plotting the differences of the spectral estimates (rather than individual phase spectral estimates) for successive movement or posture phases revealed the task modulation in a more comprehensive manner. For example the EEG spectral power modulation between movement flexion and posture flexion was derived by simple arithmetic subtraction of the spectral estimates for corresponding channels during these two phases. The scale and improved magnitude resolution of the produced plots allowed small differences to emerge in a way that can be easily identified.

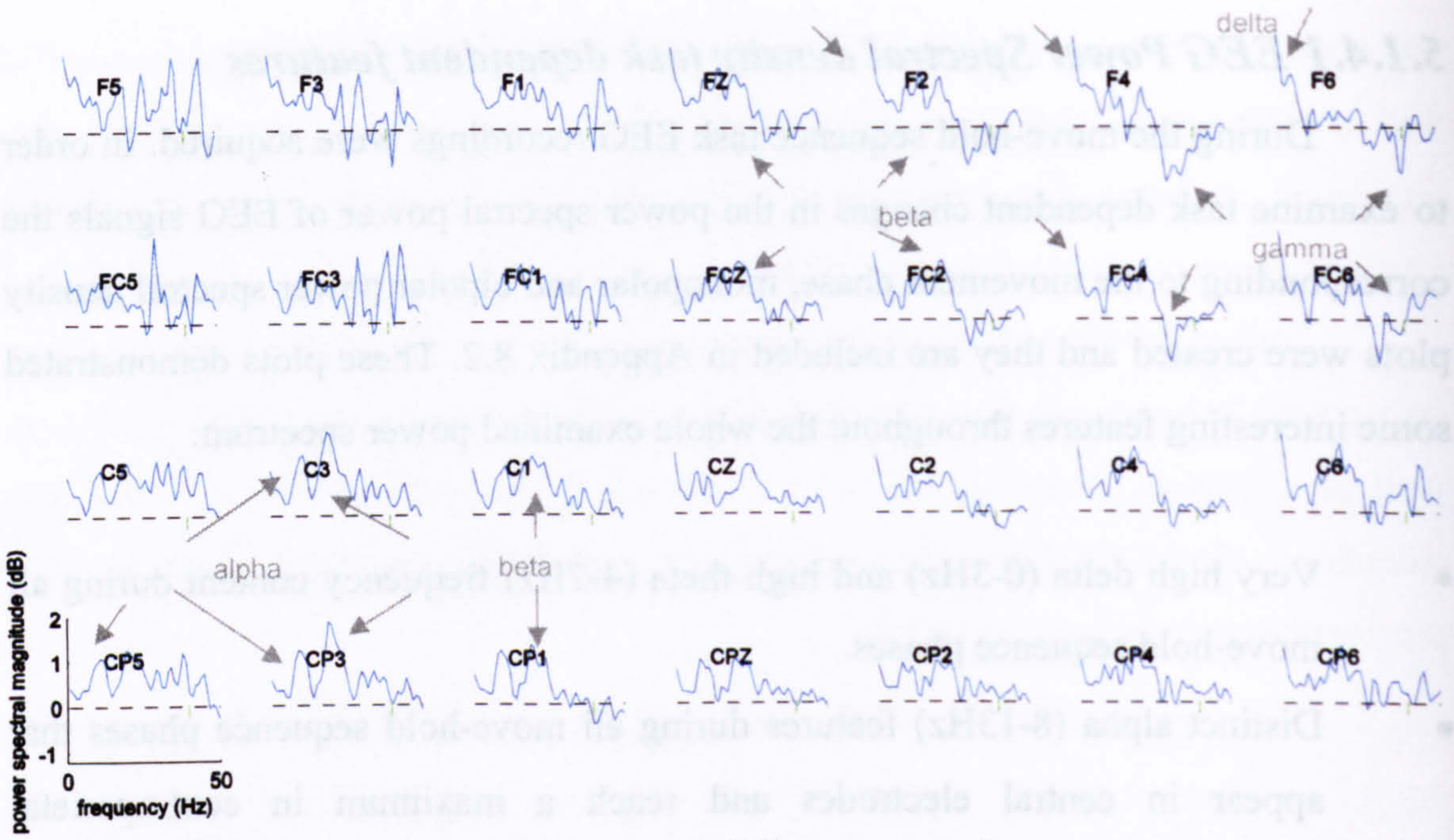

Fig. 5.22 EEG monopolar power spectral difference map between movement flexion and posture flexion; pooled power spectral maps. The labels represent the relative position of the electrodes over the head. The green vertical line indicates the magnitude of a 95% confidence interval for the spectral estimates.

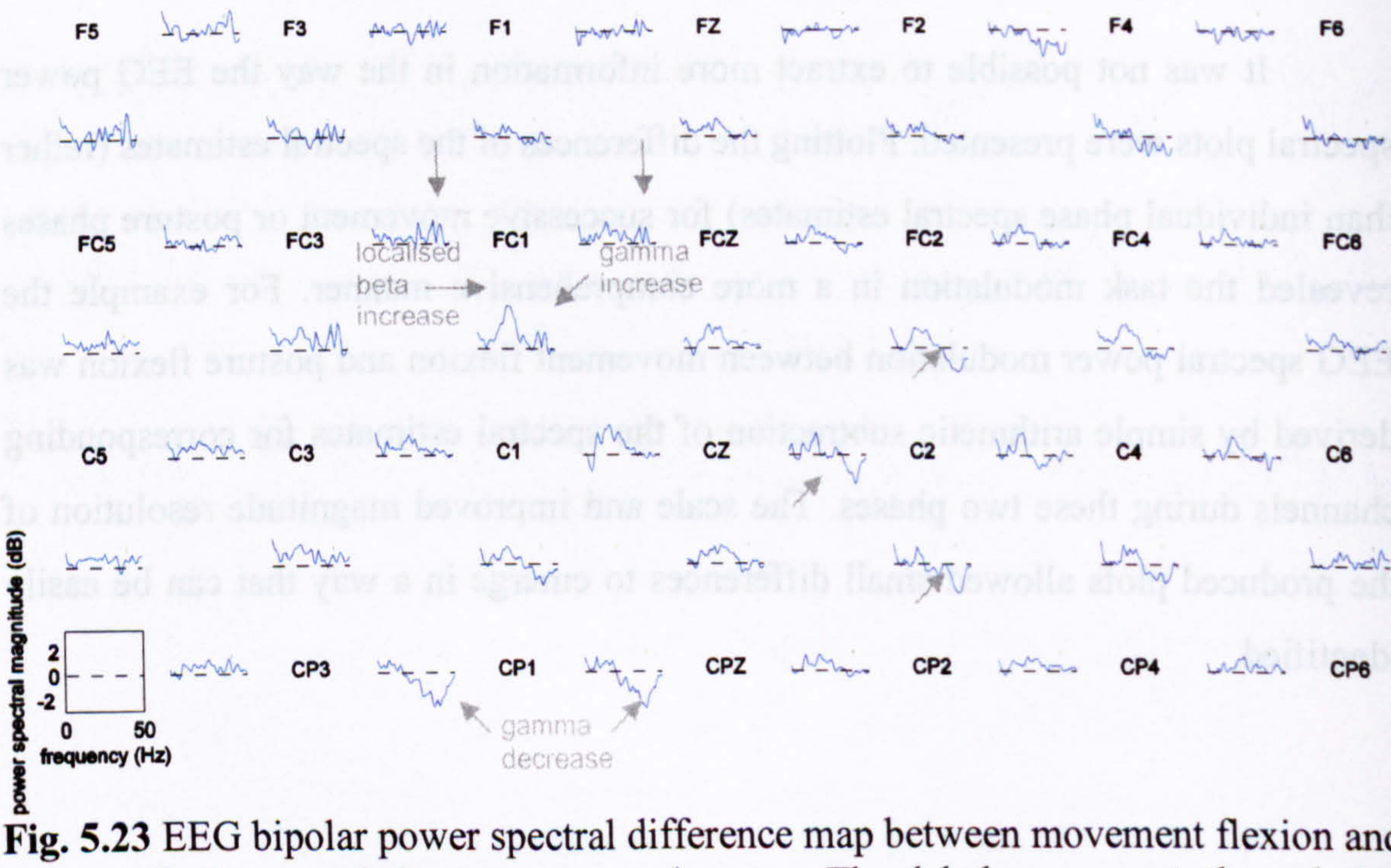

Fig. 5.23 EEG bipolar power spectral difference map between movement flexion and posture flexion; pooled power spectral maps. The labels represent the relative position of the electrodes over the head. The green vertical line indicates the magnitude of a 95% confidence interval for the spectral estimates.

5.1.4.1.1 EEG spectral changes between movement flexion and posture flexion.

Fig. 5.22 displays the monopolar EEG power spectral differences between posture flexion and movement flexion. It demonstrates an increase in the posture flexion power spectrum throughout the whole examined spectrum for the majority of the electrodes. This increase mainly took place in the alpha and beta bands. 10 and 20Hz features were higher in the contralateral central and centroparietal electrodes (C5, C3, C1, CP5, CP3 and CP1) while the main beta feature in the ipsilateral cortex was closer to 24Hz (F2, F4, FCZ, FC2, FC4, CZ, C2, C4 and C6). The most obvious decrease features were observed for the ipsilateral frontal and frontocentral electrodes in the high beta and gamma bands with negative peaks at 32 and 40Hz (FZ, F2, F4, F6, FC2, FC4 and FC6). A number of high beta and gamma increase features were present in the contralateral cortex with the most prominent located in the contralateral frontal and frontocentral areas.

Increase in the 0-5Hz power during flexion posture (compared to movement flexion) was also observed. This increase is higher in frontal and frontocentral electrodes and also higher in ipsilateral electrodes. The highest such increase was observed in F6 electrode.

Fig. 5.23 demonstrates the corresponding bipolar EEG powers spectral differences between movement flexion and posture flexion. It contained analogues changes in similar frequency bands with a different spatial distribution than the monopolar plot. Increase in the beta power during posture flexion was present for a number of electrodes mainly in frontocentral and central areas. The highest increase having a peak at 21Hz was given by the FC1-C1 bipolar electrode pair. 10Hz features were present for a number of electrodes but they were not as distinctive as the ones observed in the corresponding monopolar map. The most statisticaly significant alpha features were observed for CP5-CP3, CP3-CP1, CP1-CPz, CPz-CP2, CP2-CP4, and CP4-CP6. A considerable decrease in high beta and gamma bands was also present for contralateral and medial centroparietal electrodes as well as medial and ipsilateral frontocentral and central electrode pairs (CP3-CP1, CP1-CPZ, CZ-C2, FC2-C2, C2-CP2, C2-C4, FC4-C4 and C4-CP4). The 0-5Hz bang showed increased power for all the electrodes taking its highest in the contralateral central and frontal electrodes.

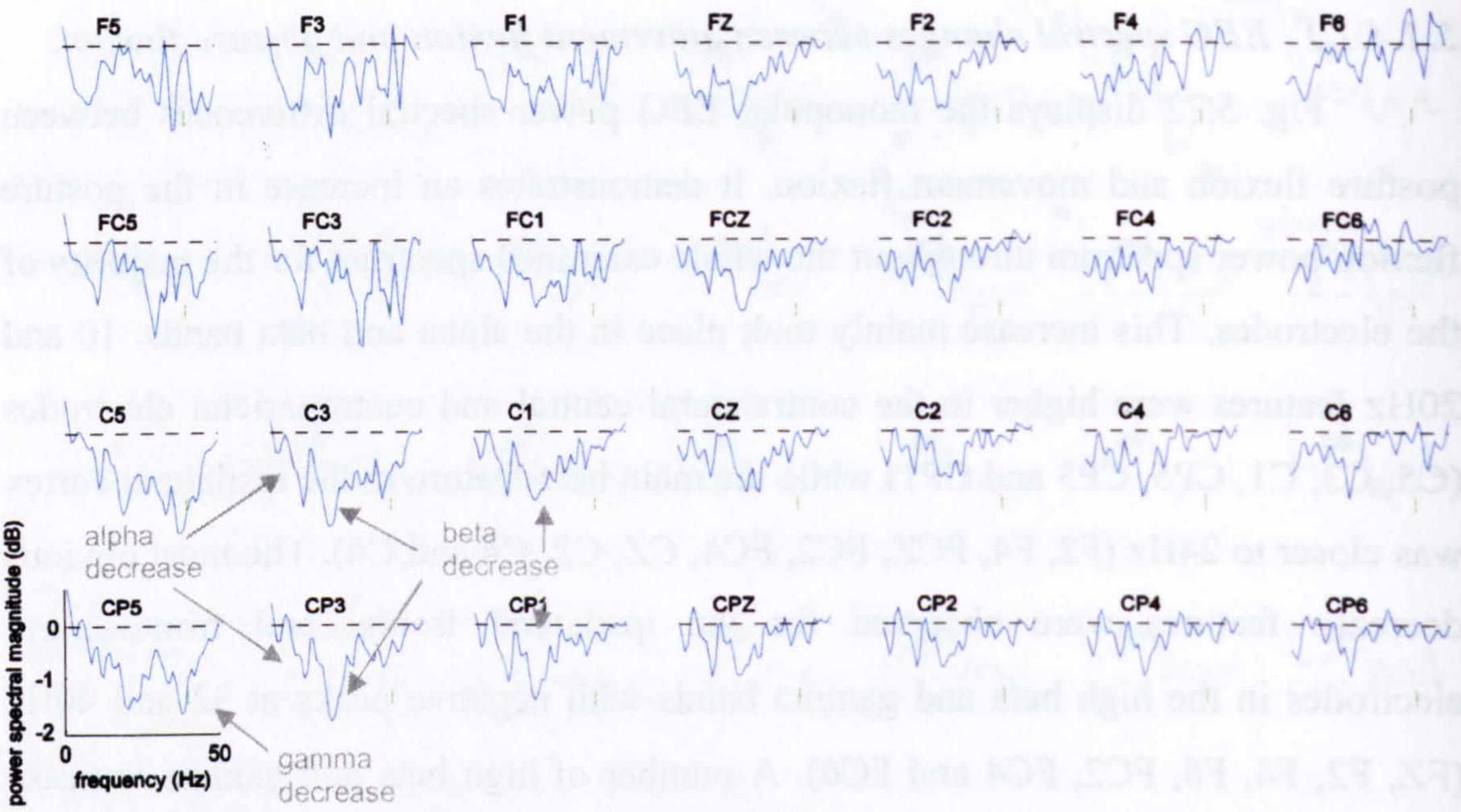

Fig. 5.24 EEG monopolar power spectral difference map between posture flexion and movement extension, pooled power spectral maps. The labels represent the relative position of the electrodes over the head. The green vertical line indicates the magnitude of a 95% confidence interval for the spectral estimates.

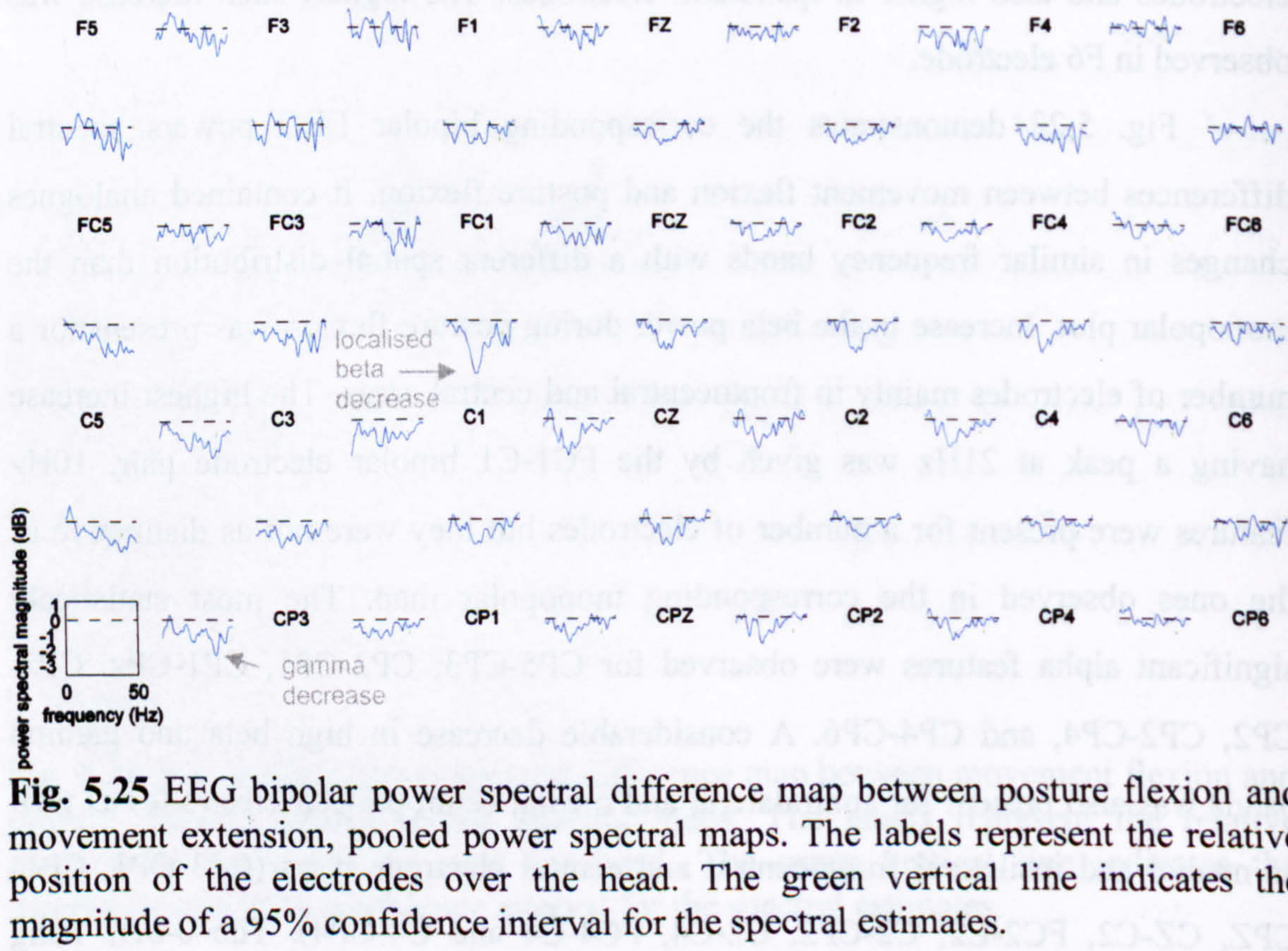

Fig. 5.25 EEG bipolar power spectral difference map between posture flexion and movement extension, pooled power spectral maps. The labels represent the relative position of the electrodes over the head. The green vertical line indicates the magnitude of a 95% confidence interval for the spectral estimates.

5.1.4.1.2 EEG spectral changes between posture flexion and movement extension.

Fig. 5.24 displays the monopolar EEG power spectral differences between posture flexion and movement extension. Spectral power for most of the electrodes has decreased over the examined frequency spectrum. The most significant changes take place in the contralateral cortex. Alpha (12Hz) beta (21Hz) and gamma (38Hz) features show a decrease especially for contralateral central and centroparietal electrodes (C5, C3, CP5 and CP3). Beta activity decreased for all the electrodes around the same 22Hz frequency. The main power increase features were observed for ipsilateral frontal electrodes at 40Hz and 46Hz (F4 and F6) and for 0-5Hz for most contralateral electrodes and especially contralateral central and centroparietal electrodes.

Fig. 5.25 demonstrates the corresponding bipolar EEG power spectral differences between posture flexion and movement extension. The most prominent feature is the feature expressing reduction in the beta band (21Hz) which appears for FC1-C1 electrode pair. Reduction of activity occurs for a number of electrodes in Frontocentral central and centroparietal electrodes. However the large and sharp decrease in the beta band appears to be localised for FC1-C1 electrode site. Decrease in the gamma coherence also appears for a number of electrodes and especially for contralateral central and centroparietal electrodes (C5-C3, C5-CP5 and CP5-CP3).

Fig. 5.26 EEG monopolar power spectral difference map between movement extension and posture extension, pooled power spectral maps. The labels represent the relative position of the electrodes over the head. The green vertical line indicates the magnitude of a 95% confidence interval for the spectral estimates.

Fig. 5.27 EEG bipolar power spectral difference map between movement extension and posture extension, pooled power spectral maps. The labels represent the relative position of the electrodes over the head. The green vertical line indicates the magnitude of a 95% confidence interval for the spectral estimates.

5.1.4.1.3 EEG spectral changes between movement extension and posture extension.

Fig. 5.26 displays the monopolar EEG power spectral differences between posture flexion and movement flexion. It demonstrates an increase in the posture flexion power spectrum throughout the whole examined spectrum for all examined electrodes. The most important increase features appear in theta, delta, alpha, beta and gamma bands. 0-5Hz shows higher increase for ipsilateral electrodes. Sharp features centred around 11Hz are very clear for central and centroparietal electrodes especially in the contralateral side. Wide beta increase features centred around 22Hz appear throughout the cortex and especially for contralateral centroparietal (C3, C1, CZ, CP5, CP3, CP1 and CPZ) and medial frontal and frontocentral electrodes (F1, FZ, F2, FC1, FCz and FC2). High beta and gamma features are also present for most monopolar power spectra.

Fig. 5.27 demonstrates the corresponding bipolar EEG power spectral differences between movement and posture extension. The vast majority of electrodes increased their spectral power during posture extension (compared to movement extension). The most prominent increase features appeared in beta band and especially for FC1-C1 electrode for which the highest increase occurs. Less important increase in the same band occurs for several frontocentral central and centroparietal electrodes. Smaller alpha increase features for posture extension appear especially in central and centroparietal electrodes. Gamma increase features are also present with the highest occurring in the ipsilateral frontal area (F2-F4 and F4-FC4) always compared to the movement extension.

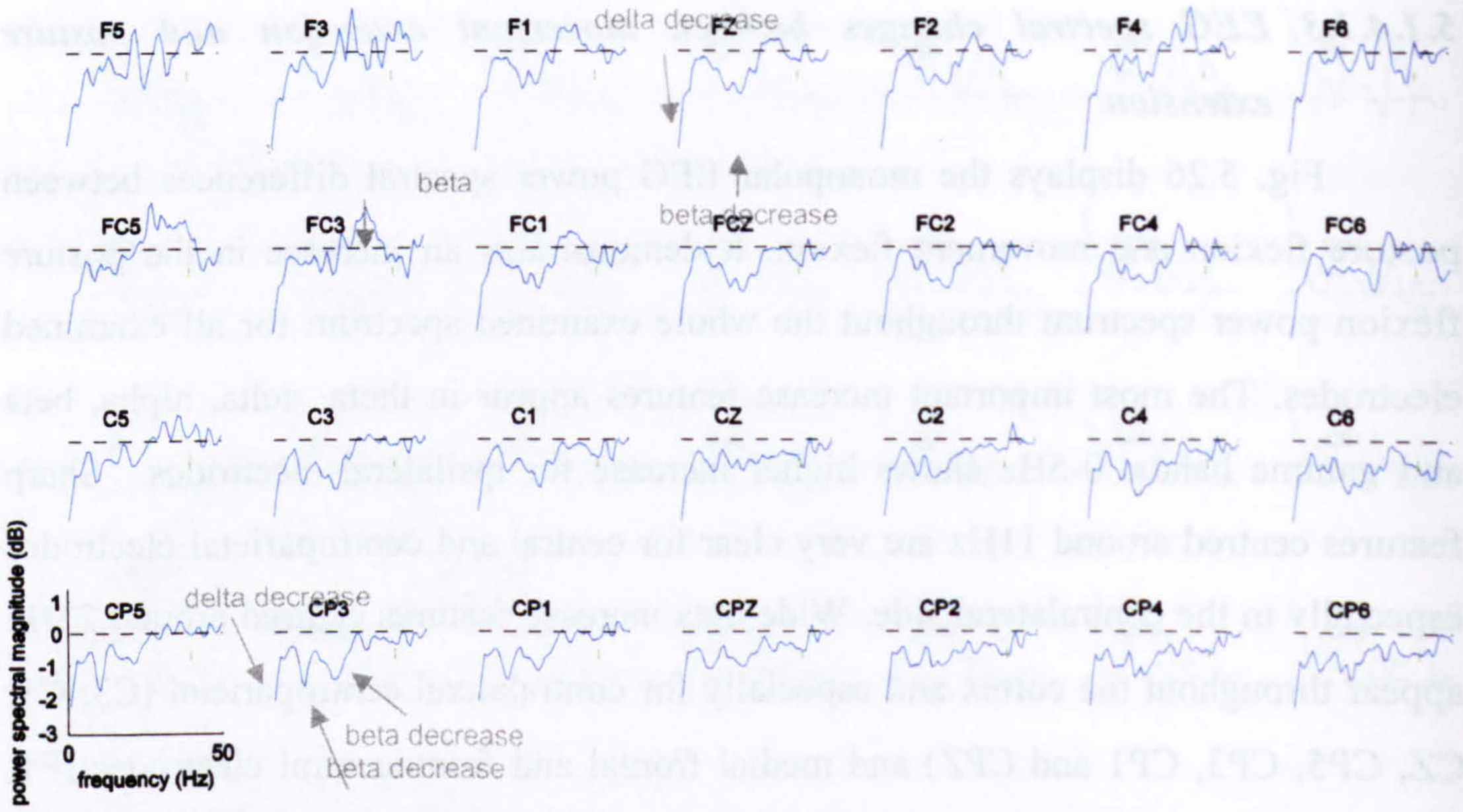

Fig. 5.28 EEG monopolar power spectral difference map between posture extension and movement flexion, pooled power spectral maps. The labels represent the relative position of the electrodes over the head. The green vertical line indicates the magnitude of a 95% confidence interval for the spectral estimates.

Fig. 5.29 EEG bipolar power spectral difference map between posture extension and movement flexion, pooled power spectral maps. The labels represent the relative position of the electrodes over the head. The green vertical line indicates the magnitude of a 95% confidence interval for the spectral estimates.

5.1.4.1.4 EEG spectral changes between posture extension and movement flexion.

Fig. 5.28 displays the monopolar EEG power spectral differences between posture extension and movement flexion. Changes were observed throughout the whole examined frequency spectrum.

0-5Hz decreased during movement flexion for all electrodes with the most substantial reduction occurring for frontal electrodes. 10Hz activity also decreased especially in contralateral central centroparietal electrodes like C5, CP5, C3, CP3, C1 and CP1 where a distinct negative peak at 11Hz is present expressing the power decrease. Beta power decrease during movement also occurs for the same set of electrodes and medial ipsilateral frontocentral and central electrodes. High beta and gamma increase during flexion movement compared to extension posture for ipsilateral and contralateral frontal and frontocentral electrodes (F5, F3, F1, FZ, F2, F4, F6, FC5, FC3, FC1, FC4 and FC6).

Fig. 5.29 demonstrates the corresponding bipolar EEG power spectral differences between posture extension and flexion movement. The most important changes appear in the beta and gamma bands. Decrease in the beta band occurs for a large number of electrodes. FC1-C1 demonstrates once more the highest change in the form of a high peak expressing the suppression in beta activity during flexion movement compared to extension posture. A large increase occurs for high beta and gamma bands for contralateral centroparietal electrodes (CP3-CP1, CP1-CPz and C1-CP1). Gamma and high beta increase also occurs for a number of electrodes in ipsilateral electrodes in frontocentral and central areas (Cz-C2, FC2-C2, C2-CP2 and C2-Cz). Small alpha suppression features are also present (FC3-C3, FC1-C1 and C1-Cz) however these features are much smaller than alpha suppression features that occurred in the corresponding monopolar map (Fig. 5.28).

5.1.4.2 Topographic maps of EEG spectral power

The results that are going to be presented are in fact a different illustration of the results presented in Fig. 5.22-Fig. 5.29 showing the spatial characteristics of EEG power differences during the four different phases of the move-hold sequence as monopolar and bipolar maps. These maps consist of plotting two dimensional plots of the frequency characteristics over a relative position that corresponds to the respective electrode site over the cortex. In this way the spatiotemporal changes over the examined spectrum were observed and the main EEG spectral power features were identified. Alpha, beta and gamma features were identified. The most distinguished features were changes in the alpha and especially the beta EEG power.

The bands were the most considerable task dependent variation occurs were identified as 8-12Hz for the alpha band and 17-23Hz for the beta band. Spectral power and changes in power within those confines were visualised as topographic maps of a scalp data field in a 2-D circular view using interpolation on a fine cartesian grid. The positions of the electrodes were also indicated on the topographic maps. By illustrating the data in this way it was possible to present the spatial, task dependent characteristics for the specific bands that changes are most likely to occur in an easy to comprehend way.

The topographic maps were presented in a configuration that also included the wrist angle information derived by the goniometer information. In this way it was possible to demonstrate in a graphical way of the movement phase that each map represents.

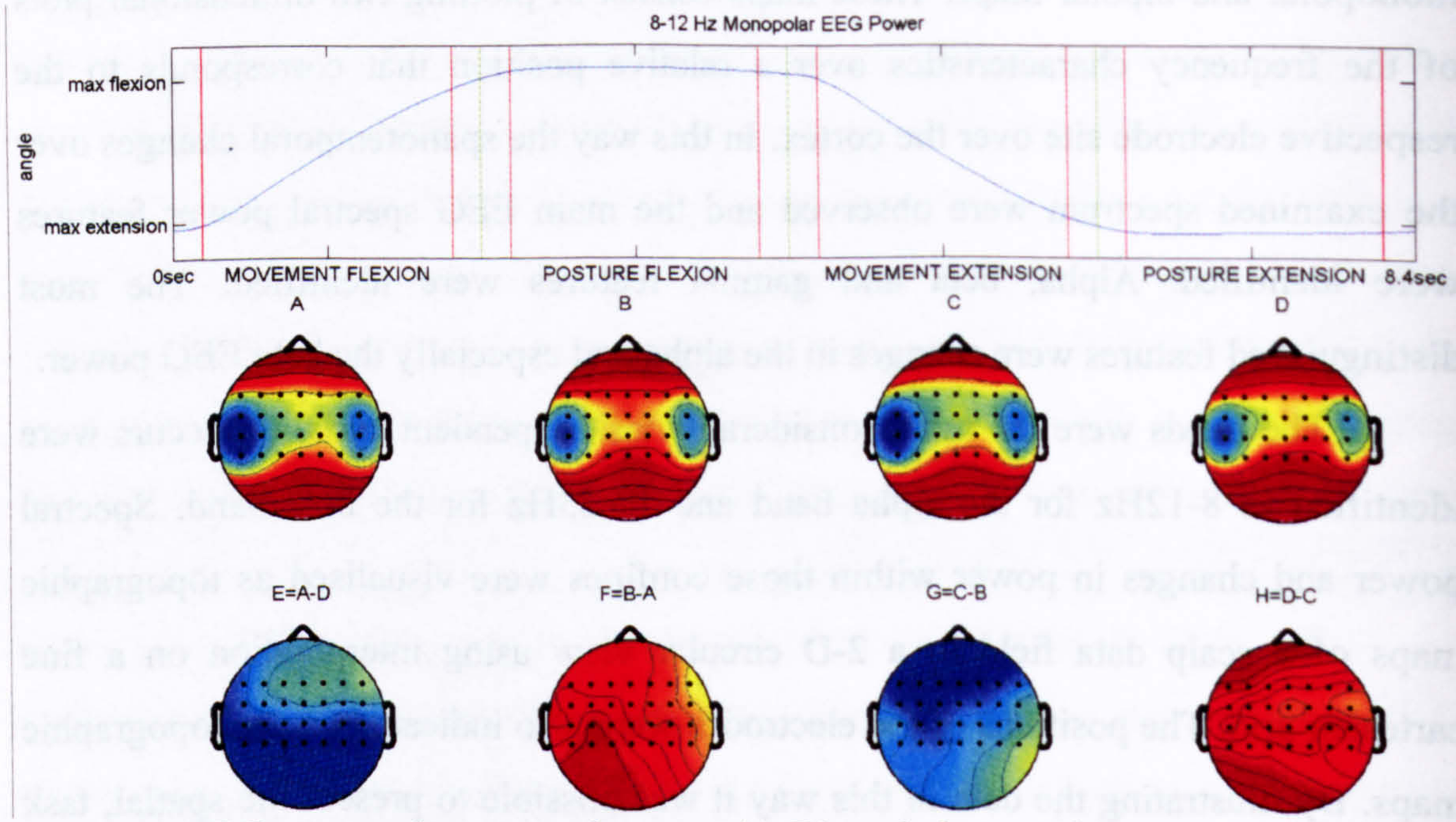

Fig. 5.30 EEG monopolar spectral power (A-D) and changes in power (E-H) within 8-12Hz band visualised as topographic maps of a scalp data field in a 2-D circular view using interpolation on a fine cartesian grid. The positions of the electrodes are indicated on the topographic maps. The maps present the spatial, task dependent characteristics for the 8-12Hz that changes are most likely to occur. Dark red represents the highest value while dark blue represents the lowest value. The top plot represents the wrist angle information derived by the goniometer demonstrating in a graphical way the movement phase that each map represents. The green vertical lines represent the audio cues while the interval between the red vertical lines represents the transition phases for which data was discarded. The difference maps are: E=A-D, F=B-A, G=C-B, H=D-C.

Fig. 5.30 shows the monopolar EEG 8-12Hz alpha spectral power modulation during the move-hold sequence. The results are pooled across 21 trials and 9 subjects as the results presented in the previous sessions. Fig. 5.30*A,B,C,D* illustrate the topographic map of interpolated absolute 8-12Hz power data while Fig. 5.30*E,F,G,H* show the difference between the current phase and the previous phase. for example Fig. 5.30*F* displays the power during posture flexion after subtracting the corresponding power during flexion movement. Because of the task dependent variations were small compared to the total power, presenting the differences increased the resolution of the given colourmap.

Fig. 5.30*A* shows the 8-12Hz monopolar alpha power during flexion movement. The highest activity for the specific frequency band can be observed for the medial electrodes while the lowest can be observed for the lateral electrodes. An asymmetry can be observed with contralateral drop in power to be greater than for the ipsilateral monopolar electrodes. A different distribution of power can also be observed for the rest of the phases with medial electrodes showing the highest activity and contralateral and ipsilateral the lower with the contralateral monopolar electrodes showing the lowest. However the overall power level appears to be higher during posture than during movement. This is confirmed by Fig. 5.30*F,H* that expresses the variation of alpha power from movement flexion to posture flexion and movement extension to posture extension. Both topographic maps show an increase in alpha power during posture. The increase is not uniform and is higher for contralateral centroparietal electrodes for flexion posture and contralateral centroparietal and frontal electrodes during posture extension. Decrease in 8-12Hz is greater for centroparietal electrodes during movement flexion and frontal electrodes during extension movement.

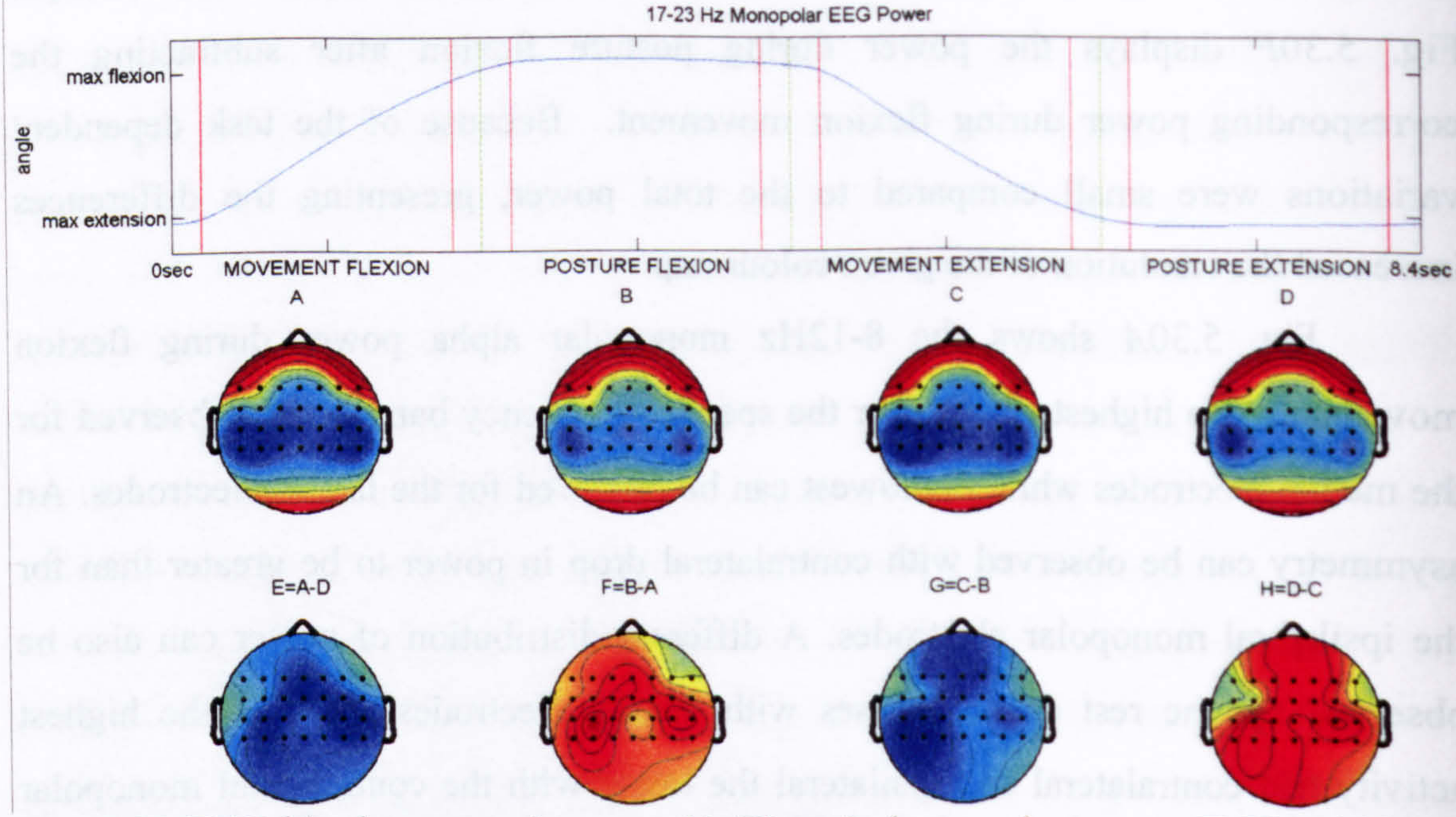

Fig. 5.31 EEG bipolar spectral power (A-D) and changes in power (E-H) within 8-12Hz band visualised as topographic maps of a scalp data field in a 2-D circular view using interpolation on a fine cartesian grid. The positions of the electrodes are indicated on the topographic maps. The maps present the spatial, task dependent characteristics for the 8-12Hz that changes are most likely to occur. Dark red represents the highest value while dark blue represents the lowest value. The top plot represents the wrist angle information derived by the goniometer demonstrating in a graphical way the movement phase that each map represents. The green vertical lines represent the audio cues while the interval between the red vertical lines represents the transition phases for which data was discarded. The difference maps are: E=A-D, F=B-A, G=C-B, H=D-C.

Fig. 5.31 demonstrates the topographic map of 8-12Hz EEG power for vertically aligned bipolar electrodes. A pattern of activity appears where a continuous trough of low activity appears for contralateral central extending to the medial frontal electrodes. A more localised low point appears in central ipsilateral electrodes. In a similar fashion to the corresponding monopolar maps in Fig. 5.30*A,B,C,D* the power at the ipsilateral site is higher than at the contralateral site. One more common feature with the corresponding monopolar maps is the suppression of alpha power during movement. The suppression is better illustrated in the 8-12Hz power differences between consequent phases shown in Fig. 5.31*E,F,G,H*. More specifically the Fig. 5.31*E* shows the difference in alpha power between movement flexion and posture extension. The alpha power follows the general power decrease while it is even further suppressed for frontal and frontocentral ipsilateral electrodes and the central and centroparietal electrodes contralateral electrodes. This suppression was inversed during flexion posture when an increase in power occurs in similar sites. The distribution of the suppression during movement extension (Fig. 5.31*G*) is slightly different, with the contralateral suppression site more frontally located. However the same pattern of activity with one ipsilateral and one contralateral site is present. Similar is the situation during posture extension where the recovery of the 8-12Hz power occurs in both ipsilateral and contralateral sites, with fontal electrodes also increasing their activity.

Both monopolar and bipolar topographic alpha power maps show distinct changes between different phases. The most important is the general power increase during posture and its suppression during movement. There are also differences between the two posture phases as well as between the two movement phases. Movement flexion and movement extension are followed by suppression of activity with a different distribution. Posture extension is connected with a different distribution in the alpha power increase than posture extension. Both general alpha power variation and suppression or rise distribution are more distinct for the monopolar maps than the bipolar. In simple terms it is easier to identify transition from one phase to the following phase by monitoring the differences of the corresponding topographic map of the alpha power spectral differences by monitoring the monopolar map than by monitoring the bipolar map.

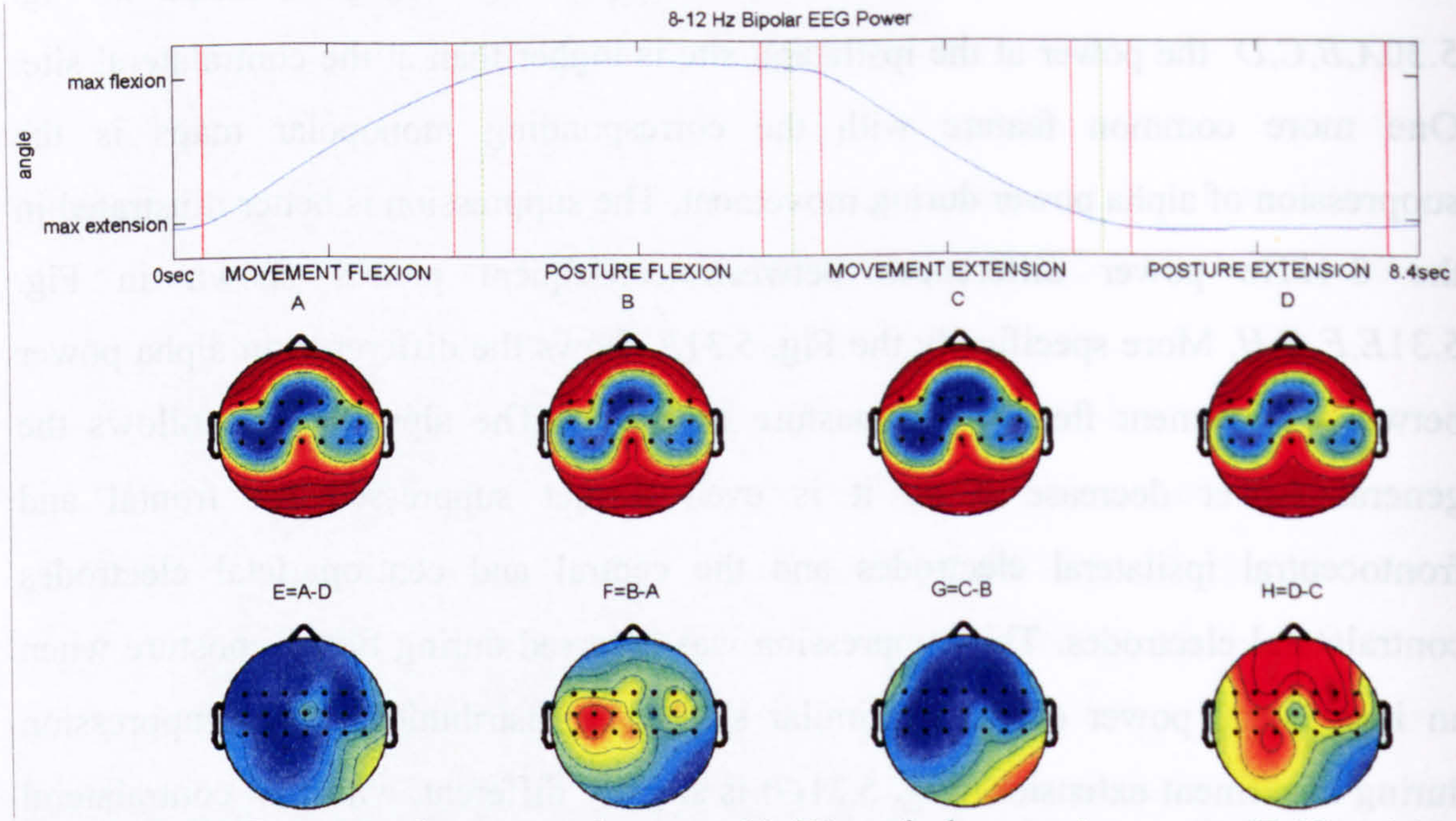

Fig. 5.32 EEG monopolar spectral power (A-D) and changes in power (E-H) within the 17-23Hz band visualised as topographic maps of a scalp data field in a 2-D circular view using interpolation on a fine cartesian grid. The positions of the electrodes are indicated on the topographic maps. The maps present the spatial, task dependent characteristics for the 8-12Hz that changes are most likely to occur. Dark red represents the highest value while dark blue represents the lowest value. The top plot represents the wrist angle information derived by the goniometer demonstrating in a graphical way the movement phase that each map represents. The green vertical lines represent the audio cues while the interval between the red vertical lines represents the transition phases for which data was discarded. The difference maps are: E=A-D, F=B-A, G=C-B, H=D-C.

Topographic maps in Fig. 5.32*A,B,C,D* show the distribution of the 17-23Hz beta power of topographic electrodes. There is a similar pattern for all three phases where alpha appears to be lower in medial frontal electrodes and show a minimum at lateral central and centroparietal electrodes. The beta power is lower for the contralateral site. The highest beta power occurs at contralateral and ipsilateral frontal electrode sites. As with central and centroparietal electrodes there is an asymmetry. This time however higher beta power occurs for the contralateral frontal monopolar electrodes.

The topographic maps also reveal a general increase of beta power during posture and suppression during movement. This modulation in power is better illustrated in the topographic maps expressing the differences in monopolar beta power (Fig. 5.32*E,F,G,H*). It is clearly demonstrated that the beta power is higher during posture than during movement. It is also demonstrated that there are two centres of the beta power suppression and increase located in the ipsilateral and contralateral central and centroparietal sites. Medial frontal and frontocentral electrodes also show analogous modulation. During movement flexion the suppression is greater at the ipsilateral site (Fig. 5.32*E*) while during movement flexion the main suppression takes place at the contralateral site (Fig. 5.32*E*). During both posture flexion and extension the main increase in power occurs at the ipsilateral site (Fig. 5.32*F,H*)

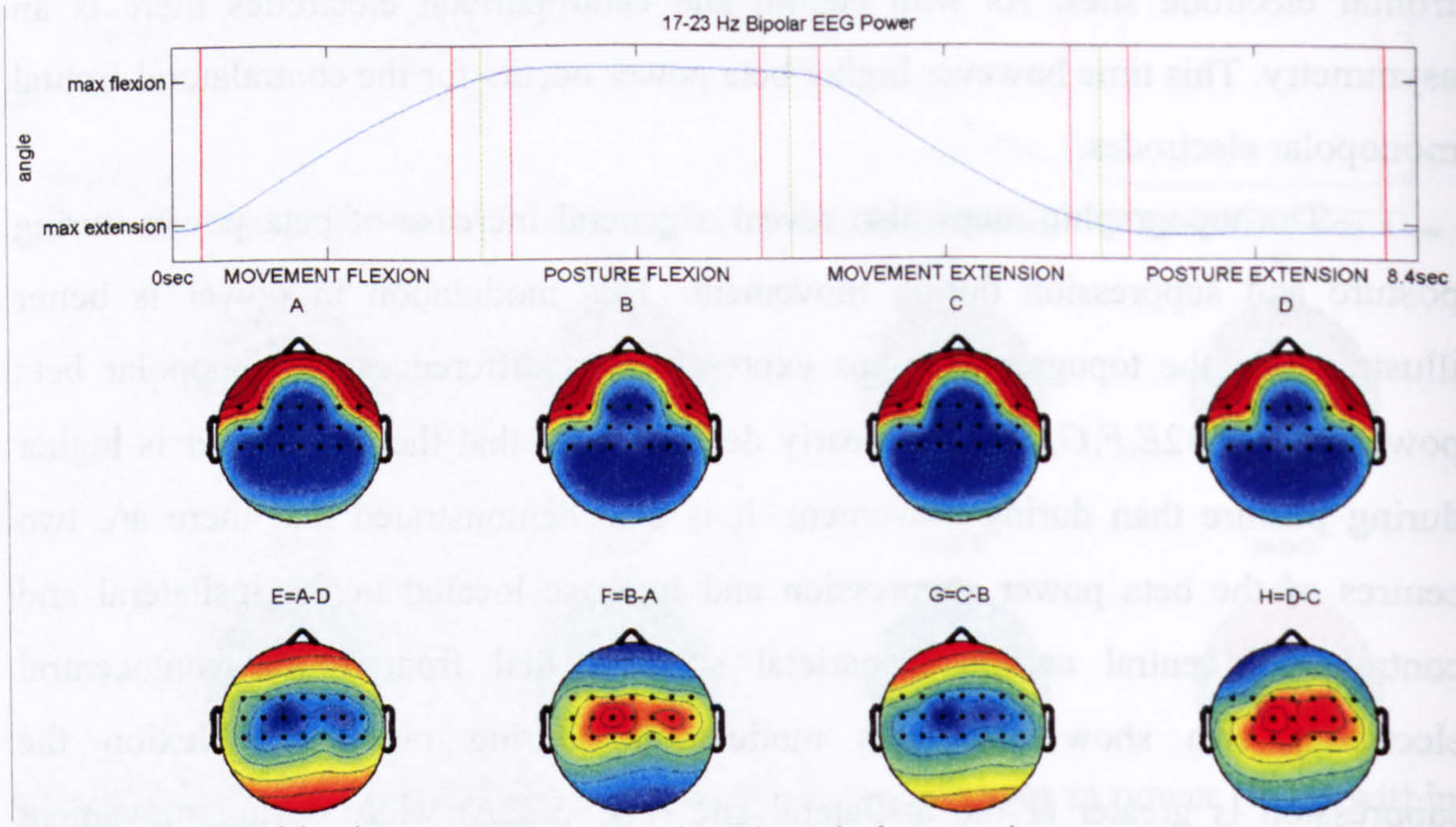

Fig. 5.33 EEG bipolar spectral power (A-D) and changes in power (E-H) within 17-23Hz band visualised as topographic maps of a scalp data field in a 2-D circular view using interpolation on a fine cartesian grid. The positions of the electrodes are indicated on the topographic maps. The maps present the spatial, task dependent characteristics for the 8-12Hz that changes are most likely to occur. Dark red represents the highest value while dark blue represents the lowest value. The top plot represents the wrist angle information derived by the goniometer demonstrating in a graphical way the movement phase that each map represents. The green vertical lines represent the audio cues while the interval between the red vertical lines represents the transition phases for which data was discarded. The difference maps are: E=A-D, F=B-A, G=C-B, H=D-C.

Fig. 5.33*A,B,C,D* show the distribution of the vertically aligned bipolar EEG channels for the 17-23 beta power during the move-hold sequence.

The corresponding power differences between consequent phases for the 17-23Hz beta band that appear in Fig. 5.33*E,F,G,H* show a similar spatial organisation. Two main centres of power suppression and recovery appear. Both overly the site that correspond to the motor cortex. The contralateral site show notably higher variation than the ipsilateral one. More specifically 17-23Hz beta band increases during posture flexion mainly over the contralateral motor cortex with smaller increase also occurring for the ipsilateral cortex. This activity is suppressed during extension movement to be re-established during posture extension. The centre of the beta power and corticomuscular coherence topographic features overlies the bipolar FC1-C1 electrode where the highest beta corticomuscular coherences occurred. This area corresponds to the contralateral primary moor cortex.

Both monopolar and bipolar topographic beta power maps show distinct changes between different phases. The most important is the general power increase during posture and its suppression during movement which also occurred for the alpha and beta band. There are small differences between the two posture phases as well as between the two movement phases for the monopolar map. For the equivalent alpha monopolar maps the differences were more noteworthy. The distribution of power change is well defined for the bipolar map. It would be possible to identify transition from movement to posture and vice versa by monitoring the increase or decrease of beta power over the FC1-C1 bipolar electrode even though it would not provide information on the nature (flexion or extension) of movement performed.

5.1.5 Summary of task dependent EEG power results.

In the last results session the pooled EEG power was examined in relation to the task performed during the move-hold sequence. That was achieved by means of two types of activity maps. The first type was a grid of two dimensional spectral power plots for the examined 0-50Hz power spectrum. The position of the plots in the grid corresponded to the relative position of the monopolar or bipolar electrode over the scalp. The second type contained spectral power and changes in power within the 8-12Hz and 17-23Hz bands where statisticaly significant task dependent changes appeared in the previous maps. The information was visualised as topographic maps of a scalp data field in a 2-D circular view using interpolation on a fine cartesian grid. Useful conclusions were made and include:

- The overall EEG spectral power was higher during posture than during movement for the whole examined spectrum (0-50Hz) with very few exemptions (mainly for a number of electrodes in the high beta and gamma bands).
- Considerable and statistically significant change features appeared in theta, delta, alpha, beta and gamma bands for both monopolar and bipolar maps. Particularly strong and well defined were features in changes of alpha and beta bands (8-12Hz and 17-23Hz)
- One of most well defined maps represented the changes in the topographic monopolar 8-12Hz map of spectral power differences which gave information about the transition from movement to posture as well as the flexion or extension type of action. 8-12Hz increased during posture following the general rise in activity.
- The topographic map representing the changes in bipolar EEG within the 17-23Hz band between phases was the most consistent in the distribution of power changes between phases. The highest variability was concentrated over the FC1-C1 electrode overlying the forearm related motor cortex site. However little information was present regarding the extension or flexion nature of movement.
- In general monopolar and bipolar EEG power appeared to contain task dependent information indicating movement or posture.

5.1.6 Corticomuscular coupling task dependent features.

In this section task dependent, corticomuscular coupling features are going to be presented. Pooled data from 9 subjects and 21 trials were examined during the four phases of the move-hold sequence (movement flexion, posture flexion, movement extension, posture extension). were pooled. The plots produced were monopolar corticomuscular maps, and bipolar corticomuscular maps. The maps were formed by plotting each estimate over the relative position of the corresponding EEG electrode. Individual corticomuscular plots containing strong coupling features are also presented and further analysed using the cumulant components analysis.

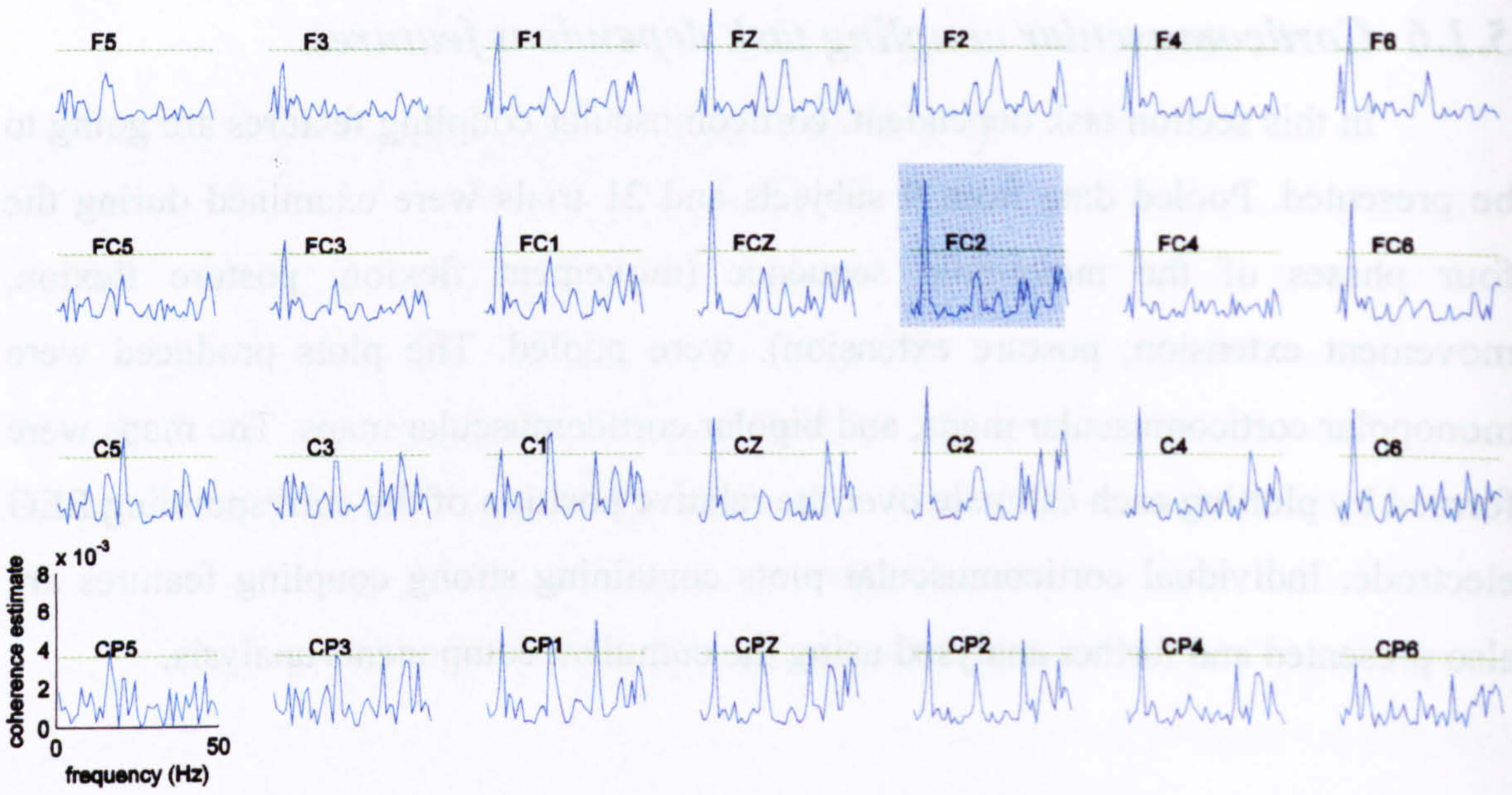

Fig. 5.34 Pooled coherence map of all subject data, between right wrist ECRL EMG and multiple monopolar EEG channels during flexion movement. The green horizontal line represents the 95% confidence interval.

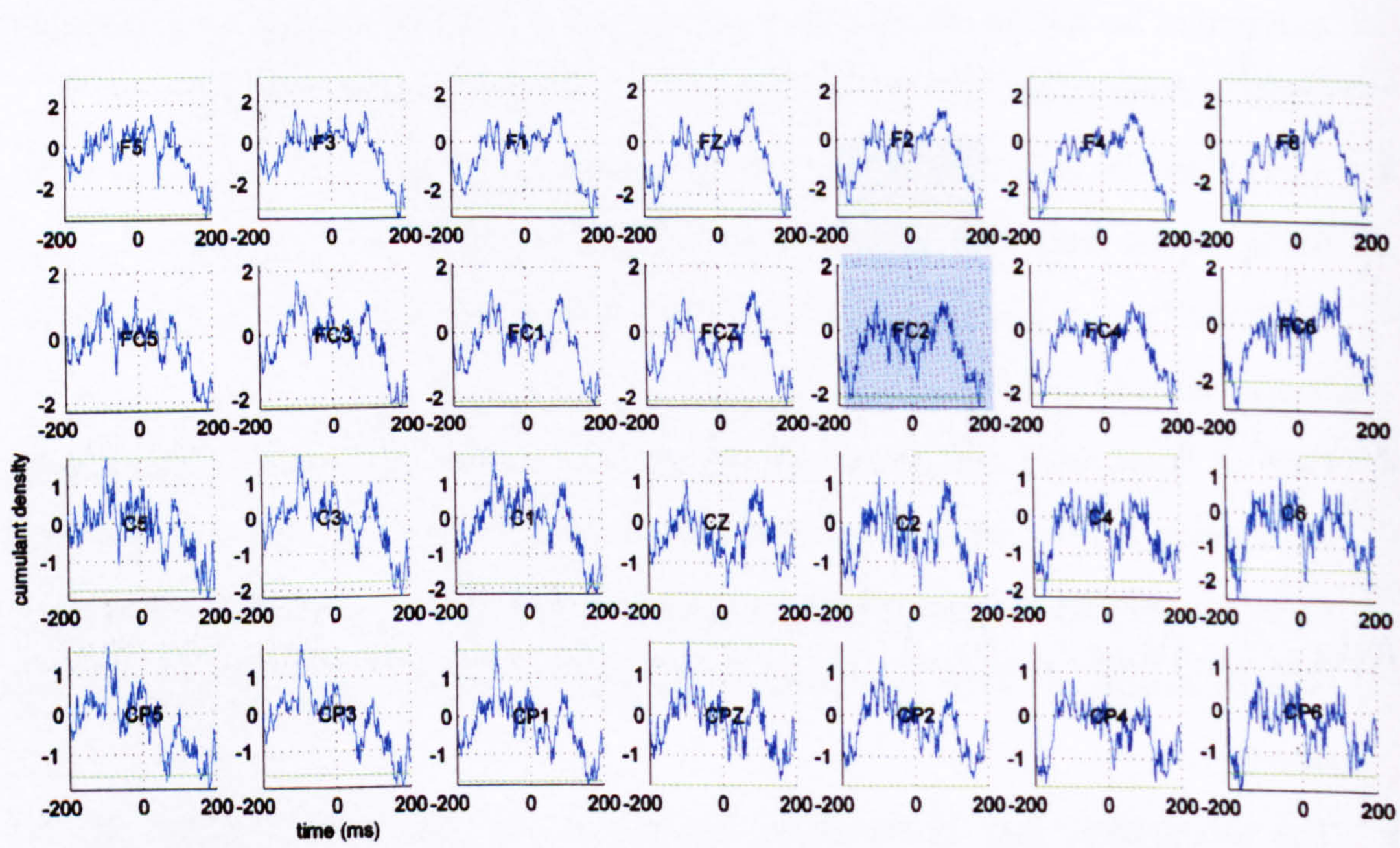

Fig. 5.35 Pooled cumulant map of all subject data, between right wrist ECRL EMG and multiple monopolar EEG channels during flexion movement. The green horizontal line represents the 95% confidence interval.

5.1.6.1 Flexion movement phase

5.1.6.1.1 ECRL coupling

Fig. 5.34 illustrates the pooled coherence estimates between the ECRL EMG and monopolar EEG recordings. The signals were recoded during the wrist movement flexion phase of the move-hold sequence task. The estimates are pooled across all subjects and trials. 6Hz corticomuscular coherence peaks can be observed over a large area, especially in the electrodes overlying medial and ipsilateral frontocentral area. The maximum coupling appears at FC2 (Fig. 5.34). Beta (21Hz) and gamma (35Hz) coherence features appear in the centroparietal row of electrodes but it is weak and not consistent for a large number of electrodes like the 6Hz feature.

The cumulant densities for ECRL EMG with the monopolar EEG channels during movement flexion (Fig. 5.35) show coupling in the 6Hz band with a similar spatial organisation to the corresponding coherence map (Fig. 5.34). Although no peaks exceed the confidence limits, the consistent shape of the cumulant plots across a widespread area, as well as the widespread 6Hz coherence appearing in the corresponding monopolar coherence map in Fig. 5.34, indicate a possible functional feature in the cumulant.

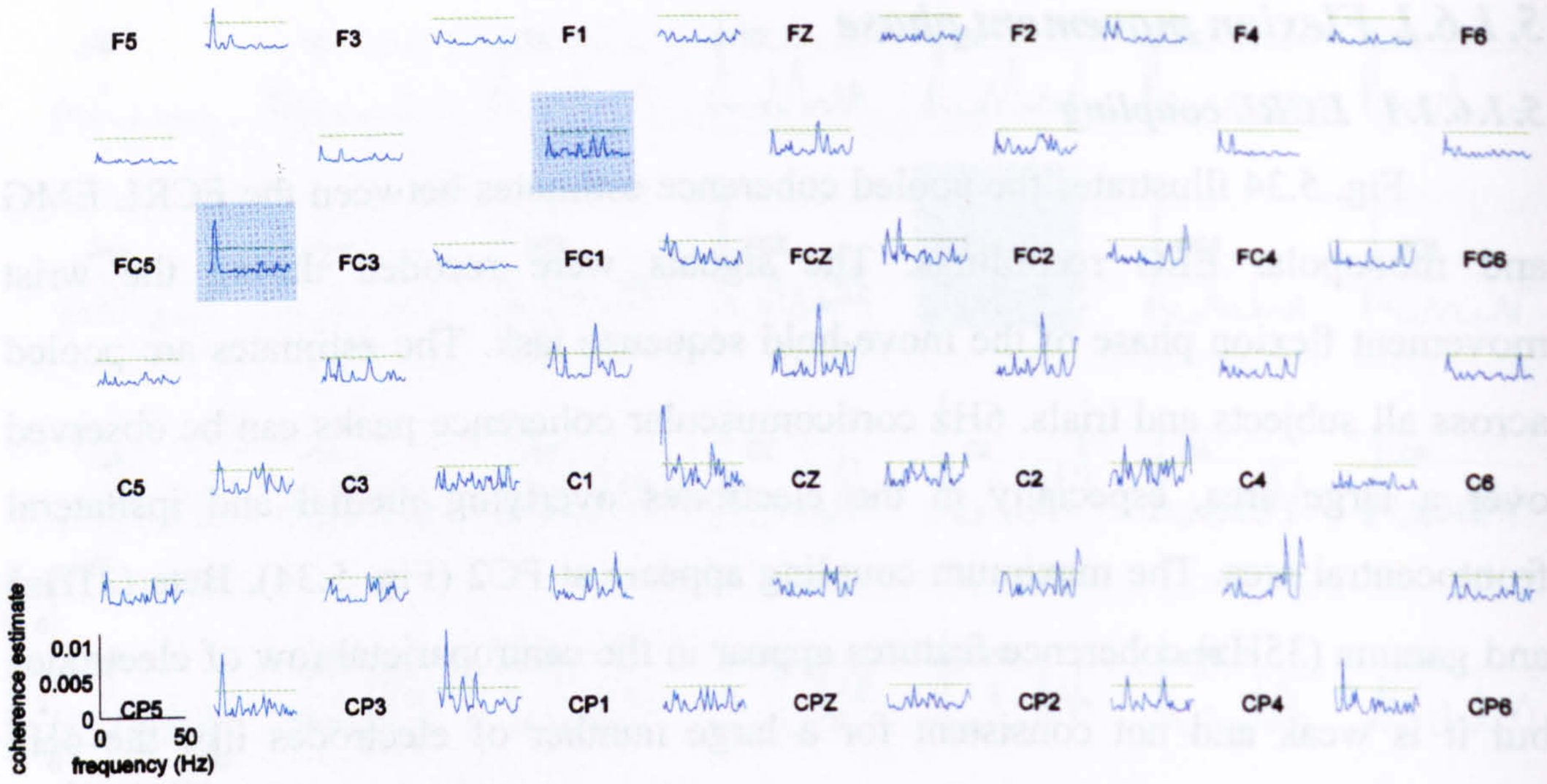

Fig. 5.36 Pooled coherence map of all subject data, between right wrist ECRL EMG and multiple bipolar EEG channels during flexion movement. The labels represent the relative position of the electrodes over the head. Coherence estimate between EMG and a bipolar EEG channel, product of two vertically or horizontally aligned monopolar ones, is plotted between the labels of the two monopolar EEG electrodes. The green horizontal line represents the 95% confidence interval.

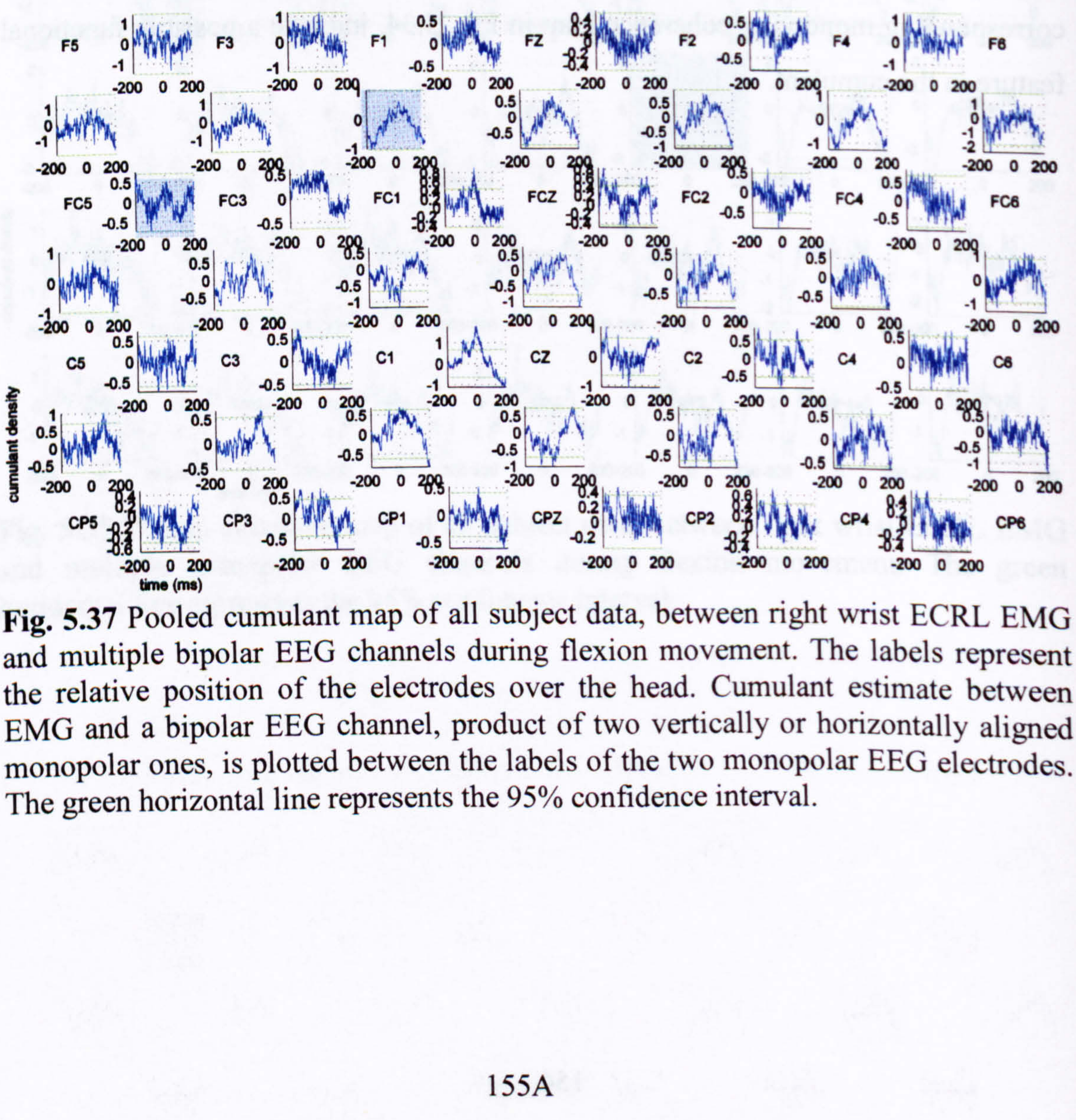

Fig. 5.37 Pooled cumulant map of all subject data, between right wrist ECRL EMG and multiple bipolar EEG channels during flexion movement. The labels represent the relative position of the electrodes over the head. Cumulant estimate between EMG and a bipolar EEG channel, product of two vertically or horizontally aligned monopolar ones, is plotted between the labels of the two monopolar EEG electrodes. The green horizontal line represents the 95% confidence interval.

Fig. 5.36 shows the coherence estimate plots between ECRL muscle and multiple bipolar EEG channels during wrist movement flexion. The bipolar EEG channels contain more localised cortical activity than the monopolar channels. The distribution of the coupling features does not resemble the monopolar map in Fig. 5.34. Local 6Hz features occur in both hemispheres, and especially contralaterally. The 6Hz coupling appears almost exclusively for bipolar electrodes of horizontal orientation (e.g. Fig. 5.36*a*). It is especially strong for CP5-CP3, CP3-CP1, CP4-CP6 and FC5-FC3 electrodes. "High beta" (28Hz) and gamma coupling, medially located in central and frontocentral areas can also be observed. The beta band feature comes in the shape of a narrow peak, which is stronger for vertically aligned bipolar electrodes, and is especially clear between the frontocentral and central row of electrodes, FC1-C1, FCZ-CZ and FC2-C2.

The movement flexion cumulant map between ECRL EMG and bipolar EEG (Fig. 5.37) does not reveal any strong or widespread coupling features. However some of the electrodes showing 6Hz coherence (e.g. FC5-FC3 and CP3-CP1) contain a rather consistent cumulant plot containing weak coupling at approximately 6Hz. In contrast weak 10Hz cumulant content appears for a few horizontal electrodes, mainly CP2 and CP4, while this coupling frequency is not obvious in the coherence map in Fig. 5.36. A 3Hz ECRL\EEG cumulant feature also spreadsaccross frontal-frontocentral rows of electrodes.

Fig. 5.38*a,b* display individual plots from Fig. 5.34 and Fig. 5.35 respectively. It illustrates the ECRL\FC2 coherence (Fig. 5.38a) and corresponding cumulant plot as well as the 5-7Hz cumulant component (Fig. 5.38b) estimated for the band of frequencies where statisticaly significant coherence is seen. While the wideband (0-500Hz) cumulant illustrates 6Hz coherence (also indicated by the corresponding coherence feature) the estimate does not exceed the 95% confidence limits. However the 5-7Hz cumulant component feature appears statistically significant as it exceeds its individual narrower confidence limits (Fig. 5.38b). The coupling appears to be "out of phase". The cumulant indicates a delay of -10ms while the corresponding phase derives a similar delay of -9.0±9.0ms (not shown)

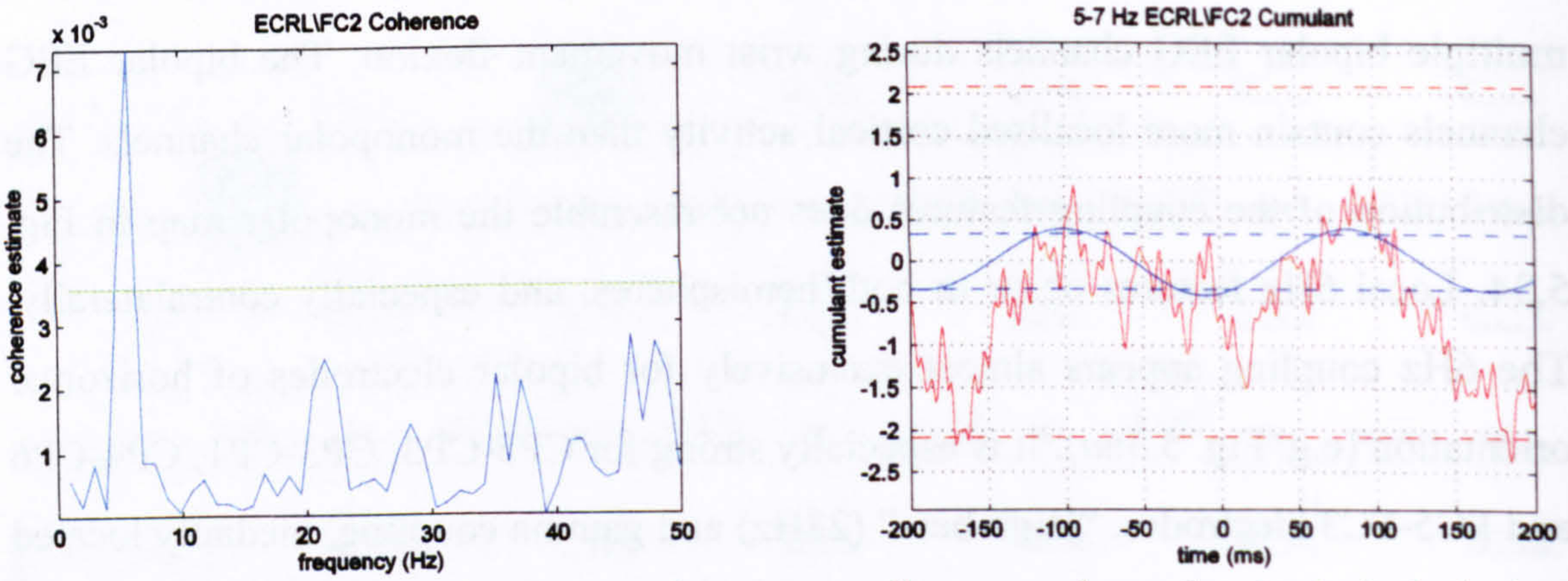

Fig. 5.38 ECRL\FC2 coherence and corresponding cumulant plot (red plot) during posture flexion. The blue plot represents the 5-7Hz cumulant component while the blue dashed lines represent the estimated upper and lower 95% confidence limits for the cumulant component.

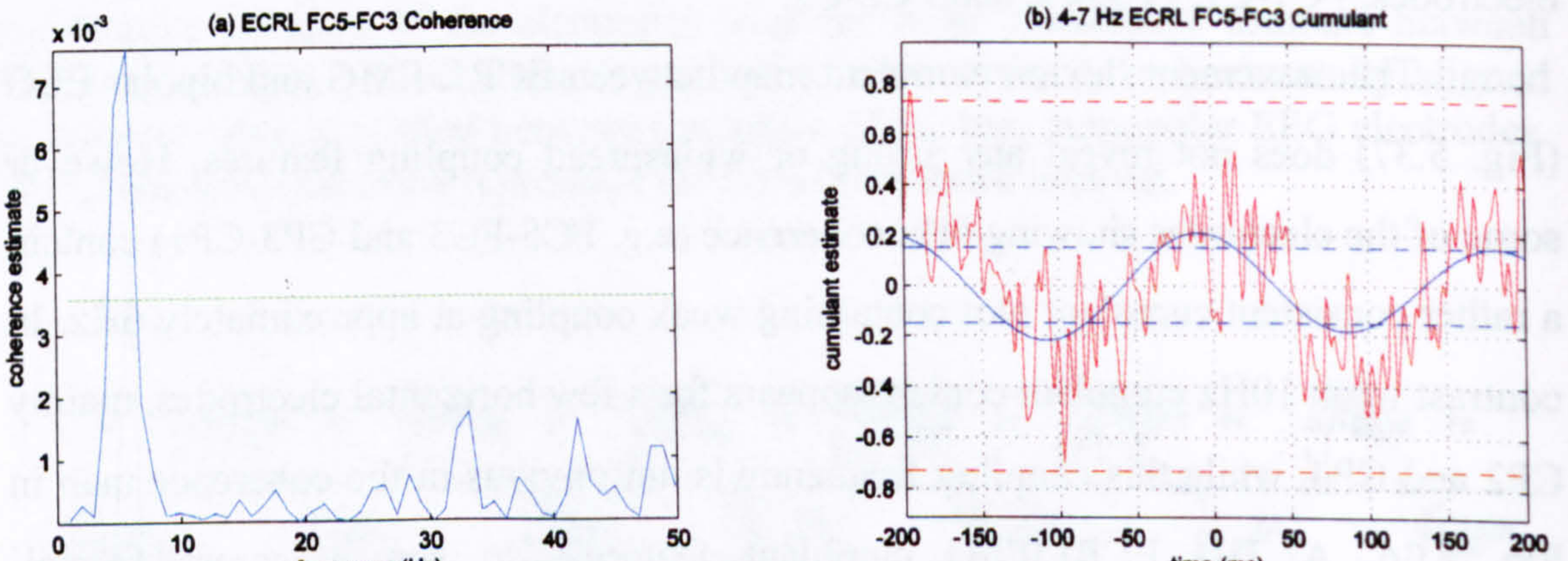

Fig. 5.39 ECRL\FC5-FC3 coherence and corresponding cumulant plot (red plot). The blue plot represents the main cumulant component for the frequency band that coherence is statistically significant while the blue dashed lines represent the estimated upper and lower 95% confidence limits for the cumulant component.

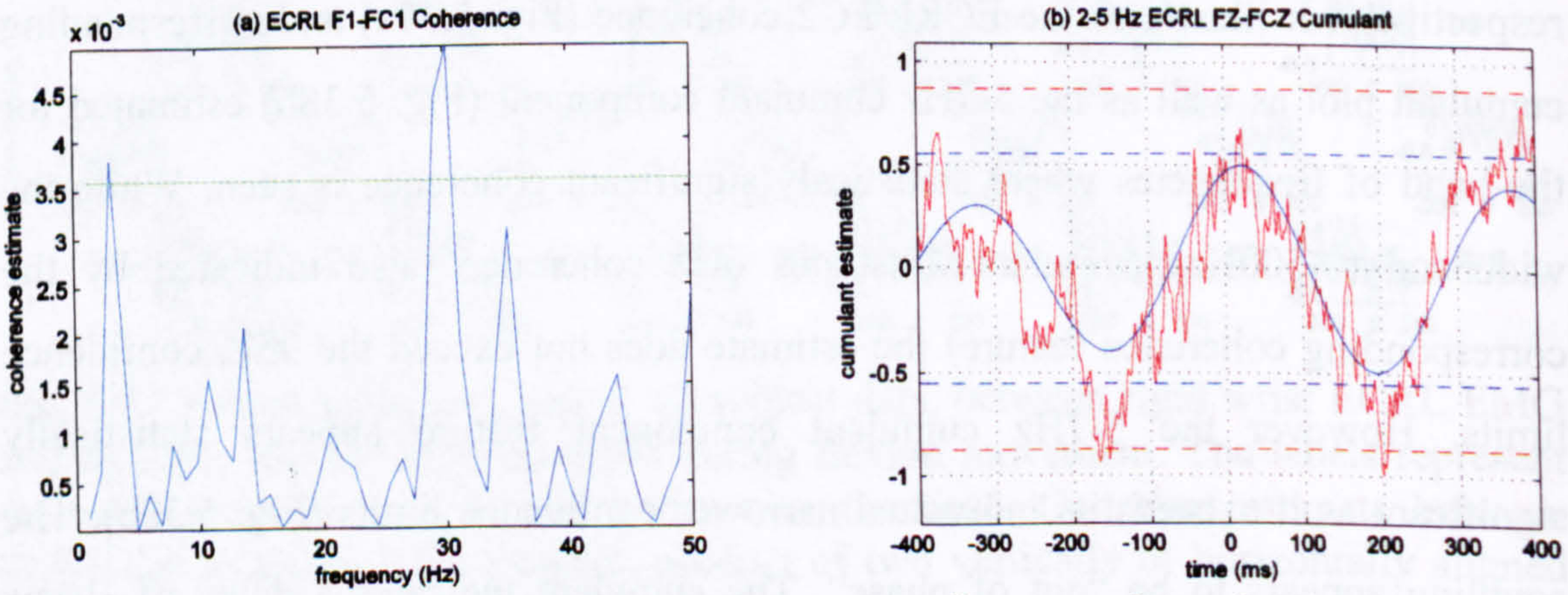

Fig. 5.40 ECRL\FZ-FCZ coherence and corresponding cumulant plot (red plot). The blue plot represents the main cumulant component for the frequency band that coherence is statistically significant while the blue dashed lines represent the estimated upper and lower 95% confidence limits for the cumulant component.

indicating that the EEG activity leads EMG by that margin (since EMG\EEG coupling is calculated, positive phase would mean that the EMG is leading the EEG).

Two individual plots from Fig. 5.36 and Fig. 5.37 are shown separately in Fig. 5.39*a,b* respectively. 4-7Hz cumulant features are evident (Fig. 5.39*a,b*) and demonstrating features similar to the monopolar corticomuscular frequency characteristics that appear in Fig. 5.38. The coherence peaks at 6Hz and the delay derived by the 4-7Hz cumulant appears to be -10ms while the corresponding phase estimate derives -8.5±24.1ms. These values are similar to the ones derived by the monopolar plot (-10ms, phase:-9.0±9.0ms). The synchronisation appears to be "in phase" while for the ECRL\FC2 pair the coupling was "out of phase". This is not an important difference since it is a matter of the orientation of the bipolar electrode. If the bipolar electrode pair (FC5-FC3) was inverted (FC3-FC5), "out of phase" synchronisation would have occurred instead. It is important to mention that while the 6Hz coupling feature is strong and shows a clear spatial organisation in the monopolar coherence and cumulant maps (Fig. 5.34, Fig. 5.35) this is not the case for the corresponding bipolar maps (Fig. 5.36, Fig. 5.37) where the features appear for a smaller number of electrodes with no clear spatial organisation.

Fig. 5.40 illustrates ECRL\FZ-FCZ coherence, the corresponding wideband cumulant plot and the 2Hz-5Hz cumulant component. While the 3Hz coherence feature is just over the significance level (Fig. 5.40*a*), the corresponding 2Hz-5Hz cumulant component does not exceed the confidence limits. However the profile of the cumulant plot is very similar for ECRL\EEG corticomuscular coherence across F5-FC5, F3-FC3, F1-FC1, FZ-FCZ, F2-FC2, F4-FC4 and F6-FC6 bipolar electrodes. The similar cumulant profile may suggest that this is a feature with functional significance. This could be the case for a number of subjects and not characterise the general population.

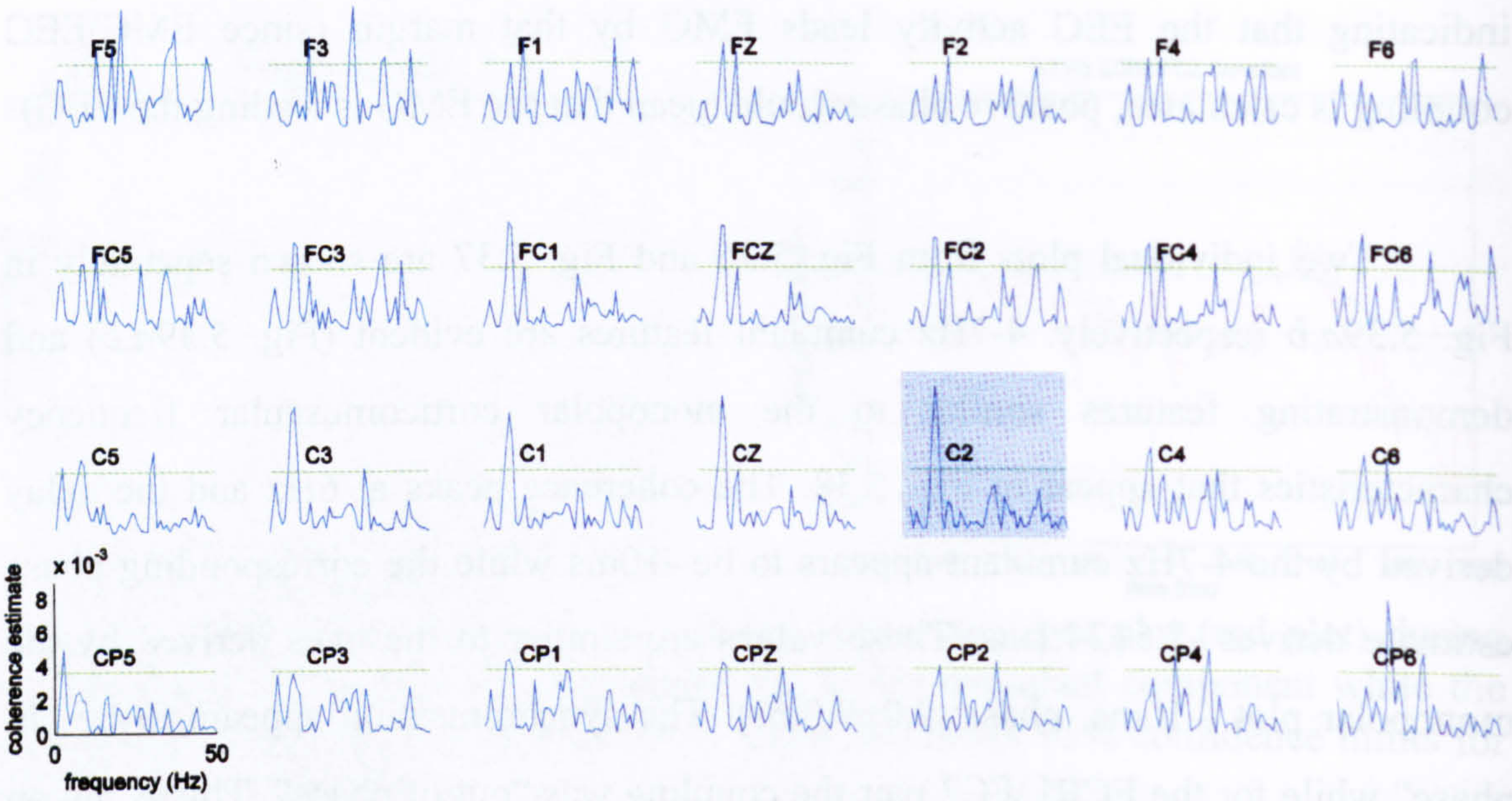

Fig. 5.41 Pooled coherence map of all subject data, between right wrist FCR EMG and multiple monopolar EEG channels during flexion movement. The green horizontal line represents the 95% confidence interval.

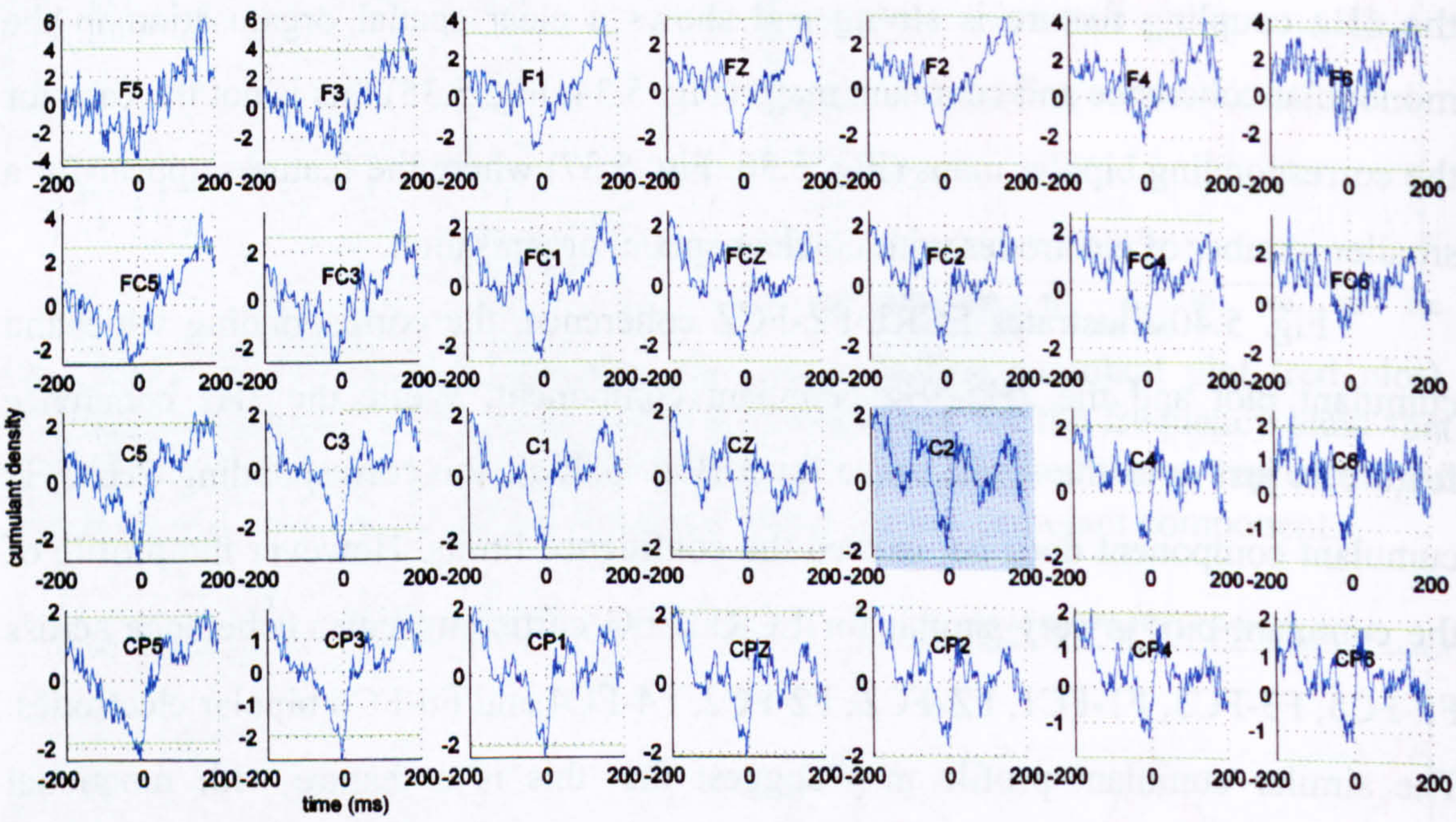

Fig. 5.42 Pooled cumulant map of all subject data, between right wrist FCR EMG and multiple monopolar EEG channels during flexion movement. The green horizontal line represents the 95% confidence interval

5.1.6.1.2 FCR coupling

Fig. 5.41 shows the coherence estimate plots between FCR muscle and multiple monopolar EEG channels during movement flexion. Alpha coupling features with a peak at 9Hz are evident over most of the cortical area. This is especially high in medial and contralateral areas with a maximum at electrode C2. Beta coupling appears in contralateral frontal and ipsilateral centroparietal areas but it is relatively weak.

The corresponding monopolar cumulant map for the same muscle in Fig. 5.42 shows coupling features just over the statistical significance level. These are connected with the 9Hz coupling appearing in the monopolar coherence map in Fig. 5.41.

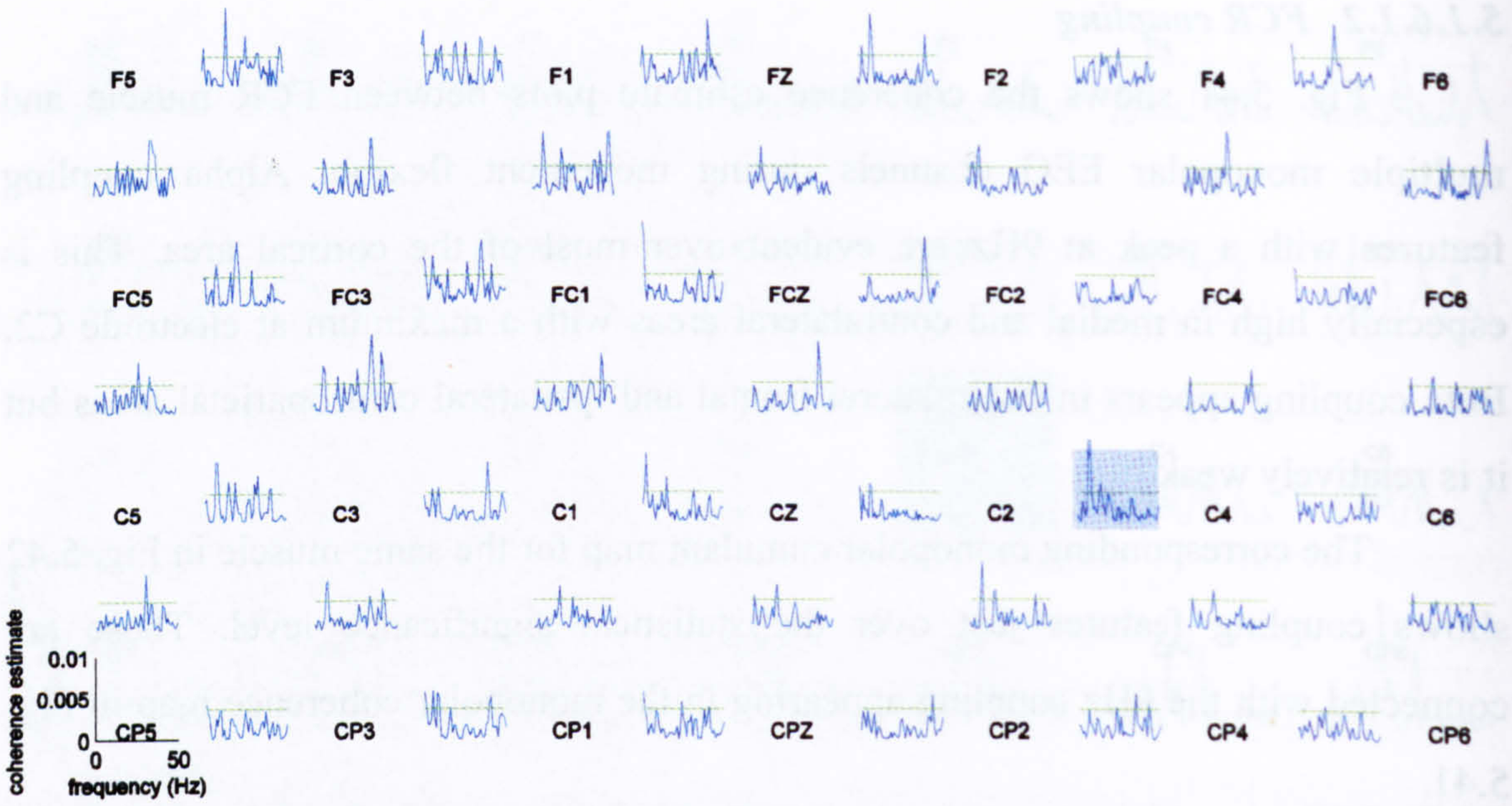

Fig. 5.43 Pooled coherence map of all subject data, between right wrist FCR EMG and multiple bipolar EEG channels during flexion movement. The labels represent the relative position of the electrodes over the head. Coherence estimate between EMG and a bipolar EEG channel, product of two vertically or horizontally aligned monopolar ones, is plotted between the labels of the two monopolar EEG electrodes. The green horizontal line represents the 95% confidence interval.

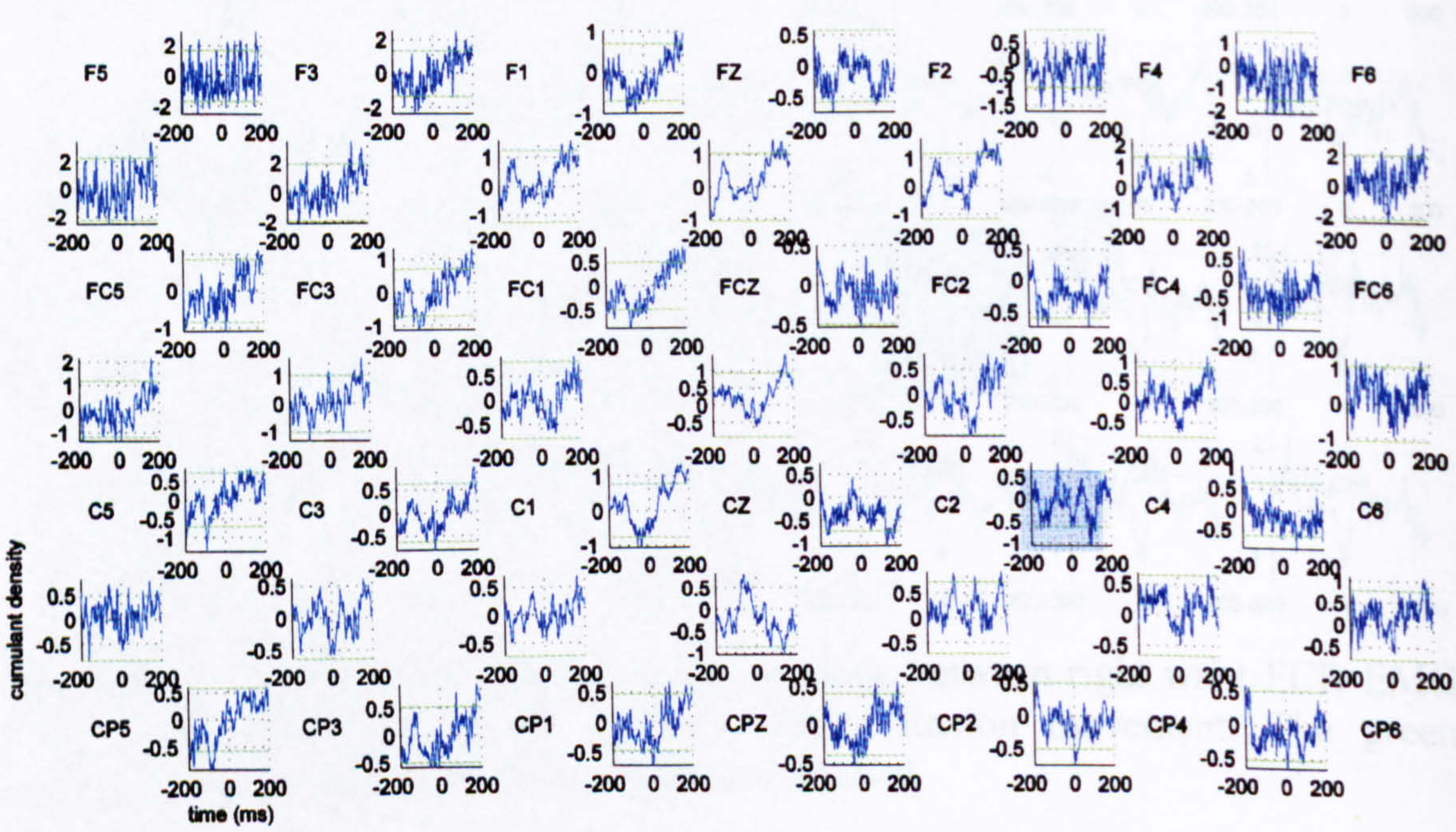

Fig. 5.44 Pooled cumulant map of all subject data, between right wrist FCR EMG and multiple bipolar EEG channels during flexion movement. The labels represent the relative position of the electrodes over the head. Cumulant estimate between EMG and a bipolar EEG channel, product of two vertically or horizontally aligned monopolar ones, is plotted between the labels of the two monopolar EEG electrodes. The green horizontal line represents the 95% confidence interval.

Fig. 5.43 shows the coherence estimate map between FCR muscle and multiple bipolar EEG channels during the movement flexion phase. It contains a plethora of coherence peaks for the whole frequency range. Narrow 9Hz peaks are the most common features. Features at the same frequency were also observed in the corresponding monopolar map (Fig. 5.41). Unlike the monopolar case, the distribution of the bipolar 9Hz coupling features do not have any obvious organisation. Well defined 28Hz coherence features appear for F4-F6 and F4-FC4 electrodes and increased gamma activity also occurs over the contralateral frontocentral area. The cumulant map (Fig. 5.44) reveals weak coupling features connected to the corresponding coherence map. C2-CP2 and C2-C4 for example show alpha coupling while F4-FC4 and F4-F6 show beta coupling.

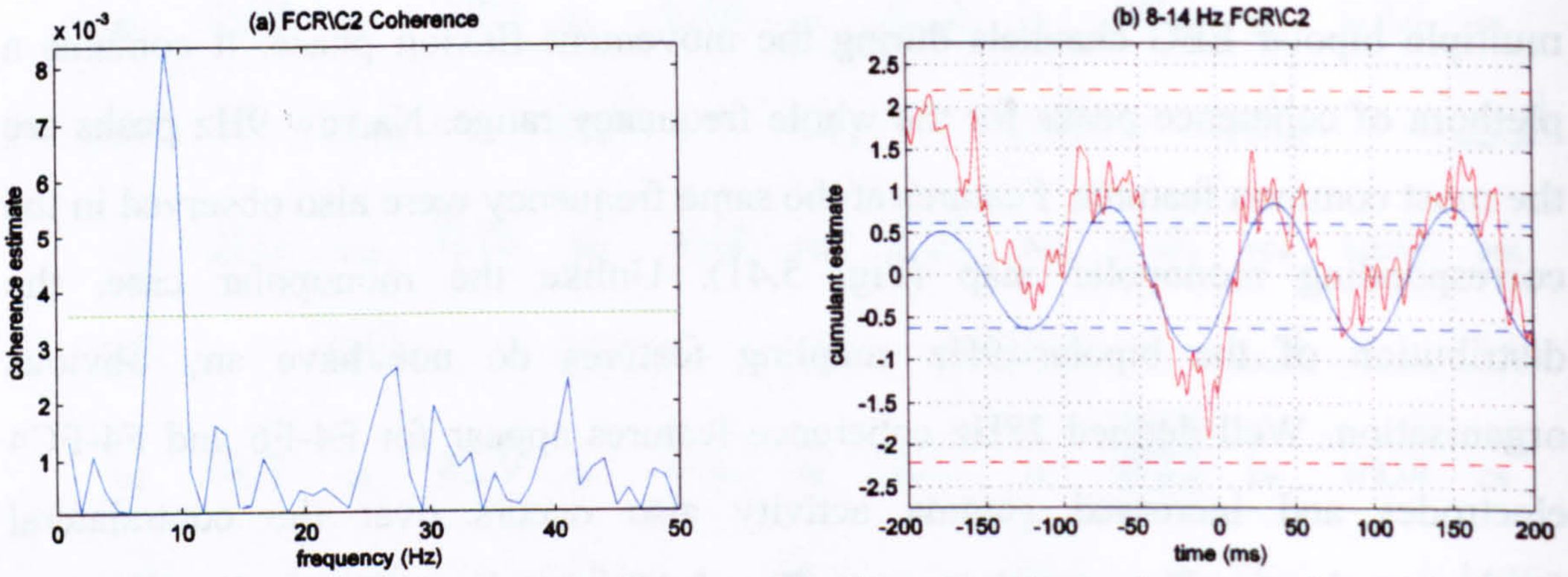

Fig. 5.45 FCR\FC2 coherence and corresponding cumulant plot (red plot). The blue plot represents the main cumulant component for the frequency band that coherence is statistically significant, while the blue dashed lines represent the estimated upper and lower 95% confidence limits for the cumulant component.

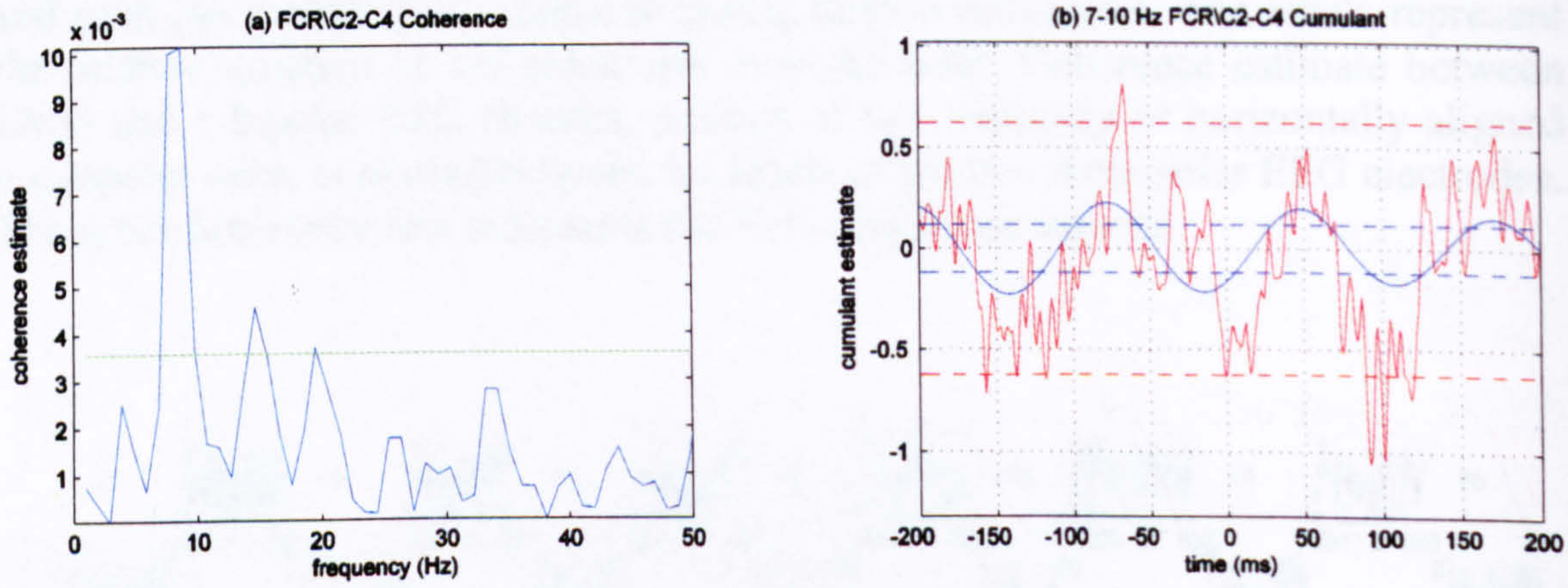

Fig. 5.46 FCR\C2-C4 coherence and corresponding cumulant plot (red plot). The blue plot represents the 7-10Hz cumulant component, while the blue dashed lines represent the estimated upper and lower 95% confidence limits for the cumulant component.

Fig. 5.45 contains the movement flexion FCR\FC2 monopolar coherence and cumulant plots highlighted in Fig. 5.41 and Fig. 5.42 respectively. It also contains the 8-12Hz cumulant component for the frequency band within which coupling is statistically significant. The synchronisation appears to be "out of phase" with the C2 leading FCR signal by 16ms (-16ms delay). The corresponding phase derives a very similar delay of -15.1±9.7ms (not shown).

The monopolar coupling feature for ECRL\FC2 displayed in Fig. 5.38 showed some similarities and differences to the corresponding FCR\FC2 features shown in Fig. 5.45. Both show "out of phase" synchronisation; however the ECRL\FC2 feature appears at the lower frequency of 6Hz while FCR\FC2 feature appears at 9 Hz. The EEG\EMG delay for FCR is in the 15ms range while the corresponding delay for ECRL the delay is in the range of 10ms.

Fig. 5.46 illustrates the FCR\C2-C4 coherence plot, cumulant and the 7-10Hz cumulant component. Fig. 5.45 shows the FCR\C2 monopolar feature that occurs in a similar frequency range. FCR\C2-C4 delay is -15ms (-14.0±15.2ms as given by the phase estimate, which is not shown), similar to the corresponding monopolar feature FCR\C2 in Fig. 5.45*b* (approximately -16ms). The monopolar feature appears in the monopolar map seen in Fig. 5.41 for a large number of electrodes with clear spatial organisation the corresponding while the 10Hz bipolar features appear for a few electrodes with no obvious organisation.

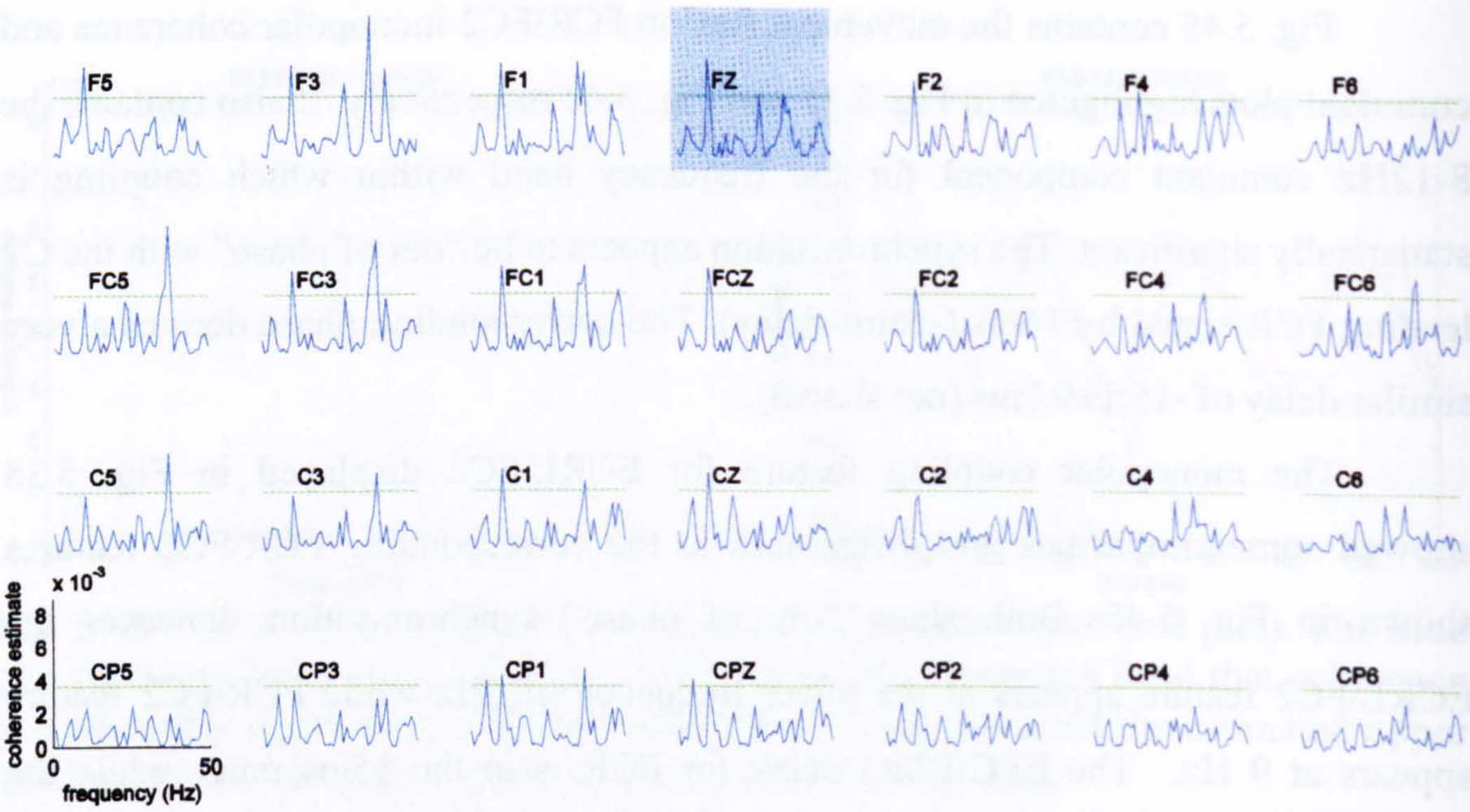

Fig. 5.47 Pooled coherence map of all subject data, between right BBLH EMG and multiple monopolar EEG channels during flexion movement. The green horizontal line represents the 95% confidence interval.

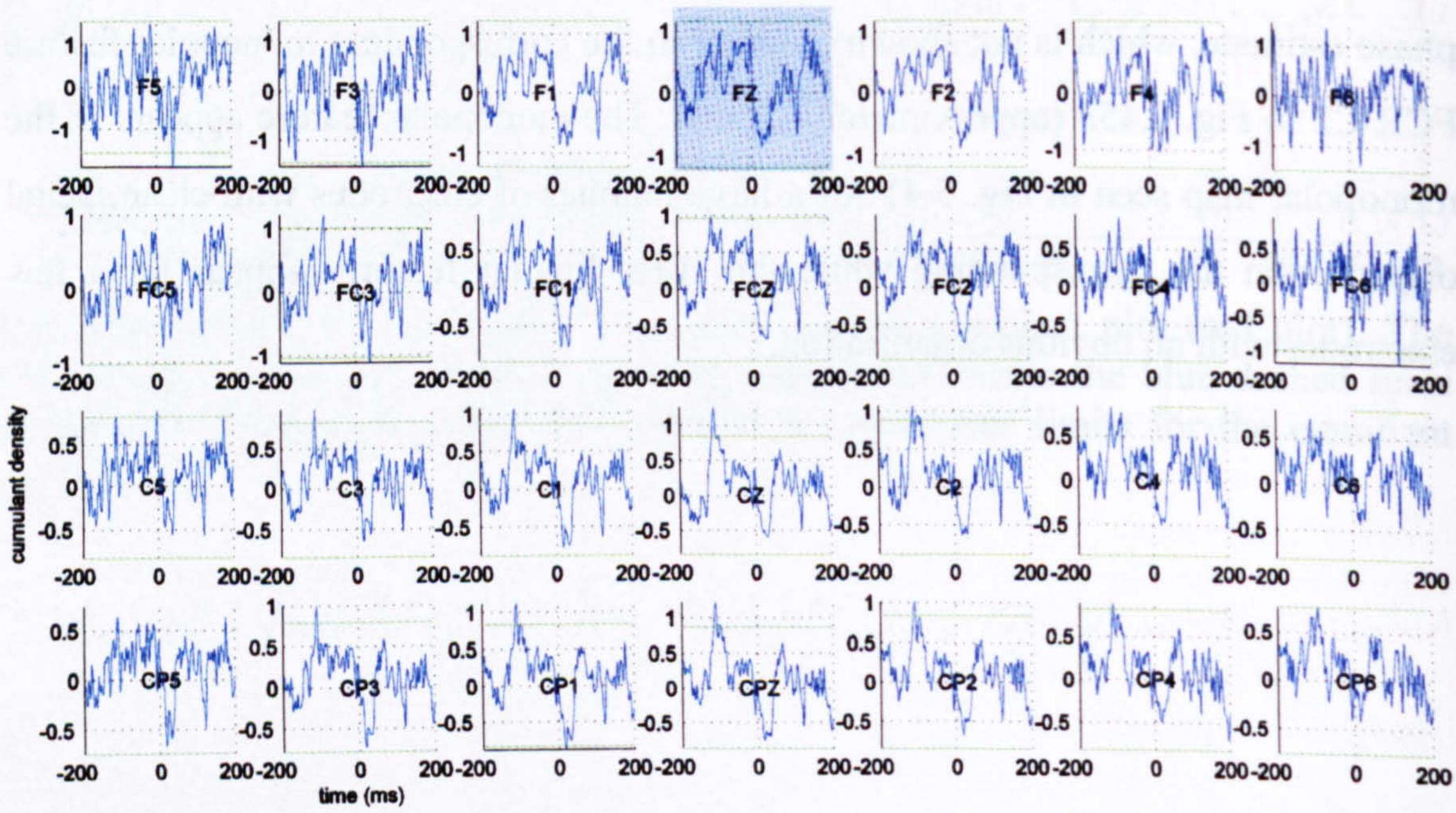

Fig. 5.48 Pooled cumulant map of all subject data, between right BBLH EMG and multiple monopolar EEG channels during flexion movement. The green horizontal line represents the 95% confidence interval

5.1.6.1.3 BBLH coupling

Fig. 5.47 shows the coherence estimate plots between BBLH muscle and the monopolar EEG channels during the movement flexion phase. The map contains small coherence features like alpha at 11Hz and gamma 35-38Hz present in contralateral frontal frontocentral and central electrodes. Alpha coupling is strongest for FZ electrode while gamma is strongest at the F3 electrode. The peaks are narrow. The contralateral hemisphere and centroparietal area show very little statistically significant coherence.

The corresponding monopolar cumulant map in Fig. 5.48 does not have clear connection with the coherence map most probably because of the fact that coherence features are narrow and not particularly strong. A large number of electrodes appear to contain a consistent trough most probably connected with the weak alpha coherence feature. The trough is more obvious for medially located electrodes.

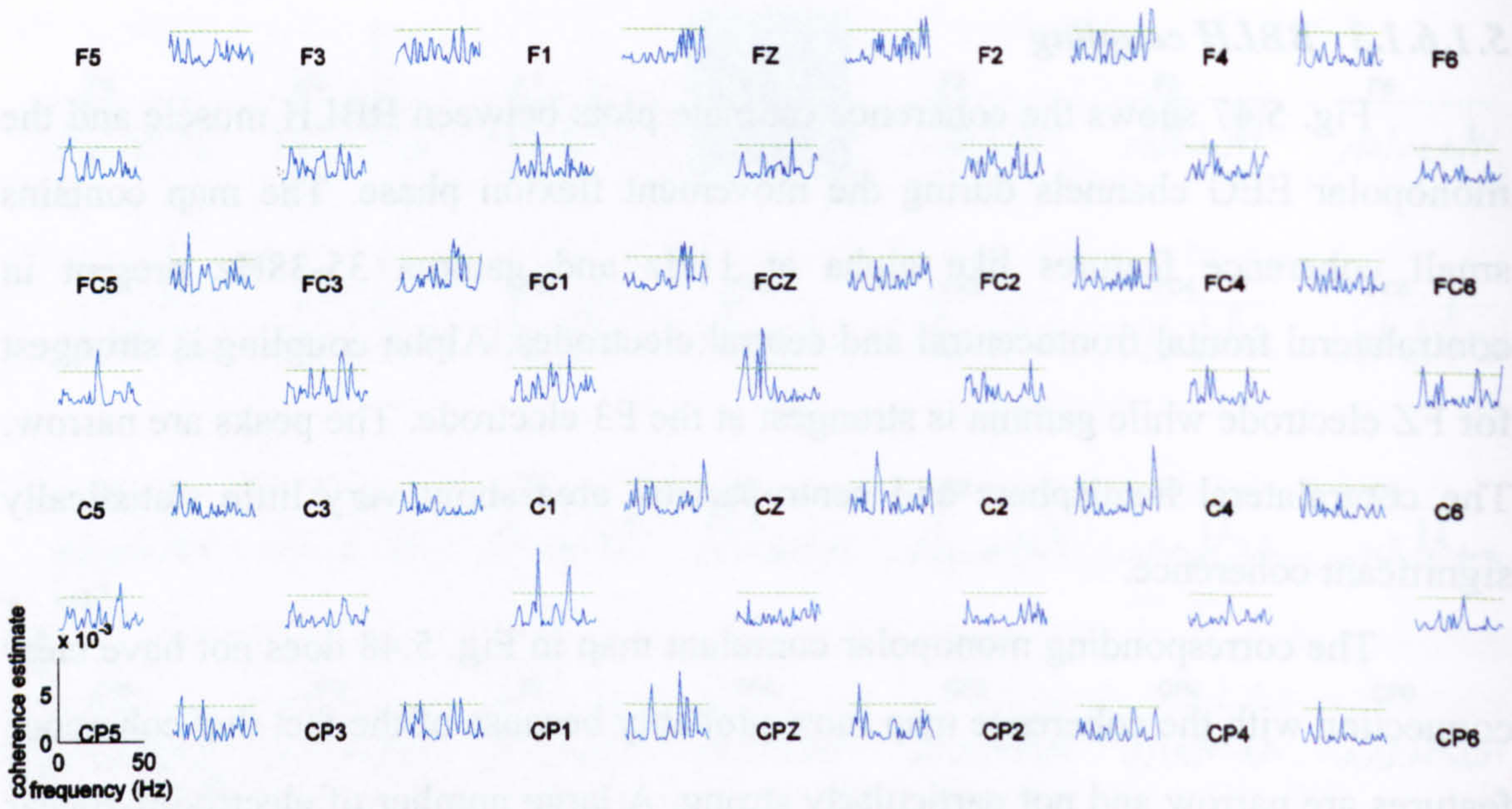

Fig. 5.49 Pooled coherence map of all subject data, between right BBLH EMG and multiple bipolar EEG channels during flexion movement. The labels represent the relative position of the electrodes over the head. Coherence estimate between EMG and a bipolar EEG channel, product of two vertically or horizontally aligned monopolar ones, is plotted between the labels of the two monopolar EEG electrodes. The green horizontal line represents the 95% confidence interval.

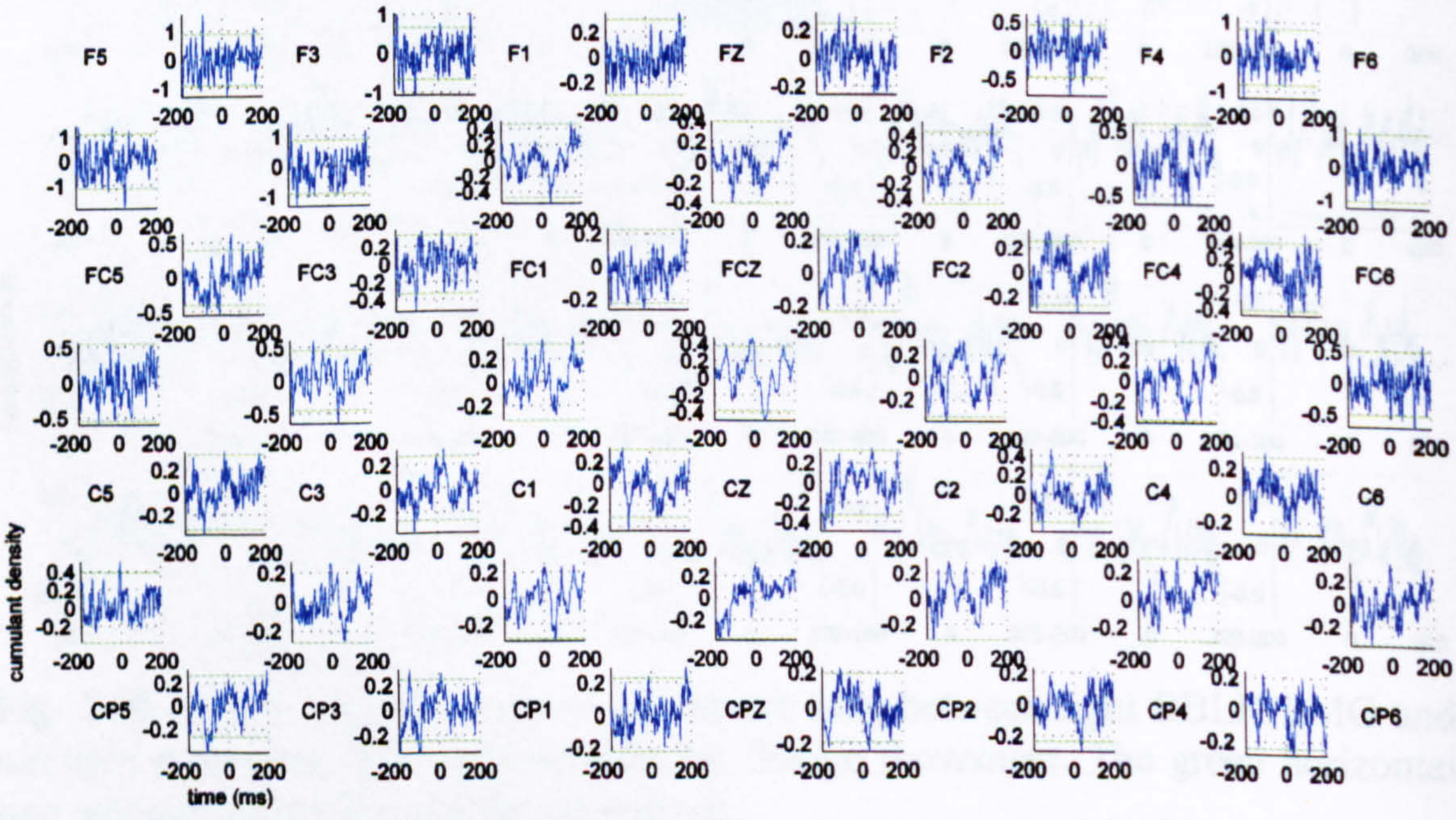

Fig. 5.50 Pooled cumulant map of all subject data, between right BBLH EMG and multiple bipolar EEG channels during flexion movement. The labels represent the relative position of the electrodes over the head. Cumulant estimate between EMG and a bipolar EEG channel, product of two vertically or horizontally aligned monopolar ones, is plotted between the labels of the two monopolar EEG electrodes. The green horizontal line represents the 95% confidence interval.

Fig. 5.49 shows the coherence estimate plots between BBLH muscle and multiple bipolar EEG channels during the movement flexion phase. BBLH acts to support the arm in a horizontal position so it would be expected the BBLH muscle to be strongly coupled with the contralateral cortex. As illustrated in the bipolar map strong beta coherence in the contralateral cortex is not present. Coherences are quite small and and with no clear spatial organisation. Fig. 5.50 illustrates the cumulant map that corresponds to the coherence map in Fig. 5.49. There is a variety of cumulant profiles which correspond to the small coherence features. However these are not statistically significant or with any sort of spatial organisation.

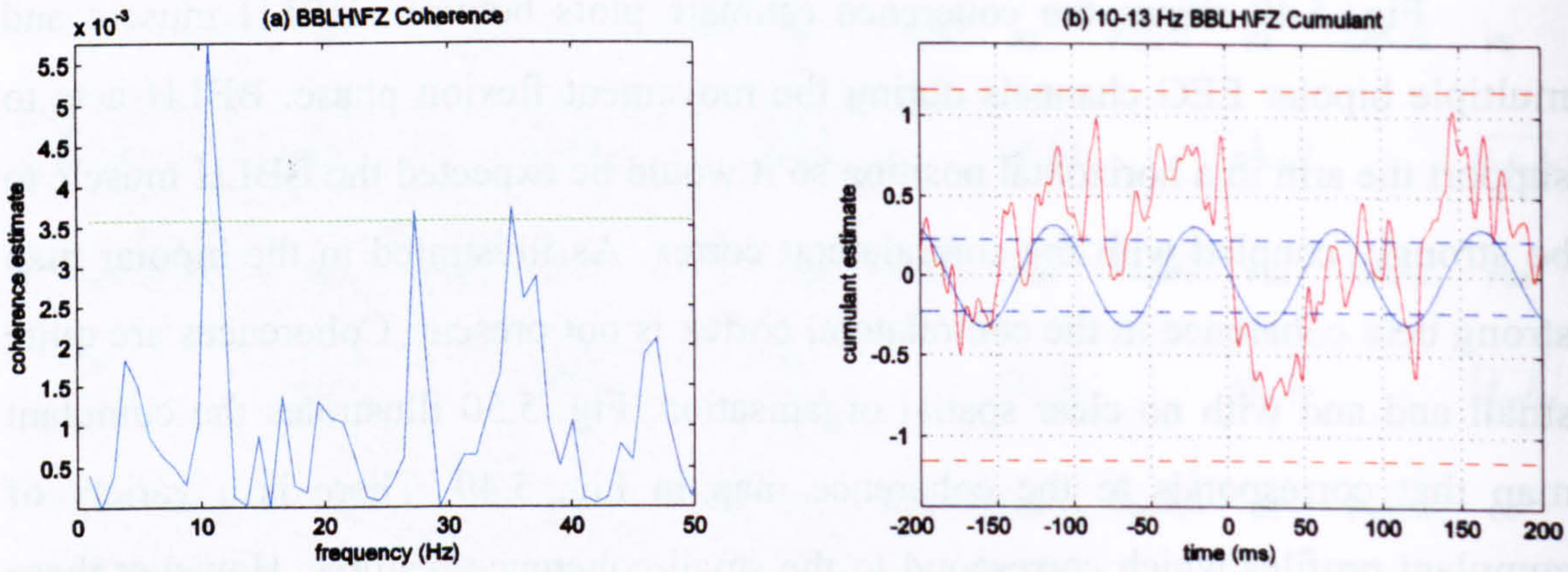

Fig. 5.51 BBLH\FZ coherence and corresponding cumulant plot (red plot). The blue plot represents the 10-13Hz cumulant component while the blue dashed lines represent the estimated upper and lower 95% confidence limits for the cumulant component

Fig. 5.51 contains the BBLH\Fz monopolar coherence and cumulants from Fig. 5.47 and Fig. 5.48 respectively. It also contains the 10-13Hz cumulant component identified from the coherence plot. The synchronisation within this band appears to be "in of phase" with the Fz leading BBLH signal. The cumulant suggests a -20ms delay. The corresponding phase derives -21.9±3.4ms (not shown).

Even though BBLH acts on elbow joint, movement around the wrist joint appears to suppress the beta coupling that is present during posture flexion (see Fig. 5.68). Intermuscular coherence plots showed that very little beta coupling was present in the ECRL\BBLH and FCR\BBLH coherences (Fig. 5.3*f,e*) compared with posture flexion (Fig. 5.8*f,e*), where all three muscles were involved in a posture task. The cortical origin of the beta band intermuscular coupling is suggested since suppression in corticomuscular coupling coincides with suppression of intermuscular coupling between FCR\ECRL and between FCR\BBLH (Fig. 5.3*d,e*).

Previous studies have reported suppression of intermuscular coherence, under similar conditions on synergistic muscles on the same joint (Mulcahy 2001). However it is now clear that suppression of corticomuscular coherence between a postural active muscle and the cortex can occur, even when a muscle in the same functional group is participating in movement acting on a different joint. Because of the fact that the forearm is not externally supported but is held only by the action of the BBLH muscle, it is possible that subtle movement of the arm could contribute to the observed suppression of the beta corticomuscular coherence. However, there are strong indications that this is not the case. As will be demonstrated later (Fig. 5.141, Fig. 5.149), statisticaly significant beta corticomuscular coherence can emerge for the BBLH EMG during continuous wrist movement, which should show similar subtle movement effect of the elbow and BBLH as the intermittent wrist movement. This suggests that the lack of beta BBLH corticomuscular coupling observed in Fig. 5.49 has functional significance.

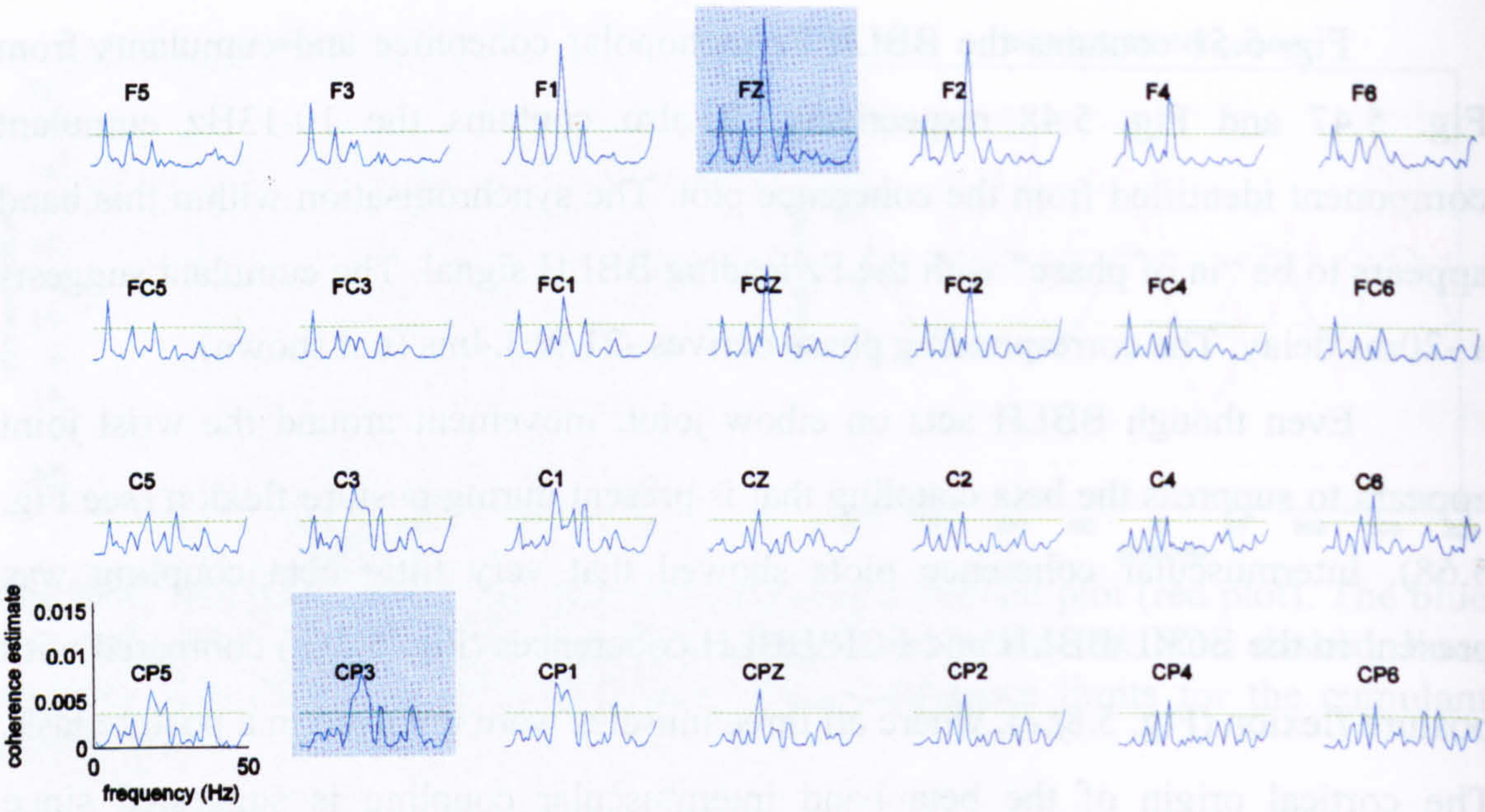

Fig. 5.52 Pooled coherence map of all subject data, between right wrist ECRL EMG and multiple monopolar EEG channels during flexion posture. The green horizontal line represents the 95% confidence interval.

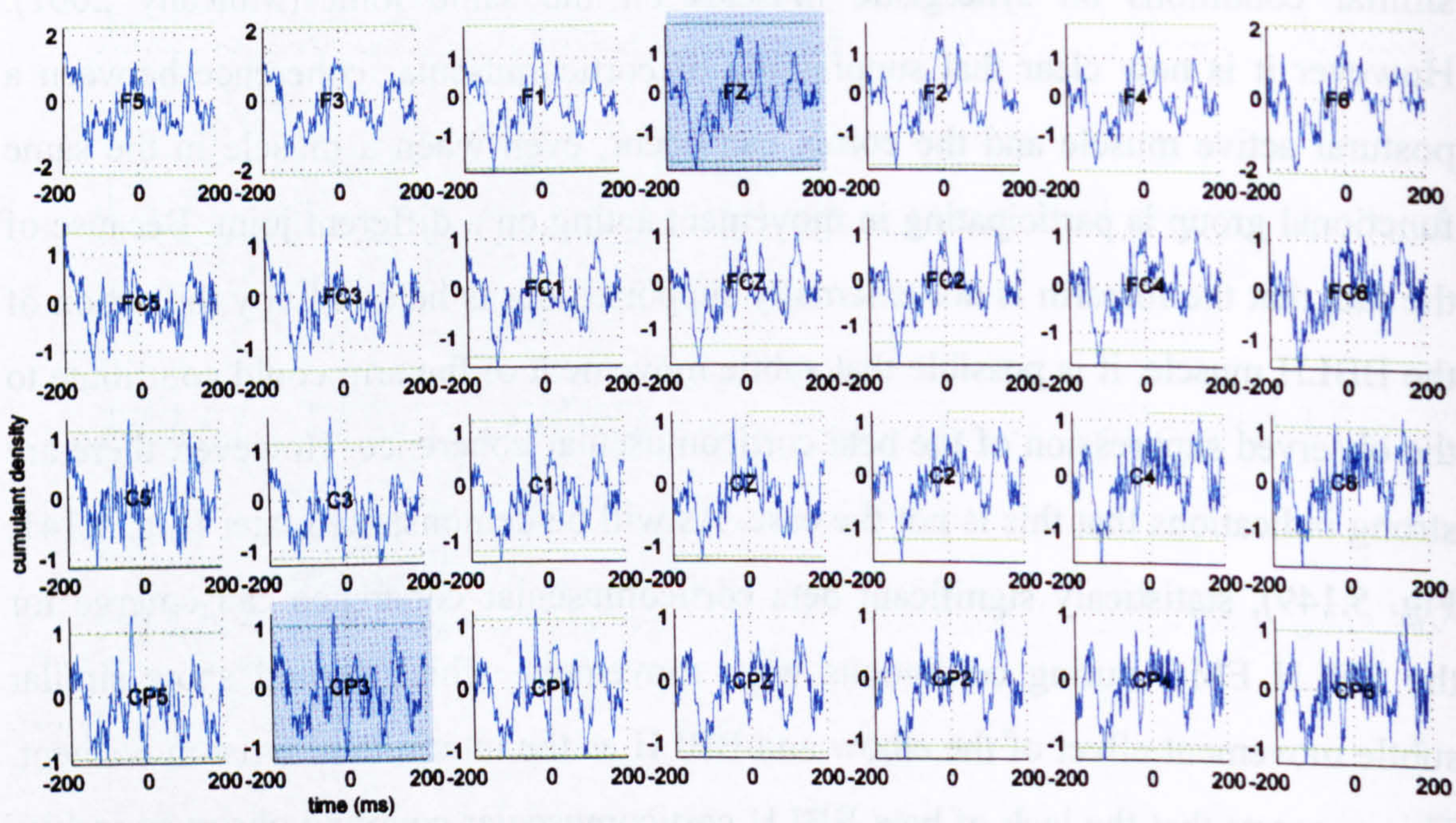

Fig. 5.53 Pooled cumulant map of all subject data, between right wrist ECRL EMG and multiple monopolar EEG channels during flexion posture. The green horizontal line represents the 95% confidence interval.

5.1.6.2 Flexion posture phase

5.1.6.2.1 ECRL coupling

Fig. 5.52 shows the coherence estimate map between ECRL muscle and multiple monopolar EEG channels during the wrist flexion hold phase. A large area of the monopolar map is coupled in the beta band with ECRL wrist antagonist. These areas are the medial frontal and frontocentral area (F1, FZ, F2, F4, FC1, FCz and FC2) and the contralateral central and centroparietal area (C3, C1, CP5, CP3, CP1 and CPz). Peaks in both areas reach maximums close to 21Hz with narrower and higher magnitude features emerging in the frontal cortex. The centroparietal coherences are wider with lower maximum. The highest coherence for the frontal cortex is observed for the Fz electrode while the centroparietal CP3 electrode gives the highest coherence value. The CP3 peak appears much broader than the Fz coherence peak. Other coupling features are a 6Hz peak in the frontal and frontocentral areas and a gamma peak at the contralateral centroparietal electrodes. A 6Hz coherence feature was present during flexion movement in ECRL but the features show different spatial distribution (Fig. 5.34).

Fig. 5.53 contains the monopolar ECRL\EEG cumulant map that corresponds to the coherence map in Fig. 5.52. It contains beta coupling features, connected to the strong beta coherence in the respective areas of the coherence map (frontocentral and contralateral central/centroparietal). As has already been mentioned, there are differences in the profile of the coherence plots in the two main areas where it occurs. This is also the case for the cumulant plots which appear different. These differences will be examined in detail in Fig. 5.57 and Fig. 5.58.

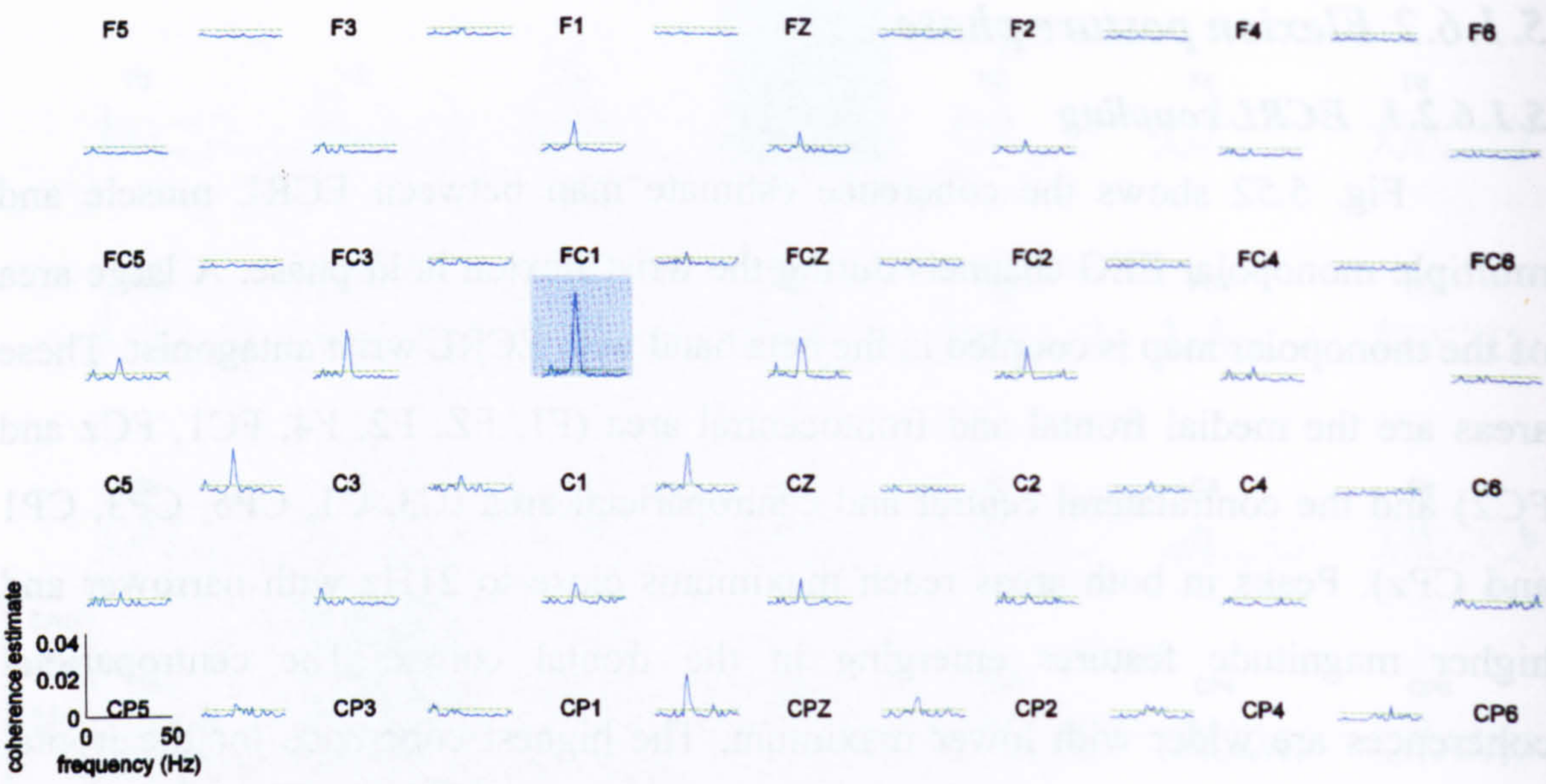

Fig. 5.54 Pooled coherence map of all subject data, between right wrist ECRL EMG and multiple bipolar EEG channels during flexion posture. The labels represent the relative position of the electrodes over the head. Coherence estimate between EMG and a bipolar EEG channel, product of two vertically or horizontally aligned monopolar ones, is plotted between the labels of the two monopolar EEG electrodes. The green horizontal line represents the 95% confidence interval.

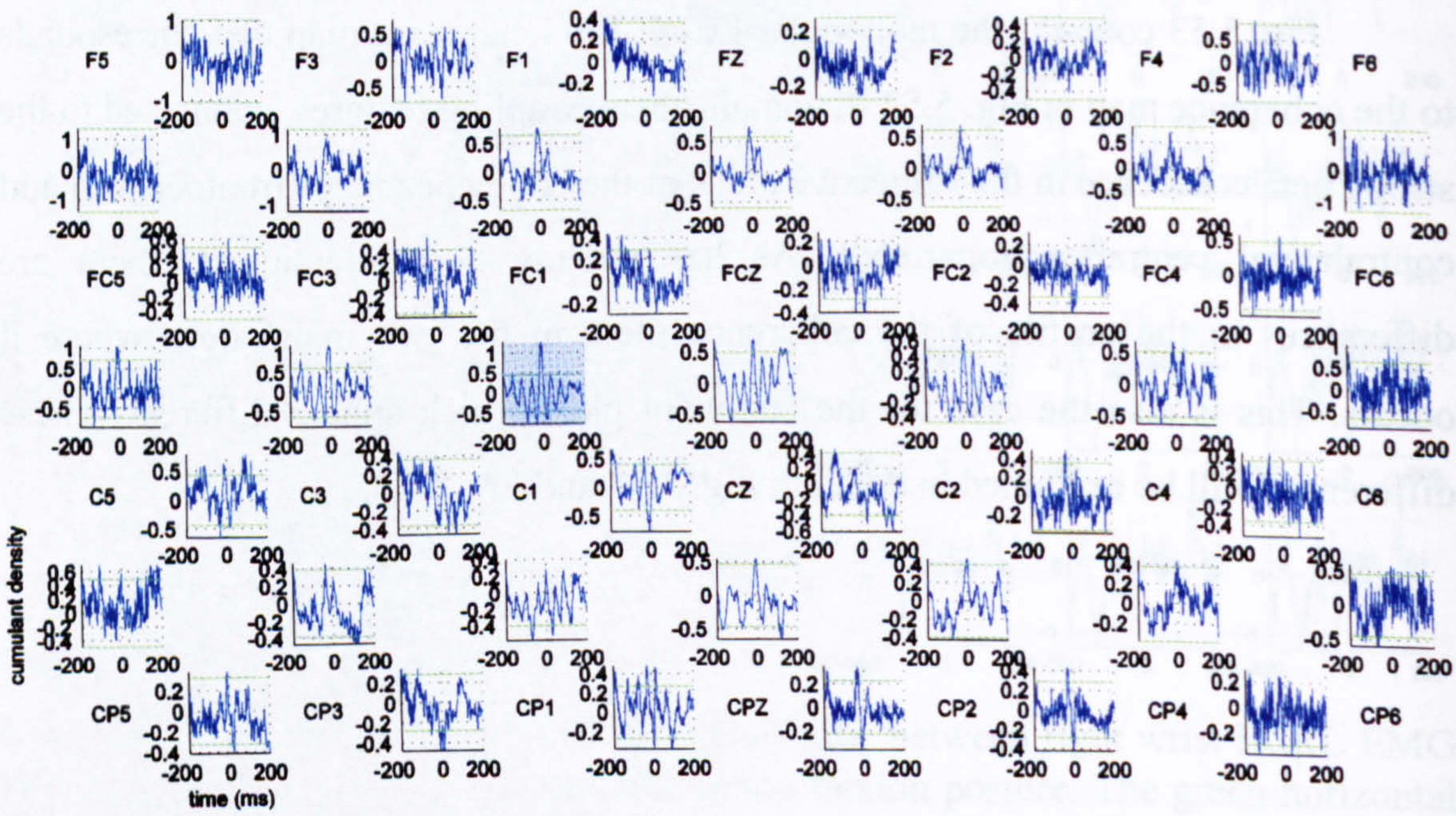

Fig. 5.55 Pooled cumulant map of all subject data, between right wrist ECRL EMG and multiple bipolar EEG channels during flexion posture. The labels represent the relative position of the electrodes over the head. Cumulant estimate between EMG and a bipolar EEG channel, product of two vertically or horizontally aligned monopolar ones, is plotted between the labels of the two monopolar EEG electrodes. The green horizontal line represents the 95% confidence interval.

The bipolar coherence map for flexed posture (Fig. 5.54) shows a very clear picture of strong coupling of the ECRL muscle with the cortex during the posture flexion phase of the task. More specifically beta coherence appears strongest in the contralateral, for frontocentral-central electrodes. The maximum coherence appears in the vertically aligned bipolar FC1-C1 electrode pair. The corticomuscular coherences for the vertically aligned electrodes are higher than for the horizontal. A statisticaly significant 6Hz feature appears for the contralateral electrodes, roughly in the same area that beta coherence appears. However, it does not seem to be a harmonic connection due to the fact that the size of the 6Hz coherence feature does not seem to be connected with the magnitude of the beta coherence peak. For example in electrode FC4-C4 the 6 and 21Hz coherence peaks have similar magnitudes while in FC1-C1 the difference is massive. Gamma coherences appear locally but they are neither strong nor having spatial organisation. The corresponding bipolar cumulant map (Fig. 5.55) also shows strong synchronisation between the contralateral hemisphere and ECRL EMG. The spatial distribution corresponds with the equivalent coherence map from Fig. 5.54. The FC1-C1 electrode shows the highest coupling. The peaks clearly show that the dominant coupling is in the beta band. The vertical electrodes are coupled "in phase" and the horizontal coupled "out of phase" coupled with the rectified EMG, presumably an effect resulting from the orientation of the bipolar EEG electrodes. ECRL\FC1-C1 coupling is "in phase" but ECRL\C1-FC1 coupling is "out of phase" coupled with the ECRL EMG.

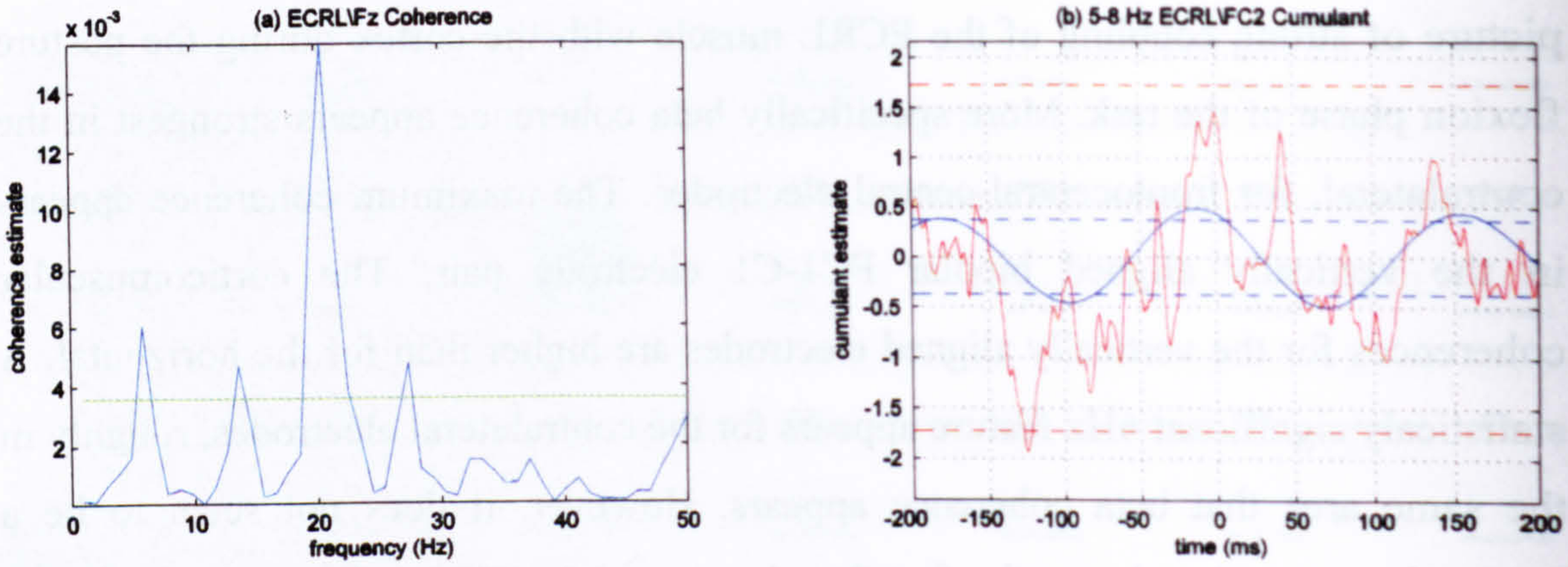

Fig. 5.56 ECRL\FZ coherence and corresponding cumulant plot (red plot). The blue plot represents the main cumulant component for the frequency band that coherence is statistically significant while the blue dashed lines represent the estimated upper and lower 95% confidence limits for the cumulant component.

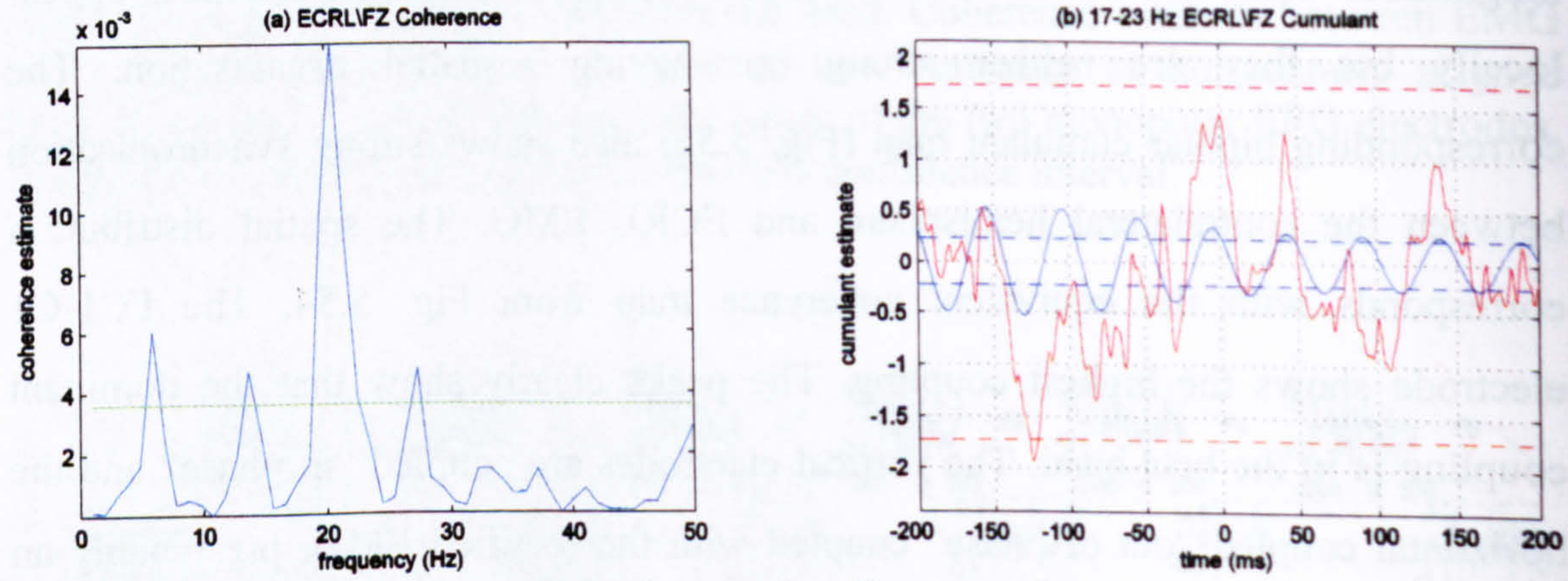

Fig. 5.57 ECRL\FZ coherence and corresponding cumulant plot (red plot). The blue plot represents the main cumulant component for the frequency band that coherence is statistically significant while the blue dashed lines represent the estimated upper and lower 95% confidence limits for the cumulant component.

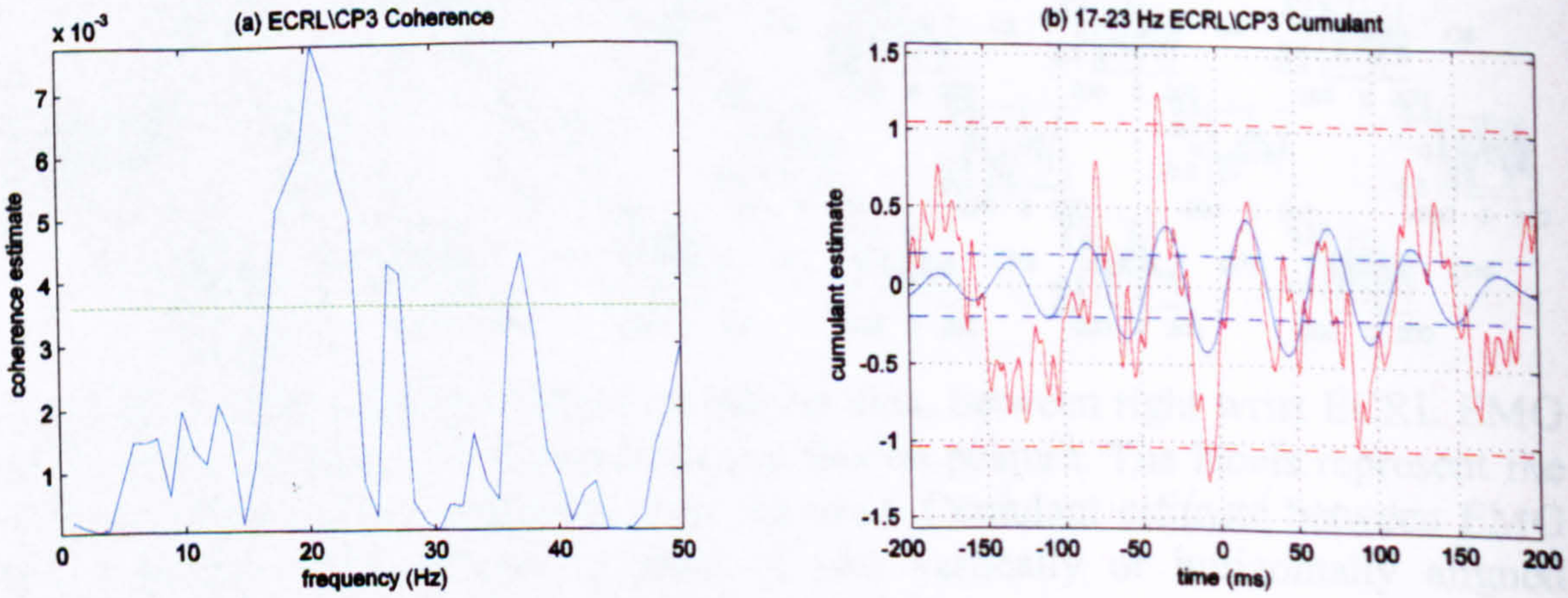

Fig. 5.58 ECRL\CP3 coherence and corresponding cumulant plot (red plot). The blue plot represents the main cumulant component for the frequency band that coherence is statistically significant while the blue dashed lines represent the estimated upper and lower 95% confidence limits for the cumulant component.

Fig. 5.57*a* shows the ECRL\Fz coherence, which is highlighted in Fig. 5.52. Fig. 5.57*b* shows the wideband cumulant plot that corresponds to Fig. 5.57*a* as well as the 17-23Hz cumulant component. "In phase" synchronisation takes place with a -6ms delay (-6.5±4.4ms as revealed by phase which is not shown). The corresponding ECRL\CP3 coherence and 17-23Hz cumulant component is shown in Fig. 5.58. CP3 has the highest beta coupling feature in the ipsilateral central and centroparietal areas. This area (as shown earlier) is strongly coupled with ECRL in the 17-23Hz band during posture. Fz activity was coupled "in phase" with ECRL in the beta band, but CP3 coupling in this band is "out of phase". The cumulant delay is -7ms (phase: -7.6±3.2ms). Fig. 5.56 shows the ECRL\Fz 5-8Hz cumulant. While the cumulant profile appears statistically significant the delay phase error is too large to give a reliable value.

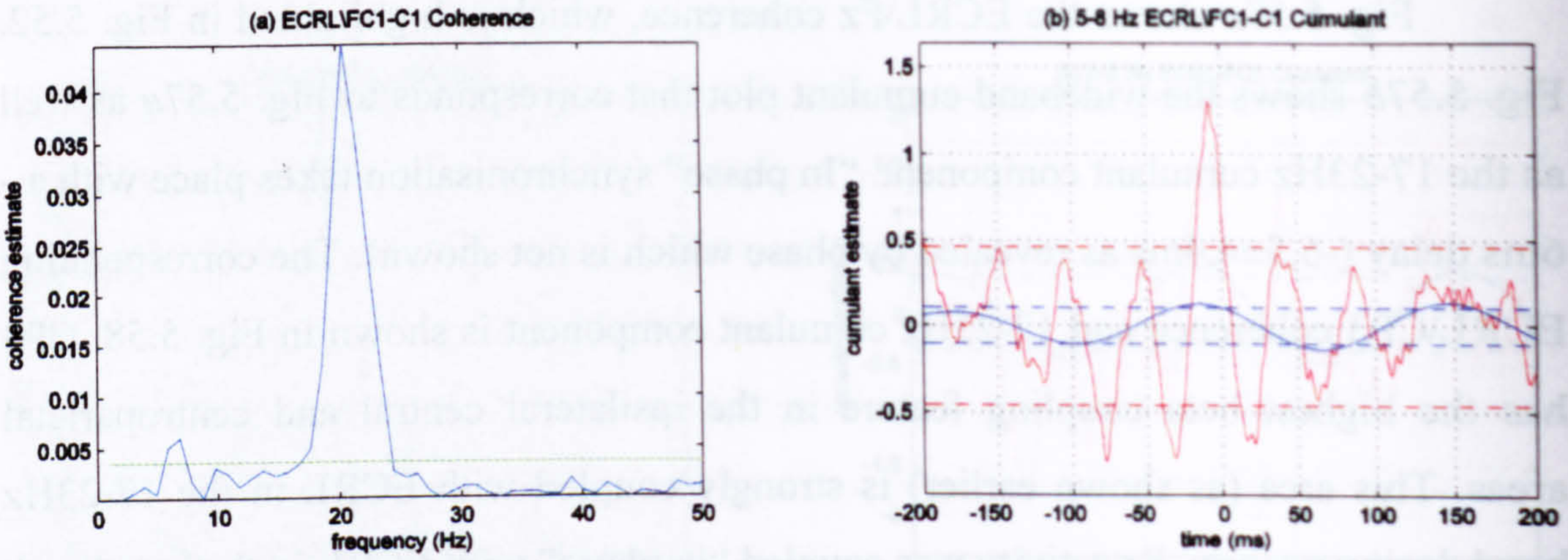

Fig. 5.59 ECRL\FC1-C1 coherence and corresponding cumulant plot (red plot). The blue plot represents the main cumulant component for the frequency band that coherence is statistically significant while the blue dashed lines represent the estimated upper and lower 95% confidence limits for the cumulant component.

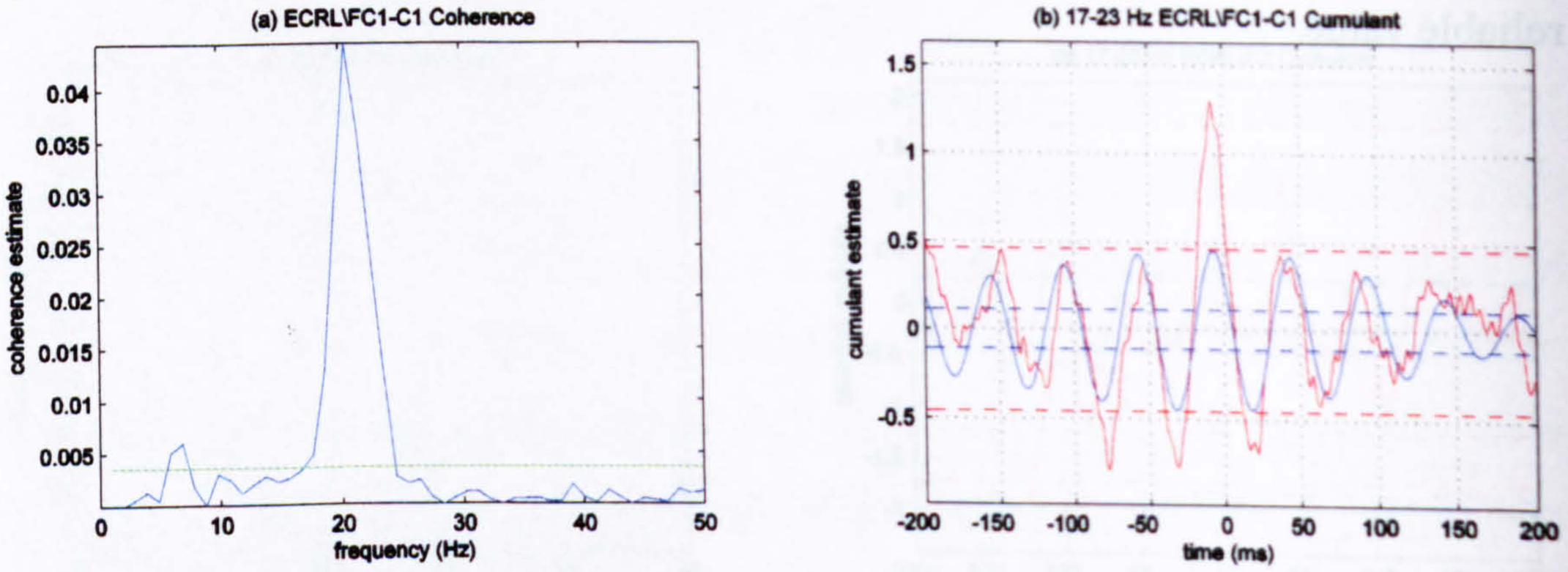

Fig. 5.60 ECRL\FC1-C1 coherence and corresponding cumulant plot (red plot). The blue plot represents the main cumulant component for the frequency band that coherence is statistically significant while the blue dashed lines represent the estimated upper and lower 95% confidence limits for the cumulant component.

Fig. 5.59*a* shows the ECRL\FC1-C1 coherence plot. Fig. 5.59*b* and Fig. 5.60*b* show the cumulant components for the 5-8Hz and 17-23Hz coupling features respectively. The 5-8Hz shows "in phase" coupling with -15ms or +66ms delay. Phase estimates could not reliably indicate the correct delay. The prominent beta feature gives a delay of -7ms (-7.5±1.6ms as derived by phase). This means that the EEG has a 7ms lead over the EMG.

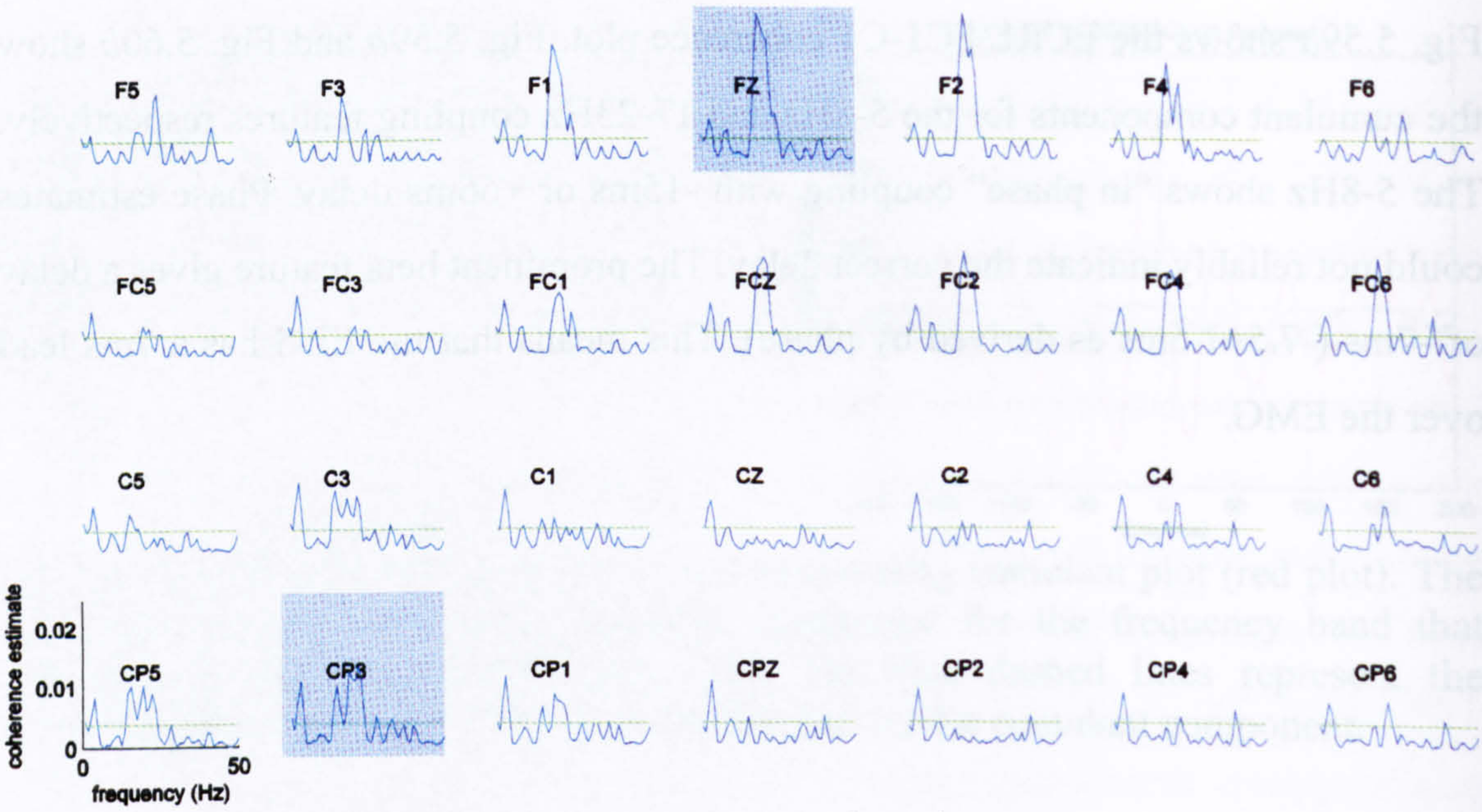

Fig. 5.61 Pooled coherence map of all subject data, between right wrist FCR EMG and multiple monopolar EEG channels during flexion posture. The green horizontal line represents the 95% confidence interval.

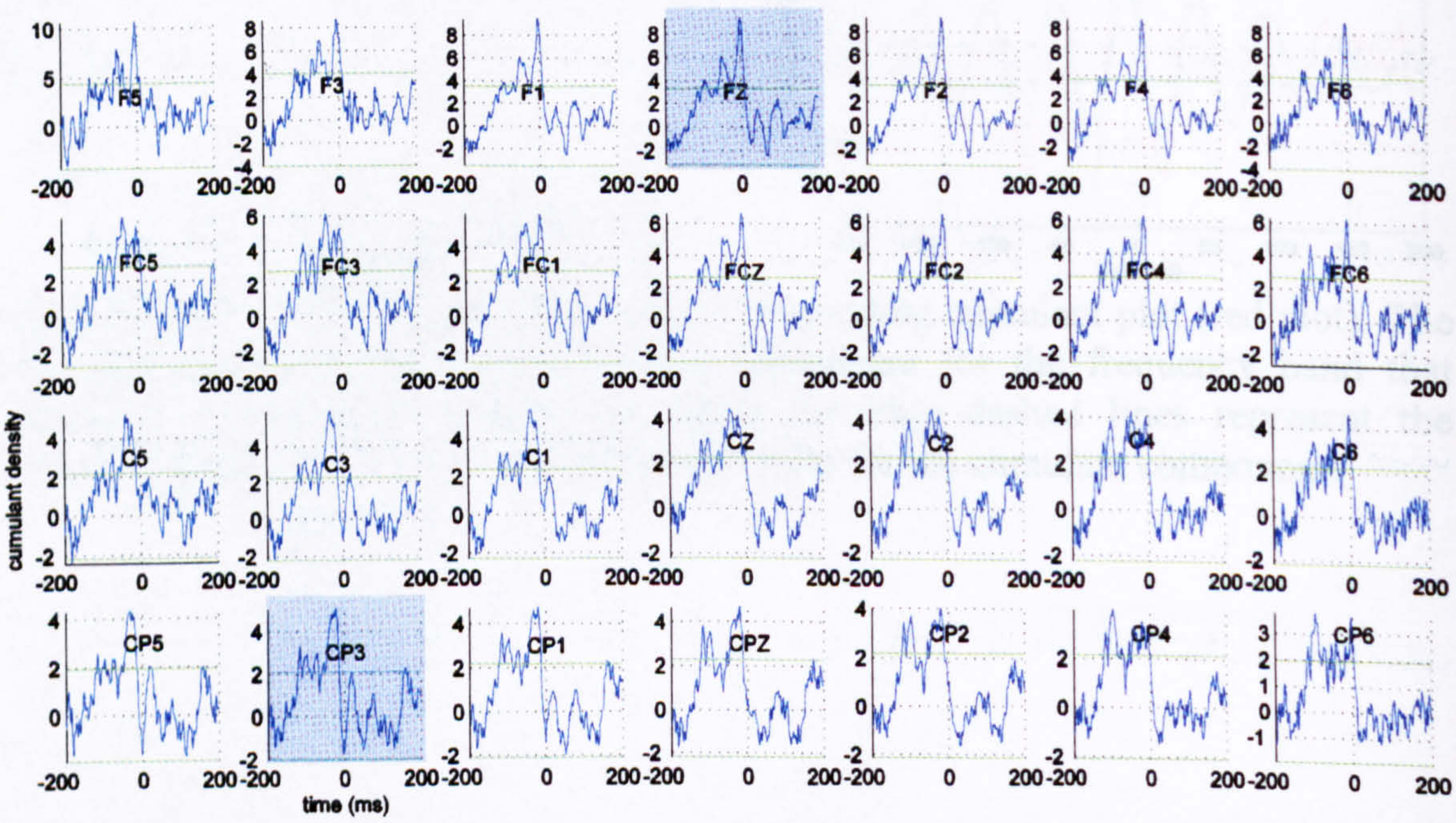

Fig. 5.62 Pooled cumulant map of all subject data, between right wrist FCR EMG and multiple monopolar EEG channels during flexion posture. The green horizontal line represents the 95% confidence interval.

5.1.6.2.2 FCR coupling

Fig. 5.61 shows the coherence estimate plots between FCR EMG and the monopolar EEG channels during the flexion posture phase. Strong beta coupling is present in the medial frontal and frontocentral areas (18-26Hz with a peak at 20Hz) and the contralateral central and centroparietal areas (14-23Hz). The peaks in the frontal and frontocentral areas appear wider and the distribution of coherence in those areas different than the corresponding ECRL map of Fig. 5.52. However, the peak frequency is still the same (21Hz). A small 4Hz coherence peak appears for the whole cortical area and some weak alpha coupling also exists for the medial frontal and frontocentral electrodes.

The monopolar cumulant map for the same muscle during flexion posture (Fig. 5.62) shows widespread features that are connected with the beta coupling features appearing in the coherence map. The plots are also influenced by a common low frequency component (most probably the 4Hz peak), which was not the case for the corresponding ECRL map (Fig. 5.53).

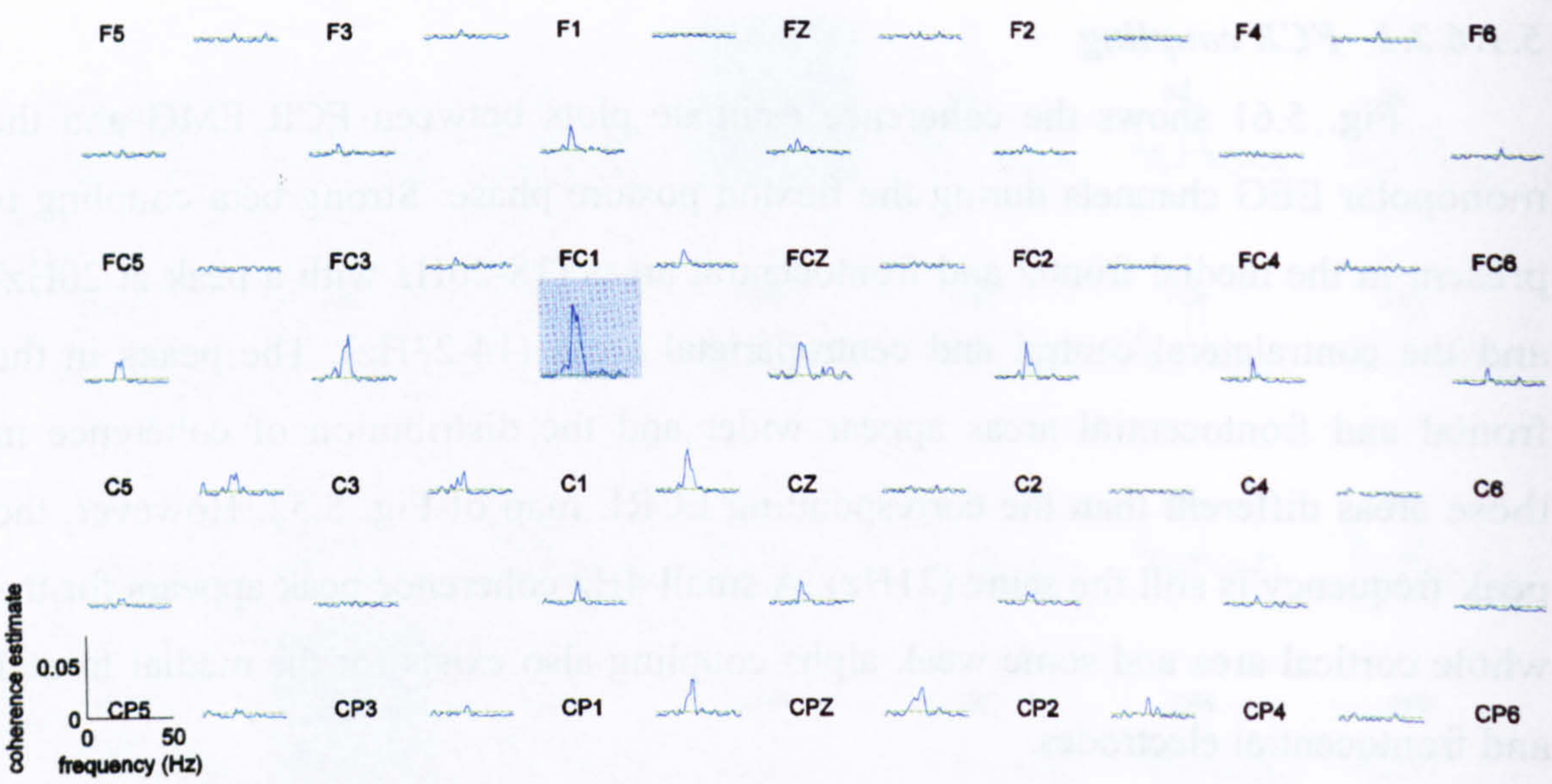

Fig. 5.63 Pooled coherence map of all subject data, between right wrist FCR EMG and multiple bipolar EEG channels during flexion posture. The labels represent the relative position of the electrodes over the head. Coherence estimate between EMG and a bipolar EEG channel, product of two vertically or horizontally aligned monopolar ones, is plotted between the labels of the two monopolar EEG electrodes. The green horizontal line represents the 95% confidence interval.

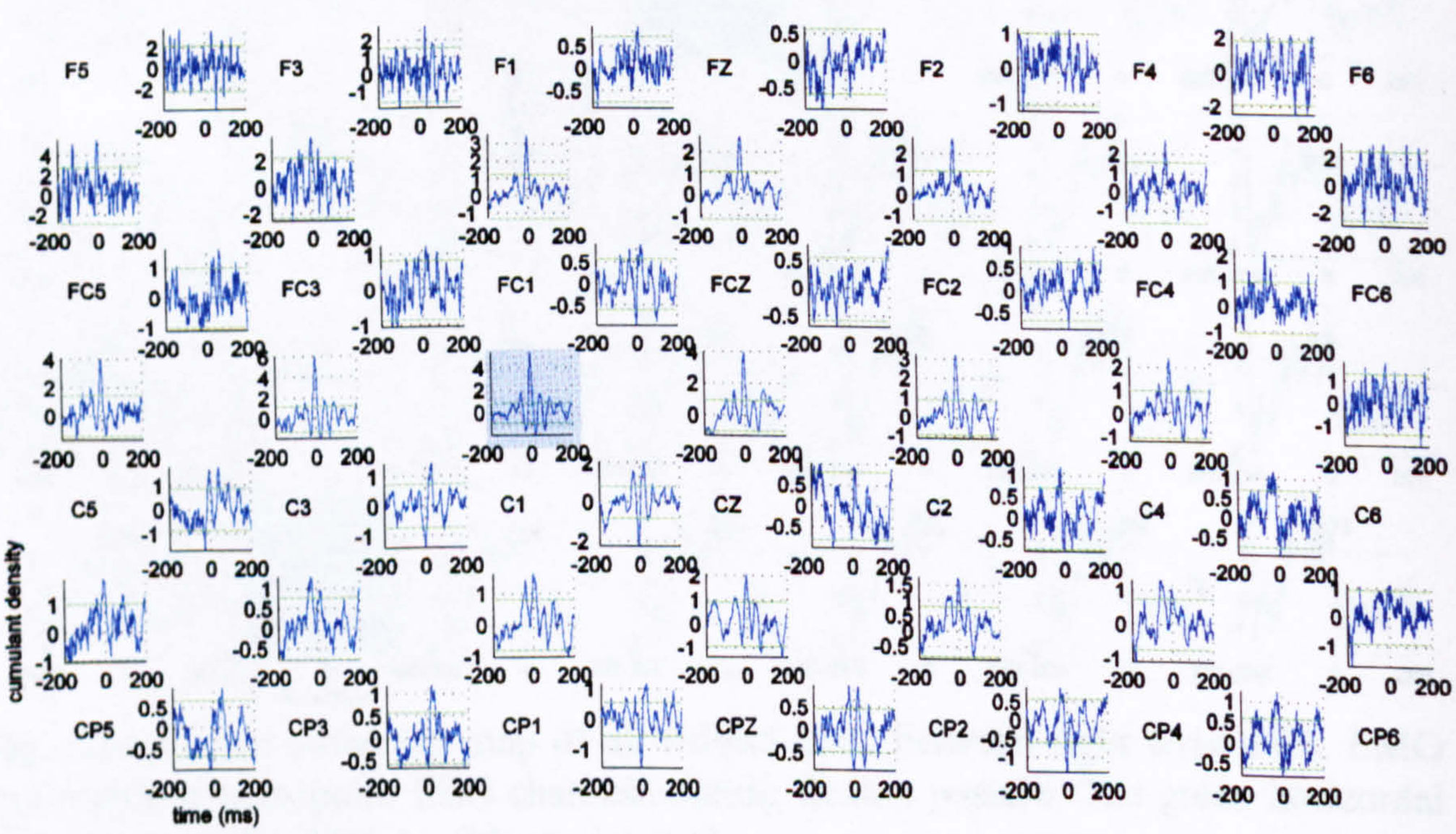

Fig. 5.64 Pooled cumulant map of all subject data, between right wrist FCR EMG and multiple bipolar EEG channels during flexion posture. The labels represent the relative position of the electrodes over the head. Cumulant estimate between EMG and a bipolar EEG channel, product of two vertically or horizontally aligned monopolar ones, is plotted between the labels of the two monopolar EEG electrodes. The green horizontal line represents the 95% confidence interval.

Fig. 5.63 shows the coherence estimates for FCR EMG (agonist) and multiple bipolar EEG channels during the posture flexion. The coupling map is very similar with the equivalent ECRL corticomuscular map shown in Fig. 5.54. Beta coherence (18-27Hz with a main peak at 20-22Hz) is very strong and widespread, and reaches its maximum in the contralateral hemisphere over the FC1-C1 electrode. The beta coupling is in general higher for the vertically than for the horizontally aligned electrodes. Comparing the results with the ECRL (antagonist) bipolar coherence map in Fig. 5.54, For FCR the ratio between and horizontal and vertical bipolar electrode coherences appears to be higher than for ECRL (Fig. 5.54). This means that there is smaller difference between FC1-C1 and C1-Cz for FCR corticomuscular coherence.

Statistically significant 5, 10, 15 and 35Hz coherence features are also present in the map for a number of electrodes. The coherence magnitudes are much smaller than the dominant 20Hz component but they may have some localised functional significance. This may well be the case especially for the 15 and 35Hz features that appear strong for some electrodes mainly in contralateral frontocentral and central electrodes (F1-FC1, FC3-C3,FC1-C1, FCz-Cz and FC2-C2).

The bipolar cumulant plots for the same muscle in Fig. 5.64 are in line with the corresponding coherence map shown in Fig. 5.63, illustrating high beta synchronisation in the same areas. Alpha coupling is also obvious in ipsilateral sites when not masked by the dominant beta synchronisation. CP4-CP6, C2-C4 and FC2-FC4 are the electrodes that show the strongest alpha coupling in the cumulant map even though C2-C4 and FC2-FC4 coherences do not reveal alpha coupling. Horizontally aligned bipolar electrodes seem more prone to the alpha coupling than vertically aligned.

Fig. 5.65 and Fig. 5.66 show the FCR\Fz and FCR\CP3 coherences, the wideband cumulants and the 17-23Hz cumulant features respectively. Fz and CP3 show the maximum coherences from respective cortical areas of high beta corticomuscular coupling during posture. The FCR\Fz figure shows "in phase" synchronisation with -4ms delay as derived by the cumulant (phase estimate: -3.8±1.9ms) while FCR\CP3 coupling was "out of phase" with similar delay at -3ms (phase estimate: -3.1±2.8ms).

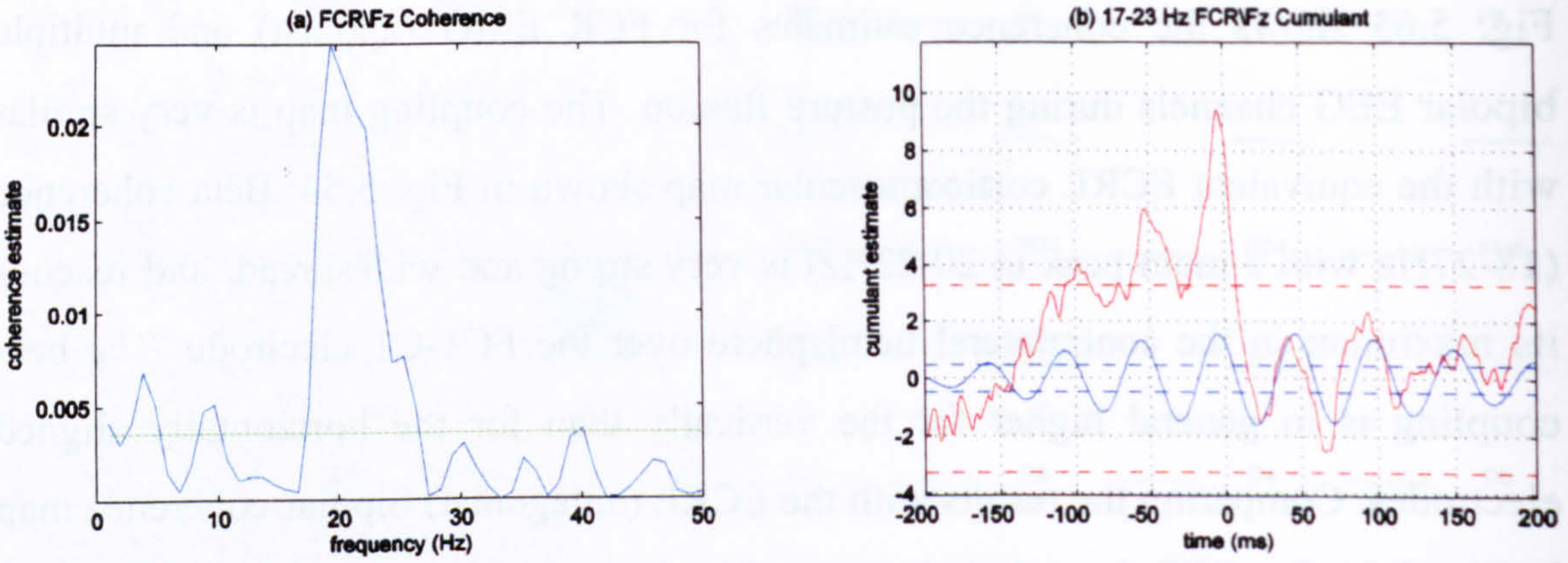

Fig. 5.65 FCR\FZ coherence and corresponding cumulant plot (red plot). The blue plot represents the 17-23Hz cumulant component, while the blue dashed lines represent the estimated upper and lower 95% confidence limits for the cumulant component.

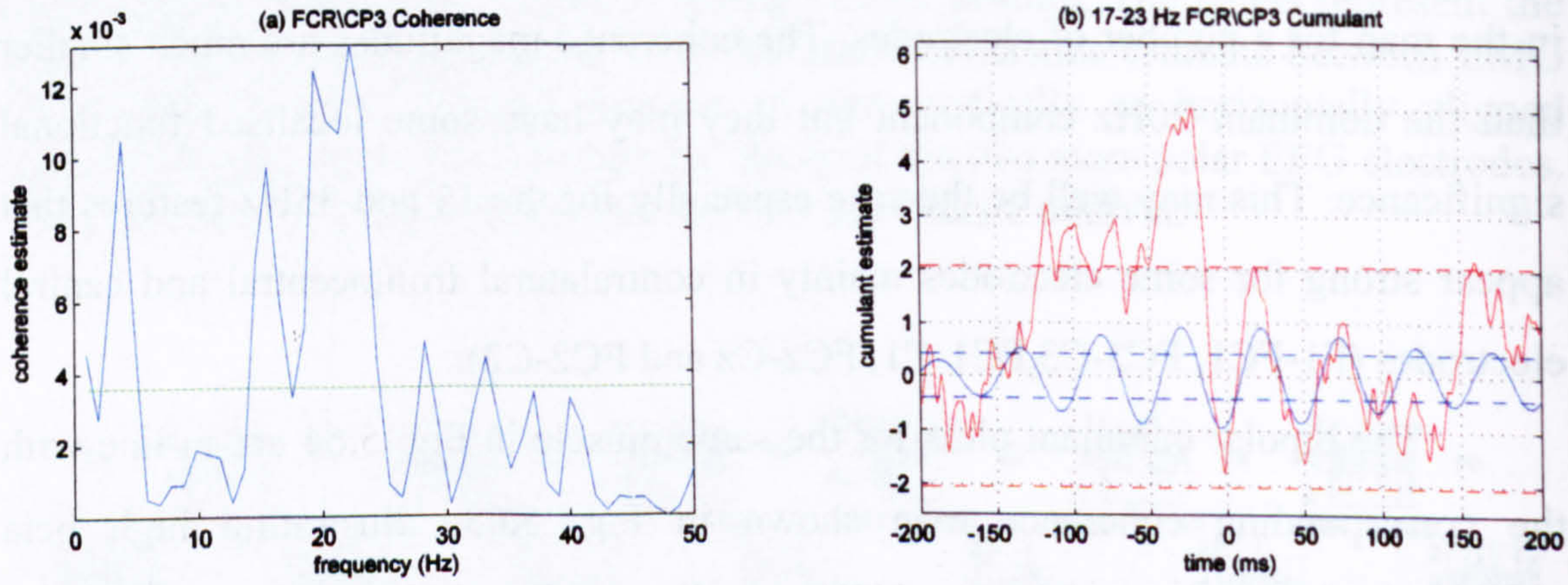

Fig. 5.66 FCR\CP3 coherence and corresponding cumulant plot (red plot). The blue plot represents the 17-23Hz cumulant component, while the blue dashed lines represent the estimated upper and lower 95% confidence limits for the cumulant component.

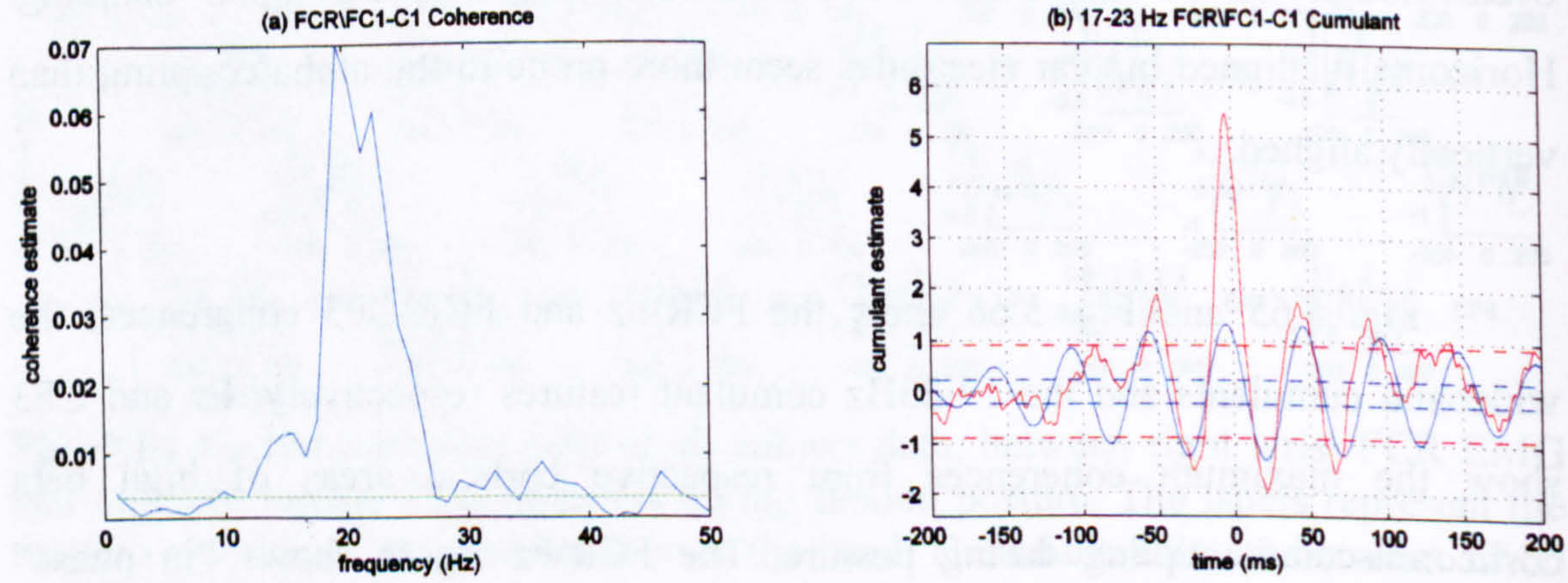

Fig. 5.67 FCR\FC1-C1 coherence and corresponding cumulant plot (red plot). The blue plot represents the 17-23Hz cumulant component, while the blue dashed lines represent the estimated upper and lower 95% confidence limits for the cumulant component.

Fig. 5.67*a* shows the most prominent beta coherence feature of the FCR bipolar map and the 17-23Hz cumulant plot. FCR\FC1-C1 show clear in phase synchronisation with -5ms delay (-4.2±1.7ms as suggested by the phase).

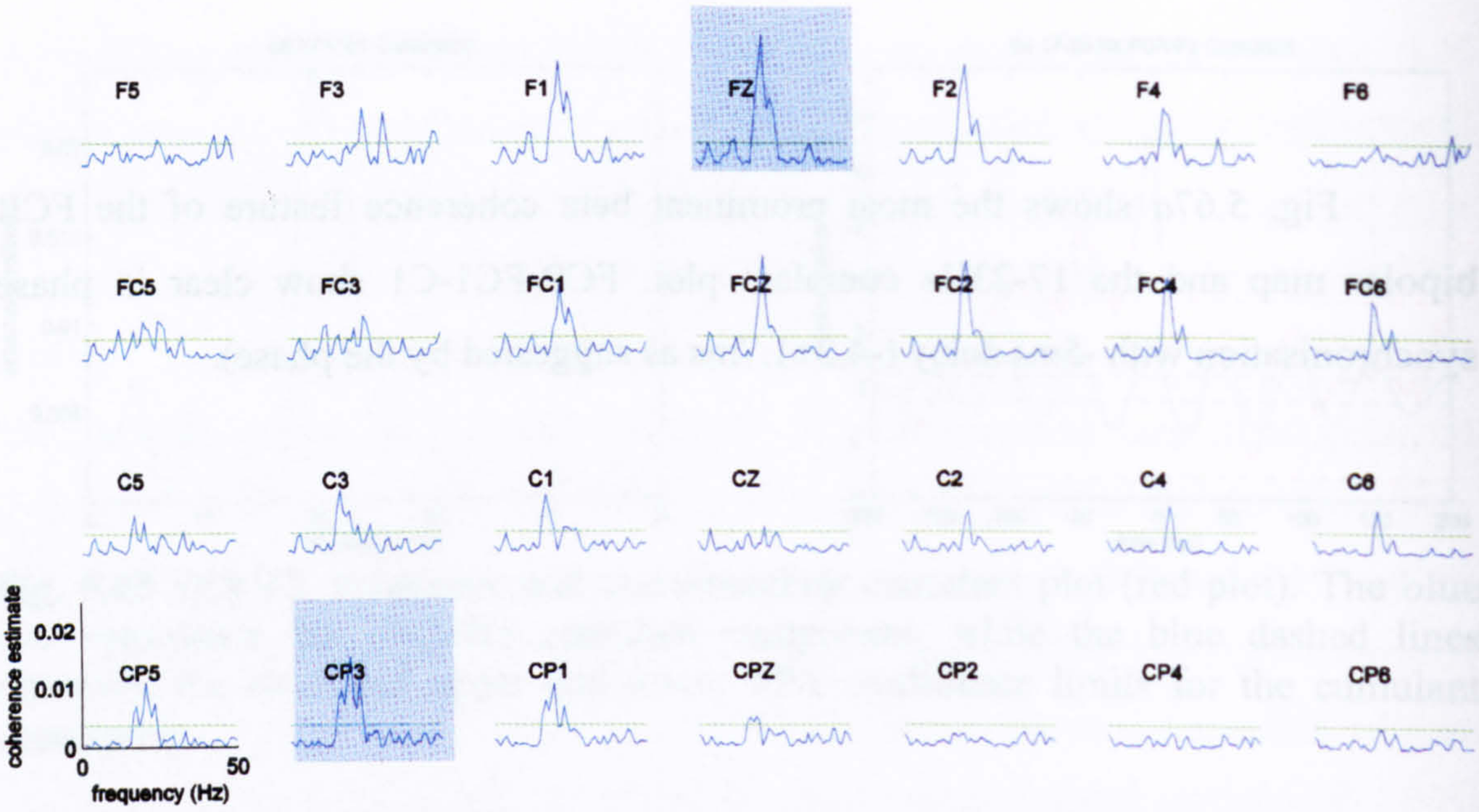

Fig. 5.68 Pooled coherence map of all subject data, between right wrist BBLH EMG and multiple monopolar EEG channels during flexion posture. The green horizontal line represents the 95% confidence interval.

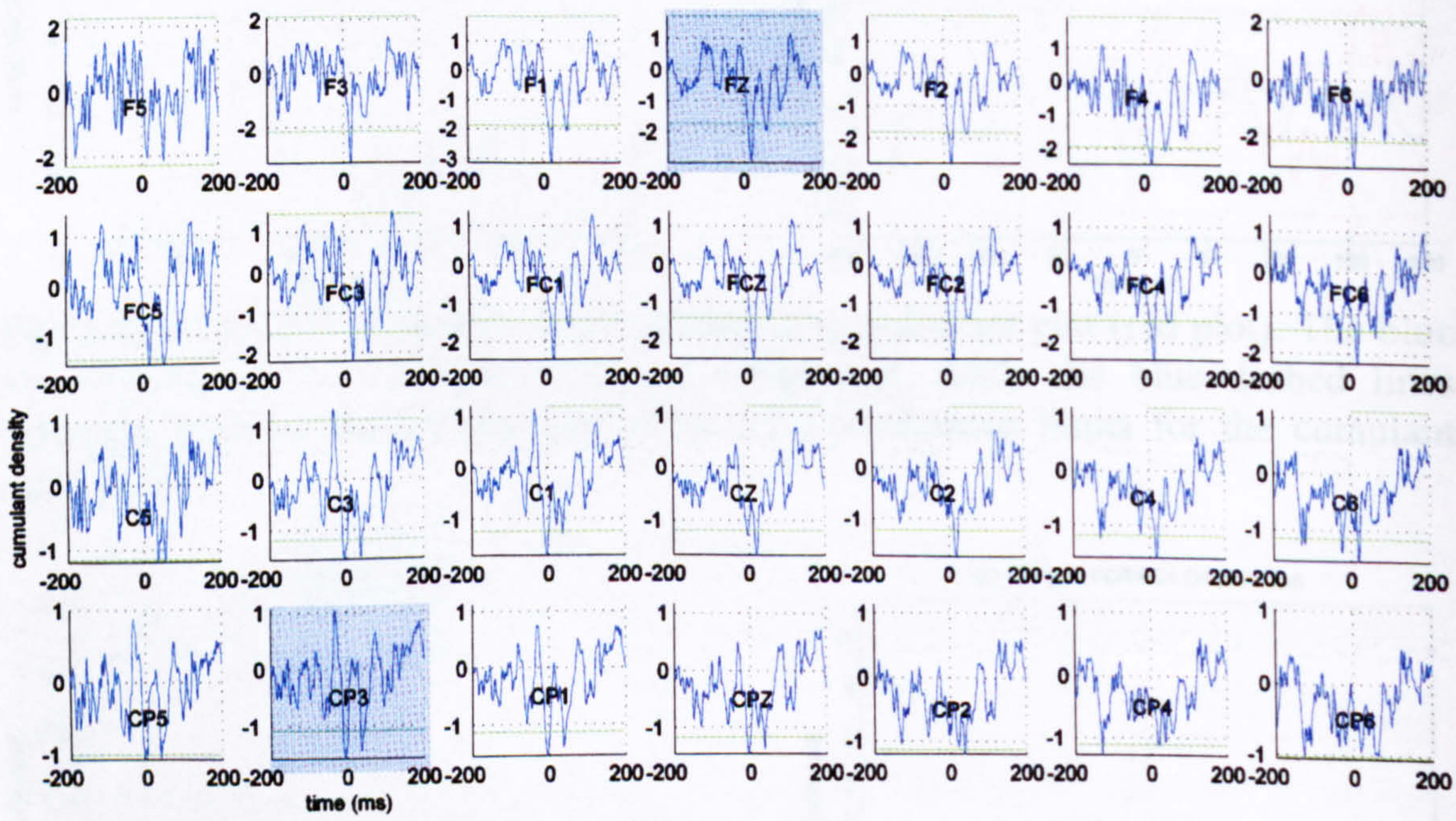

Fig. 5.69 Pooled cumulant map of all subject data, between right BBLH EMG and multiple monopolar EEG channels during flexion posture. The green horizontal line represents the 95% confidence interval.

5.1.6.2.3 BBLH coupling

Fig. 5.68 shows the coherence estimate map between BBLH EMG and monopolar EEG channels during flexion posture. Strong beta band coherence is seen mainly in the medial frontal and frontocentral areas (21Hz) as well as the contralateral central and centroparietal electrodes (17-24Hz). Alpha band coupling is almost absent except for a few frontal electrodes showing weak 13Hz. There is also very little gamma synchronisation. The corresponding cumulant map contains evidence of beta features (Fig. 5.69) in the same electrodes which show high coherence.

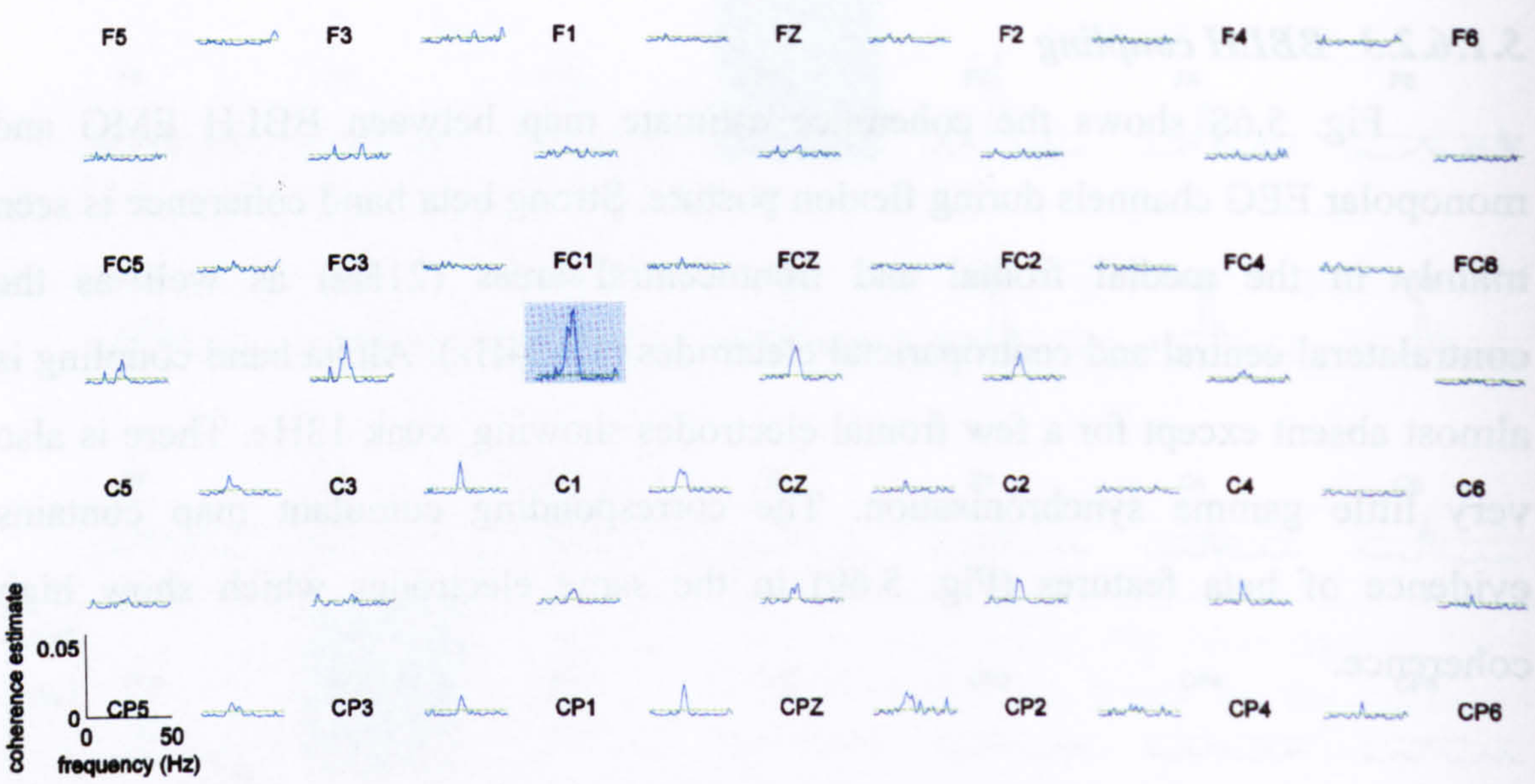

Fig. 5.70 Pooled coherence map of all subject data, between right BBLH EMG and multiple bipolar EEG channels during flexion posture. The labels represent the relative position of the electrodes over the head. Coherence estimate between EMG and a bipolar EEG channel, product of two vertically or horizontally aligned monopolar ones, is plotted between the labels of the two monopolar EEG electrodes. The green horizontal line represents the 95% confidence interval.

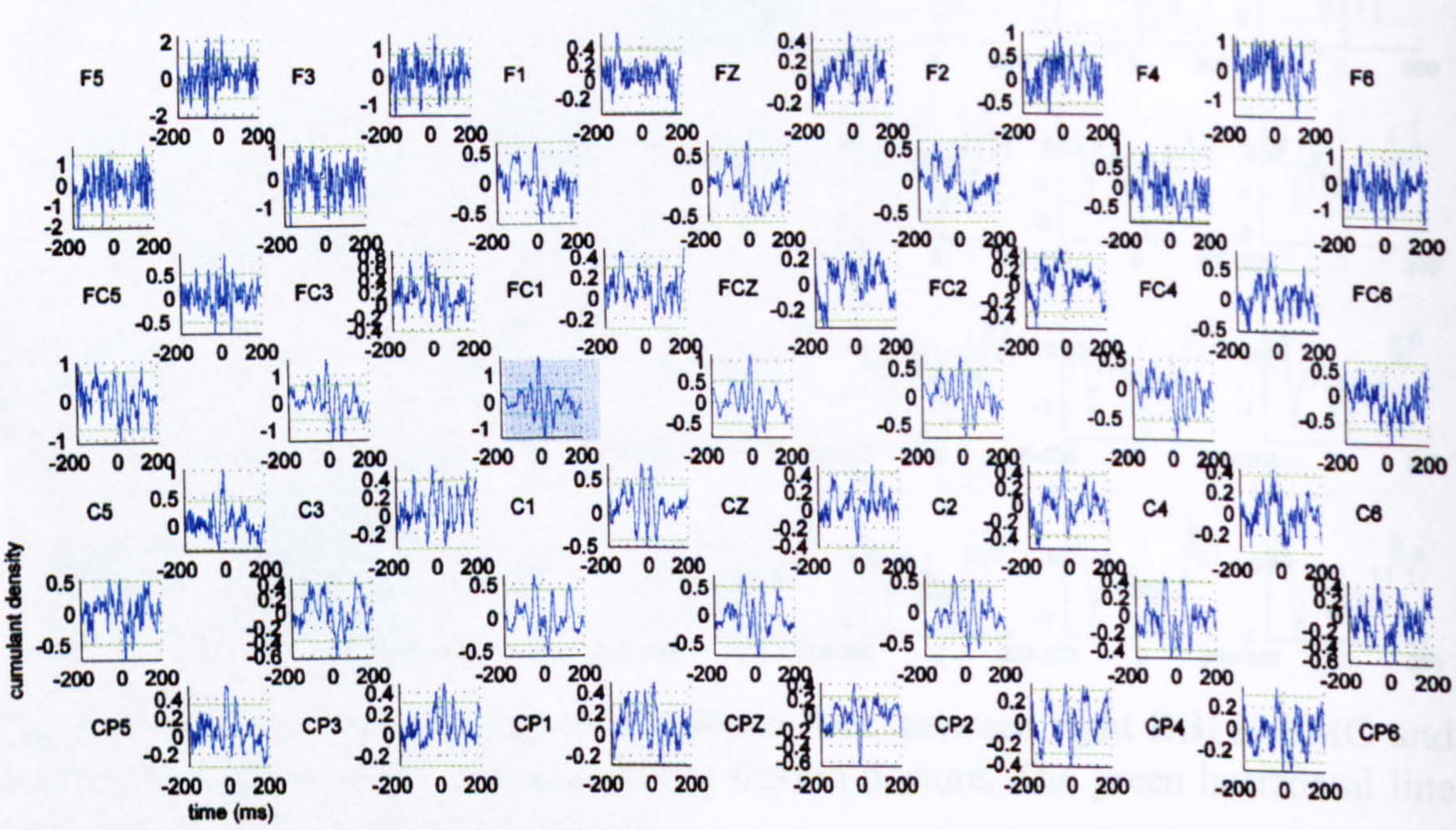

Fig. 5.71 Pooled cumulant map of all subject data, between right BBLH EMG and multiple bipolar EEG channels during flexion posture. The labels represent the relative position of the electrodes over the head. Cumulant estimate between EMG and a bipolar EEG channel, product of two vertically or horizontally aligned monopolar ones, is plotted between the labels of the two monopolar EEG electrodes. The green horizontal line represents the 95% confidence interval.

Fig. 5.70 shows the respective coherence estimate plots between BBLH and bipolar EEG channels during the posture flexion phase. It appears similar to FCR and ECRL bipolar coherence maps (Fig. 5.54, Fig. 5.63) with strong contralateral beta synchronisation that is maximal for the FC1-C1 electrode pair. The spatial distribution is slightly different with the appearance of the strong beta component for medial and ipsilateral, vertically aligned electrodes in the central and centroparietal area (Cz-CPz, C2-CP2 and C4-CP4) and the lower coherence for the contralateral vertically aligned bipolar electrodes between the frontal and frontocentral rows (e.g. F1-FC1 and Fz-FCz). Statistically significant alpha synchronisation (12-13Hz) occurs especially in the contralateral cortex (FC5-C5 and FC3-C3).

The cumulant map corresponds closely to the beta coherence map features (Fig. 5.71). Beta coupling features are present in the contralateral cortex with BBLH\FC1-C1 showing the most prominent beta coupling. CP4-CP6 shows alpha coupling despite the fact that there is no coupling in the respective coherence plot. Similar observations can be made for the equivalent FCR coherence map Fig. 5.64.

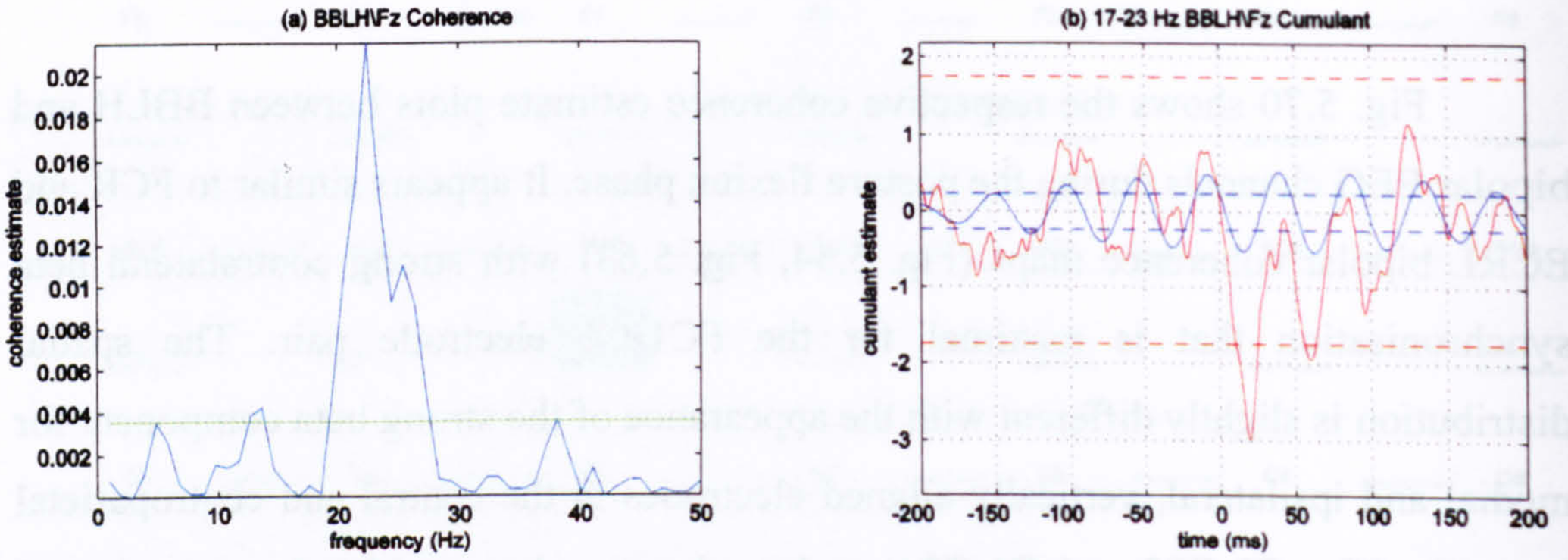

Fig. 5.72 BBLH\FZ coherence and corresponding cumulant plot (red plot). The blue plot represents the main cumulant component for the frequency band that coherence is statistically significant while the blue dashed lines represent the estimated upper and lower 95% confidence limits for the cumulant component.

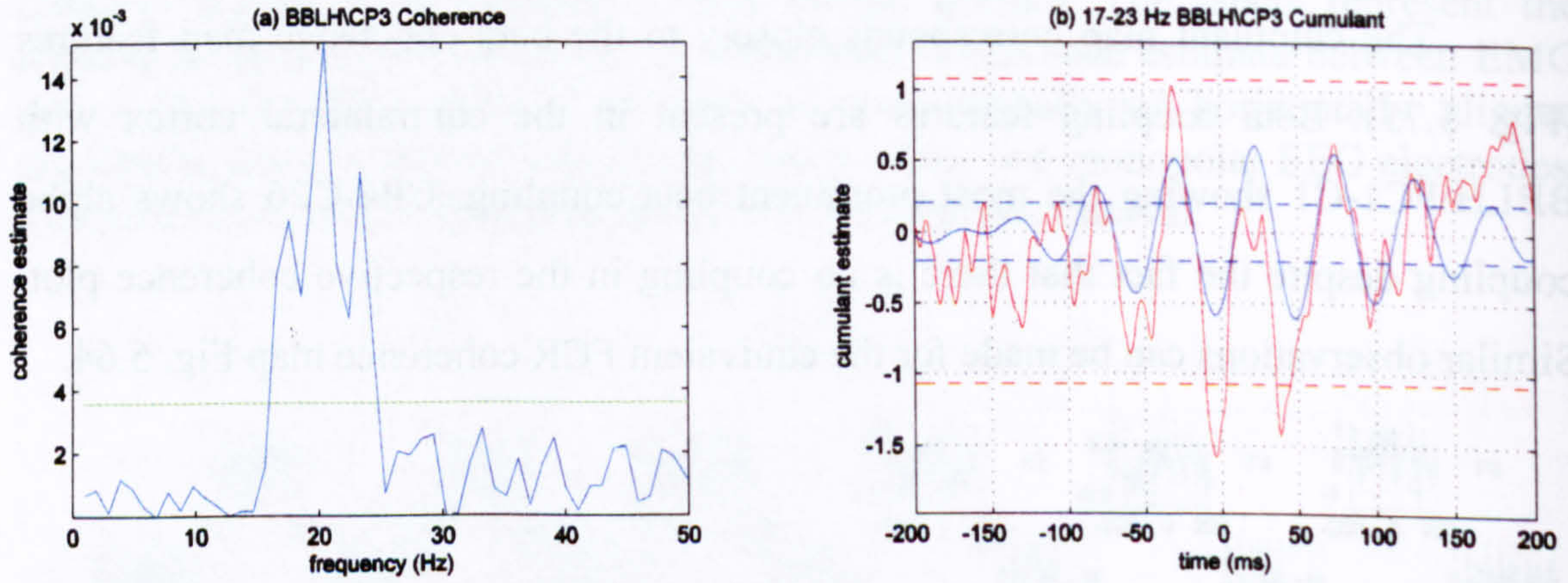

Fig. 5.73 BBLH\CP3 coherence and corresponding cumulant plot (red plot). The blue plot represents the 17-23Hz cumulant component, while the blue dashed lines represent the estimated upper and lower 95% confidence limits for the cumulant component.

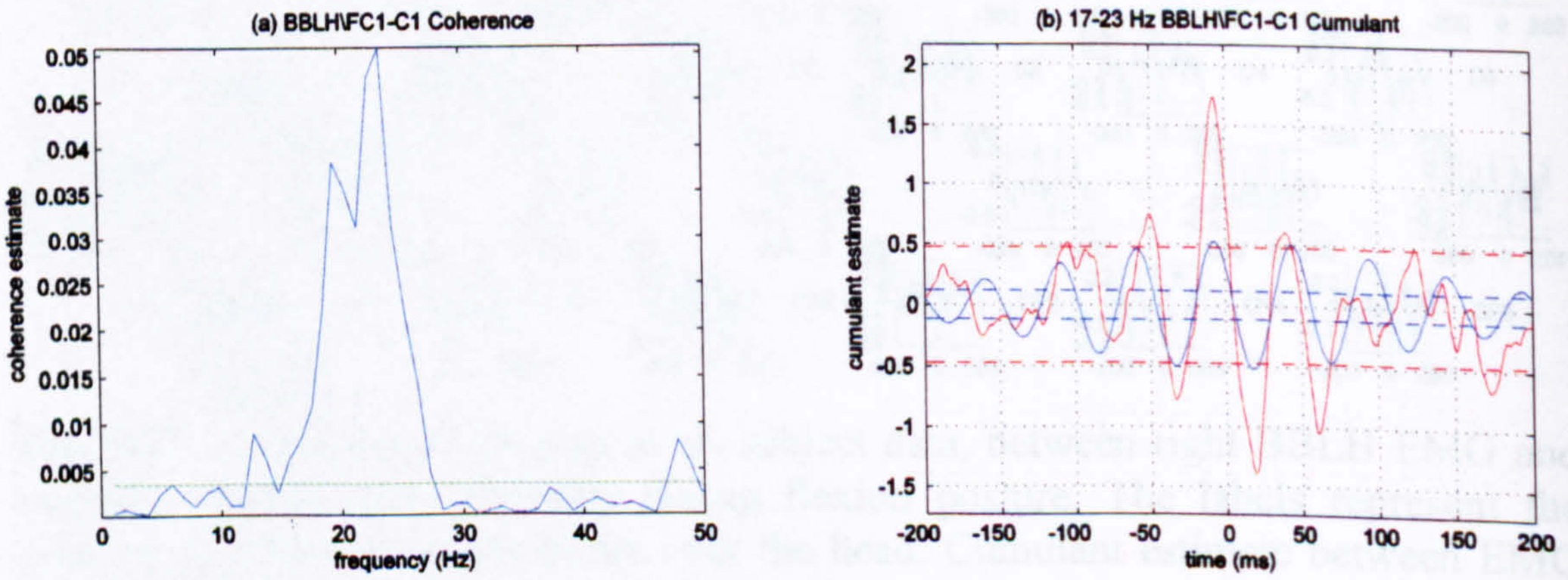

Fig. 5.74 BBLH\FC1-C1 coherence and corresponding cumulant plot (red plot). The blue plot represents the 17-23Hz cumulant component while the blue dashed lines represent the estimated upper and lower 95% confidence limits for the cumulant component.

Fig. 5.74b shows the BBLH\FC1-C1 17-23Hz component during the posture flexion phase. The delay is -8ms (phase: -7.5+-0.5ms). The absolute delay is higher than BBLH\CP3 (-4ms) while it is similar to BBLH\Fz (-7ms).

Fig. 5.72*b* and Fig. 5.73*b* show the 17-23Hz cumulant components for corticomuscular coupling between BBLH\Fz and BBLH\CP3 respectively. The BBLH\Fz 17-23Hz cumulant shows -7ms delay (-5.6±2.5ms as given by phase) while the equivalent BBLH\CP3 delay was -4ms (phase:2.2±3.2ms).

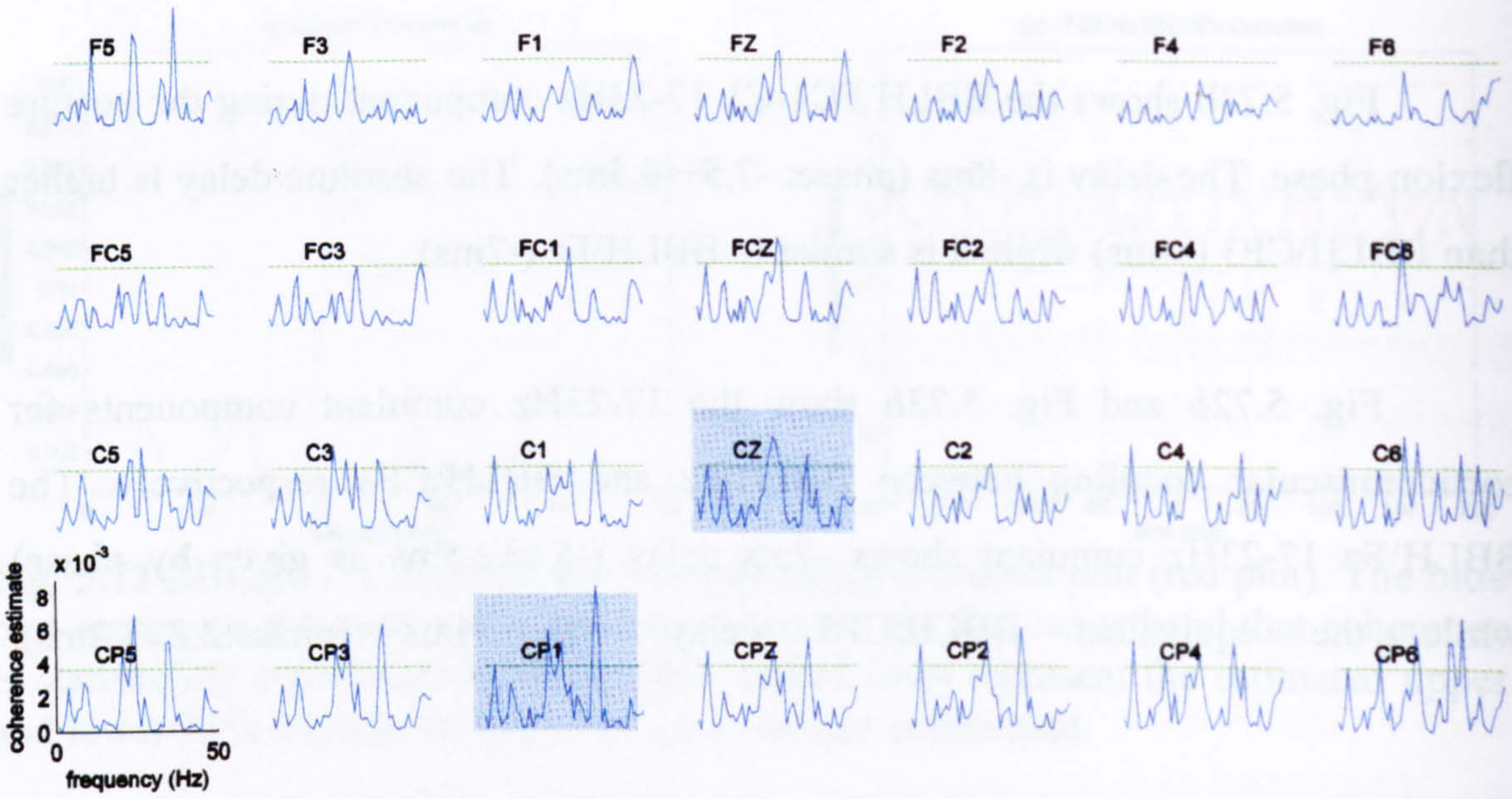

Fig. 5.75 Pooled coherence map of all subject data, between right wrist ECRL EMG and multiple monopolar EEG channels during extension movement. The green horizontal line represents the 95% confidence interval.

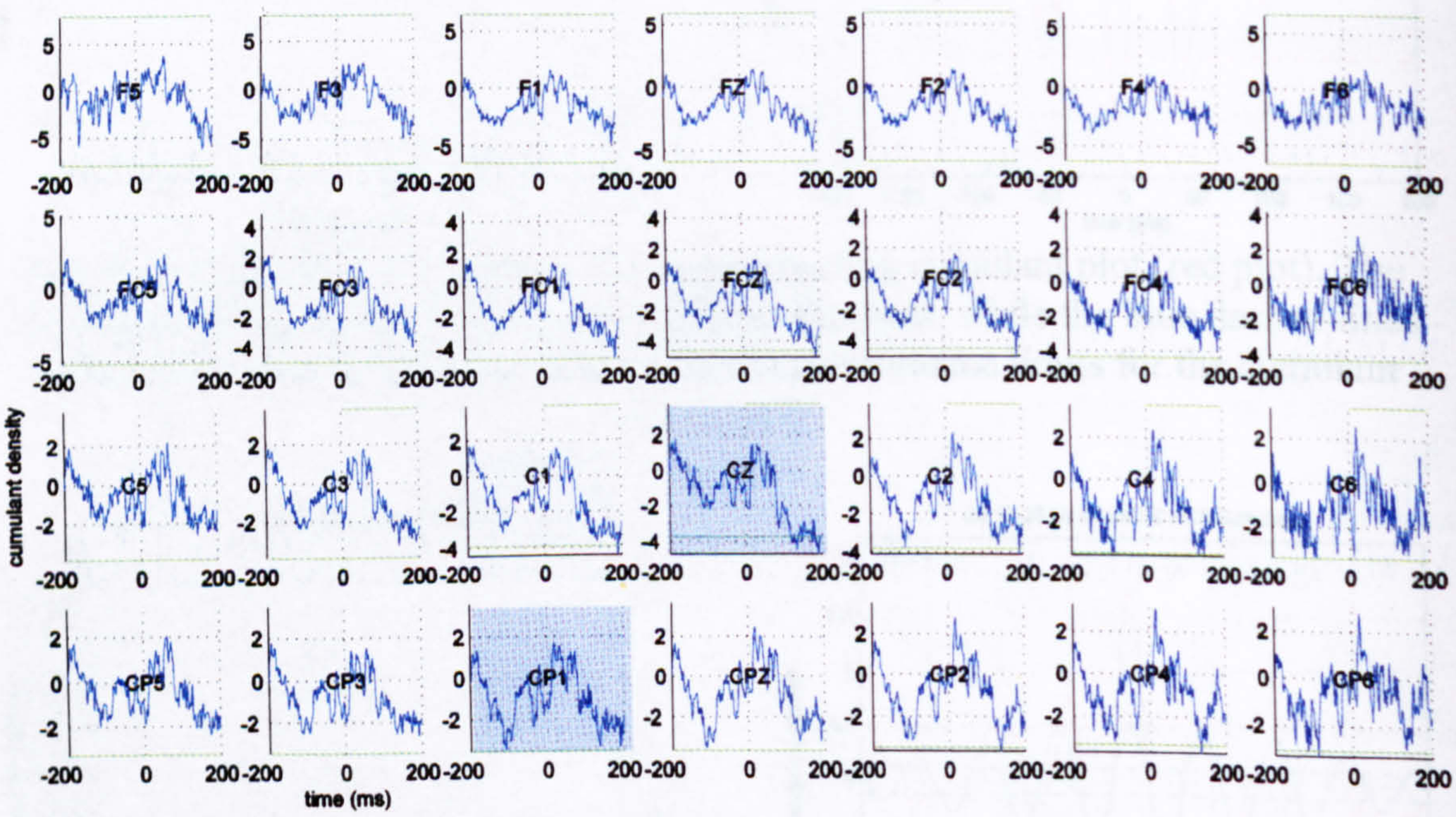

Fig. 5.76 Pooled cumulant map of all subject data, between right wrist ECRL EMG and multiple monopolar EEG channels during extension movement. The green horizontal line represents the 95% confidence interval.

5.1.6.3 Extension movement

5.1.6.3.1 ECRL Coupling

Fig. 5.75 shows the coherence estimate plots between the ECRL muscle and multiple monopolar EEG channels during wrist movement extension. In this phase this muscle acts as agonist. The strong beta coherence observed during posture flexion in the beta in medial frontal and contralateral centroparietal and central areas (Fig. 5.52) has been suppressed. Weak beta coupling features in central and centroparietal areas (Cz, CP5, CP3 and CPZ) is present. Localised coherence in the gamma band (35-38Hz) appears for a number of centroparietal, and central (C3, C1, CP5, CP3, CP1, CPZ, CP2, CP4 and CP6) as well as one frontal (F5) electrode.

The monopolar cumulant map (Fig. 5.76) shows consistent low frequency coupling over the whole cortex (approximately 3Hz). However these features are not above the confidence limits and not clearly connected with the corresponding coherence map.

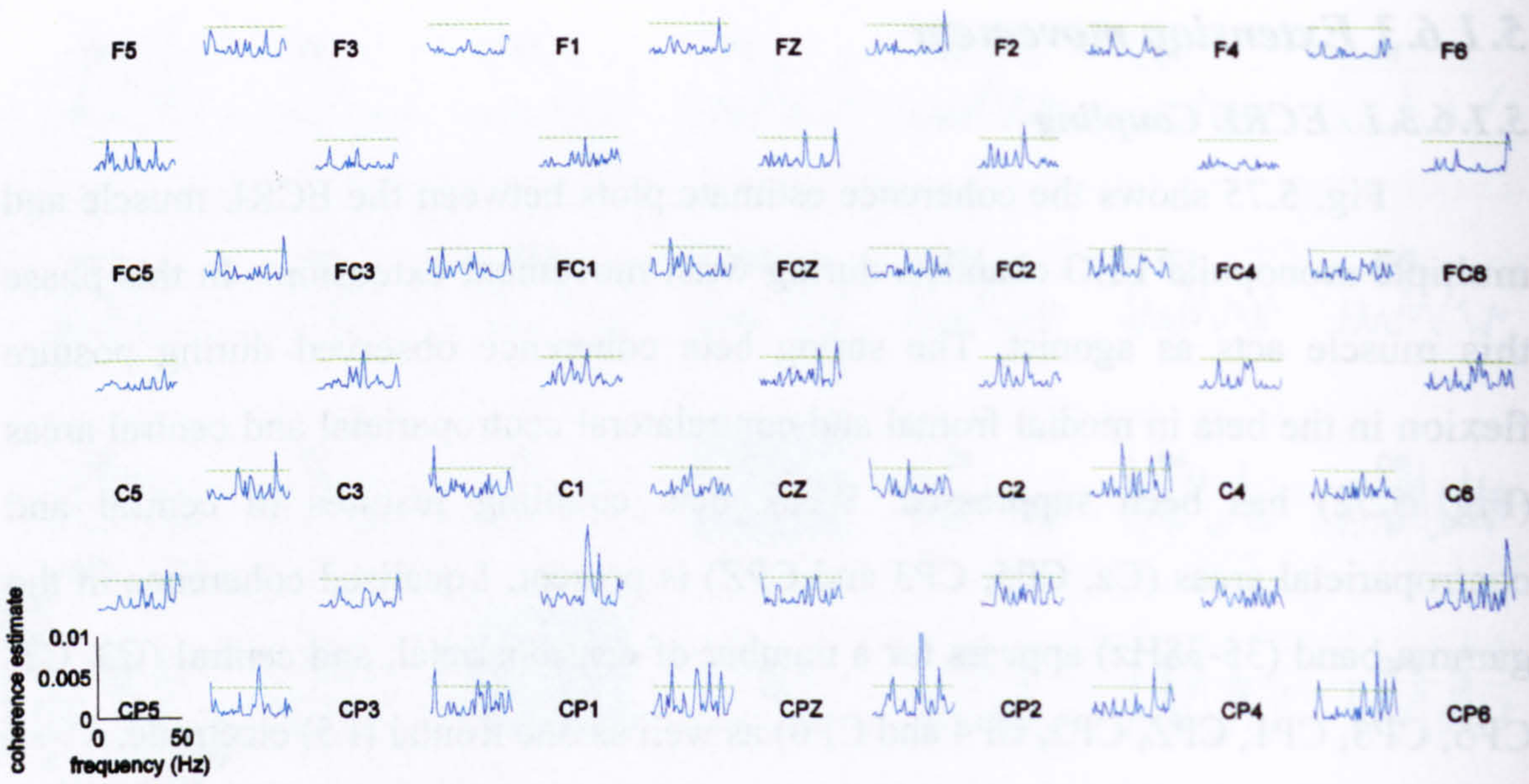

Fig. 5.77 Pooled coherence map of all subject data, between right wrist ECRL EMG and multiple bipolar EEG channels during extension movement. The labels represent the relative position of the electrodes over the head. Coherence estimate between EMG and a bipolar EEG channel, product of two vertically or horizontally aligned monopolar ones, is plotted between the labels of the two monopolar EEG electrodes. The green horizontal line represents the 95% confidence interval.

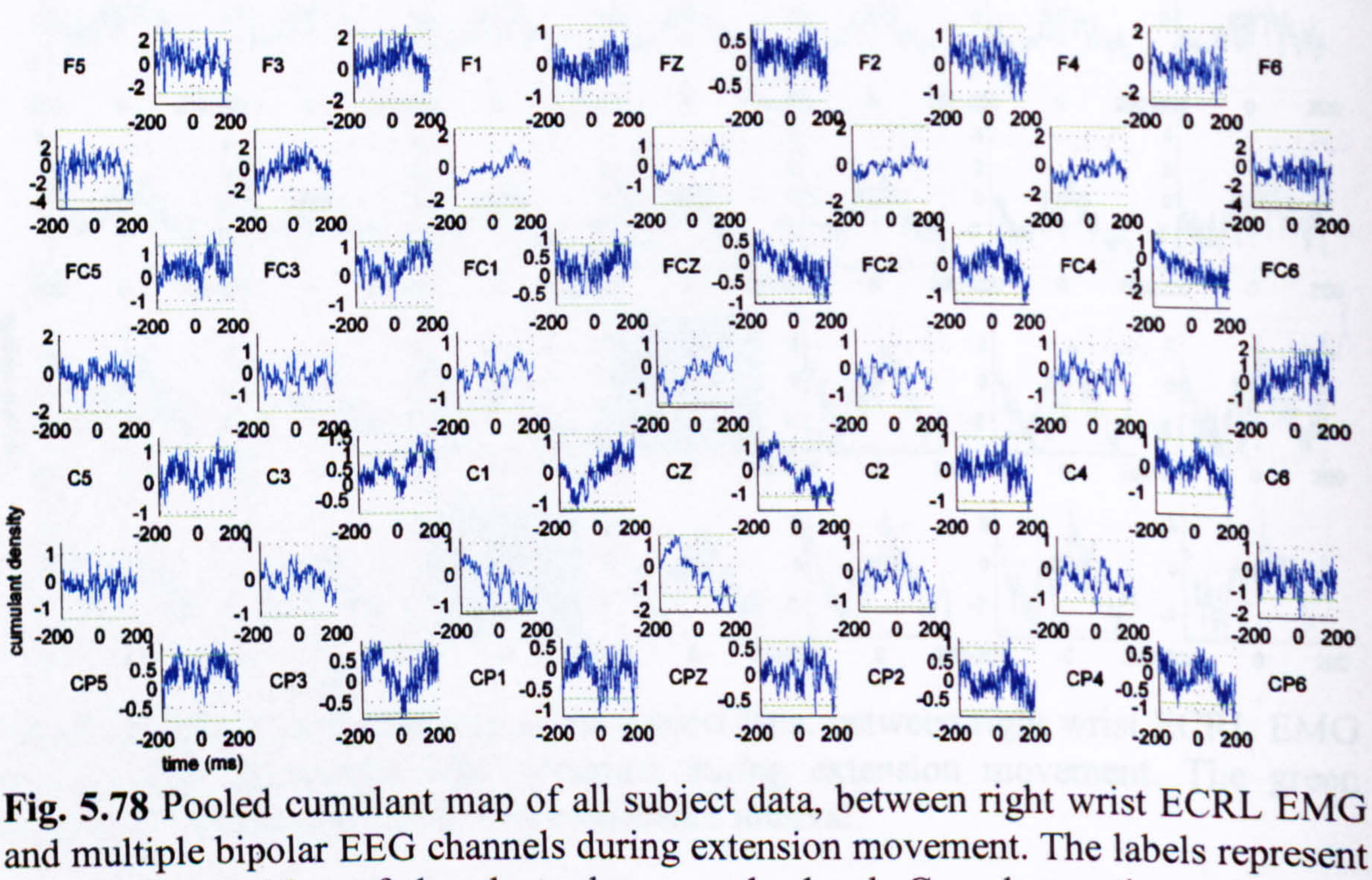

Fig. 5.78 Pooled cumulant map of all subject data, between right wrist ECRL EMG and multiple bipolar EEG channels during extension movement. The labels represent the relative position of the electrodes over the head. Cumulant estimate between EMG and a bipolar EEG channel, product of two vertically or horizontally aligned monopolar ones, is plotted between the labels of the two monopolar EEG electrodes. The green horizontal line represents the 95% confidence interval.

Fig. 5.77 shows the coherence estimate plots between ECRL muscle and multiple bipolar EEG channels during movement extension. The strong and widespread 21Hz coupling observed during posture (Fig. 5.54) is suppressed. A number of electrodes contains "high beta" (C1-CP1, CPZ-CP2 and CP5-CP3) and gamma coupling features (C2-C4, CP2-CP4 and CP4-CP6).

The beta coupling is also suppressed in the bipolar ECRL cumulant map (Fig. 5.78) where no significant coupling features can be observed. In a similar fashion to flexion movement (Fig. 5.37), 10Hz coupling appears for CPZ-CP2 and C2-CP2 electrodes. However, no analogous coupling features appear in the corresponding coherence plots in (Fig. 5.77).

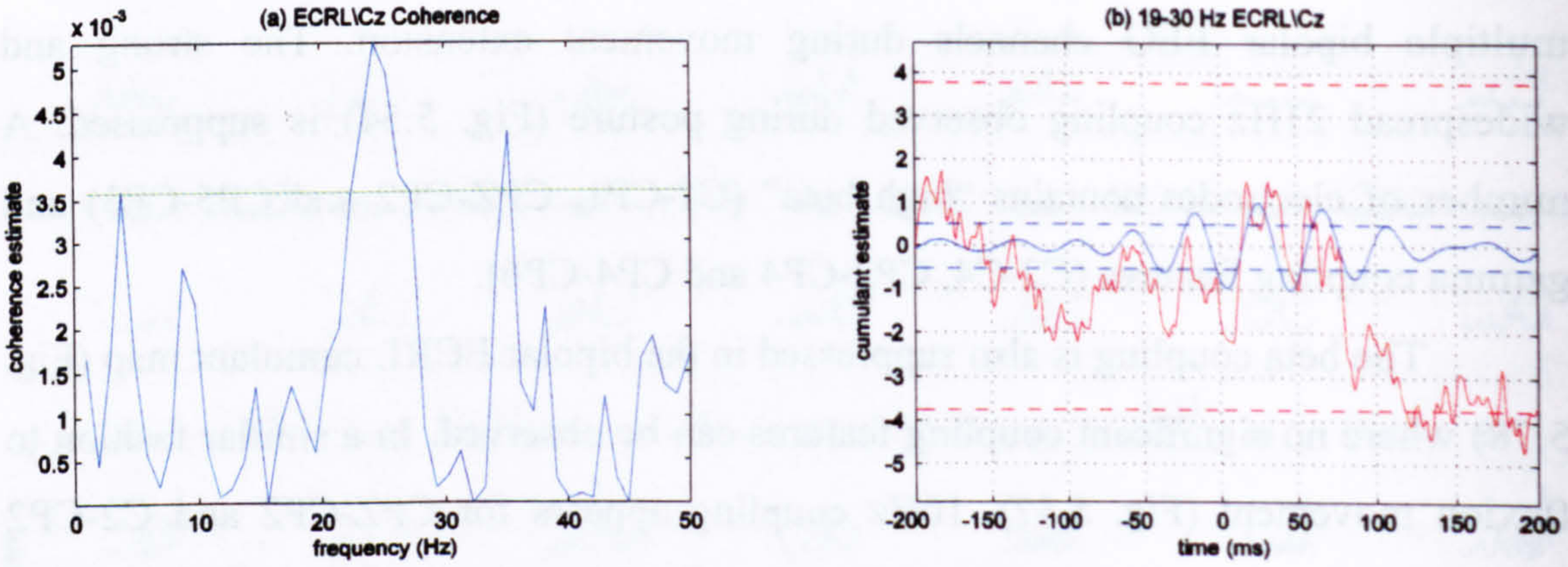

Fig. 5.79 ECRL\Cz coherence and corresponding cumulant plot (red plot) during movement extension. The blue plot represents the 19-30Hz cumulant component while the blue dashed lines represent the estimated upper and lower 95% confidence limits for the cumulant component.

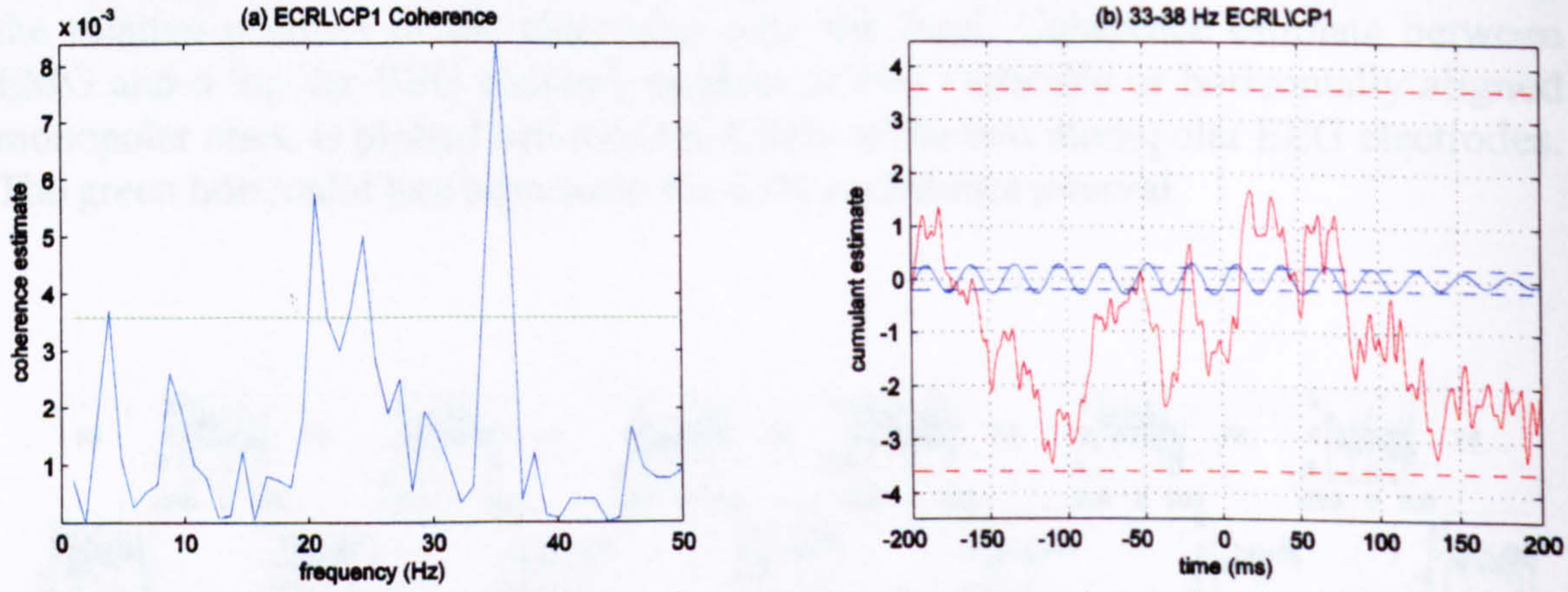

Fig. 5.80 ECRL\CP1 coherence and corresponding cumulant plot (red plot) during movement extension. The blue plot represents the 33-38Hz cumulant component while the blue dashed lines represent the estimated upper and lower 95% confidence limits for the cumulant component.

Fig. 5.79*b* shows the ECRL\Cz cumulant component for the 19-30Hz feature. The delay derived by the cumulant is not clear as an "out of phase" 5ms delay or an "in phase" 25ms can be detected. The phase plot indicates that the delay is 5.4±3.2ms supporting the "in phase" form of coupling suggesting that EMG is leading EEG.

Fig. 5.80*b* shows the ECRL\CP1 cumulant component for the 33-38Hz band. The ECRL\CP1 33-38Hz cumulant derives a delay of -5ms (phase: -5.4±1.5ms). The synchronisation appears to be "in phase" and the EEG leads the EMG as revealed by the -5ms delay.

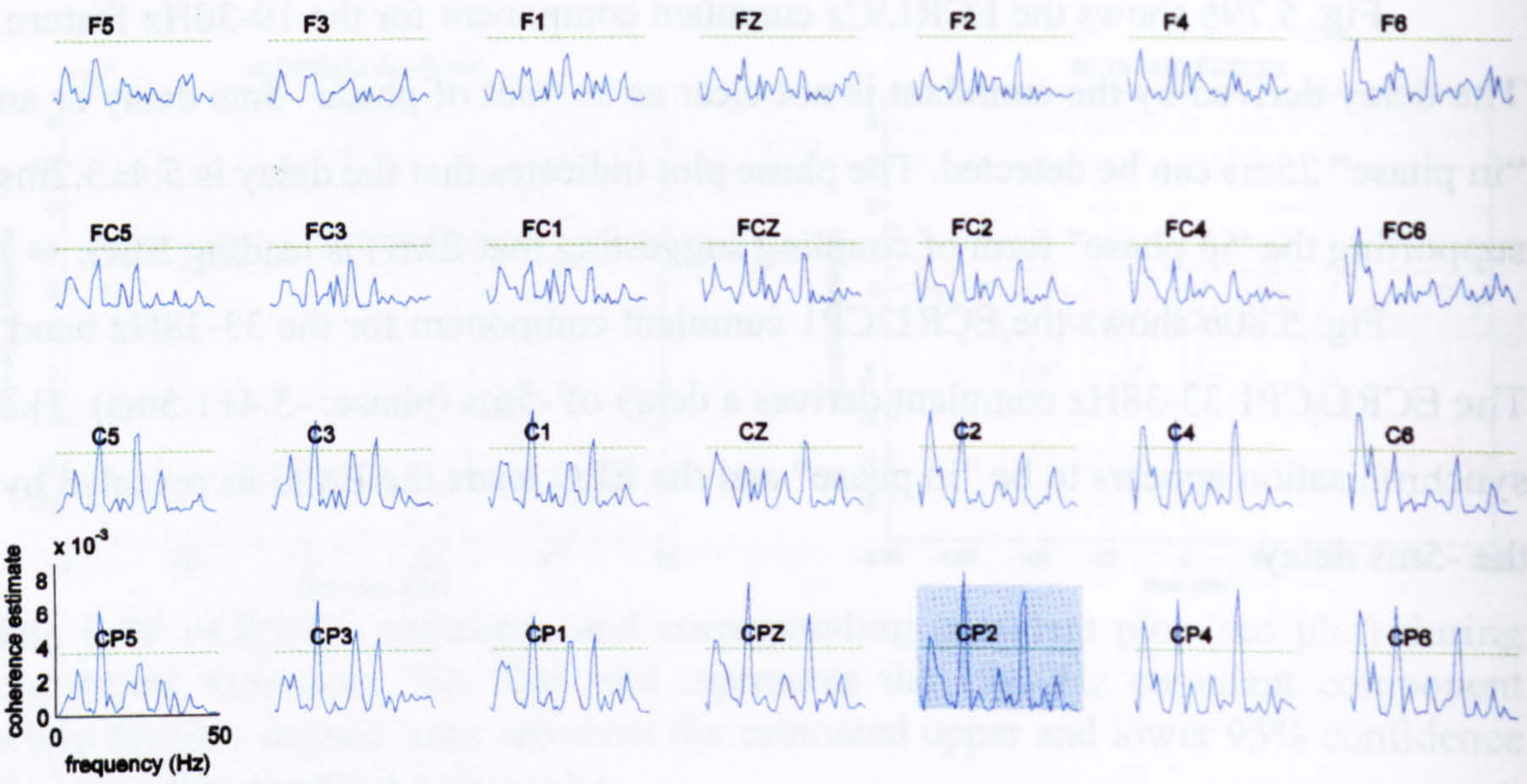

Fig. 5.81 Pooled coherence map of all subject data, between right wrist FCR EMG and multiple monopolar EEG channels during extension movement. The green horizontal line represents the 95% confidence interval.

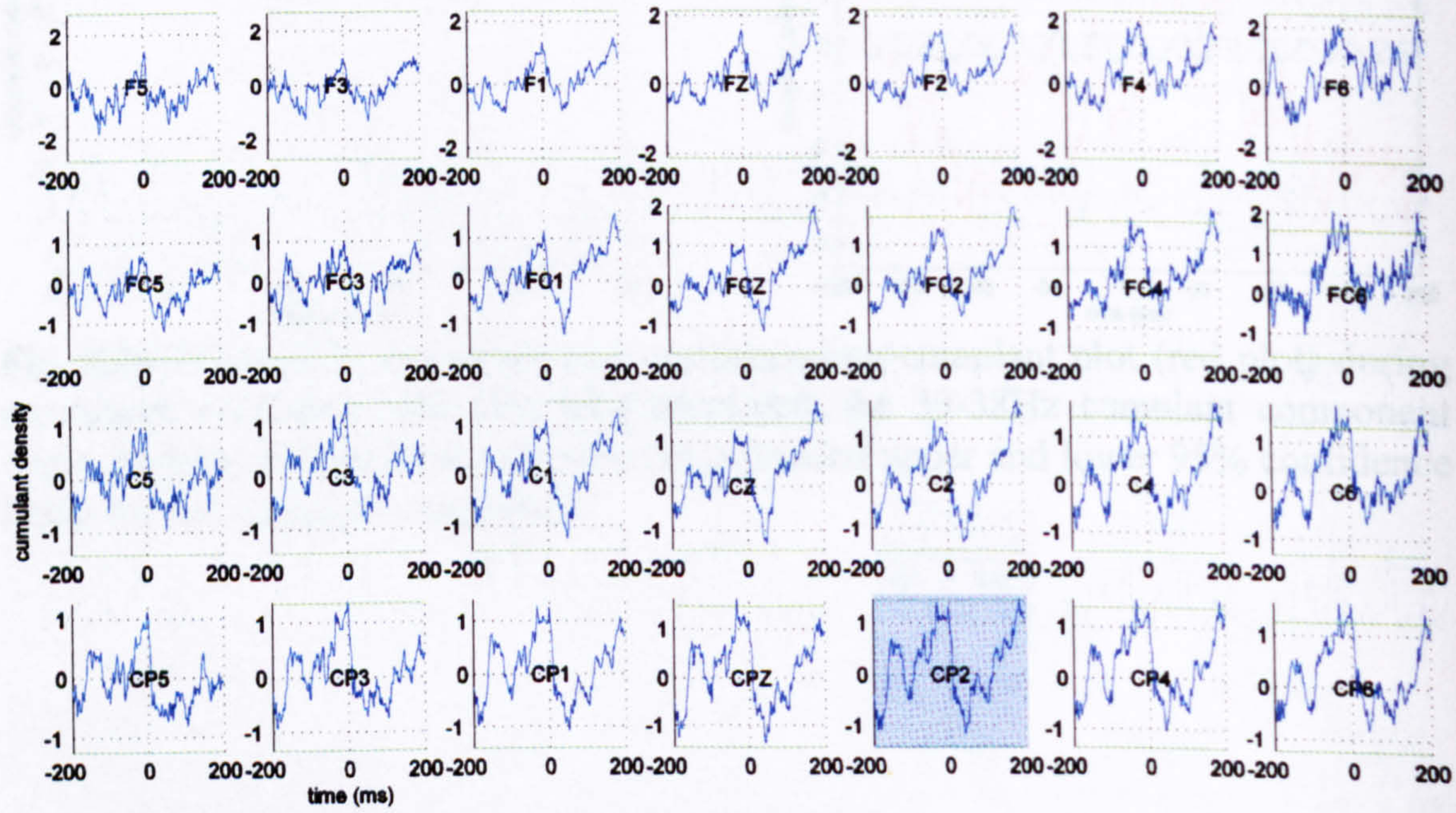

Fig. 5.82 Pooled cumulant map of all subject data, between right wrist FCR EMG and multiple monopolar EEG channels during extension movement. The green horizontal line represents the 95% confidence interval.

5.1.6.3.2 FCR coupling

Fig. 5.81 shows the coherence estimate plots between the FCR EMG and monopolar EEG channels during extension movement. The corticomuscular coherence map of the antagonist FCR shows a narrow beta peak at 15Hz across central and centroparietal electrodes. Gamma coupling (33Hz) appears for the same area while a "high beta" (26Hz) components appear in the contralateral areas and 4Hz ipsilaterally. The beta coupling observed during movement in the SMA and contralateral sensorimotor areas has been suppressed.

The cumulant map in Fig. 5.82 shows weak coupling features for central and centroparietal electrodes in the 15Hz area that are connected with the narrow coherence peaks in the same frequency range in the monopolar coherence map shown in Fig. 5.81.

Fig. 5.83 Pooled coherence map of all subject data, between right wrist FCR EMG and multiple bipolar EEG channels during extension movement. The labels represent the relative position of the electrodes over the head. Coherence estimate between EMG and a bipolar EEG channel, product of two vertically or horizontally aligned monopolar ones, is plotted between the labels of the two monopolar EEG electrodes. The green horizontal line represents the 95% confidence interval.

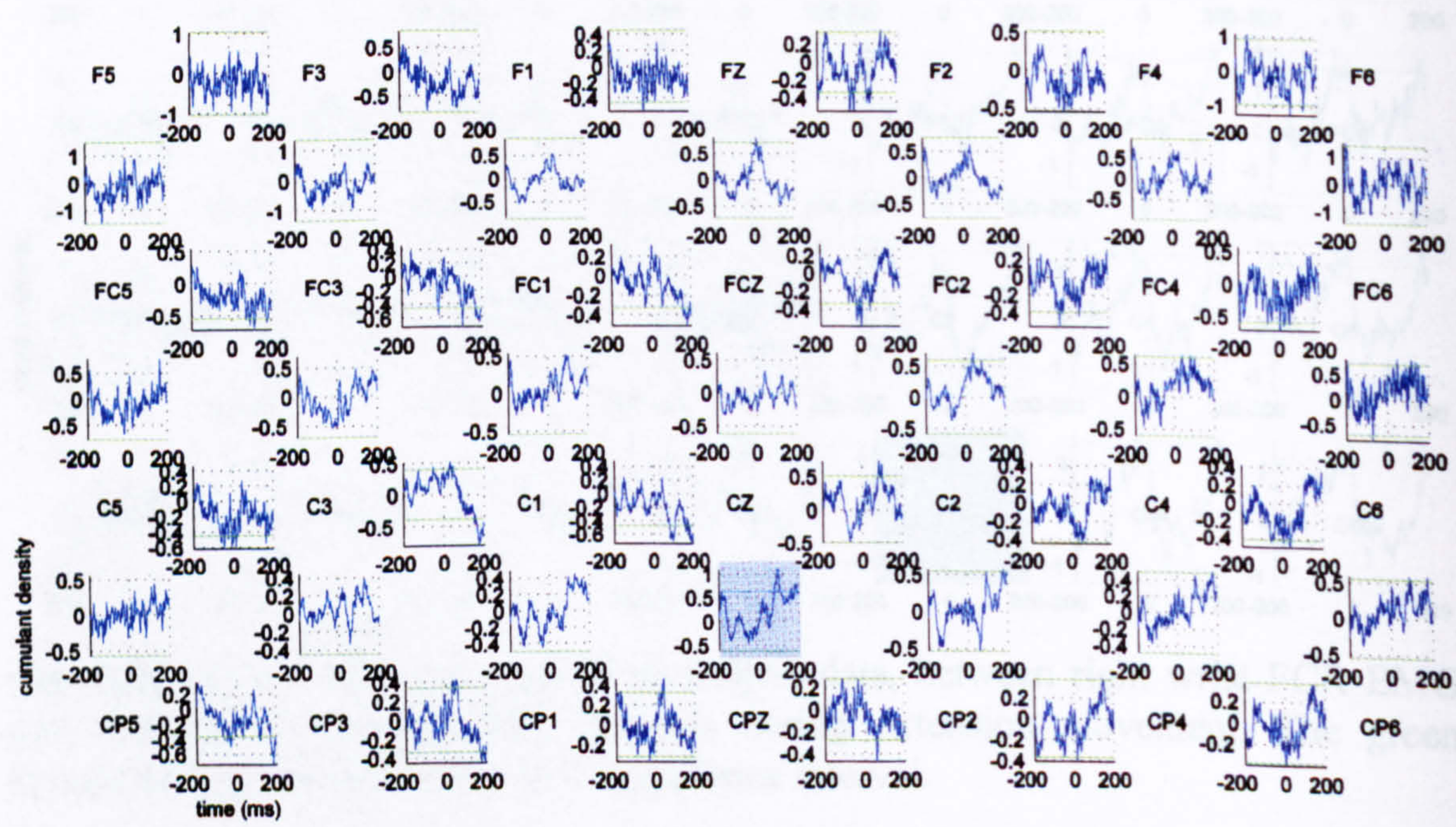

Fig. 5.84 Pooled cumulant map of all subject data, between right wrist FCR EMG and multiple bipolar EEG channels during extension movement. The labels represent the relative position of the electrodes over the head. Cumulant estimate between EMG and a bipolar EEG channel, product of two vertically or horizontally aligned monopolar ones, is plotted between the labels of the two monopolar EEG electrodes. The green horizontal line represents the 95% confidence interval.

Fig. 5.83 shows the coherence estimate plots between FCR muscle and multiple bipolar EEG channels during extension movement. The strong posture beta coherence has been suppressed. There is however localised alpha, beta and gamma peaks. The 4, 15, and 33Hz coherence components observed in the bipolar map, also appeared in the corresponding monopolar map (Fig. 5.81). 40-50Hz gamma features appeared in F1-Fz, Fz-F2, Fz-FCz, FCz-FC2, FC4-FC6, C5-C3,Cz-CPz, C2-CP2, C4-CP4, CP3-CP1 and CPz-C2. 4Hz features were present in Fz-F2, F2-F4, F4-F6, Fz-FCz, FCz-FC2, C3-C1, Cz-C2, C2-C4 and CP1-CPz electrode pairs. 15-20Hz features appeared in Fz-F2, C5-C3, C3-C1, C1-Cz, Cz-CPz, Cz-C2, CP5-CP2, and CPz-CP2, while 33Hz features existed for Fz-FCz, FC2-FC4, FC4-FC8, FC4-C4 and C5-C3 bipolar electrode pairs. Apparently there is no clear organisation in the above mentioned features.

The bipolar cumulant map does not contain any strong or widespread features for corticomuscular synchronisation. However in the ipsilateral centroparietal area alpha features appear. They are more obvious for CPZ-CP2 and CP2-CP4 channels.

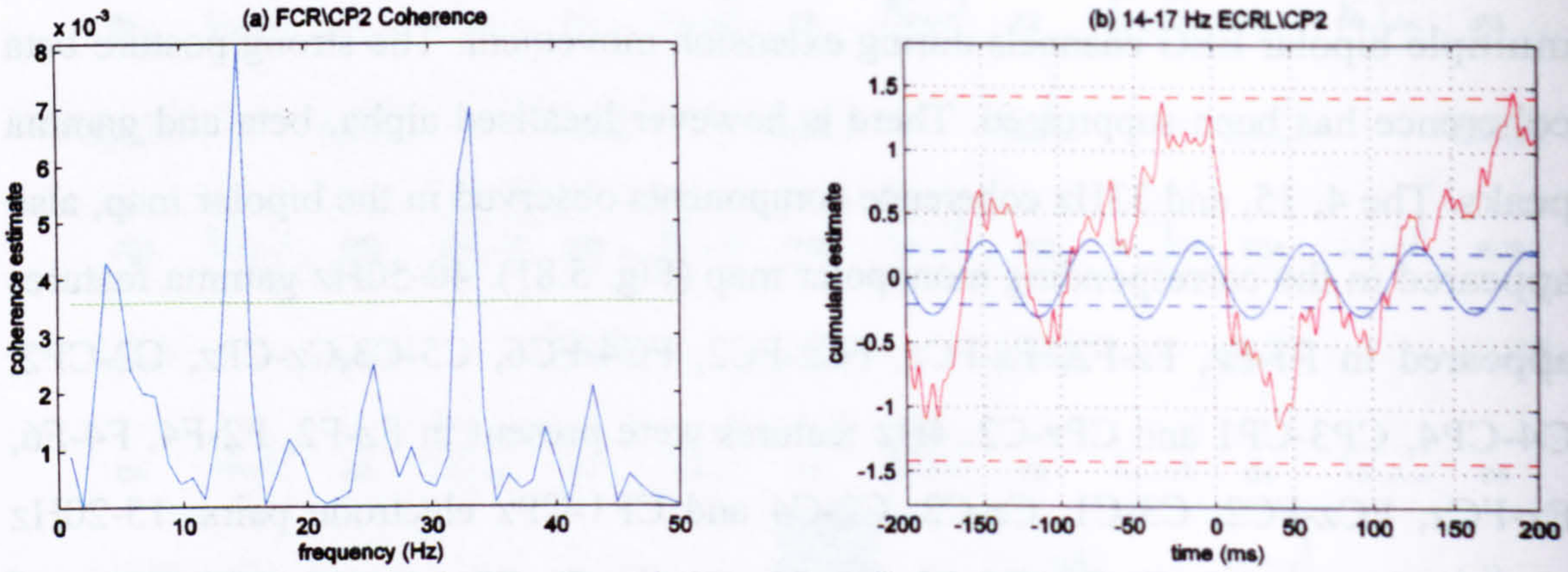

Fig. 5.85 FCR\CP2 coherence and corresponding cumulant plot (red plot) during movement extension. The blue plot represents the 14-17Hz cumulant component while the blue dashed lines represent the estimated upper and lower 95% confidence limits for the cumulant component.

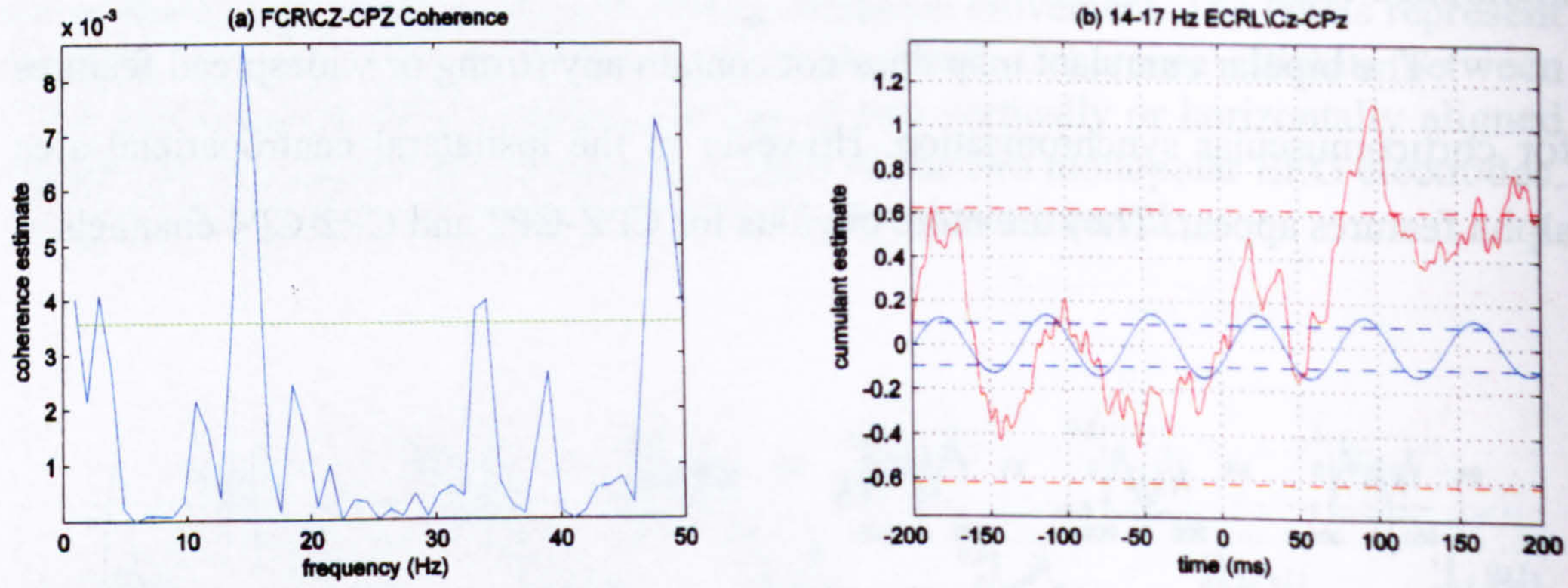

Fig. 5.86 FCR\Cz-CPz coherence and corresponding cumulant plot (red plot) during movement extension. The blue plot represents the 14-17Hz cumulant component while the blue dashed lines represent the estimated upper and lower 95% confidence limits for the cumulant component.

Fig. 5.85*b* and Fig. 5.86*b* show the 14-17Hz cumulant component for (monopolar) FCR\CP2 and (bipolar) FCR\Cz-CPz respectively. The delays measured by the cumulants are -10ms in both cases (phases gave -10.7±2.6 and -11.4±3.4 respectively). The similarities in frequency and delay suggest that the monopolar and bipolar cumulant feature are expressing the same underlying activity.

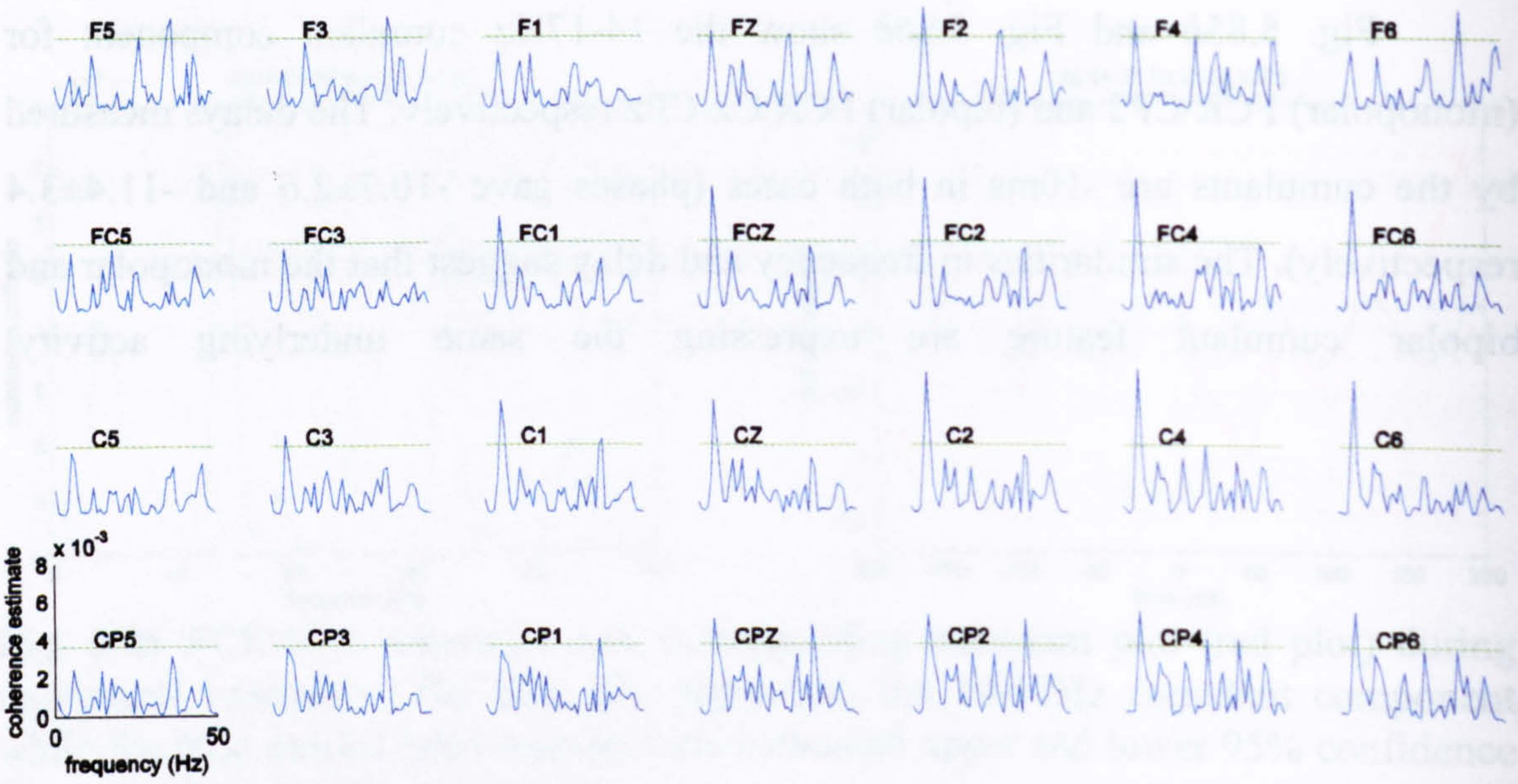

Fig. 5.87 Pooled coherence map of all subject data, between right BBLH EMG and multiple monopolar EEG channels during extension movement. The green horizontal line represents the 95% confidence interval.

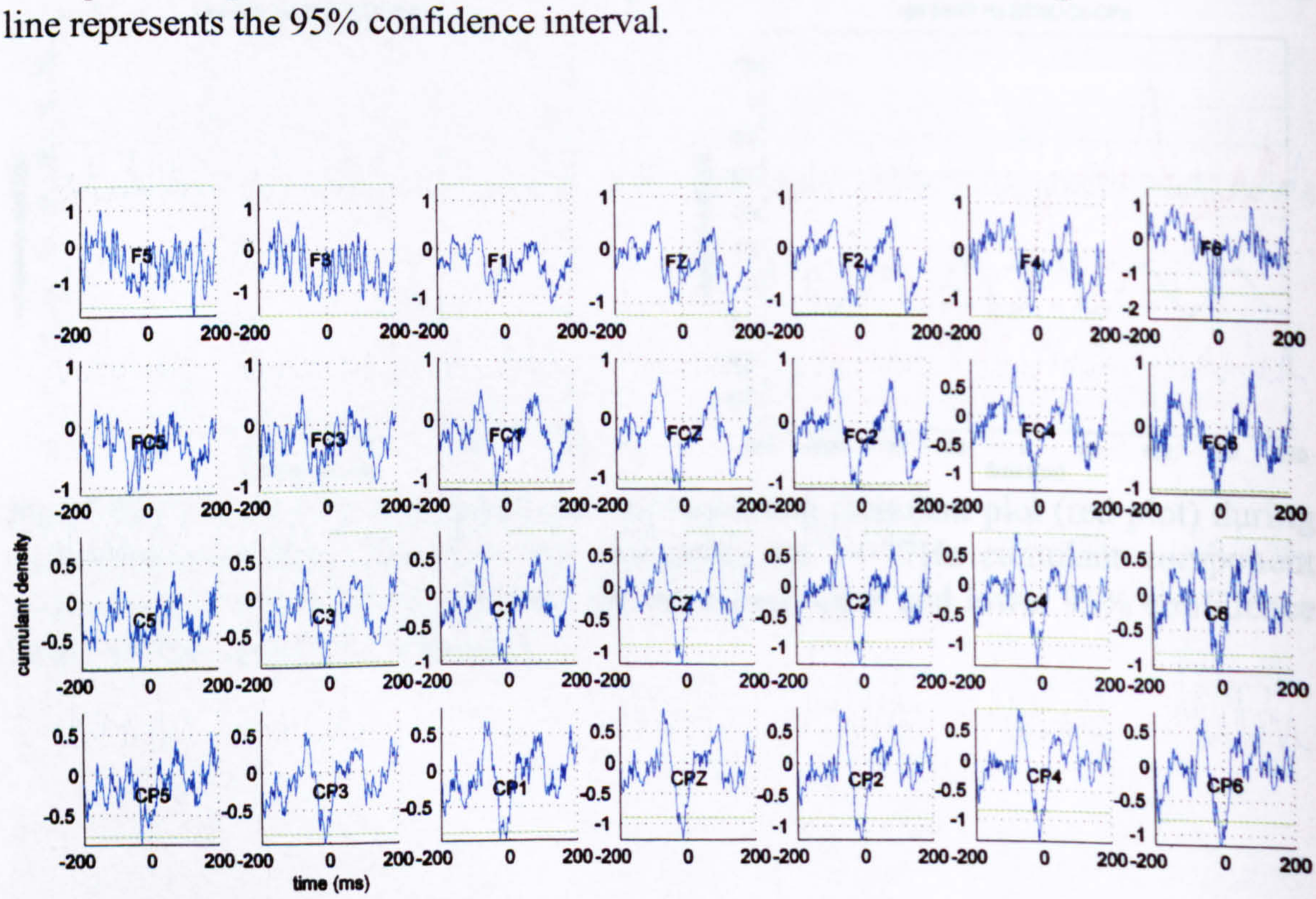

Fig. 5.88 Pooled cumulant map of all subject data, between right BBLH EMG and multiple monopolar EEG channels during extension movement. The green horizontal line represents the 95% confidence interval.

5.1.6.3.3 BBLH coupling

Fig. 5.87 shows the coherence estimate plots between BBLH EMG and monopolar EEG channels during movement extension. A widespread 6Hz narrow peak is the only important coupling feature in the monopolar coherence map. It is most apparent ipsilaterally and diminishes in amplitude towards the contralateral side. The same 6Hz synchronisation feature is also present in the corresponding cumulant map presented in Fig. 5.88.

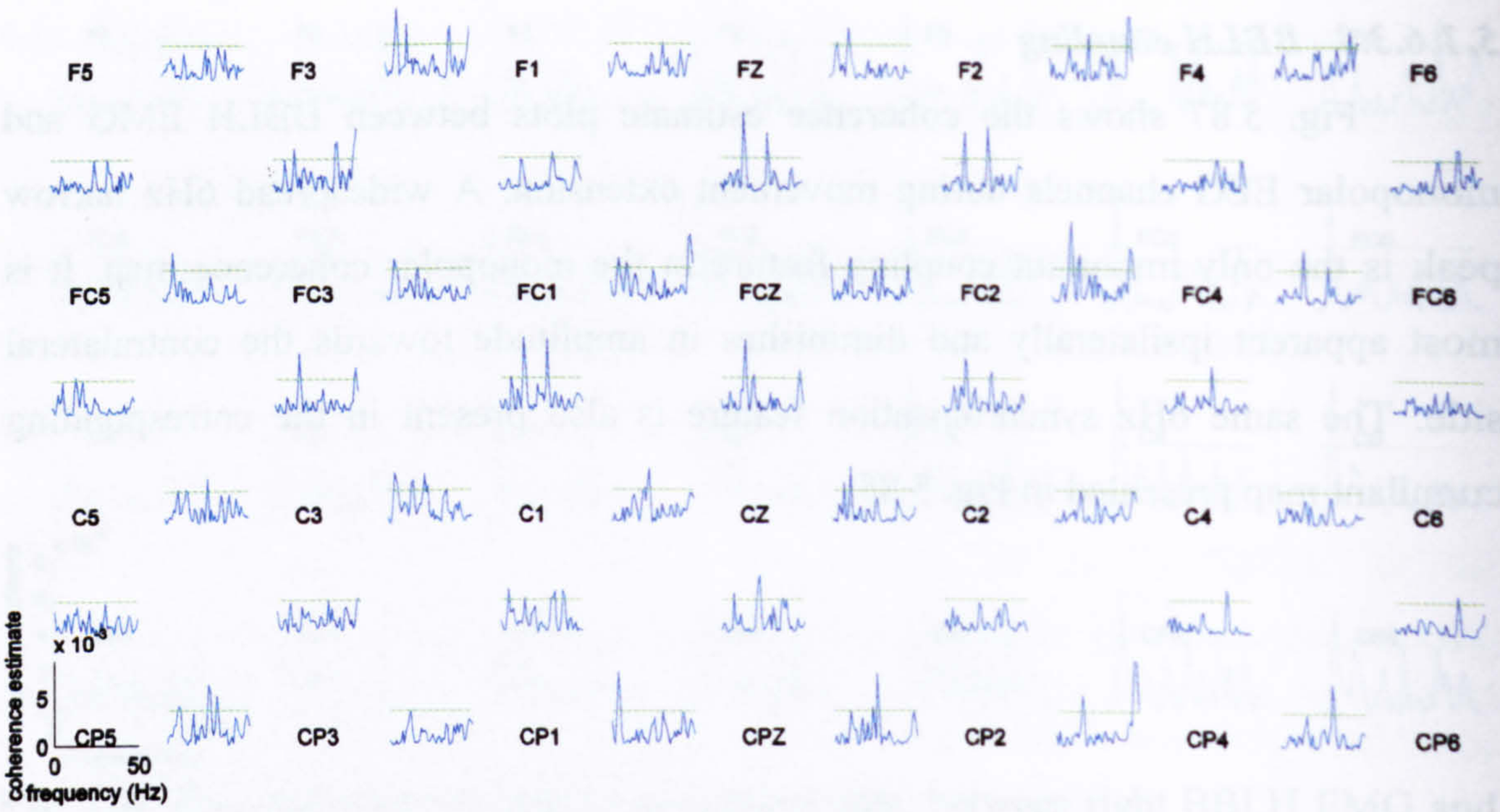

Fig. 5.89 Pooled coherence map of all subject data, between right BBLH EMG and multiple bipolar EEG channels during extension movement. The labels represent the relative position of the electrodes over the head. Coherence estimate between EMG and a bipolar EEG channel, product of two vertically or horizontally aligned monopolar ones, is plotted between the labels of the two monopolar EEG electrodes. The green horizontal line represents the 95% confidence interval.

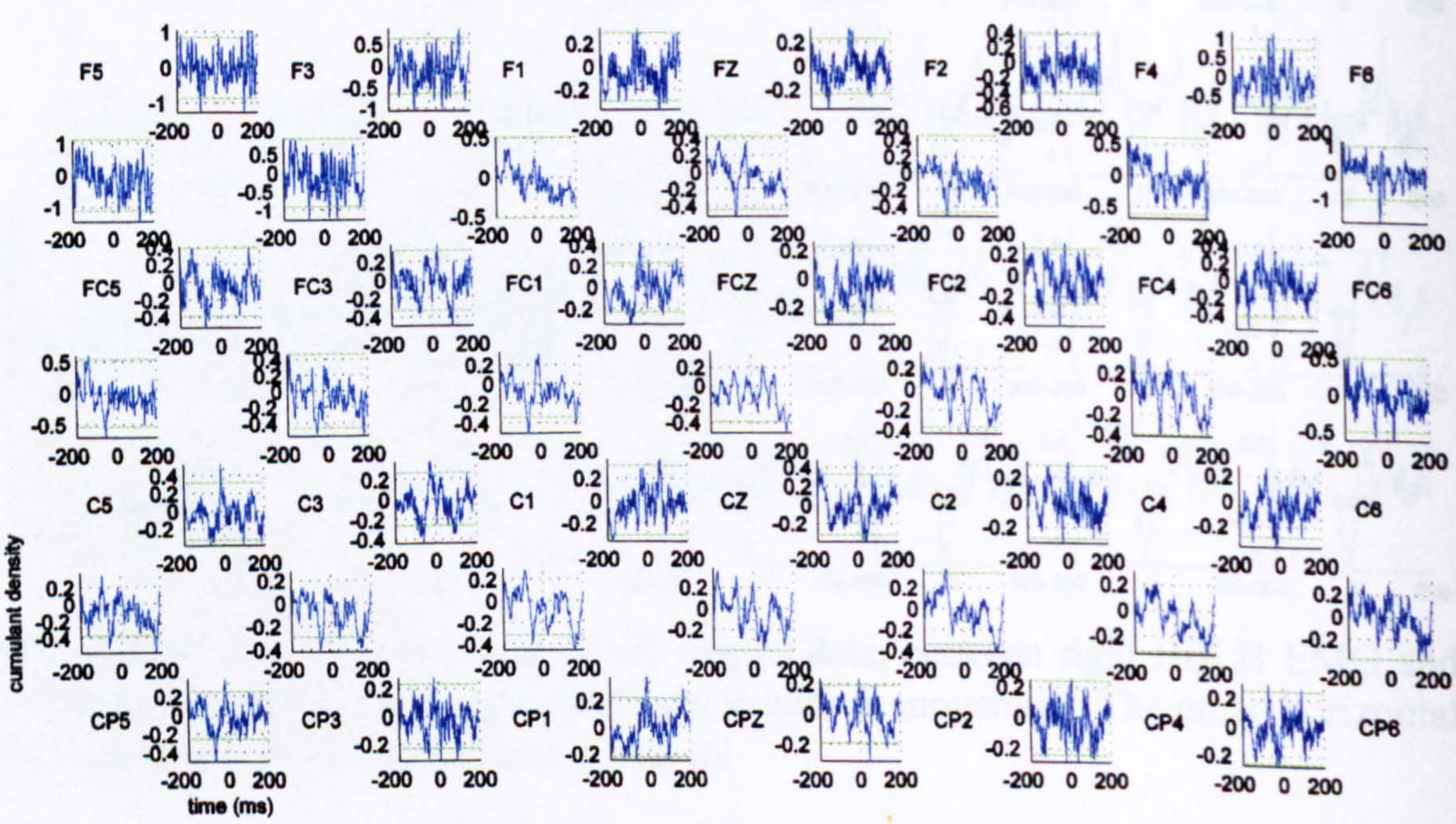

Fig. 5.90 Pooled cumulant map of all subject data, between right BBLH EMG and multiple bipolar EEG channels during extension movement. The labels represent the relative position of the electrodes over the head. Cumulant estimate between EMG and a bipolar EEG channel, product of two vertically or horizontally aligned monopolar ones, is plotted between the labels of the two monopolar EEG electrodes. The green horizontal line represents the 95% confidence interval.

Fig. 5.89 shows the coherence estimate plots between BBLH and bipolar EEG channels during the wrist movement extension phase. The strong beta coupling has been greatly suppressed despite the fact that the BBLH muscle is still involved in an isometric posture task. 16 and 29Hz peaks appear for medially located electrodes. 30 and 47Hz gamma coupling also occur for some electrodes, with no obvious organisation.

The weak beta features are not clearly represented in the corresponding cumulant map in Fig. 5.90. However some weak alpha features appear in the bipolar cumulant map despite not having a strong presence in the bipolar coherence map. These features are also widespread over a large area of the contralateral and especially ipsilateral cortices (mainly for central and centroparietal electrodes). CPZ-CP2, C4-CP4 and FC4-C4 are some of the electrodes for which these features are clearly seen.

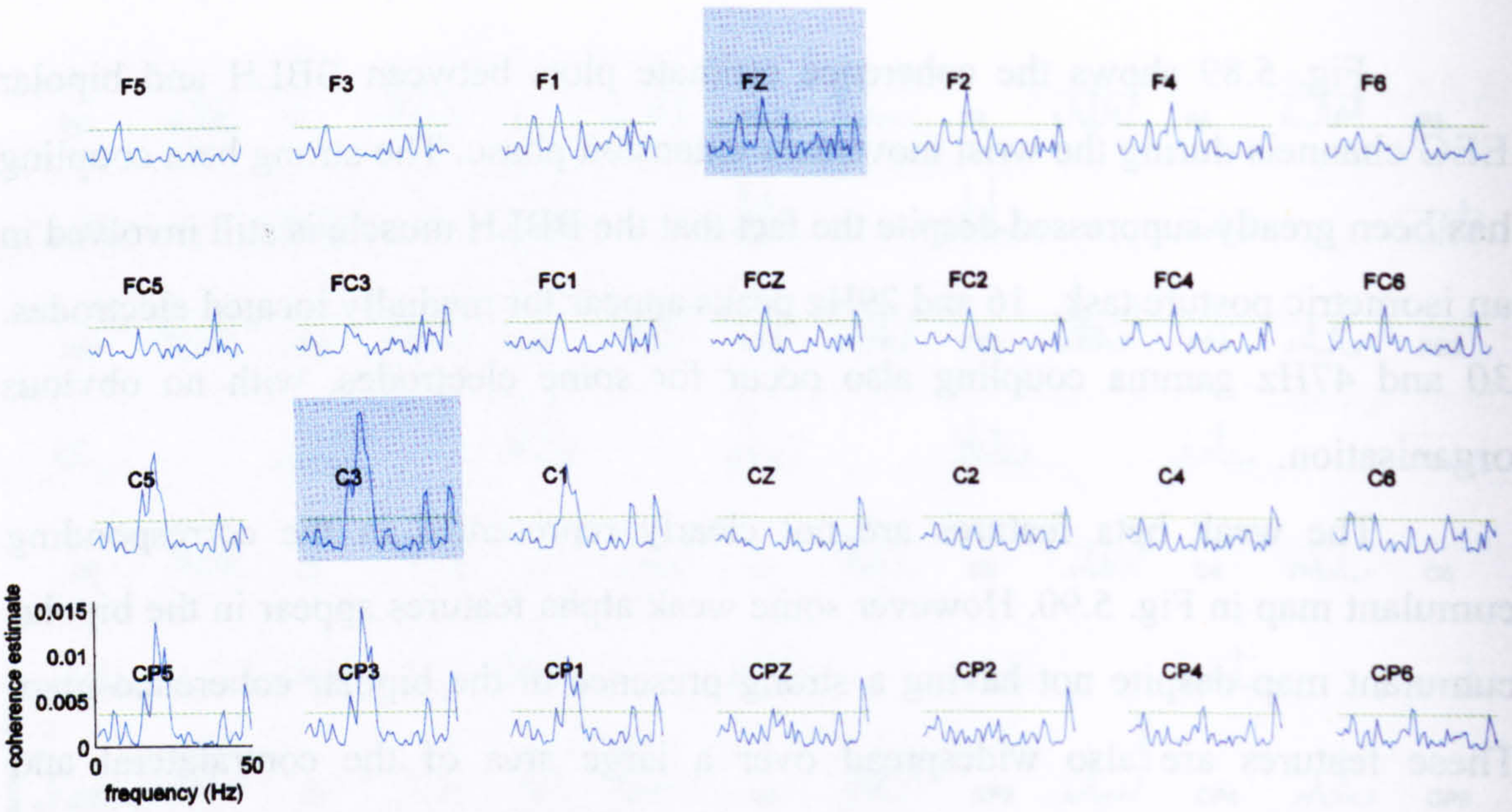

Fig. 5.91 Pooled coherence map of all subject data, between right wrist ECRL EMG and multiple monopolar EEG channels during extension posture. The green horizontal line represents the 95% confidence interval.

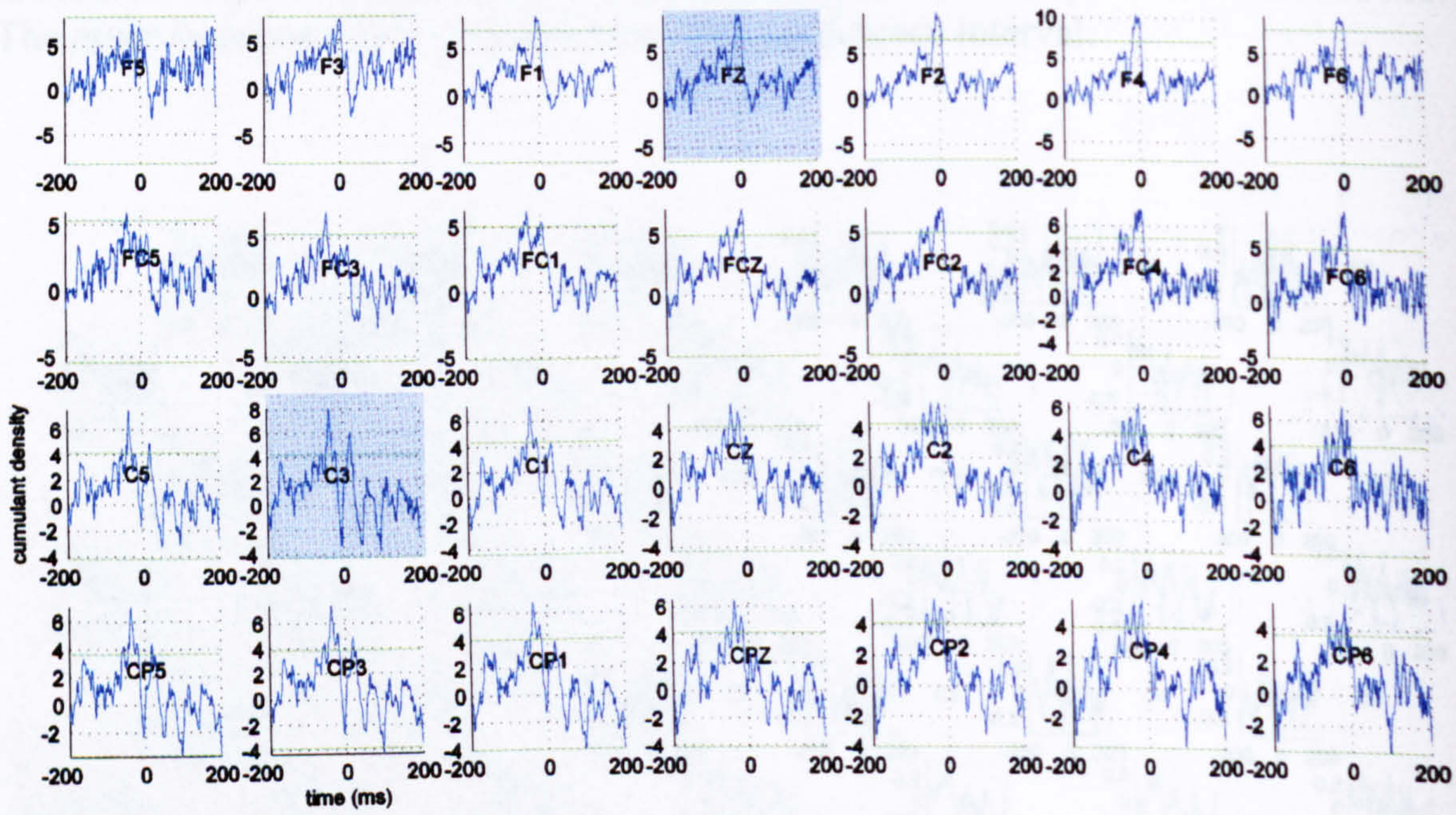

Fig. 5.92 Pooled cumulant map of all subject data, between right wrist ECRL EMG and multiple monopolar EEG channels during extension posture. The green horizontal line represents the 95% confidence interval.

5.1.6.4 Extension posture

5.1.6.4.1 ECRL coupling

Fig. 5.91 contains the coherence estimate map for the ECRL EMG (agonist) and monopolar EEG channels during extension posture. Strong beta coupling absent during the extension movement (Fig. 5.75), is now re-established during posture. Statistically significant coupling is observed in the beta band over contralateral central and centroparietal areas. The medial frontal lobe also shows beta coupling features. These features are smaller compared with the equivalent plot in Fig. 5.52 during flexion posture. The coherence is in the 14-25Hz range with a peak at 20Hz.

The monopolar cumulant map in Fig. 5.92 shows beta coupling for the same set of beta coupled electrodes as shown in the corresponding coherence map in Fig. 5.91. The coupling features do not exceed the confidence limits in all cases. However the beta coupling features are clear and widespread especially over the central and cenroparieal areas.

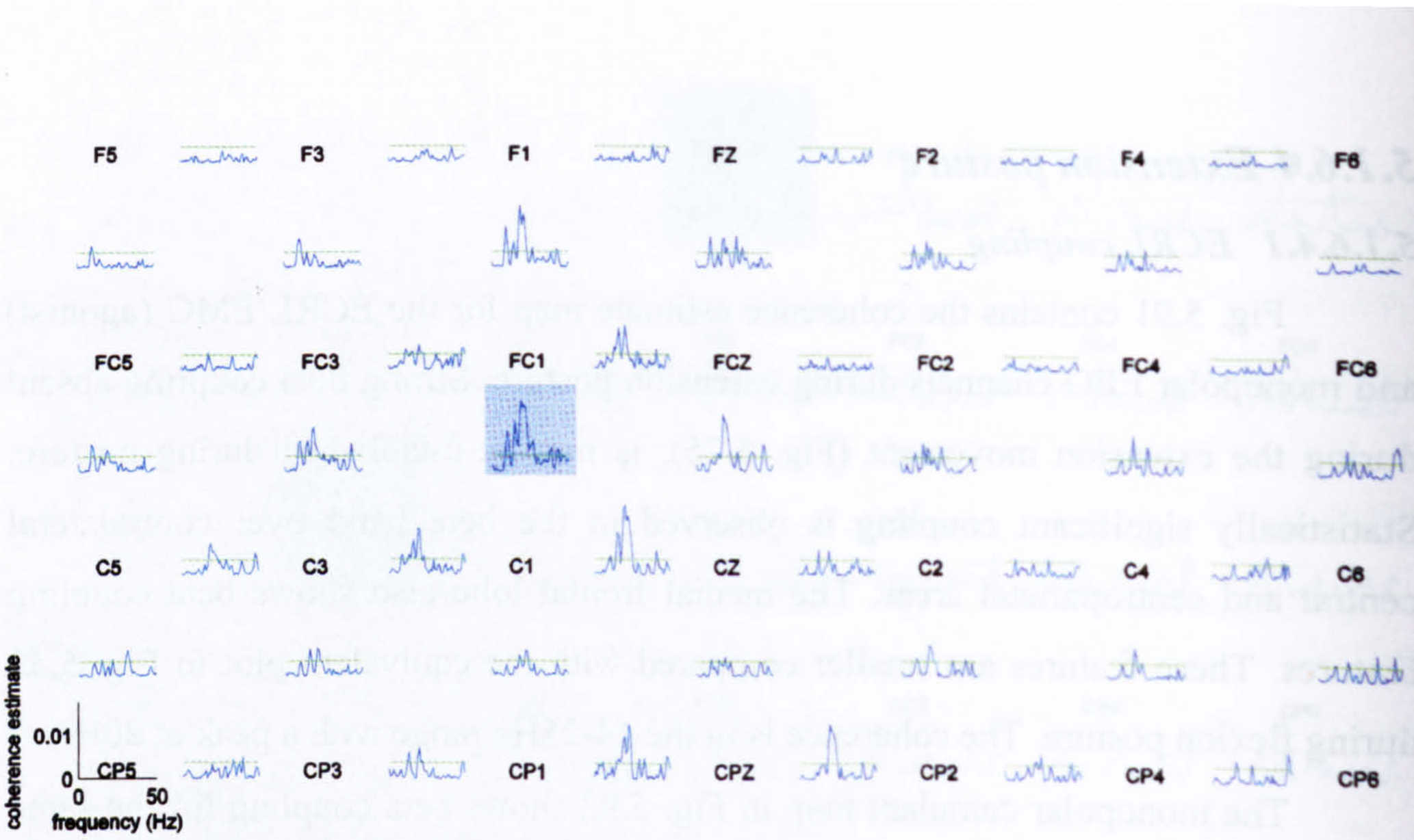

Fig. 5.93 Pooled coherence map of all subject data, between right wrist ECRL EMG and multiple bipolar EEG channels during extension posture. The labels represent the relative position of the electrodes over the head. Coherence estimate between EMG and a bipolar EEG channel, product of two vertically or horizontally aligned monopolar ones, is plotted between the labels of the two monopolar EEG electrodes. The green horizontal line represents the 95% confidence interval.

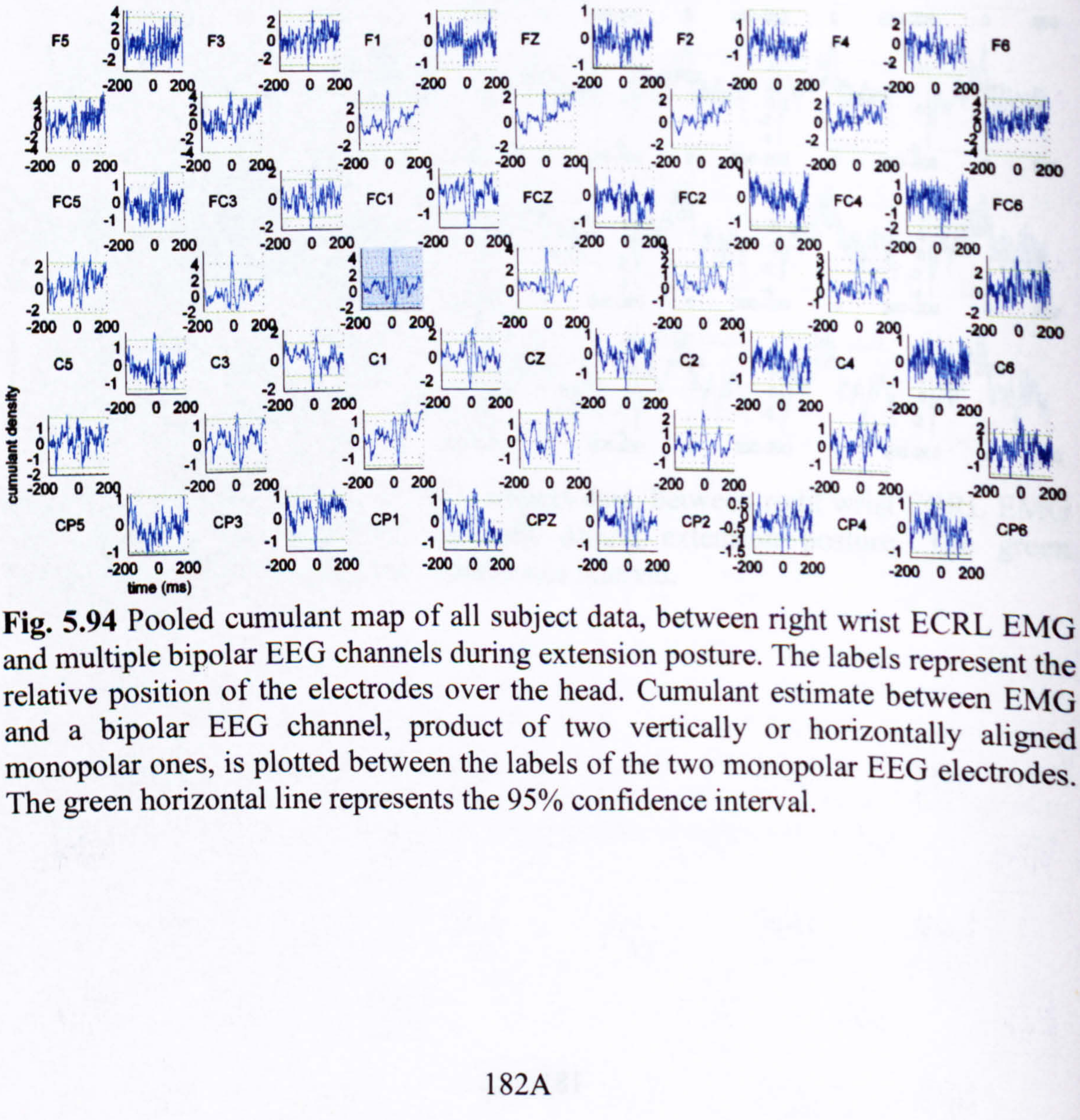

Fig. 5.94 Pooled cumulant map of all subject data, between right wrist ECRL EMG and multiple bipolar EEG channels during extension posture. The labels represent the relative position of the electrodes over the head. Cumulant estimate between EMG and a bipolar EEG channel, product of two vertically or horizontally aligned monopolar ones, is plotted between the labels of the two monopolar EEG electrodes. The green horizontal line represents the 95% confidence interval.

Fig. 5.93 contains the coherence estimate plots between the ECRL EMG and bipolar EEG channels during the posture extension phase. As expected, high beta coherence emerges during posture extension in the bipolar plot for contralateral central and frontocentral areas. The ECRL\EEG corticomuscular coherence during this posture is lower than the coherence seen when ECRL acted was coactive during flexion posture (Fig. 5.54). Distinct 10Hz and 15Hz coupling features coexist with the prominent 19-25Hz. Despite the strong alpha features in the bipolar coherence map, there is only weak occurrence of alpha coupling in the ECRL monopolar map (Fig. 5.91). This occurs mainly in the frontal lobe. Horizontally aligned C1-Cz has similar coherence magnitude to vertically aligned FC1-C1. In contrast in the corresponding map during posture flexion (Fig. 5.54), where FC1-C1 beta coherence feature was much larger than C1-Cz beta coherence feature.

The beta coupling can also be observed in the bipolar cumulant map in Fig. 5.94, for the same set of electrodes displaying statisticaly significant coherence in the bipolar coherence map. Alpha influences in the cumulant plot cannot be observed, possibly because they are masked by the prominent beta synchronisation for most of the channels.

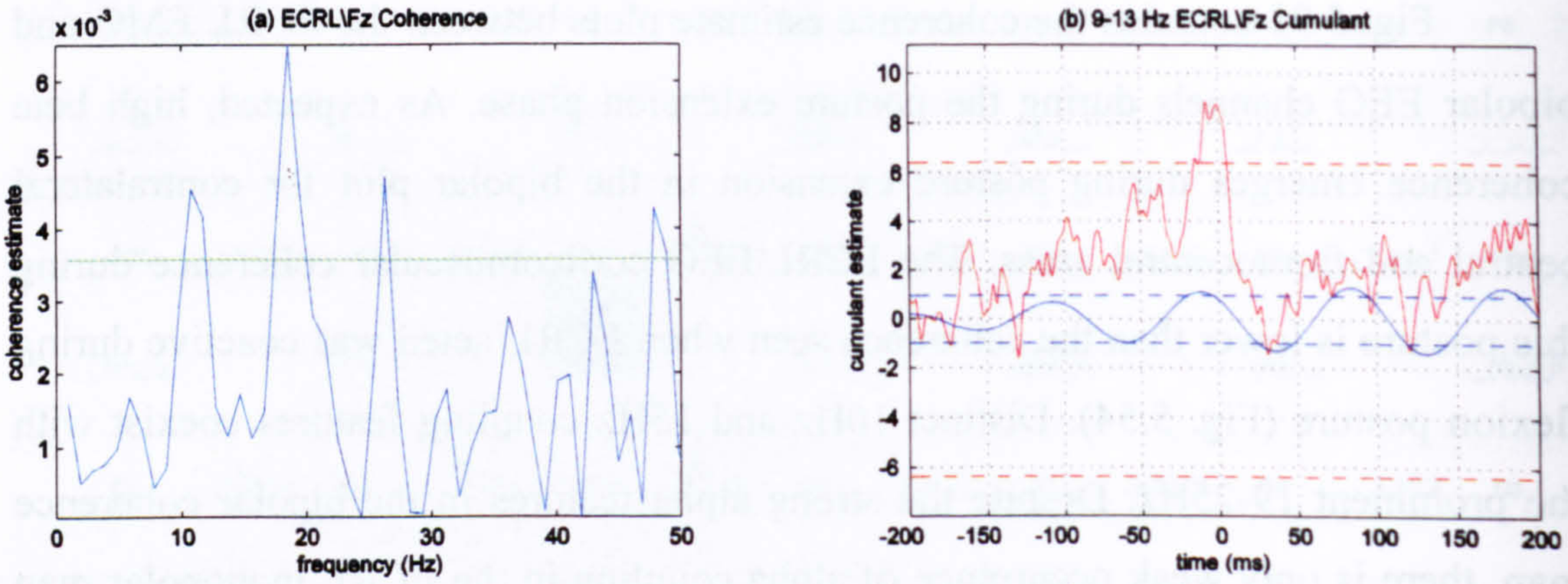

Fig. 5.95 ECRL\Fz coherence and corresponding cumulant plot (red plot) during posture extension. The blue plot represents the 9-13Hz cumulant component while the blue dashed lines represent the estimated upper and lower 95% confidence limits for the cumulant component.

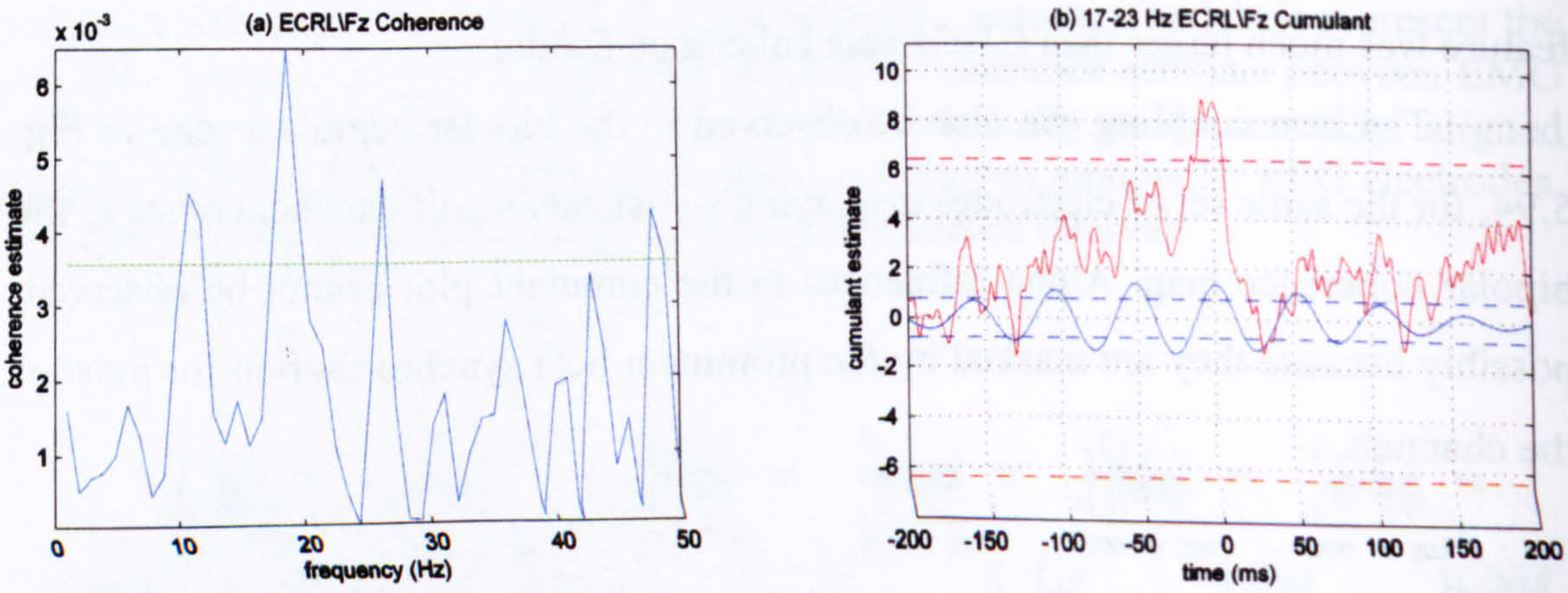

Fig. 5.96 ECRL\Fz coherence and corresponding cumulant plot (red plot) during posture extension. The blue plot represents the 17-23Hz cumulant component while the blue dashed lines represent the estimated upper and lower 95% confidence limits for the cumulant component.

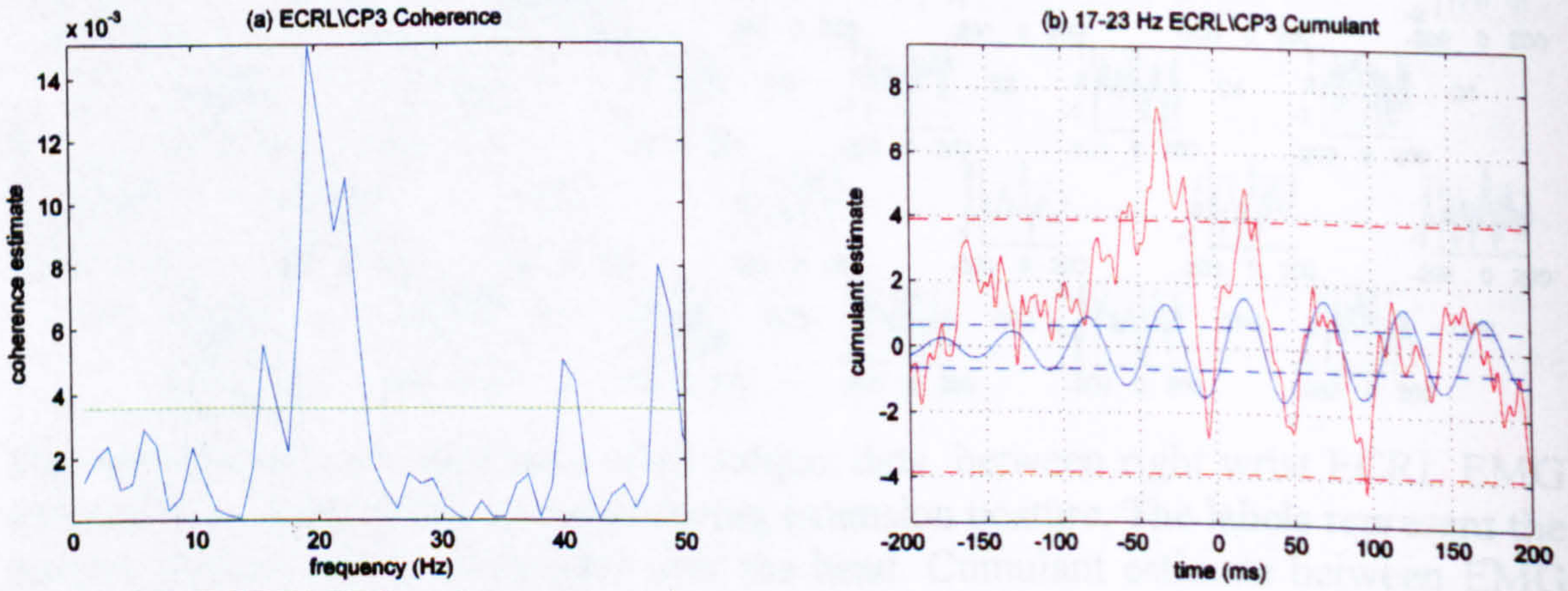

Fig. 5.97 ECRL\CP3 coherence and corresponding cumulant plot (red plot) during posture extension. The blue plot represents the 17-23Hz cumulant component while the blue dashed lines represent the estimated upper and lower 95% confidence limits for the cumulant component.

Fig. 5.95 and Fig. 5.96 show the 9-13Hz and 17-23Hz cumulant components respectively between ECRL\Fz. Both couplings are "in phase" and 9-13Hz component gives 12ms EMG\EEG delay (phase: -7.9±1.0ms) while the 17-23Hz gives a delay of 0ms (phase: -1.6±2.4ms). In both cases EEG appears to lead the EMG.

Fig. 5.97*b* shows the ECRL\CP3 17-23Hz posture extension cumulant component that corresponds to the peak of the respective coherence plot. CP3 is located in the contralateral centroparietal area which is one of the two centres of increased corticomuscular coherence during posture. The coupling appears to be "out of phase" with a delay of -7ms (phase: -3.2±4.4ms). The wideband cumulant gives a minimum at -5ms.

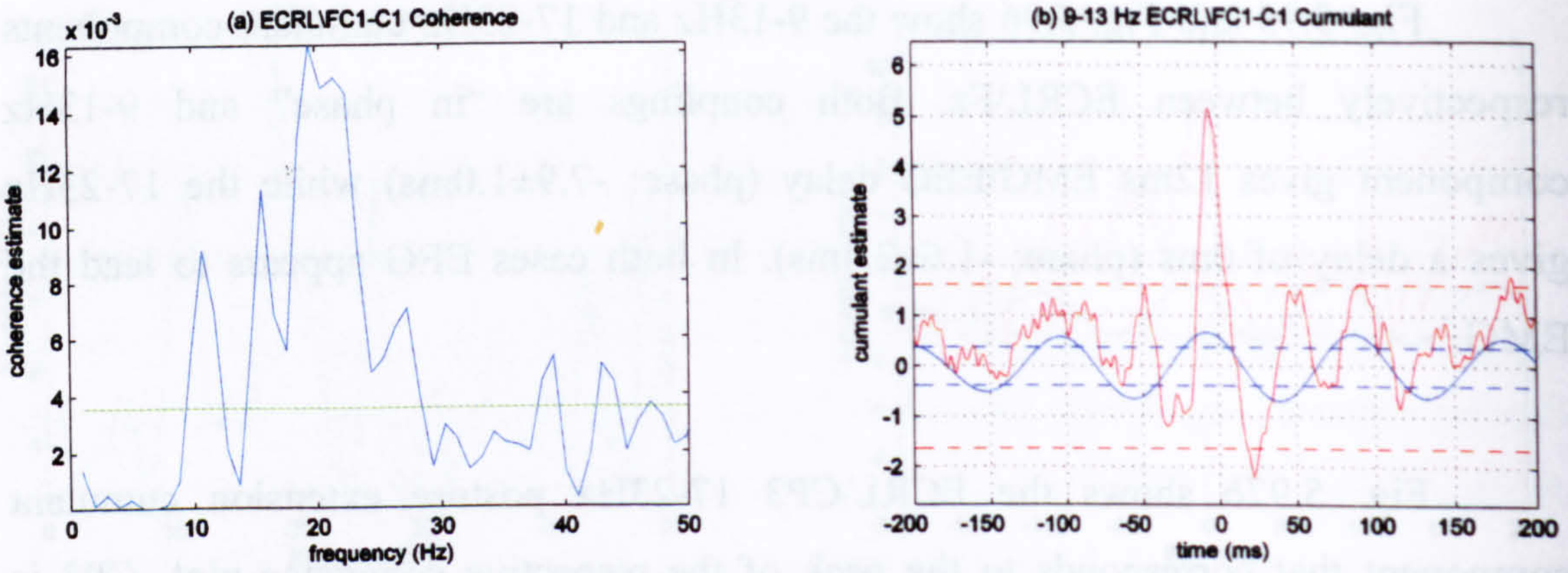

Fig. 5.98 FCR\FC1-C1 coherence and corresponding cumulant plot (red plot) during posture flexion. The blue plot represents the 9-13 cumulant component while the blue dashed lines represent the estimated upper and lower 95% confidence limits for the cumulant component.

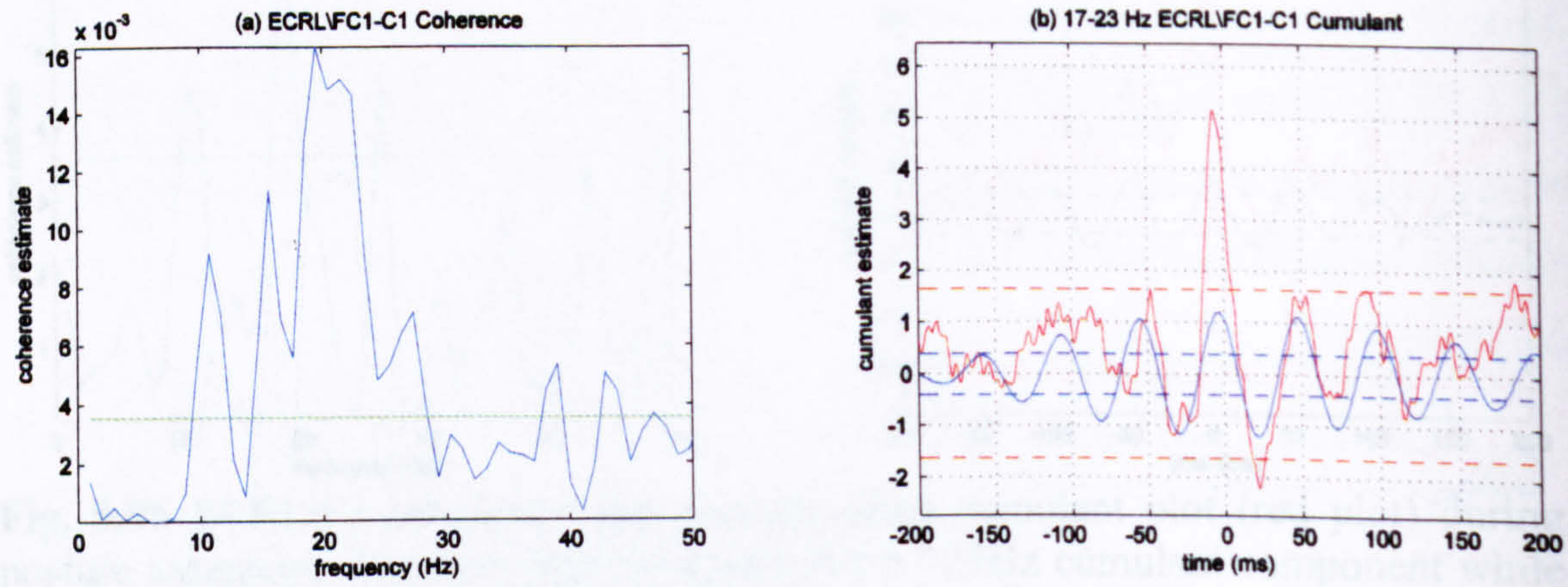

Fig. 5.99 ECRL\FC1-C1 coherence and corresponding cumulant plot (red plot) during posture extension. The blue plot represents the 17-23 cumulant component while the blue dashed lines represent the estimated upper and lower 95% confidence limits for the cumulant component.

Fig. 5.98 and figure Fig. 5.99 show the 9-13Hz and 17-23Hz cumulant components respectively. The 9-13Hz cumulant gives -8ms EMG\EEG delay (phase: -8.2±7.9ms) while the 17-23Hz component derives -4ms delay (phase: -3.8±3.0ms). Both couplings are "in phase" with the EEG leading the EMG.

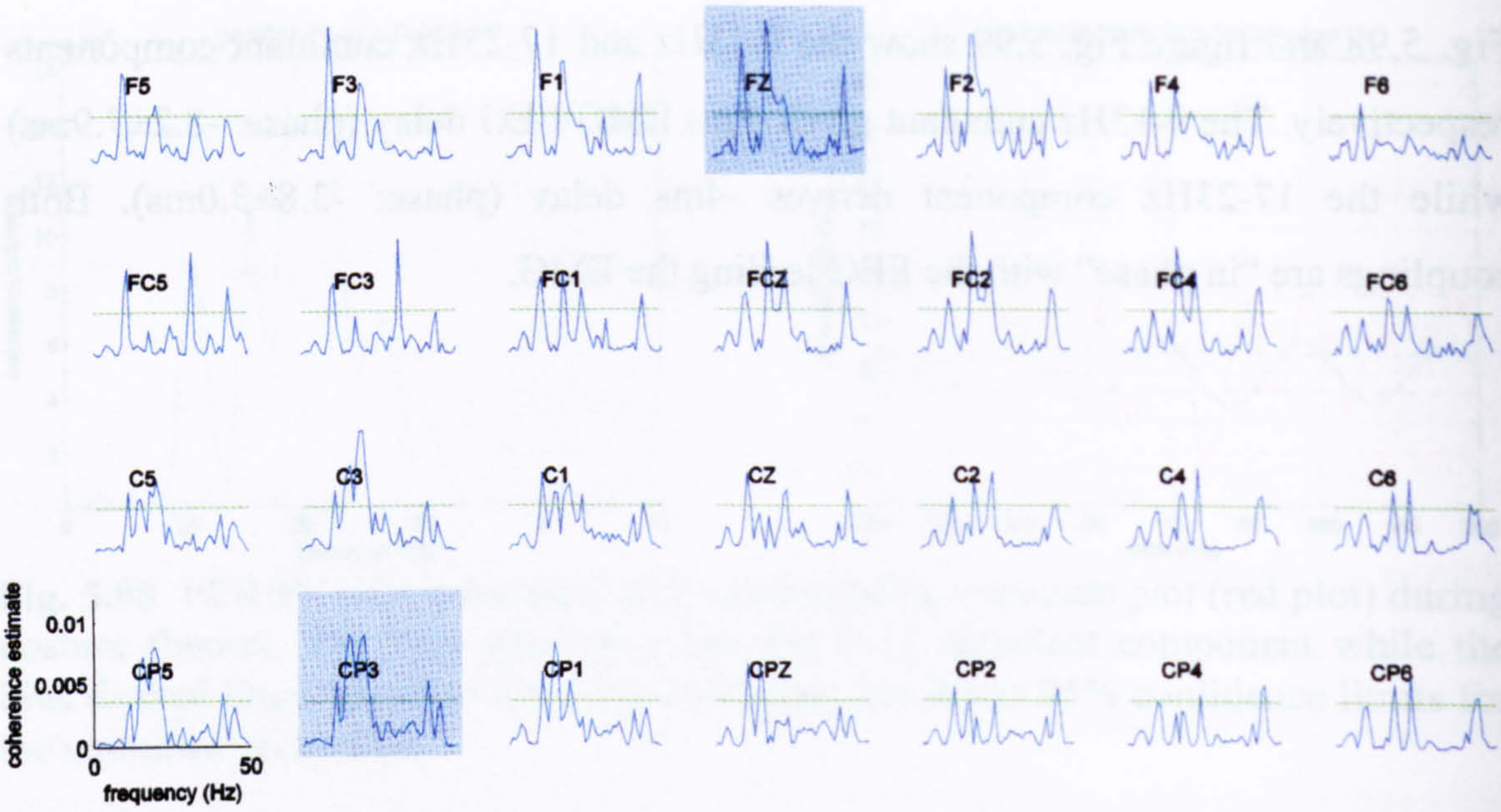

Fig. 5.100 Pooled coherence map of all subject data, between right wrist FCR EMG and multiple monopolar EEG channels during extension posture. The green horizontal line represents the 95% confidence interval.

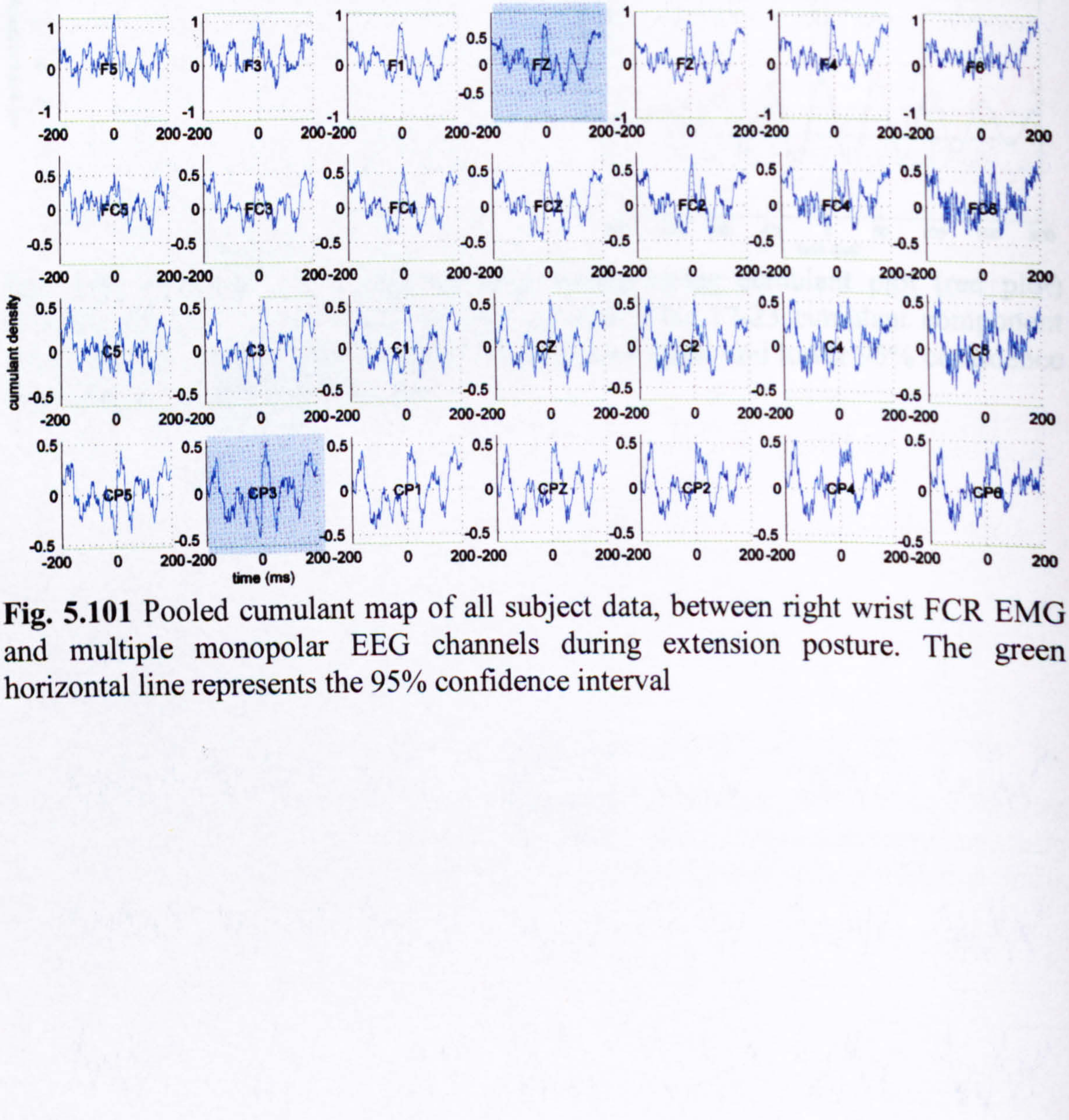

Fig. 5.101 Pooled cumulant map of all subject data, between right wrist FCR EMG and multiple monopolar EEG channels during extension posture. The green horizontal line represents the 95% confidence interval

5.1.6.4.2 FCR coupling

Fig. 5.100 shows the corticomuscular map between FCR muscle and monopolar EEG channels during the extension posture. Beta coupling is widespread across the whole cortical area. The strongest coherence appears at the contralateral centroparietal and central areas (peaks at 15Hz and 20Hz), as well as medial frontal and frontocentral areas (20Hz). Strong alpha coupling at 11Hz appears for frontal and frontocentral electrodes. Some widespread but small magnitude gamma coupling at 44Hz is also present.

The corresponding cumulant plot (Fig. 5.101) as expected is influenced by synchronisation over a wide range of frequencies, but mainly in alpha and beta bands where the alpha cumulant density features dominate the map. The alpha synchronisation is especially clear for the central and centroparietal electrodes despite the fact that for ipsilateral centroparietal electrodes, there is no statisticaly significant alpha coherence present in the corresponding coherence plots.

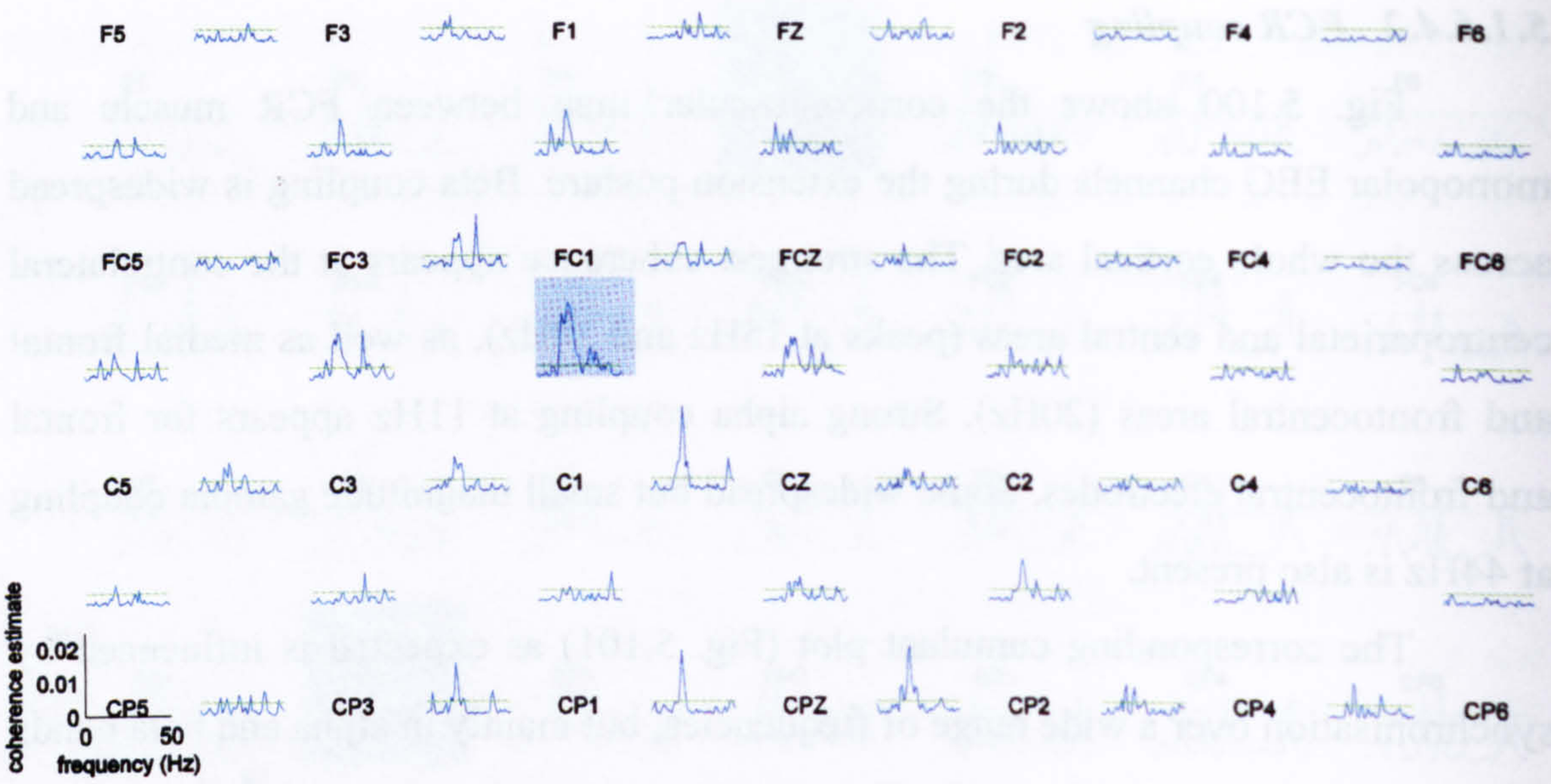

Fig. 5.102 Pooled coherence map of all subject data, between right wrist FCR EMG and multiple bipolar EEG channels during extension posture. The labels represent the relative position of the electrodes over the head. Coherence estimate between EMG and a bipolar EEG channel, product of two vertically or horizontally aligned monopolar ones, is plotted between the labels of the two monopolar EEG electrodes. The green horizontal line represents the 95% confidence interval.

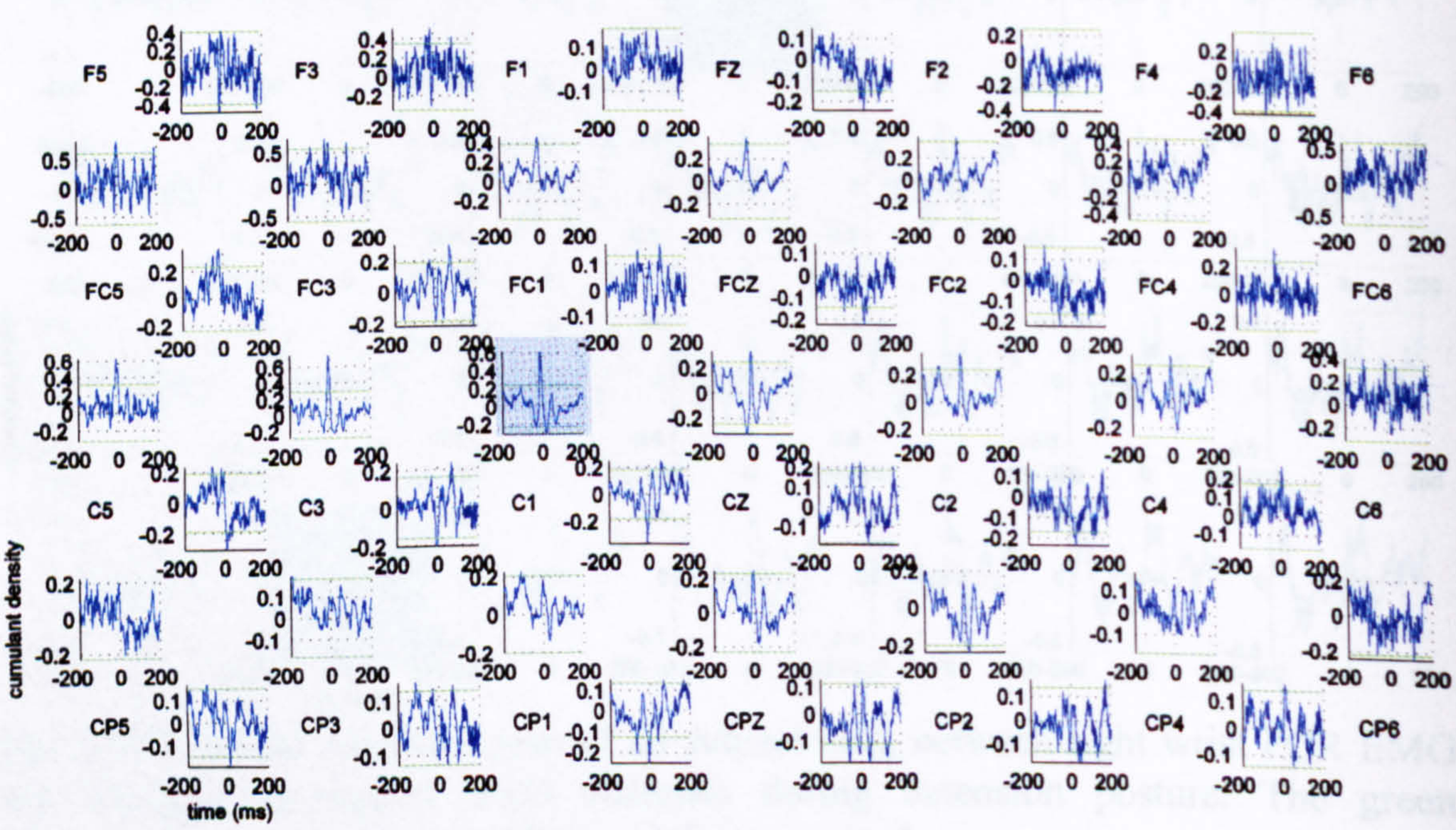

Fig. 5.103 Pooled cumulant map of all subject data, between right wrist FCR EMG and multiple bipolar EEG channels during extension posture. The labels represent the relative position of the electrodes over the head. Cumulant estimate between EMG and a bipolar EEG channel, product of two vertically or horizontally aligned monopolar ones, is plotted between the labels of the two monopolar EEG electrodes. The green horizontal line represents the 95% confidence interval.

Fig. 5.102 shows the corticomuscular map between FCR and the bipolar EEG channels during extension posture. The vertically aligned FC1-C1 bipolar electrode pair gives the highest beta coherence, with horizontal C1-CZ showing a large coupling in the same band. The 10, 15 and 20Hz components, observed in the ECRL bipolar and FCR monopolar maps can be observed here as well, but are differently distributed. Many electrodes also show increased gamma activation at approximately 35Hz and 45Hz (especially FC5-C5, FC3-C3, FC1-C1 and FCz-Cz).

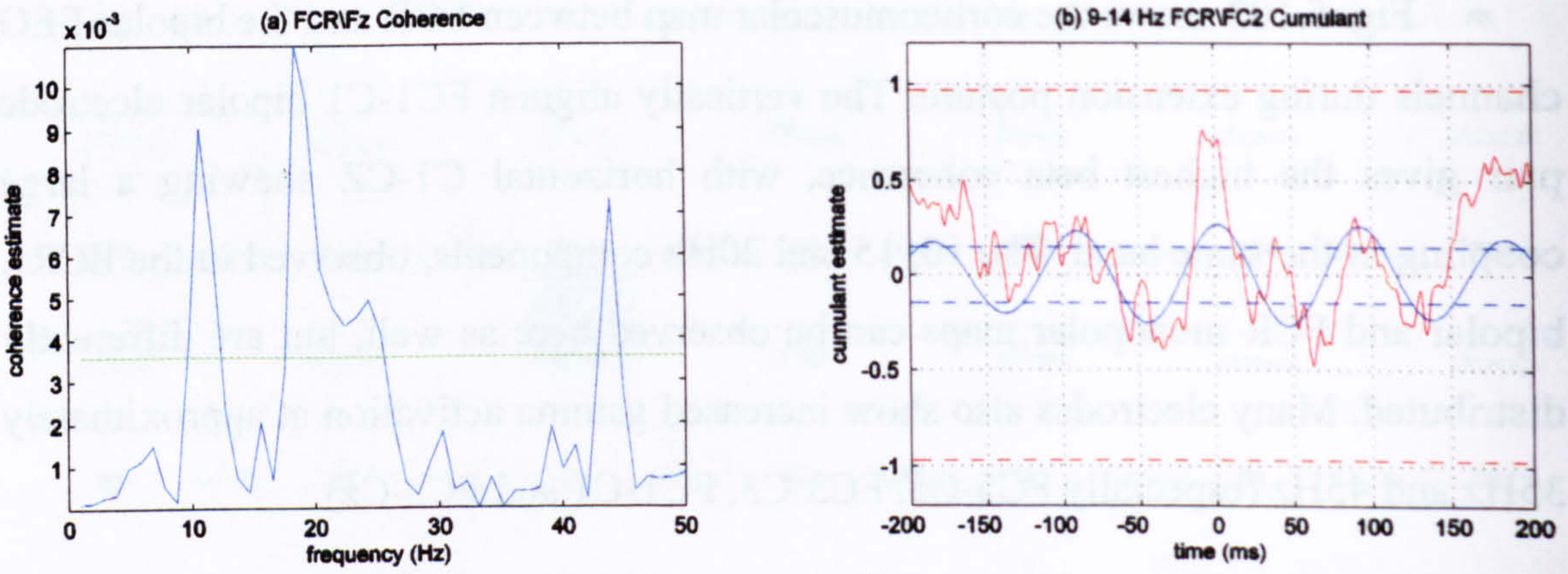

Fig. 5.104 FCR\Fz coherence and corresponding cumulant plot (red plot) during posture extension. The blue plot represents the 9-14Hz cumulant component while the blue dashed lines represent the estimated upper and lower 95% confidence limits for the cumulant component.

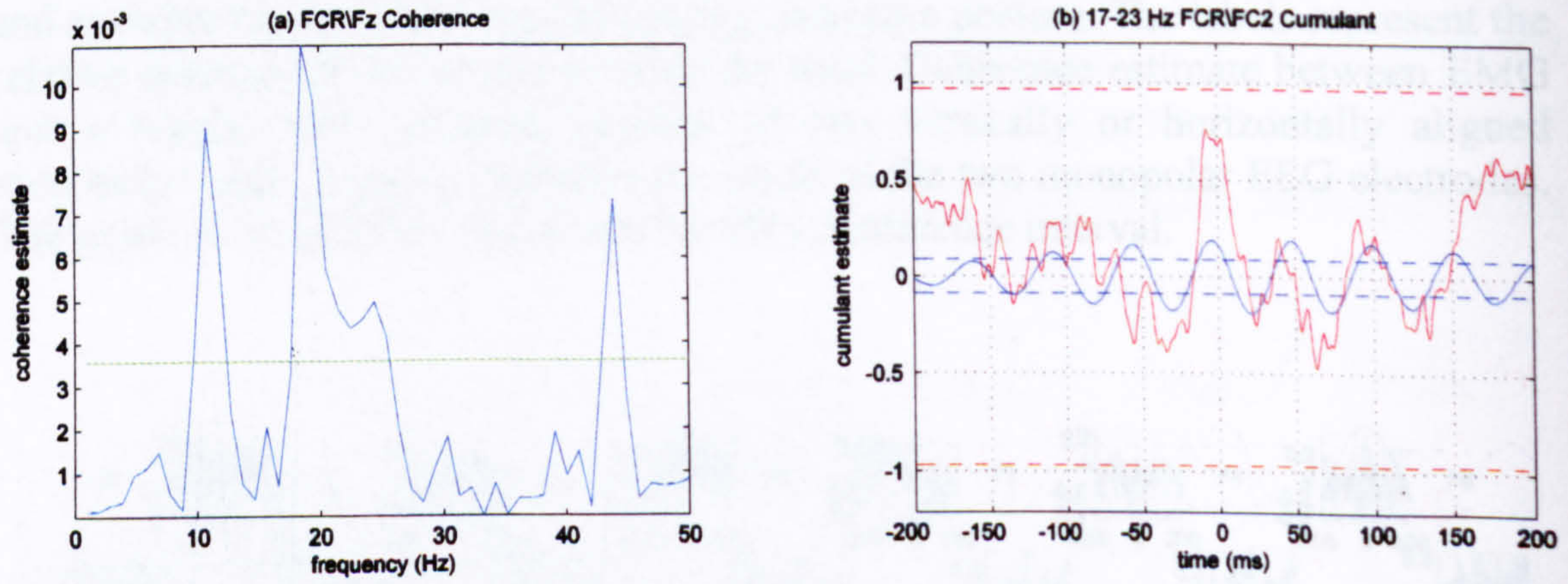

Fig. 5.105 FCR\Fz coherence and corresponding cumulant plot (red plot) during posture extension. The blue plot represents the 17-23Hz cumulant component while the blue dashed lines represent the estimated upper and lower 95% confidence limits for the cumulant component.

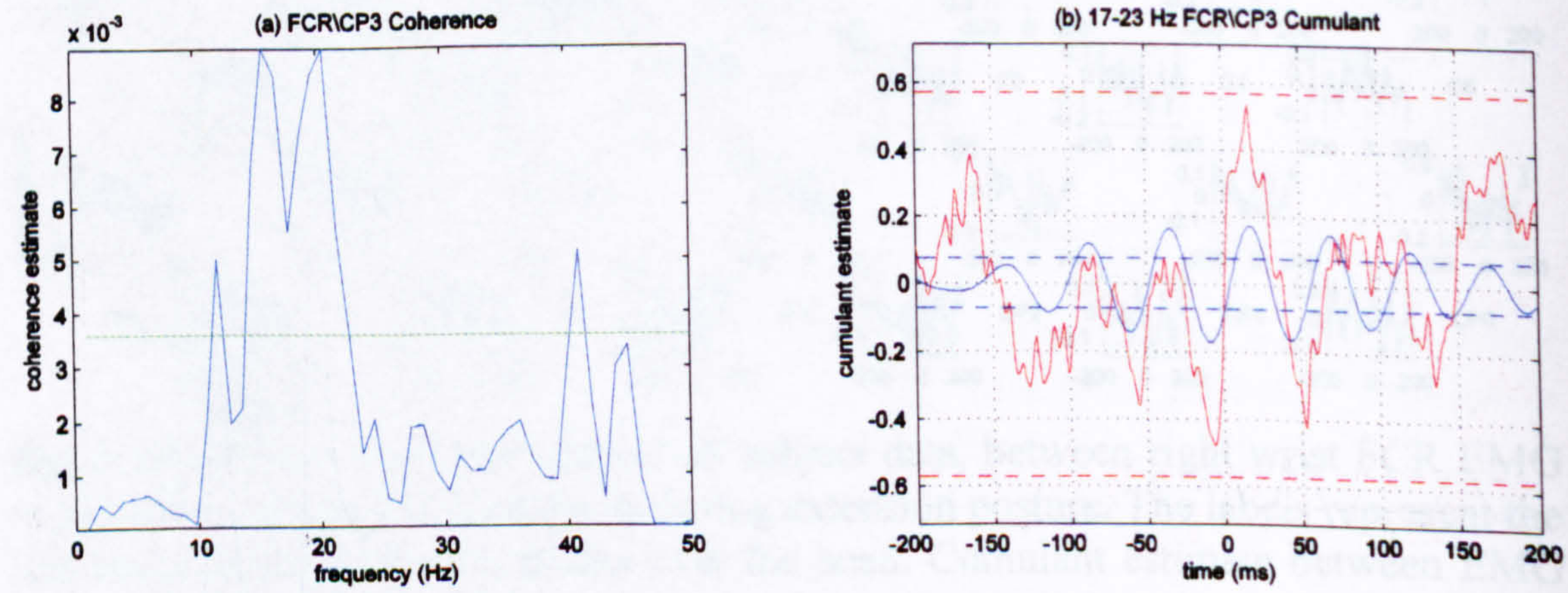

Fig. 5.106 FCR\CP3 coherence and corresponding cumulant plot (red plot) during posture extension. The blue plot represents the 17-23Hz cumulant component while the blue dashed lines represent the estimated upper and lower 95% confidence limits for the cumulant component.

Fig. 5.104b and Fig. 5.105b show the 9-14Hz and 17-23Hz FCR\Fz cumulant components respectively. The 9-14Hz gives 2ms EEG\EMG delay (phase: 0.1±6.6ms) while the 17-23Hz cumulant gives -5ms (phase: -3.5±2.34ms). The 9-14Hz may indicate that the EMG has a slight lead over the EEG signal, but lead of EEG over EMG is within the error margin.

Fig. 5.106 shows the FCR\CP3 17-23Hz cumulant component during the posture extension phase. The coupling is "out of phase" at a delay of -8ms EMG\EEG (phase suggests: -10.7±5.5ms)

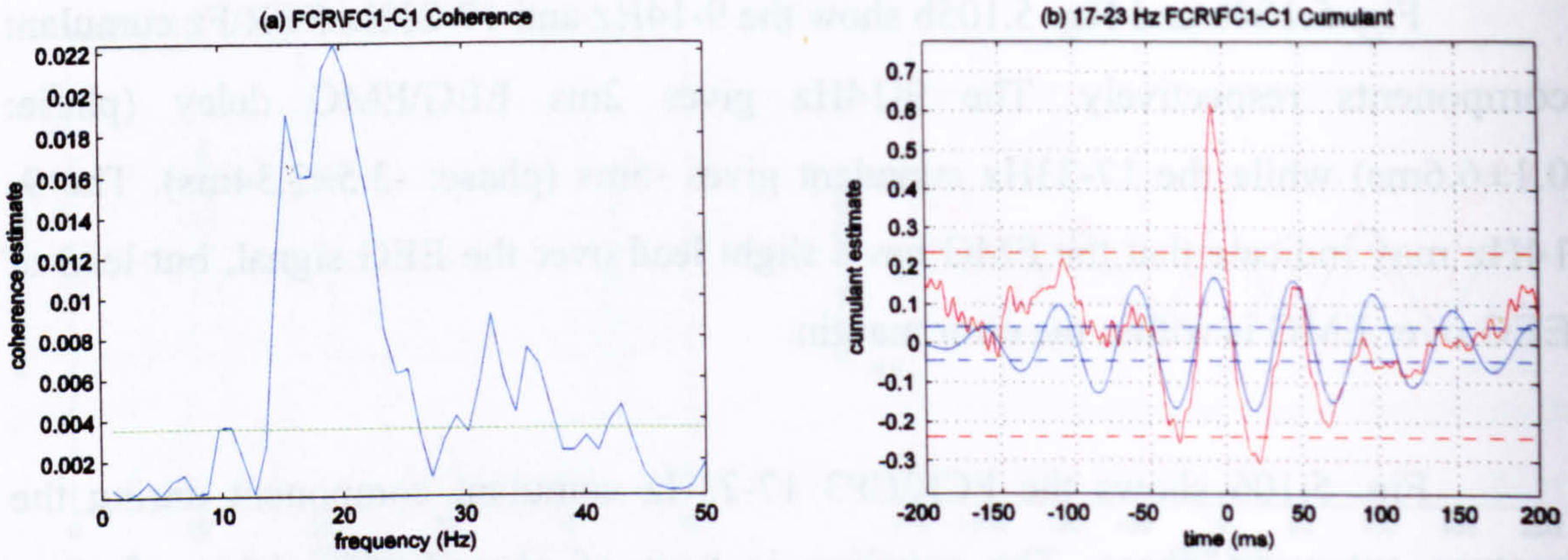

Fig. 5.107 FCR\FC1-C1 coherence and corresponding cumulant plot (red plot) during posture extension. The blue plot represents the 17-23Hz cumulant component while the blue dashed lines represent the estimated upper and lower 95% confidence limits for the cumulant component.

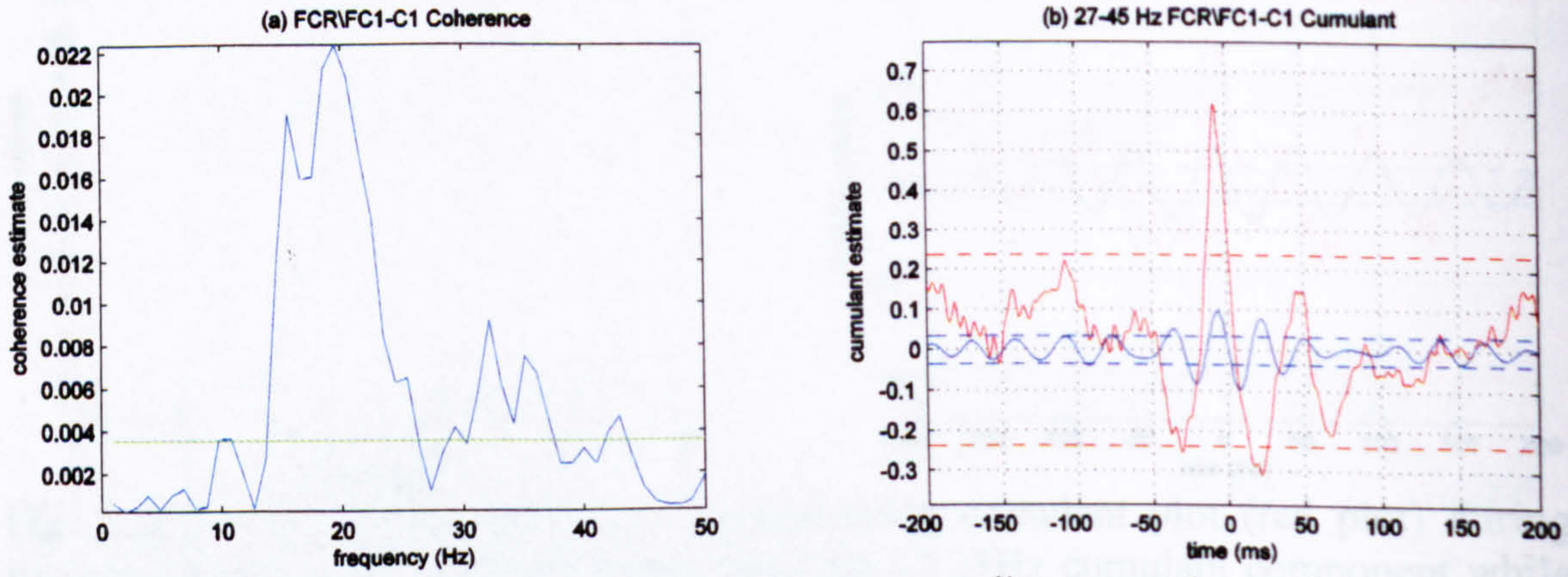

Fig. 5.108 FCR\FC1-C1 coherence and corresponding cumulant plot (red plot) during posture extension. The blue plot represents the 27-45Hz cumulant component while the blue dashed lines represent the estimated upper and lower 95% confidence limits for the cumulant component.

Fig. 5.107*b* and Fig. 5.108*b* show the 17-23Hz and 27-45Hz cumulant components of FCR\FC1-C1 wideband cumulant respectively. The 17-23Hz cumulant component derives a -7ms delay (phase: -5.9±2.2ms) while the 27-45Hz shows a very similar EMG\EEG delay of -6ms (phase: -7.5±1.6ms). Both synchronisation features reveal "in phase" coupling.

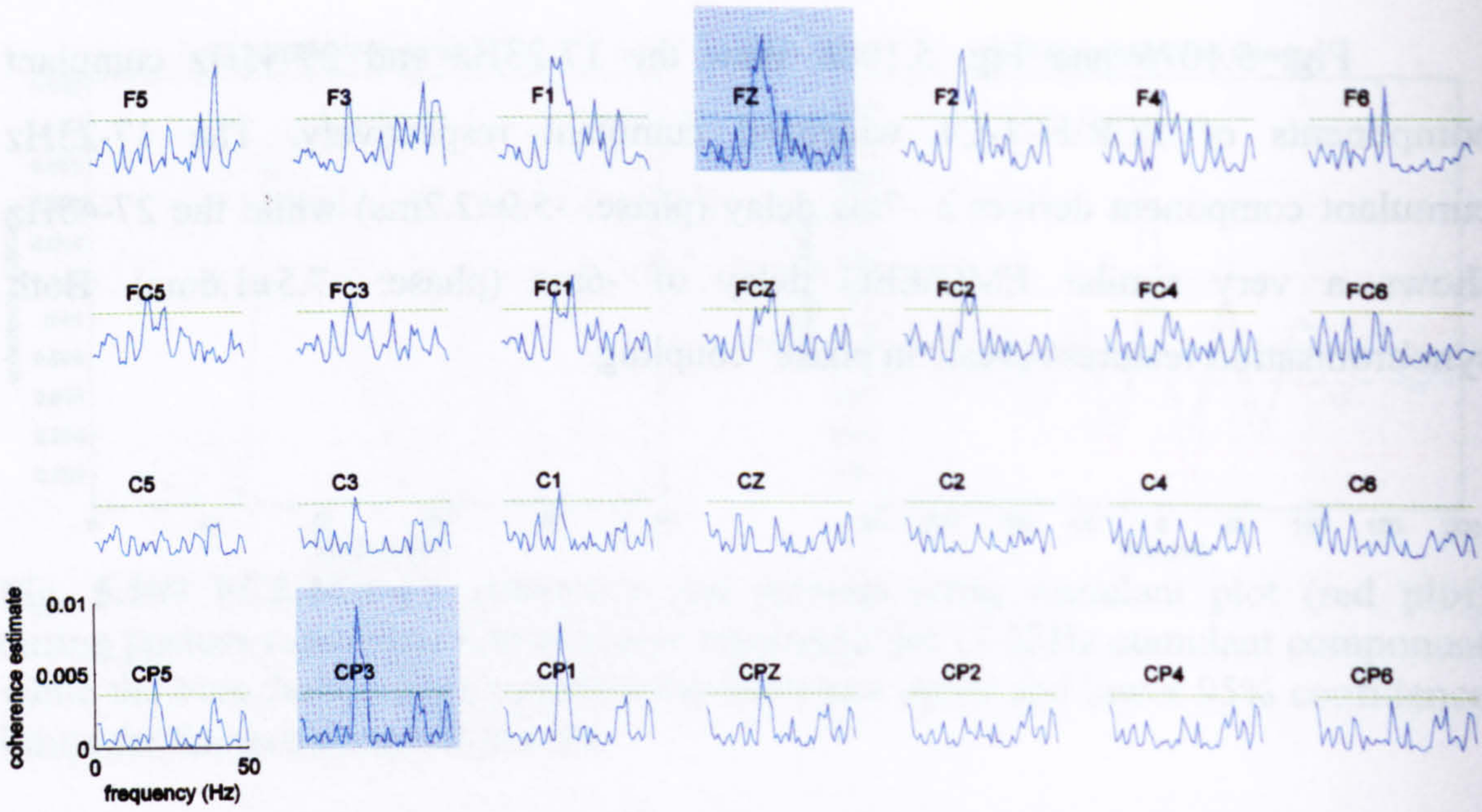

Fig. 5.109 Pooled coherence map of all subject data, between right BBLH EMG and multiple monopolar EEG channels during extension posture. The green horizontal line represents the 95% confidence interval.

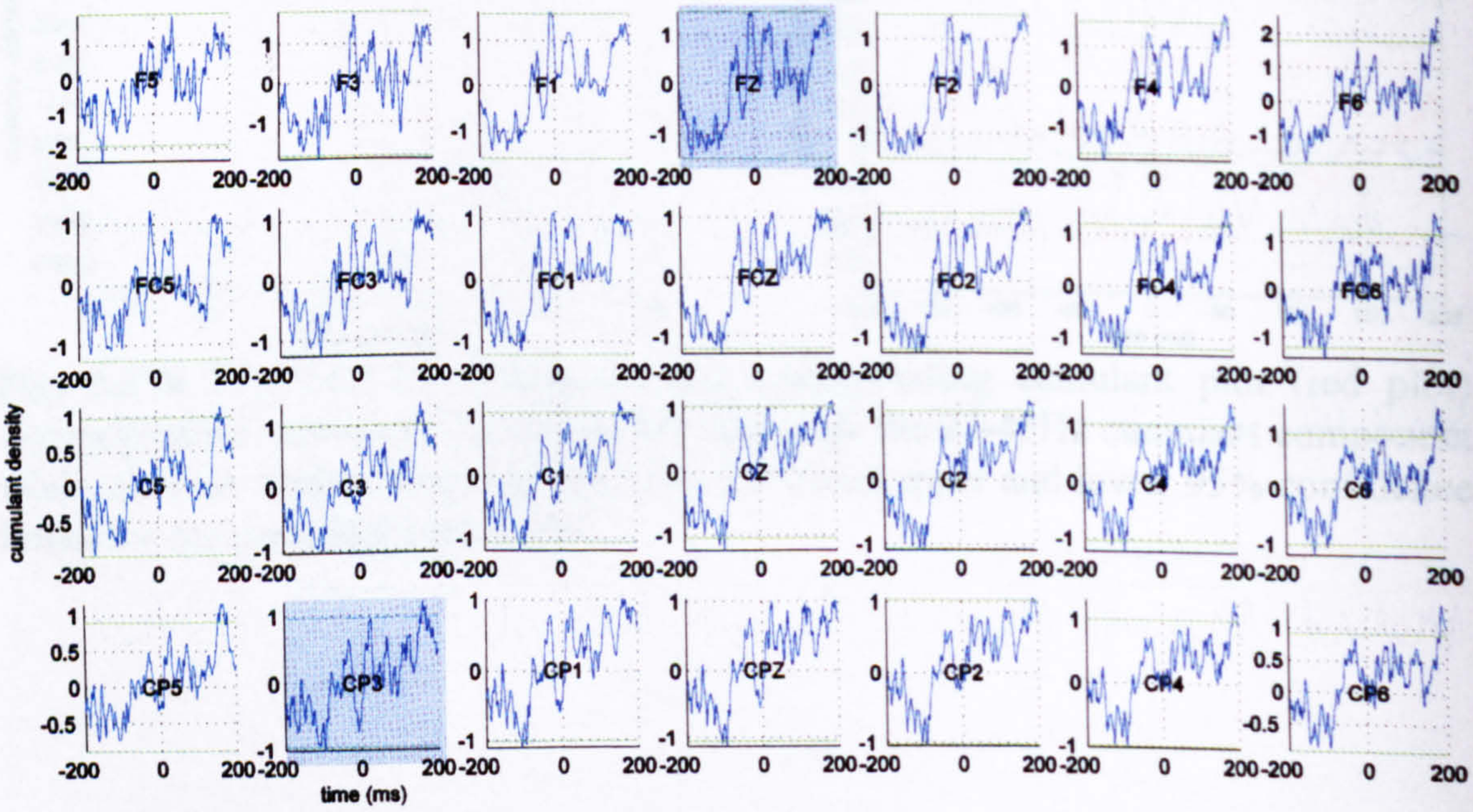

Fig. 5.110 Pooled cumulant map of all subject data, between right BBLH EMG and multiple monopolar EEG channels during extension posture. The green horizontal line represents the 95% confidence interval

5.1.6.4.3 BBLH coupling

Fig. 5.109 shows the corticomuscular map between BBLH muscle and monopolar EEG channels during extension posture. It displays high beta coupling in the medial frontal and frontoparietal area as well as contralateral central and centroparietal areas. Weak gamma coupling is present in the contralateral frontal electrodes but no alpha coupling is present. This is in contrast to the ECRL and FCR monopolar maps (Fig. 5.91, Fig. 5.100). The corresponding cumulant map (Fig. 5.110) show beta coupling for the same set of electrodes as the coherence map, with beta influences being more obvious in the frontal areas.

Fig. 5.111 shows the bipolar corticomuscular coherence map between BBLH EMG and the paired EEG channels during extension posture. The BBLH map contains the strongest beta corticomuscular coherence, for all recorded muscles during posture extension. The coherence is very much concentrated between the contralateral central and frontocentral area, with the maximum appearing at FC1-C1. Strong coherence appears for vertical oriented electrodes. 32Hz coupling appears at electrodes where high 12-25Hz beta coupling also occurs. The two features have similar distribution, which suggests the possibility that the smaller 32Hz feature may be a harmonic of the main feature. BBLH/EEG coherence map during extension posture does not contain the alpha features, observed during the corresponding map during flexion posture in Fig. 5.70.

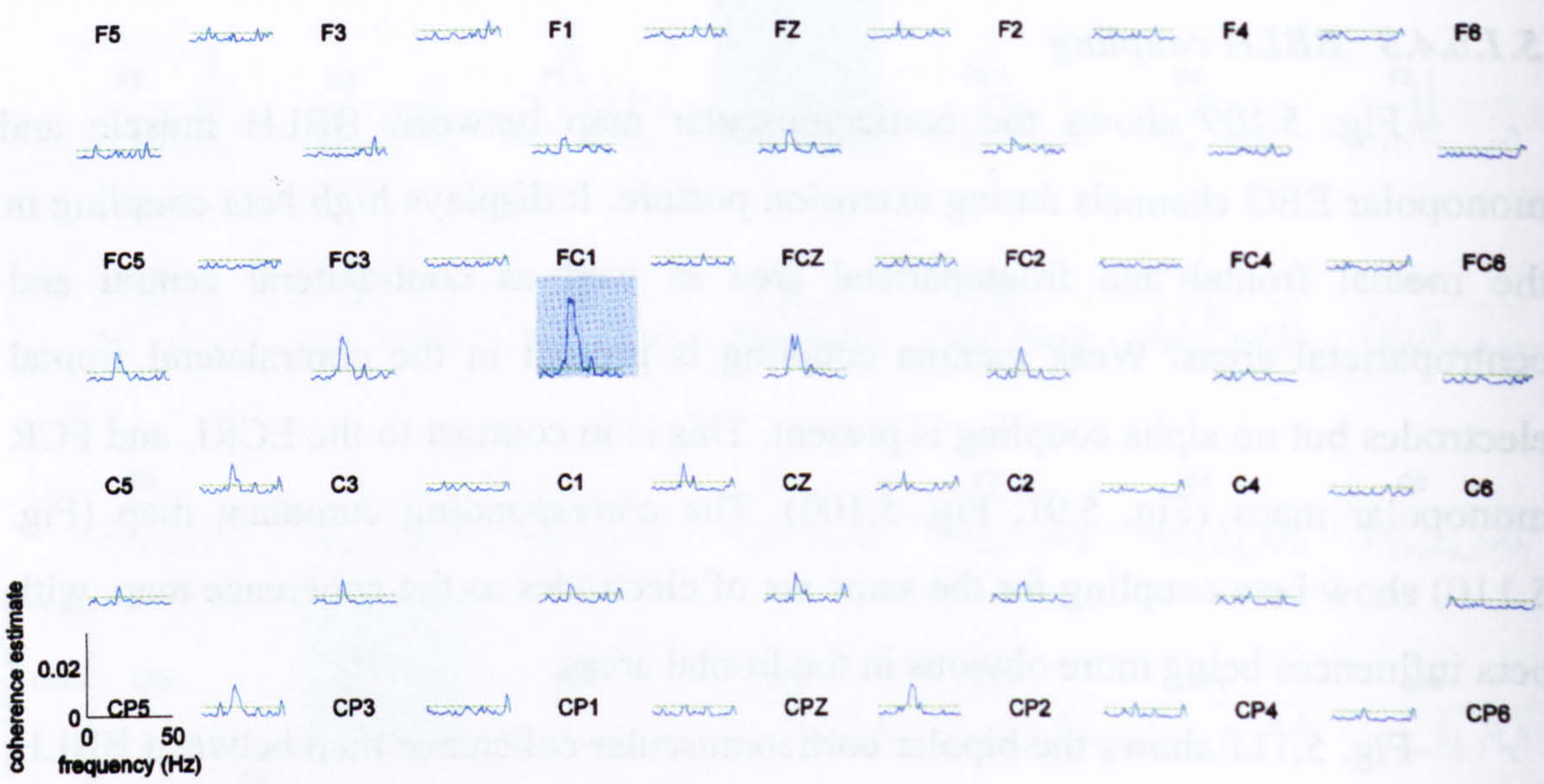

Fig. 5.111 Pooled coherence map of all subject data, between right BBLH EMG and multiple bipolar EEG channels during extension posture. The labels represent the relative position of the electrodes over the head. Coherence estimate between EMG and a bipolar EEG channel, product of two vertically or horizontally aligned monopolar ones, is plotted between the labels of the two monopolar EEG electrodes. The green horizontal line represents the 95% confidence interval.

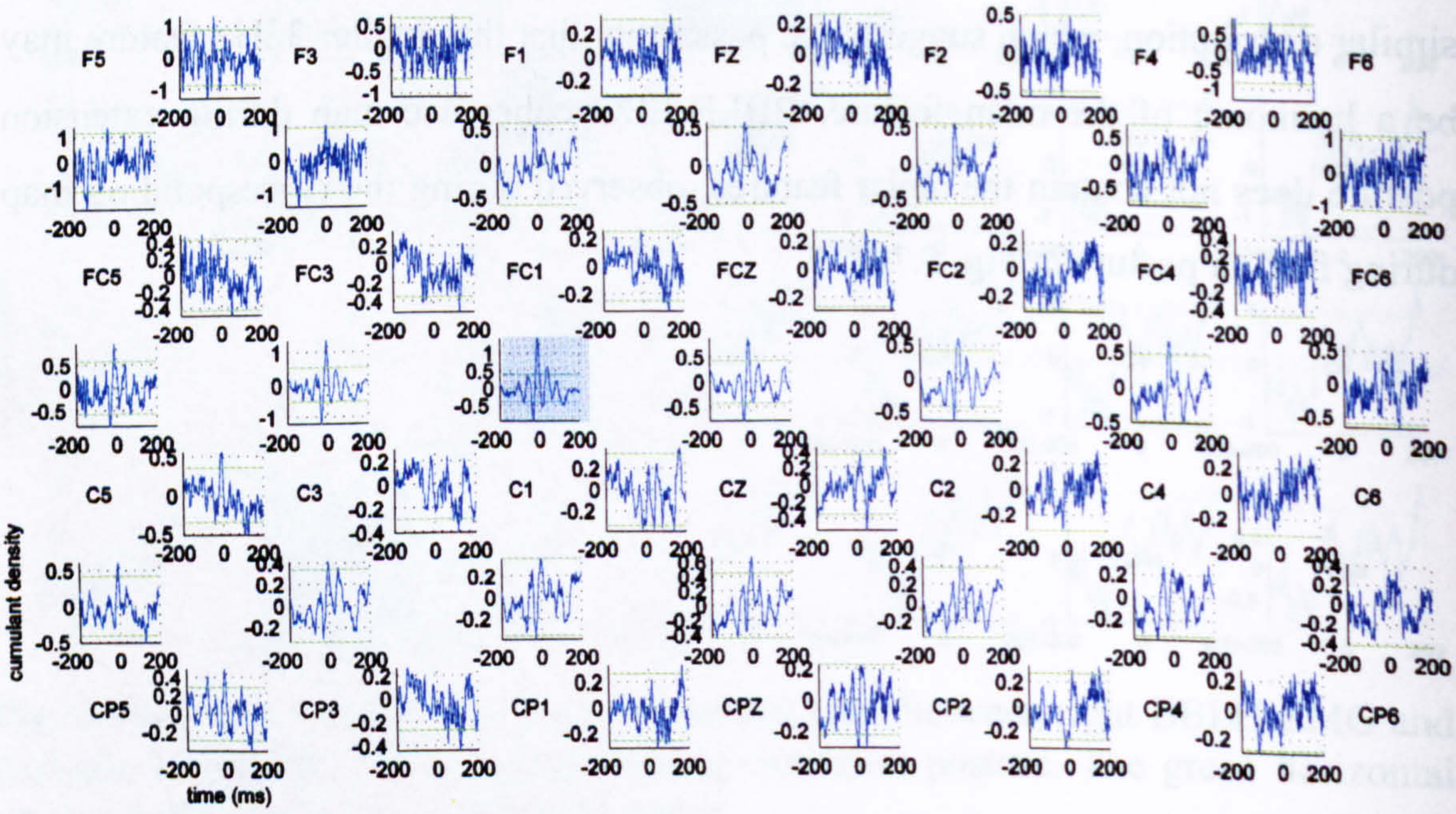

Fig. 5.112 Pooled cumulant map of all subject data, between right BBLH EMG and multiple bipolar EEG channels during extension posture. The labels represent the relative position of the electrodes over the head. Cumulant estimate between EMG and a bipolar EEG channel, product of two vertically or horizontally aligned monopolar ones, is plotted between the labels of the two monopolar EEG electrodes. The green horizontal line represents the 95% confidence interval.

Fig. 5.112 shows the corresponding BBLH/bipolar EEG cumulants and demonstrates the same strong beta coupling appearing in the coherence map. FC1-C1 electrode shows a statisticaly significant central peak, showing EEG leading the EMG signal. There is no clear indication for any alpha synchronisation.

Fig. 5.113 and Fig. 5.114 show the 17-24Hz for BBLH\Fz and BBLH\CP3 respectively. BBLH\Fz derives -7ms EMG\EEG delay (phase: -6.1±3.3ms) and "in phase" synchronisation while BBLH\CP3 derived -7ms delay (phase: -7.5±4.2ms) and "out of phase" synchronisation.

Fig. 5.115b shows the 17-23Hz cumulant for BBLH\FC1-C1 during posture extension. The EMG EEG delay is -8ms while the phase derives -8.1±1.3ms. The synchronisation is "in phase".

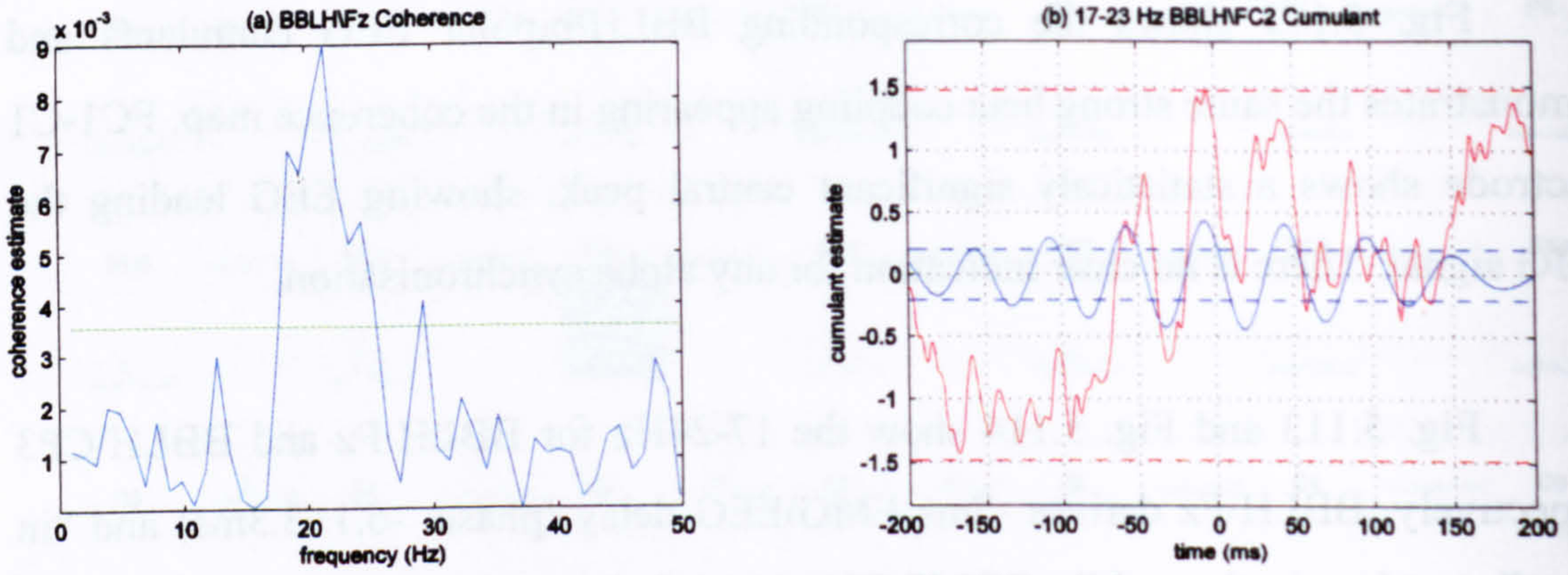

Fig. 5.113 BBLH\Fz coherence and corresponding cumulant plot (red plot) during posture extension. The blue plot represents the 17-23Hz cumulant component while the blue dashed lines represent the estimated upper and lower 95% confidence limits for the cumulant component.

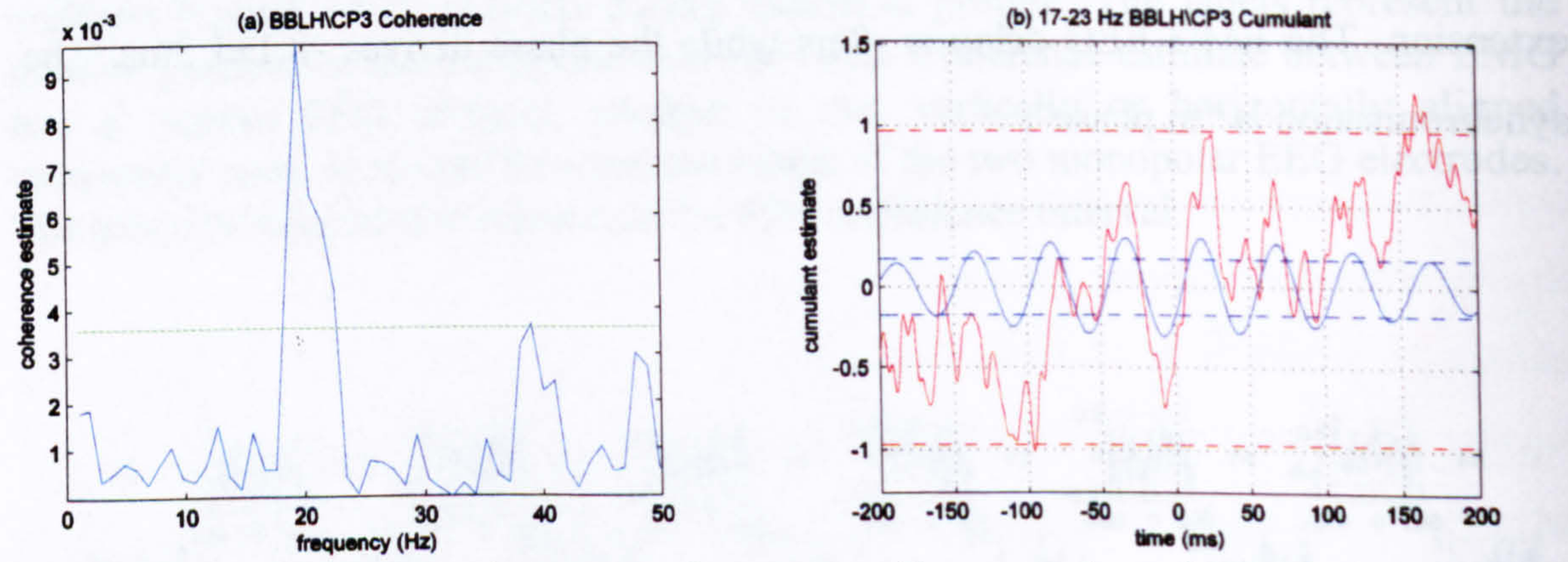

Fig. 5.114 BBLH\CP3 coherence and corresponding cumulant plot (red plot) during posture extension. The blue plot represents the 17-23Hz cumulant component while the blue dashed lines represent the estimated upper and lower 95% confidence limits for the cumulant component.

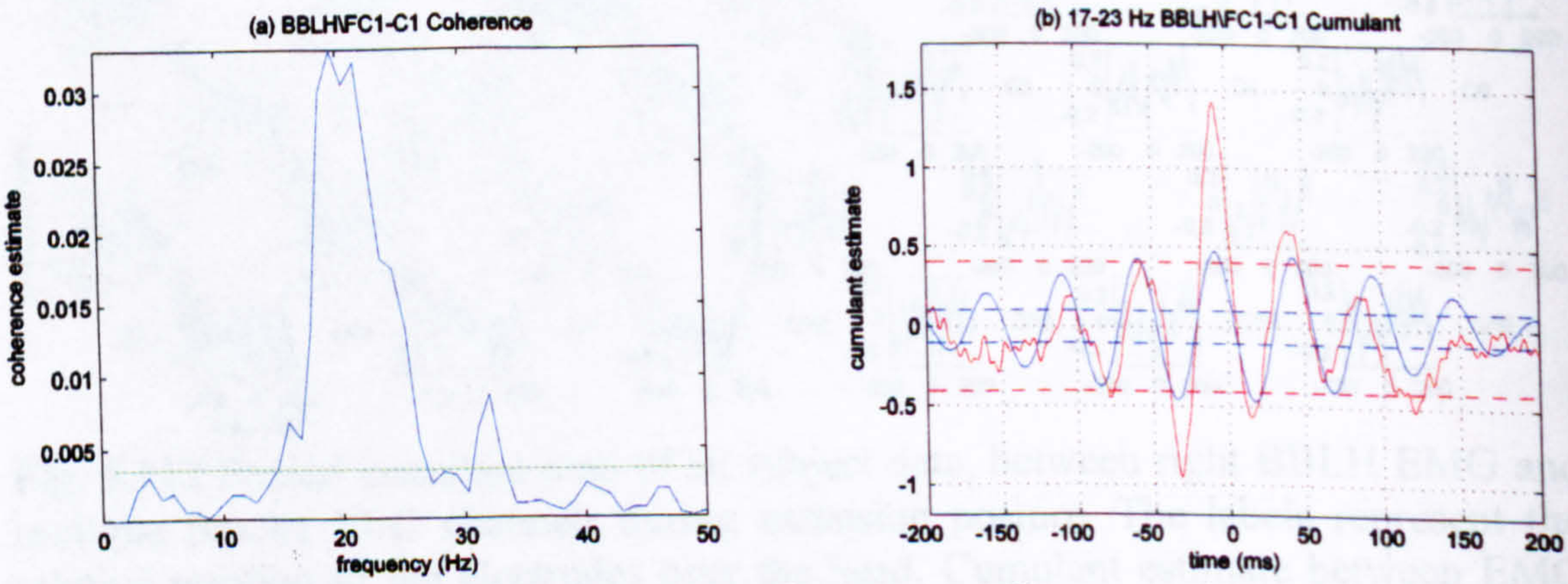

Fig. 5.115 BBLH\FC1-C1 coherence and corresponding cumulant plot (red plot) during posture extension. The blue plot represents the 17-23Hz cumulant component while the blue dashed lines represent the estimated upper and lower 95% confidence limits for the cumulant component.

5.1.6.5 Summary of corticomuscular coupling results

- Corticomuscular coherences of the wrist extensor, flexor and supporting biceps muscles were examined during the move-hold sequence. Strong beta coupling in the EEG with all three muscles was present during posture and was stronger during posture flexion phase. The beta coherence was strongest over the contralateral motor cortex (FC1-C1) for the bipolar EEG while for the monopolar sites it appeared strongest in the medial frontal and contralateral centroparietal electrodes.

- Other smaller features were also occasionally present and include alpha and gamma coupling. The amplitude of alpha coherence is not correlated with the amplitude of the beta peaks which suggest that the two features were independent. The beta features during posture were more defined and show a clearer spatial organisation in the bipolar plots than in the monopolar. The spatial organisation appeared similar for all three muscles. Cumulant estimates confirmed the presence of strong beta rhythmic features and the fact that the cortical beta band drives the muscle activity.

- During movement the strong beta coupling was suppressed for all muscles. That was the case for the supporting biceps as well, despite the fact that this muscle held the elbow position unchanged. However there were coupling features at lower frequencies and more specifically in the 6-9Hz range. These features were present as very narrow peaks mainly in the monopolar coherence maps. These features were also clear in the corresponding cumulant plots. However, they were not strictly statistically significant but because of the consistent shape seen over a wide area, these features may be effective as movement indicators in certain individuals.

- Quite defined rhythmic activity lying in the alpha range was also observed in the bipolar cumulant plots even when coherence was not statisticaly significant in that band. The cumulant features were not statistically significant and may express the coexistence of strong 10Hz frequency content during movement for both EMG

and EEG without being strongly correlated. These features should be investigated further.

- The corticomuscular delays revealed by the phase and cumulant plots for beta posture coupling features were not consistent ranging from 4-9ms with expected corticomuscular times in the range of 15ms. The conduction times for 4-8Hz movement features derived conduction times in the 15ms range.

- The model that appears to be closer to the beta corticomuscular coherence appears in Appendix 8.4.4 Example 4. The source of coupling appears to be a common oscillatory input with common poison processes, which is responsible for the high coherence, the oscillatory cumulant as well as the prominent central cumulant peak.

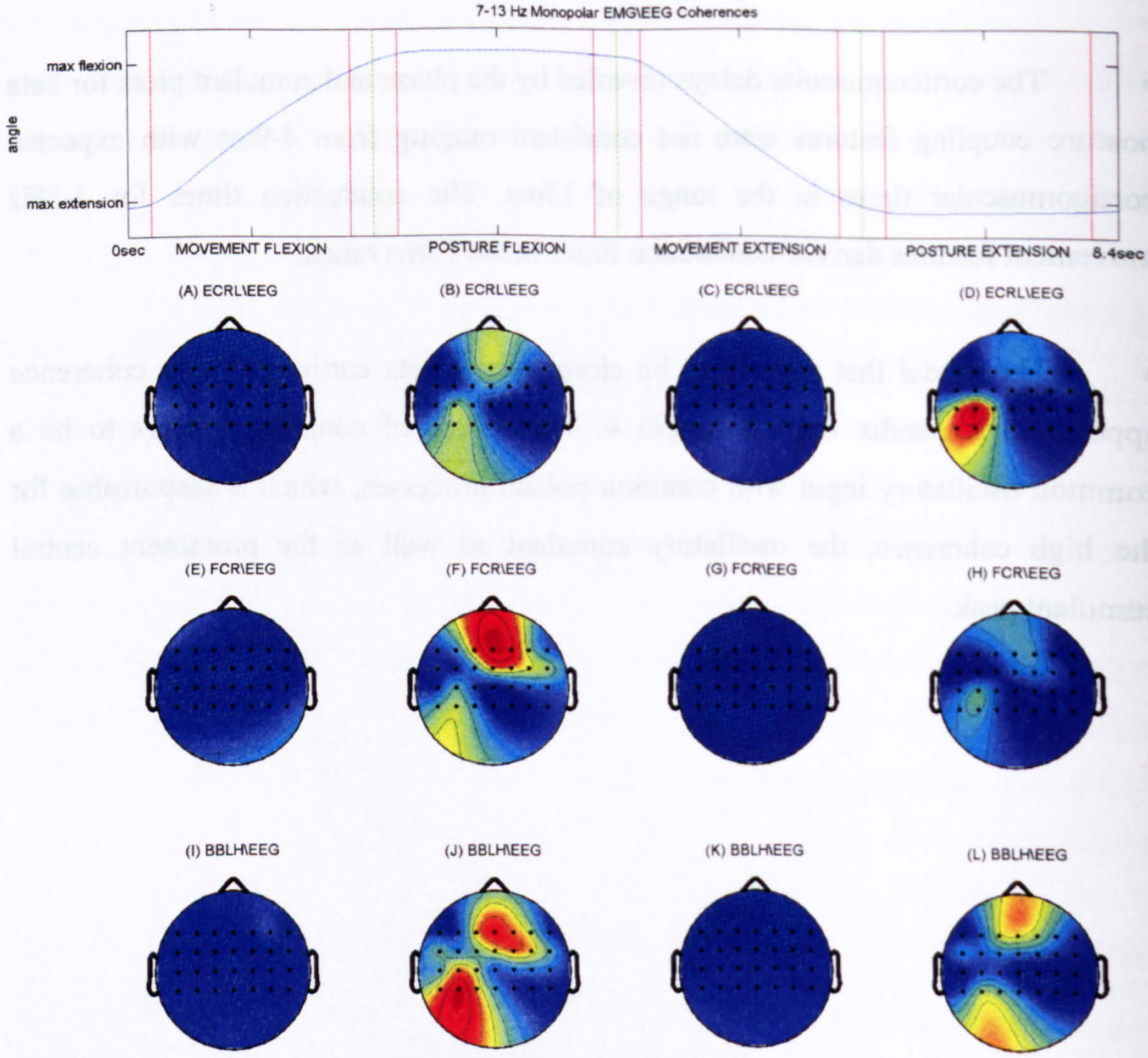

Fig. 5.116 EEG monopolar corticomuscular coherences within 17-23Hz band for during movement flexion, posture flexion, movement extension, posture extension for ECRL (*A,B,C,D*), FCR (*E,F,G,H*), BBLH (*I,J,K,L*) respectively. The coherences were visualised as topographic maps of a scalp data field in a 2-D circular view using interpolation on a fine cartesian grid. The positions of the electrodes are indicated on the topographic maps. Dark red represents the highest value while dark blue represents the lowest value. The top plot represents the wrist angle information derived by the goniometer demonstrating in a graphical way the movement phase that each map represents. The green vertical lines represent the audio cues while the interval between the red vertical lines represents the transition phases for which data was discarded.

5.1.7 Topographic coherence and cumulant maps

The results that are going to be presented are a different representation of the results presented in Fig. 5.34-Fig. 5.115. The corticomuscular characteristics during the four move-hold sequence phases were previously presented as monopolar and bipolar maps. These maps consisted of two dimensional corticomuscular estimates plotted over the relative positions of the corresponding electrode sites over the cortex. The spatiotemporal changes over the examined 0-50Hz spectrum could be observed and the main coupling features were identified. The most important task dependent characteristic identified was beta band coherence and cumulant features during posture and the suppression of those features during movement.

In this session coherence and cumulant estimates within this band will be visualised as topographic maps of a scalp data field in a two-dimensional circular view using interpolation on a fine cartesian grid. By illustrating the data in this way it will be possible to present in an easy to comprehend way the spatial, task dependent characteristics for the 17-23Hz band where changes are most likely to occur. It will also allow the approximation of the origin of the cortical source responsible for the corticomuscular association. The coherence topographic maps were presented in a configuration that displayed the wrist angle information. In this way it was possible to illustrate in a graphical way the movement phase that each map represents.

5.1.7.1 Monopolar corticomuscular coherence topographic maps

Fig. 5.116 illustrates the topographic maps of the 17-23Hz monopolar corticomuscular coherence for the three examined muscles during the four phases of the move hold sequence. The goniometer information is also displayed in order to better illustrate the association of the coherence modulation with the performed task phases. Each horizontal row of topographic maps corresponds to each of the three EMGs while the columns correspond to the indicated movement phase. It is obvious that statisticaly significant coherence features appear during posture flexion Fig. 5.116*B,F,J* and posture extension Fig. 5.116*D,H,L* while these are suppressed during movement. Increase in coherence during posture mainly occurs at contralateral central and centroparietal sites and the medial frontal and frontocentral electrodes. While coherence spatial features appear for all posture maps there are district

differences depending on the muscle examined and if the posture is flexion or extension. During posture flexion the two main ECRL\EEG corticomuscular features appear to have similar amplitude (Fig. 5.116*B*), while for FCR\EEG map (Fig. 5.116*F*) the medial frontal feature is considerably larger than the contralateral centroparietal. The opposite can be observed for BBLH\EEG topographic coherence map (Fig. 5.116*J*) where the contralateral centroparietal feature is higher than the frontal feature. During posture extension the contralateral centroparietal feature for ECRL\EEG (Fig. 5.116*D*) is higher than the medial frontal one. The corresponding features for FCR\EEG and BBLH\EEG maps (Fig. 5.116*H* and Fig. 5.116*L*) appear to have similar amplitude.

It is also important to examine the differences for individual muscles in relation to the preformed posture task, the spatial distribution of beta corticomuscular coherence in relation to posture extension or posture flexion. Comparing ECRL\EEG maps during posture flexion and posture extension (Fig. 5.116*B* and Fig. 5.116*D* respectively) important differences can be observed. During flexion posture the two features have a similar magnitude while during posture extension the contralateral centroparietal feature is considerably higher than the corresponding frontal. For FCR\BBLH posture maps (posture flexion in Fig. 5.116*F* and posture extension in Fig. 5.116*H*) the overall coherence for posture extension is noticeably lower. For the same phase the magnitudes of the two features are comparable. In contrast during posture flexion the FCR\EEG coherence is higher for the medial frontal electrodes than the contralateral centroparietal ones.

Fig. 5.116*J,L* show respectively the BBLH\EEG beta coherences maps during posture flexion and posture extension. The overall coherence level is lower during posture extension while the two features have similar size. During posture flexion the centroparietal feature is larger than the frontal. The distribution of coherences over the medial frontal cortex is different. During posture flexion the ipsilateral frontal and frontocentral electrodes show higher coherence than the corresponding electrodes during posture extension. The last observations confirm once more the fact that task modulation of BBLH corticomuscular coupling depends on the task performed by the wrist.

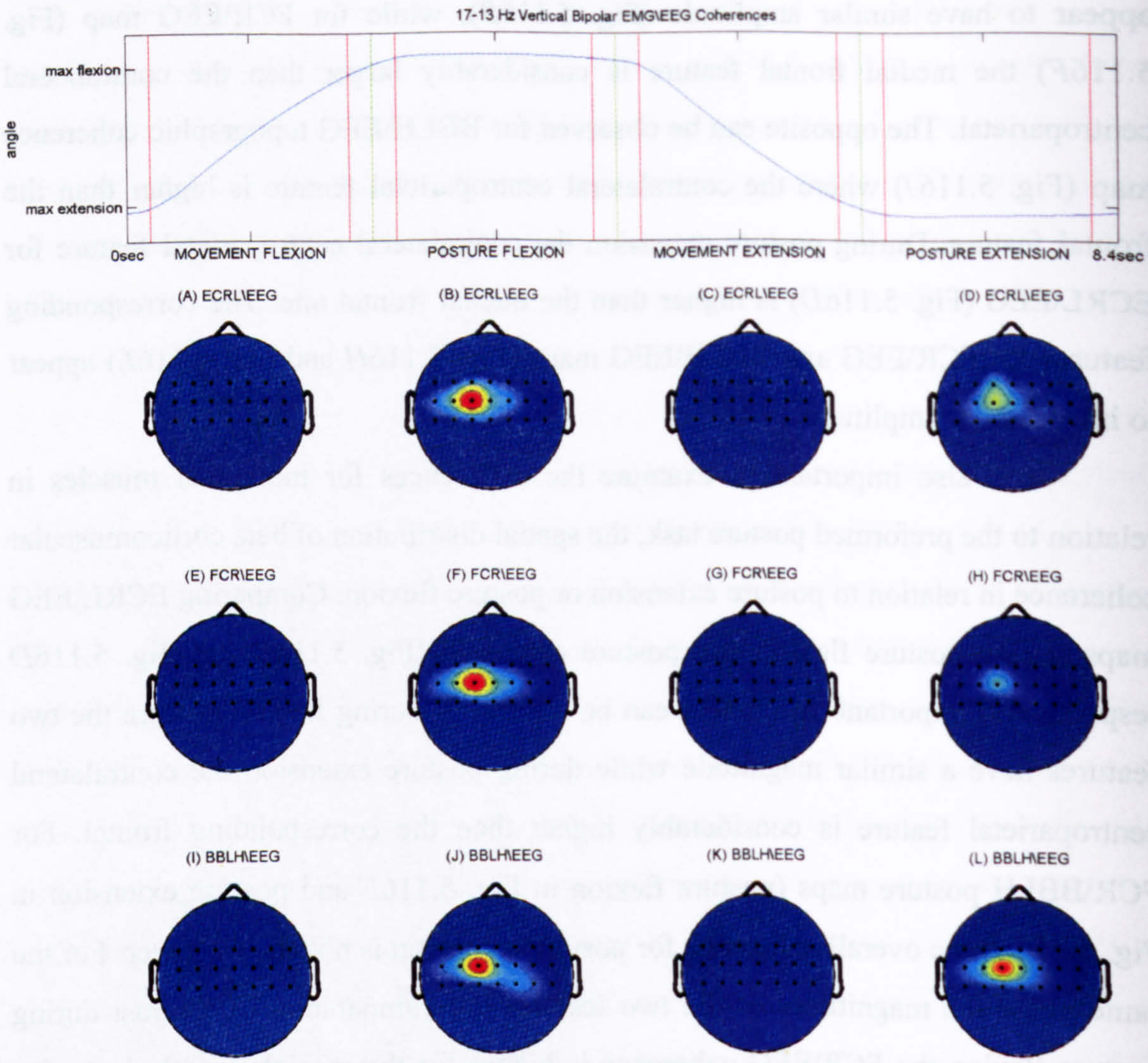

Fig. 5.117 EEG bipolar corticomuscular coherences within 17-23Hz band for during movement flexion, posture flexion, movement extension, posture extension for ECRL (*A,B,C,D*), FCR (*E,F,G,H*), BBLH (*I,J,K,L*) respectively. The coherences were visualised as topographic maps of a scalp data field in a 2-D circular view using interpolation on a fine cartesian grid. The positions of the electrodes are indicated on the topographic maps. Dark red represents the highest value while dark blue represents the lowest value. The top plot represents the wrist angle information derived by the goniometer demonstrating in a graphical way the movement phase that each map represents. The green vertical lines represent the audio cues while the interval between the red vertical lines represents the transition phases for which data was discarded.

It can also be concluded that the relative size of the two beta corticomuscular features were task specific. This may suggest that they could be utilised as a means of identifying not only posture but also distinguish posture flexion from posture extension.

5.1.7.2 Bipolar corticomuscular coherence topographic maps

Fig. 5.117 illustrates the topographic maps of the pooled beta bipolar (vertically aligned electrodes) coherences during the move hold sequence. The map contains the 17-23Hz coherence, where the most prominent corticomuscular coupling features occur for all EMGs.

The results show a very clear spatial organisation with high coherence over the contralateral motor cortex during posture flexion (Fig. 5.117*B,F,J*) and posture extension (Fig. 5.117*D,H,L*) which is suppressed during movement (Fig. 5.117*A,E,I,C,G,K*). The centre of the corticomuscular coherence is clearly located over the FC1-C1 electrode. Lower coherence is also extended over the ipsilateral cortex.

The distribution of coherences over the cortex is very similar for ECRL\EEG and FCR\EEG (agonist – antagonist) while it appeared slightly different for BBLH\EEG for which the weak ipsilateral coherence (Fig. 5.117*J*) occurs at a more posterior location than for ECRL and FCR (Fig. 5.117*B,F*) during posture flexion. The opposite is happening during posture extension where ipsilateral ECRL\EEG and FCR\EEG features (Fig. 5.117*D,H*) are stronger in more posterior electrodes than BBLH\EEG (Fig. 5.117*L*). Nevertheless the centre of high coherence remains the same.

The contralateral beta bipolar coherence feature for all three muscles is higher during posture flexion (Fig. 5.117*B,F,J*) than during posture extension (Fig. 5.117*D,H,L*). This is the case even for ECRL which acts as an antagonist during posture flexion (Fig. 5.117*B*) and as an agonist during posture extension (Fig. 5.117*D*).

Comparing the bipolar topographic maps with the corresponding monopolar in Fig. 5.116 it is obvious that the coherence posture feature is more distinct and localised in the bipolar maps. FC1-C1 electrode which actually overlies the part of

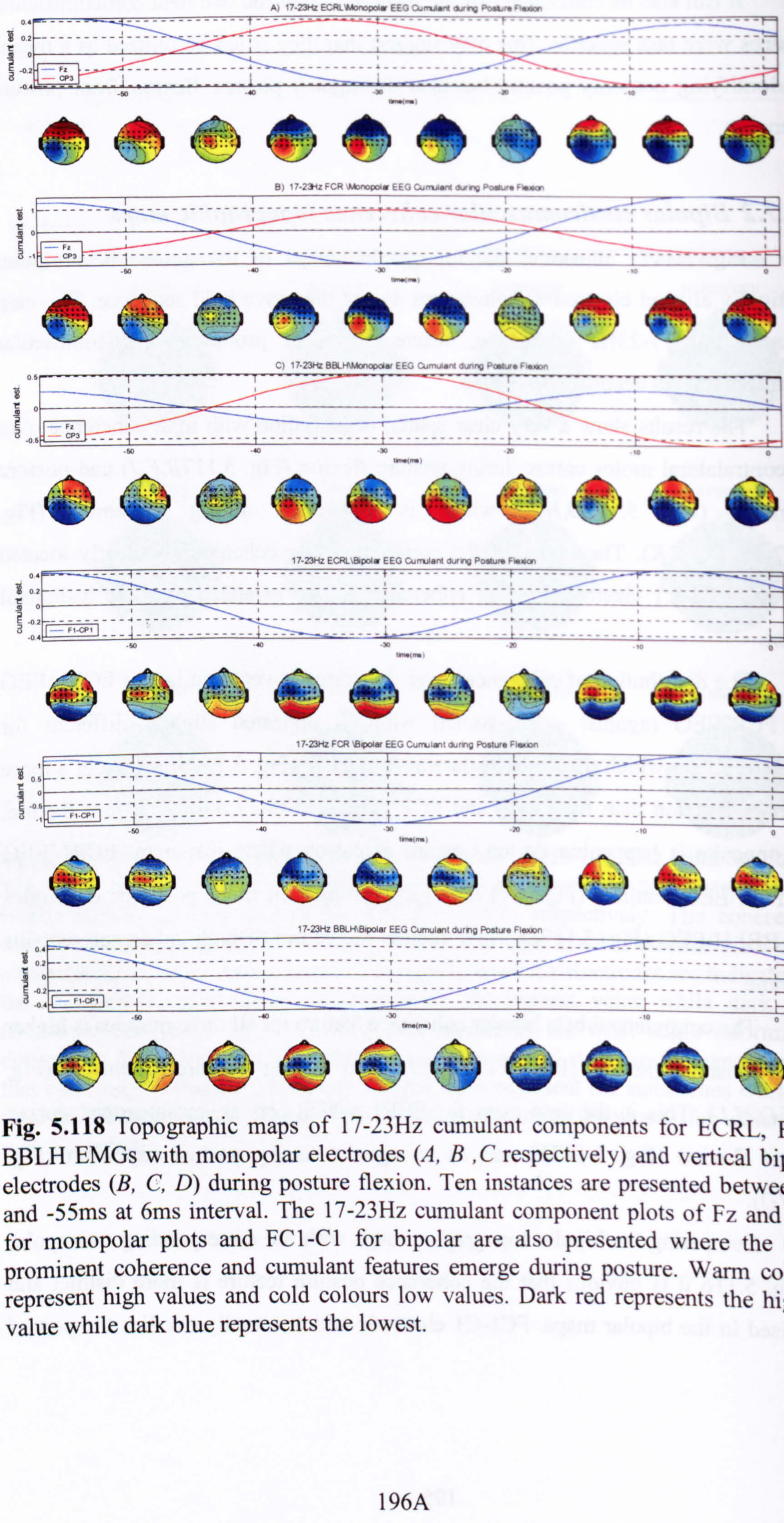

Fig. 5.118 Topographic maps of 17-23Hz cumulant components for ECRL, FCR, BBLH EMGs with monopolar electrodes (*A, B ,C* respectively) and vertical bipolar electrodes (*B, C, D*) during posture flexion. Ten instances are presented between -1 and -55ms at 6ms interval. The 17-23Hz cumulant component plots of Fz and CP3 for monopolar plots and FC1-C1 for bipolar are also presented where the most prominent coherence and cumulant features emerge during posture. Warm colours represent high values and cold colours low values. Dark red represents the highest value while dark blue represents the lowest.

the motor cortex that corresponds to the forearm muscles would derive the optimal information as a means for detecting posture. The reduction of the feature during posture extension and the slightly changed distribution of coherences (mainly over the ipsilateral cortex) could be used for differentiating posture extension from posture flexion. However the monopolar map could still be useful since it derives more unambiguous information on the type of posture (flexion or extension) by comparing the relative size of the two spatial coherence features in frontal and centroparietal electrodes.

5.1.7.3 Cumulant topographic maps

The individual corticomuscular cumulant estimates represent the envelope of averaged EEG channel timelocked to the EMG signal bursts. Furthermore the 17-23Hz cumulant component specifically represents the averaged 17-23Hz EEG frequency content timelocked to the 17-23Hz EMG bursts. Therefore the cumulant estimates in effect represent voltage (electric field), as the envelope of the averaged EEG. Therefore the resulting topographic maps represent the distribution of electric field over the cortex for an instance within the period of an approximately 20Hz corticomuscular motor command.

In other words it can be assumed that a cortical 17-23Hz oscillator generates motor descending command to the muscles because of the fact that most of the corticomuscular coherence occurs within this band. In order to detect the spatial characteristics of the cortical activity and its source, every 17-23Hz EEG pulse is averaged using the corresponding coupled 17-23Hz EEG pulse as a trigger. This results to a number of cumulant estimates; one for each channel which combined in a topographic plot give us with great accuracy the distribution of voltages for a single period of the 17-23Hz cortical rhythm generator pulse. From resulting distribution useful conclusions can be drawn regarding the origin and other characteristics.

Fig. 5.118*A,B,C* demonstrates the monopolar corticomuscular 17-23Hz cumulant topographic maps for ECRL, FCR, and BBLH EMGs respectively with monopolar EEG electrodes during posture flexion. The 17-23Hz corticomuscular cumulant component plots for Fz and CP3 are also presented as they contain the most prominent coupling features during posture. Fig. 5.118*D,E,F* show the

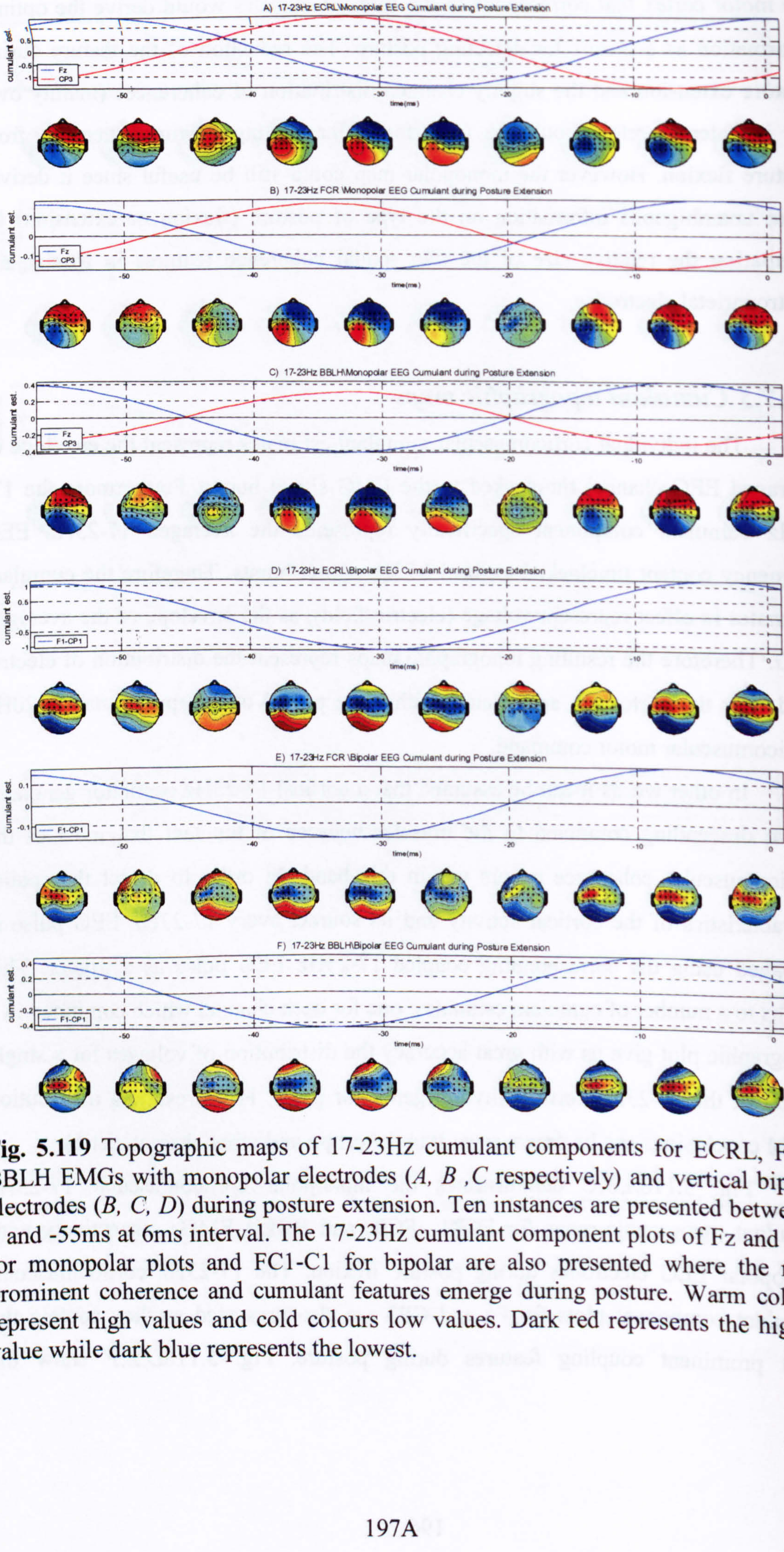

Fig. 5.119 Topographic maps of 17-23Hz cumulant components for ECRL, FCR, BBLH EMGs with monopolar electrodes (*A, B ,C* respectively) and vertical bipolar electrodes (*B, C, D*) during posture extension. Ten instances are presented between -1 and -55ms at 6ms interval. The 17-23Hz cumulant component plots of Fz and CP3 for monopolar plots and FC1-C1 for bipolar are also presented where the most prominent coherence and cumulant features emerge during posture. Warm colours represent high values and cold colours low values. Dark red represents the highest value while dark blue represents the lowest.

respective bipolar topographic maps and the 17-23Hz cumulant component for FC1-C1 which shows the strongest bipolar corticomuscular coupling features. The corresponding results for posture extension can be seen in Fig. 5.119. Ten instances of the topographic maps are illustrated between -1 and -55ms timepoints of the cumulant estimates at a 6ms interval.

As shown earlier Fz and CP3 displayed the highest coupling with EMG from posturally activated muscles. The two monopolar EEG channels represent the two cortical centres of high corticomuscular coupling. It was also shown that while Fz was "in phase" coupled with the EMG during posture, CP3 was coupled "out of phase", both at approximately 17-23Hz. This can also be observed in Fig. 5.118*A,B,C* and Fig. 5.119*A,B,C* where Fz reaches it's minimum CP3 reaches it's maximum and vice versa. Since cumulant expresses variation of electric field this means that when medial frontal and frontocentral cortex (area around Fz) is more positive, the contralateral central and centroparietal cortex (area around CP3) is more negative and vice versa. This is more evident in the corresponding monopolar cumulant topographic maps. For time point -7ms, the area around Fz is dark red which means that the voltage is maximum and positive while the dark blue in the area around CP3 means that the voltage is negative. The opposite happens at -31ms.

This is probably caused by a dipole which acts as a battery transferring electrodes from one cortical area to the other. The isocontours reveal the possible location and orientation of the dipole. The isocontours express the area along which the voltage is equal. Therefore the dipole source will be situated where the isocontours density is high. High density of isocontours means that the change in voltage per distance is high. This change can only be created by a source of activity. The orientation of the dipole should also be perpendicular to the isocontours at the point if highest density.

The hypothesis for the location of the dipole is further supported by the 17-23Hz bipolar corticomuscular cumulant topographic maps Fig. 5.118*D,E,F* and Fig. 5.119*D,E,F*. The bipolar cumulant estimates express averaged electric potential field differences between electrodes timelocked to the EMG activity. Therefore it can detect changes in voltage generated by underlying oscillators.

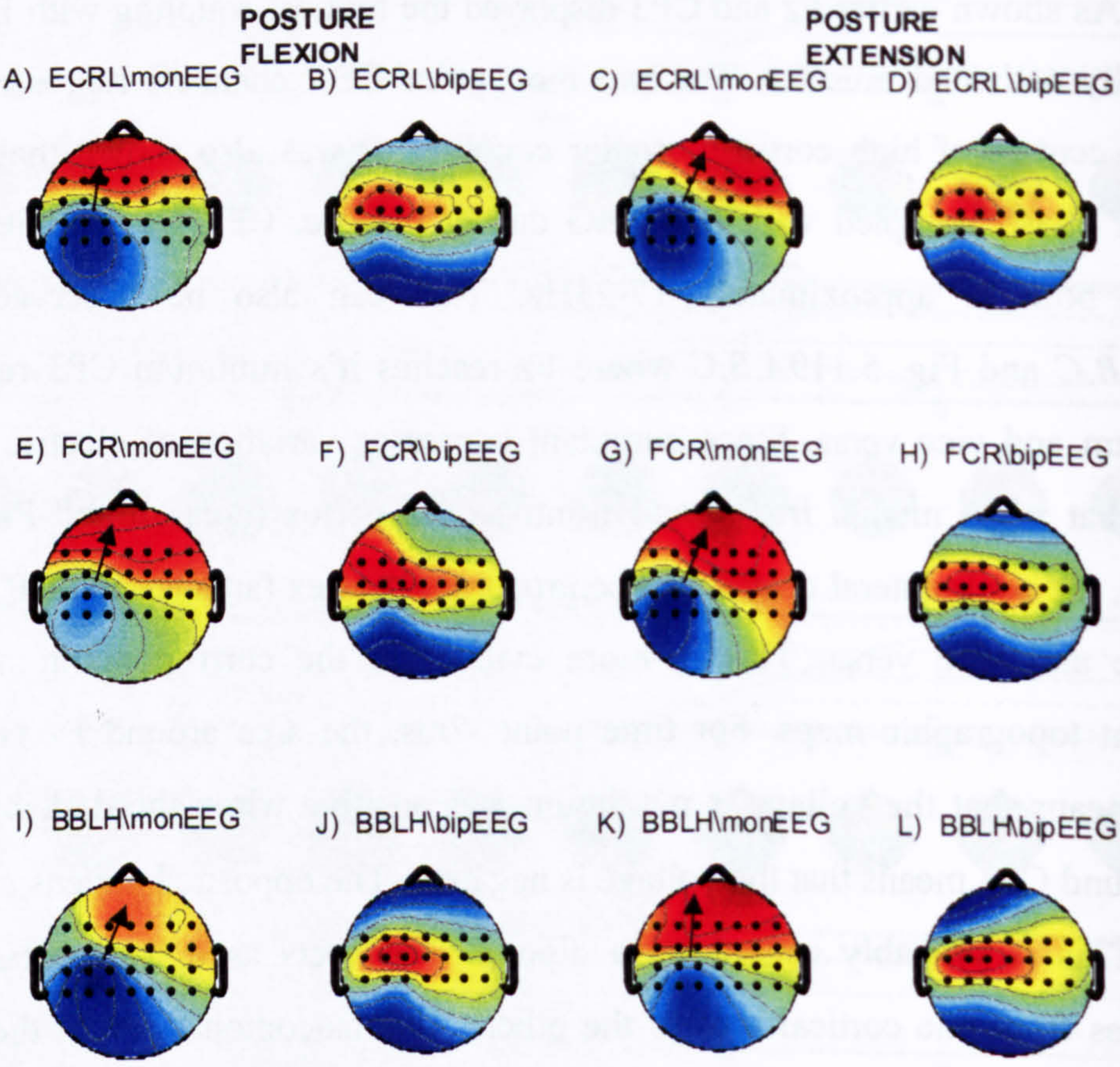

Fig. 5.120 Monopolar and bipolar cumulant topographic maps for ECRL, FCR and BBLH EMGs during posture flexion and posture extension at -7ms of the cumulant estimate. A dipole source has been experientially approximated for the monopolar plots. The location of the dipole should match the area with the highest density of isocontours. Its direction should be perpendicular to these isocontours. The location should also roughly match the area that the maximum value occurs for the bipolar map. Dark red represents the highest value while dark blue represents the lowest value.

The maximum and minimum cumulant features occur at approximately -7ms and -31ms timepoints on the cumulant estimates. At -7ms minimum voltage can be seen over the contralateral central cortex and increased voltage over the ipsilateral central cortex compared to the rest of the cortical area. The voltage in the same areas drops below zero at -31ms with the contralateral motor cortex showing the lowest value.

An experiential approximation of the dipoles at -7ms can be seen in Fig. 5.120. The bipolar recordings contain more localised activity and express activity of underling processes. In this case it is very likely to contain the dipole source associated with corticomuscular coherence. The interchanged positive and negative voltage is the result of the change in polarity of the dipole that generates oscillatory activity. The disadvantage of the bipolar configuration compared with the monopolar is the lack of information on the orientation of the dipole. Some information could be extracted by combining information from vertical and horizontal bipolar montages in order to reconstruct diagonal voltages. However a much greater number of electrodes would be required, resulting to much greater spatial resolution of information in order to obtain accurate results. This is not an issue for the results presented in this session since the monopolar montage derived adequate dipole orientation information.

5.1.7.4 Summary of topographic coherence and cumulant map results.

- Monopolar and bipolar topographic maps were produced illustrating the distribution of the 17-23Hz coherence over the cortex. This was a useful way to examine the spatial characteristics of coherence for the band that was previously shown to display the most task dependent variations.
- Monopolar topographic maps showed two centres of high 17-23Hz corticomuscular coherence during posture; medial frontal and frontocentral cortex and contralateral central and centroparietal cortex. The relative size of the maximum of each feature contains information regarding the flexed or extended type of posture. The distribution of the features (disregarding heir size) was similar for ECRL and FCR EMGs while slightly different for BBLH.
- Bipolar topographic maps showed one site of localised 17-23Hz corticomuscular coherence over the contralateral motor cortex during posture. This site closely matched the site where the highest increase in 17-23Hz spectral power occurs during posture. The distribution of corticomuscular coherences was similar for ECRL and FCR EMGs while slightly different for BBLH. The features were stronger during posture flexion than during posture extension for all three EMGs. The higher size of the peaks during posture flexion and small differences in the distribution of the features contain information regarding the type of posture performed (posture extension or posture flexion). However the relative information contained in the corresponding monopolar topographic map is clearer and easier to recognize.
- Monopolar and bipolar topographic maps were produced illustrating the distribution of the 17-23Hz cumulant estimates over the cortex. Several frames were captured over the cumulant estimate time axis. This was a useful way to examine the spatial characteristics of cumulant for the band that was previously shown to display the most task dependent variations.
- Cumulant components express the averaged EEG timelocked to the onset of EMG bursts. Therefore the collective cumulant topographic maps are a good estimation of the distribution of voltage over the scull. By confining the cumulant within the 17-23Hz band that corticomuscular coupling features occur, the

200A

distribution of voltage over the cortex generated by the cortical oscillators underling the corticomuscular coupling in this band was estimated.

- The monopolar and bipolar cortical voltage distribution revealed features of the underlying cortical oscillator. It appears to be located in the contralateral motor cortex. Earlier, bipolar coherence and spectral power showed a localised increase during posture over the same area. The isocontours of the monopolar topographic map revealed the orientation of the dipole souse. For ECRL and FCR the dipole orientation roughly follows the line connecting the electrodes showing the highest coupling features (Fz, CP3). The direction for the dipole underlying the BBLH corticomuscular activity has a direction closer to the posterior-anterior axis. While the direction of the dipoles appears relatively constant, its polarity alternates between positive and negative, justifying the term cortical oscillator.
- The estimated location and orientation of the dipole using multiple EEG closely matches analogous studies (Gross, Tass et al. 2000) using multiple MEG recordings. The magnetic field isocontours (Fig 2.22) appeared perpendicular to the electric potential field isocontours calculated in the present study, simply because of the fact that electric and magnetic fields are fundamentally perpendicular.

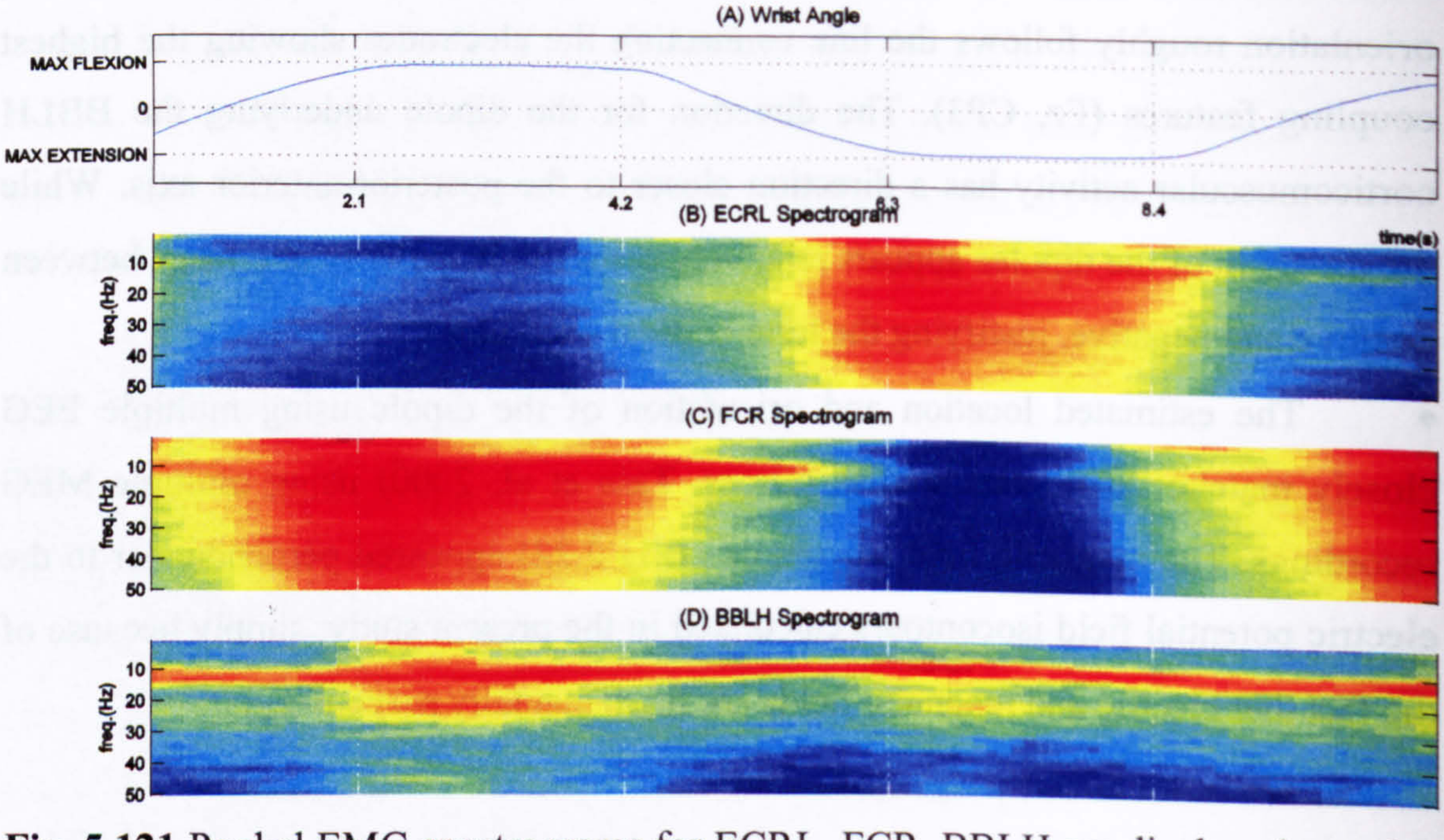

Fig. 5.121 Pooled EMG spectrograms for ECRL, FCR, BBLH are displayed together with averaged wrist angle and audio cue triggers. The plots contain the data from all 9 subjects and 21 trials and illustrate the spectral power variations in the length of one trial.

5.1.8 Time dependent frequency characteristics

In this section the EEG and EMG data sets obtained from the move-hold sequence experiment are going to be presented from a different perspective. Previously the focus was to identify task dependent features for each individual phase during the move-hold sequence by segmenting and analysing the data into four data sets. Each contained data only from a specific task (movement flexion, posture flexion, movement extension, posture extension) ignoring the data spanning the transition periods. In this section, the focus will not only be the task dependent frequency characteristics of individual tasks but also how these parameters continuously change in time during the transition from phase to phase and within each phase. Sliding-window time-frequency techniques were used in order to achieve this. Data was pooled across subjects (9 subjects) and trials (sets of four sequential phases; movement flexion, posture flexion, movement extension, posture extension) and estimates were calculated in time. This produced three dimensional matrix results where X axis represents time, Y axis represents frequency (or time for cumulant plots) and Z axis is the value of the estimate (phase, coherence, cumulant or phase). These results were plotted as images, where the Z axis was displayed as an optimised scale 256 colour intensity map.

Using this approach, it was possible to monitor the time dependent changes of the estimates. The way these estimates changed between tasks or during the same task, provide additional information that could improve our understanding of the nature of human movement, and also relevant to the design of control systems for neural prostheses.

Fig. 5.121 shows the pooled EMG spectrograms. All results are presented as one trial of the move hold sequence (movement flexion, posture flexion, movement extension, posture extension). Fig. 5.121*A* represents the averaged wrist angle information normalised to the "maximum flexion" and "maximum extension" deviations. An example of the ECRL, FCR and BBLH EMG modulation during the move-hold sequence can be seen in Fig.5.1. While the level of activity for BBLH appears quite constant, ECRL and FCR activity show great variability depending on the point in the movement sequence.

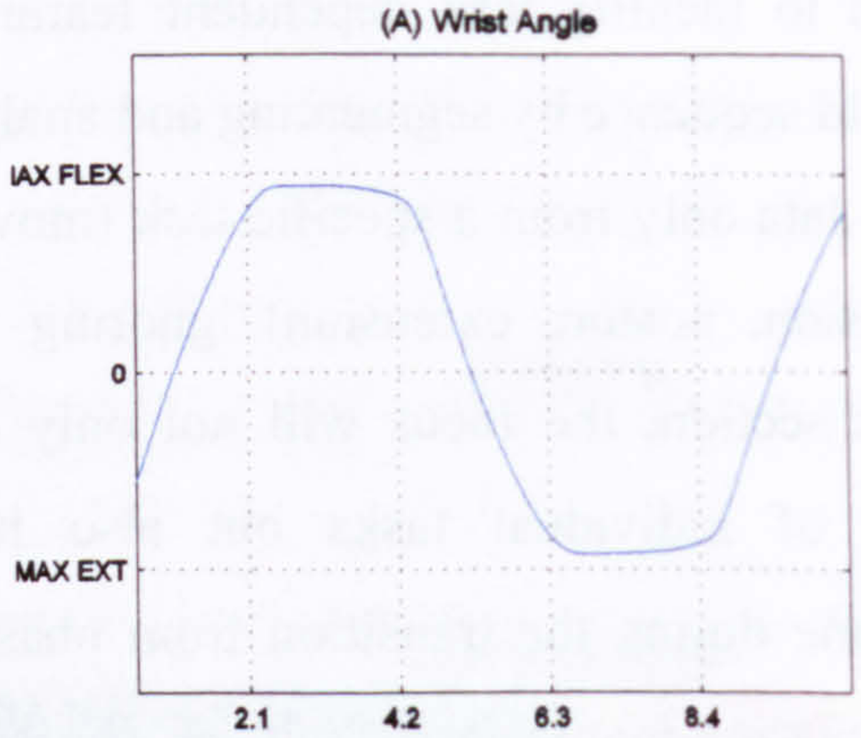

Fig. 5.122 Pooled EMG spectrogram of BBLH muscle, displayed together with averaged wrist angle and audio cue triggers. The plots contain the data from all 9 subjects and 21 trials and illustrate the spectral power variations in the length of one trial. Fig. 5.122*B* is actually identical to Fig. 5.121*D* plotted in a tighter time scale to highlight the variation of the near 10Hz carrier frequency during the move-hold sequence.

Fig. 5.121*B* shows the pooled ECRL spectrogram. During the flexion phase the antagonist ECRL activity is relatively low. However activity in the 10Hz band increases. The agonist-antagonist activity, as has been previously demonstrated (REF), appears to be modulated in 10Hz bursts. The ECRL 10Hz power during flexion movement is stronger at the beginning of the movement. The transition from movement flexion to posture flexion decreases the overall power for the ECRL muscle. During the posture flexion phase the ECRL power is relatively low except from a low activity feature in the 15-30Hz range. The 35-45Hz band activity is largely decreased compared to movement flexion. The transition from posture flexion to movement extension initiates increased activity over the whole ECRL EMG spectrum. A low frequency component (below 5Hz) is present at the onset of movement. There is no distinct 10Hz peak, despite the presence of very strong 10Hz activity in the antagonist's FCR spectrum. At the end of the extension movement a strong ECRL and FCR 5Hz power feature emerges again. At the same time a dramatic increase in the activity of the ECRL muscle takes place. At the start of the posture extension phase, a distinct FCR feature at 10Hz is apparent and persists throughout the extension movement and posture becoming narrower loosing power towards the end of the phase. Features at 19Hz, 23Hz, 30Hz and 40Hz were also present. Towards the end of the posture phase the overall power decreases, with frequencies from 30 to 45Hz decreasing faster than the 10–30Hz band. After the transition from extension posture to flexion movement there is a general decrease in activity except from the 10Hz band while decreasing in power, persists into the flexion movement phase.

Fig. 5.121*C* shows the FCR EMG spectrogram during a period of the move hold sequence. The wrist movement flexion phase is dominated by a strong, movement related 10Hz feature. A gradual increase in the whole power spectrum also occurs. In the transition from flexion posture to movement a low frequency components can bee seen to emerge. During the flexion posture high activity can be observed in the FCR spectrum. Towards the end of the phase, power is decreased and focused to occur within the 10Hz band. This 10Hz power increases and reaches a maximum with the start of the movement extension phase. Higher frequencies seem to decrease faster than low frequencies towards the end of the phase. After the start

of extension, high frequencies decrease in a more progressive way, when compared with ECRL (Fig. 5.121*B*) during the transition from extension posture to flexion movement. The 10Hz antagonist FCR power remains at a high level throughout extension movement phase. During the posture extension phase, the FCR EMG is relatively silent with a weak 10Hz component. Small 20Hz activity is also present while in the 30 to 45Hz band the activity is low. For the transition from extension posture to flexion movement there is an increase in all frequencies with an onset of 10Hz activity occurring before the increase at higher frequencies. The 10Hz power becomes increasingly stronger.

For the BBLH muscle (Fig. 5.121*D*) there is a 10Hz trail of activity throughout the move-hold sequence. The carrier frequency appears relatively constant however it actually varies from 14Hz to 9Hz depending on the wrist movement phase. During movement flexion the peak of the examined alpha band is 14Hz. During posture flexion the frequency shifts to 12Hz. During extension movement the power magnitude decreases even further to reach the minimum frequency of 9Hz just after the start of extension posture. During extension posture and flexion movement the frequency again reaches its maximum frequency of 14Hz. These changes can be better monitored in Fig. 5.122 where the BBLH spectrogram is displayed using a shorter time scale to highlight the task dependent frequency variation. In addition an 18Hz feature is seen during the first phases of wrist posture flexion and a 20-24Hz is present throughout the duration of posture. The same features emerge in the same way during posture extension. They appear considerably stronger during posture flexion than during posture extension. BBLH shows strong (wrist) task dependent modulation despite the fact that its main action during the test was to stabilise the elbow at a fixed angle. It acts as agonist on elbow, and performs a continuous contraction supporting the arm while the wrist performs the move hold sequence. It is obvious that there is a task dependent variation of the dominant BBLH alpha activity, not only in the power magnitude but in the carrier frequency as well. It appears that BBLH does not function in isolation, but as part of synergistic system. Despite the fact that BBLH is not directly involved in wrist action, its activity is task modulated according to the wrist movement, with its frequency content changing according to the task performed by the wrist.

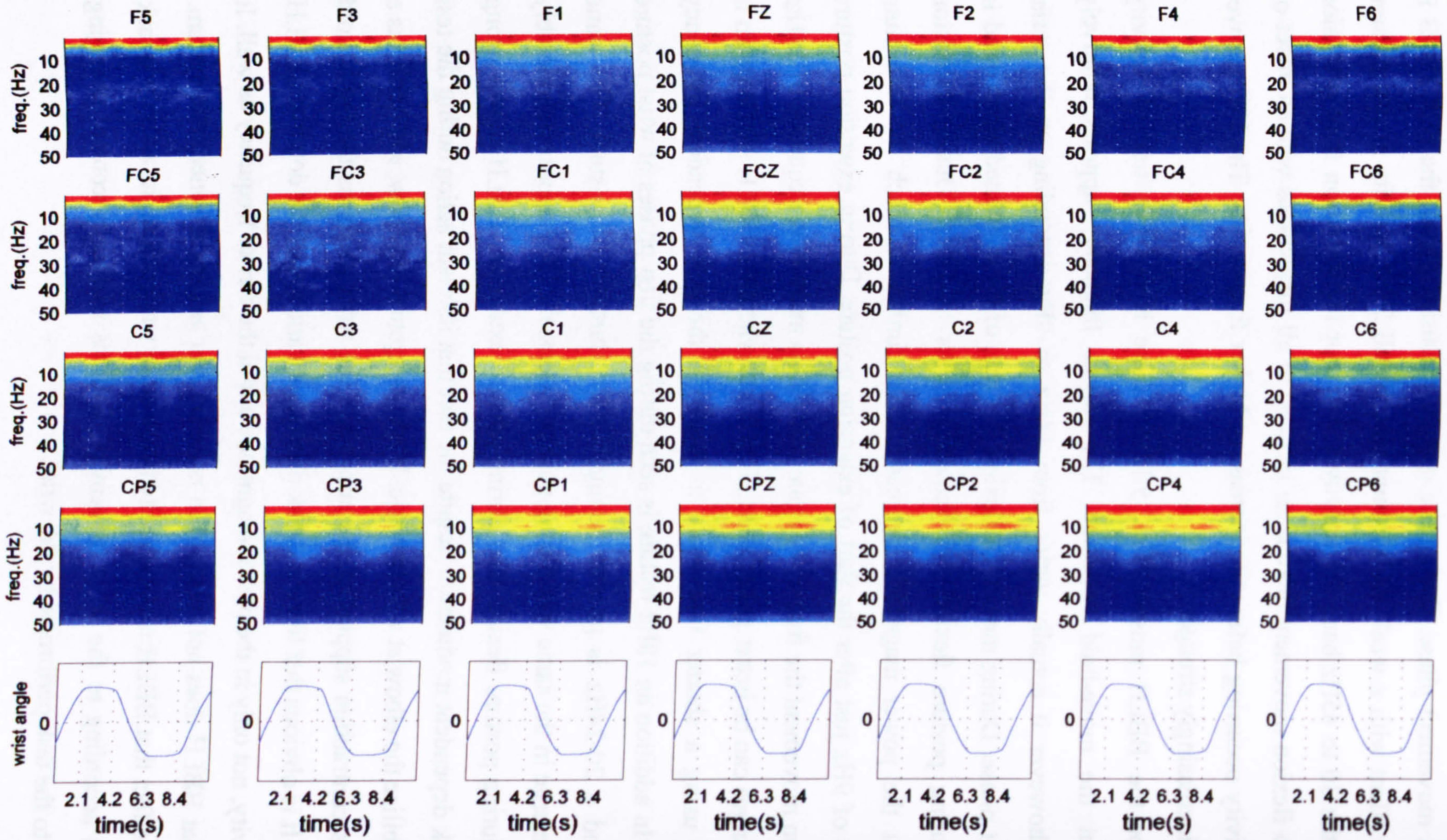

Fig. 5.123 Grid consisting of the pooled monopolar EEG spectrograms during the move-hold sequence. Each spectrogram has been individually scaled to use the full colourmap. Therefore magnitude of features for different electrodes can not be compared. Wrist angle and audio cues are also displayed.

Fig. 5.123 shows a grid consisting of the pooled monopolar EEG spectrograms during the move-hold sequence. A number of movement dependent features are present in all examined bands.

In delta band (0-3Hz), task dependent activity can be observed. This modulation is expressed as relative power increase (synchronisation) during posture and during movement. The increase during posture is higher than during movement. Desynchronisation occurs during the transition from posture to movement and vice versa. A similar pattern of activity can be observed for the theta band; however the delta features are more distinct. The theta and delta features are widespread and are present for all examined electrodes, while they appear slightly stronger in the frontal area.

The alpha band also displays task dependent features. These features have different temporal and spatial characteristics than the ones observed in the delta band. They are stronger for medially located, central and centroparietal electrodes at the medial-ipsilateral cortex. The alpha patterns show alpha synchronisation before the initiation of movement flexion and movement extension phases (or towards the end of posture flexion and posture extension phases) and desynchronisation during movement flexion and movement extension. Synchronisation at a smaller scale also occurs just before the onset of posture phases.

There is increase in beta EEG power during posture while it is suppressed during movement. The beta features are widespread and are more distinct for medial frontal electrodes while they expand laterally towards the centroparietal area. The beta feature is present for all monopolar centroparietal electrodes. The distribution of features also appears to be symmetrical over the anterior-posterior axis. Small gamma features are also present mainly during posture these features are quite small in comparison to the features already examined so they are not easily identifiable.

Fig. 5.124 displays a grid of spectrograms of the bipolar EEG electrodes (bipolar montage includes all pairs of adjacent electrodes on the vertical axis). All displayed spectrograms contain similar delta, theta alpha and gamma features with the corresponding monopolar map (Fig. 5.123) but but with different spatial characteristics. Delta band features emerge during posture and movement with the

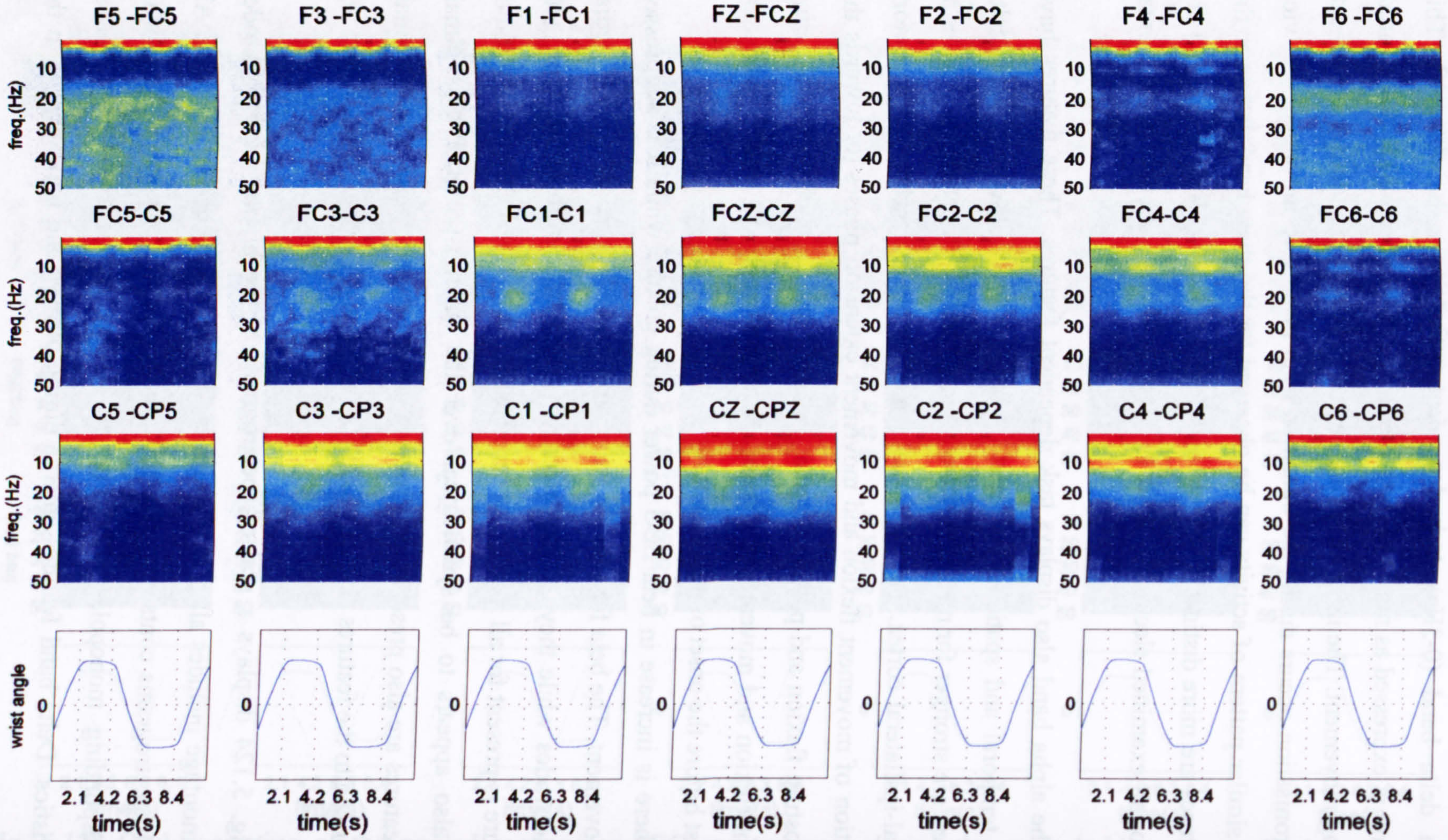

Fig. 5.124 Grid consisting of the pooled bipolar EEG spectrograms during the move-hold sequence. Each spectrogram has been individually scaled to use the full colourmap. Therefore magnitude of features for different electrodes can not be compared. Wrist angle and audio cues are also displayed. C1-CP1, FC2-C2, C2-CP2 and C4-CP4 contain artefacts, because of the proximity of the corresponding electrodes.

posture feature larger than the movement. Delta desynchronisation occurs during the transition between movement and posture phases. Similar to the corresponding monopolar spectrogram features is the bipolar alpha modulation while it appears less defined in the latter. Regarding the beta band there are clear features during posture (flexion and extension) at around 15-25Hz, reaching a maximum around 0.7 sec after the audio cue. For ipsilateral frontocentral and central electrodes small occurrence of beta power can be observed during movement, which is not obvious in the contralateral electrodes.

Fig. 5.125 and Fig. 5.126 illustrate the cortical maps consisting of time dependent intracortical coherences between adjacent electrodes on the vertical and horizontal axis respectively. Fig. 5.125 demonstrates posture specific decoupling in the beta band. The decoupling is expressed as reduction in coherence and is more distinct for the contralateral cortex between frontocentral-central electrodes. It is also present at the ipsilateral cortex where smaller beta decoupling is also present during movement. Delta intracortical coupling features are also present and resemble the power spectra features observed for monopolar and bipolar EEG spectrograms (Fig. 5.123 and Fig. 5.124). No alpha features are apparent. However alpha features appear in Fig. 5.126 at the ipsilateral cortex, mainly for FC2\FC4 intracortical time dependent coherence. It emerges as task dependent alpha decoupling during the last 1s of posture and the first 1.5s of movement. Coupling recovers at the end of movement (last 0.5s), the transition to posture and the first 1s of posture.

Fig. 5.127 contains in more detail the spectrograms of selected EEG channels from the spectrogram grid maps in Fig. 5.123 and Fig. 5.124. These channels are the monopolar FC1 (Fig. 5.127*B*) and C1 (Fig. 5.127*C*) as well as the bipolar FC1-C1 (Fig. 5.127*D*) electrode pair. The spectrograms of the FC1 and C1 monopolar channels displayed in great detail in Fig. 5.127*B,C* appear very similar and contain task related features. The most obvious is increased power during posture at around 15-25Hz. This beta synchronisation appears slightly higher during extension posture than during flexion posture. There are also delta spectral features (at approximately 2Hz) following the initiation of posture and movement. As described earlier the

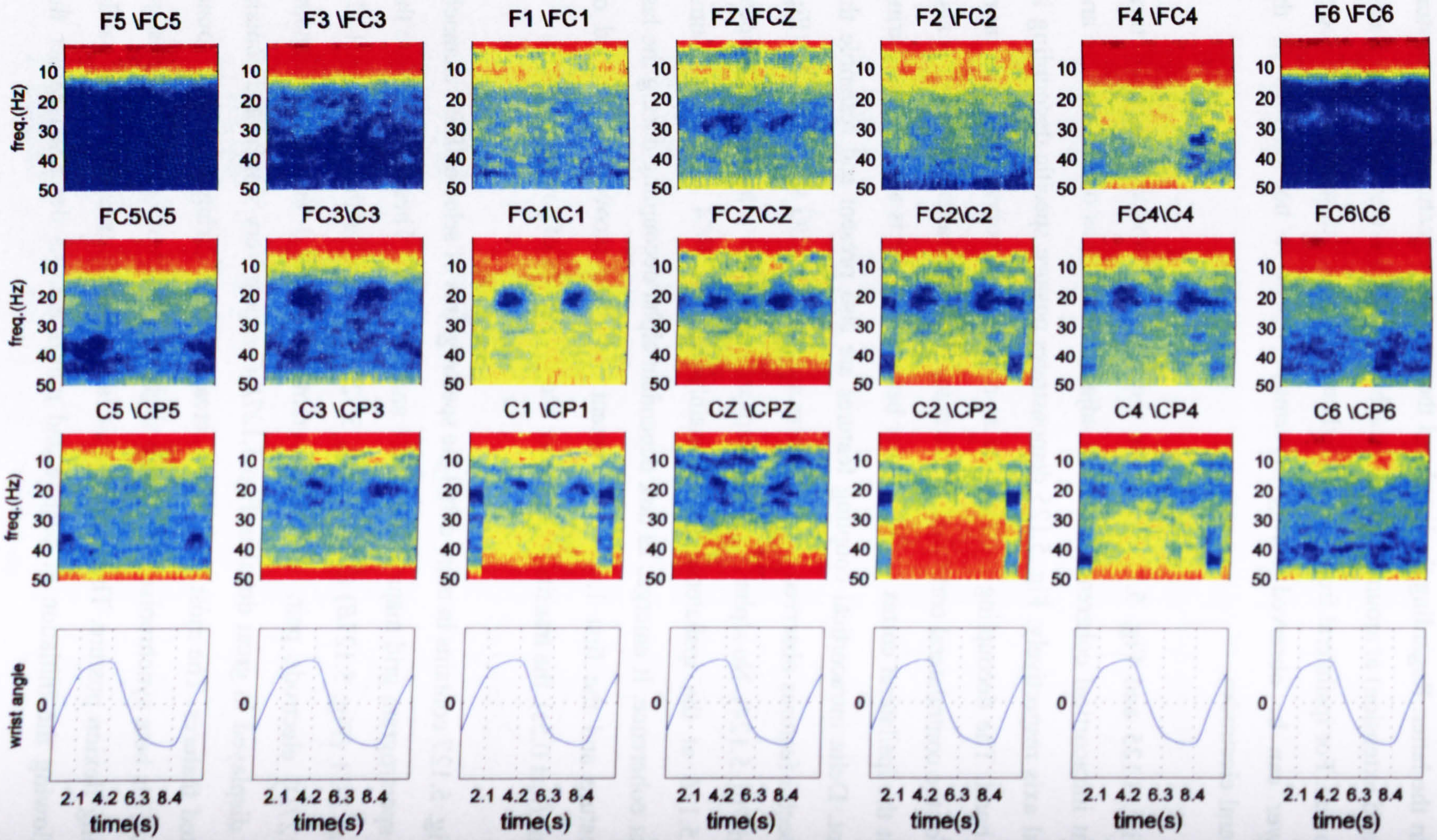

Fig. 5.125 Grid consisting of the pooled intracortical EEG time dependent coherences between monopolar electrodes on the vertical axis, during the move-hold sequence. Each coherogram has been individually scaled to use the full colourmap. Therefore magnitude of features for different electrodes can not be compared. Wrist angle and audio cues are also displayed. *C3\CP3, FC2\C2, C2\CP2, FC4\C4 and C4\CP4 contain artefacts, because of the proximity of the corresponding electrodes.*

features have greater magnitude during posture than during movement. The timing is also different with the posture delta features reaching a maximum approximately 0.6s after the audio cue while this happens 0.9s after the audio trigger during movement phases. Desynchronisation occurs during the movement-posture and posture-movement transitions. Strong 10Hz activity appears almost throughout the performed movement phases, especially for C1 channel. This feature takes its maximum at the end of the posture phase. This means that it is either a late posture component, (becoming stronger around 1.5 sec after posture commences) or that it is the cognitive product of a movement preparation state.

The spectrogram of FC1-C1 bipolar channel is illustrated in Fig. 5.127*D*. The delta, alpha and beta features are also present in the bipolar spectrogram with similar temporal characteristics to the monopolar spectrograms. The fact that these features emerge in a similar way for monopolar and bipolar channels suggest that they are not the product of auditory evoked potentials triggered by the audio cue, as these evoked potentials should be diminished in the bipolar recording. The beta features are in fact better defined than in the monopolar plots. A strong and broad (15-25Hz) beta component appears during the two posture phases, which is broader and occurs at a similar frequency as observed for the two monopolar channels. It has a peak at around 22Hz. A small beta feature is also present during movement. It is different to the one observed during posture, being narrower and with lower amplitude. The beta feature proportional increases during posture, reaches it's maximum at 0.7-0.9ms after the audio cue, and clearly decreases during the transition between posture and movement. A small beta feature remerges during movement while it decreased during the transition to posture.

Fig. 5.127*E* shows the intracortical coherence between FC1\C1 electrodes. It is evident that there is a major reduction in intracortical coherence (decoupling), during posture phases. While the beta power in the area has increased during posture (as demonstrated in the monopolar FC1, C1 and bipolar FC1-C1 spectrograms in Fig. 5.127*B,C,D*) the coherence between FC1 and C1 electrodes has decreased. The reduction occurs in the same frequency band (15-25Hz). The decrease starts soon after the audio cue and reaches a minimum level at approximately 0.9s after the audio cue for flexion and extension posture. The decoupling is not as strong towards

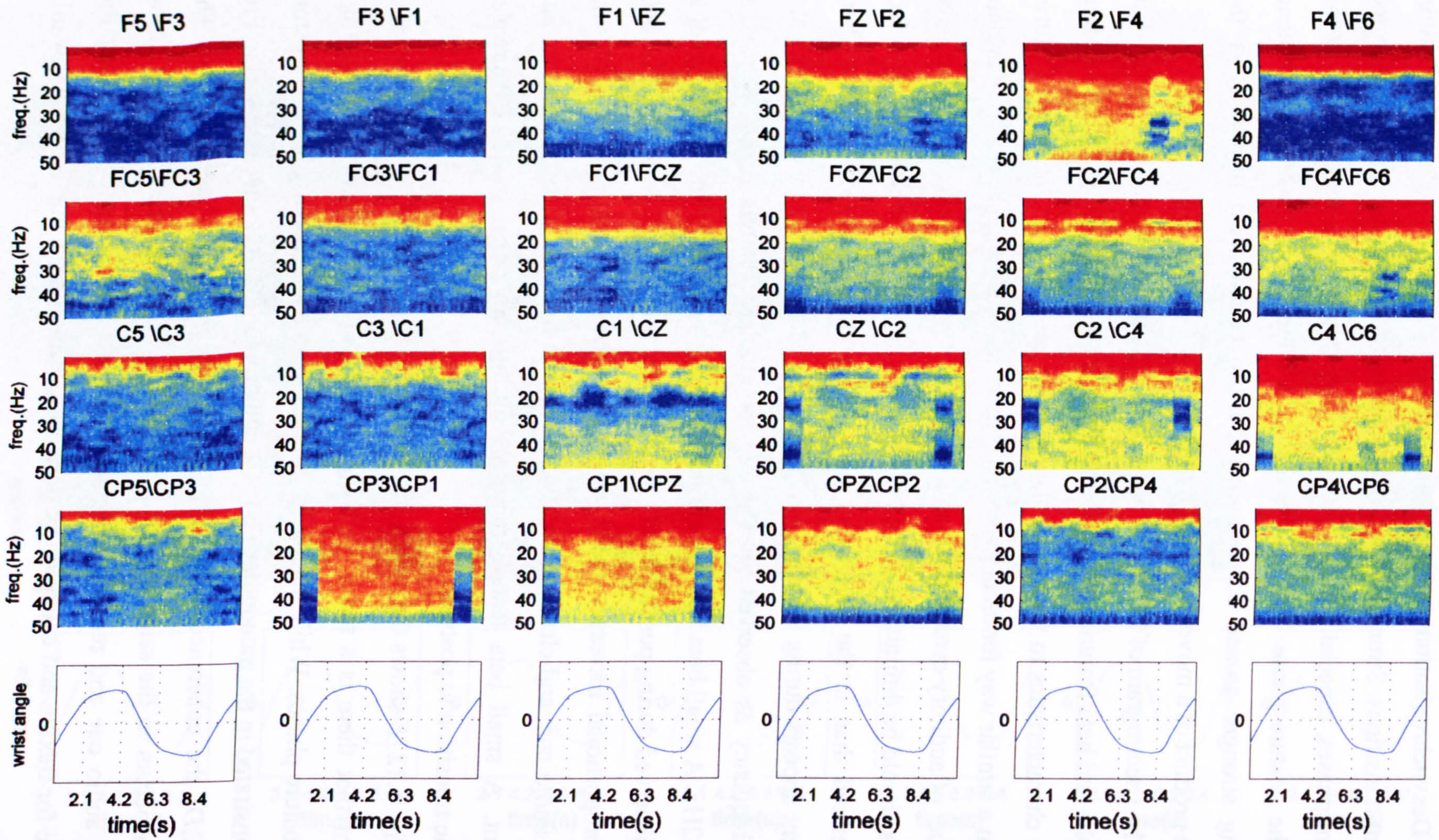

Fig. 5.126 Grid consisting of the pooled intracortical EEG time dependent coherences between monopolar electrodes on the horizontal axis, during the move-hold sequence. Each coherogram has been individually scaled to use the full colourmap. Therefore magnitude of features for different electrodes can not be compared. Wrist angle and audio cues are also displayed. CP3\CP1, CP1\CPz, Cz\C2, C2\C4 and C4\C6 contain artefacts, because of the proximity of the corresponding electrodes.

the end of the posture phase and intracortical coherence seems to recover before the second audio cue instructing the subject to move. During movement there are no strong features apart from a small trough in coherence at 21Hz for the whole duration of the wrist movement. "High beta" and gamma features are also present during posture. During posture flexion decoupling at 30Hz is present, which is more defined in the second half of the phase. In addition a 40Hz desynchronisation can be identified and is more defined in the first half of posture flexion. For posture extension there are no clearly defined features outside the ones described above.

In Fig. 5.127*F* there is a representation of the phase between the two monopolar EEG channels in time. During movement the phase is very uniform throughout the examined band. During posture clear phase modulation occurs in the same beta frequency area and with similar timing to intracortical coherence and power modulation observed in Fig. 5.127*E*. The phase starts decreasing at 16-18Hz, reaches a minimum value at 21Hz and then recovers to its near zero value at 26Hz. Its timing is similar to the coherence features with minimum value around 0.9s after the audio cues. These characteristics are clearest for the posture extension feature.

In Fig. 5.127*G* the time dependent cumulant density can be seen, which also includes task dependent modulation. There is an increase during posture and movement phases, with cumulant during posture higher compared to movement. The maximum cumulant during posture appears approximately 0.6ms after the audio cue a few ms earlier than power, coherence and phase EEG modulation (where the maximum features emerged 0.7-0.9ms after the audio prompt).

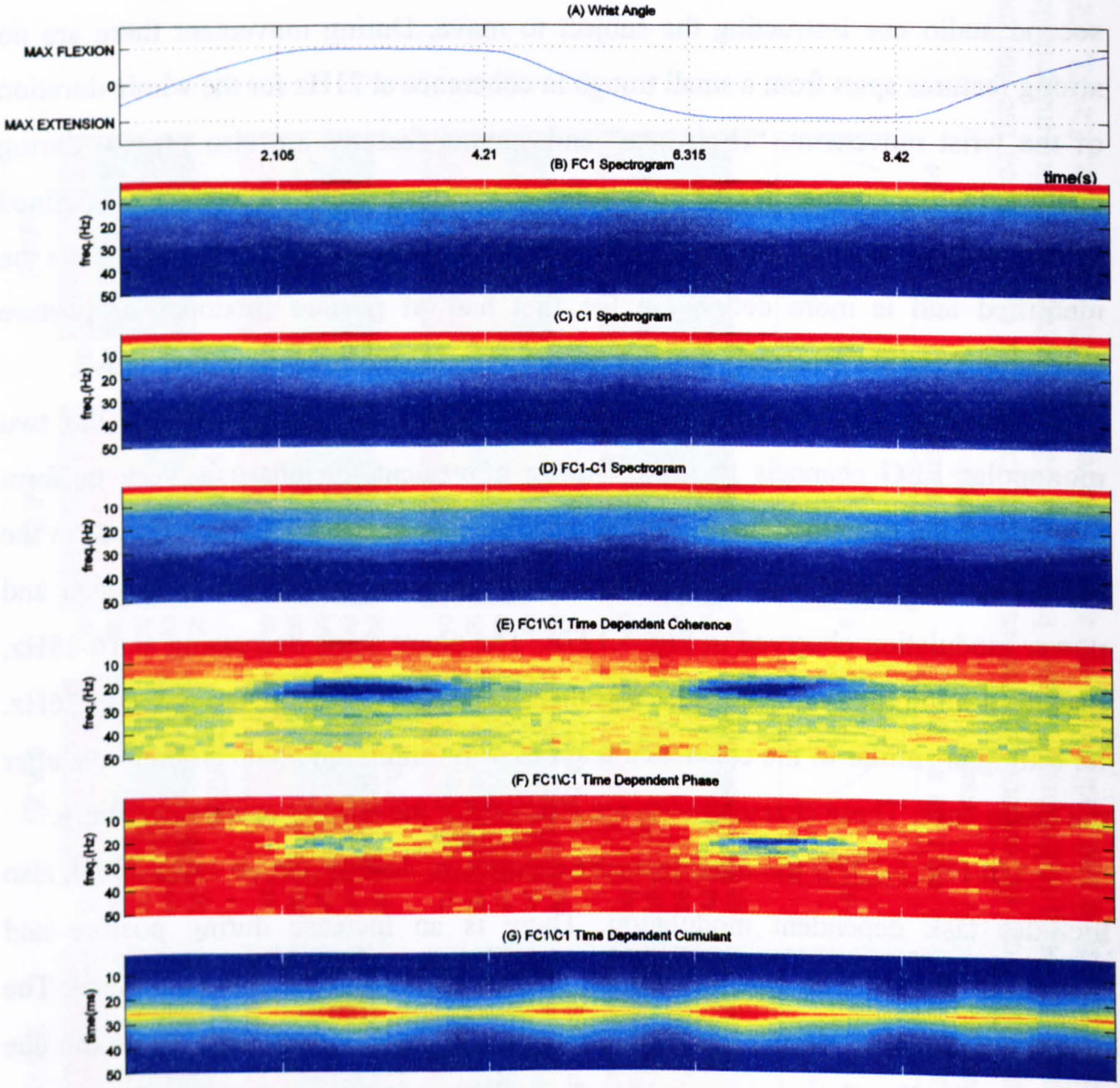

Fig. 5.127 Pooled EEG spectrograms for monopolar FC1, monopolar C1 and bipolar FC1-C1 channels are displayed together with averaged wrist angle and audio cue triggers. The plots contain the data from all 9 subjects and 21 trials and illustrate the spectral power variations in the length of one move-hold sequence trial.

Fig. 5.128 displays the time dependent coherence and cumulant estimates between all three EMG pairs, ECRL\FCR (Fig. 5.128*B,C*), FCR\BBLH (Fig. 5.128*D,E*) and ECRL\BBLH (Fig. 5.128*F,G*). There is functional coupling in the 18-26Hz area during posture flexion and posture extension for all three coherograms with peaks at approximately 21Hz. Beta coupling is not constant throughout posture phases but starts increasing soon after the establishment of posture, reaches a maximum value and declines before the end of the phase. Because of the 1024 point sliding window used for the processing, the exact time of rise or end of coherence can not be accurately defined. It appears that in most cases beta posture intermuscular coherence reaches its maximum approximately 0.9ms following the audio cue. It also seems that coherence drops towards the late stages of posture and prior to the audio cue instructing the subject to move.

For the ECRL\FCR pair (Fig. 5.128*B*), the intermuscular coherence is higher during posture extension than during posture flexion while coherence for FCR\BBLH and ECRL\BBLH pairs (Fig. 5.128*D* and *F*) is stronger during posture flexion. This means that ECRL\BBLH and FCR\BBLH coherences are higher for posture flexion but ECRL\BBLH is higher in posture extension. Different pairs of muscles reach different levels of coupling under similar conditions which under the assumption of central origin of coupling, suggests the independent control of coactive muscles by the CNS.

In the FCR\BBLH time dependent coherence (Fig. 5.128*E*) weak 10Hz is present during both posture phases, but is stronger during the posture flexion. This feature becomes stronger in the last stages of posture after the decline of the 20Hz coherence.

During movement the time dependent coherence reveals development of 10Hz intermuscular coupling. At the beginning of movement extension there is strong coherence for ECRL\FCR pair, which is strongest in the early stage of the movement but does not sustain to the end of the movement. While the 10Hz ECRL\FCR feature starts immediately with the movement phase set off, ECRL\BBLH and FCR\BBLH coherences start later (approximately 0.7ms) which suggest that these features are not directly connected, and are not the expression of the same underlying activity. This is also supported from results displayed in Fig.

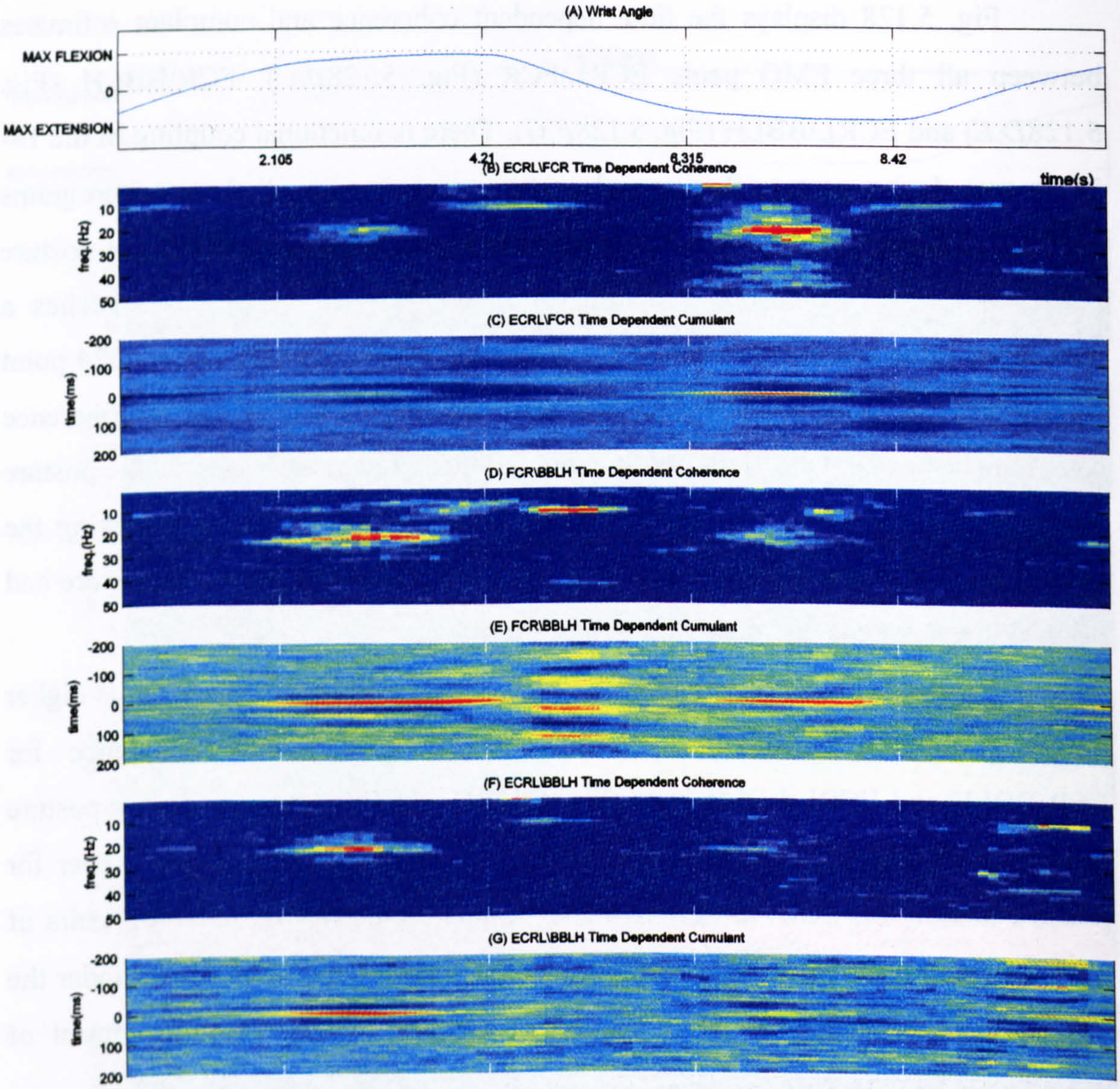

Fig. 5.128 Pooled intermuscular time dependent coherence and cumulant estimates displayed together with averaged wrist angle and audio cue triggers. The plots contain the data from all 9 subjects and 21 trials and illustrate the coherence and cumulant variations in the length of one move-hold sequence trial.

5.3*d,e,g,h* and Fig. 5.13*d,e,g,h*. while both ECRL\FCR and FCR\BBLH coherences during posture flexion (Fig. 5.3*d,e* respectively) occur at exactly the same band, the cumulant plots and delay characteristics (Fig. 5.3*g,h*) are different. During the transition from extension posture to flexion movement coherence at 10Hz between FCR and ECRL occurs. Weak coupling appears for FCR\BBLH and ECRL\BBLH.

Fig. 5.128*C,E,G* show the intermuscular time dependent cumulant estimates for all three EMG pairs, pooled across subjects and trials. For all three pairs of muscles, task dependent features can be seen. Most of these features relate to the corresponding time dependent coherence plots (Fig. 5.128*B,D,F*). For ECRL\FCR cumulant (Fig. 5.128*C*) there are clear features around time zero during posture extension and flexion, indicating strong synchronisation during these phases, and 0ms delay. The feature takes is maximum 0.9 s after the audio cue for flexion posture and 0.9 s for extension posture. The positive side-band peaks placed around 40-50ms on each side of the main peak indicate beta synchronisation. The central cumulant features start immediately and last almost throughout the posture tasks, being better defined than coherence peaks, seen in Fig. 5.128*B*. The central peak contains short term synchronisation information from the full 0-500Hz band and not only the 0-50Hz band as the coherence plot. This information is expressed by the more defined central peak. The secondary features indicating beta synchronisation are strong only for the part of posture where corresponding coherence plot is also strong.

During movement the ECRL\FCR cumulant central peak is absent and is replaced by features with 100ms period in the vertical time axis, revealing 10Hz synchronisation (Fig. 5.128*C*). The features during movement include a central trough in the cumulant density function. The trough is better defined for extension movement than for flexion. For both movement directions the synchronisation feature is more intense at the beginning and is fading out towards the end, with the trough lasting longer during extension movement than during flexion. The delay characteristics of the central trough and 10Hz cumulant can be better seen in Fig. 5.4*b*. ECRL\FCR appear as "out of phase" coupling with 0ms delay. The pictures for movement extension and posture extension are very similar to movement flexion and posture flexion.

Examining the FCR\BBLH time dependent cumulant (Fig. 5.128*D*), a central synchronisation feature can be observed at approximately time zero during posture, similar to the one observed for ECRL\FCR and ECRL\BBLH. The feature lasts longer than for the other two EMG pairs. For flexion posture the prolonged central feature appears to have two peaks during his phase. It reaches a first maximum value at 0.9s and after small decreased reaches a second one 1.6 after the audio cue. This may be connected to the double coherence features that will be shown for FCR\EEG coherence later (Fig. 5.134). The satellite features indicate that beta band coupling occurs. Alpha synchronisation can be clearly seen in the continuous time plots, with alpha coupling appearing in the late stages of posture. Stronger side-peaks appear at 100ms while secondary peaks close to ±50ms are present in the early stages and become less strong in the later posture stages.

For FCR\BBLH 10Hz synchronisation can bee seen during the movement phases, very strong during extension movement and less strong during flexion movement. The 10Hz synchronisation feature does not reach its maximum at the start of the movement phase similar to the ECRL\FCR pair but occurs well into the movement phase, and with different delay characteristics which suggests, as already mentioned different underlying processes.

ECRL\BBLH time dependent cumulant is shown in Fig. 5.128*G*. Similar to the ECRL\FCR and FCR\BBLH cumulant, a synchronisation feature is present during posture flexion, showing beta coupling. 10Hz coupling is present during movement. For movement flexion it appears stronger during the first half of the phase while during movement extension it appears later within the phase.

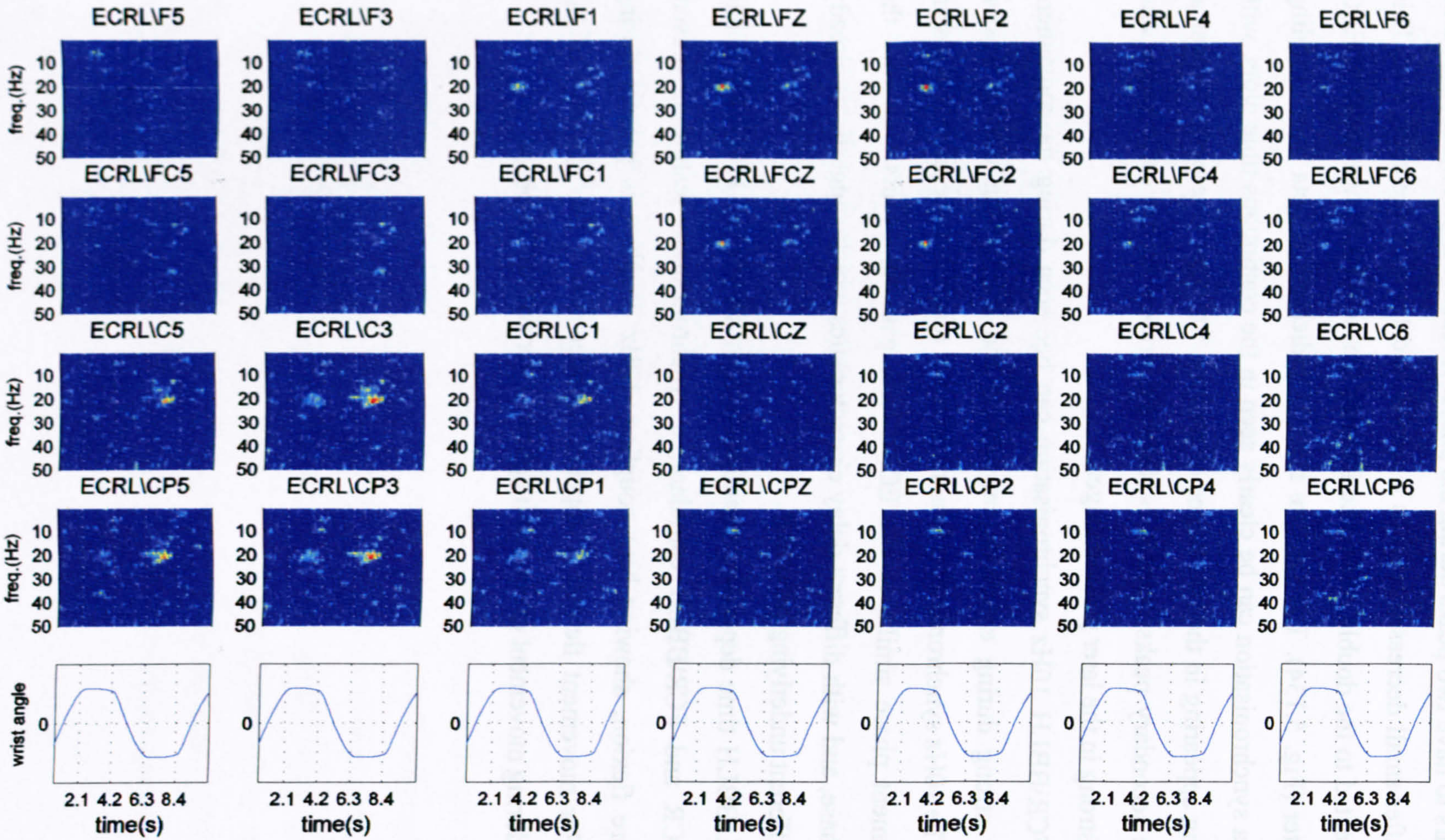

Fig. 5.129 Grid consisting of the pooled time dependent coherences between ECRL EMG and monopolar EEG spectrograms during the move-hold sequence. All time dependent coherence plots have been scaled to use the same colourmap. Therefore magnitude of features for different electrodes can be compared. The positions of the individual estimates correspond to the relative EEG electrode position. Wrist angle and audio cues are also displayed.

Fig. 5.129 illustrates a grid of the pooled time dependent coherences between ECRL EMG and monopolar EEG channels during the move-hold sequence. A number of theta, alpha and beta features can be observed. Most of the features can be are present during posture.

Beta coherence features are present in the medial frontal and front central areas as well as contralateral central and centroparietal areas during posture flexion and posture extension with ECRL\Fz and ECRL\CP3 showing the largest features. For the medial frontal and frontocentral electrodes the magnitude of corticomuscular coherence is higher during posture flexion while in central and centroparietal electrodes the highest coherence emerges during posture extension.

A distinct 10 Hz feature occurs during the last stages of the posture phase for a number of electrodes. This feature appears stronger in the ipsilateral cortex and especially in centroparietal, central and frontocentral electrodes. Its spatial distribution is very different than for the beta couplings. The most distinct alpha coupling appears in ECRL\CP6 estimate. Similar features also appear in the contralateral cortex, mainly in centroparietal and central electrodes. However the features are weak and last for a few ms around the audio cue indicating the end of posture flexion. FCR corticomuscular coherence also contains a similar feature with different spatial distribution on the cortex, as will be shown later in Fig. 5.132.

A theta coherence feature is also present mainly in the contralateral and medial frontocentral and central channels. The frequency of the feature is approximately 4Hz. The coherence emerges just after the audio cue indicating the start of the extension movement phase. A smaller feature in a similar frequency is also present in the contralateral frontal electrodes. The timing this time is different since the feature emerges just after the trigger indicating the start of posture flexion and last for approximately half the posture phase. Very small gamma activity is also present during posture flexion in ECRL\CP5 and ECRL\CP6

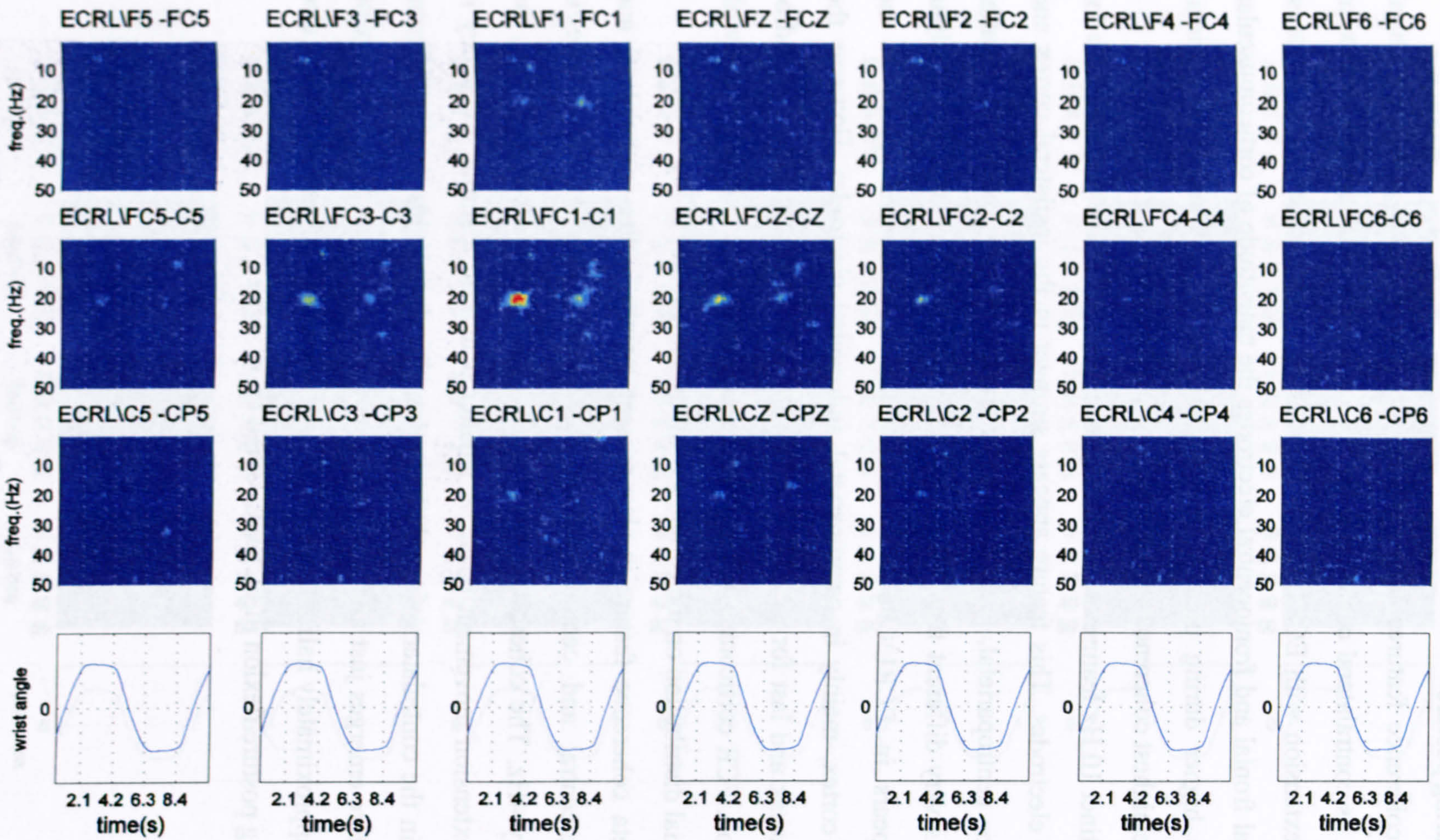

Fig. 5.130 Grid consisting of the pooled time dependent coherences between ECRL EMG and bipolar EEG spectrograms during the move-hold sequence. All time dependent coherence plots have been scaled to use the same colourmap. Therefore magnitude of features for different electrodes can be compared. The positions of the individual estimates correspond to the relative EEG electrode position. Wrist angle and audio cues are also displayed.

Fig. 5.130 illustrates a grid of the pooled time dependent coherences between the ECRL EMG and bipolar EEG channels during the move-hold sequence. A number of theta, alpha, beta and gamma features can be observed mainly during posture. The most prominent features emerge in the beta band during posture flexion and posture extension. The highest coherence occurs for ECRL\FC1-C1 estimate, and is also seen for surrounding electrodes, particularly those between the contralateral frontocentral and central area. The strongest feature also occurs during flexion posture where ECRL is coactive with FCR.

A beta feature is present in the bipolar maps during posture extension. It is stronger in ECRL\FC1-C1, ECRL\FC3-C3, ECRL\FCz-Cz and emerges in the last stage of the posture extension disappearing with movement. Weak theta features are present in the frontal-frontocentral channels. The features are similar with the features observed in the monopolar map in Fig. 5.129.

Gamma coherence also appears during posture extension. There is no clearly defined feature but sparse activity ranging from 30Hz to 45Hz, and occurring mainly during the second half of posture extension.

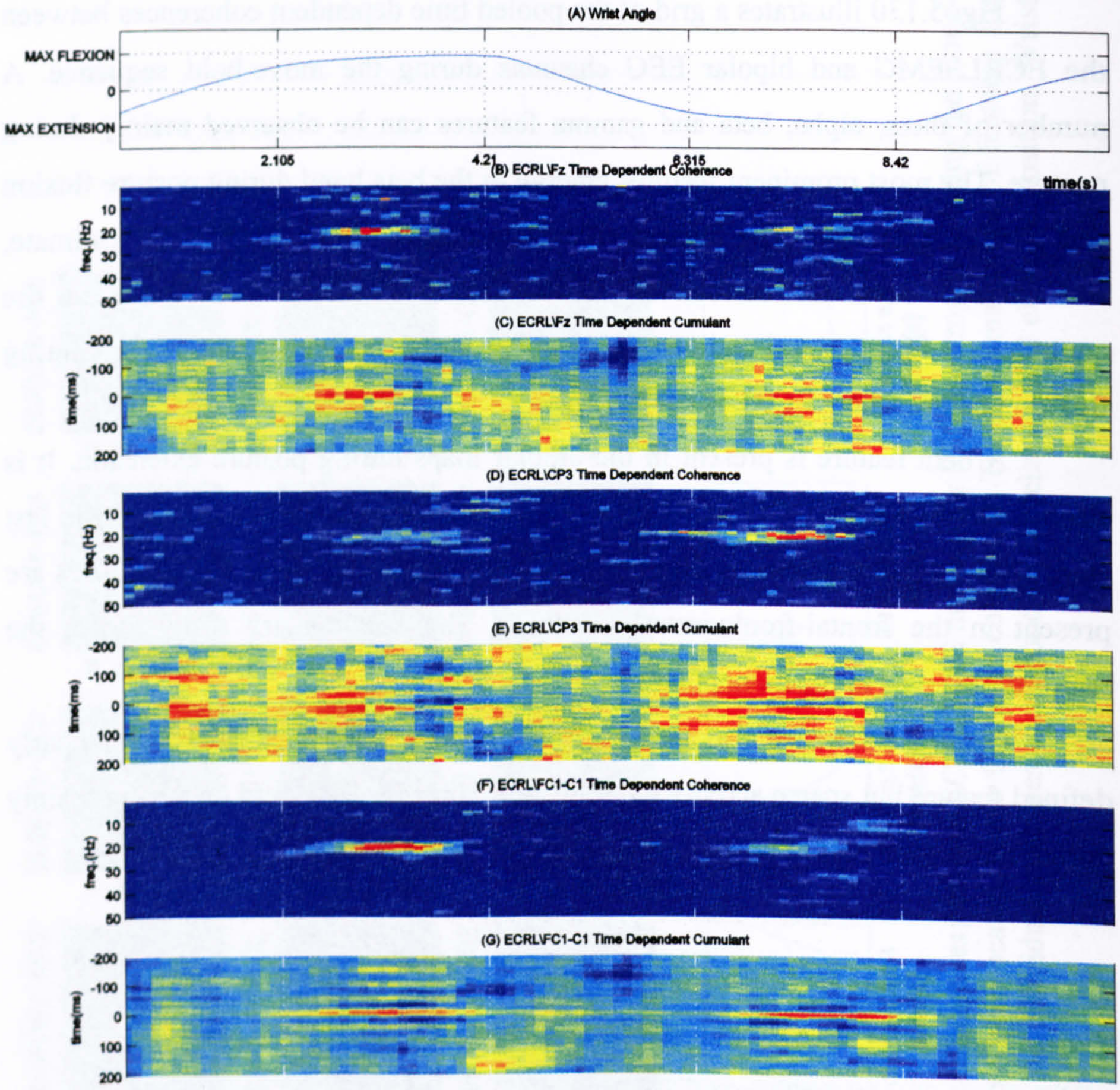

Fig. 5.131 Pooled ECRL\Fz, ECRL\CP3, ECRL\FC1-C1 corticomuscular time dependent coherence and cumulant estimates displayed together with averaged wrist angle and audio cue triggers. The plots contain the data from all 9 subjects and 21 trials and illustrate the coherence and cumulant variations in the length of one move-hold sequence trial.

Fig. 5.131*B,D,F* show the coherences in time between ECRL EMG and three EEG channels, two monopolar FZ, CP3 and one bipolar FC1-C1. As illustrated previously these channels are strongly coupled with the EMG during posture. As expected, during movement phases no significant corticomuscular coherence is seen in the examined spectrum. 10Hz coherence exists in the equivalent intermuscular ECRL\FCR coherogram Fig. 5.128*B* but not in the corticomuscular coherograms (either bipolar or monopolar). This suggests that the 10Hz intermuscular coherence is not the direct result of a process originating from a 10Hz activation of the examined cortical areas.

Flexion posture shows significant beta corticomuscular coherence between ECRL and all three EEG channels. The strongest coherence appears for the bipolar FC1-C1 channel and the weakest for the CP3 channel. The duration of the coherence does not last for the whole duration of the posture phase. It commences after the posture is established, (approximately 0.5 sec after the audio cue), and lasts around 1 second. The duration for the bipolar channel is longer during flexion posture. However once again the main coherence feature does not seem to last for the entire duration of the posture phase. The coherence trail is relatively narrow, with a range of 19-23Hz and maximum at around 21Hz. The maximum magnitude coincides with the equivalent intermuscular coherence coherograms in Fig. 5.128. The time that the maximum ECRL\Fz coherence value occurs also coincides with the maximum for the ECRL\FCR and ECRL\BBLH coherograms, which is an indication that the phenomena are related. During the extension movement there is no significant 10Hz or other feature in the examined frequency spectrum. During extension posture the bipolar coherence shows the strongest coupling. In this phase (extension posture) the ECRL\CP3 pair shows a stronger coherence than ECRL\Fz. During flexion posture ECRL\Fz appeared stronger coupled than ECRL\CP3. At the very late stage of extension movement alpha coherence is present. This appears more clearly for the bipolar EEG.

The corticomuscular time dependent cumulant estimates are going to be examined for single monopolar and bipolar EEG recordings (Fz, CP3, FC1-C1 in Fig. 5.131*C,E,G*), looking for task dependent features. Fig. 5.131*C* shows the corticomuscular cumulant estimates in time for ECRL EMG. For the monopolar Fz

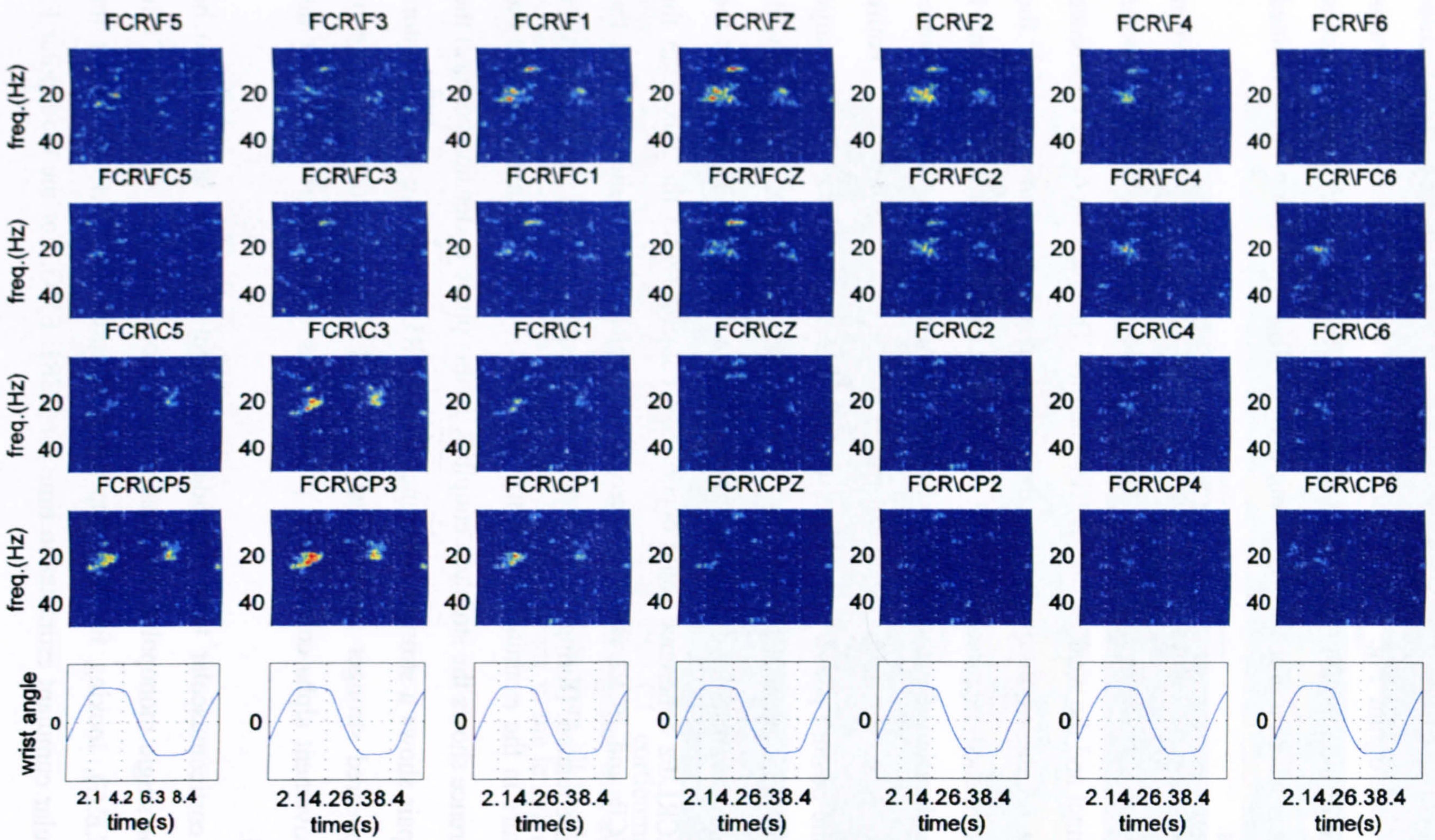

Fig. 5.132 Grid consisting of the pooled time dependent coherences between FCR EMG and monopolar EEG spectrograms during the move-hold sequence. All time dependent coherence plots have been scaled to use the same colourmap. Therefore magnitude of features for different electrodes can be compared. The positions of the individual estimates correspond to the relative EEG electrode position. Wrist angle and audio cues are also displayed.

EEG channel (Fig. 5.131*C*), 20Hz coherence with ECRL can be observed during both posture phases. The 20Hz is indicated by the spacing of the sidebands on the vertical axis (approximately ±50ms) and in the cumulant density plot between CP3 and ECRL (Fig. 5.131*E*). Coherence during extension posture where ECRL muscle is acting as agonist, especially for CP3, appears stronger than during flexion posture. Movement phases do not contain any comprehensive synchronisation features.

The cumulant densities estimated between ECRL muscle and the bipolar pairing of FC1-C1 (Fig. 5.131*G*) reveal task specific features clearer than the corresponding monopolar estimates. For both postural phases, the EEG signal appears to lead the EMG signal. The maximum central peak occurs 0.9 s after the flexion posture audio cue and 1.2s with a second one at 1.8 after the extension posture audio cue. There is clear 20Hz coupling during early posture that is suppressed during movement. The central synchronisation peaks are strong and last almost for the whole length of the posture phase. The corresponding coherence peaks do not last as long Fig. 5.131*F*. However it appears that the last part of the extension posture reveals 10Hz synchronisation since the major side-peaks come at approximately ±100ms. A similar observation was made for the equivalent time dependent coherence plot which revealed an initial 20Hz feature replaced by a 10Hz component during the last phase of posture, before the initiation of movement. This finding is in agreement with previous studies, reporting 10 and 20Hz corticomuscular synchronisation during maintained posture (Hansen, Hansen et al. 2002). The present results show that this alteration between 10 and 20Hz may take place over short time scales.

Fig. 5.132 illustrates a grid of the pooled time dependent coherences between FCR EMG and monopolar EEG channels during the move-hold sequence. A number of alpha and beta features can be observed. Most of the features are present during posture. Beta features appear for medial frontal and frontocentral electrodes as well as contralateral central and centroparietal electrodes. The beta features do not appear in the form of a single feature but as a double feature with the individual peaks occurring at different frequencies and with a few ms delay. This will be examined in more detail in Fig. 5.134. The features in central and centroparietal electrodes are

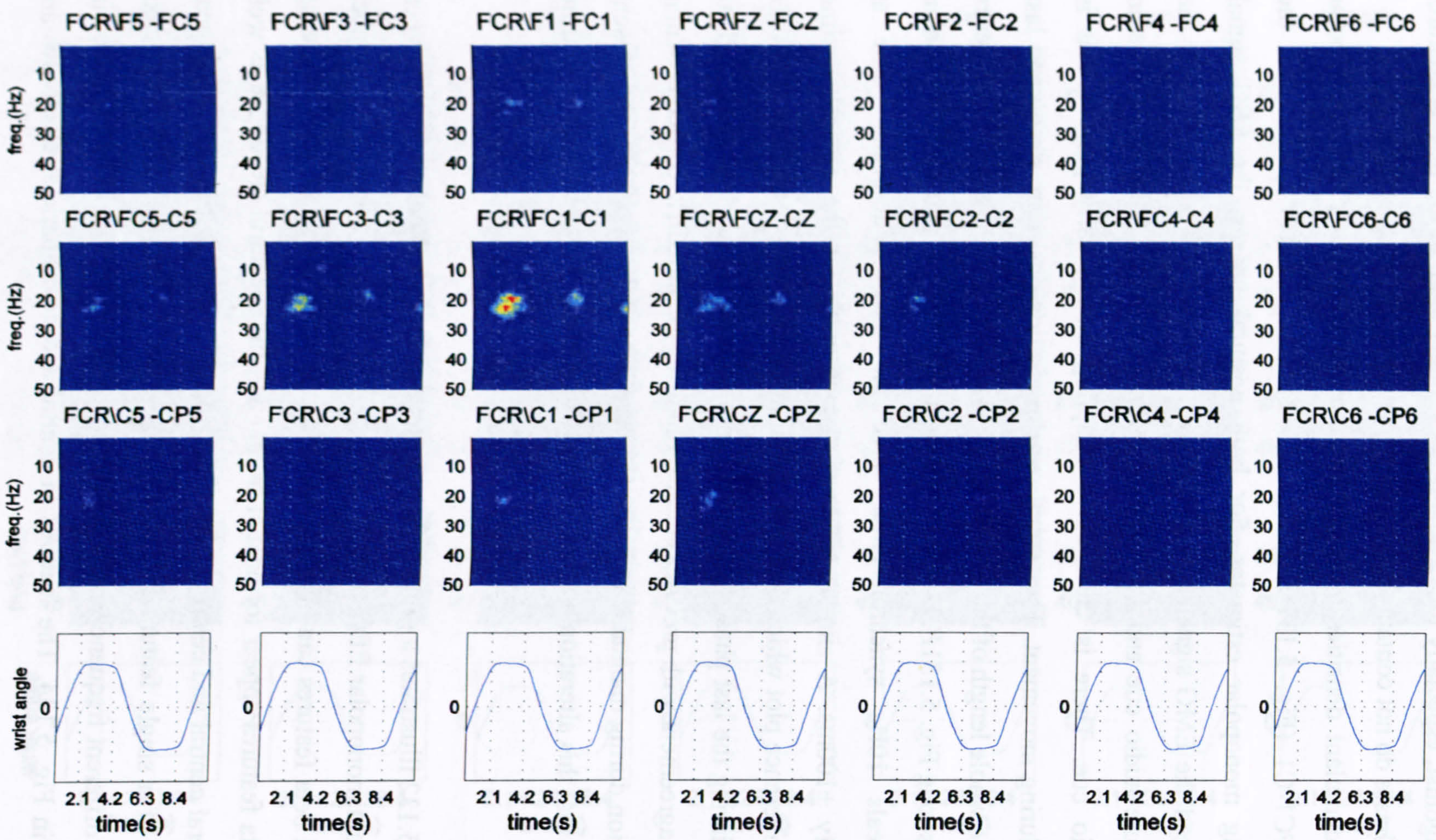

Fig. 5.133 Grid consisting of the pooled time dependent coherences between FCR EMG and monopolar EEG spectrograms during the move-hold sequence. All time dependent coherence plots have been scaled to use the same colourmap. Therefore magnitude of features for different electrodes can be compared. The positions of the individual estimates correspond to the relative EEG electrode position. Wrist angle and audio cues are also displayed.

stronger than in frontal and frontocentral for both posture phases (CP3 and Fz give the highest features respectively).

A very clearly defined alpha feature is present in the coherence map Fig. 5.132. The feature is especially strong for the medial frontal electrodes and also extends in the frontocentral and central electrodes while it appears very weak for centroparietal channels. Fz shows the strongest alpha coherence feature which appears at the last stages of posture flexion and during the transition to movement extension. This feature shows similar temporal characteristics to the 10Hz feature observed for ECRL\ monopolar EEGs coherence (Fig. 5.129). However the spatial characteristics appear different since the ECRL alpha feature seem to be stronger in the ipsilateral central and centroparietal electrodes.

A low strength 14Hz feature is also present for a large number of electrodes during movement extension. The feature is greatest for the contralateral centroparietal electrodes but it also expands into the frontal region.

Fig. 5.133 illustrates the pooled time dependent coherences between FCR and bipolar EEG spectrograms during the move-hold sequence. It shows alpha and beta features in similar frequency ranges and temporal characteristics as those present in the corresponding monopolar plots in Fig. 5.132, but with a different distribution because of the fundamental differences between monopolar and bipolar recordings. Beta coupling is stronger for the FC1-C1 bipolar electrode and surrounding bipolar electrodes. It is also stronger during posture flexion than during posture extension. The alpha feature appearing in the last stages of posture flexion and in the transition to movement extension are also strongest in the contralateral frontocentral-central row of electrodes. However this appears to be weaker than seen in the corresponding monopolar map (Fig. 5.132). FCR\Fz, FCR\CP3 and FCR\FC1-C1 time dependent coherence and the contained features is going to be presented in more detail in Fig. 5.134*F*

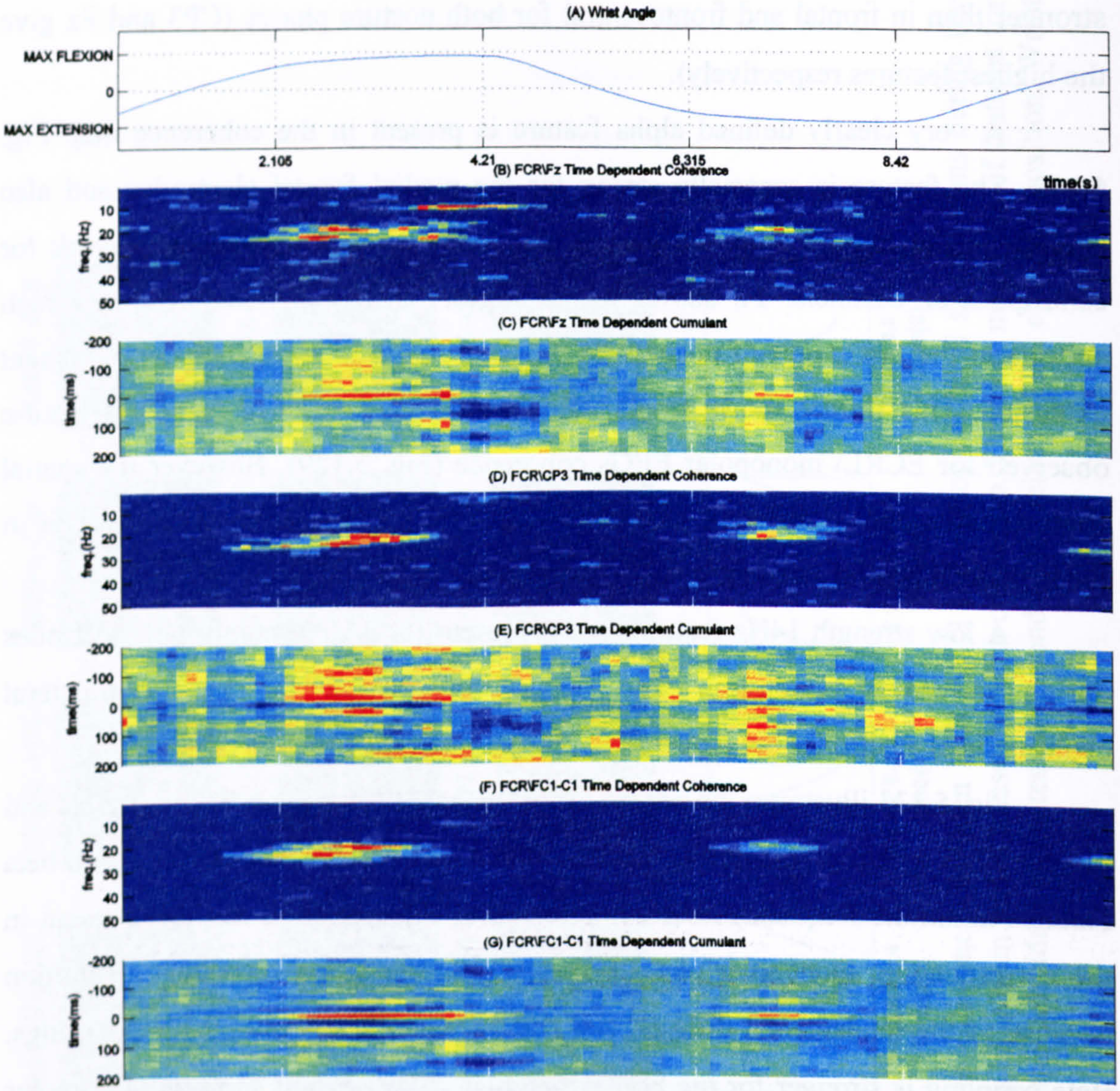

Fig. 5.134 Pooled FCR\Fz, FCR\CP3, FCR\FC1-C1 corticomuscular time dependent coherence and cumulant estimates displayed together with averaged wrist angle and audio cue triggers. The plots contain the data from all 9 subjects and 21 trials and illustrate the coherence and cumulant variations in the length of one move-hold sequence trial.

In Fig. 5.134*B,D,F* the time dependent coherences between wrist FCR EMG and Fz, CP3, FC1-C1 are presented in greater detail than in the corresponding cortical maps in Fig. 5.132 and Fig. 5.133.

As with the ECRL time dependent corticomuscular time dependent plot (Fig. 5.131), there is an increase in beta corticomuscular coherence during posture which is suppressed during movement. However, ECRL coherence during posture flexion contains one coherence feature at 21Hz, whereas the FCR corticomuscular coherogram contains 2 distinct features, (one at the same 21Hz frequency and the second at 24Hz). This is the case for monopolar (Fig. 5.134*B,D*) and the bipolar EEG (Fig. 5.134*F*) channels. The two features are not aligned in time. The 24Hz feature starts first and reaches its maximum around 0.5 sec after the audio cue. The 21Hz feature follows and reaches its maximum around 0.9 sec after the audio cue. The timing and the frequency of the 21Hz FCR\EEG corticomuscular coherence feature is closer to the corresponding ECRL\EEG corticomuscular features (Fig. 5.131) as well as equivalent ECRL\FCR intermuscular coherence feature observed during posture flexion (Fig. 5.128). During posture extension, only one 21Hz coherence feature is present in the coherogram with similar time characteristics as the equivalent feature during flexion posture. The feature takes its maximum around 0.6 seconds after the audio cue and declines before the end of the posture.

During the last one second of the flexion posture and approximately half a second in the movement extension phase a strong 10Hz coherence feature appears into the coherence for FCR\FZ (Fig. 5.134*B*) but not for FCR\CP3 (Fig. 5.134*D*). Smaller coherence (comparing with the main coherence feature) in the same frequency band is also present in the FCR\FC1-C1 time dependent coherence (Fig. 5.134*F*). As shown in Fig. 5.132 this feature is particularly strong for frontal electrodes.

The corticomuscular cumulant estimates in time for FCR EMG can be seen in Fig. 5.134*C,E,G*. During posture both monopolar EEG channels are coupled with FCR EMG in the beta band, indicated by the spacing of the peaks on the vertical axis (*C, E*). The FCR is most strongly coupled with CP3 during flexion posture, where it acts an agonist. For FZ channel coherence with FCR during extension posture is very weak and there are hardly any features defining beta synchronisation. In all other

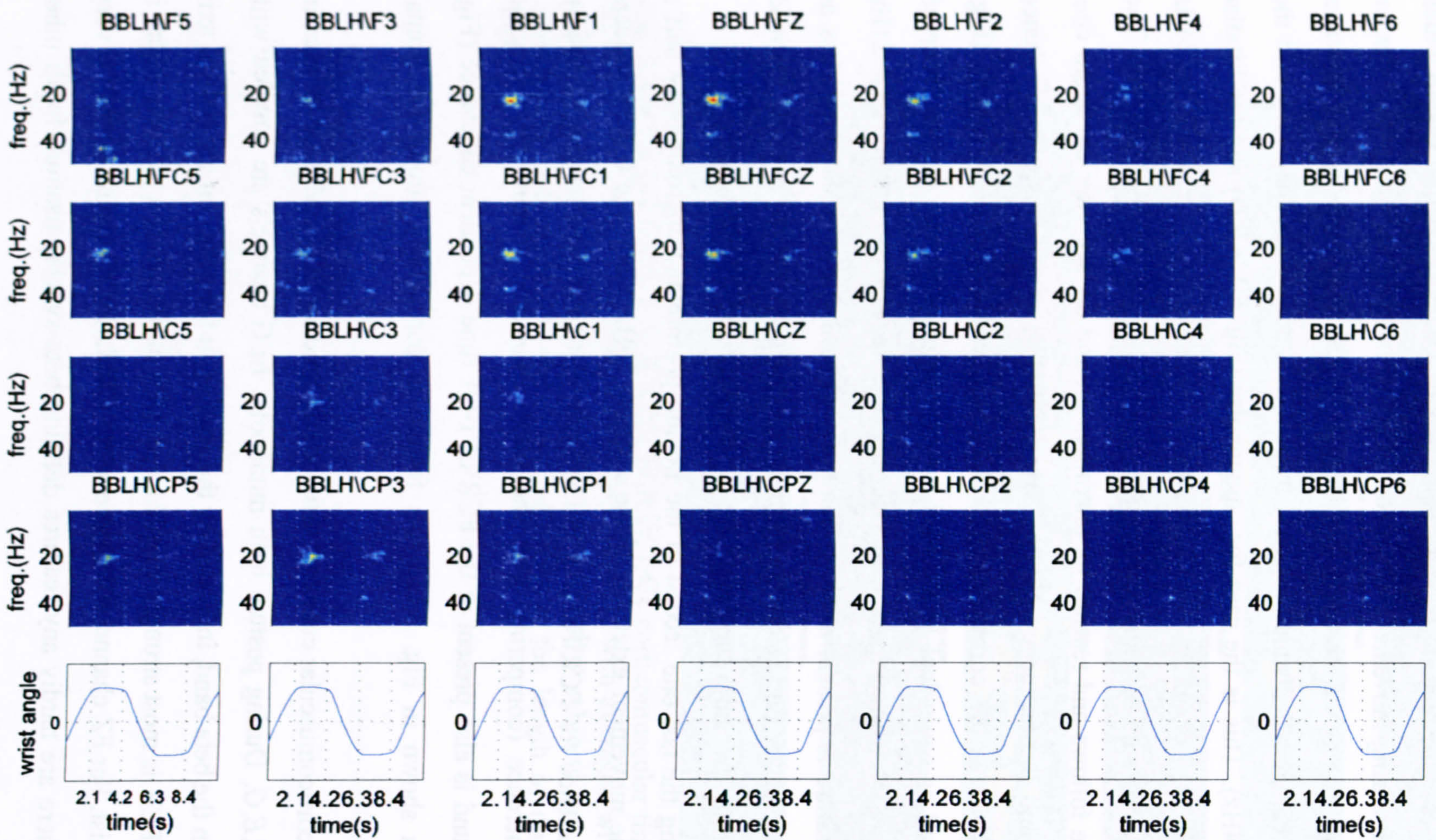

Fig. 5.135 Grid consisting of the pooled time dependent coherences between BBLH EMG and monopolar EEG spectrograms during the move-hold sequence. All time dependent coherence plots have been scaled to use the same colourmap. Therefore magnitude of features for different electrodes can be compared. The positions of the individual estimates correspond to the relative EEG electrode position. Wrist angle and audio cues are also displayed.

cases features indicating beta synchronisation are obvious. Movement phases do not contain any significant features.

A trough is also observed during and shortly after the transition from posture flexion to movement extension at approximately 100ms in the cumulant delay for FCR\CP3 in Fig. 5.134E. This is an expression of a very low amplitude coherence feature appearing at the same time in the corresponding time dependent cumulant Fig. 5.134C.

The bipolar EEG channel gives better defined synchronisation features (Fig. 5.134*H*) than the monopolar channels (Fig. 5.134*D,F*) during posture. It shows strong synchronisation during the hold flexed postural phase and a weaker coupling during maintained extension. Maximum synchronisation emerges 0.8s after the audio cue for both posture phases. Beta synchronisation is indicated by side-band features mainly during the early stages of movement. A 10Hz component replaces the 20Hz one at the end of the flexion posture phase according to the corresponding corticomuscular coherence feature. The central coherence peak is strong throughout posture alike corresponding coherence that declined before the end of posture (Fig. 5.134*G*). A 6Hz feature in the beginning of posture flexion in FCR\FC1-C1 coherogram is also present at the corresponding cumulant plot as peaks and troughs cumulant modulation spaced approximately 150ms.

Fig. 5.135 illustrates a grid of the pooled time dependent coherences between BBLH EMG and monopolar EEG spectrograms during the move-hold sequence. A number of beta and gamma features can be observed while no alpha features are evident. All features can be observed during posture. There are no obvious features during movement.

Beta features are present during posture flexion as well as posture extension. These features are stronger in the medial frontal and frontocentral as well as the contralateral central and centroparietal areas. For both areas the posture flexion feature is higher than the posture extension while the highest feature appears for Fz electrode during posture flexion. In the medial frontal and frontocentral area the coherence occurs earlier, just after the audio cue, and at a slightly higher frequency with a peak at 24Hz, than the coherence features in contralateral central and

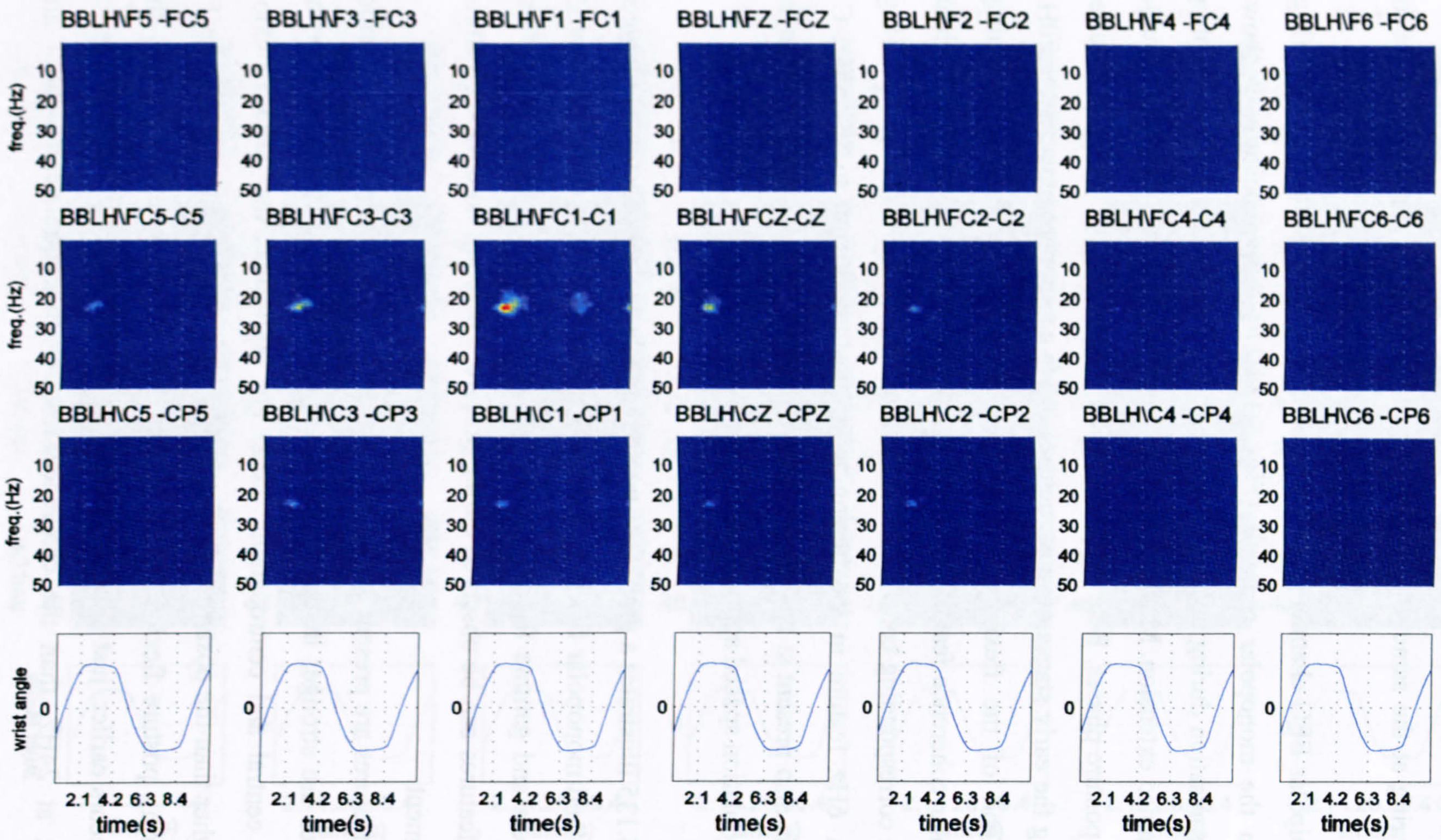

Fig. 5.136 Grid consisting of the pooled time dependent coherences between BBLH EMG and bipolar EEG spectrograms during the move-hold sequence. All time dependent coherence plots have been scaled to use the same colourmap. Therefore magnitude of features for different electrodes can be compared. The positions of the individual estimates correspond to the relative EEG electrode position. Wrist angle and audio cues are also displayed.

centroparietal electrodes. For the second area the coherence peak occurs at 21Hz. Both features decline before the end of the phase.

Gamma features are also present in most of time dependent coherence estimates at times close to the end of the movement periods. These short lasting features appear during posture flexion and posture extension just after the audio cue. Frontal and frontocentral electrodes show higher gamma coherence during posture flexion while centroparietal electrodes show higher coherence during posture extension. The distribution of gamma features appears different to the distribution of beta features.

Fig. 5.136 illustrates the grid of pooled time dependent coherences between BBLH EMG and bipolar EEG spectrograms during the move-hold sequence. Most features can be observed during posture. There are no obvious features during movement. While there are strong beta features in the same frequency range as observed in the monopolar plot (Fig. 5.135) there are less obvious gamma features which were very widespread in the monopolar plots, with similar temporal characteristics. The beta features appear during posture and they are absent during movement despite of the fact that BBLH is posturally activated in supporting the elbow. This reveals that BBLH corticomuscular coherence is modulated by the wrist activity. The maximum coherence occurs for FC1-C1 for both posture phases. The coherence of electrodes located around FC1-C1 also show high coherence with electrodes located between the frontocentral and central rows of electrodes to show higher coherence. Coherence features during posture flexion are stronger than those features observed during posture extension (Fig. 5.135, Fig. 5.136).

The bipolar beta features for contralateral centroparietal-central electrodes appears centred at 24Hz and emerge early after the audio trigger while for the medial frontal-frontocentral electrodes, the feature appears at 21Hz and occurs later within the posture phase. The frontal-frontocentral feature seems to be a fusion of the early 24Hz and later 21Hz with the first appearing stronger. These facts will be shown in greater detail in Fig. 5.137.

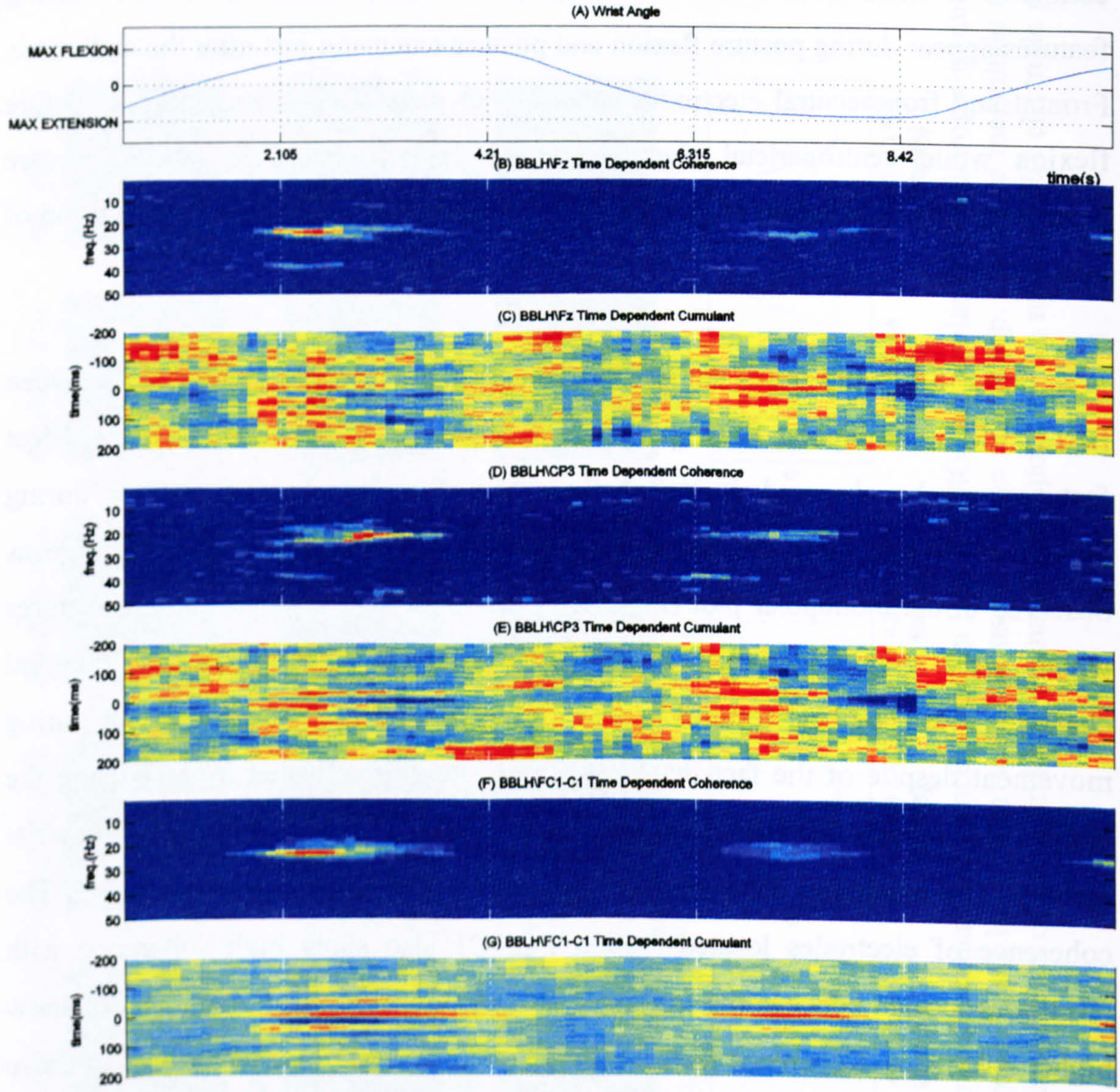

Fig. 5.137 Pooled BBLH\Fez, BBLH\CP3, BBLH\FC1-C1 corticomuscular time dependent coherence and cumulant estimates displayed together with averaged wrist angle and audio cue triggers. The plots contain the data from all 9 subjects and 21 trials and illustrate the coherence and cumulant variations in the length of one move-hold sequence trial.

Fig. 5.137 shows the detailed corticomuscular time dependent coherence and cumulant estimates for BBLH EMG with Fz, CP3 monopolar and FC1-C1 bipolar EEG channels, (see also Fig. 5.135 and Fig. 5.136). BBLH is not directly involved in the wrist movement since its main task was to support the arm in the horizontal position during the move-hold task. However its spectral power is strongly modulated with the wrist movement as shown in Fig. 5.121*D*. This is also the case for the time dependent coherence. Movement is characterised by complete suppression of beta coherence and no obvious corticomuscular coupling. During posture flexion the BBLH muscle shows significant coherence with the cortical EEG, occurring more specifically during the early stage of the flexion posture. It is maximal at 24Hz, approximately 0.4 sec after the audio cue (Fig. 5.137*C*). The timing and the frequency of this feature resembles the early feature in the FCR\CP3 coherogram during the same phase (Fig. 5.134*D*). A much weaker occurrence of a 21Hz feature is also present. For the coherogram between BBLH and CP3 (Fig. 5.137*E*) a 21Hz feature with maximum at 0.9 s after the audio cue is dominant during posture flexion. This feature resembles the late FCR\CP3 feature during the same phase (Fig. 5.134*D*). A much weaker early feature is also present at 24Hz. During posture extension where BBLH\Fz shows mainly 24Hz coherence, this time with a maximum 1.2s after the audio cue. At the same time BBLH\CP3 coherence occurs mainly at 20Hz with a maximum at 0.9s after the audio cue. Significant coherence at 24Hz is also present.

The coherogram between BBLH and bipolar FC1-C1 EEG channel (Fig. 5.137*F*) derives the highest coherence during posture. The maximum coherence is reached at 24Hz, but a weaker lower frequency feature is also present. The feature appears to be a fusion of the 24Hz and 21Hz features with the first being the dominant. Coherence takes is maximum 0.3s-0.4.s after the audio cue. One more element that appears during flexion posture in all three time dependent coherences is a gamma feature appearing at 38Hz in the monopolar and bipolar plots. It is present during the first half of the posture phase and was not observed in the ECRL and FCR time dependent corticomuscular coherences (Fig. 5.134, Fig. 5.131), or in intermuscular coherence estimates between these muscles.

In Fig. 5.137*C,E,G* the corticomuscular time dependent cumulant estimates for BBLH EMG can be seen. Wrist movement dependent synchronisation features in the BBLH cumulant plots with FZ, CP3 and FC1-C1 EEG channels are present. 20Hz coherence can be observed during posture between BBLH and the monopolar EEG channels (Fig. 5.137*C,E*). The cumulant is stronger in the early stages of posture. During movement some high magnitude features can be observed but they do not suggest any coupling in any band area.

The cumulant of BBLH with the bipolar channel (FC1-C1) reveals high 20Hz synchronisation starting very early and lasting for the whole duration of both posture phases. Unlike FCR and ECRL, the BBLH cumulant in time does not give any obvious 10Hz feature, which is also the case in the corresponding time dependent coherence plots that does not contain alpha features (Fig. 5.137*F*). The maximum central feature occurs 1.1s and 0.9s after the audio cue indicating flexion and extension posture respectively. During posture flexion however there is a smaller peak at 0.5 ms obviously corresponding to the earlier 24Hz coupling feature. Coupling during posture flexion also appears stronger than during posture extension.

5.1.8.1 Summary of time dependent frequency characteristics results

- The EMG spectrograms revealed task related components at 10Hz mainly associated with movement and 15-30Hz mainly associated with posture. 10Hz power was present for antagonist FCR during extension movement and for antagonist ECRL during flexion posture.
- The BBLH spectrogram showed activity which was task modulated by the wrist movement. 9-14Hz activity was continuously present throughout the move hold sequence while 15-30Hz components appeared during wrist posture and were mostly suppressed during wrist movement. The 9-14Hz activity of the BBLH showed frequency variation dependent on the wrist task.
- Significant ECRL\FCR, FCR\BBLH and ECRL\BBLH beta coherence features appeared in the early stages of posture phases. In the current study near 10Hz activity was also present during short posture tasks for the pooled data. For FCR\BBLH this coupling was higher at the end of the posture phase where 20Hz coherence had declined, but for ECRL\FCR coherence during extension it occurs simultaneously with the main 20Hz feature.
- The monopolar and bipolar EEG spectrograms contained task dependent features in delta, alpha and beta bands. 0-4Hz power showed an increase during early parts of posture and movement phases. Alpha activity was present throughout the move hold sequence showing an increase just before the onset of the movement task. A distinct beta feature was present during posture and was suppressed before the initiation of the movement but partially recovered during the movement. These features were better defined in the bipolar FC1-C1 channel records.
- The cortical and intracortical frequency characteristics revealed important features for cortical organisation during posture. This organisation was expressed by beta band synchronisation, as expressed by an increase in power, with simultaneous decoupling as expressed by a decrease in intracortical coherence in the same beta range of frequencies with similar temporal characteristics. These changes were also localised over the contralateral motor cortex. The range of frequencies that this simultaneous synchronisation-decoupling occurs is in the same beta (15-30Hz) range of frequencies that posture corticomuscular and intermuscular coupling occur which suggest that the phenomena are related.

- ECRL\FCR 10Hz intermuscular coherence appeared early, during the initiation of extension movement and remained strong for roughly two thirds of movement duration. Coherence in the same band occurred for FCR\BBLH pairs and ECRL\BBLH with different temporal characteristics, starting around half a second later than the ECRL\FCR 10Hz coupling feature, suggesting that the couplings are generated by different underlying physiological processes.
- Time dependent intermuscular and corticomuscular cumulant plots proved a helpful way of representing coupling information over a wide frequency spectrum and complemented the coherence estimates
- The corticomuscular time dependent coherence plots also reveal task dependent features. The most important were the coupling features that occurred in the beta band during posture. No strong coherence features were identified for movement. The strongest coherence was observed for the FC1-C1 bipolar EEG channel. The timing of intermuscular and corticomuscular coherences was similar with coherence reaching a maximum soon after the initiation of posture and declined before the end of the postural phase. For all bipolar plots, coherence was higher for the hold flexed than for the hold extended phase.
- Very interesting and comprehensive results were derived by the time dependent cumulant plots of the pooled EMG data. Coupling frequencies were clearly displayed. The duration of posture features, unlike time dependent coherence, were also clearly defined, with the short term synchronisation cumulant peaks lasting throughout the posture phase. The sidepeaks indicating 20Hz synchronisation corresponded to the equivalent coherence features. 10Hz coupling features were easily identified in the intermuscular cumulant plots during movement.
- For corticomuscular synchronisation the bipolar estimates gave more defined results than the monopolar. The central synchronisation peaks that emerged, in the time dependent cumulant plots showed more distinct, consistent and clear coupling features than the corresponding time dependent coherence plots. The central cumulant features covered nearly the whole duration of the posture tasks. The secondary satellite oscillatory features indicating beta coupling frequency were strong for a shorter period. This period matched the time that coherence features were also significant.

5.1.9 Continuous movement and maintained posture.

This experiment aimed to examine differences in corticomuscular and intermuscular estimates between maintained posture and short posture tasks, as well as continuous movement and single movement tasks interchanged with posture. It consisted of analysing the following data records:

- Maintained Posture Flexion (MPF)
- Maintained Posture Extension (MPE)
- Continuous Movement Flexion (CMF) (movement flexion segments epoched from a continuous movement task)
- Continuous Movement Extension (CME) (movement extensions segments epoched from a continuous movement task)
- Intermittent Movement Flexion (IMF) (movement flexion segments epoched from the move-hold sequence)
- Intermittent Movement Extension (IME) (movement flexion epoched segments from the move-hold sequence)
- Intermittent Posture Flexion (IPF) (posture flexion segments epoched from the move-hold sequence)
- Intermittent Posture Extension (IPE) (posture extension segments epoched from the move-hold sequence)

The analysis examined differences in the EMG frequency characteristics between MPF - IPF, MPE – IPE, CMF – IMF, CME – IME. It must be noted that all records compared had the same amount of information equal to 44.2s of data.

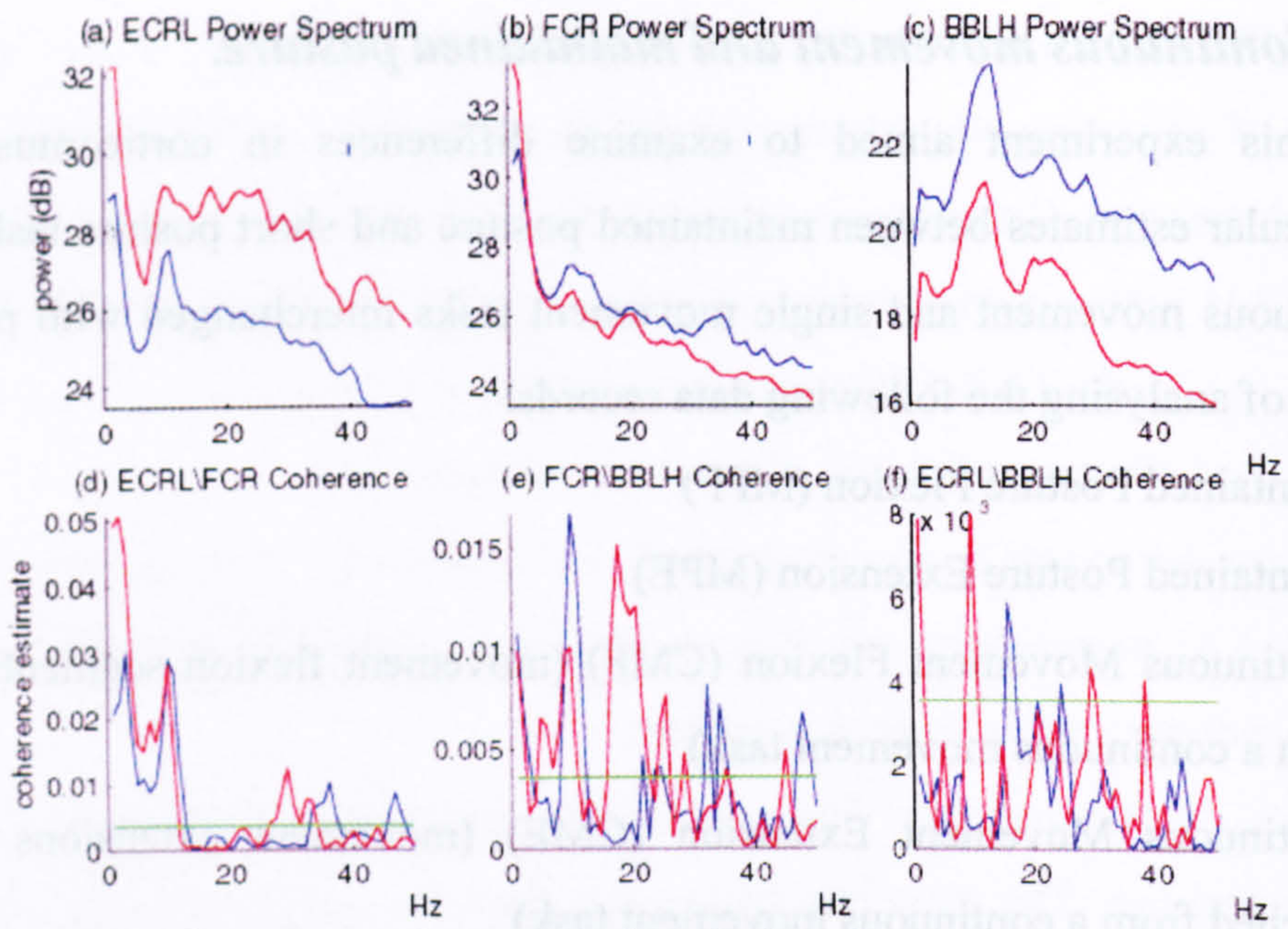

Fig. 5.138 EMG frequency characteristics during Intermittent Movement Flexion (IMF), Continuous Movement Flexion (CMF). In power spectral estimates for (a) ECRL, (b) FCR, (c) BBLH the small vertical lines at the top right give the estimated magnitude of a 95% confidence interval. The second row of plots gives the coherence estimates for (d) ECRL\FCR, (e) FCR\BBLH and (f) ECRL\BBLH. The green horizontal line represents the estimated upper 95% confidence limit.

Fig. 5.139 Pooled coherence map of all subject data, between right wrist ECRL EMG and multiple bipolar EEG channels during flexion movement (Intermittent Movement Flexion (IMF), Continuous Movement Flexion (CMF)).The green horizontal line represents the 95% confidence interval.

5.1.9.1 Intermittent and Continuous Movement Flexion

Fig. 5.138 shows the spectral estimates for ECRL and FCR and BBLH during Intermittent Movement Flexion (IMF) and Continuous Movement Flexion (CMF). The agonist FCR EMG has similar activity level for the CMF as for the IMF (Fig. 5.138*b*) with an enhanced feature centred around 20Hz. 20Hz power features are associated with posture. The antagonist ECRL spectrum however has much higher activity for all frequencies during CMF (Fig. 5.138*a*) with 15Hz-35Hz frequency band particularly enhanced. BBLH which performs a similar task in both occasions by supporting the elbow at a consents angle, is less active during the CMF. BBLH EMG maintains a similar frequency profile with a strong 10Hz peak while the beta band frequencies are slightly enhanced during the CMF (Fig. 5.138*c*).

The ECRL\FCR coherence (Fig. 5.138*d*) is stronger for low frequencies 1-10Hz during the CMF with a 10Hz peak having similar amplitude during both types of movement. There is also some low gamma or beta coupling of similar magnitude. For the FCR\BBLH coherence (Fig. 5.138*e*) there is smaller 10Hz coupling and significant 20Hz coupling emerging for CMF but not during IMF. Previous findings showing suppression of 15-25Hz intermuscular coherences when one of the synergistic muscles becomes involved in a movement task. This is the case only for IMF while for the CMF significant 20Hz coupling can still be observed despite that FCR is clearly performing movement and BBLH is performing posture. Increased 20Hz coherence can not only be observed in the FCR\BBLH coherence plot but also in the power spectra of FCR and BBLH during CMF compared to IMF (Fig. 5.138*b,c*) This feature is usually associated with posture. The ECRL\BBLH (Fig. 5.138*f*) coherence shows increased alpha coupling during CMF.

The ECRL\FCR cumulant plot (Fig. 5.138*g*) maintains its minimum near time 0ms and even though it looks as if it retains the 10Hz coupling features for the CMF, it is not as clear as for IMF because it has been influenced by the increased low frequency (<8Hz) coupling. The FCR\BBLH cumulant (Fig. 5.138*h*) is similar in both cases, revealing 20Hz and 10Hz features. The ECRL\BBLH cumulant (Fig. 5.138*i*) contains small beta features during IMF while weak 10Hz features are present in the corresponding CMF cumulant.

Fig. 5.140 Pooled coherence map of all subject data, between right wrist FCR EMG and multiple bipolar EEG channels during flexion movement (Intermittent Movement Flexion (IMF), Continuous Movement Flexion (CMF)). The green horizontal line represents the 95% confidence interval.

Fig. 5.141 Pooled coherence map of all subject data, between right BBLH EMG and multiple bipolar EEG channels during flexion movement (Intermittent Movement Flexion (IMF), Continuous Movement Flexion (CMF)). The green horizontal line represents the 95% confidence interval.

Fig. 5.139 contains the ECRL EMG corticomuscular coherence map with bipolar EEG channels during IMF and CMF. The corticomuscular coherence of the antagonist ECRL EMG is lower than the significance level at all sites for both CMF and IMF, with the exception of low frequency coupling, mainly in the contralateral cortex and small beta coupling for medial frontocentral electrodes during IMF that are not present during CMF.

Fig. 5.140 demonstrates the coherence map for the FCR EMG muscle with bipolar cortical electrodes during IMF and CMF. A significant increase occurs in the beta coherence for the CMF data compared to the IMF despite FCR performing movement. The highest increase occurs for the contralateral area and especially for the area around FC1-C1 electrode where the maximum occurs. A similar spatial coherence pattern of beta coherence was also observed during posture. Normally during movement the beta corticomuscular coherence would be expected to be suppressed.

The bipolar corticomuscular coherence maps for the BBLH muscle during flexion can be seen in Fig. 5.141. As it has already been stated the BBLH performs a posture task supporting the forearm. As it can be seen in Fig. 5.141 the beta corticomuscular feature during posture was suppressed for the IMF, despite the fact that BBLH is performing a postural task. While absent during IMF, during CMF, beta corticomuscular coupling is reinstated, in a pattern similar to the one observed during posture. A small alpha coupling feature present during the IMF task is not seen during the CMF.

FCR and BBLH EMGs displayed beta corticomuscular coupling during CMF absent during IMF. This was not the case for ECRL map where no beta coupling emerged. Observing the corresponding intermuscular coherences during the same tasks shows that the 20Hz coupling for FCR\BBLH pair has increased during CMF (Fig. 5.138*e*). FCR and BBLH are the same EMGs that demonstrated increased corticomuscular coherence. Beta intermuscular coherence for muscle pairs including the ECRL (ECRL-FCR, ECRL-BBLH) remains unchanged (Fig. 5.138*d,f*).

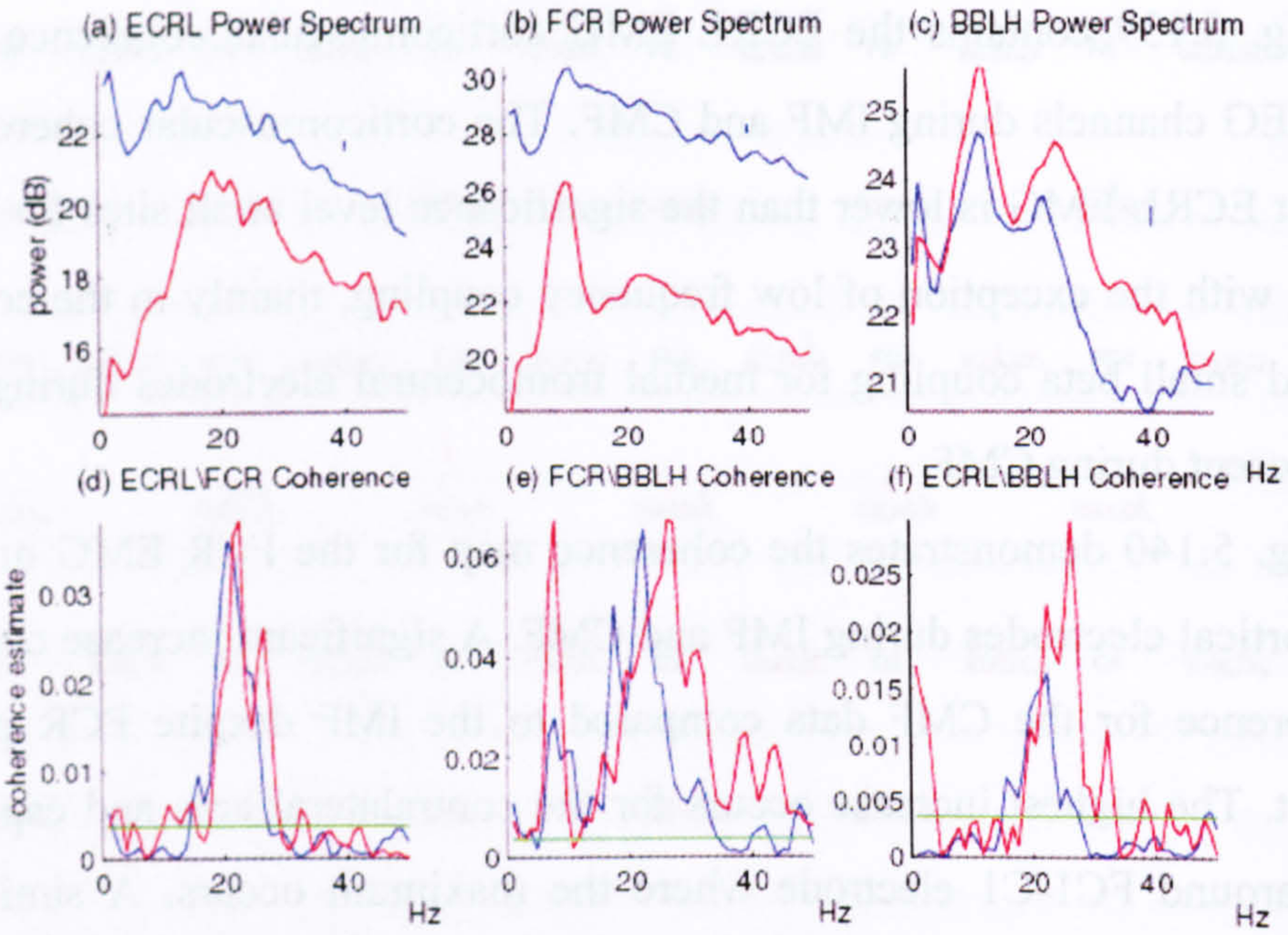

Fig. 5.142 EMG frequency characteristics during Intermittent Posture Flexion (IPF), Maintained Posture Flexion (MPF). In power spectral estimates for (a) ECRL, (b) FCR, (c) BBLH the small vertical lines at the top right give the estimated magnitude of a 95% confidence interval. The second row of plots gives the coherence estimates for (d) ECRL\FCR, (e) FCR\BBLH and (f) ECRL\BBLH. The green horizontal line represents the estimated upper 95% confidence limit.

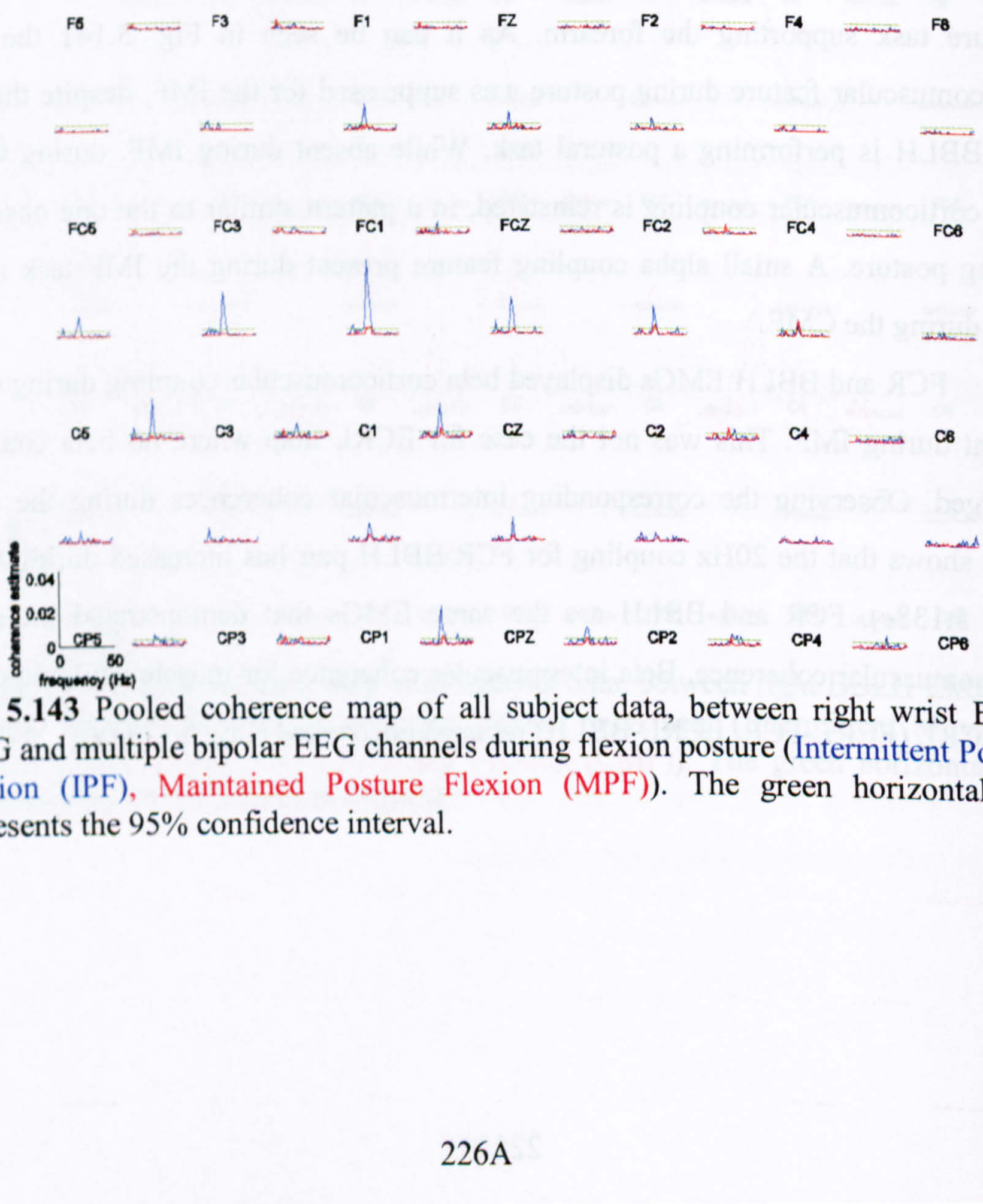

Fig. 5.143 Pooled coherence map of all subject data, between right wrist ECRL EMG and multiple bipolar EEG channels during flexion posture (Intermittent Posture Flexion (IPF), Maintained Posture Flexion (MPF)). The green horizontal line represents the 95% confidence interval.

5.1.9.2 Intermittent and Maintained Posture Flexion

Intracortical frequency characteristics during IPF and MPF are compared in Fig. 5.142. The ECRL power spectrum (Fig. 5.142*a*) shows lower spectral power for MPF with activity below 15Hz being significantly decreased compared to IPF. The FCR power spectrum (Fig. 5.142*b*) shows enhanced 10Hz and near 20Hz features during MPF. As with ECRL, the overall FCR spectral power has decreased at all frequencies during MPF task when compared with IPF. The BBLH power spectrum (Fig. 5.142*c*) has also more defined 13Hz and 18-30Hz features, higher gamma power and reduced 3Hz activity during MPF than during the IPF task. The overall power level has increased.

The ECRL\FCR coherence (Fig. 5.142*d*) still shows high beta coherence reaching similar levels and small but enhanced alpha coupling during MPF, when compared with the equivalent IPF phase. The main coherence feature is slightly shifted to higher frequencies (from 21Hz to 23Hz). In the FCR BBLH coherence (Fig. 5.142*e*) the already strong 10Hz coupling feature of the IPF, shows significant increase for the MPF, while 15-35Hz coherence is also enhanced. This time the shift to higher frequencies (from 22Hz to 26Hz) is more obvious. 35-50Hz coupling has also increased during MPF. The ECRL\BBLH coupling (Fig. 5.142*f*) has increased during the same phase, and moved to higher frequencies (from 22Hz to 2Hz). The cumulant density plots (Fig. 5.142*g,h,i*) agree with the above findings.

Fig. 5.143 shows the comparison of bipolar corticomuscular coherence for the antagonist ECRL muscle during the Intermittent Posture Flexion (IPF) and Maintained Posture Flexion (MPF). The strong IPF contralateral coherences have significantly decreased during the MPF and stay statistically significant for a number of electrodes with an area of high coherence around electrode FC1-C1. A 6Hz feature in the contralateral, frontocentral-central row of electrodes has also been suppressed during the maintained task.

The coherence map for the FCR (agonist) muscle (Fig. 5.144) shows a similar reduction in coherence for the maintained task. The coherence for the MPF is considerably reduced (more than five times for the FC1-C1 electrode) compared to

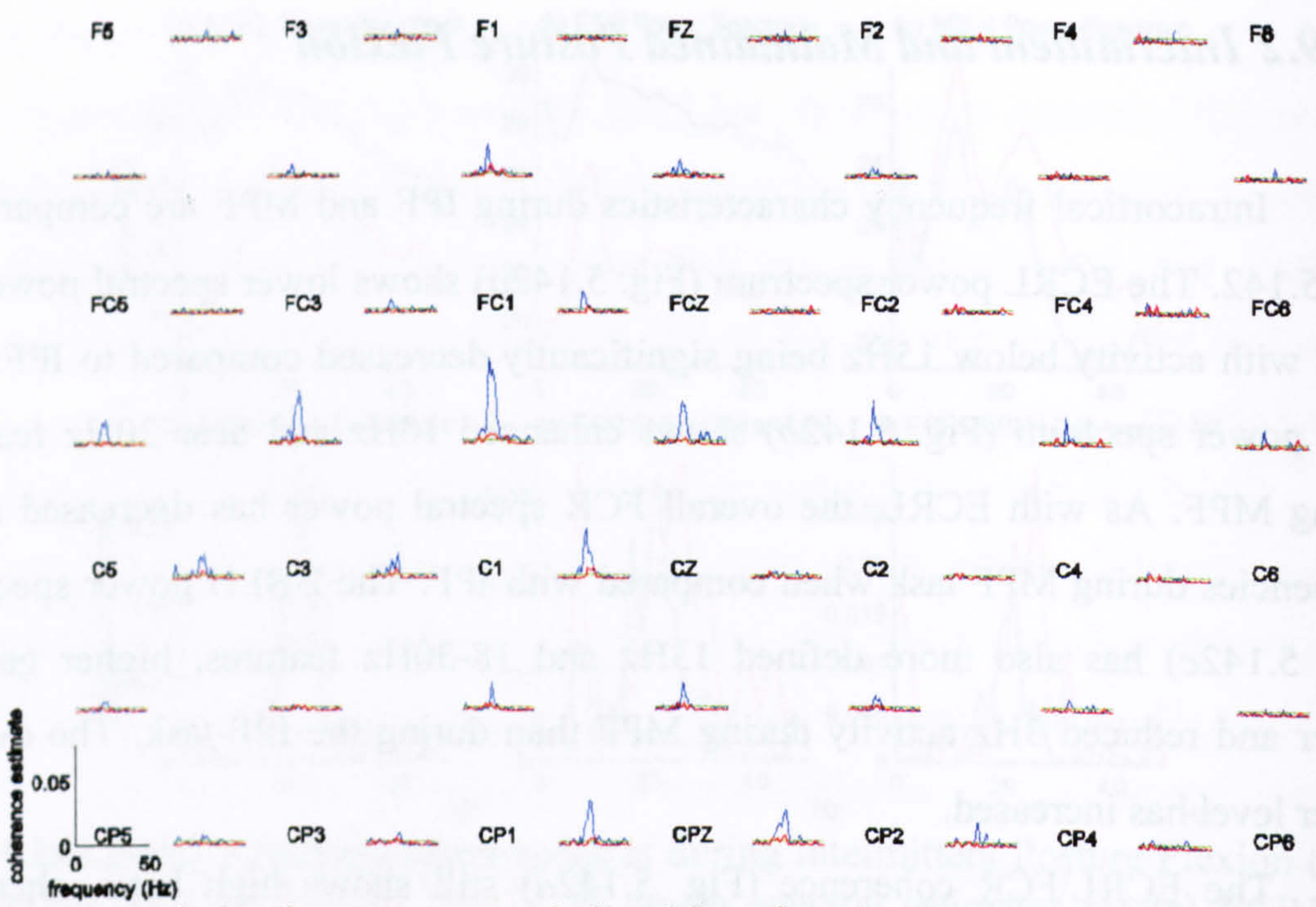

Fig. 5.144 Pooled coherence map of all subject data, between right wrist FCR EMG and multiple bipolar EEG channels during flexion posture (Intermittent Posture Flexion (IPF), Maintained Posture Flexion (MPF)). The green horizontal line represents the 95% confidence interval.

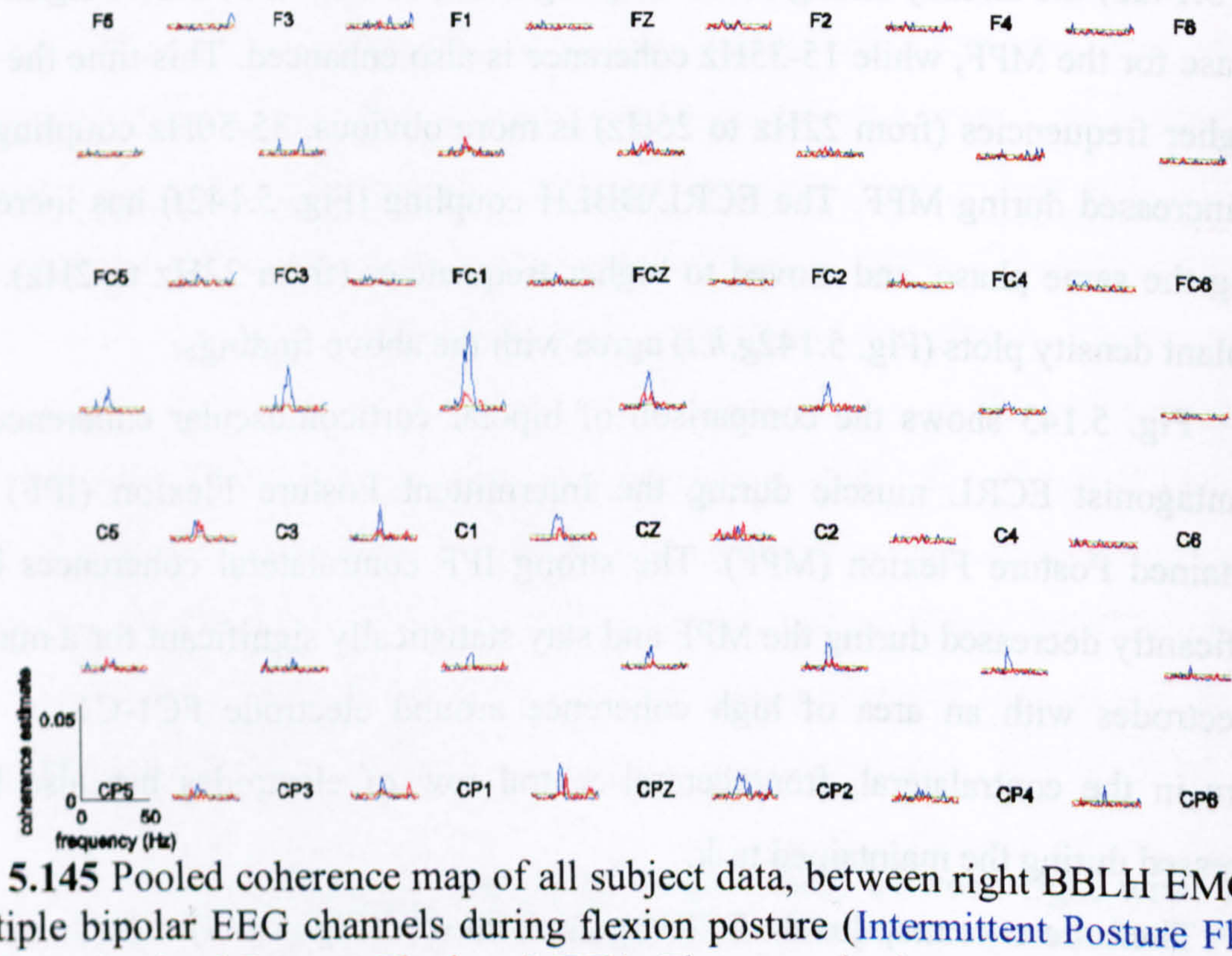

Fig. 5.145 Pooled coherence map of all subject data, between right BBLH EMG and multiple bipolar EEG channels during flexion posture (Intermittent Posture Flexion (IPF), Maintained Posture Flexion (MPF)). The green horizontal line represents the 95% confidence interval.

IPF. Despite the reduction, the FC1-C1 and neighbouring bipolar electrode coherences remain statistically significant.

A similar situation is observed for the BBLH muscle. As it is shown in **Fig. 5.145** the beta corticomuscular coherence during MPF, has greatly decreased compared with the IPF, while a number of electrodes maintains statistically significant corticomuscular coherence despite a dramatic decrease. A 13Hz feature in the central contralateral cortex has also been suppressed.

The beta intermuscular coherence magnitudes for the same phases (Fig. 5.142), appear similar for the ECRL FCR, and FCR BBLH pairs, and are enhanced for the ECRL BBLH pair during MPF.

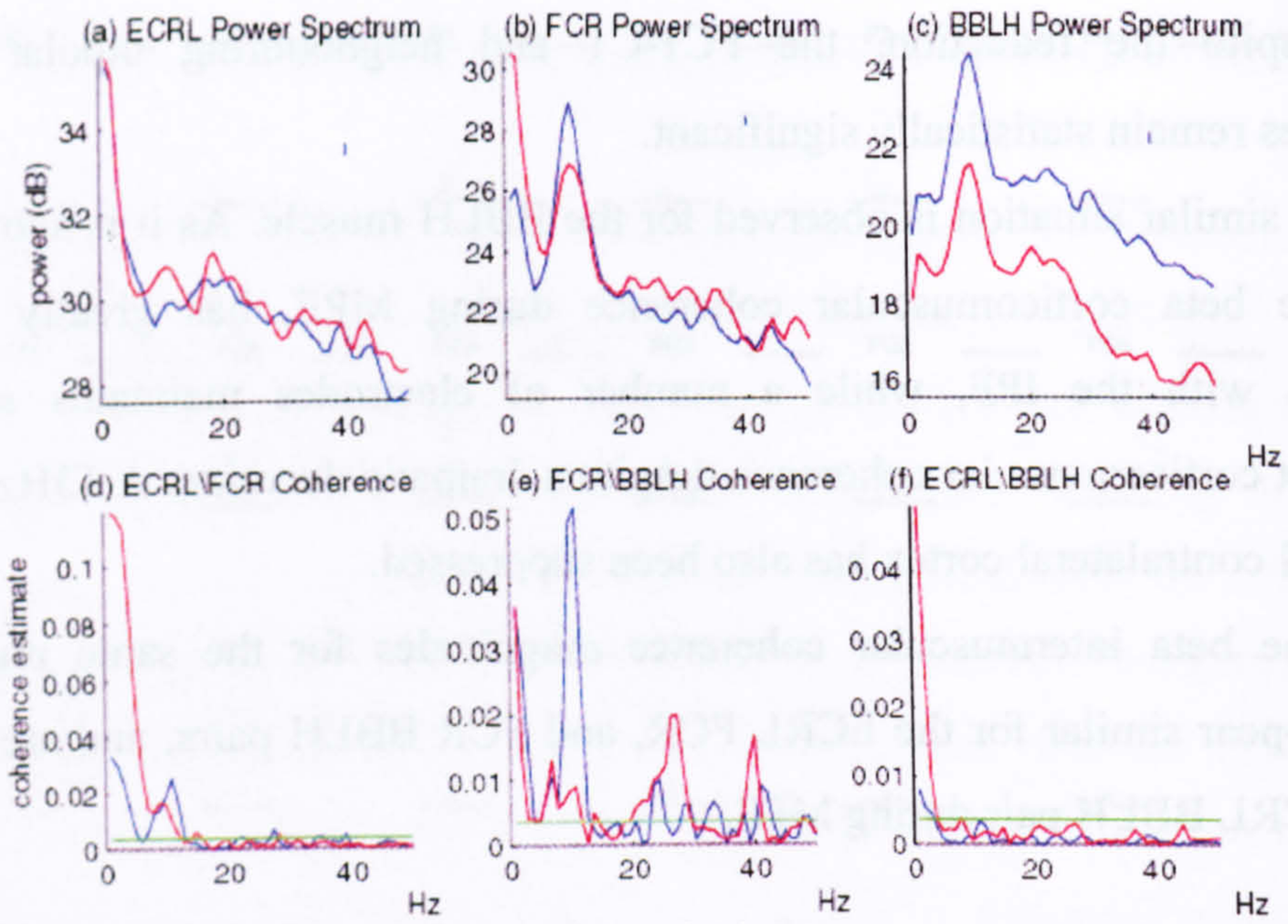

Fig. 5.146 EMG frequency characteristics during Intermittent Movement Extension (IME), Continuous Movement Extension (CME). In power spectral estimates for (a) ECRL, (b) FCR, (c) BBLH the small vertical lines at the top right give the estimated magnitude of a 95% confidence interval. The second row of plots gives the coherence estimates for (d) ECRL\FCR, (e) FCR\BBLH and (f) ECRL\BBLH. The green horizontal line represents the estimated upper 95% confidence limit.

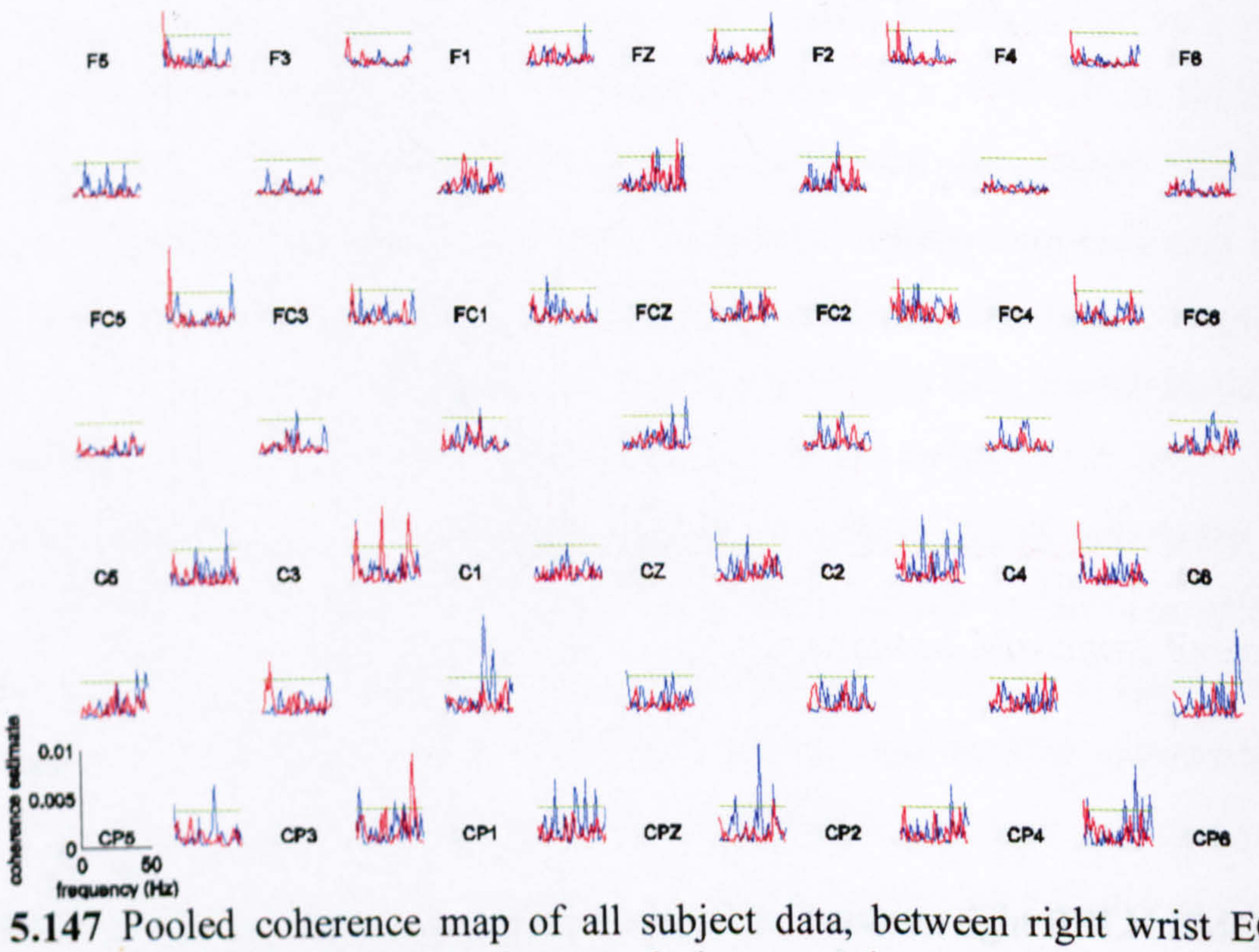

Fig. 5.147 Pooled coherence map of all subject data, between right wrist ECRL EMG and multiple bipolar EEG channels during extension movement (Intermittent Movement Extension (IME), Continuous Movement Extension (CME)). The green horizontal line represents the 95% confidence interval.

5.1.9.3 Intermittent and Continuous Movement Extension

The differences between the EMG frequency estimates for the IME and the CME are examined in Fig. 5.146. The ECRL power spectrum (Fig. 5.146*a*) shows more defined 10Hz and 20Hz features during the CME. During CME the FCR power spectrum (Fig. 5.146*b*) shows lower but still significant 10Hz activity while the BBLH power spectrum (Fig. 5.146*c*) retains the high 10Hz peak during the same task. ECRL and FCR show a similar average power level during both CME and IME, while BBLH gives lower spectral power during CME.

The ECRL\FCR coherence (Fig. 5.146*d*) shows extremely high sub 5Hz activity while the 10Hz peak is smaller during CME compared to IME. The 10Hz coupling has also been reduced for the FCR BBLH coherence (Fig. 5.146*e*) during CME, while a significant 40Hz peak appears. The most interesting observation is the significant increase in the FCR\BBLH beta band occurrence during CME. A similar observation was previously made for the CMF. As shown in Fig. 5.146*e* and Fig. 5.146*e* the 15-25Hz and 20-30Hz intermuscular coherences have increased during CMF and CME compared with the IMF and IME respectively. The ECRL BBLH coherence (Fig. 5.146*f*) shows a sub 5Hz increase in coherence during CME. Apart form that, coherence does not exceed the confidence level for the remaining of the examined spectrum.

The cumulant estimates reflect the features of the coherence plots. The ECRL\FCR cumulant (Fig. 5.146*g*) while maintaining the trough is strongly influenced from the low frequency coherence and 10Hz coupling reduction during CME, so the 10Hz coupling is not clearly demonstrated. Features signifying beta coupling, have appeared in the FCR\BBLH cumulant (Fig. 5.146*h*). However the 10Hz content in the CME is still visible since it follows a similar pattern to the plot derived from the IME data. The cumulant estimate for ECRL\BBLH (Fig. 5.146*i*) shows weak beta coupling, that is strongly influenced by the increased 0-5Hz coherence component during CME.

Fig. 5.147 is the pooled coherence map for all subject data, between right wrist ECRL EMG and multiple bipolar EEG channels during IME and CME. There is no clear pattern in the changes of beta corticomuscular coherence. C3-C1 displays

Fig. 5.148 Pooled coherence map of all subject data, between right wrist FCR EMG and multiple bipolar EEG channels during extension movement (Intermittent Movement Extension (IME), Continuous Movement Extension (CME)). The green horizontal line represents the 95% confidence interval.

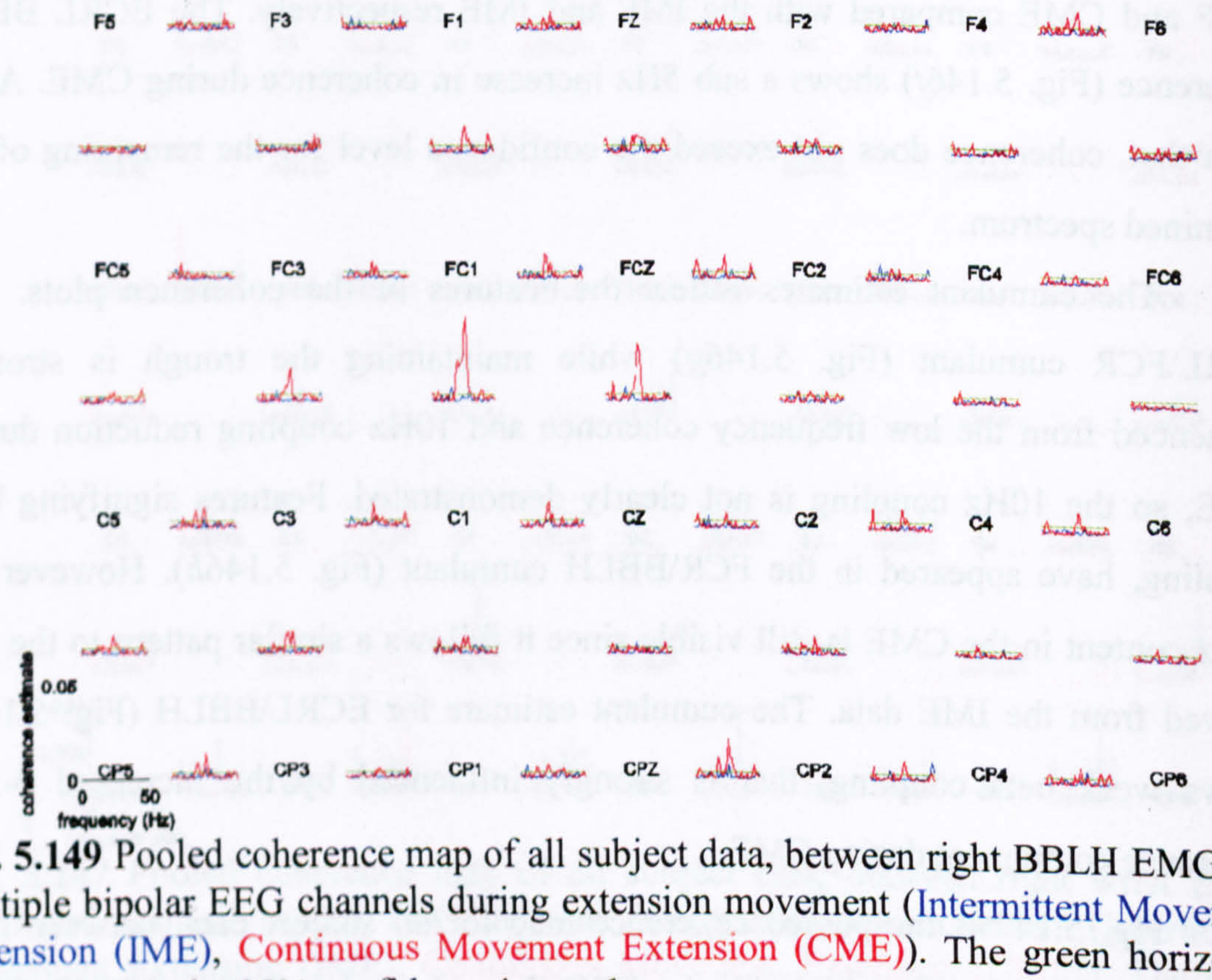

Fig. 5.149 Pooled coherence map of all subject data, between right BBLH EMG and multiple bipolar EEG channels during extension movement (Intermittent Movement Extension (IME), Continuous Movement Extension (CME)). The green horizontal line represents the 95% confidence interval.

higher coherence during CME while for C1-CP1 the largest coherence occur for the IME.

For FCR however there is significant beta coupling present during the CME as demonstrated in Fig. 5.148. The beta coherence features are much smaller than those occurred during IPE but they appear statistically significant for the FC1-C1 and surrounding electrodes, which also display maximum coherence during posture (Fig. 5.144). For IME there is no significant beta coupling. Small differences can be spotted in alpha and gamma bands, but the pattern is not as clear as with beta.

The largest features of beta corticomuscular coherence during movement occurred for the BBLH EMG during CME (Fig. 5.149). The BBLH beta corticomuscular coherence was almost completely suppressed during the wrist IME, despite of the fact that the muscle was performing a posture task. It appears that when wrist is performing continuous movement this suppression does not occur for BBLH. The coherences that appear are at the same level or even higher than during posture **(Fig. 5.145)** and have a similar distribution. This is also the case for CMF (Fig. 5.141) where BBLH beta corticomuscular coherence, suppressed during the IMF, re-emerged during the continuous movement task (CMF).

Since coherences for both FCR and BBLH EMGs with Bipolar EEGs were increased it is important to mention that as seen previously in Fig. 5.146*e*, significant beta intermuscular coupling appears between the same muscles, during CME. The substantial increase in corticomuscular coupling for BBLH, and the increase in FCR corticomuscular coupling for the same task, further suggests a link between corticomuscular and intermuscular phenomena. ECRL did not display increased beta coherence neither with the cortex nor with synergistic muscles.

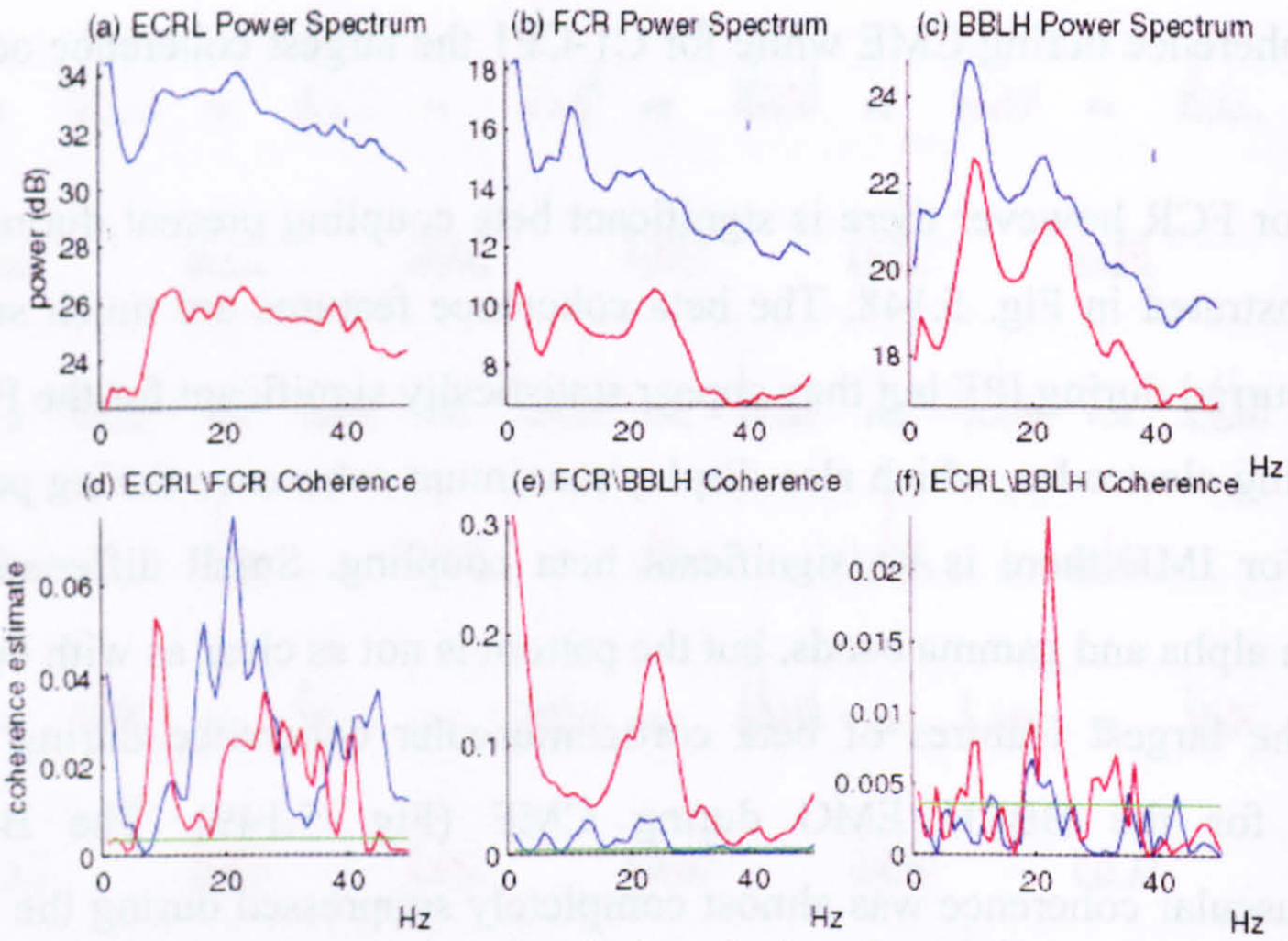

Fig. 5.150 EMG Frequency characteristics during Intermittent Posture Extension (IPE), Maintained Posture Extension (MPE). In power spectral estimates for (a) ECRL, (b) FCR, (c) BBLH the small vertical lines at the top right give the estimated magnitude of a 95% confidence interval. The second row of plots gives the coherence estimates for (d) ECRL\FCR, (e) FCR\BBLH and (f) ECRL\BBLH. The green horizontal line represents the estimated upper 95% confidence limit.

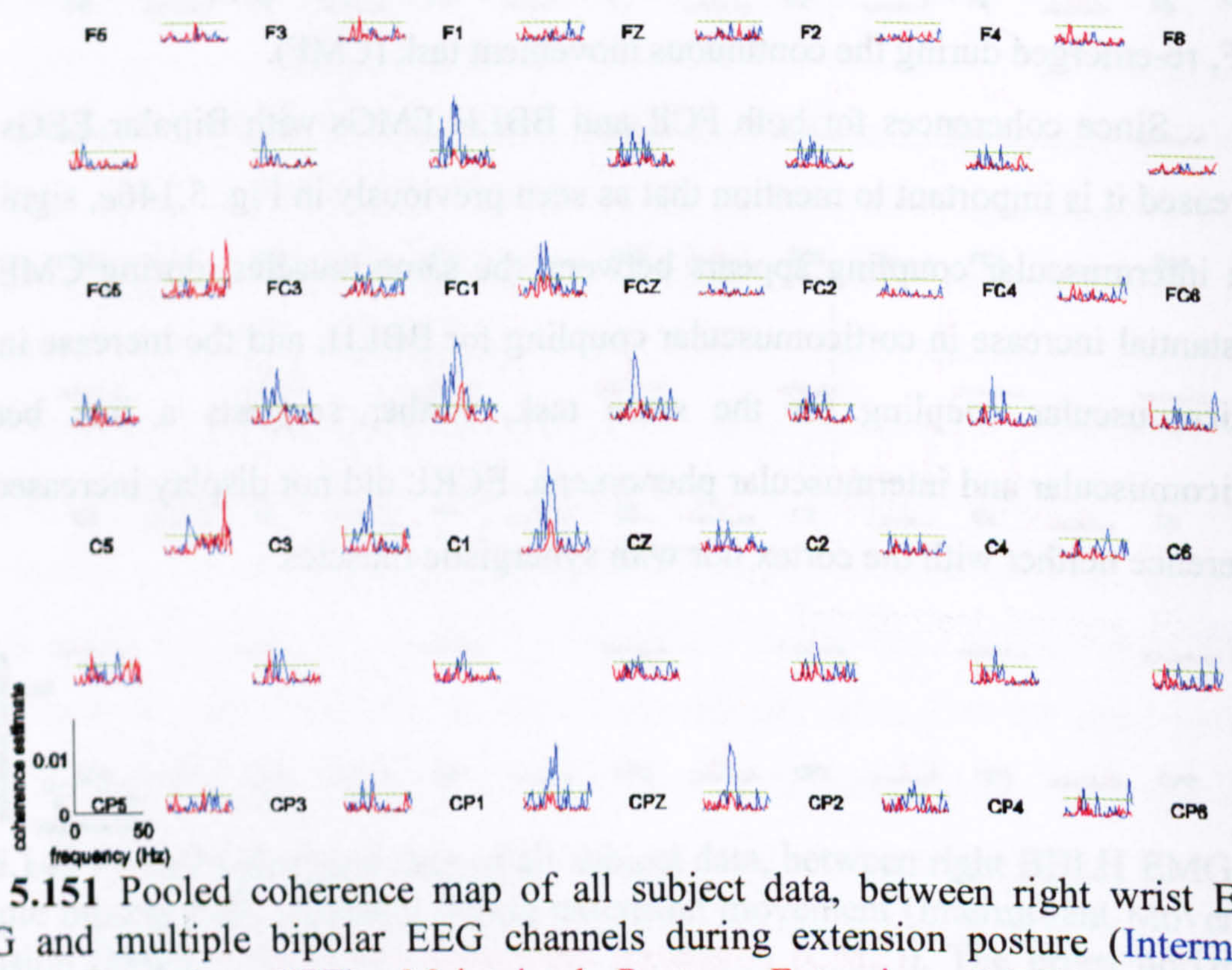

Fig. 5.151 Pooled coherence map of all subject data, between right wrist ECRL EMG and multiple bipolar EEG channels during extension posture (Intermittent Posture Extension (IPE), Maintained Posture Extension (MPE)). The green horizontal line represents the 95% confidence interval.

5.1.9.4 Intermittent and Maintained Posture Extension

The intermuscular frequency characteristics of ECRL, FCR and BBLH EMGs are compared during extension posture data derived from IPE and MPE in Fig. 5.150. The overall power for the ECRL power spectrum (Fig. 5.150*a*) for MPE is smaller, with a higher decrease in low frequencies (0-5Hz) compared to IPE. The overall FCR power spectrum level (Fig. 5.150*b*) is also lower for MPE with an enhanced 25Hz spectral power feature and smaller 10Hz feature. The BBLH power spectral profiles (Fig. 5.150*c*) are very similar, with a small decrease in the overall power for MPE.

The ECRL\FCR coherence estimate (Fig. 5.150*d*) is much altered showing high 10Hz coherence for the MPE. The IPE 15Hz-30Hz coherence has moved to higher frequencies between 18-38Hz during MPE with not so well defined central peak. The strong 35-47Hz has also been reduced to a strong but narrow 40Hz peak. The difference of the FCR\BBLH coherence during the two types of posture extension (Fig. 5.150*e*) is considerable. The vast coherence feature is man times the confidence level and much higher during MPE than during IPE for all examined frequencies and especially for beta coherence which is dominating the plot. This vast coherence feature should not be due to crosstalk because both recordings were obtained at the same experimental session, so IPE and MPE as well as CME and IME (Fig. 5.150*e*) would be expected to have similarly high coherences, which was not the case. The ECRL\BBLH coherence (Fig. 5.150*f*) shows increased alpha, significantly increased beta and some gamma coherence for the maintained posture task.

The ECRL\FCR cumulant density (Fig. 5.150*g*) is not very clear because it contains coupling over a broad spectrum of frequencies. The FCR BBLH cumulant (Fig. 5.150*h*) demonstrates the dominant beta coupling while the ECRL BBLH cumulant (Fig. 5.150*i*) shows 20 and some 10Hz coupling

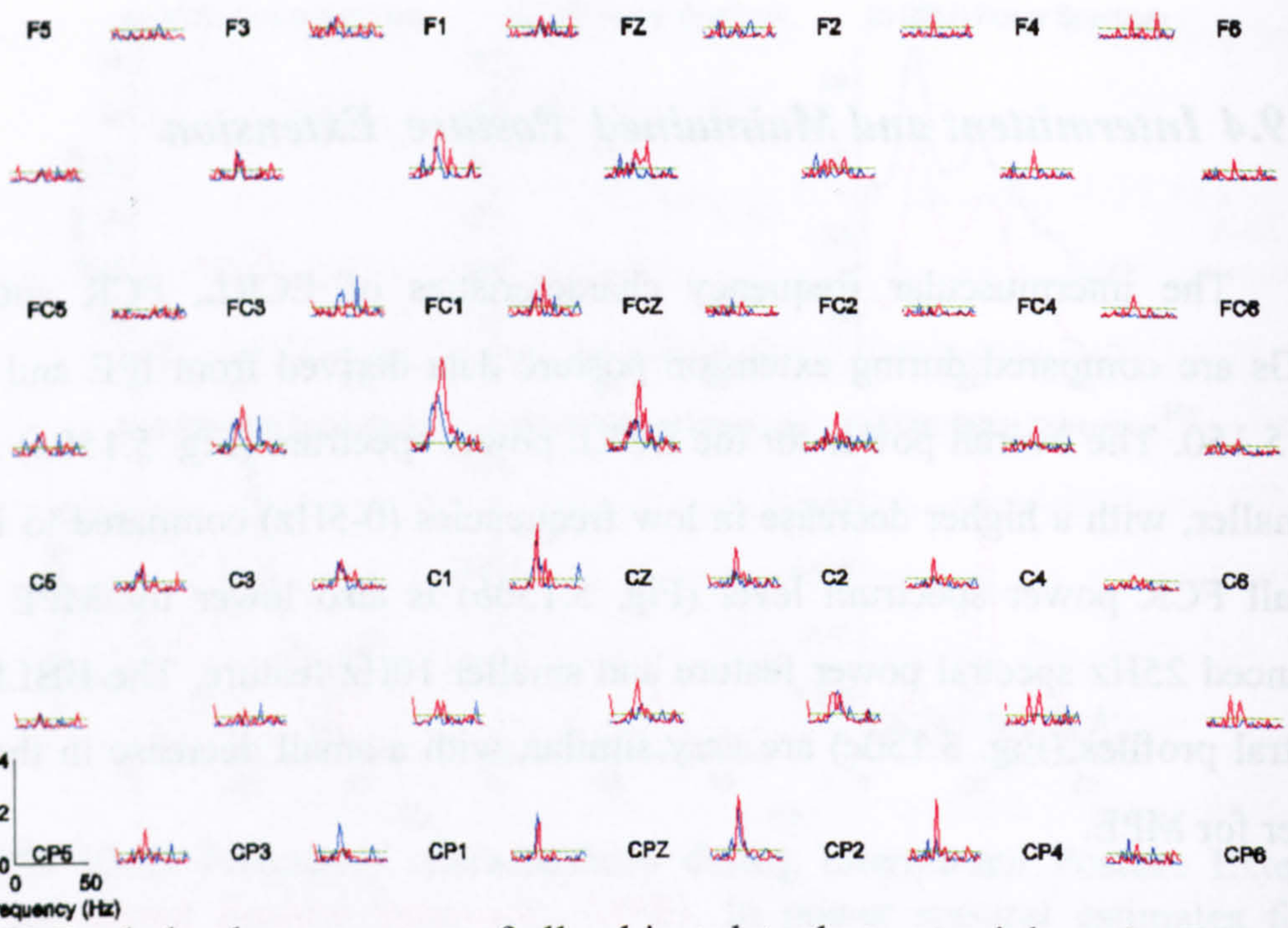

Fig. 5.152 Pooled coherence map of all subject data, between right wrist FCR EMG and multiple bipolar EEG channels during extension posture (Intermittent Posture Extension (IPE), Maintained Posture Extension (MPE)). The green horizontal line represents the 95% confidence interval.

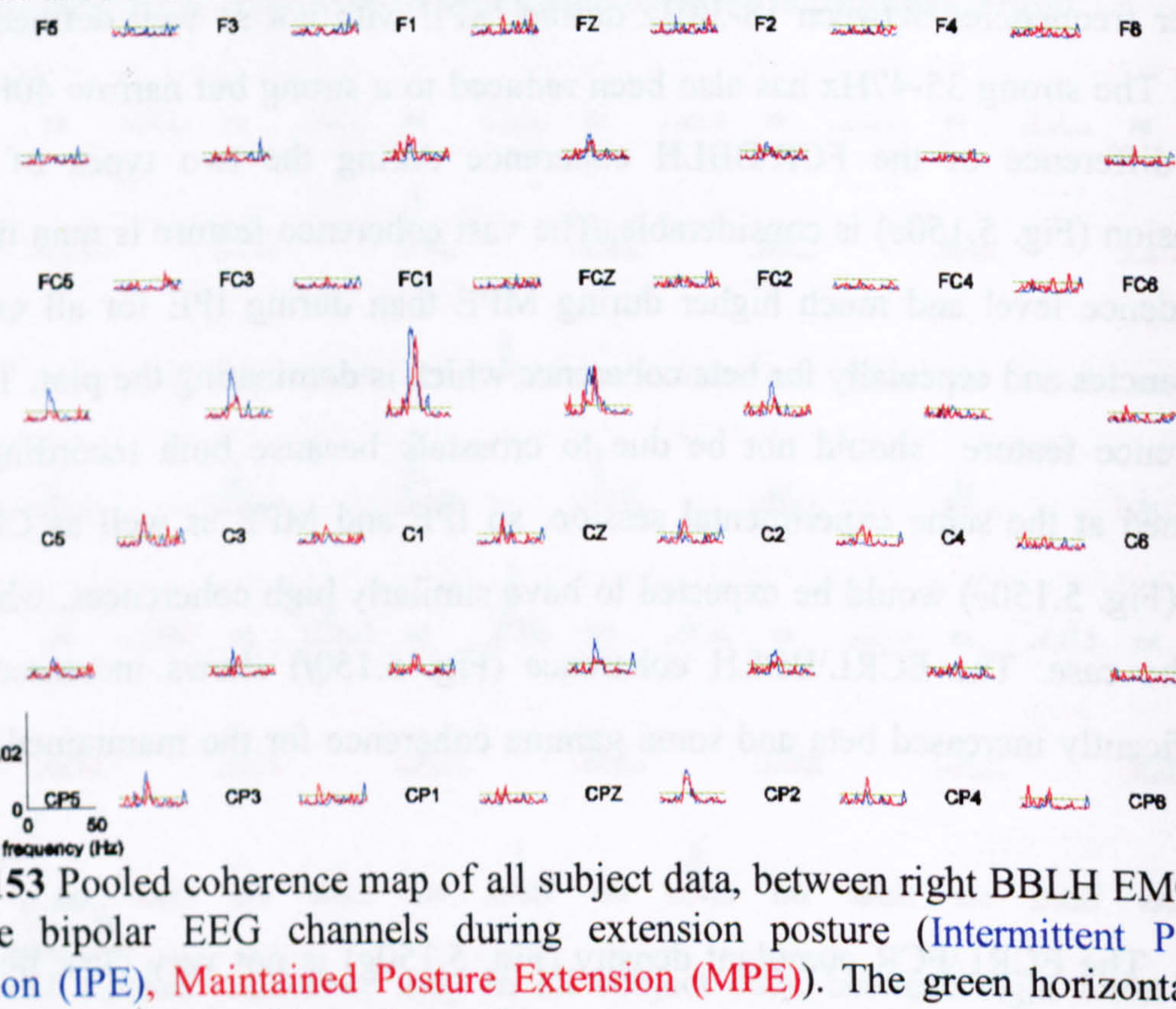

Fig. 5.153 Pooled coherence map of all subject data, between right BBLH EMG and multiple bipolar EEG channels during extension posture (Intermittent Posture Extension (IPE), Maintained Posture Extension (MPE)). The green horizontal line represents the 95% confidence interval.

Fig. 5.151 shows that the agonist ECRL beta corticomuscular coupling has significantly decreased during MPE compared to IPE. The main 20Hz coherence features have been reduced and the 10Hz and 15Hz features are almost completely suppressed during MPE trials. Coherence is almost absent from the ipsilateral cortex during MPE, where there was small but widespread beta coupling for the IPE. The maximum coherence peak still occurs for the FC1-C1 bipolar electrode pair for MPE as with IPE with the beta coherence statistically significant for a number of electrodes around their maximal feature. The main coherence feature has also shifted to higher frequencies. More specifically the peak was at 19Hz and has moved to 23Hz for MPE. A similar shift in the frequency of maximum intermuscular coherences for ECRL\FCR, ECRL\BBLH pairs of muscles during MPE as can be seen in Fig. 5.150*d,f*. Some gamma activity is also present during the same phase in the contralateral area (FC5-FC3, C5-C3).

In contrast to the ECRL, the FCR corticomuscular coherence seems to be enhanced for the MPE (Fig. 5.152). The beta coherence features look very different in shape and are slightly shifted to higher frequencies (from 19Hz to 24Hz). A similar shift for intermuscular coherences and ECRL corticomuscular coherences was observed. Beta coupling is also more widespread in the ipsilateral area. The 10Hz observed for F1-FC1, F2-FC2, FZ-FCZ and a few other electrodes for the extension posture of the move hold task has been lost as has the strong gamma features (FC3-C3 and FC3-FC1).

Fig. 5.153 gives the BBLH corticomuscular coherence map. MPE coherence with BBLH muscle is slightly lower compared to data from IPE. The difference is most noticeable for the contralateral frontocentral-central row of vertically aligned bipolar electrodes. The main coherence peaks appear at a higher frequency, (23Hz instead of 19Hz) at FC1-C1 and FCz-Cz electrode sites. Similar to BBLH, FCR and ECRL corticomuscular coherence maps (Fig. 5.151, Fig. 5.152) present a similar shift, as do the intermuscular coherences, suggesting a connection between corticomuscular and intermuscular coupling. Small gamma coupling features present

during IPE are central, centroparietal and contralateral frontal electrode sites have been suppressed during MPE.

As already seen in Fig. 5.150*e*, the intermuscular coupling for the FCR/BBLH pair changes considerably between IPE and MPE. The beta coherence has increased significantly during MPE, with wideband coherence appearing at 24Hz in the place of strong IPE coherence. Increases of a similar scale can not be observed for the corticomuscular coherence maps of FCR or BBLH, FCR\FC1-C1 coherence is slightly increased and BBLH\FC1-C1 coherence is slightly decreased for MPE. Both coherences also show a shift to higher coherences (approximately 24Hz). This fact suggests a significant degree of independence of the magnitude of intermuscular coherence from corticomuscular coherence. Very high intermuscular coherence is not the result of analogous very high corticomuscular coherence. The fact however that both intermuscular and corticomuscular coherences were shifted to frequencies close to 24Hz show strong connection between the phenomena.

5.1.9.5 Summary of continuous movement and maintained posture results

This experiment aimed to identify differences in the EMG and EEG frequency characteristics between maintained posture and intermittent posture as well as between continuous movement and intermittent movement.

- Significant differences emerged in the intermuscular and corticomuscular couplings between data derived from maintained posture and intermittent posture. During the MPF the 15-25Hz intermuscular features either reached similar levels or were greater than the ones observed during IPF. The coherence features appeared centred around slightly higher frequencies. In contrast to intermuscular increase the corresponding corticomuscular features, decreased significantly for all three muscles during the MPF.

- During the MPE, FCR\BBLH and ECRL\BBLH intermuscular coherences increased compared to IPE, with the first pair showing extremely high wideband coherence centred around 24Hz. During the MPE ECRL\FCR EMGs showed decreased peak beta coherence. However the feature was broader and the central peak was shifted to higher frequencies, with enhanced 1Hz peak also present. In the corresponding corticomuscular maps the ECRL shows clear reduction in beta coherence during MPE while for the BBLH there is a small reduction compared to IPE. For the antagonist FCR map the coupling with the contralateral cortex during the MPE has increased. The increase however does not in any case follow the large increase in the FCR\BBLH intermuscular coherence.

- During intermittent movement (IMF, IME), intermuscular coherences of coactive muscles participating in posture were suppressed when the wrist engaged in movement. During continuous movement (CMF, CME) however, beta corticomuscular coherences were considerably enhanced for FCR and BBLH muscles. The distribution of coherence features over the cortical map during

continuous movement strongly resembled posture. The intermuscular coherences in the same frequency range between FCR and BBLH EMGs was also significantly facilitated. The changes for ECRL\EEG, ECRL\FCR and ECRL\BBLH coherences were not as significant.

- The near 10Hz intermuscular coupling also showed significant variation between intermittent and maintained posture tasks, as well as continuous and intermittent movement. A considerable increase in the FCR\BBLH 10Hz coherence was observed for the MPF. An increase was also observed for the ECRL\FCR pair during MPE

5.2 ATTENTION AND COGNITIVE INFLUENCES IN CORTICOMUSCULAR COHERENCE.

5.2.1 Influence of attention in corticomuscular coherence.

The aim of this experiment was to identify the way that attention to a precision motor task affects corticomuscular and intermuscular coupling. More specifically the aim was to identify distinct changes in intermuscular and corticomuscular coupling between a forearm muscle - right extensor carpi radialis longus (ECRL), a hand muscle - right abductor pollicis brevis (APB) and the cortex. Coherence was measured during the performance of a precision task in two attentional states; a high attention (HA) and low attention (LA) states during the performance of a precision task. The task was the compression of an instrumented ring between thump and little finger with the wrist in the extended position. The force acting on the ring was fed back visually to the subject on the display of an oscilloscope. By varying the gain of the feedback signal the LA and HA levels could be set for the task which was to keep the force level steady at a target force. With high gain feedback the task required more attention since small variations in the force create larger differences from the target force. Lower gain consequently required less attention to follow the target force since variations were smaller.

Pooled intramuscular coherence estimates and corticomuscular coherence maps were produced for the examined group of nine subjects. The length of the data record for each subject for each attentional state was 180s which consisted of three separate 1min trials. EMGs from wrist ECRL and hand APB were recorded.

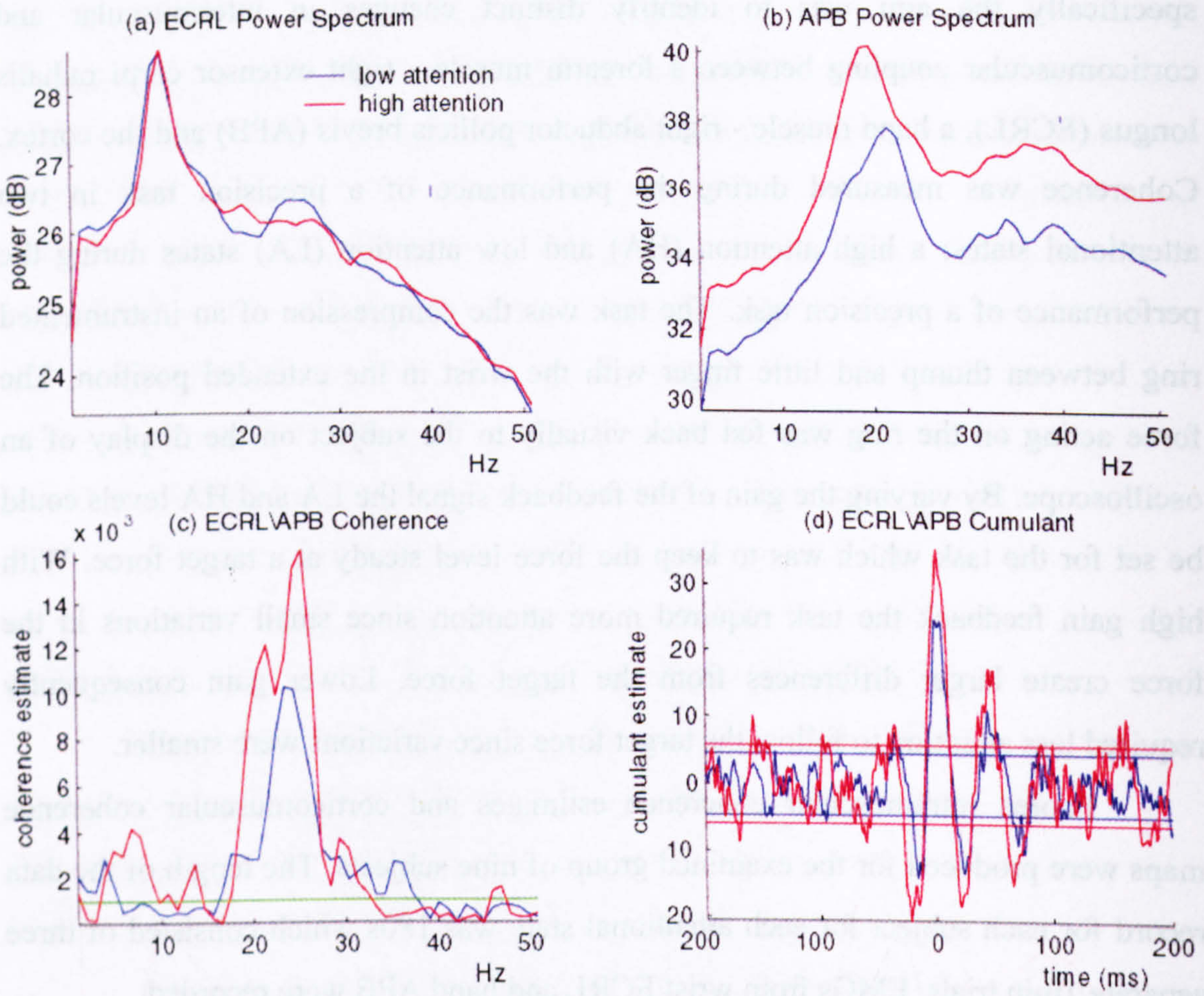

Fig. 5.154 Pooled power spectra of right ECRL (a) and APB (b), intermuscular coherence (c) and intermuscular cumulant during low motor attention (blue) and high attention (red).

In Fig. 5.154*a,b* the produced estimates for the wrist ECRL and the hand APB muscle can be seen. The HA estimates are plotted in red colour while the LA estimates are plotted in blue colour. The ECRL power spectra estimates have a prominent peak at 11Hz for both attentional states and very similar amplitude. However while the power of the HA estimate gradually declines in the 20 to 50Hz band, the power of the LA task contains a 20-30Hz feature with maximum at around 25Hz.

The APB power spectrum power during the HA task is higher in the whole examined frequency spectrum. The HA peak also is shifted to lower frequency of 19Hz rather than the 22Hz during the LA. The experiment was designed to encourage the subject to maintain a constant level of compression on the ring, with the same target force for low and high display gain (corresponding to LA and HA). EMG power revealed higher activity, despite of the fact that the target force is the same. The subjects in the HA task, possibly had to do more corrections in order to keep the compression level close to the target, which may have also resulted to greater muscular activity. Records of the force were not obtained in order to examine whether the actual variation of the force corresponds to the increased muscular activity.

For both HA and LA states, frequency components around 20Hz are present in the APB power spectra. However the peaks appear at different frequencies. During the HA state the spectrum shows a peak at 18Hz while the peak of the LA occurs at 22Hz.

The intramuscular coherence between APB and ECRL muscles (Fig. 5.154*c*) has clearly increased in the 17-30Hz area during the HA compared to the LA condition where the coherence was smaller. The peak frequency has also moved from 23Hz during the LA to 26Hz for HA. The cumulant estimate also indicates higher coupling (Fig. 5.154*d*).

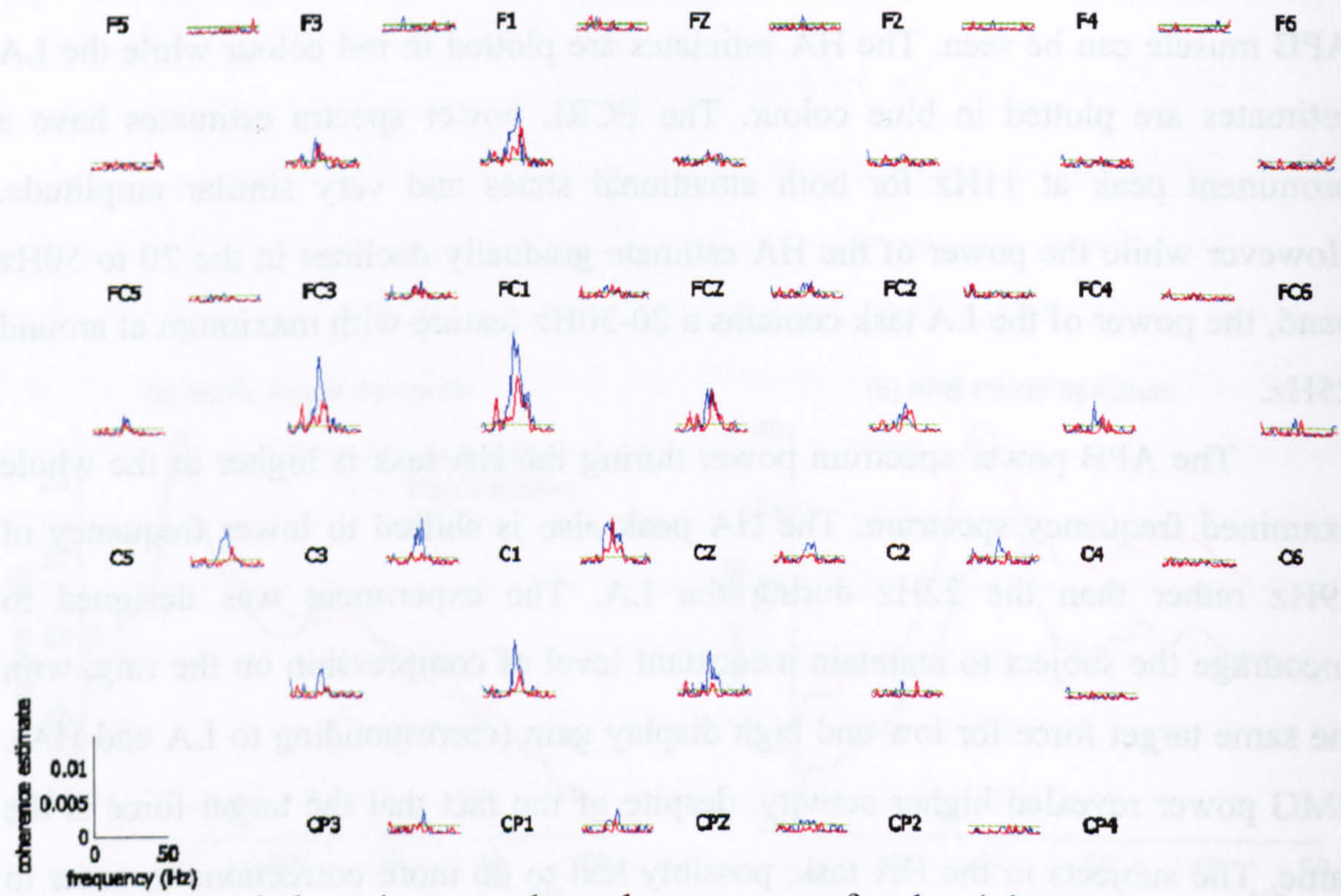

Fig. 5.155 Pooled corticomuscular coherence map for the right ECRL with bipolar EEG recordings during the precision task during low (blue) and high (red) motor attention.

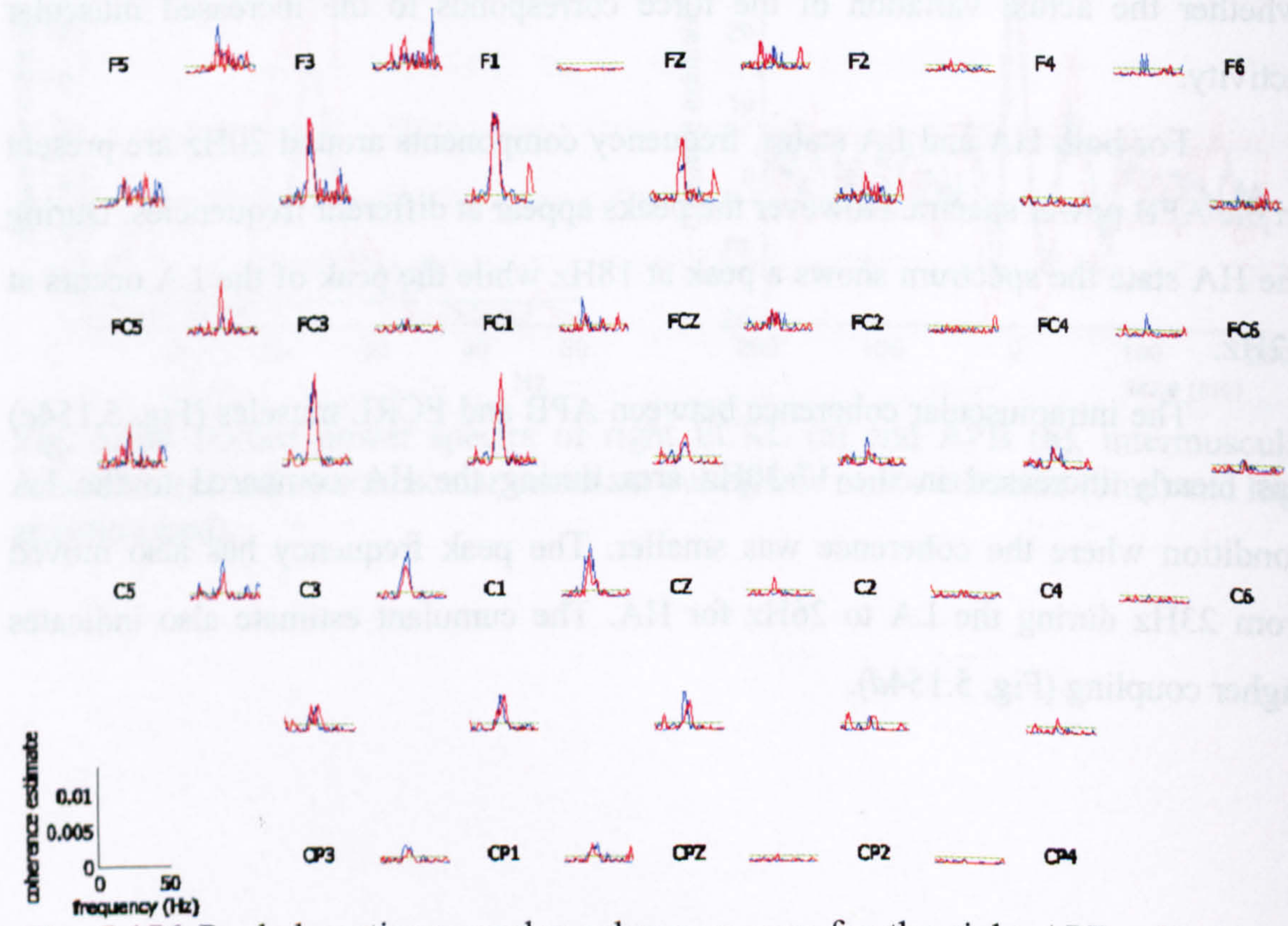

Fig. 5.156 Pooled corticomuscular coherence map for the right APB with bipolar EEG recordings during the precision task during low (blue) and high (red) motor attention.

Fig. 5.155 shows the coherence map of the wrist ECRL EMG with the bipolar montage of EEG channels. The ECRL bipolar EEG coherence montage shows strong coupling for the contralateral electrodes with a maximum at FC1-C1. The coherence is stronger for the LA state than the HA and extends over a wider area to include frontal and central centroparietal areas. The coherences for the horizontally aligned frontocentral row of electrodes are relatively low while for the central row of electrodes it is considerably larger. Alpha coupling is also present for central electrodes, especially the vertically aligned frontocentral-central row of electrodes, which appears considerably higher for the HA state.

Fig. 5.156 shows the coherences of the APB and the bipolar cortical montage. The beta coupling is again strong in the contralateral area but with the maximum activity shifted from the contralateral central area to the contralateral frontal-centrofrontal electrodes. The coherences are slightly larger for the HA that those seen for LA. The coherences for the frontal and centrofrontal electrodes contain multiple features that cover the whole spectrum while the ones in the central estimates contain a more defined 19-26Hz component. A smaller sharp peak at 32Hz is also there and is larger for low attention. The frontocentral-central vertical row of electrodes contains some gamma coupling especially for HA and not present in LA.

5.2.1.1 Summary of attentional influence results

The question of attention influences in corticomuscular coupling has been raised before (Kristeva-Feige, Fritsch et al. 2002). It may also be a factor responsible for intersubject and intrasubject differences in EEG-EMG coherence, in both normal and patients.

- The results presented showed that corticomuscular and intermuscular coherences are relatively robust under different states of attention. Despite variations between low attention and high attention conditions, beta intermuscular and corticomuscular coherences remained strong and statistically significant.
- The intermuscular coherence between the ECRL (wrist muscle) and APB (hand muscle) increased during the high attention precision task compared to the low attention task. The corticomuscular coherence for the APB increased as well. However at the same time the ECRL corticomuscular coherence clearly decreased suggesting independent control of the CNS on APB and ECRL muscles.
- The contralateral frontal cortex was strongly coupled with the APB muscle during the precision task during high attention and low attention conditions.

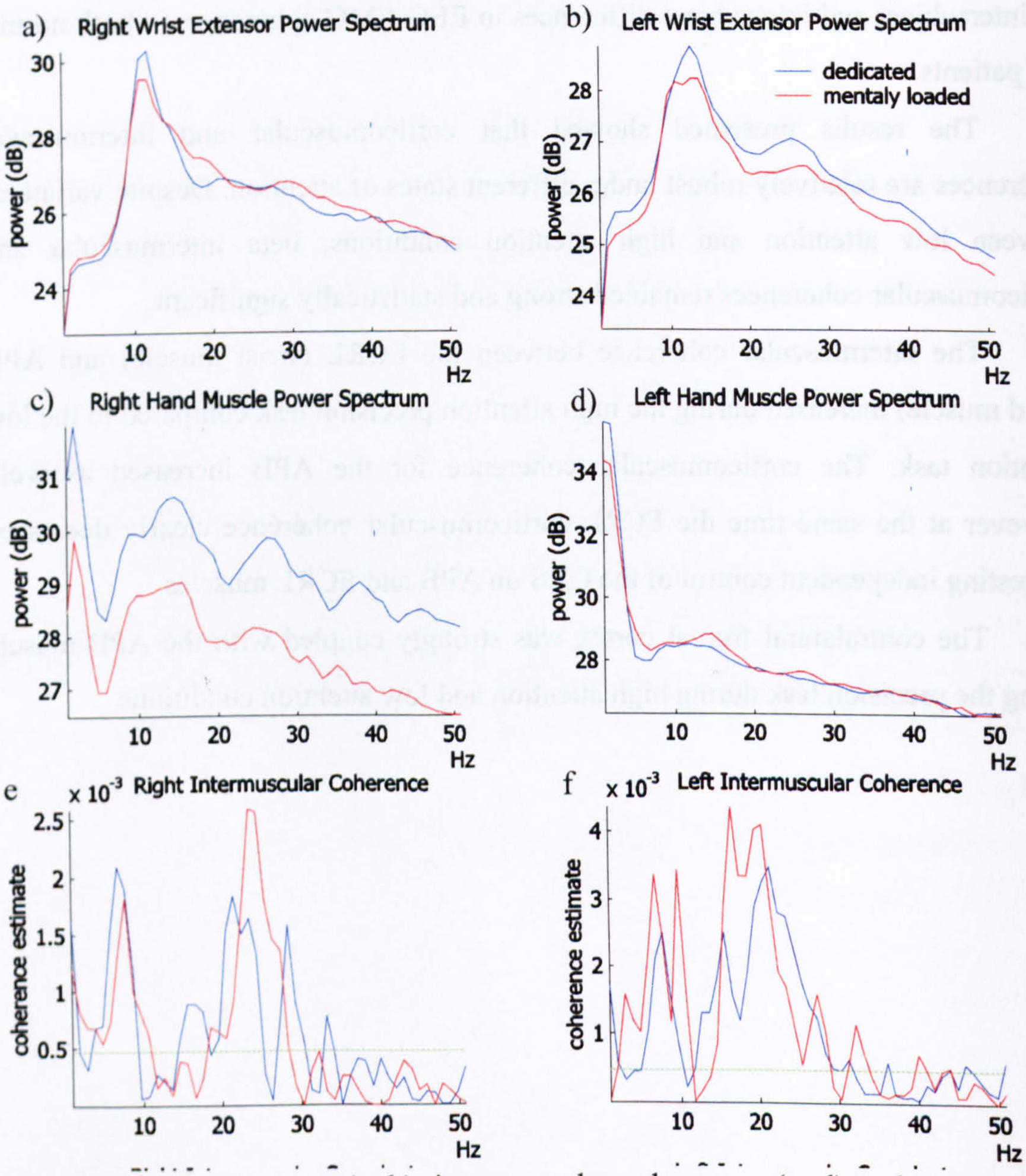

Fig. 5.157 Pooled power (a, b), intermuscular coherences (c, d) and cumulant plots (e, f) of homologues ECRL and APB muscles during dedicated performance of the elastic band precision extension task (blue) and the same task during simultaneous performance of mental arithmetic task (red).

5.2.2 Influence of cognitive loading in corticomuscular coherence

The aim of this experiment was to study the way corticomuscular and intermuscular frequency characteristics are affected by the performance of simultaneous cognitive tasks. It involved the bilateral extension of an elastic band. Subjects were instructed to keep the length of the extended elastic band constant as indicated by marks on a ruler. The constant length corresponded to a constant extension force. The experiment was conducted under two conditions; the Dedicated Performance (DP) of the task and the Cognitively Loaded (CL) state whilst carrying out complicated mental arithmetic.

Nine subjects were included in the study. EMG was recorded from left and right wrist Extensor Carpi Radialis Longus (ECRL) muscles and from left and right Abductor Pollicis Brevis (APB). EEG was also recorded from multiple cortical sites. The length of the records was 2min for the CL task and 2min for the DP task for each subject. Intermuscular frequency estimates were calculated between homologues muscles. Corticomuscular coherence maps were also produced between recorded EEG and EMG channels.

Fig. 5.157*a,b,c,d* show the pooled EMG spectral power estimates from all nine subjects. EMGs came from right ECRL *(a)*, left ECRL *(b)*, right APB *(c)*, left APB *(d)*. Despite the symmetric performance of the task the power spectra appear different between left and right sides. A 7-20Hz feature is present for both left and right ECRL power spectra. The peak for the right ECRL is wider and has a peak at a slightly higher frequency of 13Hz compared to the narrower peak centred at 11Hz for the right ECRL. A 20-30Hz component is present in the left wrist ECRL EMG while it is not as strong or it is absent in the right ECRL power. The overall power for DP and CL states are very similar.

The power for APB EMG in the 0-4Hz band is much higher than the equivalent power of the right APB. Comparing DP and CL conditions, while for left APB the spectra have very similar spectral power, the right APB power during the CL sate has been reduced compared with DP.

Fig. 5.157*e* shows the intermuscular coherences for right ECRL and right APB muscles EMG while Fig. 5.157*f* shows the intermuscular coherences between left ECRL and left APB muscles EMG. It is clear that the coupling between the left

Fig. 5.158 Pooled corticomuscular map of right ECRL coherences with bipolar EEG recordings during the dedicated (blue) and cognitively loaded (red) performance of the band extension task.

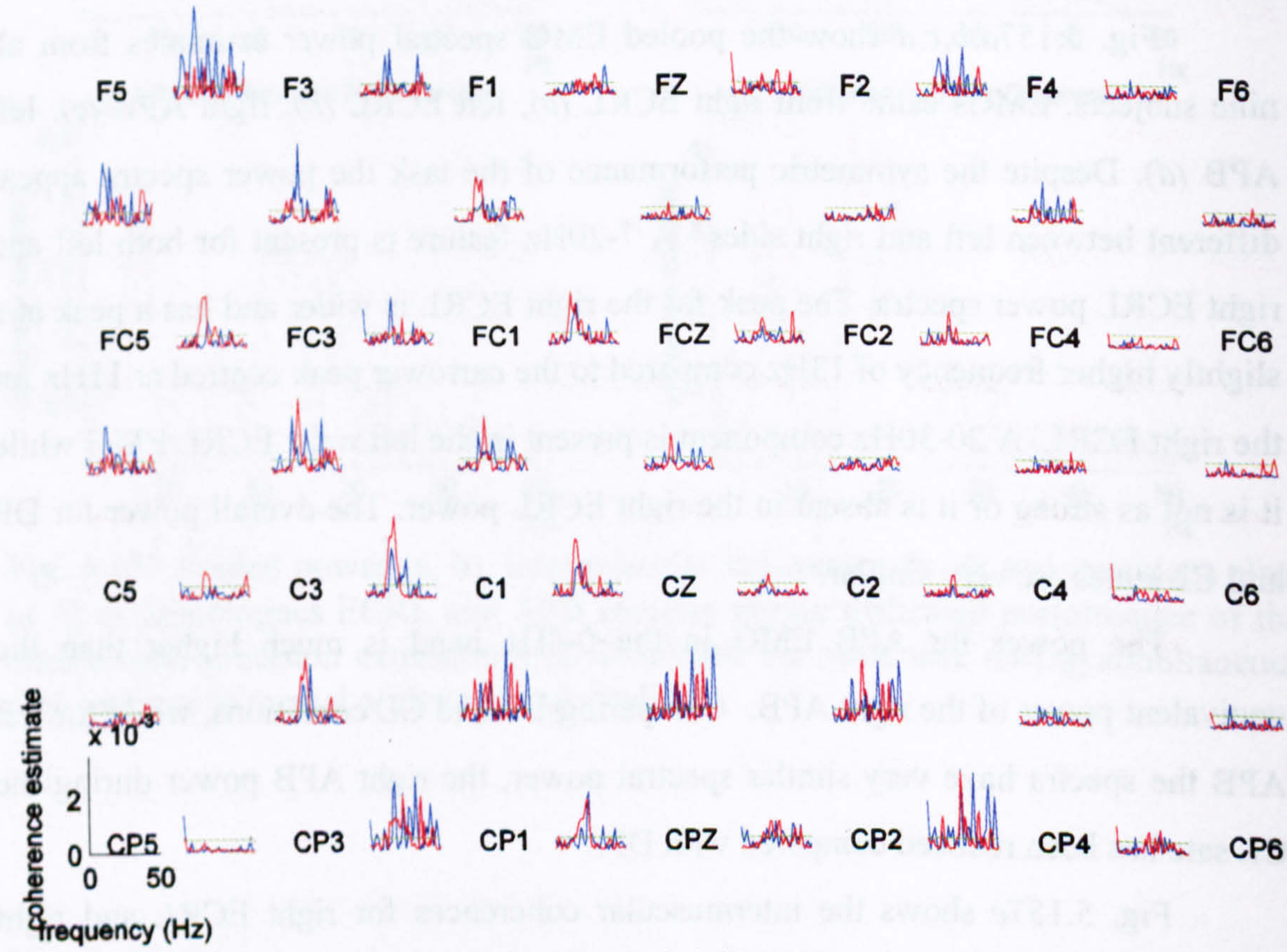

Fig. 5.159 Pooled corticomuscular map of right APB coherences with bipolar EEG recordings during the dedicated (blue) and cognitively loaded (red) performance of the band extension task.

forearm muscles is much higher than between the right forearm muscles, for both task states. Two main coupling components can be identified one in 4-12Hz band and the alpha area and one in 10-35Hz. 10-35Hz coherence on both sides appears higher during the CL task than during DP. The 4-12Hz coupling feature for the right forearm muscles is slightly stronger for the DP than the CL while for the left side where the coherence feature is much higher for the CL task.

Fig. 5.158 shows the bipolar coherence map for right ECRL muscle. Coherences in the beta band are higher on the contralateral side as expected. The strongest coherence appears for the FC1-C1. The beta coherence peak for the same electrode has a higher peak for DP task but the CL feature appears wider. The picture is not clear for the surrounding electrodes where coherence amplitudes are not significantly different for DP or CL.

Fig. 5.159 shows the bipolar coherence map for the right APB. As expected stronger coupling occurs at the contralateral side than at the ipsilateral. However the map appears different to the one observed for the bipolar wrist muscle map (Fig. 5.158). Beta coupling is dominant in contralateral central electrodes. However significant coherence is not only concentrated in beta band. A wider spectrum of frequencies is present for centroparietal areas as well as ipsilateral frontal and especially contralateral frontal electrodes. It is not clear if coherence is higher during DP or CL. During both task conditions the coherences are statistically significant.

For the left ECRL bipolar coherence plot in Fig. 5.160 there is very strong and defined contralateral beta coupling for both horizontally and vertically aligned electrodes. The coherence features are significantly stronger than the corresponding features observed for the right ECRL in Fig. 5.158. The coupling is clearly stronger for the CL task than for the DP. There is a difference in the frequency that the maximum coherence occurs at most of the strongly coupled electrode sites with the coherence during the CL task appearing at a 3-4Hz lower frequency. Apart from the dominant beta coherences, other weaker coupling can be observed. Alpha coherences emerge for the CL task for contralateral frontocentral-central electrodes while absent for the DP. Gamma features are also present for the same electrodes for both tasks.

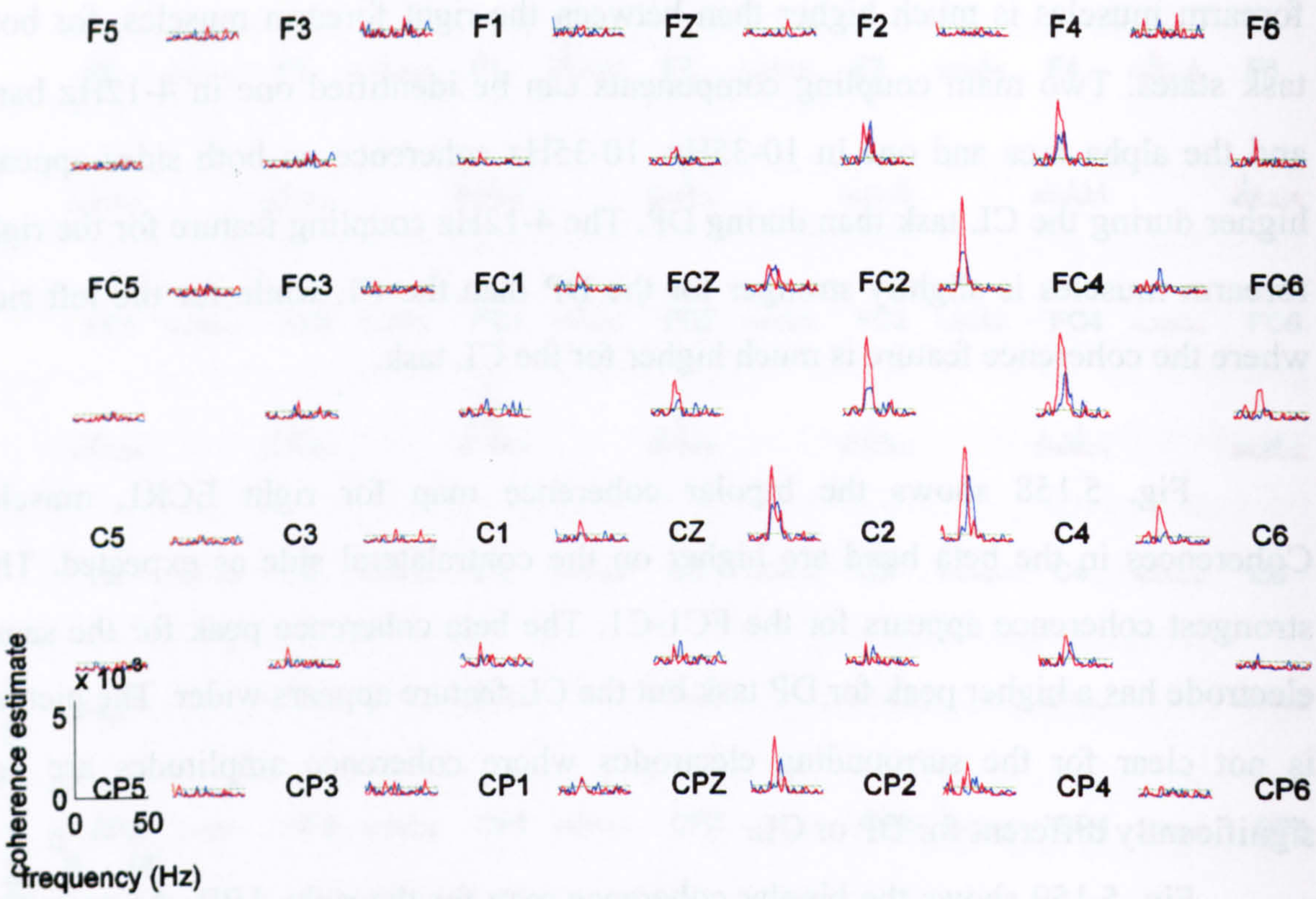

Fig. 5.160 Pooled corticomuscular map of left ECRL coherences with bipolar EEG recordings during the dedicated (blue) and cognitively loaded (red) performance of the band extension task.

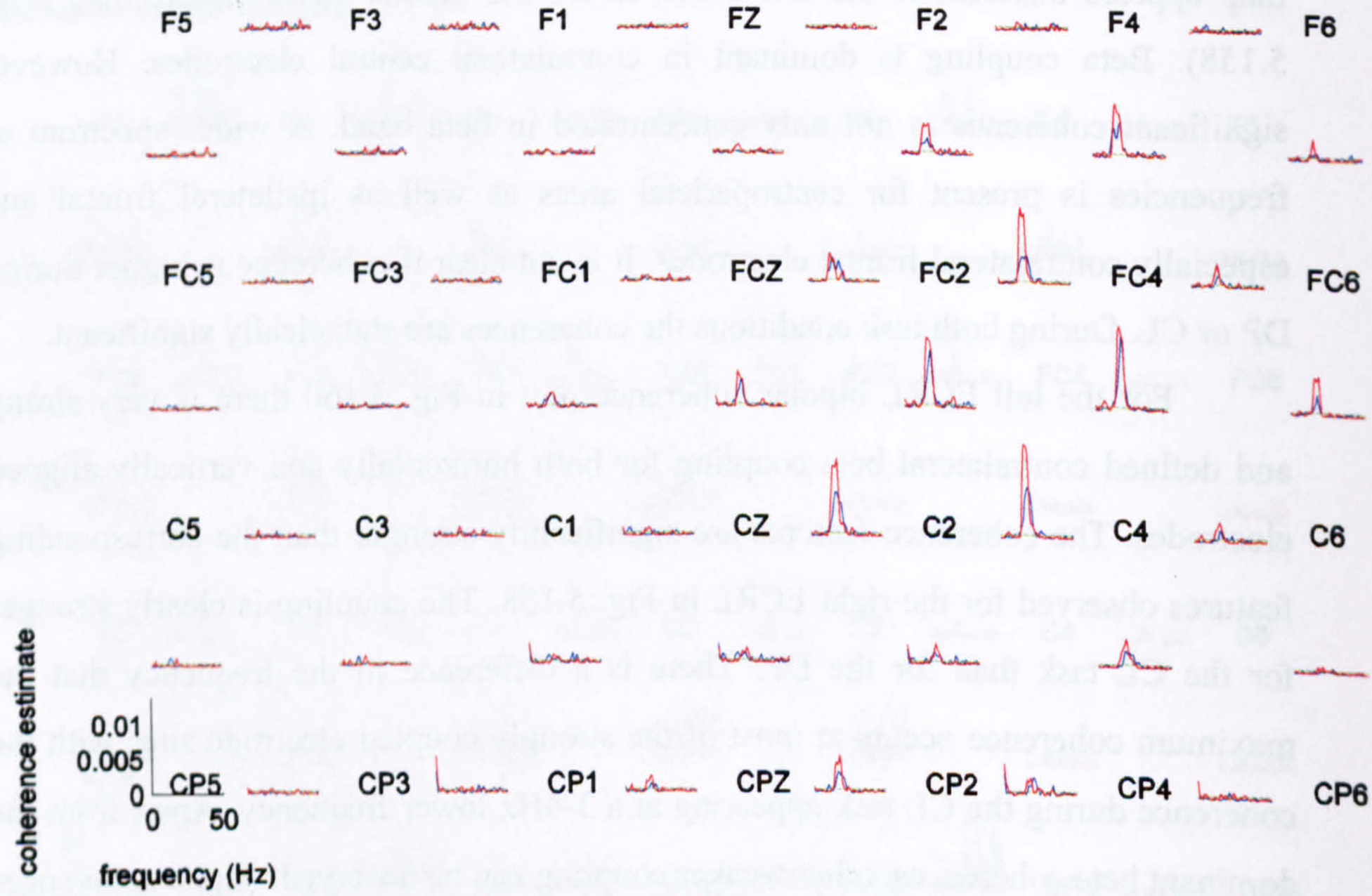

Fig. 5.161 Pooled corticomuscular map of left APB coherences with bipolar EEG recordings during the dedicated (blue) and cognitively loaded (red) performance of the band extension task.

The left APB bipolar corticomuscular coherence map in Fig. 5.161 shows coherences that appear much stronger than for the right APB (Fig. 5.159). Coherence features during the CL task are higher than for the DP task. The CL coherences occurred approximately 3Hz lower than the corresponding DP features. Alpha coherence emerge during CL while it is absent for DP. The higher left EMG coherence, the higher coherence for CL, the 3Hz shift to lower frequencies and the appearance of alpha coherence during the CL are all observed for the left ECRL corticomuscular map (Fig. 5.160) as well as left APB.

Coherence of the muscles within the left forearm (left ECRL\left APB) was significantly higher than for the right (right ECRL\right APB). Furthermore this asymmetry existed for the corticomuscular coherences as well. While the bilateral task was mechanically symmetrical the coupling of the left forearm muscles with the contralateral cortex (left ECRL\EEG and left APB\EEG) also were much stronger than of the right forearm EEG corticomuscular coherences (right ECRL\EEG and right APB\EEG).

5.2.2.1 Summary of cognitive loading influence results

In this experiment the focus was to examine how intermuscular and corticomuscular coherences are affected during a precision bilateral task, by the performance of a simultaneous cognitive task.

- The magnitude of beta intermuscular coupling was enhanced for the cognitive loaded task compared to the dedicated performance.
- Beta corticomuscular coupling also increased during the cognitive loaded task compared to the dedicated performance, for left and right forearms. The increase was higher for the left forearm that for the right.
- 4-12Hz intermuscular coupling clearly increased for the left forearm while for the right one was marginally smaller during the cognitive loaded task compared to the dedicated performance.
- There was an asymmetry in the left and right side intermuscular and corticomuscular coherences. The left forearm muscles' beta intermuscular coherence was much greater than the coherence observed for the right forearm. Furthermore the left forearm APB and ECRL beta corticomuscular coherence features with the contralateral cortex were much greater than the corresponding features observed for the right forearm corticomuscular coherence. The increased intermuscular and corticomuscular coherences for the left side were observed during both cognitive loaded and dedicated performance conditions, despite the symmetrical nature of the bilateral extension task. The coupling predominance of the left side during this bimanual task appears to have functional significance since all subjects were right handed. This should be further investigated in the future by examining left handed subjects.

5.3 *AFFERENT SENSORY INFLUENCES IN CORTICOMUSCULAR COHERENCE*

This experiment aimed to examine how corticomuscular and intermuscular frequency characteristics are affected by temporary sensory deafferentation induced using an ischemic nerve block (tourniquet induced ischemia) to the upper arm. The use of the Ischemic Nerve Block (INB) is a common method examining peripheral nervous system changes and the subsequent nervous system plasticity, caused by the lack of afferent or efferent input (Glencross and Oldfield 1975; Ziemann, Corwell et al. 1998; Ziemann, Hallett et al. 1998; Ziemann, Muellbacher et al. 2001).

INB deafferentation has been used in humans as a model of reversible short-term plasticity (Ziemann, Corwell et al. 1998). Deafferentation induces rapid plastic changes in the cerebral cortex. Several mechanisms may contribute, such as changes in neuronal membrane excitability, removal of local inhibition, or various forms of short or long term synaptic plasticity (Ziemann, Hallett et al. 1998). Long term perturbations are difficult to be replicated in normal subjects.

3 subjects participated in this study. The INB protocol followed inflating a sphygmomanometer cuff over the systolic arterial blood pressure level for a length of time around 20 minutes. The cuff was placed just above the elbow. As efferent nerve fibres are of smaller diameter than the large diameter afferent fibres they are more resistant to hypoxia. Thus, efferent fibres conduction declines at a slower rate than the function of the large afferent fibres. This usually results in a time window where efferent input to the muscles exists without or with reduced afferent feedback.

Two recordings were performed in 3 intervals during each INB session. The recordings were continuous movement for two minutes followed by two minutes of maintained extension. Both actions were performed in the vertical plane. The sequence was before the inflation of the sphygmomanometer cuff, just after the inflation of the cuff, 10 minutes after the inflation, 15 minutes after the inflation and finally just after the cuff deflation.

For the *Subject 3* the experimental protocol was slightly modified. Instead of having two separate 2 minute recordings for movement and posture the subject interchanged continuous movement with continuous extension every 10 seconds

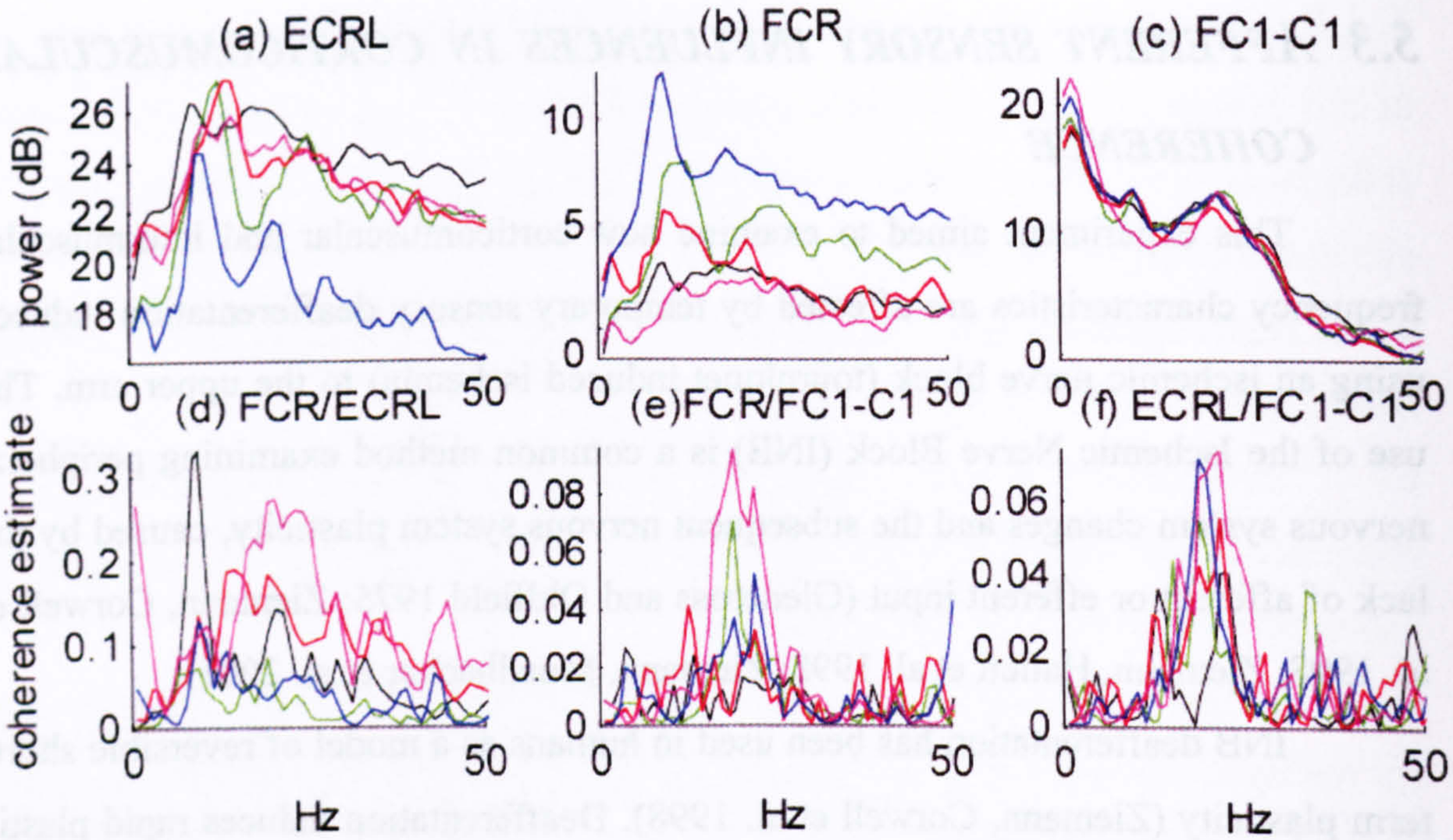

Fig. 5.162 INB results for subject 1 during posture extension. (a) ECRL power, (b) FCR power, (c) FC1-C1 power, (d) FCR\ECRL coherence, (e) FCR\FC1-C1 coherence, (f) ECRL\FC1-C1 coherence. Plots were plotted using the following colour code: (before inflation, just after inflation, 10 min after inflation, 15 min after inflation, just after deflation)

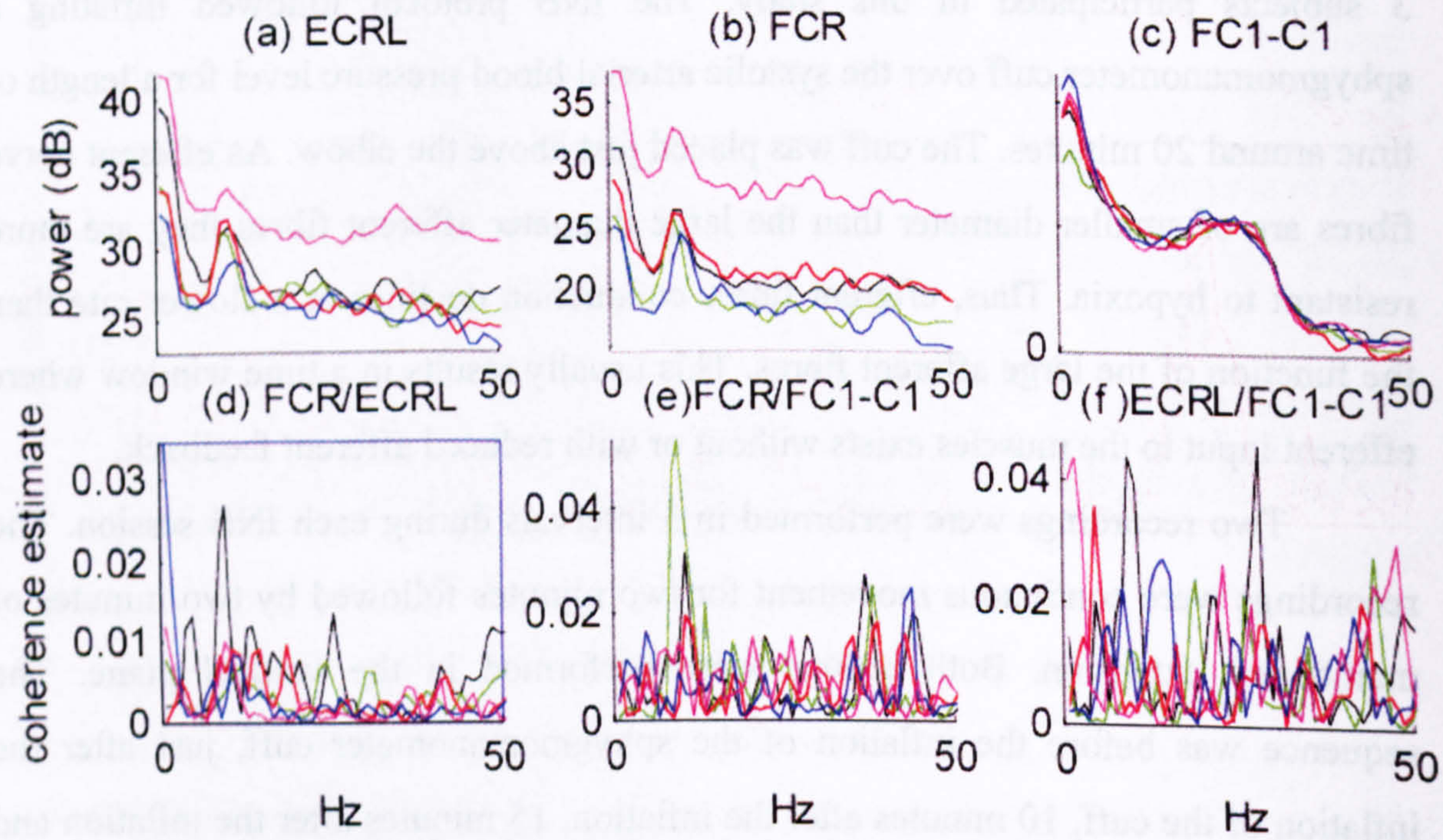

Fig. 5.163 INB results for subject 1 during movement. (a) ECRL power, (b) FCR power, (c) FC1-C1 power, (d) FCR\ECRL coherence, (e) FCR\FC1-C1 coherence, (f) ECRL\FC1-C1 coherence. Plots were plotted using the following colour code: (before inflation, just after inflation, 10 min after inflation, 15 min after inflation, just after deflation)

(indicated by regular audio cues). Each session lasted around 4 minutes which was epoched and appended into two minutes of posture and two minutes of movement.

The obtained records were pooled analysed using similar methods with analysis performed for previous experiments. Plots were plotted using the following colour code:

- Blue: before inflation
- Green: just after inflation
- Red: 10 min after inflation
- Cyan: 15 min after inflation
- Magenta: just after deflation

5.3.1 Results for Subject 1

Fig. 5.162 shows the power spectra and coherence estimates for *Subject 1* during posture extension. Fig. 5.162*a* gives the ECRL power spectra. Near 10Hz peaks, present during posture extension are enhanced during INB. After the release of the cuff the 10Hz feature is significantly reduced. The near 10Hz peaks do not occur at exactly the same frequency. Beta and "high beta" features also area also present. Their shapes do not appear consistent and they also seem to have a harmonic relationship with the 10Hz features. The overall picture shows significant variability in the agonist EMG power spectra.

Fig. 5.162*b* shows the FCR power posture extension. Near 10Hz activity is present and enhanced during the INB. The most distinct peak appears 20 min after applying the block, when the highest overall power level also occurs. Immediately after the release of the nerve block the general activity level returns to the pre-INB levels while the near 10Hz peak diminishes. Beta features that appear after 10 and 15 minutes show a harmonic relationship with the 10Hz centred peaks. On the whole there is high variability in the overall power level as well as in the distinct spectral features.

Fig. 5.162*c* shows the power spectra for FC1-C1. They remain quite consistent throughout the INB. The most significant change is the suppression of the

10Hz feature after the release of the cuff. 0-4Hz power seems to increase with the INB.

Examining the FCR/ECRL coherences in Fig. 5.162*d*, a 10Hz features appear before, during and after the INB. Despite that 10Hz EMG features were enhanced during the INB, the intermuscular coherence appears to decrease in the same frequency band. Beta coherence shows variability, having no clear connection with the progress of the INB. The highest beta coherence occurs for the session after the deflation of the cuff.

Fig. 5.162*e* gives the FCR\FC1-C1 coherence. The corticomuscular coherence for the antagonist muscle shows an enhanced beta coupling during the INB. The maximum coherence appears after the deflation for the cuff. There is no noticeable alpha coherence feature. Fig. 5.162*f* shows the agonist ECRL\FC1-C1 coherence. The corticomuscular coherence shows enhanced coupling during the INB and after the deflation of the cuff, where the highest coherence occurs.

Fig. 5.163*a* shows the power spectrum of ECRL during movement. The spectral content of the FCR EMG does not change dramatically. The 10Hz peak feature appears pretty constant, compared with the near 10Hz feature observed during extension posture which varied considerably. The overall power level appears higher after the deflation of the cuff. Similar is the picture for the FCR muscle (Fig. 5.163*b*). The FC1-C1 spectra (Fig. 5.163*c*) contain high 0-5Hz power as well as a distinct beta component and alpha features. The plots are very consistent during the INB.

Despite the strong 10Hz feature in ECRL and FCR power spectra the intermuscular FCR/ECRL coherence (Fig. 5.163*d*) shows a clear 10Hz coupling feature only before the inflation of the cuff. The FCR\FC1-C1 coherence (Fig. 5.163*e*) shows 10Hz coupling which is enhanced after the inflation of the cuff but then declines with time during the INB. Gamma activity at around 40 and 45Hz is present with no clear connection to the INB the INB. Similar is the picture for the coherence between ECRL and FC1-C1.

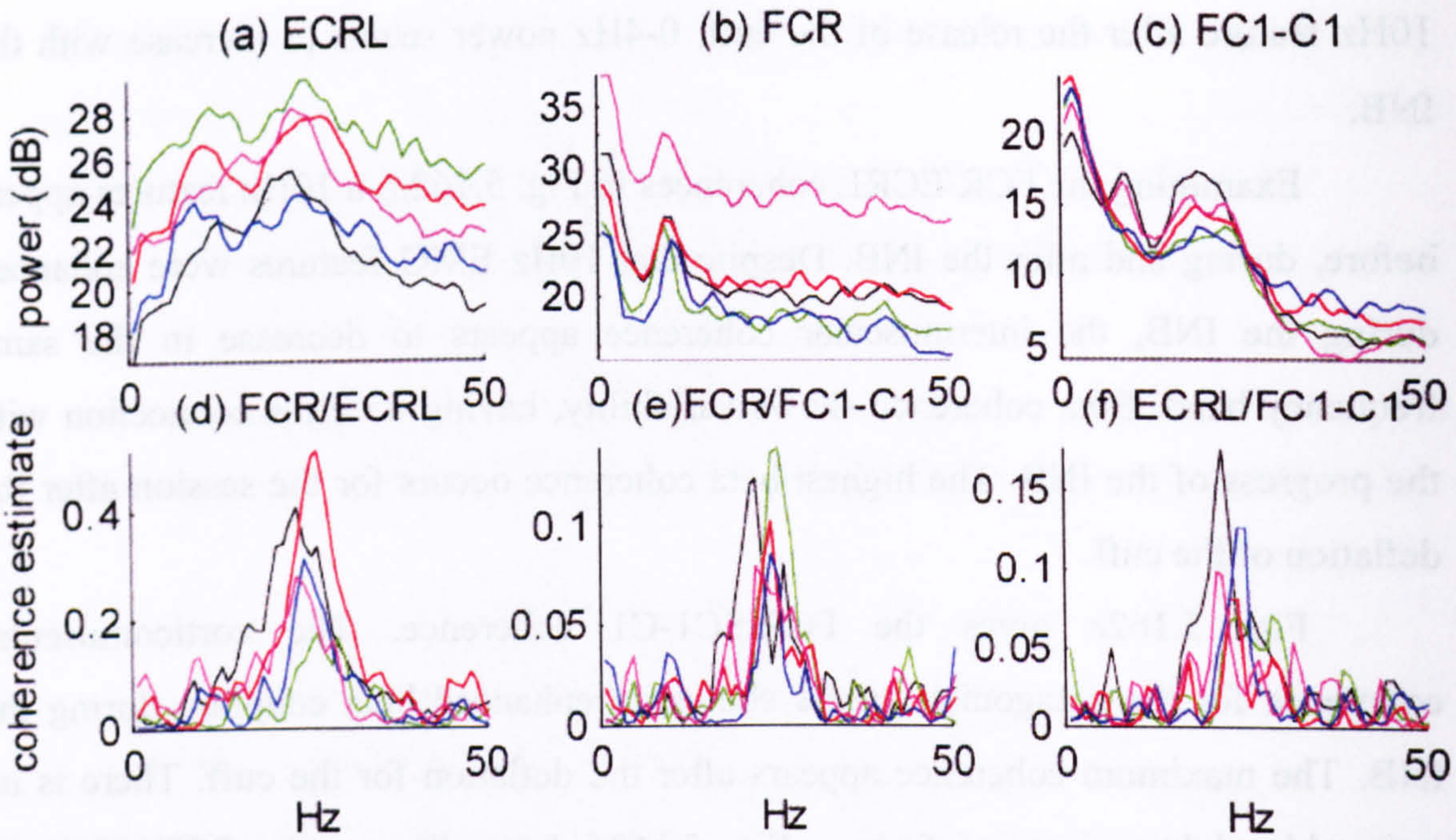

Fig. 5.164 INB results for subject 2 during posture extension. (a) ECRL power, (b) FCR power, (c) FC1-C1 power, (d) FCR\ECRL coherence, (e) FCR\FC1-C1 coherence, (f) ECRL\FC1-C1 coherence. Plots were plotted using the following colour code: (before inflation, just after inflation, 10 min after inflation, 15 min after inflation, just after deflation)

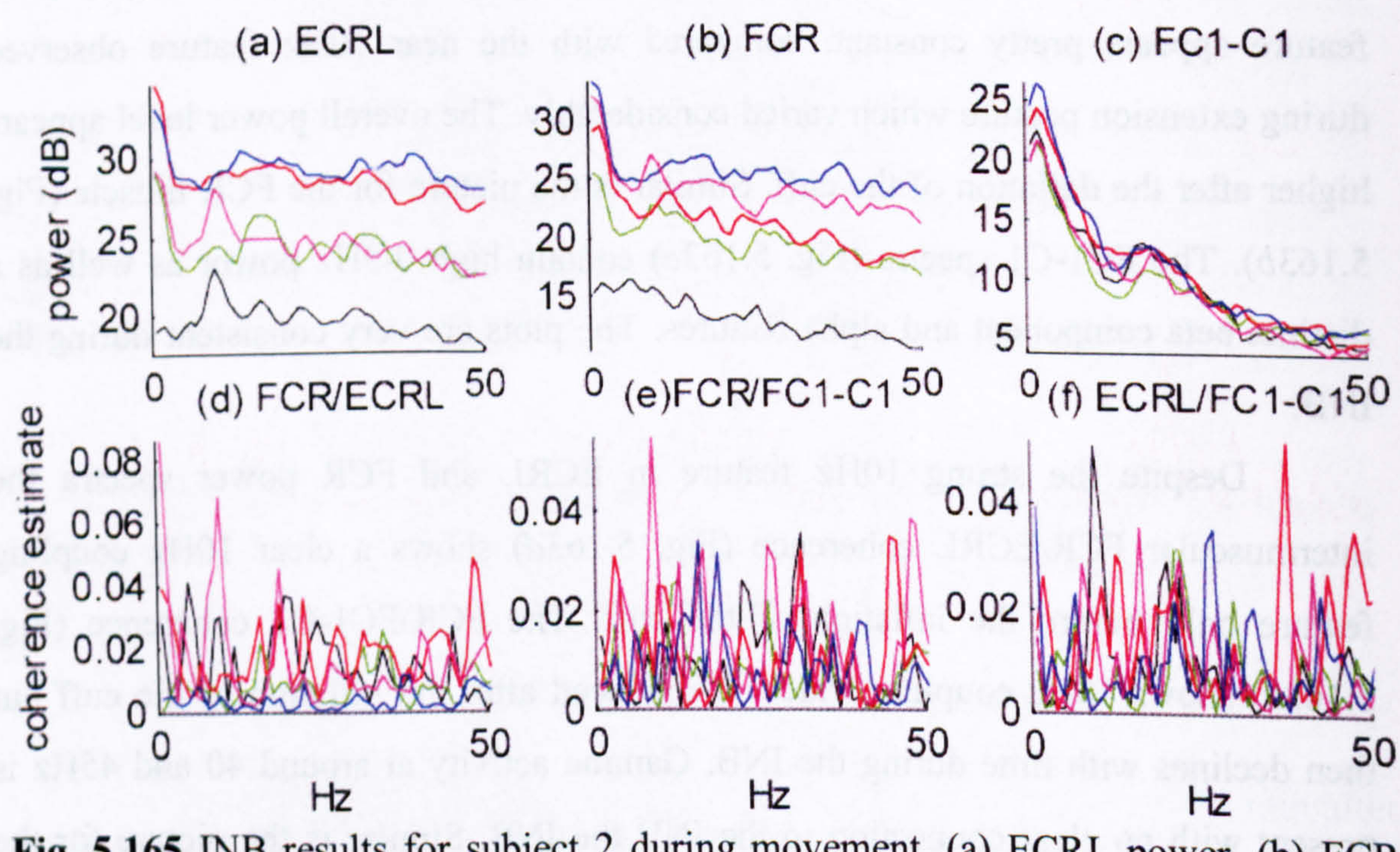

Fig. 5.165 INB results for subject 2 during movement. (a) ECRL power, (b) FCR power, (c) FC1-C1 power, (d) FCR\ECRL coherence, (e) FCR\FC1-C1 coherence, (f) ECRL\FC1-C1 coherence. Plots were plotted using the following colour code: (before inflation, just after inflation, 10 min after inflation, 15 min after inflation, just after deflation)

5.3.2 Results for Subject 2

Fig. 5.164*a* gives the power spectral of ECRL for *Subject 2* during posture extension. The 10Hz peak seems to be enhanced with the INB and declines after the release of the block. A similar observation was made for *Subject 1*. Beta features appear to have a more consistent form than for *Subject 1*. The overall picture shows again significant variability in the shape of the agonist EMG power spectra, especially for the near 10Hz peaks, which do not occur at exactly the same frequency. In FCR power spectra (Fig. 5.164*b*), near 10 and 20Hz features are present, during and after the INB with increasing overall power level. Immediately after the release of the nerve block the spectral power returns to the pre-INB levels. There is little variability in the overall shape of the power spectra. Fig. 5.164*c* shows the FC1-C1 spectra which contains a persistant 10 Hz feature before and after the INB, witch is suppressed during the INB. Beta features are present and weaken during the INB, to return to the pre-INB levels after the release of the cuff.

FCR/ECRL coherence in Fig. 5.164*d*, does not show high alpha coupling. Intermuscular beta coupling shows some variability but in general it remains high. The highest beta coupling occurs just after the inflation of the cuff and the highest 10 min after the inflation. The corticomuscular coherences for the antagonist FCR muscle (*e*) show significant beta coupling during all phases. Fig. 5.164*f* shows the coherence for ECRL\FC1-C1 corticomuscular coherence. The beta corticomuscular coherence appears slightly suppressed but still high during and after the INB.

Fig. 5.165 gives the frequency characteristics of the recorded signals during continuous movement. ECRL power (Fig. 5.165 *a*) shows a 10Hz feature before inflation and after the release of the cuff, which is suppressed during the INB. The power spectrum of the FCR EMG (Fig. 5.165 *b*) does not show any clear features and a 10Hz feature is obvious only after the deflation of the cuff. The overall level of power appears higher during and after the INB, compared to the power before the inflation, as was at case for ECRL. FC1-C1 power (Fig. 5.165 *c*) shows high "low frequency" power, a distinct beta component and no distinct alpha features. The spectra are quite consistent throughout the INB. The FCR/ECRL, FCR\FC1-C1and ECRL\FC1-C1 coherences (Fig. 5.165 *d,e,f*) do not show any important features

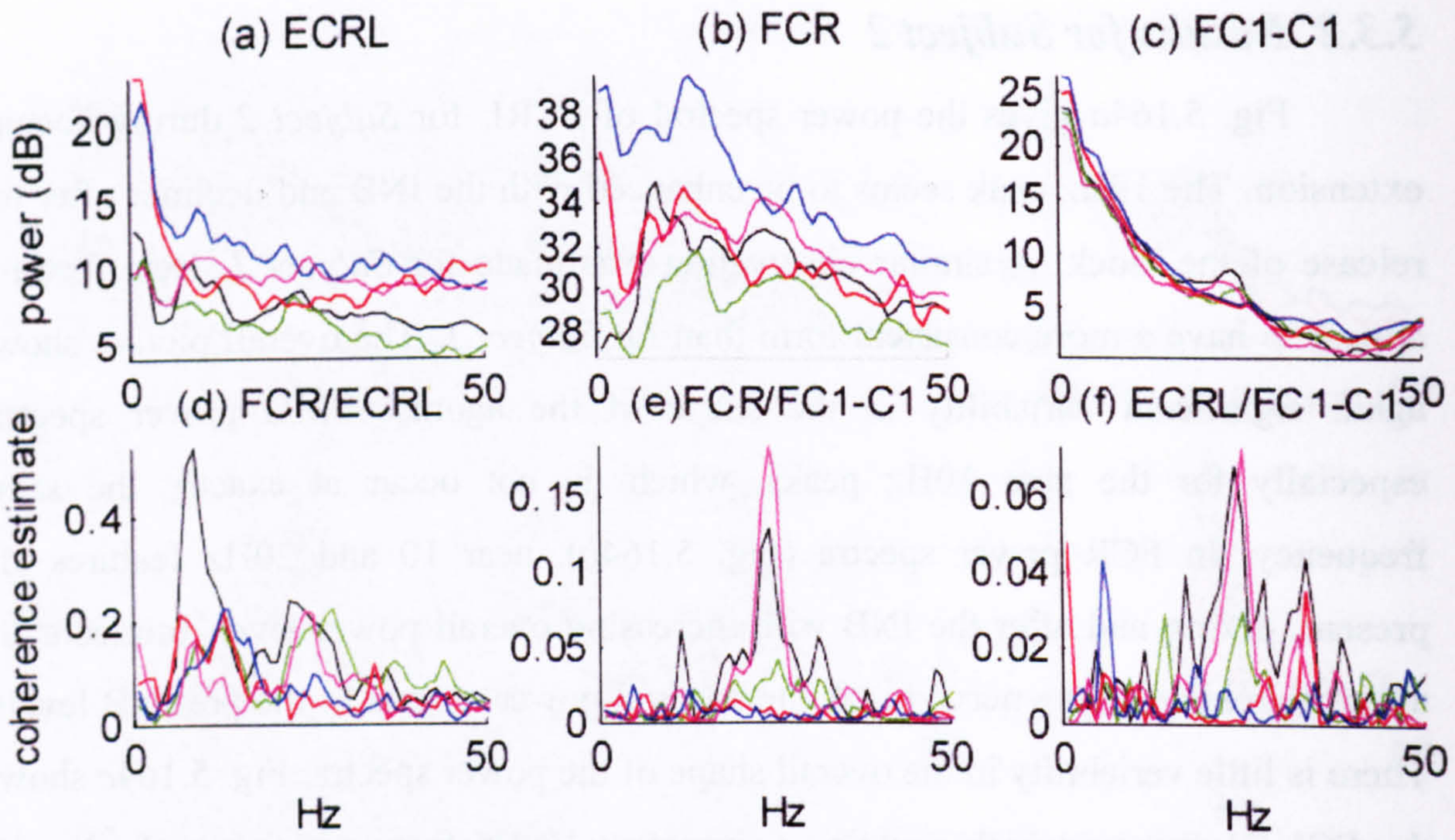

Fig. 5.166 INB results for subject 3 during posture extension. (a) ECRL power, (b) FCR power, (c) FC1-C1 power, (d) FCR\ECRL coherence, (e) FCR\FC1-C1 coherence, (f) ECRL\FC1-C1 coherence. Plots were plotted using the following colour code: (before inflation, just after inflation, 10 min after inflation, 15 min after inflation, just after deflation)

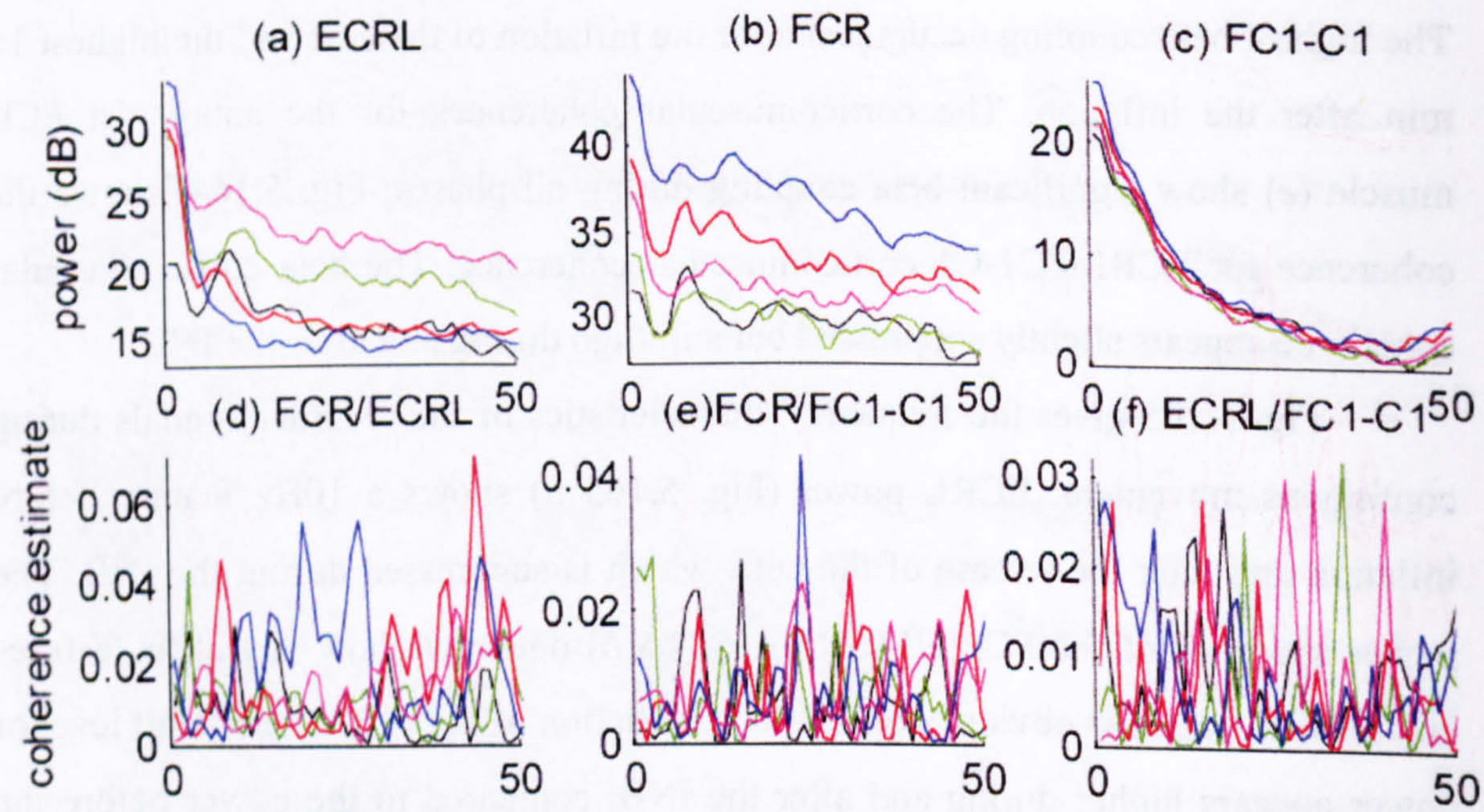

Fig. 5.167 INB results for subject 3 during movement. (a) ECRL power, (b) FCR power, (c) FC1-C1 power, (d) FCR\ECRL coherence, (e) FCR\FC1-C1 coherence, (f) ECRL\FC1-C1 coherence. Plots were plotted using the following colour code: (before inflation, just after inflation, 10 min after inflation, 15 min after inflation, just after deflation)

5.3.3 Results for Subject 3

During the posture extension task near 10Hz, 15Hz and 25Hz features are present in ECRL and FCR spectra (Fig. 5.166*a,b*) but with high variability, and no clear connection to the phases before, during and after the INB. The Fig. 5.166*c* gives the FC1-C1 bipolar EEG power. There is no clear 10Hz peak while a 25Hz feature is present. The feature declines with the INB and does not recover after the deflation.

The FCR/ECRL coherence can be seen in Fig. 5.166*d*. A very strong 10 Hz feature is suppressed during the INB and does not recover after the deflation of the cuff. 25Hz coupling is also observed but decreases during the INB and recovers afterwards. The corticomuscular coherence for the FCR muscle shows significant beta coupling before, and after the INB. Coupling just after the inflation it is decreased but is still significant, while coherence for the progressed stages of the INB appears very low. High alpha coupling is also present before the application of the INB.

The ECRL/FC1-C1 coherence is displayed in Fig. 5.166*f*. Beta corticomuscular coherence appears high before and after the INB, while suppressed during the INB.

Fig. 5.167 shows the results for *Subject 3* during continuous movement. For the ECRL muscle (Fig. 5.167*a*) suppression of 10Hz feature occurs at the 15 min INB. No other change related with to the INB is present. The power spectrum of the FCR EMG (Fig. 5.167*b*) shows clear 10Hz features. The overall power appears higher during and after the INB compared to the power before the cuff inflation. The FC1-C1 spectrum (Fig. 5.167*c*) does not contain any alpha or beta features while no obvious changes can be observed that can be observed during the INB.

FCR/ECRL, FCR\FC1-C1 and ECRL\FC1-C1 coherences (Fig. 5.167*d,e,f*) do not show any distinct features related to INB.

5.3.4 Summary

The aim of this experiment was to examine whether perturbations of the peripheral nervous system can affect the corticomuscular and intramuscular frequency characteristics. The results illustrated a significant intersubject and intrasubject variability of the frequency characteristics.

- *Subject 1* showed an increase of posture beta corticomuscular coherence for ECRL and FCR during the INB. The corticomuscular coherence progressively increased during the INB, with maximum coherence occurring after the release of the block. Intermuscular coherence also displayed variability with the largest coherence appearing after the release of the INB. There was no clear connection between the sequence of the recordings during the block and the magnitude of the peaks. A clear connection of intermuscular coherence and loss of afferent input was not evident. 10Hz posture intermuscular coherence was clearly suppressed with INB despite the significant increase in the corresponding EMG activity.
- *Subject 2* maintained high corticomuscular coherence as well as intermuscular coherence throughout the INB. Beta EEG power declined during the INB but partially recovered amplitude after the release. The alpha EEG power feature was suppressed during INB, and re-emerged after the release of the block. The corresponding EMG alpha and beta spectral peaks were present during the INB.
- *Subject 3* showed a progressive decrease of corticomuscular coherence during the INB. The coupling feature diminished during the late stages, returning to the pre-INB levels after the release of the block. This progressive reduction should be connected with the ongoing decrease of the afferent activity, induced by the ischemia of the neural tissue. Reduction in beta coupling also occurred for the intermuscular coherence between agonist and antagonist. A similar reduction also occurred in the beta EEG power. Alpha intermuscular and corticomuscular coherences were also suppressed during the INB.
- During continuous movement none of the subjects demonstrated consistent changes for intermuscular coherence characteristics.

6 DISCUSSION

6.1 INTRODUCTION

The growing interest in the study of brain activity involved in motor control and development of robust methods of intention detection for use in the activation and regulation of prosthetic devices and communication aids for the severely motor disabled were the driving force behind the work carried out within this thesis. The aim of the experiments performed was to identify task dependent corticomuscular features in EEG and EMG signals, and consider their use for intention detection.

The patient groups that could benefit from neuroprosthetic systems are quite diverse. They can be grouped into two main groups; patients with or without residual voluntary control. The first group consists of amputees, incomplete spinal cord injured patients, hemiplegics etc. The second group include "locked-in" patients including these with high complete spinal cord injury, degenerating neuropathies etc. Patients with voluntary control in principle should be able to use neuroprosthetic systems that react to EEG and/or EMG signal characteristics and may also utilise the corticomuscular synchronisation. For "locked-in" patients only EEG is available to be utilised for neuroprosthetic control.

EEG and EMG signals are known to reflect the rhythmic activity in the nervous system. The current study used advanced time-frequency analysis techniques on forearm muscle EMGs and recording of multichannel EEG electrodes in order to examine the spatial and temporal characteristics of activity representative of a wide area of the cortex. Task dependant changes in frequency content and corticomuscular coherence were monitored during a sequence of simple posture and movement tasks. These signals were expressed as EEG and EMG power, as well as corticomuscular and intermuscular coupling estimates such as coherence, cumulant and phase estimates.

The connection between corticomuscular coupling and changing levels of motor attention or cognitive loading was also examined in order to consider the robustness of the examined signals. This form of evaluation is an important aspect of the intention detection not often considered by researchers e.g. (Wolpaw et al. 2002).

Similarly, because this study only examined normal subjects, temporary deprivation of sensory feedback using an INB was used to study how pathologic deafferentation may affect the frequency characteristics and corticomuscular coupling. Subjects with sensory deficits may not show similar features to these seen in EEG and EMG recordings in normal subjects. These experiments were therefore intended to examine to what extend the task dependencies in EEG/EMG coupling are affected by the loss of feedback from ascending sensory signals.

6.1.1 Novel methodological and analytical features

The study employed novel methodological and analytical features combined with methods validated from previous studies (Halliday et al. 1995; Halliday, 1998; Mulcahy, 2001). The analysis of the results involved analysis of pooled records obtained from different subjects. Pooled estimates (Amjad et al. 1997) give numerical results calculated over all available data, giving a population result in contrast to having to consider trials separately. Pooled coherence analysis is an established method, useful to summarize a large data set, and avoids presenting individual data in the form of a "typical" example (Halliday and Rosenberg 1999). It is recognised that significant intersubject variability in corticomuscular coherence has been observed (Kilner et al. 1999), thus presentation of selected data sets from an individual can often lead to misleading conclusions, by emphasizing features not typical of the population as a whole (Fetz 1994). Within the framework of this thesis, the primary aim was to examine the typical population movement related behaviour that can be considered significant for the entire population group studied. The results suggested that movement related characteristics exist and could be used for intention detection systems. However clinical applications should consider the variability within the general population result and customise the intention detection systems to the task dependencies of the individual. A customisation process will probably require the use of automatic feature extraction and classification systems (Pfurtscheller et al. 2000) that will relate the individual task dependent features to the intention command. These systems will also have to be able to deal with, and potentially benefit from central and peripheral neuroplasticities. New task dependencies may be

developed or enhanced during training and continuous use of the system by the users, giving a need for systems to be adaptive.

In this study a main novel methodological feature involved the assessment of corticomuscular estimates during short posture tasks and maintained posture tasks, as well as between short movements and continuous movement.

An additional important novel methodological feature was the performance of a symmetrical bilateral isometric extension task that demonstrated a significant asymmetry between left and right side corticomuscular and intermuscular associations.

Equally important were the novel analysis techniques used. The estimation of cumulant components corresponding to coupling in specific frequency bands proved a useful tool for the interpretation of complex cumulant plots. Coupling features in different frequency bands may be the result of different underlying physiological mechanisms which have different functional significance.

A new method was devised for the calculation of the phase estimate of rectified "out of phase" coupled EMG signals. The coupling was converted into "in phase" by inverting one rectified EMG, which provided a robust estimate of the delay, which was not possible before. The method also applied for "out of phase" coupled EEG and rectified EMG signals.

A new approach was also developed for generating pooled time (cumulant) and frequency (spectral power, coherence) domain estimates over time. It consisted of pooling movement phases aligned as short disjoint sections across different trials and subjects. It generated good quality results with high time and frequency resolution providing an insight of how each frequency characteristic changes in time during posture and movement as well as during transitions between tasks. It successfully overcame the compromise between time and frequency resolution demands often met in this type of study.

6.1.2 Main findings

The experimental protocols and analytical methodologies have produced original results and findings. The most important findings of this study are:

Time dependent frequency estimates in time (and especially time dependent power, coherence and cumulant) gave a very comprehensive picture of task dependent features throughout the duration of repeated movement and posture tasks as well as during the transition between tasks.

Signals within the beta band demonstrated the clearest task dependent features. EEG and EMG power, intermuscular coupling, corticomuscular coupling showed synchronisation in the beta band during posture that is suppressed during movement. Intracortical coherence showed beta band decoupling during posture, an expression of increased organised cortical activity in this band.

Beta power and corticomuscular coupling has been shown to be strongly associated with posture. However the present study has also shown that it may not be essential for the establishment of posture as has been previously suggested (Baker et al. 1999). It appears to be greatly dependent on movement performed in neighbouring joints since beta EMG power and corticomuscular coherence associated with biceps during posture of elbow was suppressed during short duration wrist movement tasks.

The posture specificity of beta band activity was also challenged since continuous wrist movements also revealed beta intermuscular and corticomuscular coherence for muscles involved in movement.

Important differences were identified in frequency characteristics between maintained posture and short posture tasks as well as continuous movement and short movement tasks. These results demonstrated that the CNS may adopt different strategies for the performance of similar tasks according to the broader movement context.

Important asymmetry was identified in the intermuscular and corticomuscular coherences between the left and right sides during a symmetrical bilateral isometric extension task. The left forearm corticomuscular coherences with the contralateral cortex were higher than the corresponding right forearm corticomuscular coherences. This

asymmetry was also reflected in the intermuscular coherence since coherence between left forearm homologues muscles was higher than for the right.

EEG power in alpha, delta and theta bands showed clear task dependent variations during the move-hold sequence which have not been reported in previous studies.

The role of alpha band in EMG was thoroughly investigated. Alpha EMG activity emerged during wrist movement primarily in antagonist muscles, rather than the agonist. The agonist\antagonist EMGs were strongly coupled at 10Hz confirming the biphasic double pulse model suggested by (Vallbo and Wessberg 1993). Using the novel analytical features described earlier, important attributes of that model are presented in the present study. The most important is the "out of phase", 0ms delay between agonist and antagonist which strongly suggests a central origin for the 10Hz modulation.

For BBLH which acted to support the forearm during the wrist move-hold sequence, a strong alpha feature was evident in the EMG and it showed a well defined frequency variation (9-14Hz) dependent on the position of the wrist. This finding demonstrates the fact that even small variations in a frequency feature may be functionally significant. It may also be concluded that tracking techniques that frequency tracking techniques focusing on narrow bands may not be as effective in detected task dependencies.

It has also been demonstrated with the use of cumulant components that coupling in the same frequency band during different movement phases may be the result of different underlying mechanisms. It has also been demonstrated that coupling in the same frequency band for different pairs of muscles may also be the result of different neurological processes.

Increased motor attention in a precision task lead to increases in intermuscular coherence and corticomuscular coherence for the hand musculature involved, but it simultaneously decreased in the corticomuscular coherence for wrist muscles. This demonstrated that corticomuscular coherences of synergistic muscles can increase and decrease independently according to the task requirements.

Cognitive loading did not appear to decrease intermuscular and corticomuscular couplings. Furthermore increased cognitive loading appeared to enhance these coherences.

INB results were not conclusive because of the small number of subjects and the variability observed in the results between the subjects. Results obtained from one of the subjects are in agreement with previous findings (Pohja and Salenius 2003) showing a decrease in the strength of frequency features as INB progresses. This was not seen in the other two subjects.

Additional evidence was provided suggesting that the source of the underlying corticomuscular coherence is an oscillating dipole generated within the contralateral motor cortex. The dipole direction oscillates from positive to negative at the beta frequency. Its orientation (for wrist muscles) was diagonal, lying approximately on the axis connecting the centroparietal and frontal electrode sites.

Significant evidence was provided illustrating that different oscillators may be driving synergistic muscles. This was suggested by small differences in the centre beta frequencies of corticomuscular coupling as well as the orientation of the corresponding cortical dipoles for the individual muscles.

6.2 TASK DEPENDENT RHYTHMIC EMG-EEG FEATURES

6.2.1 Introduction

The main aim of the study was to identify task related features in the temporal and spatial characteristics of EMG and EEG frequency estimates. These estimates include spectral power, coherence, cumulant and phase. Multichannel EEG signals from 28 cortical electrodes as well as EMG signals from ECRL, FCR and BBLH muscles were examined during the repetition of a sequence of move-hold tasks.

Task dependent variations during movement and posture were identified. Because of the dynamic nature of the examined signals, it was also useful to examine the way the time dependent frequency characteristics change in time, over a wide range of frequencies (0-50Hz) not only during a movement or posture but also during the transition between two successive tasks. This information may be relevant for the control of neural prostheses as well as for the improvement of our understanding of the dynamic nature of the control of human movement. Considering the low signal to noise ratio content of the examined signals, real time intention detection methods will require the use of the most sensitive available task related information.

6.2.2 EMG task related features

8-12Hz modulation within the EMG, and the level of motor-unit synchronisation, has been associated with the control of voluntary dynamic movements (Vallbo and Wessberg 1993; Wessberg and Vallbo 1995; Wessberg and Kakuda 1999). Modulation in the 15-35Hz EMG activity has been mainly associated with posture (Farmer et al. 1993; Conway et al. 1995; Halliday et al. 1999). It has also been suggested that the rhythmic modulation of motor-unit synchronisation in these two frequency ranges might be interrelated, such that both rhythms occur simultaneously in the EMG, but are conversely enhanced or weakened in task-specific fashion during a movement or a postural task (Wessberg and Kakuda 1999).

The EMG power spectral plots and spectrograms (time dependent power spectral plots) during the move hold sequence revealed task related components present at 8-

12Hz during movement and at 15-25Hz mainly during posture. However the association was not always clear and well defined, displaying rather poor task dependency. Such that 8-12Hz features also occurred during both posture and movement and the 15-25Hz features were masked by the overall increase in activity during posture.

Intermuscular coupling displayed more consistent task dependent features than the corresponding power spectra. The most notable feature was the strong agonist antagonist coupling at 8-12Hz during movement. Previous studies have demonstrated for finger movements that the near 10Hz agonist and antagonist EMG modulations come in a form of biphasic motor output giving bursts in agonist muscles that are followed by a braking burst in the antagonist at 8-12Hz (Vallbo and Wessberg 1993).

The present study demonstrated that the 10Hz EMG modulation occurs primarily in the antagonist whereas the agonist power spectrum was often not dominated by a 10 Hz peak during the wrist movement. Similar observations have also been reported for finger muscles where the 8-12Hz flexor antagonist power was greater than the extensor agonist power during extension (Mulcahy 2001). Yet, in the present study, despite the absence of a clear ECRL 10Hz power feature, ECRL\FCR coherence plots during movement flexion revealed strong coupling in the above frequency range. The lack of a clear 10Hz feature in the EMG power spectra and spectrogram does not mean low power content within this frequency, since the power of agonist ECRL was higher than for FCR. 10Hz power is probably masked by the generally high activity over the spectrum.

These observations partially confirm previous findings suggesting that 8-12Hz finger agonist and antagonist modulations come in a form of biphasic motor output. However, it would appear that the agonist muscle may be able to increase power in a more smooth way while the breaking action of the antagonist contributes more to the expression of the 10Hz movement tremor. The concentric and eccentric nature of contraction of agonist antagonist may be a contributing factor in the production of a more distinct frequency feature for the antagonist muscle. While this was not described in the Vallbo (1993) study it was evident in the acceleration records as individual 8-10Hz cycles are asymmetrical with decelerations showing higher peaks than the preceding accelerations (Vallbo and Wessberg 1993).

The cumulant estimates between agonist and antagonist can give more insight into the association. The cumulant component for the 8-12Hz coupling (as well as the phase) of EMG signals revealed interesting features regarding the origin of this biphasic motor command. The "out of phase" nature of coupling as well as the near 0ms delay indicate a central origin for the 10Hz signals and provide further evidence to support previous studies already suggesting that the coupling is not the result of a reflex loop and is of central origin (Vallbo and Wessberg 1993; Wessberg and Vallbo 1995; Wessberg and Vallbo 1996). The present study demonstrated that the agonist-antagonist signals are almost perfectly out of phase, a finding which can not be easily reconciled with a reflex mechanism given the conduction distances and times available.

Although EEG has been used to reveal oscillatory activity and corticomuscular coherence in the beta band there has been no consistent evidence for the existence of an alpha central descending motor command during movement. However EEG results are often poorly localised and are not clearly related to ongoing moor activity (McAuley and Marsden 2000). New recording techniques such as MEG have been used for the study of central oscillatory motor activity and have provided with some evidence for alpha central motor activity. However most of the evidence suggesting the central origin of the 8-12Hz tremor is indirect, by ruling out reflex loops contributions that can make to rhythmicities. Despite of this evidence the peripheral mechanisms that may contribute to the primarily central 8-12Hz tremor are being reconsidered (McAuley and Marsden 2000).

FCR EMG had a clear spectral 9Hz feature during extension movement while it had an 11Hz spectral feature during posture flexion. This small but noticeable difference may suggest that the underlying physiological mechanism may be different, despite both occurring in the alpha range. This was clearer for corticomuscular coherences in the same alpha range. For example the FCR\BBLH pair displayed high 8-12Hz intermuscular coherence during movement flexion as well as movement extension. Strong coupling also occurred in a similar band during posture flexion, but not during posture extension. Furthermore the cumulant profile was different revealing different timing characteristics for the detected coupling. For example, coherence during

movement was "in phase", while during posture extension it was "out of phase", supporting the suggestion that 8-12Hz movement and posture coupling features are the expression of different underlying mechanisms.

This finding is not in line with the majority of the studies investigating the 8-10Hz EMG discontinuities, which have suggested that the frequency occurrences during posture and movement are related phenomena (Wessberg and Kakuda 1999). However, as the present study illustrated this may not be the case. Both movement and posture tremor demonstrate EMG-acceleration coherence in the area of 8-10Hz. High motoneuron-acceleration coherence in the area of 8-10Hz may be observed for movement tremor, but for postural tremor this is not the case. This suggests that the two phenomena are observed as activity in the same frequency range rather than being a related process.

8-12Hz coupling was also observed between the same pair of muscles during different tasks (posture and movement) and likely arising by different physiological processes. Different physiological mechanisms may also be implicated for the generation of 8-12Hz corticomuscular coupling during movement between different sets of muscles. ECRL\FCR and FCR\BBLH show high 8-12Hz intermuscular coupling during flexion movement. The cumulant components and phases for the specific band were "out of phase" with a delay close to 0ms for ECRL\FCR but were "in phase" between FCR\BBLH (FCR leads BBLH by 21ms, despite the BBLH being the most proximal of the pair to the CNS). Given corticomuscular conduction times and peripheral reflex loop delays, different intermuscular coupling delays suggest different neuronal pathways. Similar findings were observed for movement flexion. One more indication that a different underlying mechanism is responsible for the two coupling features is the general lack of coherence for the ECRL\BBLH muscle pair. If ECRL\FCR and FCR\BBLH were coupled at 8-12Hz under the influence of a common rhythmical input then it would be expected that ECRL\BBLH would also be coupled in the same band. Equally convincing evidence for the different nature of near 10Hz coherence features appeared in the relevant time dependent coherence plots. While the ECRL\FCR 10Hz coherence starts immediately after the initiation of movement the

FCR\BBLH coherence feature emerged after the start of movement (approximately 0.7ms). The different temporal characteristics lend support to the idea that different physiological processes may contribute to generate coupling that has a similar frequency.

The BBLH spectrogram contained a continuous showing spectral feature in the 9-14Hz band which was strong throughout the move-hold sequence. Careful observation demonstrated that this feature showed task dependent frequency variations. While this task dependency of the spectral power in the 9-14Hz band has not been reported before, it is a good example of the dynamic way that physiological systems behave. It is not clear what physiological process generates this frequency variation, or if different mechanisms may be engaged during different phases of movement. Even small variations in the emerging frequencies may have important functional significances which are not obvious from frequency tracking using narrow bands (Mulcahy 2001).

The BBLH also displayed 15-25Hz during wrist posture phases. However this activity (corticomuscular and intermuscular couplings as well as power) was significantly suppressed during wrist movement. This was unexpected based on previous discussions of the role of corticomuscular coherences (Conway et al. 1995; Salenius et al. 1997; Conway et al. 1998). As with the 9-14Hz band examined earlier this clearly illustrates that the frequency content of EMG is modulated not only with the task that a specific muscle is performing but also by the task that the synergistic group of muscles it couples to are engaged in. This task dependency of the spectral power in the 15-25 Hz band has not been reported before and also support previous observations that the drive to muscles depends on functional rather than anatomical organization (Gibbs et al. 1995). What has been reported is that a common drive in this frequency range was observed between muscles coactive in postural tasks (Gibbs et al. 1995). Furthermore it has been reported that when either of the muscles becomes involved in movement this coupling was usually lost (Mulcahy 2001). Motor-unit synchronization generated by central presynaptic common drive is considered to be the main source of this frequency modulation and importantly this activity appears to be suppressed during movement (Farmer et al. 1993; Conway et al. 1995; Halliday et al. 1999). Consequently it was

suggested that the near 15-25Hz intermuscular coupling feature is functionally significant for the establishment of muscle synergies during posture.

When single slow wrist motions (2s flexion and extension) were combined with short periods of wrist posture (2s held extended or flexed) with the forearm stabilised by voluntary contraction of the BBLH muscle, ECRL, FCR and BBLH demonstrated increased 15-25Hz coupling during posture (Conway et al. 1998). This was expressed by clearly defined ECRL\FCR, FCR\BBLH, ECRL\BBLH 15-25 Hz coupling while no coherence was present during movement. The coherence features shared some common characteristics including the peak frequency (approximately 22Hz). They also took their maximum value approximately 0.8s after the audio movement cue. However, the coupling features did not last until the end of the phase and declined approximately 0.5s before the end of the short posture task. The fact that fixed interval audio cues were used to instruct the subjects to move or hold, has to be taken under consideration. The reduction in coherence before the onset of the movement could be caused by the subject anticipating the trigger for the next movement. The reduction could alternatively be a normal variation of coupling during posture maintenance. It has been shown that periods of enhanced and suppressed intermuscular coherence have been reported during long maintained posture tasks (15min) for individual subjects (Hansen et al. 2002). The latter could explain the decline of coherence in short lasting postural tasks seen in the present study. In the present study, maintained posture records of approximately 45s derived equal or significantly higher intermuscular coherence features than appended short (2s) posture records, but the variations in time were not examined. The anticipated and predictable time of the end of the short posture phase is quite likely to have contributed to the observed coherence pattern. This anticipation may be connected with the attention of the subject, which may influence the level of synchrony and coherence, (Schmied et al. 2000).

The replacement of beta with alpha coherence during maintained posture has also been reported before (Hansen et al. 2002) where it was observed that rhythmic activity in a muscle switched from "in phase" 15–35Hz coherent synchronisation to a central trough featuring 7–12Hz coherence during continuous recordings. Some recordings

illustrated that the two patterns may coexist, but the results suggested that one or the other dominates at different times and that the switch from one pattern to the other may take place within a rather short time span (Hansen et al. 2002). The results in the present study are in line with these findings. 10 Hz intermuscular coupling was present during short posture tasks for the pooled data. For FCR\BBLH this coupling appears higher towards the end of the posture phase where 20 Hz coherence had already declined. For ECRL\FCR EMGs 10 Hz coherence measured during extension posture occurred simultaneously with the main 20 Hz feature. Therefore it was demonstrated that 10 Hz intermuscular coupling may also occur during short posture tasks.

As mentioned before, during posture flexion a three way synchronization occurred in the 15-25Hz band with each wrist muscle strongly coupled to each other and both coupled to the biceps. Cumulant and phase plots derived sharp peaks and delay for all three coherences at less than 3ms. The small latency together with the sharp central peaks confirm to the suggestion that the underling cause is short term synchronization most probably as a consequence of a central common presynaptic drive to the muscles (Farmer et al. 1993; Conway et al. 1995; Halliday et al. 1999). If a peripheral reflex mechanism was involved, longer latencies should have been observed. It important to mention that no noticeable delay emerged between BBLH and the wrist muscles, despite BBLH having shorter corticomuscular conduction time, due to its proximity to the CNS. This indicates that the CNS probably compensates for this delay which is programmed in the corresponding neuronal circuit.

It is important to note that the magnitude of the 15-25Hz ECRL\FCR coherence during posture extension 15-25 Hz coherence feature was higher than the magnitude of the corresponding feature during posture flexion. However for FCR\ECRL and ECRL\BBLH coherences the corresponding features were clearly higher during posture flexion. This fact indicates independent organisation of coupling between different pairs of muscles can exist according to the task performed. This is also further supported by the different profile of the coherence features during posture flexion and posture extension for the same pair of muscles, and the shift in coherence peaks to slightly higher frequencies (2-3Hz) during posture extension. This is a further indication that the

15-25Hz corticomuscular coupling feature is not hardwired and can show variability according to the performed task.

Comprehensive results were also derived from the time dependent intermuscular cumulant plots during the move-hold sequence. Coupling features were visible. The durations of different features were also clearly defined for the pooled data. During posture, the central cumulant peaks in intermuscular plots (and the secondary features) indicating 20Hz synchronisation were in line with the corresponding time dependent coherence features. The central peaks in the time dependent cumulant plots defined the duration of posture more clearly than the beta coherence features, which declined before the end of the phase. In posture tasks where the 15-25Hz coupling was replaced by a 10Hz feature (eg. FCR\BBLH during flexion posture), the corresponding 20 Hz sidepeaks at ±50ms were replaced by features indicating 10 Hz synchronization with the central peak being unchanged. 10 Hz coupling features could be also easily identified in the intermuscular cumulant plots during movement. Features like the sharp negative cumulant trough for ECRL\FCR, indicating out of phase short term synchronisation were also very clearly illustrated.

Apart from 8-12Hz and 15-25Hz intermuscular coupling and power features, the most significant feature observed was 35-45Hz intermuscular coherence and 0-6Hz power and coherence features. During posture extension significant coherence was present in the 35-45Hz band. The cumulant component and phase estimates derived a near 0ms delay, which suggests short term synchronisation as an underlying cause. The functional significance of the feature is not clear and a similar feature is not present during posture flexion. 0-6Hz features usually occurred during the transition from posture to movement and vice versa. Their temporal characteristics and functional significance were not very clear.

6.2.3 EEG and corticomuscular characteristics

6.2.3.1 EEG Characteristics

The EEG spectrograms (monopolar and bipolar) revealed significant spatial and temporal task dependent features during the performance of the move-hold sequence. A

task dependent synchronisation-desynchronisation pattern was identified in the delta frequency band, which was well defined, widespread and present at all examined monopolar and bipolar electrodes. A similar pattern also appeared in the intracortical time dependent coherence estimates, suggesting that the observed synchronisation-desynchronisation pattern follows a very similar coupling-decoupling pattern.

These features are thought to be the expressions of movement related slow cortical potentials. Slow cortical potentials in the form of electric or magnetic fields have been described in the literature, mainly for self paced movements rather than guided sequence of movements with fixed intervals (Nagamine et al. 1996; Stancak and Pfurtscheller 1996; Pineda et al. 2000; Wolpaw et al. 2002). These are usually examined only as the pattern of rise of electric potential (or magnetic) field before and after the onset of the movement without examining the frequency content of the pattern. Frequencies also in the theta and delta range are not normally examined thoroughly, as studies have traditionally focused on frequencies above the alpha range. Therefore it is believed that the movement related delta features reported in the present study have not been reported on before. However, their functional significance is not clear, and further work is required to clarify the functional significance and origin of those features and evaluate any potential clinical relevance. The widespread occurrence of the features over multiple electrode sites is also a challenging issue to clarify.

Alpha cortical task dependent power variations were also clearly identified in the EEG spectrograms. A pattern of alpha activity was always well defined throughout the move hold sequence with task related synchronisation occurring before the onset of the movement. This synchronisation most probably expressed a preparatory state of the subject in anticipation of the next cue for movement. It could also be related with to cortical activity at a late stage of posture. The alpha synchronisation feature was present in both monopolar and bipolar EEG recordings mainly at the central and centroparietal areas. A feature in the same frequency range is present in intracortical time dependent coherence and was expressed as decoupling mainly over the ipsilateral motor cortex. Decoupling does not necessarily contradict synchronisation since both can express underlying cortical activity. Studies on 8-12Hz "mu" rhythm, have shown

desynchronisation over the sensorimotor cortices prior to voluntary movement (Pfurtscheller et al. 1997). In the present study synchronisation was observed. However the experimental protocols for most "mu" rhythms studies have been different, which may explain the differences. The most important difference is that action follows a rest phase while in the present thesis posture follows movement and vice versa.

The beta EEG spectral features were the most distinct task dependent features in the monopolar as well as the bipolar spectrograms. 15-25Hz power variations were best defined in FC1-C1 bipolar electrode pair. This suggests localised activity. Beta synchronisation was present during posture and was suppressed during movement. For contralateral electrodes weak beta features re-emerged during movement, while the power in that band was completely suppressed during the transition from posture to movement and vice versa.

The intracortical frequency characteristics revealed important features of cortical organisation during posture. This was expressed by decoupling in the beta band. The decoupling occurred despite a simultaneous increase in the beta EEG power of monopolar and bipolar EEG channels. These findings agree with the view that cortical information content is highest when neurons are differentially and independently active with the overall activation showing no regular time course (Feige 1996). The decrease of beta intracortical coupling expresses high information content related to the posture task. The range of frequencies that this decoupling occurs over is in the same range as with cortical spectral power, corticomuscular and intermuscular coupling features which suggest that the phenomena are related.

The intracortical phase also displayed task modulation and was another indication of the central task dependencies in the beta band. The phase delay modulation may be expressing organised synchronous activity of small populations of neurons, where the near 0ms phase delay indicates strong wideband idling activity. These populations may be the source of the oscillations and provide input to corticospinal neurones that communicate with the spinal motor pools. More work is needed in this area. Experimental setups and simulation studies aimed at studying the phase

characteristics of intracortical signals must be designed and performed to examine this hypothesis.

6.2.3.2 Corticomuscular characteristics

Previous work has demonstrated the existence of coupling between hand muscle EMG and the corresponding muscle motor areas of the contralateral cortex (Conway et al. 1995). The coupling occurred in the same frequency range as intermuscular coherence during posture and was suppressed during movement.

The findings in the present study confirmed these previous findings regarding corticomuscular coherence (Conway et al. 1995) (Conway et al. 1999) (Halliday et al. 1998). Time dependent coherence and cumulant plots demonstrated task dependent variations in a comprehensive manner. All three EMGs appeared to be coupled with the EEG in a similar pattern and similar frequency range. The coupling features appeared to be associated with the corresponding features in intermuscular coherence, beta cortical synchronization and beta intracortical decoupling. Beta coupling occurred during posture while no strong coherence features were identified during movement. The features observed for the FC1-C1 bipolar EEG channel displayed the strongest corticomuscular synchronisation. The timing of intermuscular and corticomuscular coherences was similar to coherences visible a few ms after the audio cue, reaching their maximum at approximately 0.8 sec after the audio cue and ending before the end of the posture phase.

For all bipolar EEG time dependent corticomuscular plots, coherence was higher during posture flexion than for posture extension. This shows some sort of preference from the CNS in wrist motion involving posture flexion. However, ECRL\FCR intermuscular coherence was higher during the posture extension phase despite the fact that corticomuscular coherences were largest during posture flexion. This fact demonstrates a degree of independence between amplitudes of corticomuscular and intermuscular coherences, despite the strong association of the phenomena. Stronger corticomuscular coherences for two EMGs do not necessarily result to stronger intermuscular coherence for the muscle pairing. This supports the hypothesis that

different central oscillators are producing the corticomuscular coherences for individual muscles.

Corticomuscular time dependent cumulant plots gave a clear picture of the corticomuscular coupling pattern in the beta frequency band during the move-hold sequence. During posture tasks, the sharp central peak features indicative of short term synchronisation were clearly visible. These central peaks spanned nearly the whole duration of the posture tasks unlike coherence features that decline before the end of posture phase. The secondary cumulant secondary features, whose distance (lag) from the central peak indicate the frequency of coupling, usually lasted for shorter periods than the central peak. This period roughly matched the time that beta corticomuscular coherence features were also significant in the corresponding time dependent coherence plots.

The coupling features present in the cumulant plots were much more consistent and defined than their corresponding coherence plots. Time dependent cumulant plots proved an excellent way of representing coupling information over a wide frequency spectrum. The representation appeared in a clear and comprehensive form. A plethora of features were present in the monopolar and bipolar plots. Despite the fact that their underling mechanism and functional significance is not clear this may provide an important source of signals for use in movement intention detection systems.

The corticomuscular delays revealed by the phase and cumulant plots for beta posture coupling features were not consistent ranging from 4-9ms, lower than the corticomuscular conduction times which are in the range of 15ms. The conduction times for 4-8Hz movement features derived conduction times in the more realistic 15ms range. It is not clear whether the delay derived by phase and cumulant estimates corresponds to the real corticomuscular conduction time (Gross et al. 2000). Transcranial magnetic stimulation studies have demonstrated corticomuscular conduction times in the range of 15ms (Rothwell et al. 1991). However a number of studies have shown contradicting results. It was not within the aims of the current study to examine the issue in depth. Further studies should be performed to investigate the corticomuscular times in greater detail.

6.2.3.3 Spatial organisation of corticomuscular features

The temporal characteristics of EMG power, corticomuscular coherence and cumulant estimates of corticomuscular synchronisation were successfully revealed by the time dependent plots. Taking advantage of the 28 channel EEG recording configuration, a range of maps was generated illustrating the spatial characteristics of the identified features. The spatial characteristics can provide evidence on the origin of the activity contributing to some of the movement related features. Furthermore knowledge on the characteristics of these signals may also have clinical implications. Any commercial intention detection system will need to use a restricted number of recorded channels, in order to minimise the hardware and processing resources required. Therefore cortical recordings should be strategically mapped to sites where the highest movement information content can be acquired.

The most important EEG power and coherence task dependent variations occurred in the delta, alpha and beta band. While all the spectral bands displayed spatial patterns, the topographic maps of the bipolar EEG power variations from movement to posture and from posture to movement gave the most consistent results. It displayed that the beta synchronisation-desynchronisation during posture-movement respectively, occurred in a distinct pattern mainly overlying the contralateral motor cortex.

The monopolar coherence maps revealed two centres of high beta corticomuscular coherence over the cortex associated with posture; medial frontal and frontocentral (maximum for Fz channel) as well as contralateral central and centroparietal electrodes (maximum for CP3). The corresponding cumulant estimate maps revealed important differences regarding the two areas of beta monopolar corticomuscular coherence. While Fz and the surrounding electrodes appeared to be coupled "in phase" with the forearm EMGs, CP3 and the surrounding electrodes were coupled "out of phase" with EMG. This observation, combined with the corresponding bipolar corticomuscular coherence and cumulant estimates indicating maximum coherence at FC1-C1 electrode site, suggest that a cortical oscillator over the contralateral motor cortex is responsible for the couplings seen in both monopolar and

bipolar setups. The centre of the oscillating dipole source for FCR and ECRL was approximately sited at the FC1-C1 electrode pair. The orientation is diagonal, approximately parallel to the axis connecting Fz with CP3 sites. The dipole direction (polarity) appeared constant but its strength oscillates at the 17-23Hz frequency.

The results reported in this study are consistent with the hypothesis that oscillatory activity in the primary motor cortex drives the spinal motoneuron pool during isometric muscle contraction and during the hold phase of a tracking task by modulating the firing probability of populations of motor units (McAuley et al. 1997). This hypothesis was also largely confirmed by the topographic cumulant maps of posture 17-23Hz component estimates. The individual corticomuscular cumulant estimates represent the envelope of averaged EEG channel activity timelocked to the strongly coupled EMG bursts. The 17-23Hz cumulant component specifically represents the averaged 17-23Hz EEG timelocked to the coupled 17-23Hz EMG features. Therefore the cumulant estimates in effect represent a cortical electric potential field, (i.e. the envelope of the averaged EEG). Therefore the resulting cumulant topographic maps represent the distribution of electric potential field over the cortex generated by a cortical oscillator. The electric potential field isocontours in such monopolar and bipolar maps supported the existence of the dipole source as described above.

These findings are in line with previous findings involving MEG activity (Gross et al. 2000). The averaged MEG signal timelocked to the motor units of the right extensor indicis muscle demonstrated damped oscillations similar to the ones obtained by bipolar cumulant estimates. The spatial distribution of the magnetic field at the time of the first negative peak preceding the EMG onset showed a dipolar field pattern modelled by a single dipole in the hand area of the left primary motor cortex as illustrated in Fig. 2.22. The corresponding electric potential field pattern that resulted from the present study is in line with the magnetic field and the two fields appear to be orthogonal, as expected. The EEG results of the present study are exceptional considering that the much smaller number of 28 electrodes was used compared to the 122 electrodes used for the MEG study (Gross et al. 2000).

One more interesting finding was that the dipole orientation for BBLH was slightly different to the one identified for FCR and ECRL during posture. While the centre appeared to localise to FC1-C1 site the orientation was more parallel to the anterior-posterior axis rather than the Fz-CP3 axis. This combined with the previous findings regarding the slightly higher coherence frequency (23-24Hz) for BBLH compared to FCR and ECRL (20-21Hz) of the CNS acts to control individual muscles.

6.3 *COMPARISON OF INTERMITTENT MOVEMENT AND POSTURE WITH CONTINUOUS MOVEMENT AND MAINTAINED POSTURE*

This component of the study compared data from posture and movement performed as maintained, continuous or intermittent actions.

6.3.1 Differences between maintained posture – intermittent posture

Significant differences were observed when Intermittent Posture and Maintained Posture were compared. During the MPF, intermuscular coherence features had similar or higher magnitude, while corticomuscular features decreased significantly compared to the IPF. During the MPE, the intermuscular and corticomuscular coherences varied, increasing or decreasing in comparison to IPE. There was no direct connection in the magnitude of corticomuscular features and intermuscular features since they increased or decreased independently. If there is a direct dependency between intermuscular and corticomuscular coherences and both phenomena were the expression of the same direct cortical motor command, analogous corticomuscular-intermuscular coupling variations would have been observed.

The current study also demonstrates that beta corticomuscular coupling features can also be partially suppressed during maintained posture. The decrease in maintained corticomuscular compared with the intermittent coherence observed is in line with MEG\EMG data (Kilner et al. 2000) where coherence for a 3min maintained steady grasp was significantly lower than the corticomuscular coherence observed just after a movement.

These findings as well as previous studies support the suggestion of independent control of the synergistic muscles by the CNS. The beta range synchronization is regarded as an "indicator" of efficient motoneuron recruitment associated with a minimum of computational effort (Baker et al. 1999; Brown 2000). It is also possible that the maintained or short posture temporal modulation expresses two different functions of coherent oscillatory activity, one that is related to maintained contractions and another that is related to the changes in the motor state (Kilner et al. 2000).

It has also been suggested that 20-30Hz cortical oscillations may not be caused by a single generator (Baker et al. 1999). Evidence has been provided that one component of the 20Hz EEG recorded over the sensorimotor cortex was motor in origin, whilst another was a harmonic of 10Hz rhythms, thought to originate from somatosensory cortex (Salmelin and Hari 1994; Salenius et al. 1997). The existence of two or more distinct types of 20 Hz cortical rhythms could explain the observed differences. It is possible that multiple underlying phenomena and mechanisms may be responsible for activity which overtly appears similar in electrophysiological recordings (Baker et al. 1999). The independent suppression or strengthening of those features may account for the different shape of the beta corticomuscular features and the frequency change.

6.3.2 Differences between intermittent movement – continuous movement

The comparison of results obtained from Intermittent Movement and Continuous Movement were equally interesting. For the IM, it was observed that the beta intermuscular coherences between all three coactive muscles present during posture were suppressed when the wrist engaged in movement. The suppression of beta corticomuscular coherence was the case for all muscles including BBLH which was active in supporting the forearm position.

During the CM beta intermuscular and corticomuscular coherences emerged for FCR and BBLH muscles with the contralateral cortex which were suppressed during the IM. The distribution of coherence features over the cortical map strongly resembled results obtained during posture.

The current results challenge the functional significance of intermuscular and especially corticomuscular coherence, in the beta band and its relation to posture. It was demonstrated that significant coupling in this band can also appear during movement and more specifically during wrist CM combined with synergistic elbow posture. So far strong beta coupling had been observed mainly during posture.

It is important to mention that two coherence peaks were identified in the posture time dependent FCR corticomuscular estimate; one at 21Hz and one at 24Hz. The 24Hz feature was also associated with BBLH activity. During continuous movement the corticomuscular features that emerge for FCR was centred at 24Hz, the 21Hz feature was suppressed. It may be that the functional association between FCR and BBLH, in relation to the postural activation of the BBLH is responsible for the emergence of beta corticomuscular coherence during FCR movement. This is supported from data by Mulcahy where continuous wrist movement with forearm support (therefore BBLH was inactive) did not reveal significant beta corticomuscular coherence for FCR (Mulcahy 2001).

All the results presented in this thesis suggest that the functional connection between FCR and BBLH is more important than between ECRL and BBLH. These differences may have evolutionary origin. As one considers changes in motor activity from lower mammals to higher primates, one of the major changes one observes lies in the cortical control of forelimb muscles. In man and primates effective synergistic action of wrist and elbow flexors may be vital for the execution of important hand tasks like feeding, or perform simultaneous elbow and wrist or hand tasks and may be a critical factor for survival.

Based on the previous findings the direct functional link between beta corticomuscular and intermuscular coupling during posture is being challenged. Beta corticomuscular coherence was seen to decrease during MPF while the corresponding intermuscular coherence features increased. During MPE beta intermuscular coherence was seen to increase in a much larger scale than the corresponding corticomuscular coherences for the same pair of muscles (FCR\BBLH). The descending command may be further modulated and amplified, at supraspinal level, most probably by the cerebellar or spinal level processes. The cerebellum has been reported to contribute to automatic movements that require little attention, while more cortical activity is allocated to difficult and unpractised movements that require more attention (Jenkins et al. 1994) (Jueptner and Weiller 1998) (Grossberg and Paine 2000). The influences of peripheral mechanisms (mechanical resonance, unfused motor units, feedback loops etc.) in the

central corticomuscular motor control have also to be considered (McAuley and Marsden 2000). The methodology used in this thesis combined peripheral and central recordings, and identified brain oscillations that are strongly manifested or absent in the periphery. However there is the possibility that some peripheral rhythmic oscillations are either peripheral artefacts or not of functional significance. Association of oscillatory features might also reflect that common anatomical pathways are involved during processing and conveyance of motor commands and not actual functional coupling (McAuley and Marsden 2000).

6.4 *EFFECTS OF ATTENTION IN CORTICOMUSCULAR COUPLING*

The question if attention influences corticomuscular coupling has been raised before (Kristeva-Feige et al. 2002) as it may be a factor responsible for intersubject and intrasubject differences in EEG-EMG coherence, in both healthy and patient populations. Increased attentional demand is one of the factors responsible for the high rejection rates of conventional upper limb neuroprostheses (Greatting 1991; Wright et al. 1995). It is important that neuroprosthetic control will not require the full attention of the user, even though a moderate level of attention will always be needed. Similarly, short lapses in attention, or short attention shifts, should not affect seriously the control of the device. The results presented in this study illustrate that corticomuscular and intermuscular coherences are relatively robust under different levels of attention. The precision task investigating attentional demand involved compression of an instrumented ring between two fingers while recording from a hand muscle (APB) and a wrist muscle (ECRL) during visual feedback of the grip force under low attention and high attention conditions (controlled by modifying the gain of the feedback signal).

The beta intermuscular coherence between ECRL and APB muscles was statistically significant during both high and low attention tasks. When higher motor attention was required, an increase in the beta intermuscular coherence was observed. The APB corticomuscular coherence with the contralateral EEG also increased during the high attention task compared to the low attention coherence. These results are in line with previous studies showing higher intermuscular coupling features during execution of more difficult and therefore more attentional demanding tasks (Bray 1999).

In contrast to the increase of ECRL\APB intermuscular coherence and APB corticomuscular coherence, ECRL corticomuscular coherence was clearly reduced during the high attention state. APB has a more critical role in the performance of the precision task and this is reflected in the increase of the beta corticomuscular coherence with the contralateral cortex. This may result to the reduction of the decrease of ECRL beta corticomuscular coherence that has a less critical role.

Since APB\EEG coherence increased, while ECRL\EEG coherence decreased it appears that the CNS provides independently channels of information flow to synergistic

muscles. These results agree with theories of limited attention capacity in the sense that more coherence appears for the more important channel than for the less important one. Therefore the CNS may be allocating limited resources according to the demands of the individual task.

It is not yet clear whether a common generator is driving synergistic muscles and producing corticomuscular and intermuscular coupling in the beta band. The present study provides some evidence against the common generator hypothesis. The beta range synchronization is regarded as an "indicator" of efficient motoneuron recruitment (Baker et al. 1999; Brown 2000). It is possible that the corticomuscular network works in this mode when the attentive resources are directed towards the motor task. The results of this experiment clearly support this suggestion by demonstrating that the level of corticomuscular coherences can change independently for different synergistic muscles under different attentional conditions since during high attention an increase in corticomuscular coupling was observed for the hand muscle but a decrease was observed for the wrist muscle.

The increased coupling with APB, observed from frontal lobe electrodes during the attention demanding task is no surprise considering the fact that the frontal lobe has been implicated in attentional mechanisms. More specifically, the frontal cortex has a critical role of in the attention control of movements as it has been shown to impair attention control of unpractised movements during motor learning in man (Richer et al. 1999). It also seems to be widely accepted that the frontal lobes are important when attention must be sustained over time (Rueckert and Grafman 1998).

6.5 *EFFECTS OF COGNITIVE LOADING IN CORTICOMUSCULAR COHERENCE*

This experiment's focus was to examine how intermuscular and corticomuscular frequency characteristics are affected during a precision task, by a simultaneous performance of an attention demanding cognitive task. The experiment involved the extension of an elastic band between left and right hands to a constant length under two conditions; a dedicated performance of the task and a cognitively loaded condition in which the task was performed with the subject simultaneously carrying out a mental arithmetic task. EMG was recorded from left and right wrist ECRL muscles and from left and right APB muscles.

Two main components were identified in the intermuscular coherence of homologues muscles for both arms; an alpha and a beta feature. The magnitude of beta intermuscular coupling was clearly enhanced during the cognitive task on both sides. Similarly corticomuscular coherence for left and right sides was found not changed or became slightly enhanced during the performance of the cognitively loaded task.

The attention demanding mental arithmetic task may occupy a segment of the attentional capacity. In that sense a limited motor attention channel (because of increased cognitive load) would have resulted in decreased coherence, which was not the case. This may suggest that cognitive tasks do not interact with descending motor signal and the mechanisms generating intermuscular coupling, or that a central mechanism compensates for the execution of a cognitive task and broadens the available attention channel. The cognitive task may have also compelled the subject to allocate more attention to the motor task to compensate for the cognitive resources used in the arithmetic task, increasing the attentional capacity. In every aspect cognitive loading of the type required in this experiment does not decrease beta intermuscular EMG synchronisation features. This result enhances the potential for the signals to be used for intention detection.

The previous findings are not in line with a study aiming to investigate the effects of attention on beta range EMG\EEG synchronisation (Kristeva-Feige et al.

2002). In this study beta corticomuscular coherences decreased below the statistical significance level when attention was divided between a motor task and a mental arithmetic task. However in the referred to study none of the 10 subjects investigated showed broad coherence peaks.

A very important result was the significant asymmetry seen for corticomuscular and intramuscular coherences during the bimanual task. The intermuscular coherences of homologues muscles within the left forearm were significantly higher than within the right forearm. Furthermore, this asymmetry also occurred for corticomuscular coherences. Coupling of both left APB and ECRL EMGs with the contralateral cortex was significantly higher than the corresponding right forearm EMGs corticomuscular coupling, despite the mechanical symmetry of the bilateral task. This observation suggests a connection between corticomuscular and intermuscular coherence phenomena, since the significant difference between left and right corticomuscular coherence was reflected in the intermuscular coherence. The independent left-right control of descending motor command channels is suggested by the strong asymmetry. This was further supported by the lack of bilateral intermuscular coherence. Importantly all subjects were right handed. In right handed individuals the left arm is less skilful at performing precision tasks. Therefore the CNS may allocate more resources to the non dominant side to meet the demands of the performed task. Higher intermuscular coupling features that have been reported during more complex tasks, than simple and familiar tasks (Bray 1999).

The observed coherence asymmetry may have important implications if the examined signal characteristics are used for neuroprosthetic control. As shown before, the attention demanding cognitive task does not decrease the task related corticomuscular and intermuscular characteristics. Yet it was shown that a simultaneous attention demanding motor task (in this case the left forearm involved in the bilateral task), may decrease the magnitude of the right forearm corticomuscular or intermuscular coherence. Bilateral tasks are very common in everyday life and therefore left and right sided sources of activity may alter in unpredictable ways.

Experiments by Mulcahy, (2001) on amputees performing bilateral tasks have shown that amputation significantly affects corticomuscular coherence even for the intact side. For a group of 8 amputees performing an extension bimanual posture little or no corticomuscular coherence was observed for either the amputated or normal side (Mulcahy 2001). 4 patients showed beta intermuscular coupling features in the normal limb while only one showed clear stump intermuscular coherence. However these results were not conclusive because of issues concerning mainly the quality of stump EMG recordings. More experiments have to be conducted.

In another study involving amputees, movement of the intact hand showed a level of fMRI activation similar to movement of the right dominant hand in the healthy controls, while during imagination of moving the phantom hand, patients showed significantly higher activation in the contralateral primary motor and somatosensory cortices compared with imagination of hand movements in the controls (Lotze et al. 2001). Therefore it is important to further study the relation of coherence to handiness and what happens following amputation of dominant or non dominant arms.

All aspects of simultaneous motor control have to be further examined since it may not only be bilateral tasks that affect the intention indicators but other kinds of motor activity. This is very important for the evaluation of this methodology for neuroprosthetic control, since the effectiveness in real life situations has to be eventually examined and not just in experimental sessions with dedicated subjects.

6.6 *EFFECTS OF DEAFFERENTATION IN CORTICOMUSCULAR COHERENCE*

The aim of the INB experiment was to examine whether corticomuscular and intramuscular frequency characteristics are affected by INB induced deafferentation. Direct influences from deprivation of the sensory input, or indirectly trough plastic changes in the CNS occurring as a result of the lack of sensory input, may be an inhibiting factor for the robustness of the examined intention indicators in clinical applications.

The results illustrated significant variability between subjects. For *Subject 1*, beta corticomuscular coherence during posture increased during the INB. The biggest increase seen in FCR corticomuscular coherence. In this subject the maximum coherence occurred after the release of the INB. This fact combined with the observation that the changes were not relative to the progress of the block may suggest that the changes were not purely the results of loss of afferent activity. The EEG beta spectral power did not show significant change. Intermuscular coherence also changed, and the largest coherence appeared after the block release, as was the case for the corticomuscular coherence. There was no clear connection in coherence changes with the sequence of the recordings during the progress of the block. However the changes suggest that afferent feedback may play a role in establishing corticomuscular coherence.

For *Subject 2*, high beta corticomuscular and intramuscular coherence features occurred before and throughout the duration of the INB. The beta EEG power however declined with the INB progress. Alpha EEG power diminished during the INB and reappeared only after the release of the block. The changes in afferent activity may be underlying the observed changes.

Subject 3 showed a progressive decrease of corticomuscular coherence during the INB. The coupling level diminished during the late stages, returning to the pre-ischemic levels after the release of the block. This progressive reduction could be connected with the decreasing level of afferent feedback, induced by the INB. A similar

pattern of reduction in beta coupling also occurred for the intermuscular coherence between agonist and antagonist. A very important feature was the corresponding reduction of beta EEG spectral power. The beta feature was a small narrow feature occurring at exactly the same frequency range as the coupling feature. This a very good illustration that the perturbation of the peripheral nervous system can induce immediate changes in the function of the central nervous system. These changes are short term changes since immediately after the release of the block, both EEG and corticomuscular coherences recover to pre-ischemic levels.

No consistent reduction in the peak frequency of the posture beta coupling occurred during the INB. If such a reduction was observed that would mean that the prolonged efferent and afferent fibres conduction times would have contributed. Thus a feedback loop was not essential for the beta corticomuscular synchronisation, suggesting that it is centrally driven. Similar results have also been reported in previous studies (McAuley et al. 1997; Pohja and Salenius 2003). The lack of change in coherent frequency in the MEG/EMG coherence observed during ischemia, indicated that a feedback loop is not essential for the generation of corticomuscular coherence (Pohja and Salenius 2003). Also the modulation peripheral feedback by local anaesthesia, by increasing feedback delays with extra loading or by varying firing frequencies (contraction strength) did not alter the occurrence of the 20Hz frequency peaks in EMG, tremor and muscle vibration recordings (McAuley et al. 1997).

Reduction in the MEG/EMG coherence has been observed in previous studies during ischemia, with the coherence level returning to the pre-INB levels after the ischemia had ended (Pohja and Salenius 2003). In the same study the reduction was also observed for the non ischemic arm as well. The decrease in strength of coherence compared with both pre-ischemia and post-ischemia may be attributed to the reduction of sensory information and/or to a change in central state (short term plasticity). Acute ischemic nerve block has been shown to induce focal increase in excitability in the hand motor representation in both the deafferented hemisphere and the contralateral one (Werhahn et al. 2002). The results of the Pohja (2003) study strongly resemble the results obtained from *Subject 3* where both corticomuscular and intramuscular coherence

levels declined with the progress of the INB and recovered to the pre-ischemic levels after the release of the cuff. A similar change in the central state may be reflected in the results of *Subject 2* where despite strong coherence, beta EEG activity during posture decreases with the progression of ischemia, only to reappear after the release of the INB. For *Subject 1* where increased coherence is observed, cortical activation may have been enhanced because the subject struggled to keep the contraction steady, possibly due to partial motor conduction block in addition to the sensory block. It has been shown that subjects tend to underestimate the extension of the movement in the ischemic limb (Goodwin et al. 1972). Therefore, the decrease in sensory feedback may indirectly induce the increase in strength of coherence.

The fact that the deafferented as well as the intact limb may be affected is also supported by amputee data. Unilateral wrist amputees performing bimanual wrist extension tasks show little or no corticomuscular coherence (Mulcahy 2001). The lack of corticomuscular coherence in amputees suggests that long term plastic changes in central state may occur on both hemispheres after amputation or loss of sensory input. This may not be a surprise given that short term changes have been observed for INB in normal subjects (Pohja and Salenius 2003).

The effects of deafferentation have also been studied by examining patients suffering from pseudochoreoathetosis after pathological deafferentation (Timmermann et al. 2001). This condition is characterised by continuous involuntary finger movements. Strong corticomuscular coherence resembling corticomuscular features seen during posture was observed for this group of patients during rest (whilst involuntary movements occurred) despite the lack of sensory input. This finding suggested that beta corticomuscular coherence does not require sensory data. This is also in line with the observation of beta intramuscular coherence in a patient suffering from severe peripheral deafferentation(Farmer et al. 1993).

In contrast to the previous study Kilner (2004) suggested that the presence of sensory afferent signals are necessary for the modulation of 15-30Hz oscillations in the motor system. For a task that required a hold-move-hold pattern of grip force to be exerted on a compliant object with the dominant right hand, significant task-related

modulation of 15-30Hz coherence between EMG activity in hand muscles in the control subjects. In contrast, the deafferented subject showed very low levels of significant coherence in the 15-30Hz range and no peak at this frequency in the power spectra of her EMG activity (Kilner et al. 2004).

The results presented are not conclusive and contradict previous research findings. The small number of subjects limited the potential for interpretation. However the value of the INB experiment results was significant for this thesis. It points out the unpredictable nature of the examined signals and the difficulties that will be faced in applications that aim to utilise the examined signals in prosthetic control. However the possibility of using these signals as movement intention indicators still exists. Any neuroprosthetic control mechanism will have to be customised for each individual user utilising any individual task dependent frequency features. Successful implementation of such systems on all patients is however quite unlikely since some patients may not be suitable for this kind of treatment.

Regarding the INB experiment, larger numbers of patient groups have to be examined, using a more complete experimental protocol that will also examine the progress of the deafferentation in afferent conduction capability, in order to produce more conclusive results.

6.7 *IMPLICATIONS FOR NEUROPROSTHETIC CONTROL*

As mentioned earlier the growing interest in the development of robust methods of intention detection for use in prosthetic devices and communication aids for the severely motor disabled was one of the main driving forces behind the work carried out in this thesis. Task dependent corticomuscular features were identified. The task specific behaviour of the studied signals may provide the basis for effective neuroprosthetic control providing the robustness of the signals are adequate. The present study did not aim to provide methods for intention detection. The aim was to provide the foundation that such methods will be developed in the future.

The potential for use of the examined signals in intention detection has been mixed. The EMG spectral power did not show potential because of the great variations which mask more task specific features. Furthermore 8-12Hz power was present during posture as well as movement and 15-25Hz features, normally associated with movement were not strong.

Intermuscular coupling showed more potential. There were no significant wideband variations as with spectral power. Changes were task specific and mainly concentrated in 8-12Hz and 15-25Hz (or 15-35Hz). Well defined coupling features were present in coherences between agonist and antagonist. Coherence at 10Hz was associated with movement and at 15-25Hz with posture. Continuous movement did not change this pattern significantly since agonist\antagonist 10Hz peak was not affected. Maintained posture did not have negative effect on the task specific coupling pattern since 15-25Hz peaks remained statistically significant, many times over the confidence level. The only concern was the high 10Hz coherence of agonist\antagonist during maintained posture extension, which undermines the movement specificity of the 8-12Hz band. However, since the similar features are generated by different physiological processes, their cumulant and phase delay characteristics are going to be different. Therefore using 8-12Hz cumulant component and phase delay estimate would be able to differentiate between movement and posture. The role of the cumulant could be even more significant since time dependent cumulant plots demonstrated more defined

cumulant peaks than coherence features during posture. Intermuscular coherences of ECRL and FCR with BBLH also derived additional task related coupling features.

It was very important to find that posture intermuscular coherence was not affected by the simultaneous performance of a cognitive task (in fact it was increased). It was also not affected by performing the task in high or low attention conditions. This was very important since any clinical neuroprosthetic application should not require the full attention of the subject (event though moderate attention will always be required), and the system should be able to be used while performing other cognitive tasks. Similar to intermuscular coherence corticomuscular coherence appeared robust under these conditions.

EMG intention detection systems however would not suit certain patient groups where there is no residual voluntary motor control. Here only EEG may serve as a window into the patients intention. EEG spectral power showed three bands where task dependent features were evident; delta, alpha and beta. The clearest association was beta synchronisation during posture, especially in bipolar montages. Alpha and delta bands showed more complex patterns of task related synchronisation-desynchronisation. While their functional significance is not clear they may have potential for use in neuroprosthetic control when combined with automatic feature extraction and classification systems (Pfurtscheller et al. 2000; Wolpaw et al. 2002). In this respect the delta band may be extremely important since it was detected by all examined electrodes.

Among the EEG frequency characteristics, intracortical coupling showed the most defined task related features and has the greatest potential for use in neuroprosthetic control. Beta band decoupling was associated with posture, and coexisted with beta band synchronisation for the examined electrodes as revealed by time dependent coherence and spectral power plots respectively.

Corticomuscular coupling also contained significant task dependent features at 15-25Hz associated with movement. Coherence and cumulant gave well defined features. The features were also robust in low and high motor attention tasks as well as during the performance of a mental arithmetic task. However beta corticomuscular coherence was not as robust as intermuscular coherence during maintained posture and

continuous movement tasks. During maintained posture flexion for example, ECRL and FCR beta corticomuscular coherences showed a significant decease (however remaining above the statistical significance level at FC1-C1 electrode). During continuous wrist movement, beta corticomuscular coherence (associated with posture) emerged for FCR, which contradicted the association of movement with the suppression of beta coherence. There is good indication that this coherence feature is an expression of the CNS motor command to BBLH (which is posturally activated). This feature has a peak at 24Hz while the FCR posture corticomuscular feature should appear at 21Hz. Therefore there are task specific features that could resolve such issues and support the use of corticomuscular coherence as reliable movement intention detection system. Still any use of EMG limits applications to groups of patients with residual voluntary control.

The bilateral extension task generated some concerns regarding the low corticomuscular coherence for the dominant forearm during bilateral tasks. However, as mentioned before plasticity induced by amputation may change this.

Finally the INB experiment, due to the small number of subjects, did not reveal any conclusive results. All three subjects behaved in a different way. Furthermore past studies also give mixed messages regarding the effect of deafferentation or other sensory perturbations on the examined signals.

It is fair to say that the present study has given encouraging results regarding the use of the examined signals and the frequency characteristics in neuroprosthetic control. Such applications however will have to be subject specific, and use advanced feature extraction systems in order to overcome intersubject and intrasubject variability. Through training and use of the system, the user could also develop new task dependent relationships, or enhance the already existing by taking advantage of the plasticity of the CNS and PNS.

The current study will possibly open the way for further research benefiting the quality of life of patients with motor disabilities like spinal cord injured patients, amputees and stroke patients. The design that could benefit those motor impaired groups is the utilisation of functional components in order to bypass or replace the affected, non-functional components or assist the residual components. For example a large part

of the paralysed musculature as well as the peripheral nervous system of a hemiplegic patient will still be functional, but the lack of an effective motor command from the higher centres of the central nervous system (CNS) to the legs makes the patient immobile.

Muscles of the contralateral side or weak muscles on the affected side of the body could provide control signal for functional electrical stimulation (FES) systems to innervate muscles that are completely paralysed. The same concept could be applied in the control of a neuroprosthetic arm for amputees. Here, the missing skeletomuscular structure could be replaced with an electromechanical prosthesis. The missing motor command could be provided by EMG signal from the muscles of the stump, or other muscles like muscles of the shoulders and the back or even EEG signal. Locked in patients could also modulate their EEG signal in order to operate assistive or communicating devices using brain computer interfaces.

Using as control indicators physiological signals that are closely associated to task performance such a system should function in a more natural manner than present systems that require a lengthy training process. The advantage of reduced training may lead to better uptake and smaller rejection rates compared to current systems. The way to make optimal use of the body's integral physiological signals and to extract the maximum of the relevant information will be the key to delivering effective neuroprosthetic devises for the motor disabled.

7 CONCLUSION

7.1 SUMMARY OF THESIS

Since the early descriptions of the relation of CNS rhythmic activity to body tremors a considerable amount of work has investigated the properties of central oscillations and their physiological manifestations in the periphery. This thesis has attempted to investigate the motor related activity of the CNS and its potential for use in neuroprosthetic control through examining central and peripheral oscillations.

Task dependent 15-25Hz intermuscular coherence was observed between muscles acting around the wrist during intermittent posture. This coherence was increased during maintained posture. 15-25Hz corticomuscular coherence was also observed during posture. Simultaneously EEG synchronisation and intracortical decoupling was observed in the beta (15-25Hz) band supporting the idea of a cortical origin to the intermuscular and corticomuscular coupling observed during posture tasks. Cortical oscillating dipoles modulated in the beta band during posture were identified arising from contralateral motor cortex in the same areas where 15-25Hz EEG synchronisation-decoupling were observed.

The strong beta corticomuscular coherence observed during intermittent posture flexion was decreased during maintained posture flexion. In contrast intermuscular coherence that increased during the maintained task. During a high attention precision task the hand muscle beta corticomuscular coherences for the hand muscle and the intermuscular coherence between the wrist and hand EMG were increased (compared to the attention task). In contrast corticomuscular coherence for the wrist extensor muscle decreased. These results suggest independent central control over synergistic muscles according to the task needs. This was also supported by the detection of differences in CNS dipole oscillator orientation for different muscles.

During movement tasks 8-12Hz coherence was observed between agonist and antagonist EMGs while their coupling was out of phase with a 0ms delay supporting the hypothesis of a central origin of this modulation. 8-12Hz rhythmic modulations were

also observed in the EMG spectral power during movement and were most apparent in the antagonist muscle EMG during movement (especially for wrist flexor during wrist movement extension).

The unexpected influence of the wrist movement on the frequency content, and corticomuscular characteristics of biceps EMG was also an important finding. The 15-25Hz biceps EMG power and corticomuscular coherence were suppressed during intermittent wrist movement. However during continuous wrist movement the beta corticomuscular coherence for biceps muscles re-emerged. Furthermore strong beta corticomuscular coherence was also observed for the wrist flexor EMG, with a distribution over the scalp resembling that seen during posture. The wrist flexor corticomuscular coherence during wrist movement is probably related to the simultaneous postural activation of biceps. The last finding suggests a special functional relationship between wrist flexor and biceps muscles. This relationship is also supported by the fact that biceps intermuscular coherence was always higher with the wrist flexor than the wrist extensor during both posture flexion and posture extension tasks.

Increased motor attention amplified corticomuscular coherence for the hand muscle that was directly involved in the precision task; however, the corticomuscular coherence for the wrist extensor muscle decreased despite a rise in intermuscular coherence. Cognitive loading also appeared to amplify the corticomuscular and intermuscular coherences. These findings demonstrated high adaptability of the CNS to the functional demands required for the successful performance of the task. This adaptability was also demonstrated by the higher intermuscular coherence seen between the left forearm muscles and the corresponding corticomuscular coherences when compared to the right forearm corticomuscular coherences during the bilateral extension task in right handed subjects.

Finally the INB appeared to affect the corticomuscular coupling, but the results were not conclusive.

7.2 *FUNCTIONAL SIGNIFICANCE*

There is the question of whether the corticomuscular and intermuscular characteristics could be an epiphenomenon, and have no functional significance. There are certain facts that arise from the findings of this thesis that suggest this.

- Considerable variability was observed in the occurrence of beta corticomuscular and intermuscular coherences between subjects.
- The time distribution of coherence features during short posture tasks was not uniform and declined before the end of the task.
- Posture was established with and without significant coherence for biceps.
- Beta corticomuscular coherence was observed in muscles involved in movement (wrist flexors during continuous movement).
- There was no clear connection between the magnitude of beta intermuscular coherence and the corresponding corticomuscular coherence features.

Other findings in this thesis argue in favour of coherence between cortex and muscle being related to specific parameters of motor control.

- The association of posture with 15-25Hz features in EEG synchronisation-decoupling, intermuscular coherence and corticomuscular and its suppression during movement.
- The localisation of the posture related oscillating dipole source and EEG beta synchronisation-decoupling over the anatomically correct contralateral motor cortex.
- The robustness and meaningful variations in intermuscular and corticomuscular coherences under different attention and cognitive conditions.
- The left-right asymmetry in the magnitude of intermuscular and corticomuscular coherences.

There is also the possibility that the observed intermuscular and corticomuscular features do not express a clear functional or a by-product relationship but a mixture of both. According to Rosenblum, (2001) coherence can be the result of the output of two oscillators, having their own rhythms when the oscillators are coupled. However coherence could be also generated by the mixture of signals generated by two independent oscillators. This will mean that signal from one oscillator may find its way in the neural pathway where the other output of the other oscillator is measured. Nevertheless either epiphenomenon or having functional significance, corticomuscular and intermuscular characteristics, where present, appear to have task dependent behaviour and are relatively robust. Therefore the use of such features for neuroprosthetic control remains a strong possibility.

7.3 FUTURE WORK

The methodology used in this thesis combined peripheral and central recordings, and identified brain oscillations that associate with motor output. This approach is particularly suited to human investigations because of obvious limitations in direct central recordings. Although EEG reveals much oscillatory brain activity, the oscillations are usually poorly localised and often not clearly connected with motor activity. Furthermore, peripheral oscillations are a summation of a number of oscillations across the frequency range and include mechanical resonances that vary with the mass and stiffness of the limb segment. This makes the proposition and proving of a new hypotheses a complex process.

- Future work should be directed towards the use of relatively new recording techniques like MEG and high resolution EEG. For best results the two complementary techniques should be combined to reveal more localised and complete information. This will be useful especially for the detection of small differences between oscillating dipole characteristics for different muscles and different tasks. Changes in the dipole orientation in relation to the direction of movement or force should also be subject of further studies

- Cortical beta synchronisation and decoupling should be further examined. The intersubject variability in relation to corticomuscular and intermuscular coherence variability should be studied. Changes in cortical activity in relation to the direction of movement or applied force should be also examined. The influence of imaginary tasks in cortical synchronisation and decoupling will also help towards the development of efficient neuroprosthetic devices for patients with no voluntary control.

- The contradicting and not consistent corticomuscular conduction times as revealed by corticomuscular synchronisation estimates like cumulant and phase is an issue that has not received a satisfactory answer. The effect of different types of EMG and EEG filtering on calculated delays should be examined. Hilbert transform based techniques should also be compared with FFT algorithms, as they appear to derive more accurate estimates for non linear systems.

- The task dependencies of the identified alpha and delta EEG spectral power features should be further examined. The role of attention and anticipation for the production of these bands should be examined by modifying the experimental protocols to use variable intervals between different tasks and/or self guided movements rather than movements guided by audio cues.

- The role of the CNS in sensory information processing should be examined. This could be achieved by examining the cortical activation during repetitive peripheral stimulation by means of muscle, nerve or cutaneous electrical (or magnetic) stimulation or muscle vibration. Coherence, cumulant, phase, delay characteristics and frequency response between the stimulation trigger process and the resulting EEG will reveal an insight to CNS processing of afferent information.

- The role of handedness in corticomuscular coherence should be examined by comparing left and right handed subjects, performing unilateral and related or unrelated bilateral tasks.

- Further experiments using INB on a larger scale should also be performed. The number of subjects should be higher in order to cover the existing subject variability, or select a subject group with high beta corticomuscular coherence. The protocol should be based on the move-hold sequence experimental protocol with intermittent posture and movement tasks. The modulatory effect of ischemia and the progress of deafferentation should be examined by measuring the latencies of early somatosensory evoked fields and the magnitude and time course of an H-reflex.

- Considering the limitations for invasive procedures in human subjects repetitive TMS (rTMS) could be a useful tool for examining the influences of cortical activation in the periphery. Technology is now able to deliver high frequency rTMS of between 1-60Hz which covers the frequency band that was investigated in this thesis. Stimulation of the motor cortex and the study of the coupling estimates (coherence, cumulant, delay) between the stimulation trains and the resulting EMG response will reveal features of the CNS motor control. The latencies measured will also provide more evidence on the actual corticomuscular conduction times.

- Single movement trial experiments in normal subjects and patients should be performed, assessing the robustness and the signal-to-noise ratio of the examined signals. The single trial studies should be also combined with advanced classification techniques that will automatically associate the subject specific task dependences to the desired task. There is a great variety of methods that could be used. Bearing in mind that the patient population is quite diverse, specific patient groups should be targeted, the user requirements of the control system defined and the classification systems should be implemented and evaluated off line and on line for testing and evaluation.

8 *BIBLIOGRAPHY*

Akshoomoff, N. A. and E. Courchesne (1992). "A new role for the cerebellum in cognitive operations." Behav Neurosci 106(5): 731-8.

Akshoomoff, N. A., E. Courchesne and J. Townsend (1997). "Attention coordination and anticipatory control." Int Rev Neurobiol 41: 575-98.

Alexander, G. E., M. R. DeLong and P. L. Strick (1986). "Parallel organization of functionally segregated circuits linking basal ganglia and cortex." Annu Rev Neurosci 9: 357-81.

Al-Falahe, N. A., M. Nagaoka and A. B. Vallbo (1990). "Lack of fusimotor modulation in a motor adaptation task in man." Acta Physiologica Scandinavica 140(1): 23-30.

Al-Falahe, N. A., M. Nagaoka and A. B. Vallbo (1991). "Dual response from human muscle spindles in fast voluntary movements." Acta Physiologica Scandinavica 141(3): 363-371.

Allanson, J. (2000). Supporting the Development of Electrophysiologically Interactive Computer Systems. Computing Department. Lancaster, Lancaster University.

Allen, G., R. B. Buxton, E. C. Wong and E. Courchesne (1997). "Attentional activation of the cerebellum independent of motor involvement." Science 275(5308): 1940-3.

Amjad, A. M., D. M. Halliday, J. R. Rosenberg and B. A. Conway (1997). "An extended difference of coherence test for comparing and combining several independent coherence estimates: theory and application to the study of motor units and physiological tremor." J Neurosci Methods 73(1): 69-79.

Andres, F. G., T. Mima, A. E. Schulman, J. Dichgans, M. Hallett and C. Gerloff (1999). "Functional coupling of human cortical sensorimotor areas during bimanual skill acquisition." Brain 122(Pt 5): 855-70.

Aoki, F., E. E. Fetz, L. Shupe, E. Lettich and G. A. Ojemann (1999). "Increased gamma-range activity in human sensorimotor cortex during performance of visuomotor tasks." Clin Neurophysiol 110(3): 524-37.

Aylward, E. H., A. L. Reiss, M. J. Reader, H. S. Singer, J. E. Brown and M. B. Denckla (1996). "Basal ganglia volumes in children with attention-deficit hyperactivity disorder." J Child Neurol 11(2): 112-5.

Baker, S. N. (2000). "'Pooled coherence' can overestimate the significance of coupling in the presence of inter-experiment variability [2]." Journal of Neuroscience Methods 96(2): 171-172.

Baker, S. N., J. M. Kilner, E. M. Pinches and R. N. Lemon (1999). "The role of synchrony and oscillations in the motor output." Experimental Brain Research 128(1-2): 109-117.

Baker, S. N., E. Olivier and R. N. Lemon (1997). "Coherent oscillations in monkey motor cortex and hand muscle EMG show task-dependent modulation." Journal of Physiology 501(1): 225-241.

Baker, S. N., E. M. Pinches and R. N. Lemon (2003). "Synchronization in monkey motor cortex during a precision grip task. II. effect of oscillatory activity on corticospinal output." J Neurophysiol 89(4): 1941-53.

Baker, S. N., R. Spinks, A. Jackson and R. N. Lemon (2001). "Synchronization in monkey motor cortex during a precision grip task. I. Task-dependent modulation in single-unit synchrony." J Neurophysiol 85(2): 869-85.

Ball, T., A. Schreiber, B. Feige, M. Wagner, C. H. Lucking and R. Kristeva-Feige (1999). "The role of higher-order motor areas in voluntary movement as revealed by high-resolution EEG and fMRI." Neuroimage 10(6): 682-694.

Barrios Cerrejon, M. and J. Guardia Olmos (2001). "[Relation of the cerebellum with cognitive function: neuroanatomical, clinical and neuroimaging evidence]." Rev Neurol 33(6): 582-591.

Braitenberg, V., D. Heck and F. Sultan (1997). "The detection and generation of sequences as a key to cerebellar function: experiments and theory." Behav Brain Sci 20(2): 229-45; discussion 245-77.

Bray, K. M. (1999). A study of motor unit synchronisation in geriatric and lacunar stroke populations. Department of Bioegineering. Glasgow, University of Strathclyde.

Breasted, J. H. (1930). The Edwin Smith Surgical Papyrus. Chicago, The University of Chicago Press.

Bremner, F. D., J. R. Baker and J. A. Stephens (1991). "Correlation between the discharges of motor units recorded from the same and from different finger muscles in man." J Physiol 432: 355-80.

Bremner, F. D., J. R. Baker and J. A. Stephens (1991). "Effect of task on the degree of synchronization of intrinsic hand muscle motor units in man." J Neurophysiol 66(6): 2072-83.

Bremner, F. D., J. R. Baker and J. A. Stephens (1991). "Variation in the degree of synchronization exhibited by motor units lying in different finger muscles in man." J Physiol 432: 381-99.

Briand, K. A., W. Hening, H. Poizner and A. B. Sereno (2001). "Automatic orienting of visuospatial attention in Parkinson's disease." Neuropsychologia 39(11): 1240-9.

Broadbent, D. E. (1958). Perception and communication. New York,, Pergamon Press.

Brown, P. (2000). "Cortical drives to human muscle: the Piper and related rhythms." Prog Neurobiol 60(1): 97-108.

Brown, P. and C. D. Marsden (1998). "What do the basal ganglia do?" Lancet 351(9118): 1801-4.

Brown, P. and C. D. Marsden (1999). "Bradykinesia and impairment of EEG desynchronization in Parkinson's disease." Mov Disord 14(3): 423-9.

Brown, P., J. C. Rothwell, J. M. Stevens, A. J. Lees and C. D. Marsden (1997). "Cerebellar axial postural tremor." Mov Disord 12(6): 977-84.

Brown, P., S. Salenius, J. C. Rothwell and R. Hari (1998). "Cortical correlate of the Piper rhythm in humans." J Neurophysiol 80(6): 2911-7.

Bruehlmeier, M., V. Dietz, K. L. Leenders, U. Roelcke, J. Missimer and A. Curt (1998). "How does the human brain deal with a spinal cord injury?" Eur J Neurosci 10(12): 3918-22.

Calford, M. B. and R. Tweedale (1990). "Interhemispheric transfer of plasticity in the cerebral cortex." Science 249(4970): 805-7.

Candia, V., T. Elbert, E. Altenmuller, H. Rau, T. Schafer and E. Taub (1999). "Constraint-induced movement therapy for focal hand dystonia in musicians." Lancet 353(9146): 42.

Carrier, L., E. Brustein and S. Rossignol (1997). "Locomotion of the hindlimbs after neurectomy of ankle flexors in intact and spinal cats: model for the study of locomotor plasticity." J Neurophysiol 77(4): 1979-93.

Caton, R. (1875). "The electrical currents of the brain." British Medical Journal 2: 278.

Classen, J., C. Gerloff, M. Honda and M. Hallett (1998). "Integrative visuomotor behavior is associated with interregionally coherent oscillations in the human brain." J Neurophysiol 79(3): 1567-73.

Classen, J., J. Liepert, S. P. Wise, M. Hallett and L. G. Cohen (1998). "Rapid plasticity of human cortical movement representation induced by practice." J Neurophysiol 79(2): 1117-23.

Cohen, D. (1968). "Magnetoencephalography: evidence of magnetic fields produced by alpha-rhythm currents." Science 161(843): 784-6.

Cohen, D. (1972). "Magnetoencephalography: detection of the brain's electrical activity with a superconducting magnetometer." Science 175(22): 664-6.

Cohen, L. G., S. Bandinelli, T. W. Findley and M. Hallett (1991). "Motor reorganization after upper limb amputation in man. A study with focal magnetic stimulation." Brain 114(Pt 1B): 615-27.

Cohen, L. G., S. Bandinelli, H. R. Topka, P. Fuhr, B. J. Roth and M. Hallett (1991). "Topographic maps of human motor cortex in normal and pathological conditions: mirror movements, amputations and spinal cord injuries." Electroencephalogr Clin Neurophysiol Suppl 43: 36-50.

Cohen, L. G., U. Ziemann, R. Chen, J. Classen, M. Hallett, C. Gerloff and C. Butefisch (1998). "Studies of neuroplasticity with transcranial magnetic stimulation." J Clin Neurophysiol 15(4): 305-24.

Cohen, R. A., Y. A. Sparling-Cohen and B. F. O'Donnell (1993). The neuropsychology of attention. New York ; London

New York, Plenum Press, c1992., Plenum Press.

Conway, B. A., P. Biswas, D. M. Halliday, S. F. Farmer and J. R. Rosenberg (1997). "Task-dependent changes in rhythmic motor output during voluntary elbow movement in man." Journal of Physiology 501.P: 48-49P.

Conway, B. A., D. M. Halliday, K. Bray, M. Cameron, D. McLelland, E. Mulcahy, S. F. Farmer and J. R. Rosenberg (1998). "Inter-muscle coherence during co-contraction of finger and wrist muscles in man." The Journal of Physiology(509.P): 175-176P.

Conway, B. A., D. M. Halliday, S. F. Farmer and J. R. Rosenberg (1995). On the relation between motor-unit discharge and physiological tremor. In Alpha and Gamma motor systems. New York and London, Plenum Press.

Conway, B. A., D. M. Halliday, S. F. Farmer and J. R. Rosenberg (1995). " On the relation between motor-unit discharge and physiological tremor. In Alpha and Gamma motor systems. ed. Taylor, A., Gladden, M.H., Durbaba., R." Plenum Press, New York and London. pp. 596-598.

Conway, B. A., D. M. Halliday, S. F. Farmer, U. Shahani, P. Maas, A. I. Weir and J. R. Rosenberg (1995). "Synchronization between motor cortex and spinal motoneuronal pool during the performance of a maintained motor task in man." Journal of Physiology 489(3): 917-924.

Conway, B. A., D. M. Halliday and J. R. Rosenberg (1999). "Rhythmic cortical activity and its relation to the neurogenic components of normal and pathological tremors." Progress in Brain Research 123(pp 437-444).

Cordo, P. and S. Harnad, Eds. (1994). Movement Control, Cambridge University Press.

Cotterill, R. M. (2001). "Cooperation of the basal ganglia, cerebellum, sensory cerebrum and hippocampus: possible implications for cognition, consciousness, intelligence and creativity." Prog Neurobiol 64(1): 1-33.

Coull, J. T., R. S. Frackowiak and C. D. Frith (1998). "Monitoring for target objects: activation of right frontal and parietal cortices with increasing time on task." Neuropsychologia 36(12): 1325-34.

Courchesne, E., J. Townsend, N. A. Akshoomoff, O. Saitoh, R. Yeung-Courchesne, A. J. Lincoln, H. E. James, R. H. Haas, L. Schreibman and L. Lau (1994). "Impairment in shifting attention in autistic and cerebellar patients." Behav Neurosci 108(5): 848-65.

Crago, P. E., H. J. Chizeck, M. R. Neuman and F. T. Hambrecht (1986). "Sensors for use with functional neuromuscular stimulation." IEEE Trans Biomed Eng 33(2): 256-68.

Creasey, G. H., K. L. Kilgore, D. L. Brown-Triolo, J. E. Dahlberg, P. H. Peckham and M. W. Keith (2000). "Reduction of costs of disability using neuroprostheses." Assist Technol 12(1): 67-75.

Crone, N. E., D. L. Miglioretti, B. Gordon and R. P. Lesser (1998). "Functional mapping of human sensorimotor cortex with electrocorticographic spectral analysis. II. Event-related synchronization in the gamma band." Brain 121(Pt 12): 2301-15.

Crone, N. E., D. L. Miglioretti, B. Gordon, J. M. Sieracki, M. T. Wilson, S. Uematsu and R. P. Lesser (1998). "Functional mapping of human sensorimotor cortex with electrocorticographic spectral analysis. I. Alpha and beta event- related desynchronization." Brain 121(Pt 12): 2271-99.

Daum, I. and H. Ackermann (1995). "Cerebellar contributions to cognition." Behav Brain Res 67(2): 201-10.

Decety, J., D. Perani, M. Jeannerod, V. Bettinardi, B. Tadary, R. Woods, J. C. Mazziotta and F. Fazio (1994). "Mapping motor representations with positron emission tomography." Nature 371(6498): 600-2.

Deiber, M. P., R. Caldara, V. Ibanez and C. A. Hauert (2001). "Alpha band power changes in unimanual and bimanual sequential movements, and during motor transitions." Clin Neurophysiol 112(8): 1419-35.

Delorme, A. and S. Makeig (2004). "EEGLAB: an open source toolbox for analysis of single-trial EEG dynamics including independent component analysis." J Neurosci Methods 134(1): 9-21.

Dengler, R., W. Wolf, P. Birk and A. Struppler (1984). "Synchronous discharges in pairs of steadily firing motor units tend to form clusters." Neurosci Lett 47(2): 167-72.

Dewan, E. M. (1967). "Occipital alpha rhythm eye position and lens accommodation." Nature 214(92): 975-7.

Dietz, V., E. Bischofberger, C. Wita and H. J. Freund (1976). "Correlation between the dischanges of two simultaneously recorded motor units and physiological tremor." Electroencephalogr Clin Neurophysiol 40(1): 97-105.

Doya, K. (2000). "Complementary roles of basal ganglia and cerebellum in learning and motor control." Curr Opin Neurobiol 10(6): 732-9.

Drake, R. A. (1991). "Processing persuasive arguments: recall and recognition as a function of agreement and manipulated activation asymmetry." Brain Cogn 15(1): 83-94.

Duval, C., M. Panisset, G. Bertrand and A. F. Sadikot (2000). "Evidence that ventrolateral thalamotomy may eliminate the supraspinal component of both pathological and physiological tremors." Exp Brain Res 132(2): 216-22.

Elble, R. J. and J. E. Randall (1976). "Motor-unit activity responsible for 8- to 12-Hz component of human physiological finger tremor." J Neurophysiol 39(2): 370-83.

Elble, R. J. and J. E. Randall (1978). "Mechanistic components of normal hand tremor." Electroencephalogr Clin Neurophysiol 44(1): 72-82.

Eslinger, P. J. and K. R. Biddle (2000). "Adolescent neuropsychological development after early right prefrontal cortex damage." Dev Neuropsychol 18(3): 297-329.

Evarts, E. V. (1968). J Neurophysiol 31: 14.

Farmer, S. F., F. D. Bremner, D. M. Halliday, J. R. Rosenberg and J. A. Stephens (1993). "The frequency content of common synaptic inputs to motoneurones studied during voluntary isometric contraction in man." J Physiol 470: 127-55.

Farmer, S. F., D. M. Halliday, B. A. Conway, J. A. Stephens and J. R. Rosenberg (1997). "A review of recent applications of cross-correlation methodologies to human motor unit recording." Journal of Neuroscience Methods 74(2): 175-187.

Farmer, S. F., L. M. Harrison, D. A. Ingram and J. A. Stephens (1991). "Plasticity of central motor pathways in children with hemiplegic cerebral palsy." Neurology 41(9): 1505-10.

Farmer, S. F., M. Swash, D. A. Ingram and J. A. Stephens (1993). "Changes in motor unit synchronization following central nervous lesions in man." J Physiol 463: 83-105.

Farwell, L. A. and E. Donchin (1988). "Talking off the top of your head: toward a mental prosthesis utilizing event-related brain potentials." Electroencephalogr Clin Neurophysiol 70(6): 510-23.

Feige, B. (1996). Oscillatory brain activity and its analysis on the basis of MEG and EEG. Institut fur Experimentelle Audiologie, Westfalischen Wilhelms Universitat Munster.

Feige, B., R. Kristeva-Feige, S. Rossi, V. Pizzella and P. M. Rossini (1996). "Neuromagnetic study of movement-related changes in rhythmic brain activity." Brain Res 734(1-2): 252-60.

Ferree, T. C., P. Luu, G. S. Russell and D. M. Tucker (2001). "Scalp electrode impedance, infection risk, and EEG data quality." Clin Neurophysiol 112(3): 536-44.

Fetz, E. E. (1994). Are movement parameters recognizably coded in the activity of single neurons. Movement Control. P. C. a. S. Harnard. Cambridge, UK:, Cambridge Univ. Press: p. 77-88.

Fish, B. J. (2002). EEG primer; basic principles of digital and analog EEG, Elsevier.

Florence, S. L., T. A. Hackett and F. Strata (2000). "Thalamic and cortical contributions to neural plasticity after limb amputation." J Neurophysiol 83(5): 3154-9.

Fromherz, P. (2002). "Electrical interfacing of nerve cells and semiconductor chips." Chemphyschem 3(3): 276-84.

Gallese, V., L. Fadiga, L. Fogassi and G. Rizzolatti (1996). "Action recognition in the premotor cortex." Brain 119 (Pt 2): 593-609.

Georgopoulos, A. P., J. F. Kalaska, R. Caminiti and J. T. Massey (1982). "On the relations between the direction of two-dimensional arm movements and cell discharge in primate motor cortex." J Neurosci 2(11): 1527-37.

Georgopoulos, A. P., J. F. Kalaska, R. Caminiti and J. T. Massey (1983). "Interruption of motor cortical discharge subserving aimed arm movements." Exp Brain Res 49(3): 327-40.

Gerloff, C., J. Richard, J. Hadley, A. E. Schulman, M. Honda and M. Hallett (1998). "Functional coupling and regional activation of human cortical motor areas during simple, internally paced and externally paced finger movements." Brain 121(Pt 8): 1513-31.

Gibbs, J., L. M. Harrison and J. A. Stephens (1995). "Organization of inputs to motoneurone pools in man." J Physiol 485(Pt 1): 245-56.

Glencross, D. J. and S. R. Oldfield (1975). "The use of ischemic nerve block procedures in the investigation of the sensory control of movements." Biol Psychol 2(3): 227-36.

Goodwin, G. M., D. I. McCloskey and P. B. Matthews (1972). "The persistence of appreciable kinesthesia after paralysing joint afferents but preserving muscle afferents." Brain Res 37(2): 326-9.

Greatting, M. D. (1991). Myoelectric Prostheses in Upper Extremity Amputees: Cost, Mechanical Reliability and Long-Term Wear Rate. American Academy of Orthopaedic Surgeons 1991 Annual Meeting.

Green, J. B., E. Sora, Y. Bialy, A. Ricamato and R. W. Thatcher (1998). "Cortical sensorimotor reorganization after spinal cord injury: an electroencephalographic study." Neurology 50(4): 1115-21.

Gross, J., P. A. Tass, S. Salenius, R. Hari, H. J. Freund and A. Schnitzler (2000). "Cortico-muscular synchronization during isometric muscle contraction in humans as revealed by magnetoencephalography." J Physiol 527 Pt 3: 623-31.

Grossberg, S. and R. W. Paine (2000). "A neural model of cortico-cerebellar interactions during attentive imitation and predictive learning of sequential handwriting movements." Neural Netw 13(8-9): 999-1046.

Grusser, S. M., C. Winter, M. Schaefer, K. Fritzsche, T. Benhidjeb, P. Tunn, P. M. Schlag and H. Flor (2001). "Perceptual phenomena after unilateral arm amputation: a pre-post- surgical comparison." Neurosci Lett 302(1): 13-6.

Hallett, M. (1998). "Overview of human tremor physiology." Mov Disord 3: 43-8.

Halliday, D. M., B. A. Conway, S. F. Farmer and J. R. Rosenberg (1998). "Using electroencephalography to study functional coupling between cortical activity and electromyograms during voluntary contractions in humans." Neuroscience Letters 241(01): 5-8.

Halliday, D. M., B. A. Conway, S. F. Farmer and J. R. Rosenberg (1999). "Load-independent contributions from motor-unit synchronization to human physiological tremor." Journal of Neurophysiology 82(2): 664-675.

Halliday, D. M. and J. R. Rosenberg (1999). Time and frequency domain analysis of spike train and time series data. Modern Techniques in Neuroscience Research. U. Windhorst and H. Johansson, Springer-Verlag: Ch 18, 503-543.

Halliday, D. M., J. R. Rosenberg, A. M. Amjad, P. Breeze, B. A. Conway and S. F. Farmer (1995). "A framework for the analysis of mixed time series/point process data--theory and application to the study of physiological tremor, single motor unit discharges and electromyograms." Prog Biophys Mol Biol 64(2-3): 237-78.

Hansen, S., N. L. Hansen, L. O. Christensen, N. T. Petersen and J. B. Nielsen (2002). "Coupling of antagonistic ankle muscles during co-contraction in humans." Exp Brain Res 146(3): 282-92.

Hari, R. and S. Salenius (1999). "Rhythmical corticomotor communication." Neuroreport 10(2): R1-10.

Harkema, S. J. (2001). "Neural plasticity after human spinal cord injury: application of locomotor training to the rehabilitation of walking." Neuroscientist 7(5): 455-68.

Hauber, W. (1998). "Involvement of basal ganglia transmitter systems in movement initiation." Prog Neurobiol 56(5): 507-40.

Hefftner, G., W. Zucchini and G. G. Jaros (1988). "The electromyogram (EMG) as a control signal for functional neuromuscular stimulation--Part I: Autoregressive modeling as a means of EMG signature discrimination." IEEE Trans Biomed Eng 35(4): 230-7.

Hikosaka, O., K. Sakai, S. Miyauchi, R. Takino, Y. Sasaki and B. Putz (1996). "Activation of human presupplementary motor area in learning of sequential procedures: a functional MRI study." J Neurophysiol 76(1): 617-21.

Hiraiwa, A., K. Shimohara and Y. Tokunaga (1990). "EEG topography recognition by neural networks." Engineering in Medicine and Biology Magazine, IEEE 9(3): 39-42.

Hoffman, D. S. and P. L. Strick (1999). "Step-tracking movements of the wrist. IV. Muscle activity associated with movements in different directions." J Neurophysiol 81(1): 319-33.

Hole, J. W. and N. A. Corbett, Eds. (1992). Essentials of Human Anatomy and Physiology. Dubuque, Iowa, William C. Brown.

Indovina, I. and J. N. Sanes (2001). "Combined visual attention and finger movement effects on human brain representations." Exp Brain Res 140(3): 265-79.

James, W. (1890). Principles of Psychology. New York, Holt.

Jenkins, I. H., D. J. Brooks, P. D. Nixon, R. S. Frackowiak and R. E. Passingham (1994). "Motor sequence learning: a study with positron emission tomography." J Neurosci 14(6): 3775-90.

Johnson, M. W. and P. H. Peckham (1990). "Evaluation of shoulder movement as a command control source." IEEE Trans Biomed Eng 37(9): 876-85.

Johnson, M. W., P. H. Peckham, N. Bhadra, K. L. Kilgore, M. M. Gazdik, M. W. Keith and P. Strojnik (1999). "Implantable transducer for two-degree of freedom joint angle sensing." IEEE Trans Rehabil Eng 7(3): 349-59.

Jueptner, M., K. M. Stephan, C. D. Frith, D. J. Brooks, R. S. Frackowiak and R. E. Passingham (1997). "Anatomy of motor learning. I. Frontal cortex and attention to action." J Neurophysiol 77(3): 1313-24.

Jueptner, M. and C. Weiller (1998). "A review of differences between basal ganglia and cerebellar control of movements as revealed by functional imaging studies." Brain 121(Pt 8): 1437-49.

Kahneman, D. (1973). Attention and effort. Englewood Cliffs, N.J.,, Prentice-Hall.

Kakei, S., D. S. Hoffman and P. L. Strick (1999). "Muscle and movement representations in the primary motor cortex." Science 285(5436): 2136-9.

Kalin, N. H., C. Larson, S. E. Shelton and R. J. Davidson (1998). "Asymmetric frontal brain activity, cortisol, and behavior associated with fearful temperament in rhesus monkeys." Behav Neurosci 112(2): 286-92.

Kandel, E. R., J. H. Schwartz and T. M. Jessel, Eds. (2000). Principles of Neural Science, McGraw-Hill.

Kandel, E. R., J. H. Schwartz and T. M. Jessell, Eds. (1995). Essentials of neural science and behavior, Appleton & Lange.

Karl, A., N. Birbaumer, W. Lutzenberger, L. G. Cohen and H. Flor (2001). "Reorganization of motor and somatosensory cortex in upper extremity amputees with phantom limb pain." J Neurosci 21(10): 3609-18.

Karnath, H. O., M. Himmelbach and C. Rorden (2002). "The subcortical anatomy of human spatial neglect: putamen, caudate nucleus and pulvinar." Brain 125(Pt 2): 350-60.

Karni, A., G. Meyer, P. Jezzard, M. M. Adams, R. Turner and L. G. Ungerleider (1995). "Functional MRI evidence for adult motor cortex plasticity during motor skill learning." Nature 377(6545): 155-8.

Kaul, R. A., N. I. Syed and P. Fromherz (2004). "Neuron-semiconductor chip with chemical synapse between identified neurons." Phys Rev Lett 92(3): 038102.

Kawato, M. (1999). "Internal models for motor control and trajectory planning." Curr Opin Neurobiol 9(6): 718-27.

Kawato, M. and D. Wolpert (1998). "Internal models for motor control." Novartis Found Symp 218: 291-304; discussion 304-7.

Keirn, Z. A. and J. I. Aunon (1990). "A new mode of communication between man and his surroundings." IEEE Trans Biomed Eng 37(12): 1209-14.

Kennedy, P. R. and R. A. Bakay (1998). "Restoration of neural output from a paralyzed patient by a direct brain connection." Neuroreport 9(8): 1707-11.

Kennedy, P. R., R. A. Bakay, M. M. Moore, K. Adams and J. Goldwaithe (2000). "Direct control of a computer from the human central nervous system." IEEE Trans Rehabil Eng 8(2): 198-202.

Kermadi, I. and J. P. Joseph (1995). "Activity in the caudate nucleus of monkey during spatial sequencing." J Neurophysiol 74(3): 911-33.

Kilner, J. M., S. N. Baker, S. Salenius, R. Hari and R. N. Lemon (2000). "Human cortical muscle coherence is directly related to specific motor parameters." J Neurosci 20(23): 8838-45.

Kilner, J. M., S. N. Baker, S. Salenius, V. Jousmaki, R. Hari and R. N. Lemon (1999). "Task-dependent modulation of 15-30 Hz coherence between rectified EMGs from human hand and forearm muscles." Journal of Physiology 516(2): 559-570.

Kilner, J. M., R. J. Fisher and R. N. Lemon (2004). "Coupling of oscillatory activity between muscles is strikingly reduced in a deafferented subject compared with normal controls." J Neurophysiol 92(2): 790-6.

Kirkwood, P. A., T. A. Sears, D. Stagg and R. H. Westgaard (1982). "The spatial distribution of synchronization of intercostal motoneurones in the cat." J Physiol 327: 137-55.

Klimesch, W., M. Doppelmayr, D. Röhm, D. Pöllhuber and W. Stadler (2000). "Simultaneous desynchronization and synchronization of different alpha responses in the human electroencephalograph: a neglected paradox?" Neuroscience Letters 284(1-2): 97-100.

Klimesch, W., H. Schimke, M. Doppelmayr, B. Ripper, J. Schwaiger and G. Pfurtscheller (1996). "Event-related desynchronization (ERD) and the Dm effect: Does alpha desynchronization during encoding predict later recall performance?" International Journal of Psychophysiology 24(1-2): 47-60.

Knowlton, B. J., J. A. Mangels and L. R. Squire (1996). "A neostriatal habit learning system in humans." Science 273(5280): 1399-402.

Koch, C. and I. Segev (1998). Methods in Neuronal Modeling: From Ions to Networks. Cambridge, MA, The MIT Press.

Koster, B., M. Lauk, J. Timmer, T. Winter, B. Guschlbauer, F. X. Glocker, A. Danek, G. Deuschl and C. H. Lucking (1998). "Central mechanisms in human enhanced physiological tremor." Neuroscience Letters 241(2-3): 135-138.

Kozelka, J. W. and T. A. Pedley (1990). "Beta and mu rhythms." J Clin Neurophysiol 7(2): 191-207.

Kristeva-Feige, R., C. Fritsch, J. Timmer and C. H. Lucking (2002). "Effects of attention and precision of exerted force on beta range EEG-EMG synchronization during a maintained motor contraction task." Clin Neurophysiol 113(1): 124-31.

Kugelberg, E. and L. Widen (1954). "Epilepsia partialis continua." Electroencephalogr Clin Neurophysiol Suppl 6(3): 503-6.

Kuhlman, W. N. (1978). "EEG feedback training: enhancement of somatosensory cortical activity." Electroencephalogr Clin Neurophysiol 45(2): 290-4.

LaBerge, D. (1997). "Attention, awareness, and the triangular circuit." Conscious Cogn 6(2-3): 149-81.

Lakie, M., E. G. Walsh and G. W. Wright (1984). "Resonance at the wrist demonstrated by the use of a torque motor: an instrumental analysis of muscle tone in man." J Physiol 353: 265-85.

Lauer, R. T., P. H. Peckham, K. L. Kilgore and W. J. Heetderks (2000). "Applications of cortical signals to neuroprosthetic control: a critical review." IEEE Trans Rehabil Eng 8(2): 205-8.

Leiner, H. C., A. L. Leiner and R. S. Dow (1986). "Does the cerebellum contribute to mental skills?" Behav Neurosci 100(4): 443-54.

Leiner, H. C., A. L. Leiner and R. S. Dow (1993). "Cognitive and language functions of the human cerebellum." Trends Neurosci 16(11): 444-7.

Lessard, N., M. Pare, F. Lepore and M. Lassonde (1998). "Early-blind human subjects localize sound sources better than sighted subjects." Nature 395(6699): 278-80.

Levy, W. J., Jr., V. E. Amassian, M. Traad and J. Cadwell (1990). "Focal magnetic coil stimulation reveals motor cortical system reorganized in humans after traumatic quadriplegia." Brain Res 510(1): 130-4.

Liberson, W. T., H. J. Holmquest, D. Scott and M. Dow (1961). "Functional electrotherapy: stimulation

of the peroneal nerve synchronized with the swing phase of the gait of hemiplegic

patients." Arch Phys Med Rehabil. 42: 101-105.

Lotze, M., H. Flor, W. Grodd, W. Larbig and N. Birbaumer (2001). "Phantom movements and pain. An fMRI study in upper limb amputees." Brain 124(Pt 11): 2268-77.

Lusted, H. S. and R. B. Knapp (1996). "Controlling computers with neural signals." Sci Am 275(4): 82-7.

Magill, R. A. (2004). Motor Learning. Concepts and Appl. New York, McGraw-Hill.

Manabe, Y., K. Kashihara, T. Ota, T. Shohmori and K. Abe (1999). "Motor neglect following left thalamic hemorrhage: a case report." J Neurol Sci 171(1): 69-71.

Mandl, G. (2000). Central Nervous System Lecture Notes. Montreal, McGill University.

Marsden, J. F., K. J. Werhahn, P. Ashby, J. Rothwell, S. Noachtar and P. Brown (2000). "Organization of cortical activities related to movement in humans." J Neurosci 20(6): 2307-14.

Marshall, J. and E. G. Walsh (1956). "Physiological tremor." J Neurochem 19(4): 260-7.

Matsuzaka, Y., H. Aizawa and J. Tanji (1992). "A motor area rostral to the supplementary motor area (presupplementary motor area) in the monkey: neuronal activity during a learned motor task." J Neurophysiol 68(3): 653-62.

Mayston, M. J., L. M. Harrison, R. Quinton, J. A. Stephens, M. Krams and P. M. Bouloux (1997). "Mirror movements in X-linked Kallmann's syndrome. I. A neurophysiological study." Brain 120(Pt 7): 1199-216.

Mayston, M. J., L. M. Harrison and J. A. Stephens (1999). "A neurophysiological study of mirror movements in adults and children." Ann Neurol 45(5): 583-94.

Mayston, M. J., L. M. Harrison, J. A. Stephens and S. F. Farmer (2001). "Physiological tremor in human subjects with X-linked Kallmann's syndrome and mirror movements." J Physiol 530(Pt 3): 551-63.

McAuley, J. H., S. F. Farmer, J. C. Rothwell and C. D. Marsden (1999). "Common 3 and 10 Hz oscillations modulate human eye and finger movements while they simultaneously track a visual target." J Physiol 515(Pt 3): 905-17.

McAuley, J. H. and C. D. Marsden (2000). "Physiological and pathological tremors and rhythmic central motor control." Brain 123(Pt 8): 1545-67.

McAuley, J. H., J. C. Rothwell and C. D. Marsden (1997). "Frequency peaks of tremor, muscle vibration and electromyographic activity at 10 Hz, 20 Hz and 40 Hz during human finger muscle contraction may reflect rhythmicities of central neural firing." Exp Brain Res 114(3): 525-41.

McFarland, D. J., A. T. Lefkowicz and J. R. Wolpaw (1997). "Design and operation of an EEG-based brain-computer interface (BCI) with digital signal processing technology." Behav Res Meth Instrum Comput 29: 337-345.

Metman, L. V., J. S. Bellevich, S. M. Jones, M. D. Barber and L. J. Streletz (1993). "Topographic mapping of human motor cortex with transcranial magnetic stimulation: Homunculus revisited." Brain Topogr 6(1): 13-9.

Middleton, F. A. and P. L. Strick (1998). "The cerebellum: an overview." Trends Neurosci 21(9): 367-9.

Middleton, F. A. and P. L. Strick (2000). "Basal ganglia and cerebellar loops: motor and cognitive circuits." Brain Res Brain Res Rev 31(2-3): 236-50.

Milner, T. E. (2002). "Adaptation to destabilizing dynamics by means of muscle cocontraction." Exp Brain Res 143(4): 406-16.

Mima, T. and M. Hallett (1999). "Corticomuscular coherence: a review." J Clin Neurophysiol 16(6): 501-11.

Mima, T. and M. Hallett (1999). "Electroencephalographic analysis of cortico-muscular coherence: reference effect, volume conduction and generator mechanism." Clin Neurophysiol 110(11): 1892-9.

Mima, T., T. Matsuoka and M. Hallett (2001). "Information flow from the sensorimotor cortex to muscle in humans." Clin Neurophysiol 112(1): 122-6.

Mima, T., T. Nagamine, A. Ikeda, S. Yazawa, J. Kimura and H. Shibasaki (1998). "Pathogenesis of cortical myoclonus studied by magnetoencephalography." Ann Neurol 43(5): 598-607.

Mima, T., T. Nagamine, N. Nishitani, N. Mikuni, A. Ikeda, H. Fukuyama, T. Takigawa, J. Kimura and H. Shibasaki (1998). "Cortical myoclonus: sensorimotor hyperexcitability." Neurology 50(4): 933-42.

Mima, T., N. Simpkins, T. Oluwatimilehin and M. Hallett (1999). "Force level modulates human cortical oscillatory activities." Neurosci Lett 275(2): 77-80.

Mima, T., J. Steger, A. E. Schulman, C. Gerloff and M. Hallett (2000). "Electroencephalographic measurement of motor cortex control of muscle activity in humans." Clin Neurophysiol 111(2): 326-37.

Morasso, P. and V. Sanguineti (1997). Self-organization, computational maps, and motor control. Amsterdam ; New York, Elsevier.

Mulcahy, E. (2001). An identification of task dependent frequency characteristics in normal and amputee EEG and EMG for use in intention detection for neuroprosthetic control. Department of Bioegineering. Glasgow, University of Strathclyde.

Munih, M. and M. Ichie (2001). "Current Status And Future Prospects For Upper and Lower Extremity Motor System Neuroprostheses." Neuromodulation 4: 176-186.

Murro, A. (1999). Clinical Neurophysiology Medical College of Georgia Course Syllabus. Augusta.

Murthy, V. N. and E. E. Fetz (1992). "Coherent 25- to 35-Hz oscillations in the sensorimotor cortex of awake behaving monkeys." Proc Natl Acad Sci U S A 89(12): 5670-4.

Murthy, V. N. and E. E. Fetz (1996). "Oscillatory activity in sensorimotor cortex of awake monkeys: synchronization of local field potentials and relation to behavior." J Neurophysiol 76(6): 3949-67.

Murthy, V. N. and E. E. Fetz (1996). "Synchronization of neurons during local field potential oscillations in sensorimotor cortex of awake monkeys." J Neurophysiol 76(6): 3968-82.

Mushiake, H., M. Inase and J. Tanji (1991). "Neuronal activity in the primate premotor, supplementary, and precentral motor cortex during visually guided and internally determined sequential movements." J Neurophysiol 66(3): 705-18.

Mushiake, H. and P. L. Strick (1995). "Pallidal neuron activity during sequential arm movements." J Neurophysiol 74(6): 2754-8.

Nagamine, T., M. Kajola, R. Salmelin, H. Shibasaki and R. Hari (1996). "Movement-related slow cortical magnetic fields and changes of spontaneous MEG- and EEG-brain rhythms." Electroencephalogr Clin Neurophysiol 99(3): 274-86.

Navas, F. and L. Stark (1968). "Sampling or intermittency in hand control system dynamics." Biophys J 8(2): 252-302.

Neuper, C. and G. Pfurtscheller (1996). "Post-movement synchronization of beta rhythms in the EEG over the cortical foot area in man." Neuroscience Letters 216(1): 17-20.

Neuralpro (2002). "neuralpro project." www.utwente.nl/bmti/neuralpro.

Ogawa, S. and T. M. Lee (1990). "Magnetic resonance imaging of blood vessels at high fields: in vivo and in vitro measurements and image simulation." Magn Reson Med 16(1): 9-18.

Ogawa, S., T. M. Lee, A. R. Kay and D. W. Tank (1990). "Brain magnetic resonance imaging with contrast dependent on blood oxygenation." Proc Natl Acad Sci U S A 87(24): 9868-72.

Ogawa, S., T. M. Lee, A. S. Nayak and P. Glynn (1990). "Oxygenation-sensitive contrast in magnetic resonance image of rodent brain at high magnetic fields." Magn Reson Med 14(1): 68-78.

Pardo, J. V., P. T. Fox and M. E. Raichle (1991). "Localization of a human system for sustained attention by positron emission tomography." Nature 349(6304): 61-4.

Passingham, R. E. (1996). "Attention to action." Philos Trans R Soc Lond B Biol Sci 351(1346): 1473-9.

Pauluis, Q. (2000). "Statistical signs of common inhibitory feedback with delay." Neural Comput 12(11): 2513-8.

Penfield, W. (1975). The Mystery of the Mind, Princeton University Press.

Penfield, W. and E. Boldrey (1937). "Somatic motor and *sensory representation in* the cerebral cortex of man as studies by electrical stimulation." Brain 60: 389-443.

Peru, A., M. Leder and S. Aglioti (2000). "Right-sided neglect following a left subcortical lesion." Rev Neurol (Paris) 156(5): 475-80.

Pfurtscheller, G. (1989). "Spatiotemporal analysis of alpha frequency components with the ERD technique." Brain Topography 2(1-2): 3-8.

Pfurtscheller, G. (2003). "Induced Oscillations in the Alpha Band: Functional Meaning." Epilepsia 44(s12): 2-8.

Pfurtscheller, G., D. Flotzinger, W. Mohl and M. Peltoranta (1992). "Prediction of the side of hand movements from single-trial multi-channel EEG data using neural networks." Electroencephalography & Clinical Neurophysiology 82(4): 313-315.

Pfurtscheller, G., D. Flotzinger, M. Pregenzer and D. McFarland (1995). "EEG-based Brain Computer Interface (BCI). Search for optimal electrode positions and frequency components." Medical Progress through Technology 21(3): 111-121.

Pfurtscheller, G. and F. H. Lopes da Silva (1999). "Event-related EEG/MEG synchronization and desynchronization: Basic principles." Clinical Neurophysiology 110(11): 1842-1857.

Pfurtscheller, G. and C. Neuper (1997). "Motor imagery activates primary sensorimotor area in humans." Neuroscience Letters 239(2-3): 65-68.

Pfurtscheller, G., C. Neuper, C. Andrew and G. Edlinger (1997). "Foot and hand area mu rhythms." International Journal of Psychophysiology 26(1-3): 121-135.

Pfurtscheller, G., C. Neuper, C. Guger, W. Harkam, H. Ramoser, A. Schlogl, B. Obermaier and M. Pregenzer (2000). "Current trends in Graz Brain-Computer Interface (BCI) research." IEEE Trans Rehabil Eng 8(2): 216-9.

Pfurtscheller, G., C. Neuper, H. Ramoser and J. Muller-Gerking (1999). "Visually guided motor imagery activates sensorimotor areas in humans." Neuroscience Letters 269(3): 153-156.

Pfurtscheller, G., K. Pichler-Zalaudek, B. Ortmayr, J. Diez and F. Reisecker (1998). "Postmovement beta synchronization in patients with Parkinson's disease." Journal of Clinical Neurophysiology 15(3): 243-250.

Pfurtscheller, G., M. Pregenzer and C. Neuper (1994). "Visualization of sensorimotor areas involved in preparation for hand movement based on classification of mu and central beta rhythms in single EEG trials in man." Neuroscience Letters 181(1-2): 43-46.

Pfurtscheller, G., K. Zalaudek and C. Neuper (1998). "Event-related beta synchronization after wrist, finger and thumb movement." Electroencephalography & Clinical Neurophysiology: Electromyography & Motor Control 109(2): 154-160.

Picard, N. and P. L. Strick (2001). "Imaging the premotor areas." Curr Opin Neurobiol 11(6): 663-72.

Pineda, J. A., B. Z. Allison and A. Vankov (2000). "The effects of self-movement, observation, and imagination on mu rhythms and readiness potentials (RP's): toward a brain-computer interface (BCI)." IEEE Trans Rehabil Eng 8(2): 219-22.

Piper, H. (1907). On rhythmical muscle contractions, Pflugers Arch: 301–38.

Pohja, M. and S. Salenius (2003). "Modulation of cortex-muscle oscillatory interaction by ischaemia-induced deafferentation." Neuroreport 14(3): 321-4.

Portas, C. M., G. Rees, A. M. Howseman, O. Josephs, R. Turner and C. D. Frith (1998). "A specific role for the thalamus in mediating the interaction of attention and arousal in humans." J Neurosci 18(21): 8979-89.

Porter, R. and R. Lemon (1993). Corticospinal function and voluntary movement. Oxford, Eng.

Posner, M. I. and G. J. DiGirolamo. (1998). Conflict, target detection and cognitive control. The Attentive Brain. R. Parasuraman. Cambridge, MA, The MIT Press.

Prats-Vinas, J. M. (2000). "[Does the cerebellum play a part in cognitive processes?]." Rev Neurol 31(4): 357-9.

Prinz, A. A. and P. Fromherz (2003). "Effect of neuritic cables on conductance estimates for remote electrical synapses." J Neurophysiol 89(4): 2215-24.

QuickCap_manual (1998). Quick-Cap EEG Electrode Positioning System - Users Guide, NeuroMedical Supplies.

Rafal, R. D. and M. I. Posner (1987). "Deficits in human visual spatial attention following thalamic lesions." Proc Natl Acad Sci U S A 84(20): 7349-53.

Ramachandran, V. S. and W. Hirstein (1998). "The perception of phantom limbs. The D. O. Hebb lecture." Brain 121(Pt 9): 1603-30.

Rao, S. M., J. R. Binder, P. A. Bandettini, T. A. Hammeke, F. Z. Yetkin, A. Jesmanowicz, L. M. Lisk, G. L. Morris, W. M. Mueller, L. D. Estkowski and et al. (1993). "Functional magnetic resonance imaging of complex human movements." Neurology 43(11): 2311-8.

Rauch, F. and J. Rittweger (2001). "What is new in neuro-musculoskeletal interactions?" J Musculoskel Neuron Interact 2001 1(4): 393-398.

Regalado, A. (2001). Top ten emerging technologies. MIT Technology Review.

Richer, F., M. J. Chouinard and I. Rouleau (1999). "Frontal lesions impair the attentional control of movements during motor learning." Neuropsychologia 37(12): 1427-35.

Rizzolatti, G., L. Fadiga, V. Gallese and L. Fogassi (1996). "Premotor cortex and the recognition of motor actions." Brain Res Cogn Brain Res 3(2): 131-41.

Rizzolatti, G., L. Riggio, I. Dascola and C. Umilta (1987). "Reorienting attention across the horizontal and vertical meridians: evidence in favor of a premotor theory of attention." Neuropsychologia 25(1A): 31-40.

Roelcke, U., A. Curt, A. Otte, J. Missimer, R. P. Maguire, V. Dietz and K. L. Leenders (1997). "Influence of spinal cord injury on cerebral sensorimotor systems: a PET study." J Neurol Neurosurg Psychiatry 62(1): 61-5.

Rosenberg, J. R., A. M. Amjad, P. Breeze, D. R. Brillinger and D. M. Halliday (1989). "The Fourier approach to the identification of functional coupling between neuronal spike trains." Prog Biophys Mol Biol 53(1): 1-31.

Rossini, P. M. and F. Pauri (2000). "Neuromagnetic integrated methods tracking human brain mechanisms of sensorimotor areas 'plastic' reorganisation." Brain Res Brain Res Rev 33(2-3): 131-54.

Rothwell, J. C., P. D. Thompson, B. L. Day, S. Boyd and C. D. Marsden (1991). "Stimulation of the human motor cortex through the scalp." Exp Physiol 76(2): 159-200.

Routhier, F., C. Vincent, M. J. Morissette and L. Desaulniers (2001). "Clinical results of an investigation of paediatric upper limb myoelectric prosthesis fitting at the Quebec Rehabilitation Institute." Prosthet Orthot Int 25(2): 119-31.

Ruben, J., J. Schwiemann, M. Deuchert, R. Meyer, T. Krause, G. Curio, K. Villringer, R. Kurth and A. Villringer (2001). "Somatotopic organization of human secondary somatosensory cortex." Cereb Cortex 11(5): 463-73.

Rueckert, L. and J. Grafman (1998). "Sustained attention deficits in patients with lesions of posterior cortex." Neuropsychologia 36(7): 653-60.

Rushworth, M. F., A. Ellison and V. Walsh (2001). "Complementary localization and lateralization of orienting and motor attention." Nat Neurosci 4(6): 656-61.

Rushworth, M. F., P. D. Nixon and R. E. Passingham (1997). "Parietal cortex and movement. I. Movement selection and reaching." Exp Brain Res 117(2): 292-310.

Salenius, S., M. Kajola, W. L. Thompson, S. Kosslyn and R. Hari (1995). "Reactivity of magnetic parieto-occipital alpha rhythm during visual imagery." Electroencephalogr Clin Neurophysiol 95(6): 453-62.

Salenius, S., K. Portin, M. Kajola, R. Salmelin and R. Hari (1997). "Cortical control of human motoneuron firing during isometric contraction." J Neurophysiol 77(6): 3401-5.

Salenius, S., R. Salmelin, C. Neuper, G. Pfurtscheller and R. Hari (1996). "Human cortical 40 Hz rhythm is closely related to EMG rhythmicity." Neuroscience Letters 213(2): 75-78.

Salmelin, R. and R. Hari (1994). "Spatiotemporal characteristics of sensorimotor neuromagnetic rhythms related to thumb movement." Neuroscience 60(2): 537-50.

Schmahmann, J. D. and J. C. Sherman (1998). "The cerebellar cognitive affective syndrome." Brain 121(Pt 4): 561-79.

Schmied, A., S. Pagni, H. Sturm and J. P. Vedel (2000). "Selective enhancement of motoneurone short-term synchrony during an attention-demanding task." Exp Brain Res 133(3): 377-90.

Schurmann, M. and E. Basar (2001). "Functional aspects of alpha oscillations in the EEG." Int J Psychophysiol 39(2-3): 151-8.

Scott, T. R. D. and M. Haugland (2001). "Command and control interfaces for advanced neuroprosthetic applications." Neuromodulation 4(4): 161-171.

Sears, T. A. and D. Stagg (1976). "Short-term synchronization of intercostal motoneurone activity." J Physiol 263(3): 357-81.

Shinoda, Y., J. Yokota and T. Futami (1981). "Divergent projection of individual corticospinal axons to motoneurons of multiple muscles in the monkey." Neurosci Lett 23(1): 7-12.

Sochurkova, D. and I. Rektor (2003). "Event-related desynchronization/synchronization in the putamen. An SEEG case study." Exp Brain Res 149(3): 401-4.

Spehlmann, R., B. J. and F. M.D (1999). EEG primer. Amsterdam ; New York

Stam, C. J., J. P. Pijn, P. Suffczynski and F. H. Lopes da Silva (1999). "Dynamics of the human alpha rhythm: evidence for non-linearity?" Clin Neurophysiol 110(10): 1801-13.

Stancak, A., Jr. (2000). "The electroencephalographic beta synchronization following extension and flexion finger movements in humans." Neurosci Lett 284(1-2): 41-4.

Stancak, A., Jr., B. Feige, C. H. Lucking and R. Kristeva-Feige (2000). "Oscillatory cortical activity and movement-related potentials in proximal and distal movements." Clin Neurophysiol 111(4): 636-50.

Stancak, A., Jr. and G. Pfurtscheller (1996). "Mu-rhythm changes in brisk and slow self-paced finger movements." Neuroreport 7(6): 1161-4.

Steriade, M., S. Datta, D. Pare, G. Oakson and R. C. Curro Dossi (1990). "Neuronal activities in brain-stem cholinergic nuclei related to tonic activation processes in thalamocortical systems." J Neurosci 10(8): 2541-59.

Steriade, M., D. A. McCormick and T. J. Sejnowski (1993). "Thalamocortical oscillations in the sleeping and aroused brain." Science 262(5134): 679-85.

Sterr, A., M. M. Muller, T. Elbert, B. Rockstroh, C. Pantev and E. Taub (1998). "Perceptual correlates of changes in cortical representation of fingers in blind multifinger Braille readers." J Neurosci 18(11): 4417-23.

Stroeve, S. and S. Gielen (2001). "Correlation Between Uncoupled Conductance-Based Integrate-and-Fire Neurons Due to Common and Synchronous Presynaptic Firing." Neural Comp. 13(9): 2005-2029.

Sutter, E. E. and D. Tran (1992). "The field topography of ERG components in man-I. The photopic luminance response." Vision Res 32(3): 433-46.

Sutton, R. S. and A. G. Barto (1998). Reinforcement learning : an introduction. Cambridge, Mass., MIT Press.

Taub, E., N. E. Miller, T. A. Novack, E. W. Cook, 3rd, W. C. Fleming, C. S. Nepomuceno, J. S. Connell and J. E. Crago (1993). "Technique to improve chronic motor deficit after stroke." Arch Phys Med Rehabil 74(4): 347-54.

Thulborn, K. R., J. C. Waterton, P. M. Matthews and G. K. Radda (1982). "Oxygenation dependence of the transverse relaxation time of water protons in whole blood at high field." Biochim Biophys Acta 714(2): 265-70.

Timmermann, L., J. Gross, F. Schmitz, H. J. Freund and A. Schnitzler (2001). "Involvement of the motor cortex in pseudochoreoathetosis." Mov Disord 16(5): 876-81.

Todorov, E. (2000). "Direct cortical control of muscle activation in voluntary arm movements: a model." Nat Neurosci 3(4): 391-8.

Toro, C., C. Cox, G. Friehs, C. Ojakangas, R. Maxwell, J. R. Gates, R. J. Gumnit and T. J. Ebner (1994). "8-12 Hz rhythmic oscillations in human motor cortex during two-dimensional arm movements: Evidene for representation of kinematic parameters." Electroencephalography & Clinical Neurophysiology: Electromyography & Motor Control 93(5): 390-403.

Toro, C., G. Deuschl, R. Thatcher, S. Sato, C. Kufta and M. Hallett (1994). "Event-related desynchronization and movement-related cortical potentials on the ECoG and EEG." Electroencephalography & Clinical Neurophysiology: Electromyography & Motor Control 93(5): 380-389.

Townsend, J., E. Courchesne, J. Covington, M. Westerfield, N. S. Harris, P. Lyden, T. P. Lowry and G. A. Press (1999). "Spatial attention deficits in patients with acquired or developmental cerebellar abnormality." J Neurosci 19(13): 5632-43.

Trehub, A. (1991). The Cognitive Brain. Cambridge, MA, The MIT Press.

Turak, B., J. Louvel, P. Buser and M. Lamarche (2002). "Event-related potentials recorded from the cingulate gyrus during attentional tasks: a study in patients with implanted electrodes." Neuropsychologia 40(1): 99-107.

Uellendahl, J. E. (2000). "Upper extremity myoelectric prosthetics." Phys Med Rehabil Clin N Am 11(3): 639-52.

Vaillancourt, D. E. and K. M. Newell (2000). "Amplitude changes in the 8-12, 20-25, and 40 Hz oscillations in finger tremor." Clin Neurophysiol 111(10): 1792-801.

Vallbo, A. B. and J. Wessberg (1993). "Organization of motor output in slow finger movements in man." Journal of Physiology 469(pp 673-691).

Vaughan, T. M., L. A. Miner, D. J. McFarland and J. R. Wolpaw (1998). "EEG-based communication: analysis of concurrent EMG activity." Electroencephalogr Clin Neurophysiol 107(6): 428-33.

Vendrell, P., C. Junque, J. Pujol, M. A. Jurado, J. Molet and J. Grafman (1995). "The role of prefrontal regions in the Stroop task." Neuropsychologia 33(3): 341-52.

Wang, H. C., A. J. Lees and P. Brown (1999). "Impairment of EEG desynchronisation before and during movement and its relation to bradykinesia in Parkinson's disease." J Neurol Neurosurg Psychiatry 66(4): 442-6.

Ward, L. M. (2001). "Human neural plasticity." TRENDS in Cognitive Sciences 5(8): 325-327.

Welford, A. T. (1952). "The psychological refractory period and the timing of high-speed performance - a review and a theory." British Journal of Psychology 43: 2-19.

Werhahn, K. J., J. Mortensen, A. Kaelin-Lang, B. Boroojerdi and L. G. Cohen (2002). "Cortical excitability changes induced by deafferentation of the contralateral hemisphere." Brain 125(Pt 6): 1402-13.

Wessberg, J. and N. Kakuda (1999). "Single motor unit activity in relation to pulsatile motor oufput in human finger movements." Journal of Physiology 517(1): 273-285.

Wessberg, J. and A. B. Vallbo (1995). "Coding of pulsatile motor output by human muscle afferents during slow finger movements." Journal of Physiology 485(1): 271-282.

Wessberg, J. and A. B. Vallbo (1996). "Pulsatile motor output in human finger movements is not dependent on the stretch reflex." Journal of Physiology 493(3): 895-908.

Wilson, R. A. and F. C. Keil, Eds. (1999). The MIT encyclopedia of the cognitive sciences, MIT Press.

Winfree, A. T. (1980). The geometry of biological time. New York, Springer Verlag.

Wise, S. P. and R. Shadmehr (2002). Motor Control. Encyclopedia of the Human Brain, Elsevier Science. 3: 1-21.

Wolpaw, J. R., N. Birbaumer, W. J. Heetderks, D. J. McFarland, P. H. Peckham, G. Schalk, E. Donchin, L. A. Quatrano, C. J. Robinson and T. M. Vaughan (2000). "Brain-computer interface technology: a review of the first international meeting." IEEE Trans Rehabil Eng 8(2): 164-73.

Wolpaw, J. R., N. Birbaumer, D. J. McFarland, G. Pfurtscheller and T. M. Vaughan (2002). "Brain-computer interfaces for communication and control." Clin Neurophysiol 113(6): 767-91.

Wolpaw, J. R. and D. J. McFarland (1994). "Multichannel EEG-based brain-computer communication." Electroencephalogr Clin Neurophysiol 90(6): 444-9.

Wolpaw, J. R., D. J. McFarland, G. W. Neat and C. A. Forneris (1991). "An EEG-based brain-computer interface for cursor control." Electroencephalogr Clin Neurophysiol 78(3): 252-9.

Wolpaw, J. R., D. J. McFarland and T. M. Vaughan (2000). "Brain-computer interface research at the Wadsworth Center." IEEE Trans Rehabil Eng 8(2): 222-6.

Wolpaw, J. R. and A. M. Tennissen (2001). "Activity-dependent spinal cord plasticity in health and disease." Annu Rev Neurosci 24: 807-43.

Wright, T. W., A. D. Hagen and M. B. Wood (1995). "Prosthetic usage in major upper extremity amputations." J Hand Surg [Am] 20(4): 619-22.

Yao, D., L. Wang, R. Oostenveld, K. D. Nielsen, L. Arendt-Nielsen and A. C. Chen (2005). "A comparative study of different references for EEG spectral mapping: the issue of the neutral reference and the use of the infinity reference." Physiol Meas 26(3): 173-84.

Yousry, T. A., U. D. Schmid, H. Alkadhi, D. Schmidt, A. Peraud, A. Buettner and P. Winkler (1997). "Localization of the motor hand area to a knob on the precentral gyrus. A new landmark." Brain 120(Pt 1): 141-57.

Ziemann, U., B. Corwell and L. G. Cohen (1998). "Modulation of plasticity in human motor cortex after forearm ischemic nerve block." J Neurosci 18(3): 1115-23.

Ziemann, U., M. Hallett and L. G. Cohen (1998). "Mechanisms of deafferentation-induced plasticity in human motor cortex." Journal of Neuroscience 18(17): 7000-7007.

Ziemann, U., W. Muellbacher, M. Hallett and L. G. Cohen (2001). "Modulation of practice-dependent plasticity in human motor cortex." Brain 124(Pt 6): 1171-81.

9 APPENDICES

9.1 APPENDIX 1 - SUBJECT VARIABILITY

The data used to produce the graphs presented in the results chapter were pooled records for all nine subjects in the studied subject group. Pooled frequency characteristics like coherence estimates presented the common features of the studied population. However different subjects may demonstrate widely different frequency characteristics, for virtually identical simple motor tasks. Furthermore pooled results may misrepresent the common population features.

For this reason the examined frequency characteristics were constructed for individual subjects. This gave us the chance to compare the results and evaluate the variability of the calculated plots in the subject group for performing the same simple tasks.

Significant variability was observed in the occurrence and magnitude of coherence features. However most subjects demonstrate task related features especially for extension movement and extension posture.

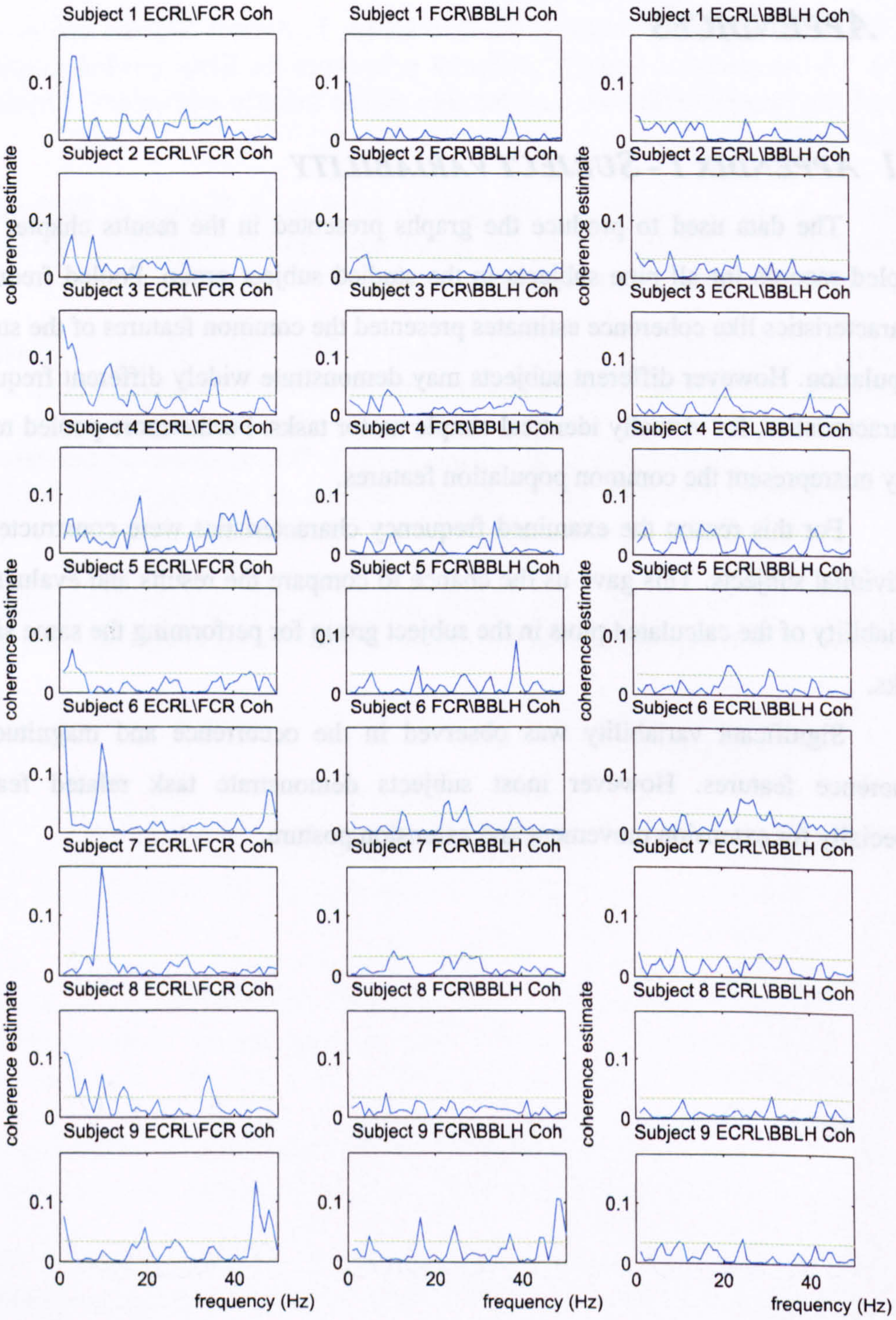

Fig. 9.1 Plot displaying subject variability for intermuscular coherence during movement flexion. ECRL\FCR, FCR\BBLH and ECRL\BBLH coherences are displayed for all 9 subjects.

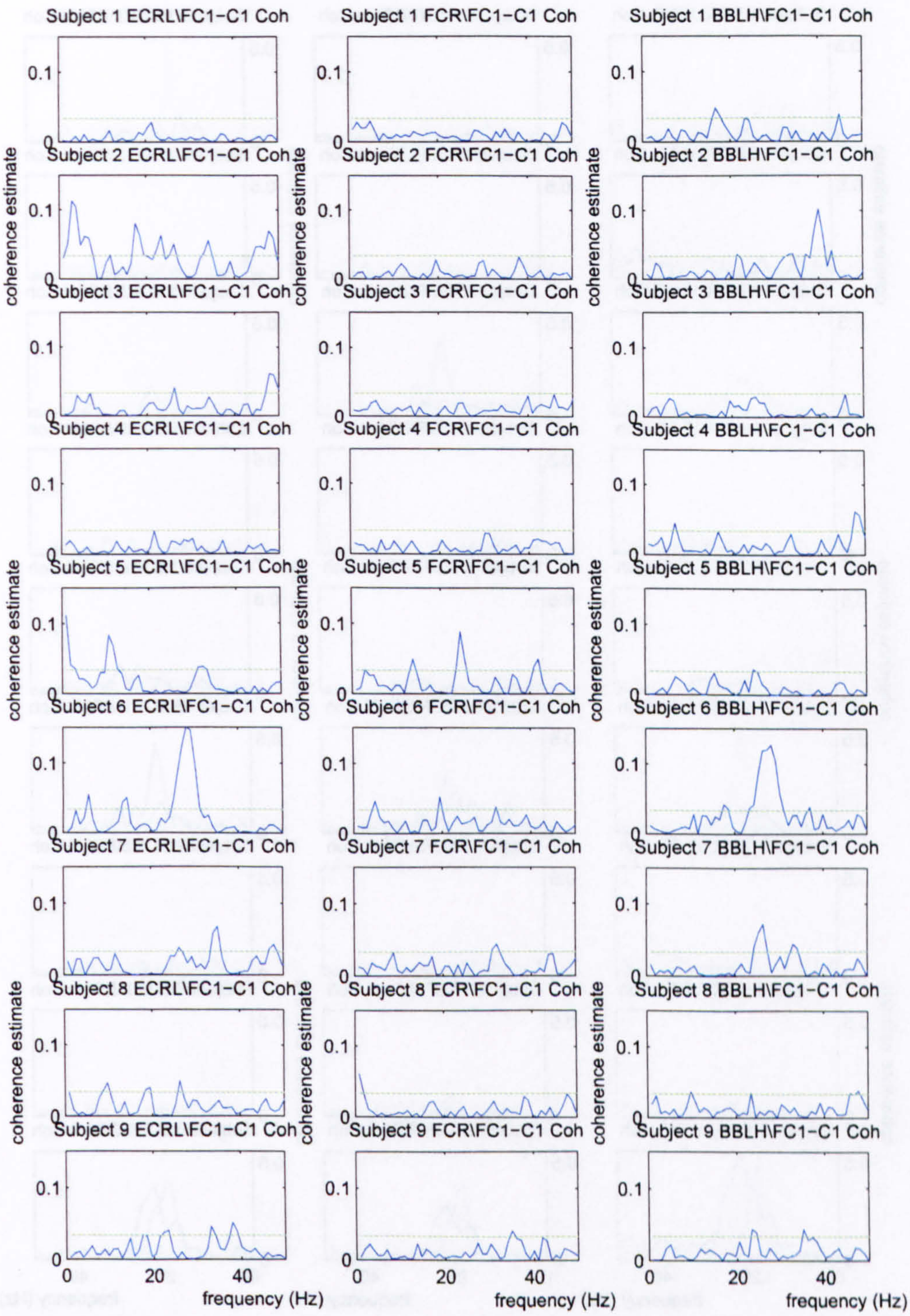

Fig. 9.2 Plot displaying subject variability for corticomuscular coherence during movement flexion. ECRL\FC1-C1, FCR \FC1-C1 and BBLH\FC1-C1 coherences are displayed for all 9 subjects.

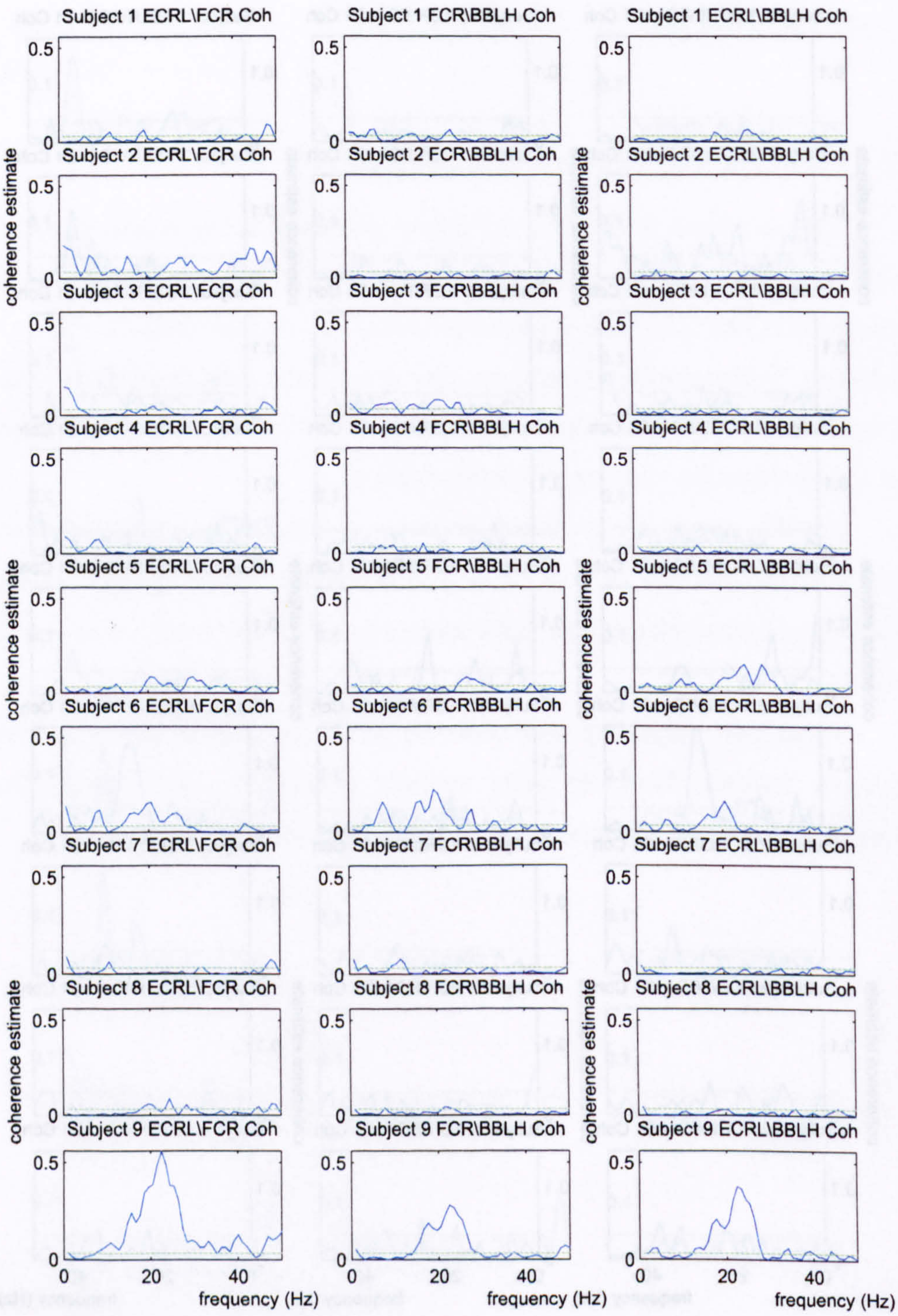

Fig. 9.3 Plot displaying subject variability for intermuscular coherence during posture flexion. ECRL\FCR, FCR\BBLH and ECRL\BBLH coherences are displayed for all 9 subjects.

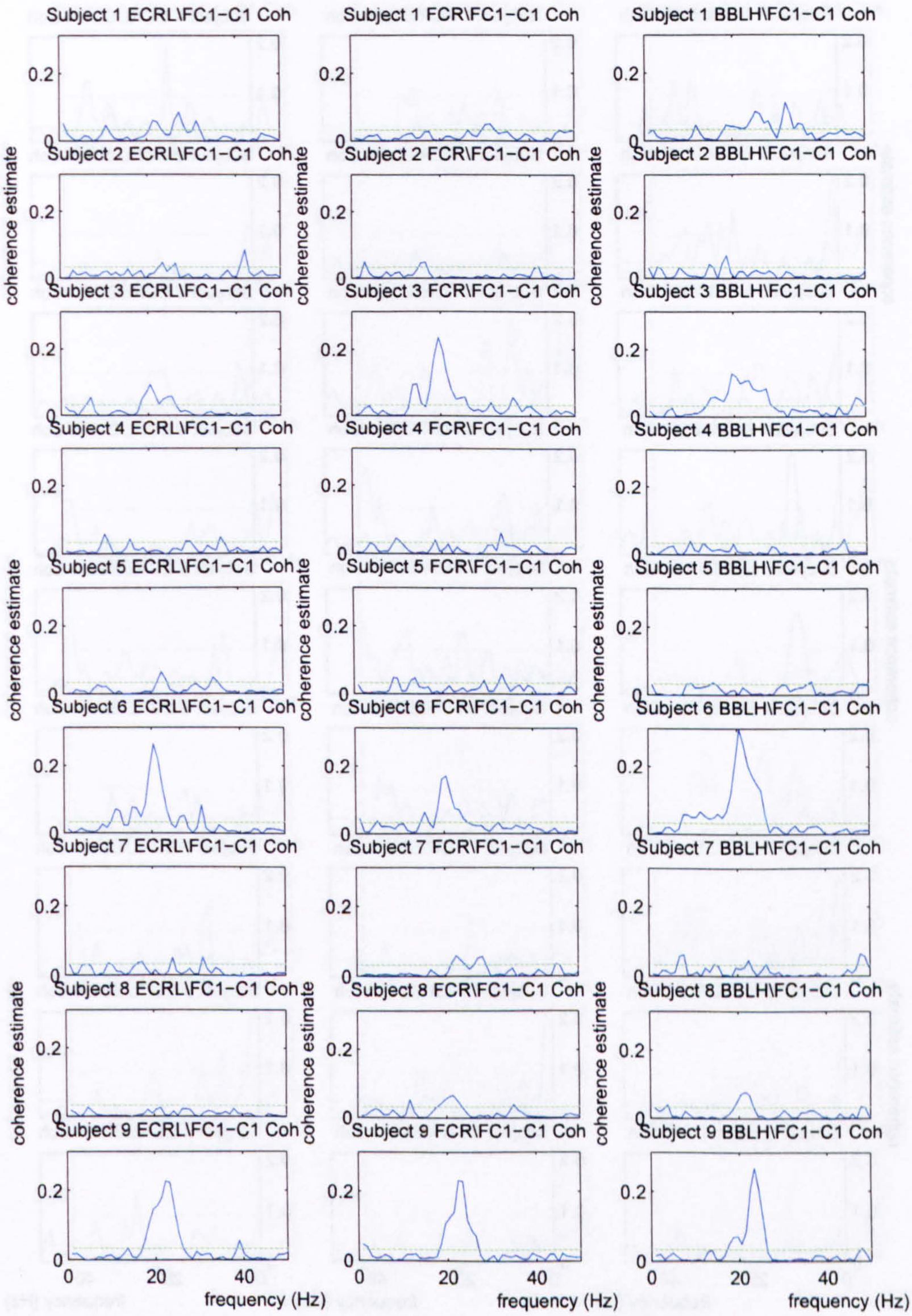

Fig. 9.4 Plot displaying subject variability for corticomuscular coherence during posture flexion. ECRL\FC1-C1, FCR\FC1-C1 and BBLH\FC1-C1 coherences are displayed for all 9 subjects.

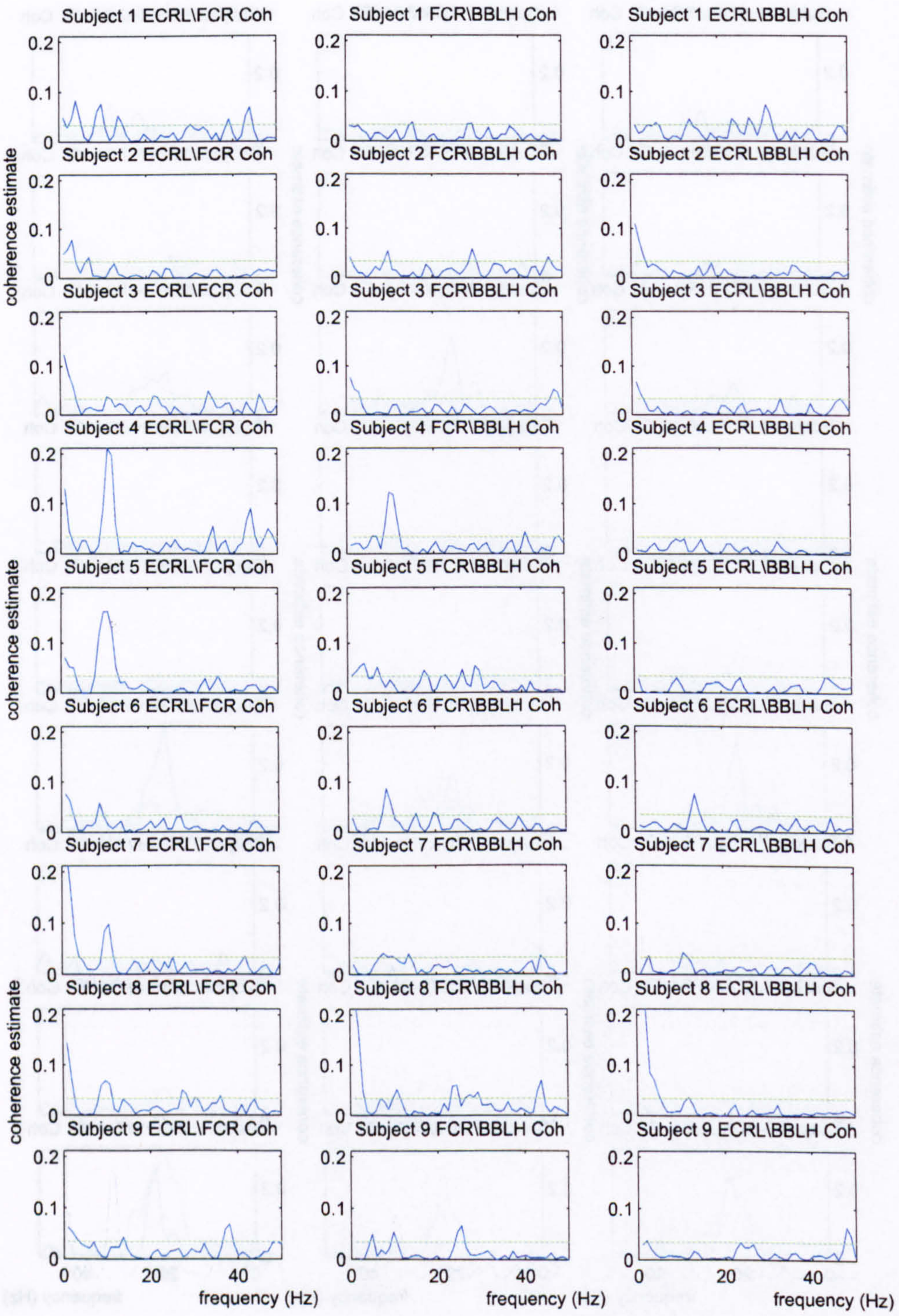

Fig. 9.5 Plot displaying subject variability for intermuscular coherence during movement extension. ECRL\FCR, FCR\BBLH and ECRL\BBLH coherences are displayed for all 9 subjects.

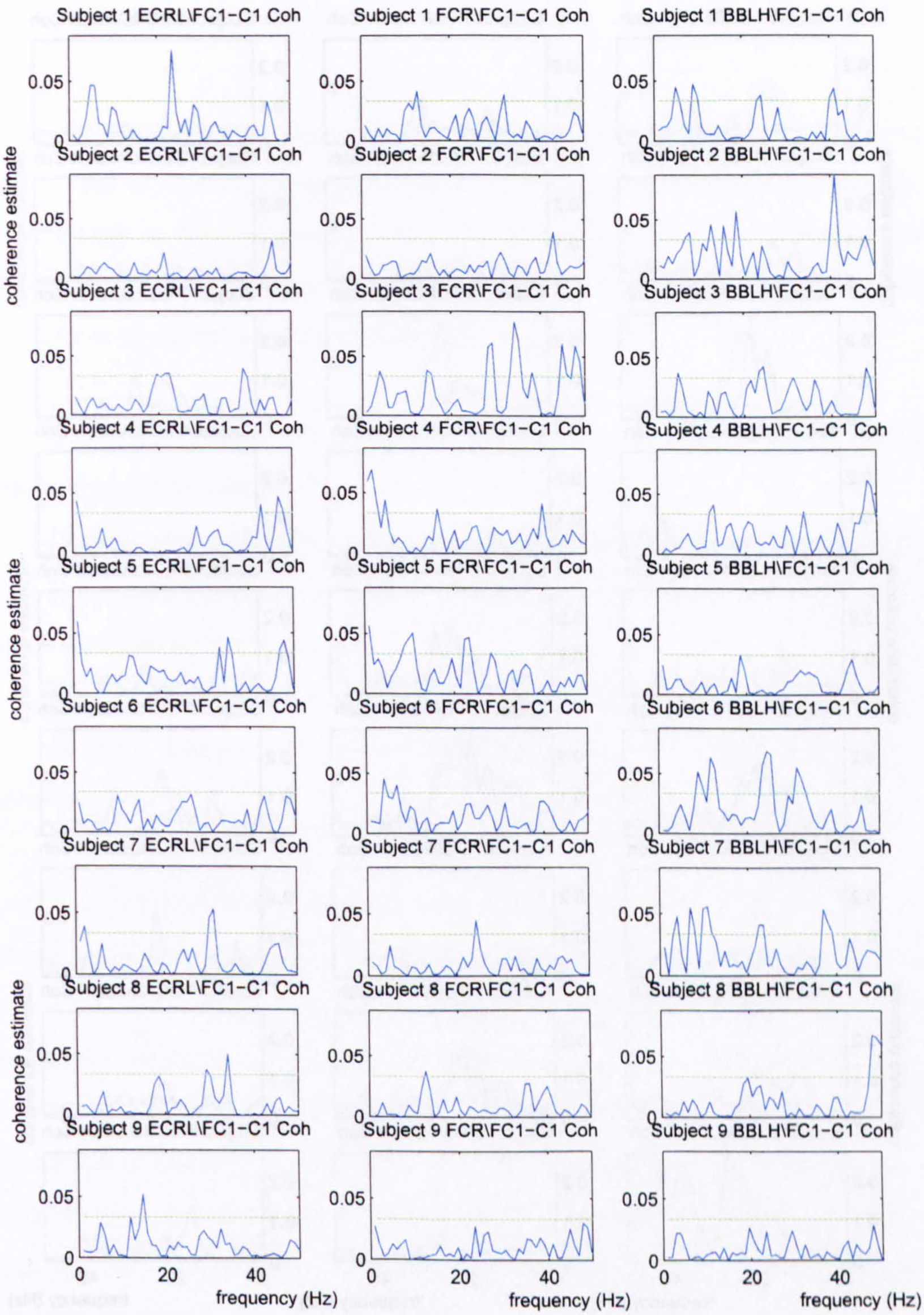

Fig. 9.6 Plot displaying subject variability for corticomuscular coherence during movement extension. ECRL\FC1-C1, FCR\FC1-C1 and BBLH\FC1-C1 coherences are displayed for all 9 subjects.

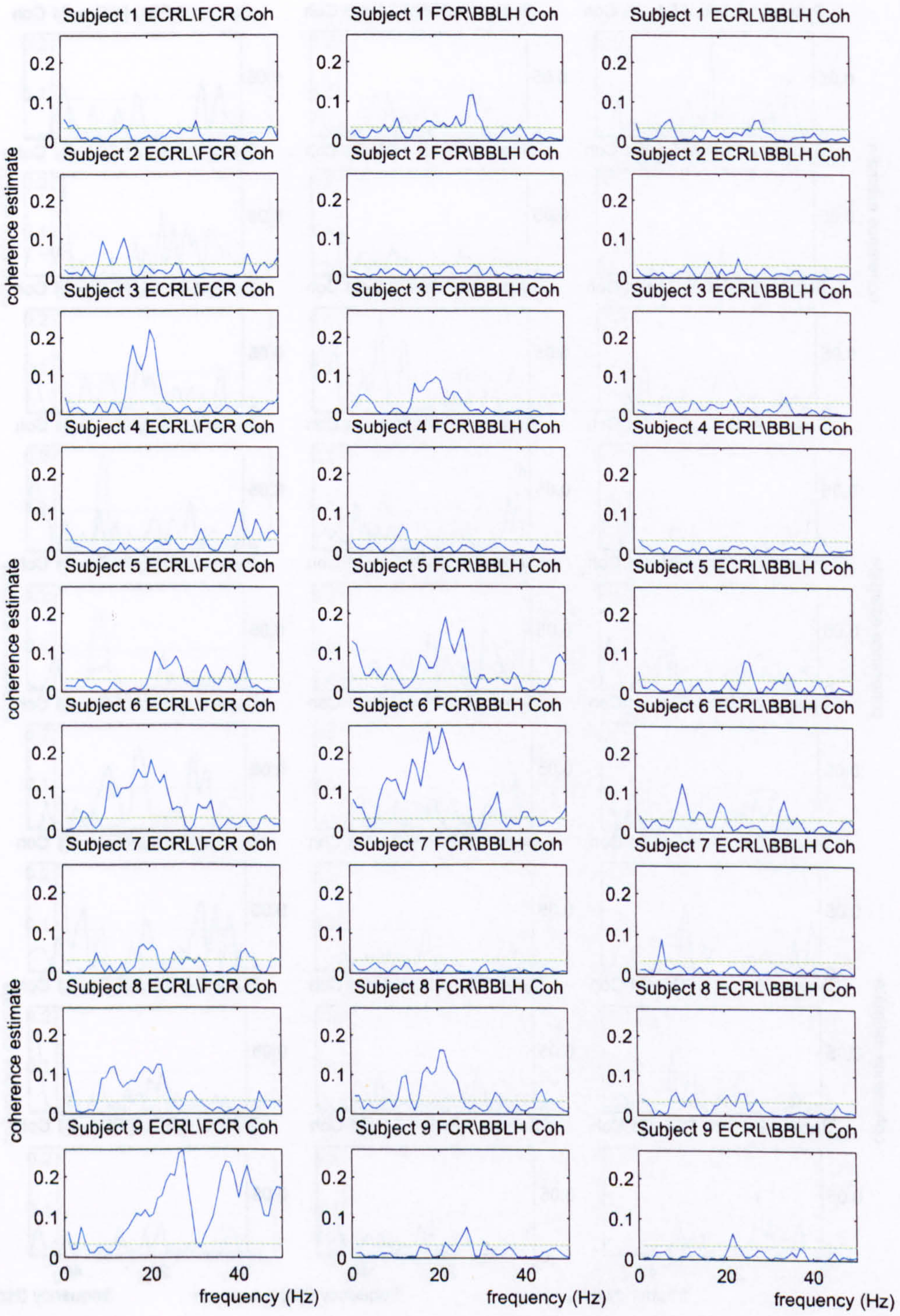

Fig. 9.7 Plot displaying subject variability for intermuscular coherence during posture extension. ECRL\FCR, FCR\BBLH and ECRL\BBLH coherences are displayed for all 9 subjects.

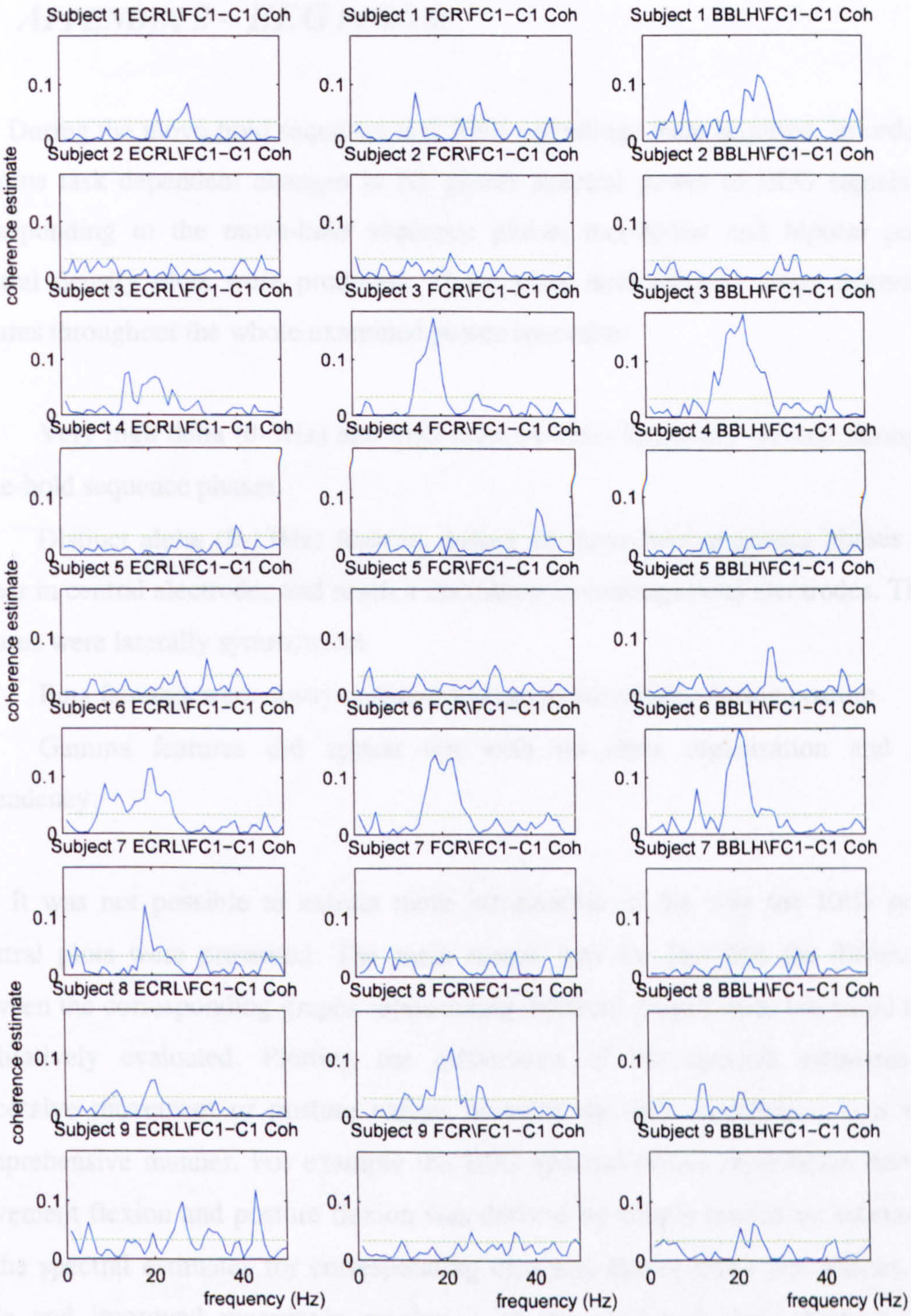

Fig. 9.8 Plot displaying subject variability for corticomuscular coherence during posture extension. ECRL\FC1-C1, FCR\FC1-C1 and BBLH\FC1-C1 coherences are displayed for all 9 subjects.

9.2 *APPENDIX 2 – EEG POWER*

During the move-hold sequence task EEG recordings were acquired. In order to examine task dependent changes in the power spectral power of EEG signals the corresponding to the move-hold sequence phase, monopolar and bipolar power spectral density plots were produced. These plots demonstrated some interesting features throughout the whole examined power spectrum:

- Very high delta (0-3Hz) and high theta (4-7Hz) frequency content during all move-hold sequence phases.
- Distinct alpha (8-13Hz) features during all move-hold sequence phases that appear in central electrodes and reach a maximum in centroparietal electrodes. These features were laterally symmetrical.
- Beta features were always present and increased mainly during posture.
- Gamma features did appear but with no clear organisation and task dependency.

It was not possible to extract more information in the way the EEG power spectral plots were presented. The main reason was the fact that the differences between the corresponding graphs representing different phases were too small to be qualitatively evaluated. Plotting the differences of the spectral estimates for successive movement or posture phases revealed the task modulation in a more comprehensive manner. For example the EEG spectral power modulation between movement flexion and posture flexion was derived by simple arithmetic subtraction of the spectral estimates for corresponding channels during these two phases. The scale and improved magnitude resolution of the produced plots allowed small differences to emerge in a way that can be easily identified. The differences of the spectral estimates for successive movement or posture phases are presented in the Results 5.1.4.1 section (EEG Power Spectral density task dependent features)

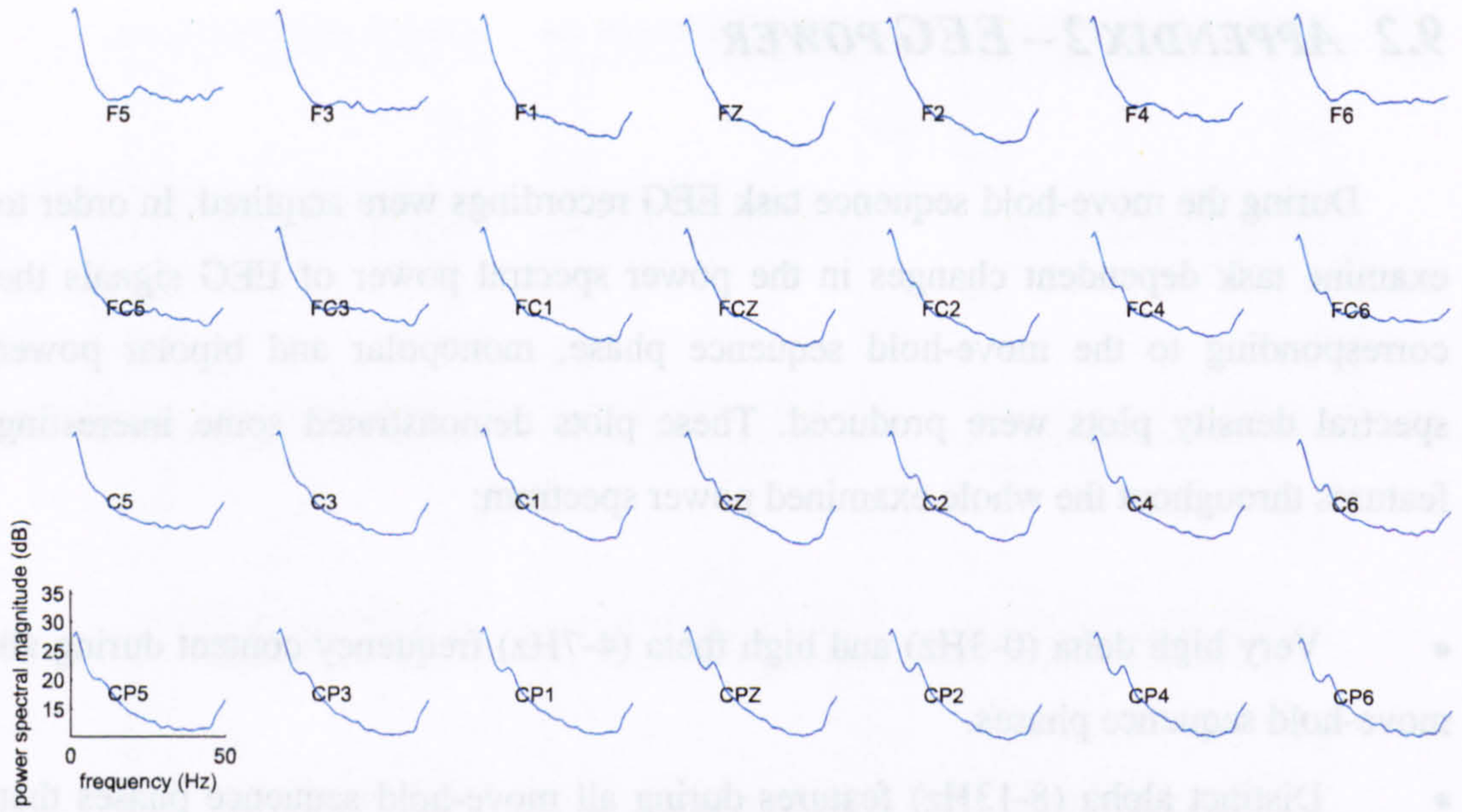

Fig. 9.9 Monopolar EEG power spectra during movement flexion

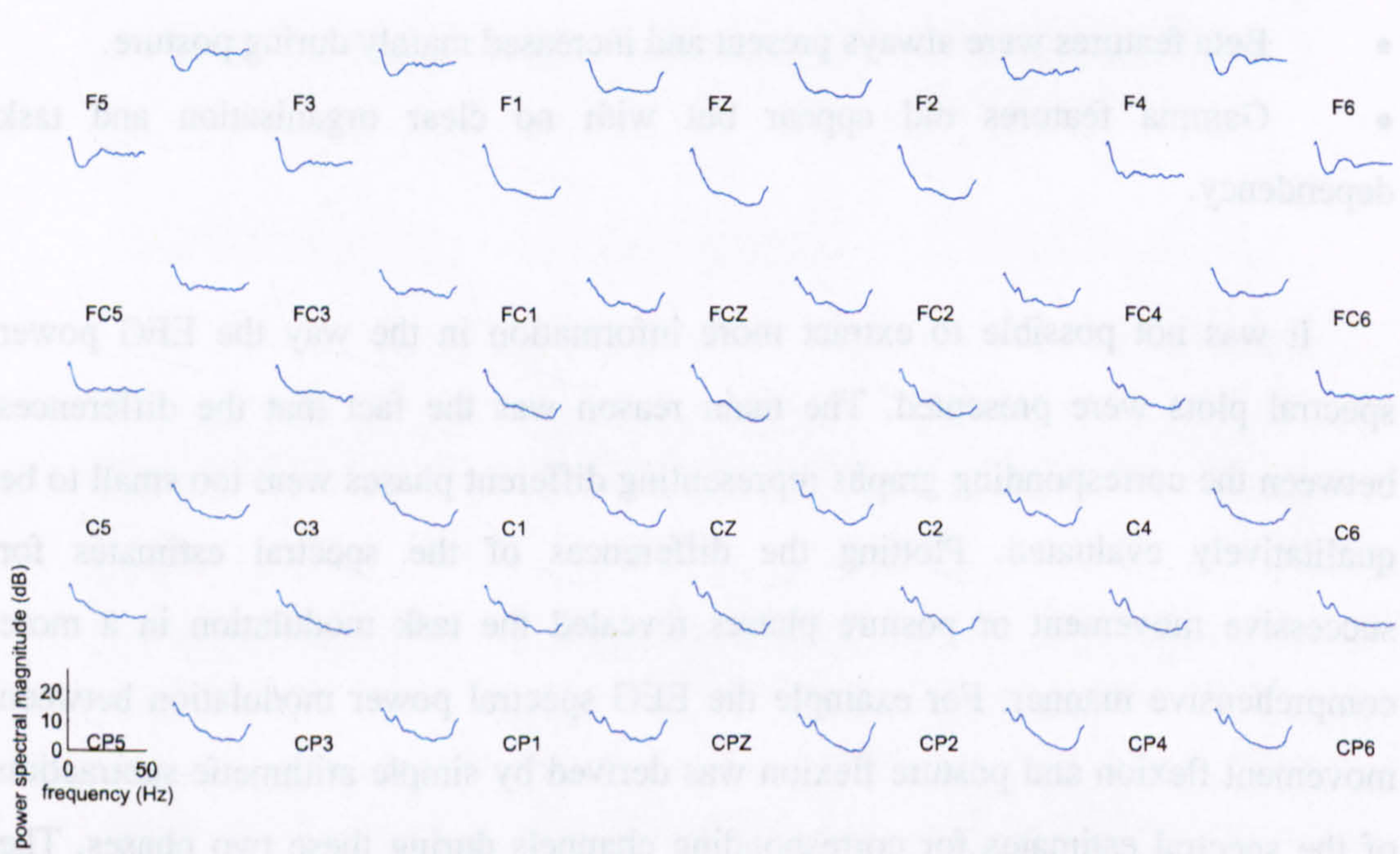

Fig. 9.10 Bipolar EEG power spectra during movement flexion

Fig. 9.11 Monopolar EEG power spectra during posture flexion

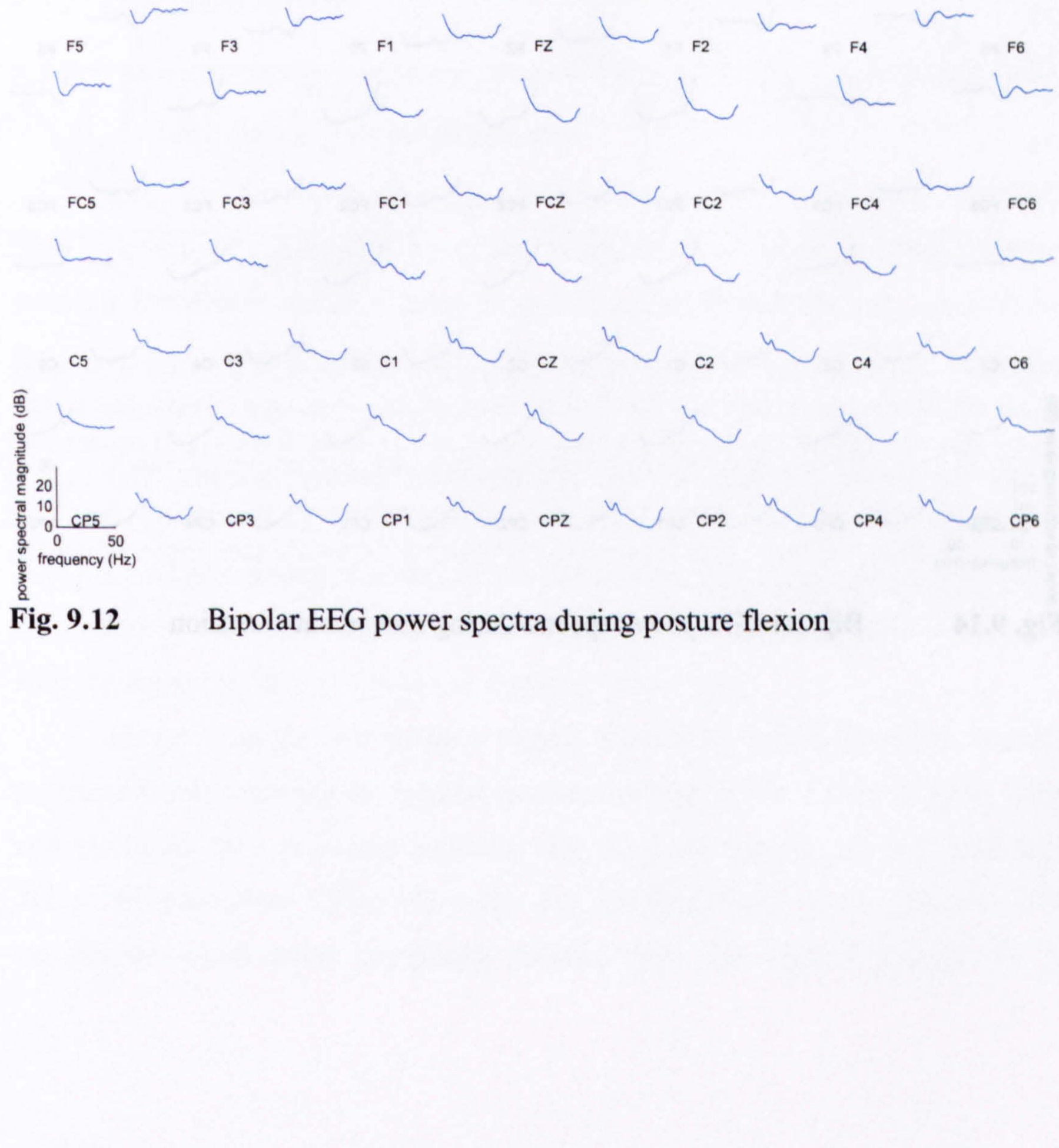

Fig. 9.12 Bipolar EEG power spectra during posture flexion

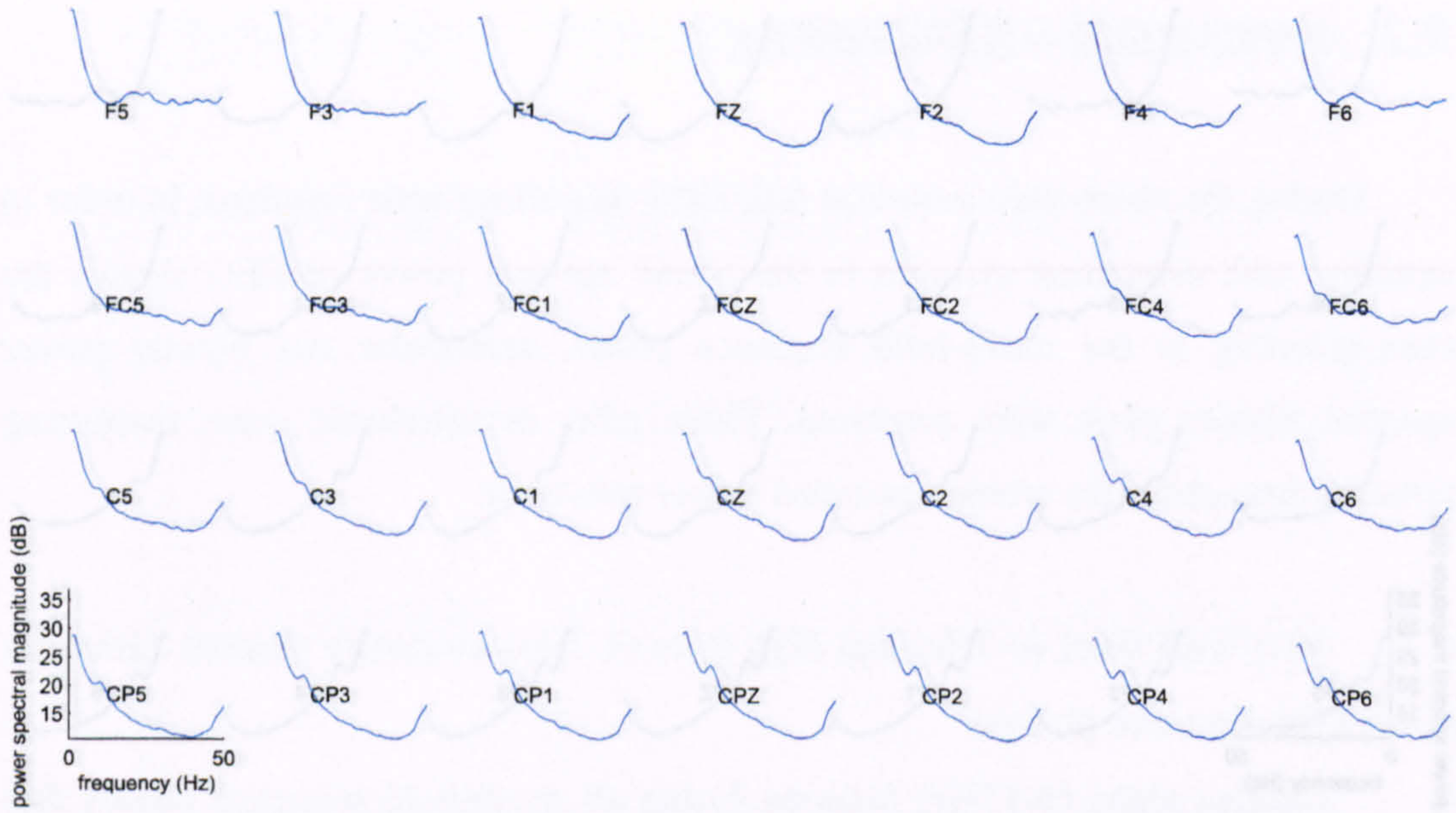

Fig. 9.13 Monopolar EEG power spectra during movement extension

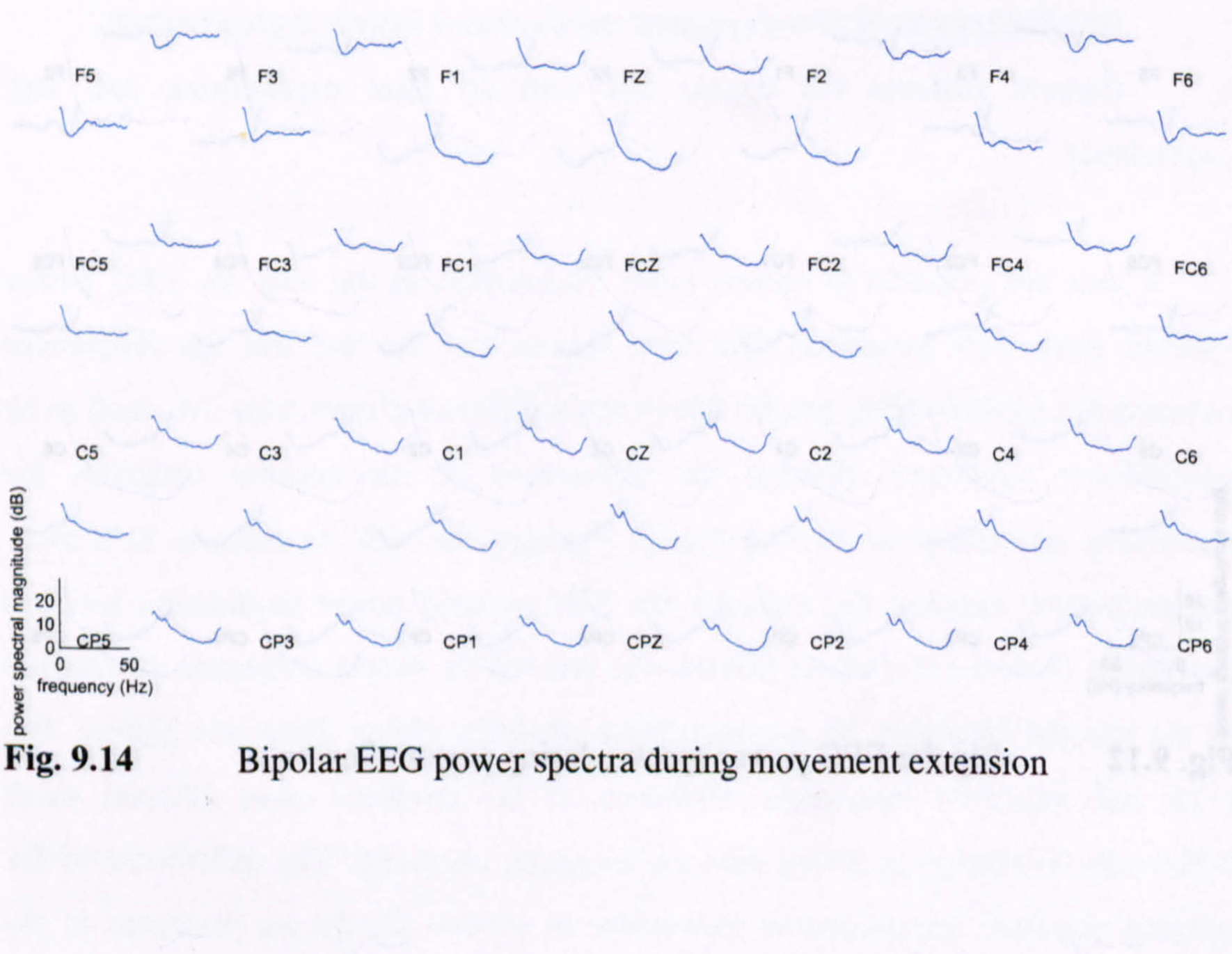

Fig. 9.14 Bipolar EEG power spectra during movement extension

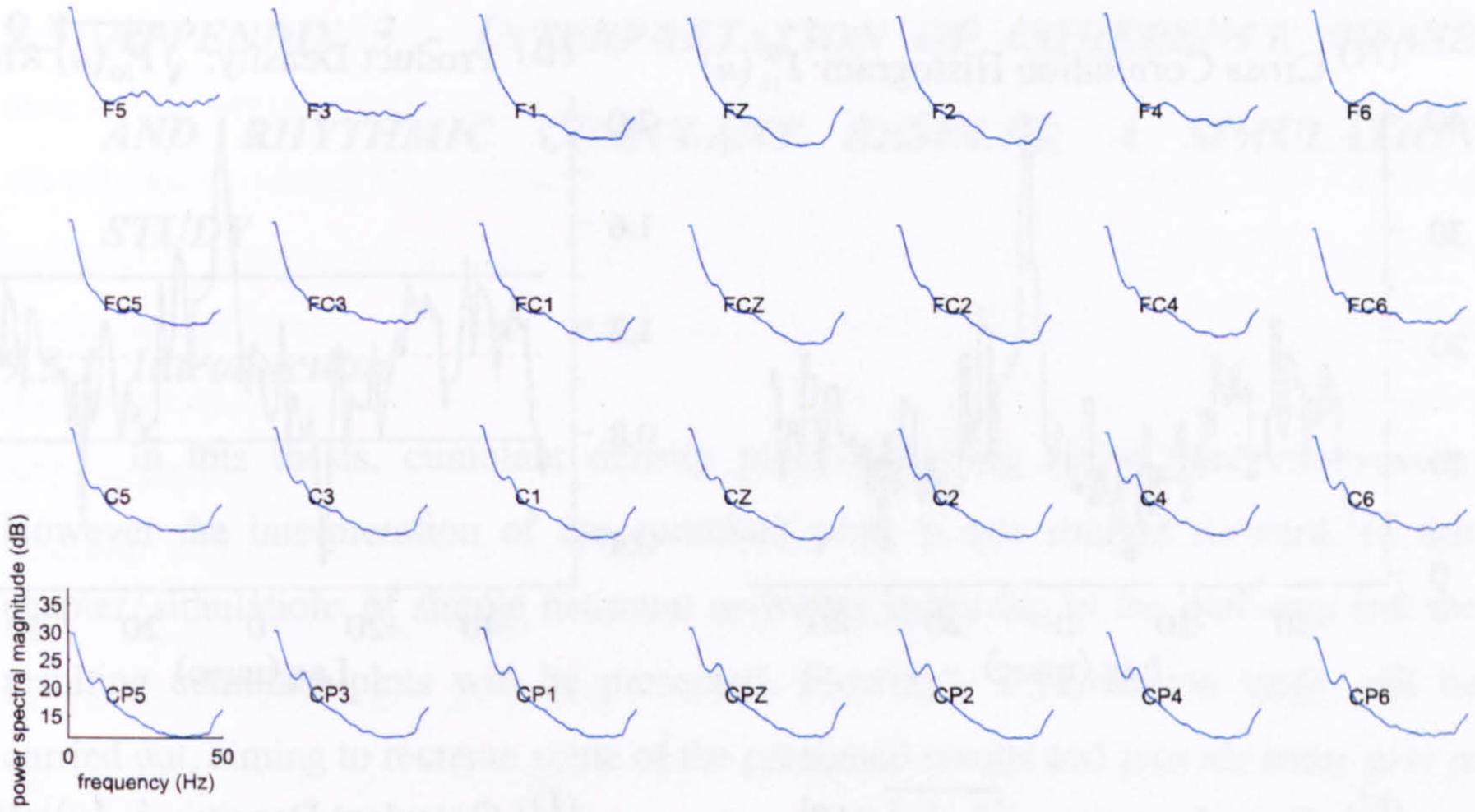

Fig. 9.15 Monopolar EEG power spectra during posture extension

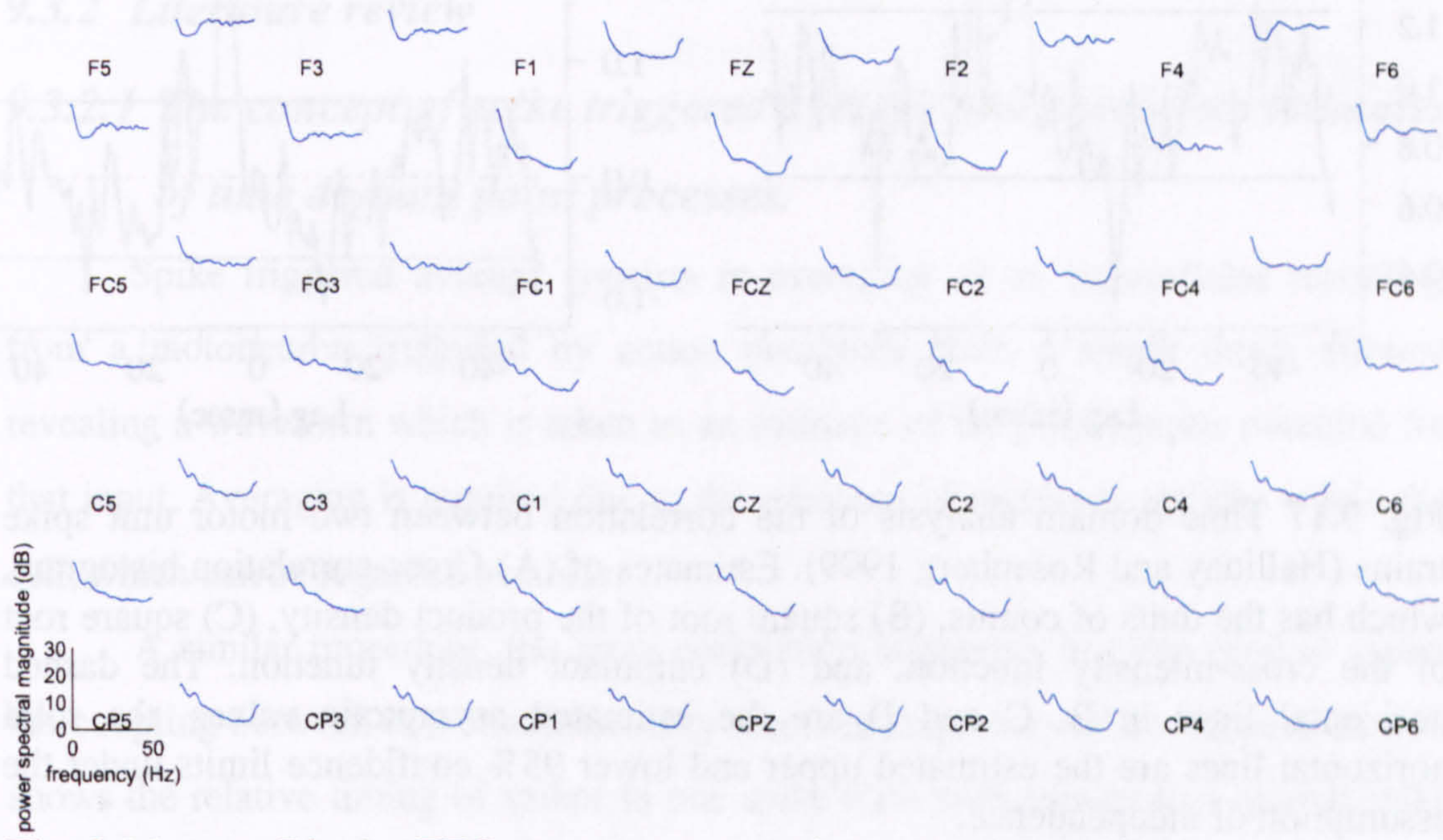

Fig. 9.16 Bipolar EEG power spectra during posture extension

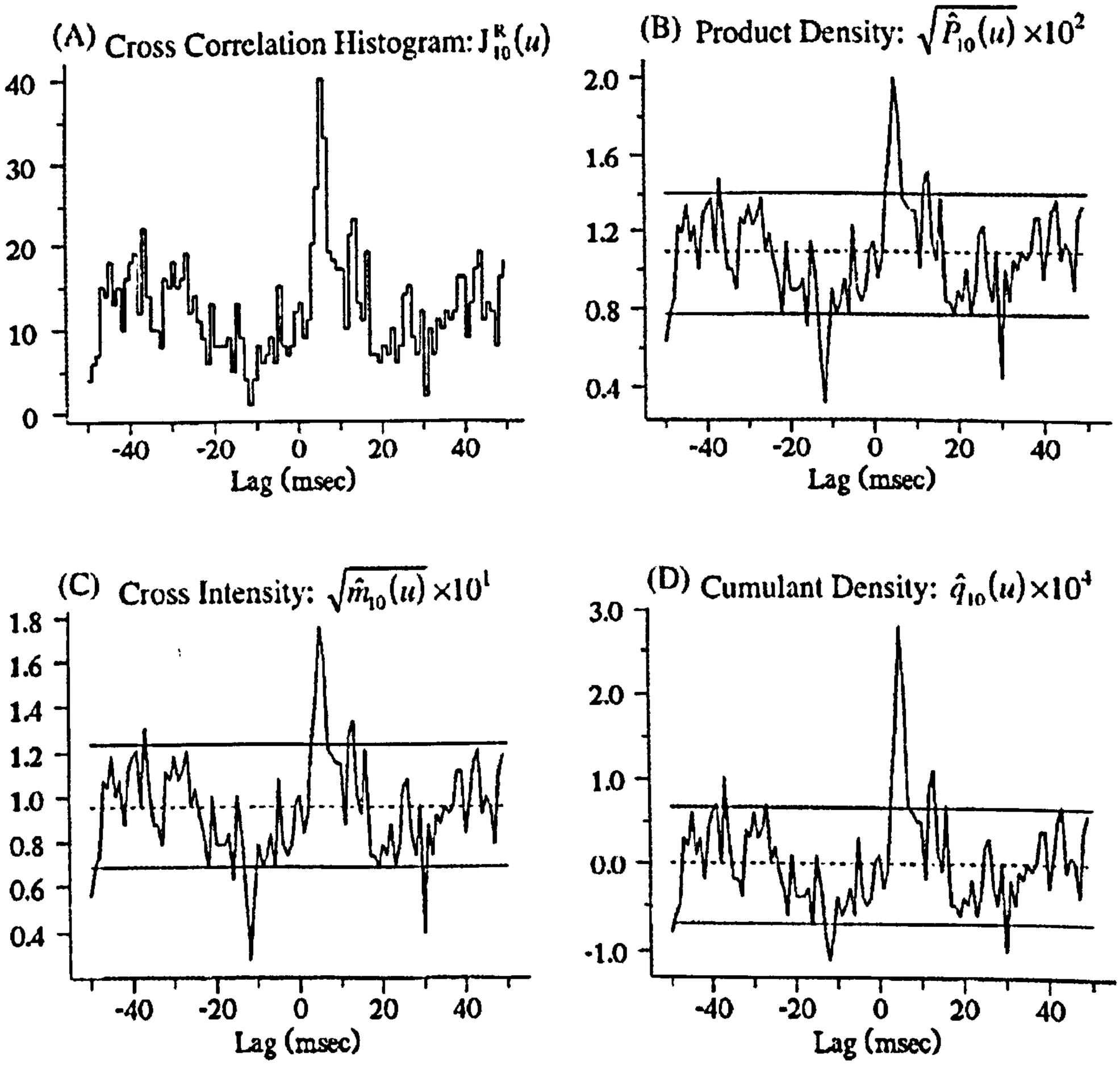

Fig. 9.17 Time domain analysis of the correlation between two motor unit spike trains (Halliday and Rosenberg 1999). Estimates of (A) Cross-correlation histogram, which has the units of counts, (B) square root of the product density, (C) square root of the cross-intensity function, and (D) cumulant density function. The dashed horizontal lines in B, C and D are the estimated asymptotic values, the solid horizontal lines are the estimated upper and lower 95% confidence limits under the assumption of independence.

9.3 APPENDIX 3 - INTERPRETATION OF COHERENCE PHASE AND RHYTHMIC CUMULANT RESULTS; A SIMULATION STUDY

9.3.1 Introduction

In this thesis, cumulant density plots are going to be used extensively. However the interpretation of the cumulant plots is not straight forward. In this chapter, simulations of simple neuronal networks appearing in the literature and the resulting cumulant plots will be presented. Flowingly a simulation study will be curried out, aiming to recreate some of the presented results and provide some new in order to give insight to the interpretation of the cumulant analysis results and frequency domain results in general.

9.3.2 Literature review

9.3.2.1 The concept of spike triggered average and parameter estimates of time domain point processes.

Spike triggered average consists in averaging of an intracellular recording from a motoneuron triggered by action potentials from a single intact afferent revealing a waveform which is taken as an estimate of the postsynaptic potential for that input. Averaging is required due to the presence of unrelated activity within the cell, which can be regarded as noise.

A similar procedure, the cross-correlation histogram is often used to assess the coupling between two simultaneously recorded sequences of action potentials. It shows the relative timing of spikes in one spike train with respect to a second spike train where in this case it is the timing of spikes in one spike train, which is averaged with respect to the timing of spikes in a second spike train.

Except from the two methods already mentioned a number of time domain parameters, estimates can be used to characterize interactions between spike trains and stochastic time processes including the cumulant density we have described before. All procedures effectively reveal any correlation between two signals. With an almost certain noise component present cases the signals studied can be

considered as stochastic processes. Fig. 8.17 adapted from (Halliday and Rosenberg 1999) shows the estimates of (A) the cross-correlation histogram, (B) the square root of the product density, (C) the square root of the cross-intensity function, and (D) the cumulant density function between two motor units spike trains. The close relationship between the cross-correlation histogram and the other three parameter estimates is clearly demonstrated in this figure. The three parameter estimates all have the same basic shape determined from the cross-correlation histogram. The main difference is in the asymptotic value and upper and lower confidence limits of the three estimates, which reflect the different probability descriptions.

A large peak at lag u=+5ms, exceeds the upper confidence limit in all parameter estimates, indicating correlated motor unit activity. Also present are smaller oscillatory features on either side of the central peak, these features are often referred to as sidebands and taken to reflect the presence of common rhythmic inputs. The confidence limits in the three parameter estimates indicate that these features are only of marginal significance at the 5% level.

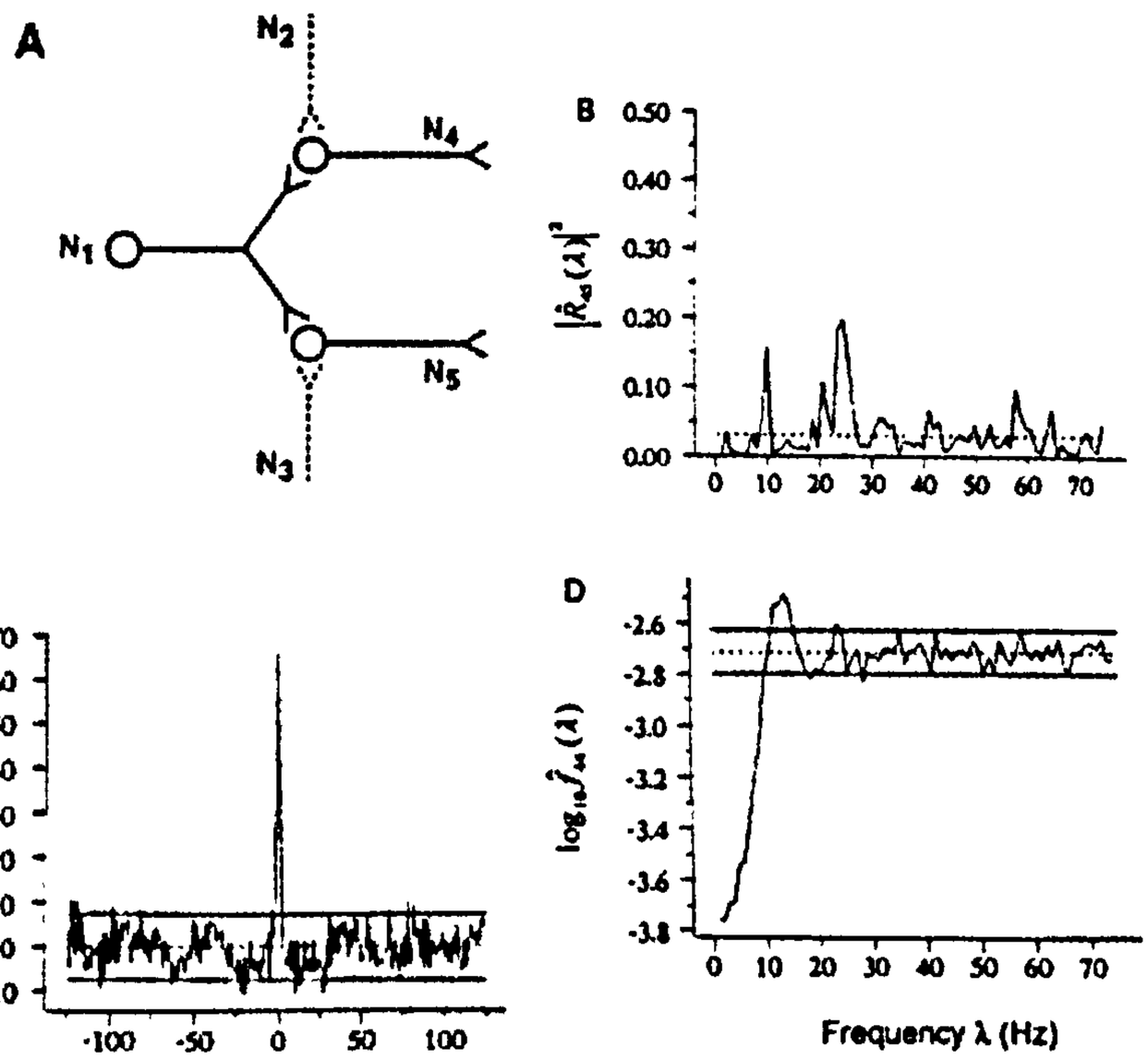

Fig. 9.18 Paired neurones with a single common excitatory input (Halliday and Rosenberg 1999)

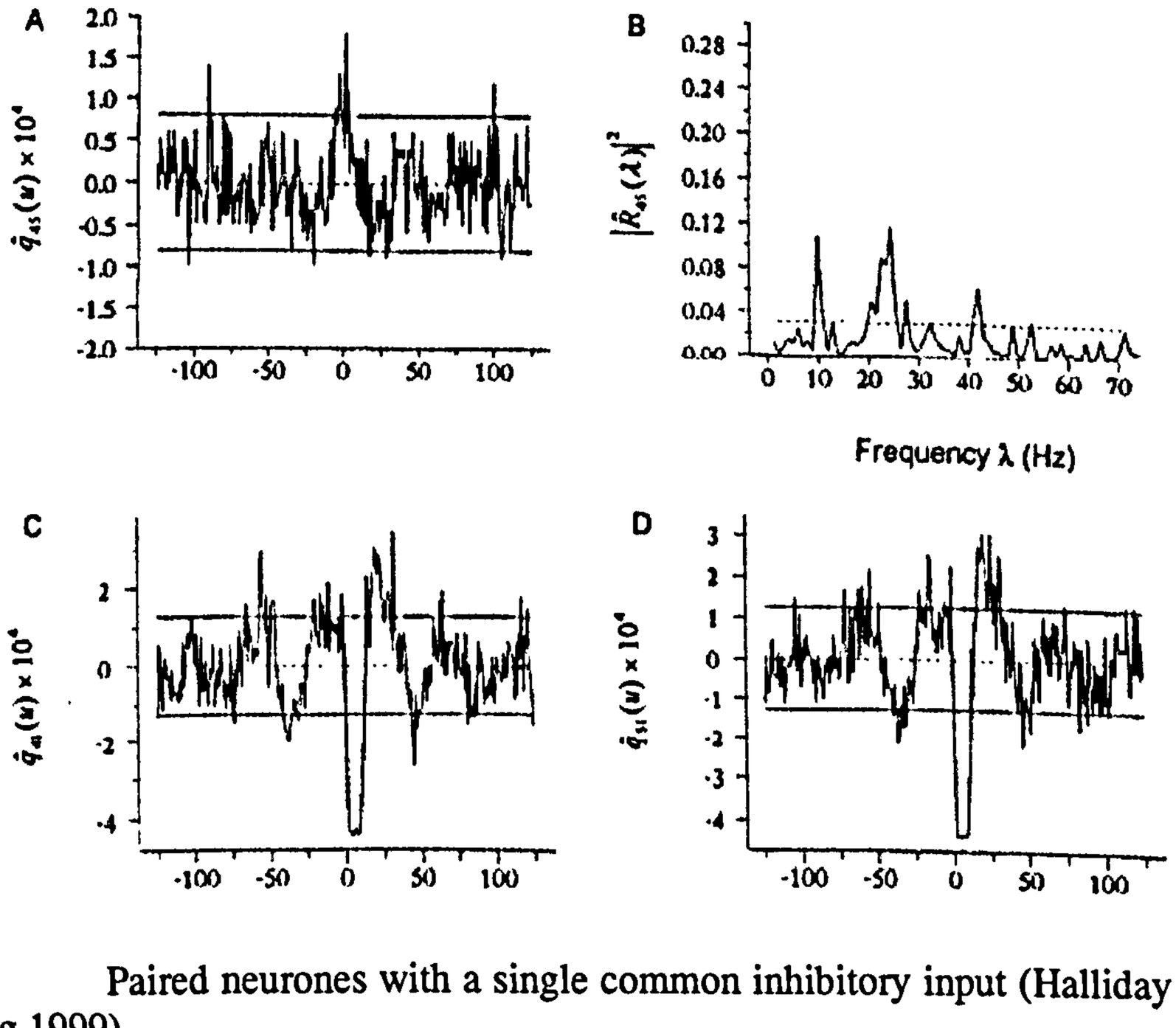

Fig. 9.19 Paired neurones with a single common inhibitory input (Halliday and Rosenberg 1999).

9.3.2.2 Simple neuronal networks

Simulation studies of simple neuronal networks will be presented. These examples will give an outline of what cumulant analysis can reveal about the structure of a simple network

9.3.2.2.1 Paired neurones with a single common excitatory input.

In Fig. 8.18 we can see a simple neuronal network, consisting of two neurons receiving a common excitatory input and independent inputs. *N*1 represents the single common input, a 10 Hz sinusoidally modulated spike train with Gaussian distribution of intervals, to two neurones whose output spike trains are represented by *N*4 and *N*5 while *N*2 and *N*3 are independent inputs to the paired neurones. Peaks in the coherence estimated from a sample of the discharges from the pair of neurones driven by the common input reflect the two dominant frequency components in the spectrum of the common input. The cross-covariance plot gave a high and narrow peak at lag u=0ms. The peak in the N4 autospectrum in Fig. 8.18, represents the mean firing rate of the corresponding neuron.

9.3.2.2.2 Paired neurones with a single common inhibitory input.

This time the single input, *N*1, common to processes *N*4 and *N*5 is inhibitory. In this example the three pair wise cross-covariances would allow the identification of a common inhibitory input from *N*1 to *N*4 and *N*5 (Fig. 8.19). Common inhibition gave a peak in the cross-covariance centred near lag u=0ms. The magnitude of this peak was smaller than for the excitatory common input Fig. 8.18.

The coherence plot is similar to the one obtained for common excitation, containing two major frequency components. One of the oscillation of the common input and one of the mean firing rate of the common input.

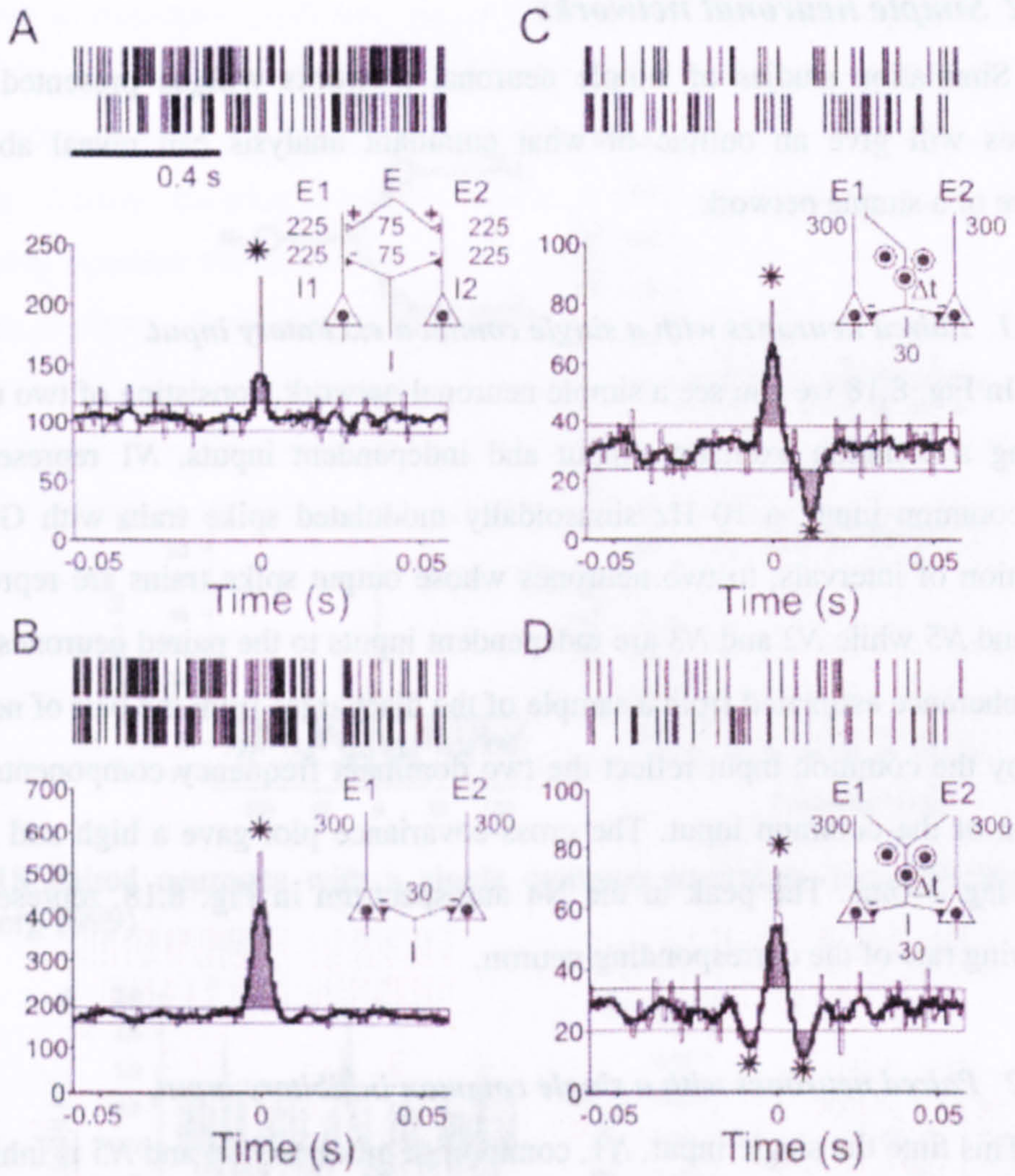

Fig. 9.20 Balanced excitation-inhibition in simple counting neurons. (A) Common excitatory and inhibitory inputs produced a sharp central peak. Rasters of the first 1 s of the cell discharge are shown at the top. Twenty seconds of activity in total were simulated. (B) The common source of excitatory inputs was removed. The common inhibitory inputs were adjusted to resemble the properties of somatic inhibition. (C) Delayed common inhibitory feedback from one excitatory pathway. (D) Delayed common inhibitory feedback from both excitatory pathways. The central peak was flanked by symmetrical troughs (Pauluis 2000).

9.3.2.2.3 Balanced excitation-inhibition in simple counting neurons

The counting model proposed by Shadlen and Newsome was used for the following simulation. Two cells were simulated with independent random trains of events for inputs, with a Poisson distribution with 50 Hz mean frequency. In the first simulation (Fig. 8.20*A*), 75 of 300 of each of the excitatory and inhibitory inputs were common to the two cells, while the rest of them were independent, which produced a narrow cross-correlation peak, similar to the one seen in Fig. 8.18 (Pauluis 2000).

For the simulation in Fig. 8.20*B*, only 30 inhibitory inputs were simulated, shared between the two cells with no common excitatory drive present. A central peak appeared in the cross correlation histogram exhibited, but no trough was present.

The effect of a delayed inhibitory feedback was examined in the next simulation. As shown in Fig. 8.20*C*, such a model produced a trough on one side of the central peak. The generation of the inhibitory input time course as a scaled-down version of a higher-rate process meant that the coefficient of variation of the inhibitory firing was lower than previously, producing the reduced output firing rate compared to previous simulations.

The final simulation tested the effect of constructing the common inhibitory drive by scaling down and averaging both excitatory sources, according to the following equation:

This simulation generated a cross correlation histogram with a central peak surrounded by symmetrical troughs (Fig. 8.20*D*). Fig. 8.20*D* suggests that network oscillations are not required to produce collateral troughs in a cross correlation histogram and that a delayed common inhibitory feedback.

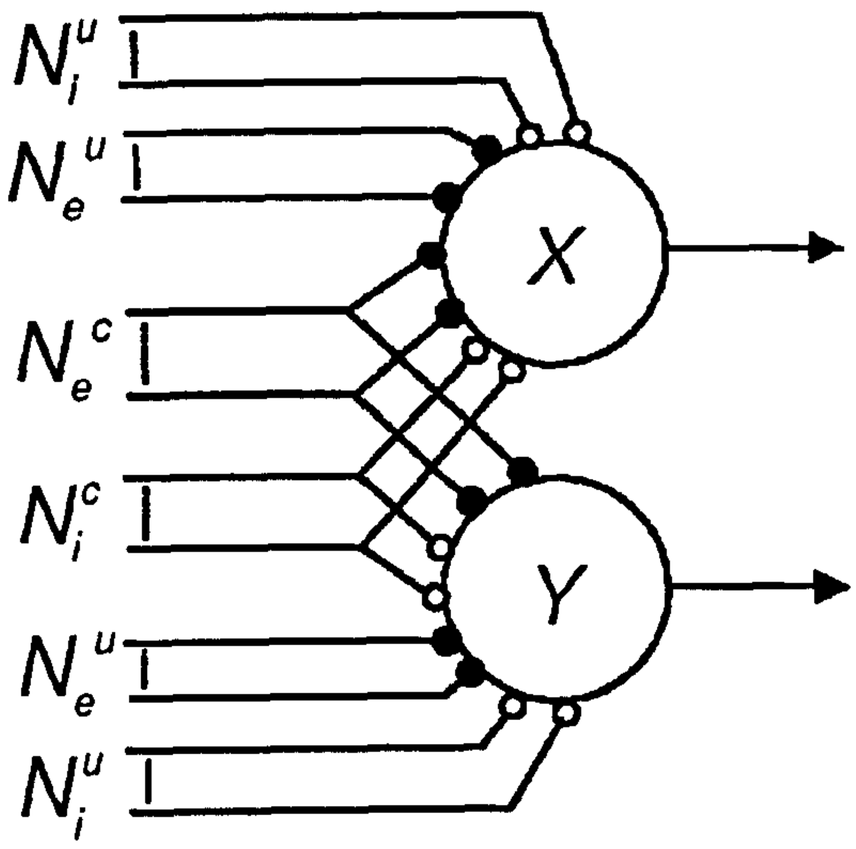

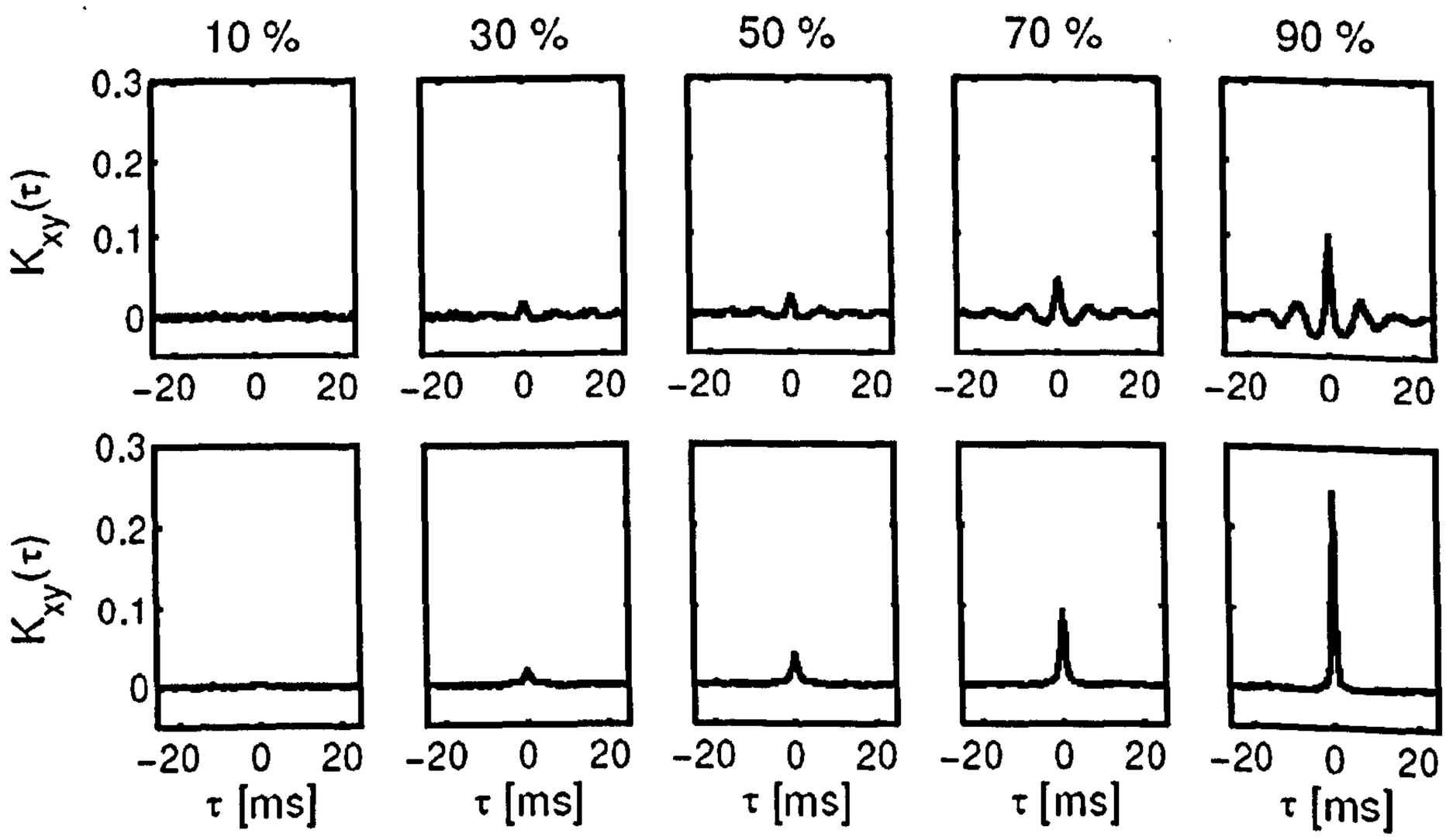

Fig. 9.21 Cross-correlation between output spikes of two conductance based integrate and fire neurons X and Y with partially common excitatory (le D 100 Hz) and inhibitory input (upper row: λi=30 Hz, bottom row: λi=90 Hz). The columns represent 10%, 30%, 50%, 70%, and 90% common excitatory and inhibitory input. Averages are over 16,500 to 25,000 spikes; bin size is 0.5 ms (Stroeve and Gielen 2001).

9.3.2.2.4 Neurons with partially common excitatory and/or inhibitory input sources without correlation

The correlation between the firing of two neurons with partially common excitatory and/or inhibitory input sources without correlation in the input streams of each single neuron is now seen in Fig. 8.21.

The cross-correlation of neural activity of two neurons with both common excitatory and inhibitory inputs, for various ratios of common input, and both for a low (30 Hz) and a high (90 Hz) inhibitory frequency is seen in Fig. 8.21. The cross-correlation had only a single central peak for 90 Hz, whereas it is oscillatory for 30Hz due to the small coefficient of variation of the neurons with low inhibitory input. This means that after synchronous spiking of the two neurons due to the common input, there is a large probability that both neurons will fire again after a time equal to the interspike interval $\langle ISI \rangle$. The oscillation frequency equals $\langle ISI \rangle^{-1}$. The coefficient of variation is much higher for 90Hz common input and the cross-correlation is not oscillatory. Second, as expected the zero-time increases with the proportion of common input (Stroeve and Gielen 2001).

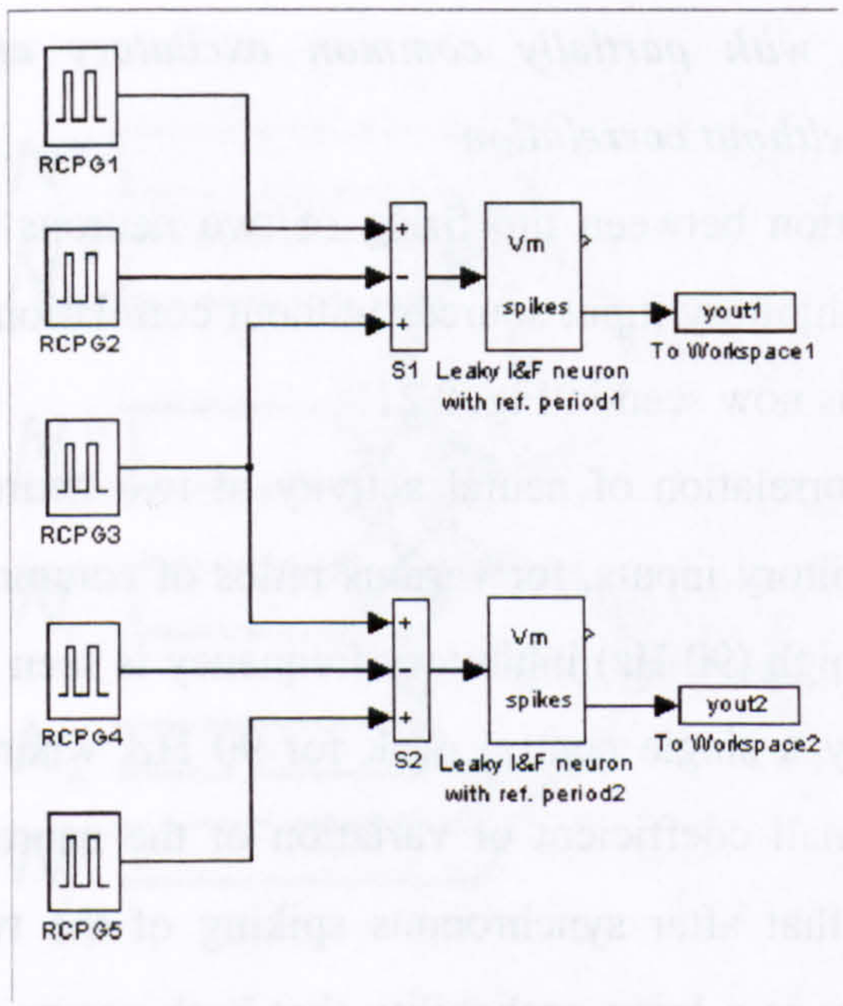

Fig. 9.22 The figure shows two neurones (threshold 5mV, refractory period 5ms, capacitance 1nF, resistance 20MOhms) that are receiving a common excitatory input, and independent excitatory and inhibitory inputs.

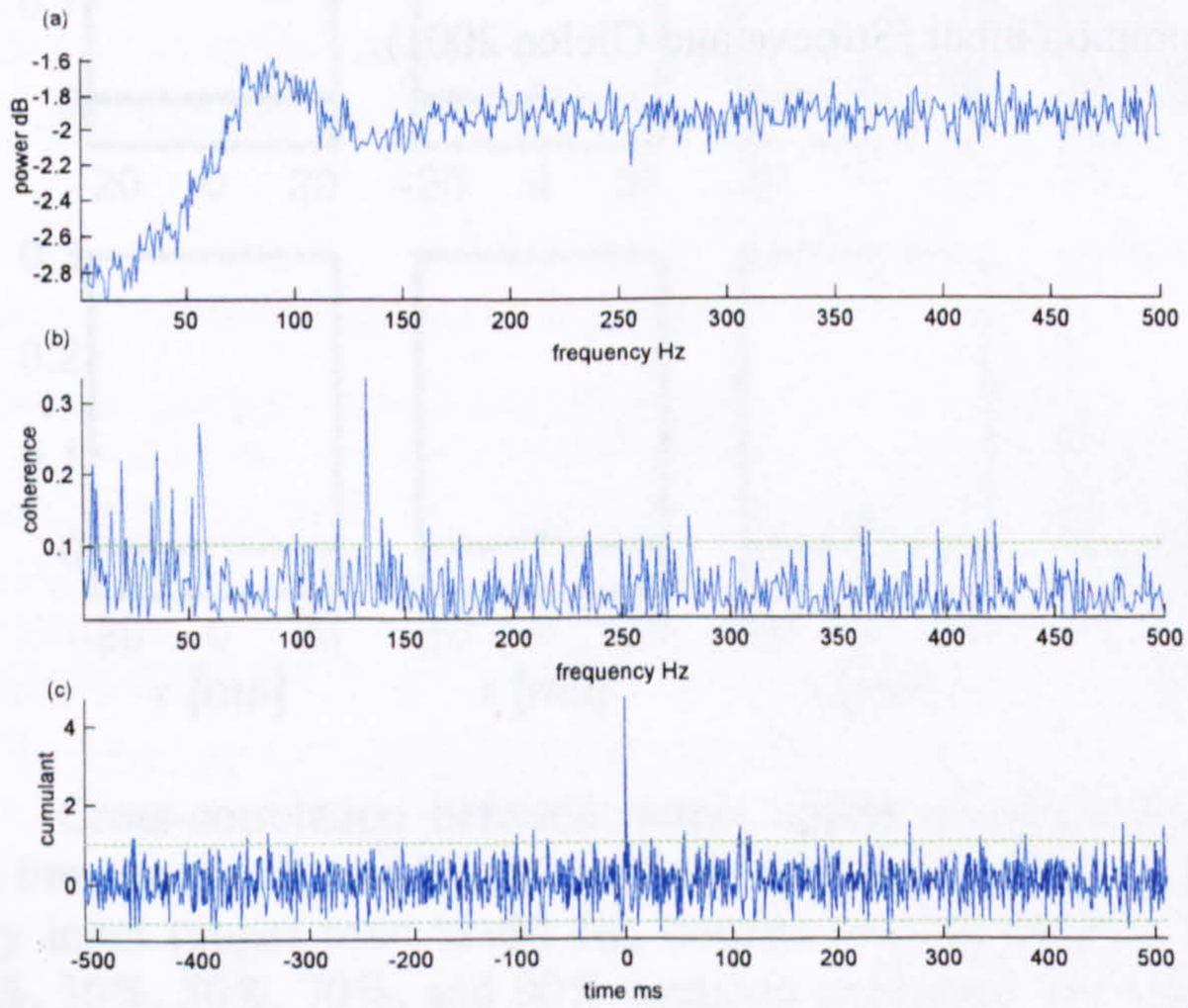

Fig. 9.23 (a) shows the power spectrum of *yout1*, very similar to the power spectrum of *yout2*. (b) shows the coherence and (c) shows the cumulant between outputs *yout1* and *yout2*.

9.3.3 Simulation study

Neurones usually receive a large number of common and independent inputs. Given the simultaneous measurement of a number of spike trains, the systematic application of cumulant coherence and phase measures is a powerful tool for determining patterns of neuronal connectivity. The simulated systems are simple neuronal networks, based on the literature presented before or built on purpose. These simple systems may form the basis for explaining the function of more complex networks than those discussed.

9.3.3.1 Example 1 - Neurones receiving a common excitatory input

Two neurones are receiving a common excitatory input (Fig. 8.22). The common input consists of 20 excitatory Poisson spike processes, each with a mean interspike interval of 20 ms. The independent excitatory and inhibitory inputs share the same properties as the common input, each consisting of 20 Poisson spike processes, with a mean interval of 20 ms. Threshold level for the two neurones at 5mv and 5ms refractory period result to 76Hz output mean firing rate. In figure Fig. 8.23*a*, the power spectrum of output *yout1* (which is very similar to the autospectrum of the *yout2*) can be seen. It contains a peak close to the mean output frequency. The coherence plot (Fig. 8.23*b*) reveals broad coupling throughout the spectrum, with 0-50 Hz the area showing the highest coupling. Despite the common maximum for *yout1* and *yout2* power spectra, there is no clear coherence peak in that area. In Fig. 8.23*c* the cumulant density can be seen. This is also common result for physiological signals as well. As it will be shown later, often increased power in the same band does not result in coupling for the same band. A central narrow peak at zero ms exceeding the confidence limit is the main characteristic in the cumulant plot. The fact that the peak occurs at zero ms reveals that there is no delay for one of the two inputs. In case a small time delay is introduced in the input of one of the two neurons the central peak will be shifted accordingly. The distance of the central peak from zero can reveal the length of the delay.

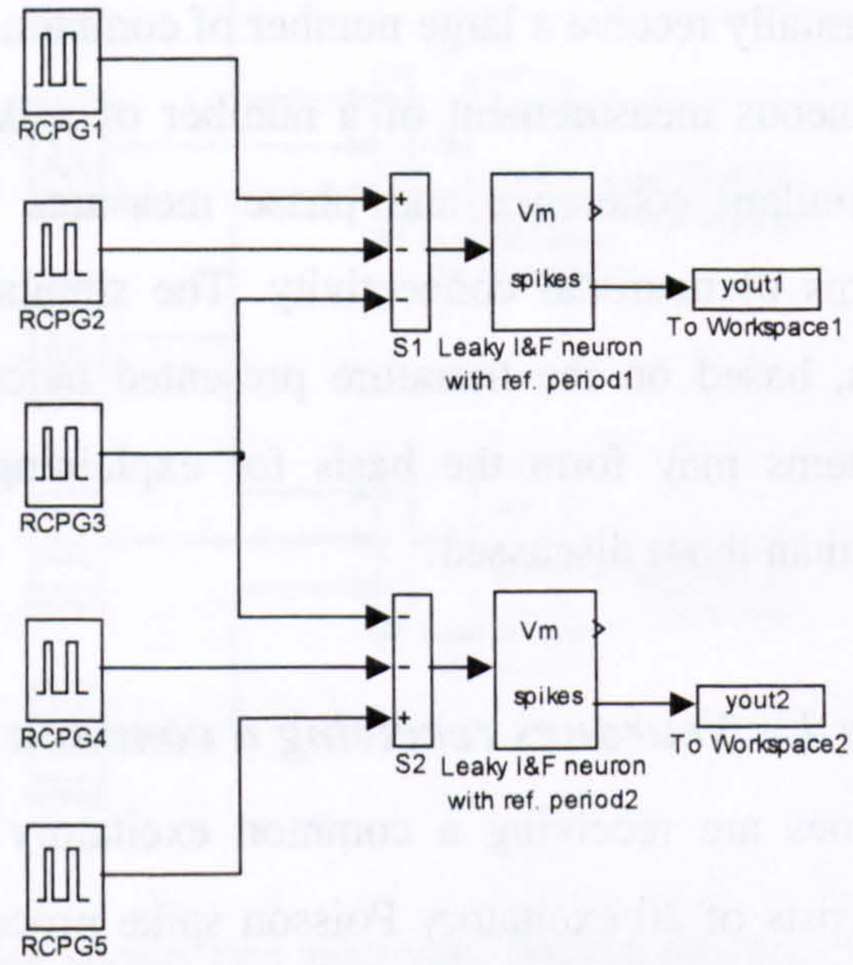

Fig. 9.24 The figure shows two neurones (threshold 5mV, refractory period 5ms, capacitance 1nF, and resistance 20MOhms) are receiving a common excitatory input, and independent excitatory and inhibitory inputs.

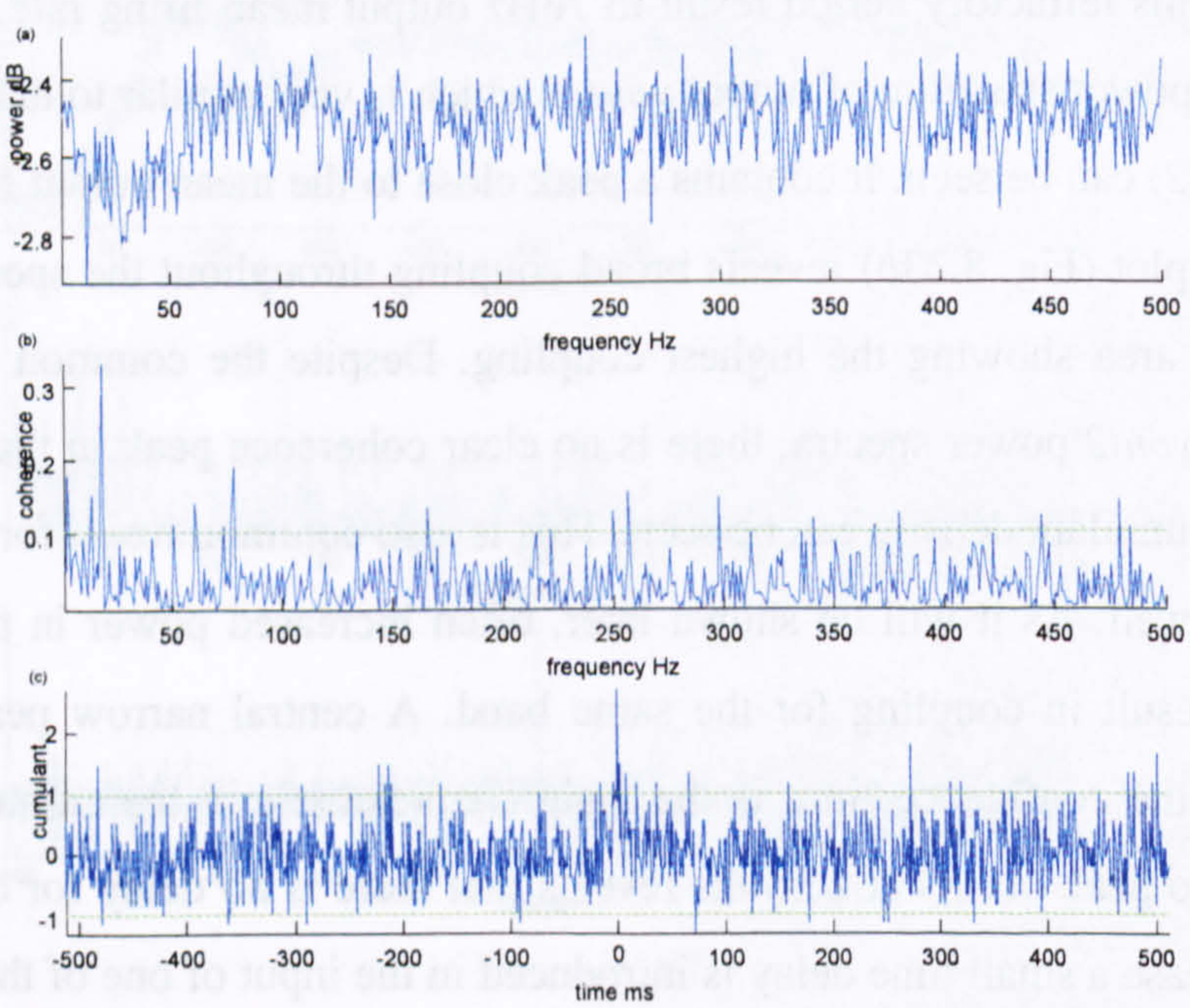

Fig. 9.25 (a) shows the power spectrum of *yout1*, very similar to the power spectrum of *yout2*. (b) shows the coherence and (c) shows the cumulant between outputs *yout1* and *yout2*.

9.3.3.2 Example 2 - Neurones receiving a common inhibitory input

Two neurones are receiving a common inhibitory input. In Fig. 8.24 the simulation network can be seen. The common input consists of 35 excitatory Poisson spike processes, each with a mean rate of 20 ms. The independent excitatory inputs share the same properties, each consisting of 40 Poisson spike processes, with a mean rate of 20 ms. The independent inhibitory inputs consist if 5 Poison spike processes with a mean rate of 20Hz. The threshold level for the two neurones is 5 mV. In contrast with the previous example a trough in the power spectrum can be seen in the mean output frequency band. Fig. 8.25*a* gives the autospectrum of yout1 output, which is very similar to the one of *yout2*. In Fig. 8.25*b,c* the coherence cumulant and cumulant plots can be seen. A central peak at zero ms exceeding the confidence interval is the main characteristic in the cumulant plot. Coherence over the confidence limit can be observed for the whole spectrum, with the low frequencies again showing higher coherence.

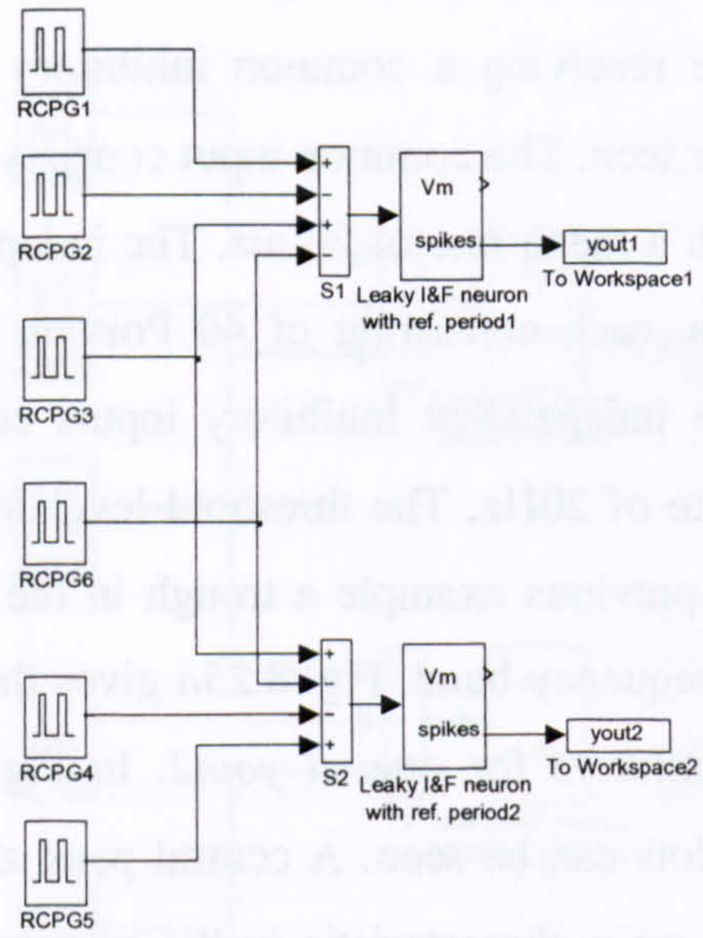

Fig. 9.26 The figure shows two neurones (threshold 5mV, refractory period 5ms, capacitance 1nF, resistance 20MOhms) are receiving a common excitatory input, and independent excitatory and inhibitory inputs.

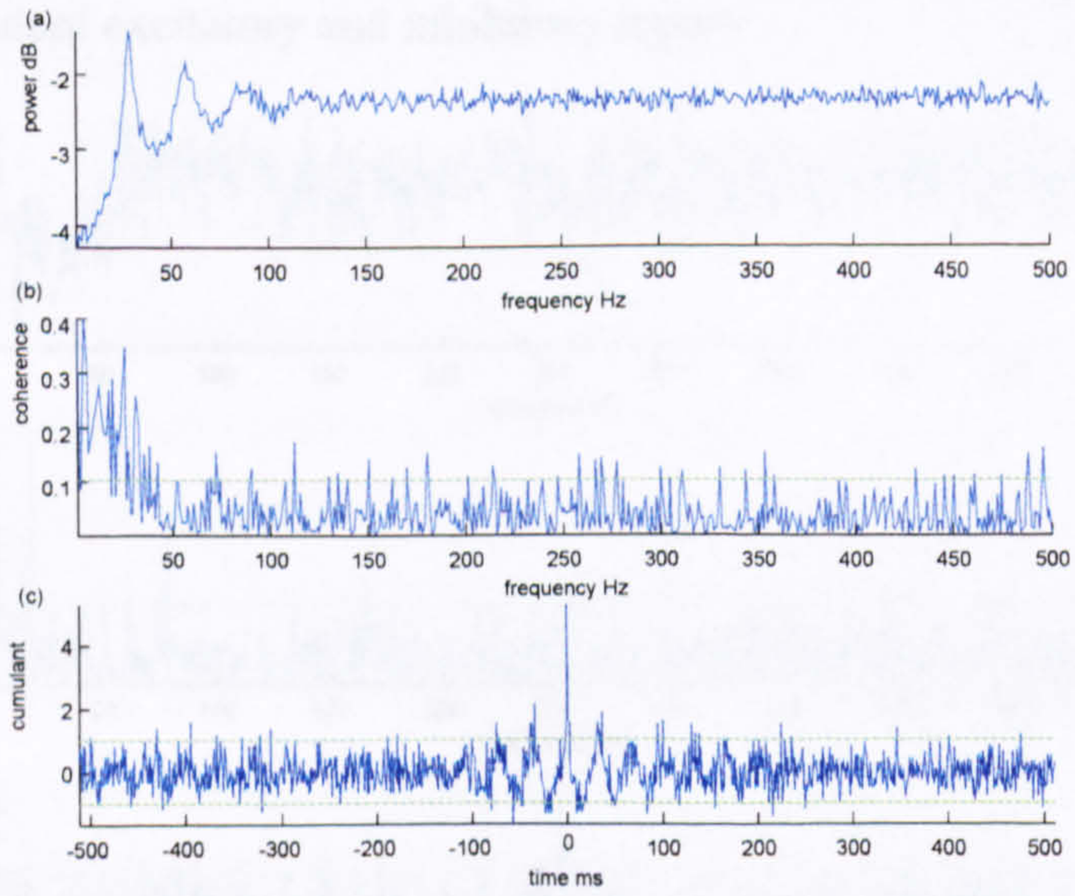

Fig. 9.27 (a) shows the power spectrum of *yout1*, very similar to the power spectrum of *yout2*. (b) shows the coherence and (c) shows the cumulant between outputs *yout1* and *yout2*.

9.3.3.3 Example 3- Non oscillatory inputs producing oscillatory output

This model (Fig. 8.26) is going to demonstrate the fact that non oscillatory inputs can produce oscillatory output cumulant plot. Two neurones are receiving a common excitatory and a common inhibitory input as well as independent inhibitory and excitatory independent processes. The common input is comprised by 90 excitatory Poisson spike processes (100 Hz mean rate each) and 90 inhibitory Poisson spike processes (30 Hz mean rate each). Each of the independent excitatory and inhibitory inputs consist of 10 Poisson spike processes that share the same properties as the common inputs. 85mv of threshold level and 15 ms of absolute refractory period result to 27 Hz output mean rates.

The autospectrum (Fig. 8.27a) shows a peak at 27 Hz which also is the mean output firing rate. It is also characterised by strong harmonics of this frequency. Broad coherence, strong in the 0-50Hz area can also be observed (Fig. 8.27b), without any well defined peak. Small coherence peaks over the confidence interval can be observed for the rest of the coherence spectrum. The cumulant plot (Fig. 8.27c) has a visibly oscillatory shape which also possesses a prominent narrow peak at 0 ms. The frequency indicated by the secondary peaks is around 27 Hz. The oscillation frequency is clearly defined by the mean output frequency.

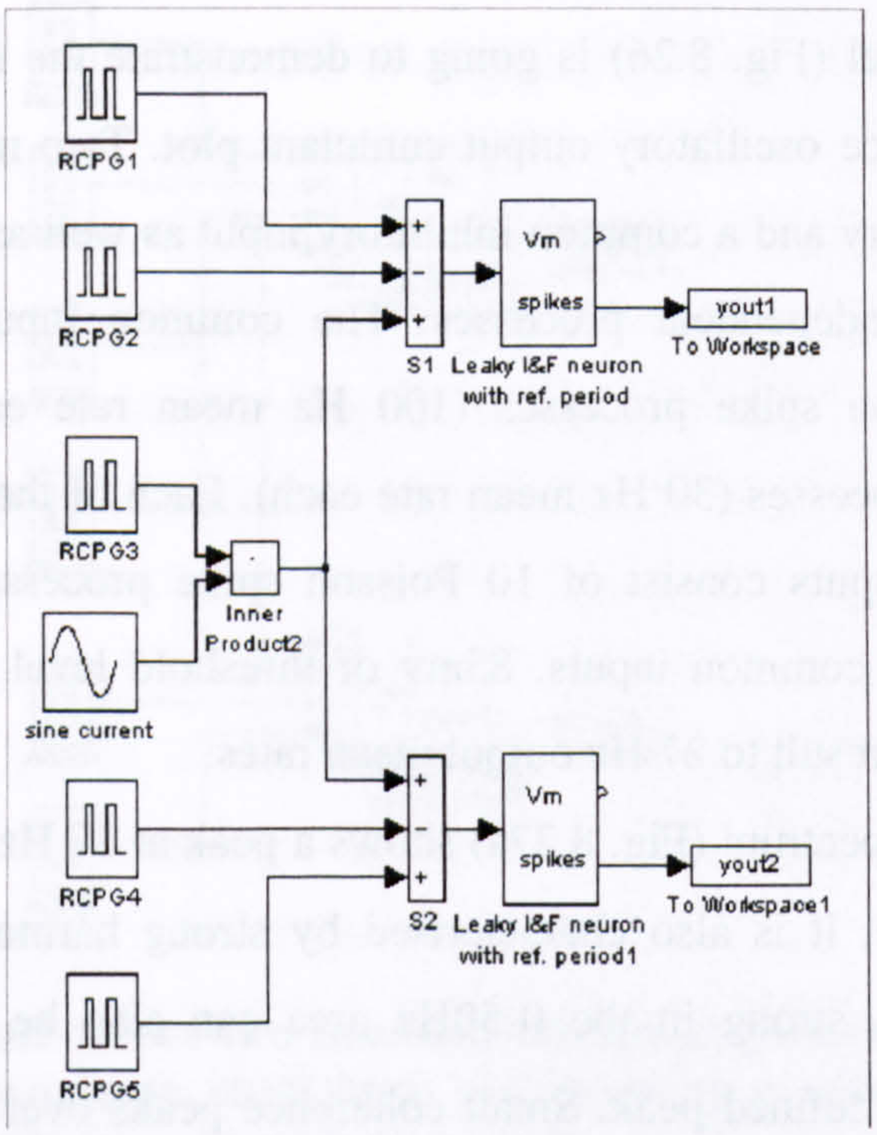

Fig. 9.28 The figure shows two neurones (threshold 5mV, refractory period 5ms, capacitance 1nF, resistance 20MOhms) are receiving a common oscillatory input with common excitatory poison processes, and independent excitatory and inhibitory inputs.

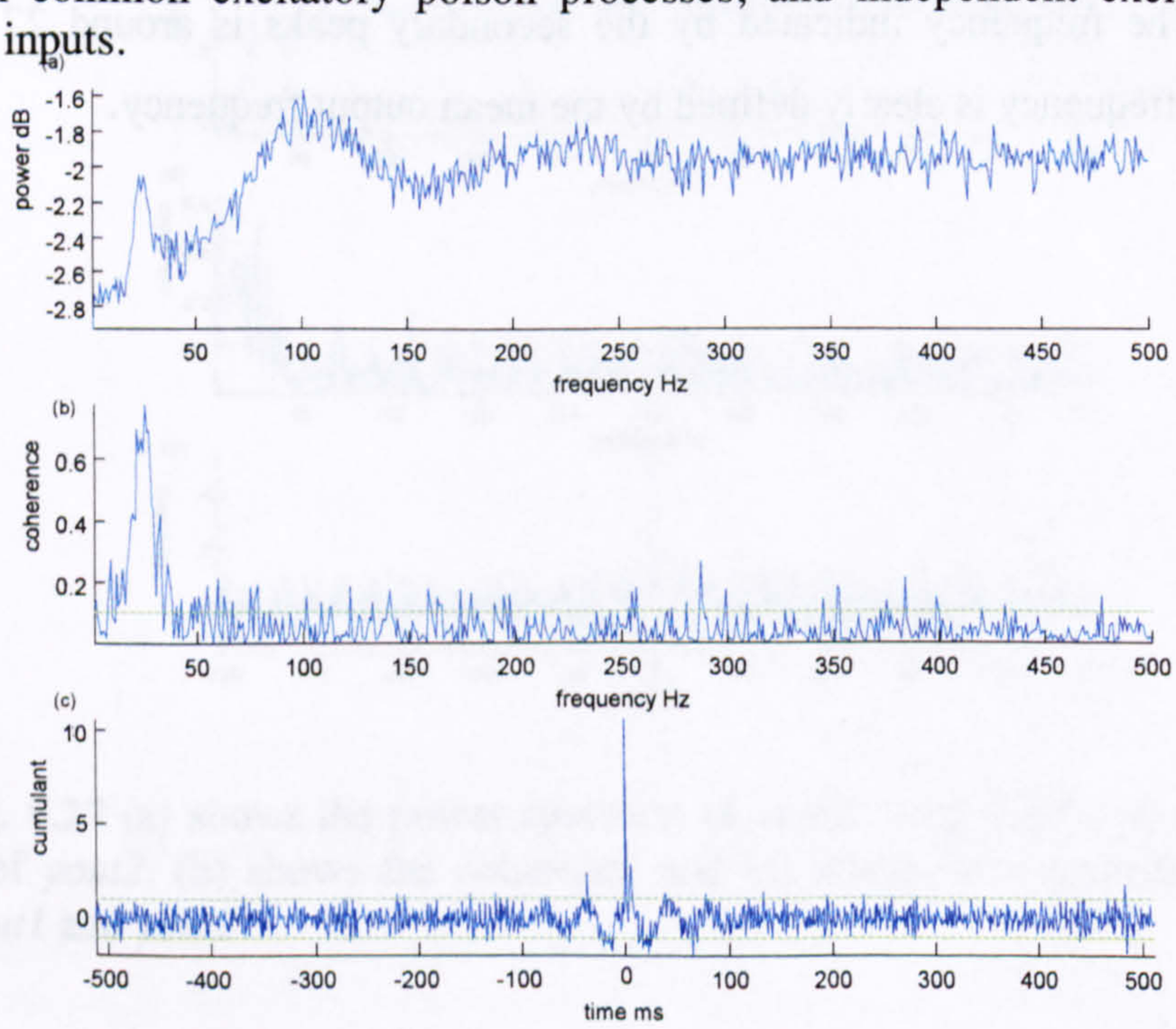

Fig. 9.29 (a) shows the power spectrum of *yout1*, very similar to the power spectrum of *yout2*. (b) shows the coherence and (c) shows the cumulant between outputs *yout1* and *yout2*.

9.3.3.4 Example 4 - Common oscillatory inputs

The next two simulations will demonstrate the effect of common oscillatory Poisson processes in frequency characteristics of neuronal output. While in the previous examined model non oscillatory inputs resulted in oscillatory shape cumulant this time oscillatory inputs will result in oscillatory cumulant plots. The first model is illustrated in Fig. 8.28. The common input is comprised by 20 common Poisson processes, with 20 ms mean rate each, modulated by a sinusoidal signal with period 25Hz. For the second model illustrated in Fig. 8.30 the input comes in the form of independent Poisson process sets (20 processes with 20ms mean rate each), for each cell, modulated by a common sinusoidal signal, with the same characteristics as for the previous model. For both models each cell also receives independent inhibitory and excitatory Poisson inputs.

The comparative results can be seen in Fig. 8.29 and Fig. 8.31. The output power spectra are extremely similar. The coherence analysis plots are quite similar especially around the frequency of high coherence. A closer look however can reveal certain differences. First of all the maximum coherence is slightly larger for the first model Fig. 8.29a (common Poisson inputs) than for the second Fig. 8.31a (common modulating signal). Secondly while the coupling for the second model is concentrated around the frequency of the modulating signal, for the first model more widespread coherence can be observed, mainly in the 0-70 Hz area, and also peaks arise over the confidence limit throughout the whole spectrum. This "additional" coherence is indeed similar to the coherence observed in Fig. 8.23 where the input consisted of only of excitatory Poisson inputs without modulating signal.

The cumulant plot has been significantly affected. In both cases it has an oscillatory shape but for the first model a significant narrow central peak can be observed in Fig. 8.29b that is not present for the common modulating signal in Fig. 8.31b. This peak is similar to the one observed in Fig. 8.23 and is obviously created by the common Poisson inputs.

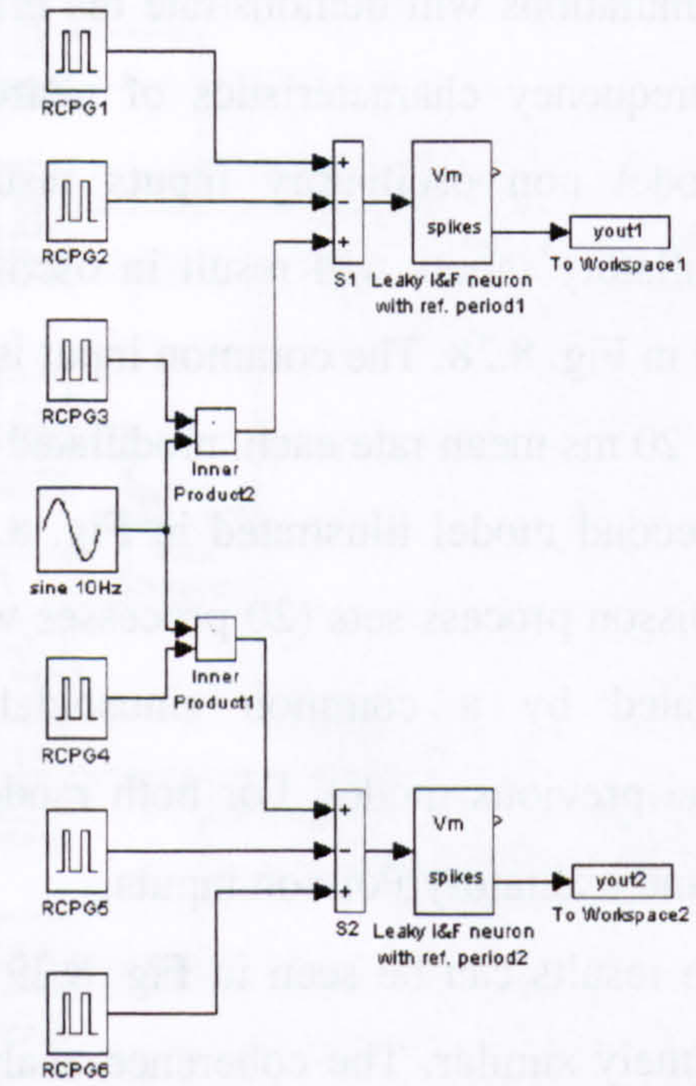

Fig. 9.30 The figure shows two neurones (threshold 5mV, refractory period 5ms, capacitance 1nF, resistance 20MOhms) are receiving a common oscillatory input with independent excitatory poison processes, and independent excitatory and inhibitory inputs.

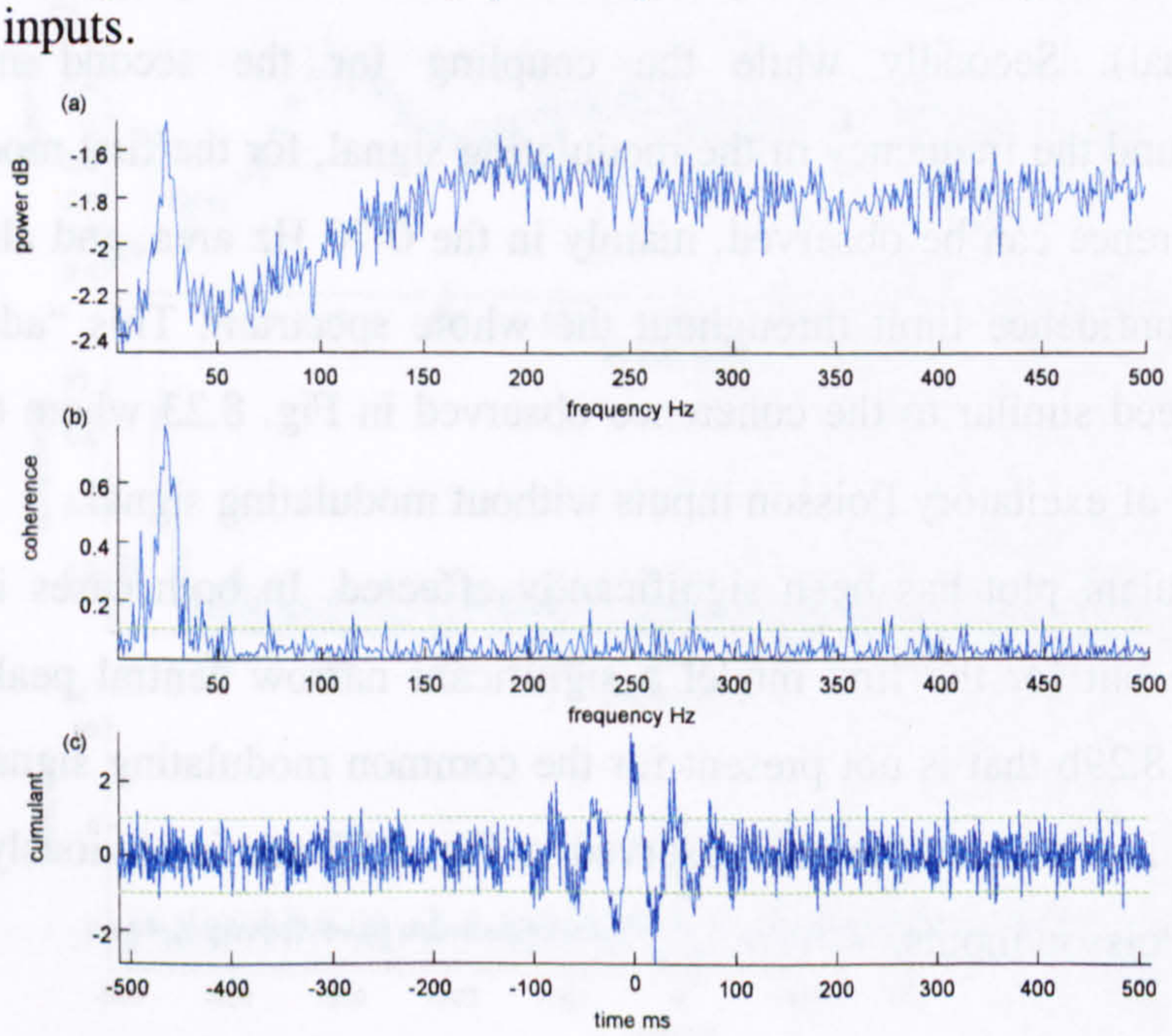

Fig. 9.31 (a) shows the power spectrum of *yout1*, very similar to the power spectrum of *yout2*. (b) shows the coherence and (c) shows the cumulant between outputs *yout1* and *yout2*.

9.4 *APPENDIX 4 - INFORMATION FOR VOLUNTEERS*

Purpose of the investigation

The aim of the project is to investigate the physiological mechanisms of human movement. The results of this investigation on normal subjects will be used as an aid for patients (mainly amputees) in the form of prosthetic devices that will be able to detect the patients intention for movement by processing signals taken from superficial electrodes from the amputated limb and be able to control neuroprosthetic devices.

Methodology and procedures

The investigation includes a spectrum of methods. Not all of them are going to be used for the current experimental setup. The investigator will give you more details on which of the methods are going to be used.

EEG recordings

EEG electrodes are going to be placed on the head and will record brain activity in the form of small currents flowing on the skin of the head.

EMG recordings

EMG electrodes are going to be placed on the skin overlying muscles of which the activity we wish to record.

Electrical stimulation

Short current pulses will flow through strategically placed electrodes simulating nerves or muscles.

Ischemic nerve block

The blood flow in the upper limb will be blocked by inflating a sphygmomanometer cuff over the blood pressure for approximately 20min.

Potential hazards

There is a small risk of allergic reaction because of the electrodes, the electrolyte gel or the adhesive tape that is going to be used. If you have experienced in the past such a reaction you should inform the investigator.

During the ischemic nerve block there is a small risk of blood clots, especially in female subjects using contraception. All female patients should be excluded from this specific procedure.

All the methods to be used have been described as safe in previous experimental and clinical applications. The equipment to be used complies with the safety standards and the investigators have extended experience using it. However there is always a negligible danger of an electric shock in case of catastrophic malfunction of the equipment.

Even though the methods o be used are safe, they can be uncomfortable for some subjects. Nerve and muscle electrical stimulation cause a tickling sensation that can become painful. The subjects have the right to stop the experiment at any time and for any reason.

Participant consent form

Subject name :_____

Date of birth :_____

	Please tick	YES	NO
• Have o read the information sheet?		☐	☐
• Have you had the opportunity to ask questions and discuss the study with the investigator?		☐	☐
• Have you received satisfactory answers to all your questions?		☐	☐
• Have you received enough information about the study?		☐	☐

Who have you spoken to?_____

• Do you understand you are free to withdraw from the study at any time, without having to give a reason?	☐	☐
• Do you agree to take part in the study?	☐	☐

Signed_____

Name in block letters_____

Date_____

Name of witness in block letters_____

Signature of witness_____

Date_____